PETROLOGY AND GEOCHEMISTRY

OF THE CENTRAL MINDANAO VOLCANIC ARC,

SOUTHERN PHILIPPINES

A thesis

submitted in fulfillment

of the requirements for the Degree

of

Doctor of Philosophy in Geology

in the

University of Canterbury

by

ERNESTO SOLIMAN G. CORPUZ

University of Canterbury

1992

In memory of my brother, Benjamin

CONTENTS

LIST OF FIGURES

Page

LIST OF TABLES

APPENDICES

ABSTRACT

This paper presents the regional geology, geochemistry and petrogenesis of volcanic rocks from Central Mindanao Volcanic Arc (CMVA), Philippines. This NNW-trending arc, from Lat 6°N-Long 125°E to Lat 9°15'-Long 125°30'E occurs parallel to the Philippine Trench and to regional structures E of Lake Lanao. CMVA centres occur 150-200 km above a W-dipping subduction system. Subduction associated with the Philippine Trench probably produced the CMVA.

CMVA can be grouped into 3 volcanically and seismically active arc segments from N to S: i) Misamis, ii) Bukidnon and iii) Davao. Camiguin Island is the most active volcanic field and resulted from SE-NW progression of volcanism from late Pliocene-Pleistocene lavas of Butay, Cabuan, Mt Ginsiliban and Mt Mambajao to Pleistocene-Recent lavas of Mt Catarman and Hibok-Hibok. Stratigraphy of historical deposits from Hibok-Hibok shows a range of volcanic products typical of other centres: domes, lava flows and pyroclastic flows.

The rocks of CMVA are crystal-rich (40-50 vol% average) with a main phenocryst assemblage of plagioclase (An_{84-31}) + clinopyroxene (augite, diopside) ± olivine (Fo_{84-72}). Ti-magnetite usually crystallised late. Two types of andesite occur: pyroxene (augite ± enstatite) and hornblende (magnesium-ferri hornblende) andesite. Two dacite types are also recognised. Type 1 dacite (Mt Katanglad, Butay) usually has fine grained plagioclase + clinopyroxene whereas Type 2 dacite (Hibok-Hibok, Mt Apo) has medium-coarse grained amphibole ± biotite. Phenocryst chemistry shows that with increasing bulk-rock SiO_2, plagioclase, olivine, clinopyroxene and Ti-magnetite follow chemical trends consistent with equilibrium crystallisation. Exceptions occur in basaltic andesite and some SiO_2-rich andesite in which olivine is Fe-enriched, plagioclase is more calcic than in basalts (An_{78-84} vs An_{50-78}) and there is a large incidence of reverse zoning in clinopyroxene.

The most widespread lavas are medium-K calcalkaline (CA) basalt, andesite and dacite with occasional low-K and high-K CA lavas. Major and trace element variations are similar with other island arc basalt (IAB) and exhibit the characteristic depletion in Zr, Ti, Y and to a lesser extent, of Ce relative to N-MORB. N-MORB normalised trace element contents are generally >1.0 and have low Zr/Nb ratios (7-14) indicating an E-MORB/OIB type mantle wedge. All CMVA basalt-basaltic andesites have lower Mg#, Cr and Ni relative to primitive MORB, probably a result of olivine-dominated fractionation. Silica activity (-0.33 to -0.36 log units) and crystallisation temperatures (1,090 - 1,161°C) of CMVA basalts suggest a source region geochemically between olivine tholeiite and alkaline olivine basalt. Basaltic analyses, corrected for olivine fractionation, suggest primitive CMVA compositions resemble magnesian MORBs. Assuming equilibrium batch melting, CMVA parental magmas segregate from residues at 10-15 kbar after 10-14% partial melting. The resultant melts are LIL-element enriched with high Ba/Nb and Ce/Nb ratios indicating a slab contribution although crustal contamination was probably low, based on low Rb/Sr ratios (0.015-0.026) relative to other IAB (0.03) and continental crust (0.12). Andesite and dacite can be modelled satisfactorily by low pressure closed-system crystal fractionation. The main fractionating assemblage is olivine + clinopyroxene + plagioclase ± Ti-magnetite in basalt-basaltic andesite melts whereas plagioclase + amphibole ± Ti-magnetite fractionate from basaltic andesites to form SiO_2-rich andesite and dacite. Magma mixing and assimilation probably occurred at Mt Apo.

In summary, the deeper seismic zone beneath CMVA relative to other island arcs may be explained by lateral transport of fluids from subducted slab (Davies and Stevenson, 1992) using a slab-induced convection model (Tatsumi, 1986; Saunders et al, 1991). Partial melts segregate at depth (spinel peridotite field) to form olivine or nepheline to diopside-normative tholeiites. As these magmas ascend, they cool, become more dense and pond at the lower crust where they differentiate to high-Al basalt and basaltic andesite. Diapirs then migrate from lower crust to shallow magma chambers (< 5 km) where extensive fractional crystallisation results in andesitic magmas. Disequilibrium features of phenocrysts from basaltic andesites support the concept of mixing between a lower basaltic layer and an upper intermediate composition layer. Predominance of intermediate to SiO_2-rich lavas suggest that i) most eruptions tap only the upper portion of compositionally-zoned chambers and/or ii) magma chambers are at a mature stage of chemical evolution.

CHAPTER I GENERAL INTRODUCTION

1.1. INTRODUCTION

The Central Mindanao Volcanic Arc (CMVA) is a volcanically-active region in the southern Philippines. Despite recent volcanism, the geology, composition and tectonic association of this arc are poorly understood. This study investigates the regional geochemical characteristics and proposes a model of geochemical evolution for the CMVA. New geologic data complement this geochemical study.

A fundamental question is whether central Mindanao volcanoes resulted from subduction in the southern Philippines or perhaps evolved from back-arc spreading. The diffuse distribution of volcanic centres precludes a simple relationship with a single subduction zone. The possibility that central Mindanao volcanoes resulted from two arc systems will be examined in this study.

This study defines the CMVA as the region from approximately Lat 6°N, Long 125°E to Lat 9°15', Long 125°30'E (Fig. 1-1). Because there are many volcanoes in the CMVA, only those major centres which are the most active are investigated. The geochemical study emphasises the northern CMVA centres because this portion of the CMVA, based on recent activity and volcanic geology, presents the greatest volcanic risk.

1.2. REGIONAL SETTING OF THE PHILIPPINES

The Philippines is a region of broad deformation and active seismicity due to the interaction of the Eurasian and Philippine Sea Plates (Fig. 1-1). Relative to Eurasia, the Philippine Plate appears to have a general clockwise rotation at a rate

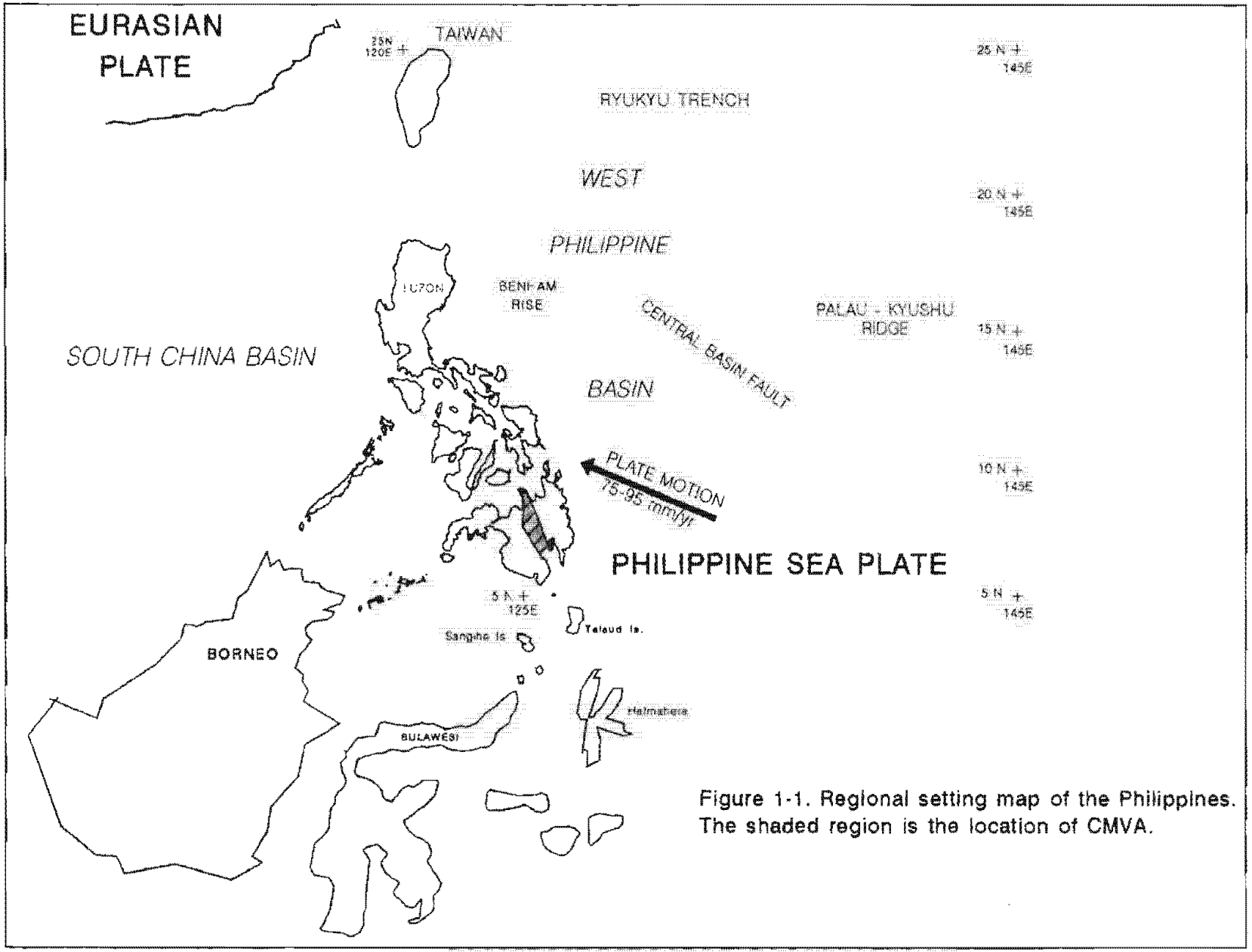

Figure 1-1. Regional setting map of the Philippines. The shaded region is the location of CMVA.

of 1.5° to 2.0° per Ma around a pole of rotation sited at just north of Tokyo (Ranken et al, 1984). Such rotation has resulted in oblique convergence between the two plates with the West Philippine Sea Plate moving WNW at about 75 - 95 mm/yr towards the passive continental margin of mainland Asia. Deformation along the Philippine-Eurasian Plate boundary is accommodated in the Philippine region where marginal basins, subduction zones and major strike-slip faults have developed.

1.3. PRESENT DAY TECTONICS

The Philippines consists of a main composite island arc comprising the Luzon, Visayas, and Mindanao islands (Fig. 1-2). The primary north-south cluster of islands runs from 117°E to 127°E and from 5°N to 20°N. Included in this convergent tectonic setting is the Sulu-Zamboanga ridge, an island arc connecting mainland Mindanao to Borneo. To the north, the Babuyan and Batan islands form the longitudinal arc-ridge between Luzon and Taiwan. Southwest of Luzon is the Palawan ridge, part of the North Palawan-Reed Bank microcontinent derived from the Eurasian Plate. Thus the Philippines is a complex mosaic of island arcs and allochthonous terranes.

At present, the Philippines is wedged between 2 opposing subduction zones where oceanic crust of marginal basins is being underthrust. The 2 main subduction zones are the East Luzon Trough-Philippine Trench system and the Manila-Negros-Cotabato Trench system (Fig. 1-3).

1.3.1. EASTERN CONVERGENT MARGIN

The West Philippine Basin (Fig. 1-1) is being underthrust along the East Luzon Trough-Philippine Trench system (Fig. 1-3). The East Luzon Trough is a NE-trending deep from 15.5°N to 18.5°N separating the Luzon margin from the Benham Rise to the east. Shallow seismicity along the East Luzon Trough is characterised by thrust faulting (Hamburger et al, 1983) which suggests active

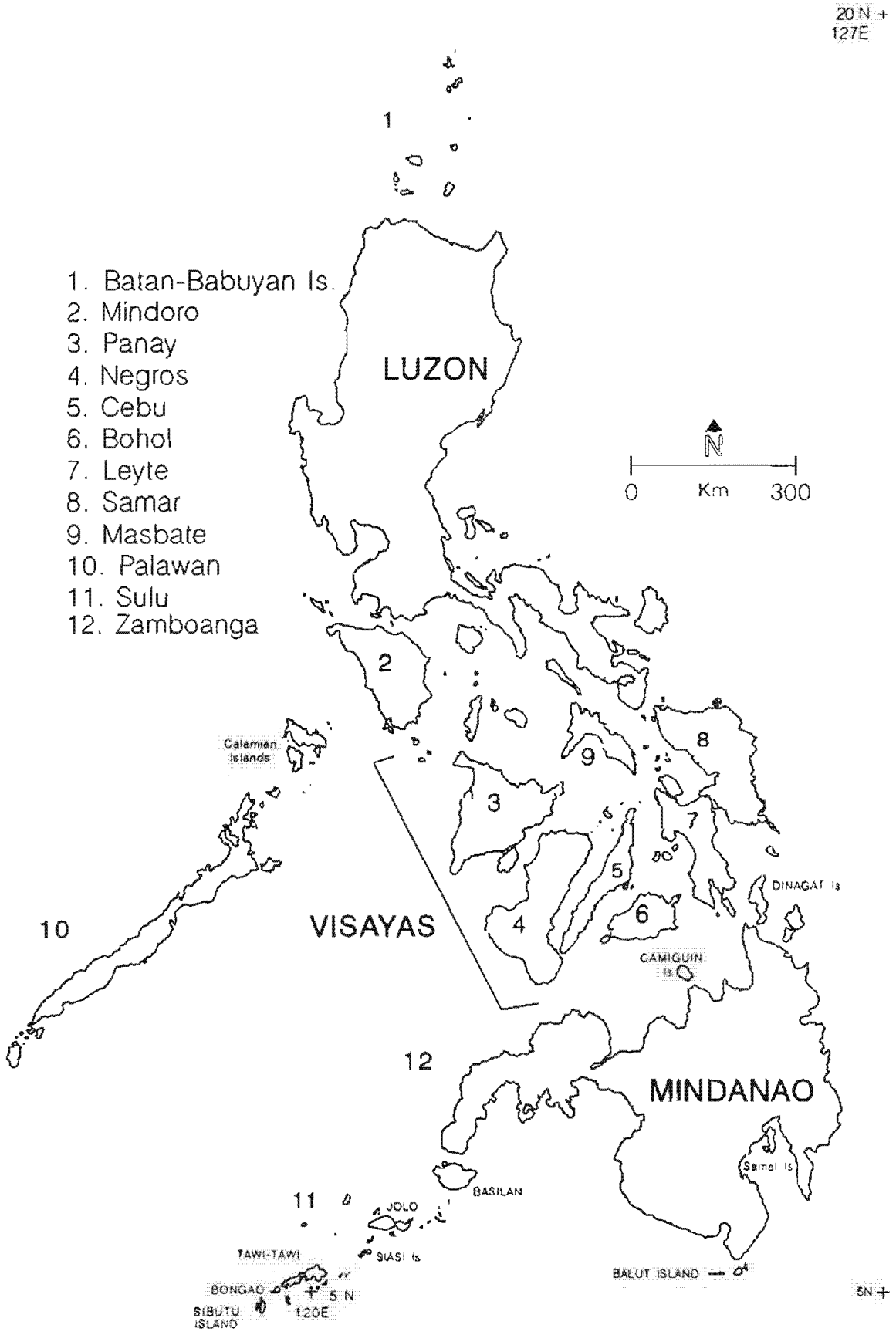

Figure 1-2. Sketch map showing main islands of the Philippines.

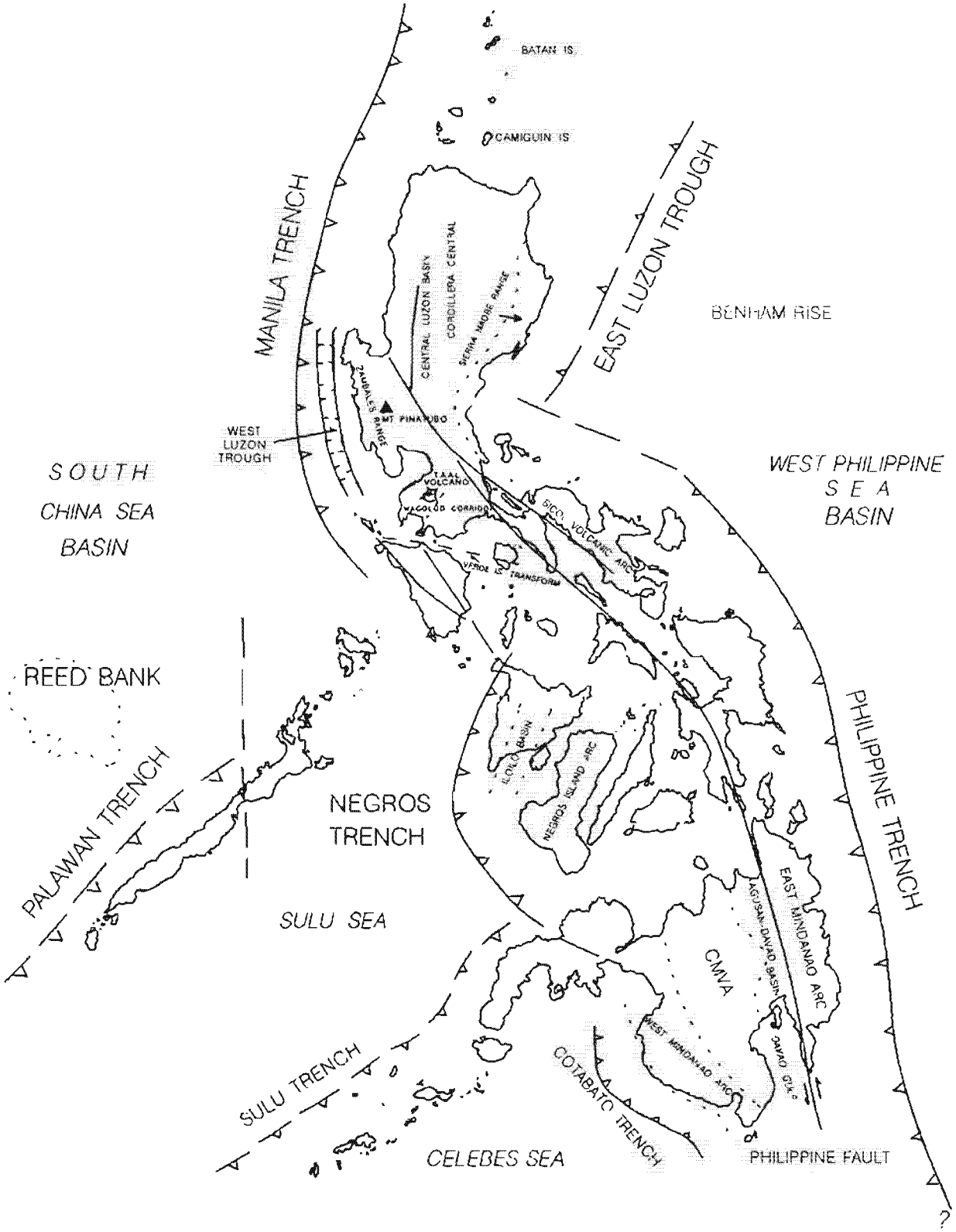

Figure 1-3. Map of the Philippine region showing tectonic elements of the South China and West Philippine Sea Plate boundary.

subduction. In contrast, the region to the north near Taiwan is distinguished by strike-slip faulting which probably marks a major change in the nature of tectonism between east and north Luzon (Lewis and Hayes, 1983).

Convergence of the Eurasian and West Philippine Plates has resulted in the Sierra Madre Range in E Luzon (Fig. 1-3), a convex eastward arcuate belt of mafic to ultramafic rocks and deformed sediments (Karig, 1973). The range includes an ophiolite slab, part of a relict subduction zone present before the East Luzon Trough. At present, subduction along the East Luzon Trough is not deep enough to generate volcanic activity, as indicated by the lack of concentrated seismic activity deeper than 70 km (Hamburger et al, 1983). At the southern end of the East Luzon Trough is a shallow ESE-WNW trough identified by Seno and Kurita (1978) as a trench-trench transform separating the East Luzon Trough from the main Philippine Trench.

Subduction along the Philippine Trench is defined by a Wadati-Benioff zone from 6°N to 15°N with a fault plane that dips variably (24° $\pm$ 10° to 45° $\pm$ 15°). The seismic zone associated with this trench dips westward and is defined by both shallow earthquakes near the trace of the trench and intermediate to deep focus earthquakes (Cardwell et al, 1980). Subduction of the northern portion of the trench has produced the Bicol Volcanic Arc (Fig. 1-3), a series of active and solfataric volcanoes from Luzon to Leyte islands .

1.3.2. Western Convergent Margin

West of the Philippines is the South China Basin, the westernmost marginal basin of the Pacific. The South China Basin has higher than normal heat flow (Karig, 1971) and probably evolved by opening of the South China Sea away from mainland China, perhaps similar to the evolution of the Japan Sea (Taylor and Hayes, 1983). The crust of the South China Basin is oceanic with a thickness of 5 - 6 km. Earthquakes studied by Acharya and Aggarwal (1980) indicate a seismic

zone extends to about 240 km depth and suggests eastward underthrusting of the Eurasian Plate beneath Luzon.

To the south of the South China Basin is the Reed Bank (Fig. 1-3) which separates the South China Basin from an extinct subduction zone associated with the Palawan Trough. The Reed Bank complex appears related with the Palawan and Calamian Islands, SW Mindoro and NE Panay Islands which are composed of a highly deformed basement complex of metasediments and silicic plutons. This terrane was classified as a "stable region" by Gervasio (1966) because of minimal seismic activity and was thought to be part of the Borneo Block (Ben-Avraham and Uyeda, 1973). The lack of seismic activity of Palawan and associated islands is probably because this region belongs to a microcontinental fragment that may have rifted from mainland China prior to Oligocene (Taylor and Hayes, 1980). In the western Philippines, eastward subduction between the Manila and Negros Trench systems (Fig. 1-3) is absent probably because the north Palawan microcontinental crust has impinged on a former oceanic zone near Mindoro, Panay and northwestern Zamboanga. This mid-Miocene collision (Hamilton, 1979; Cardwell et al, 1980; McCabe et al, 1982) terminated active subduction and volcanism in northern Zamboanga Peninsula until resumption of subduction during the Late Miocene.

At present, subduction of the South China Basin occurs along the Manila, Negros, and Cotabato Trenches. The Manila Trench is the longest contiguous trench in western Philippines, marking east-dipping consumption of the South China Basin between Palawan and Mindoro at 13°N to northern Luzon at 21°N. Subduction of the South China Basin beneath Luzon is indicated by underthrusting (Acharya and Aggarwal, 1980) although seismic activity is sparse and no deep focus earthquakes occur. The most intense seismic activity occurs along the Verde Island Transform near the southern terminus of the Manila Trench. The Wadati-Benioff zone in this area is nearly vertical and shallows to 40° to the north. The seismic

zone associated with the Manila Trench extends to 220 - 240 km (Cardwell et al, 1980; Acharya and Aggarwal, 1980). Subduction along the Manila Trench has produced a non-volcanic outer ridge and sediment-filled forearc basin (West Luzon Trough). On the west coast of Luzon is the Zambales Range, an ophiolite slab probably of Eocene age that originated from close to the equator (Schweller and Karig, 1979; Fuller et al, 1983; Hawkins and Evans, 1983).

The West Luzon volcanic arc consists of Miocene to Recent volcanic centres extending 900 km from Mindoro in SW Luzon to the Coastal Range in Taiwan (Defant et al, 1989). The volcanoes are irregularly distributed which suggest the occurrence of several arc segments. Volcanoes from Camiguin to Batan Island of northern Luzon to Mt Pinatubo in central Luzon are the most active while volcanic centres in SW Mindoro are now inactive (Fig. 1-3). Quaternary and Recent volcanoes of the West Luzon Arc occur where the top of the inclined seismic zone is about 100 km deep (Cardwell et al, 1980). However, volcanoes of SW Luzon lie over a significantly deeper portion of the seismic zone, away from the main axis of the West Luzon Arc. These volcanoes were attributed to a fracture zone or "leaky" transform (Divis, 1980) that trends nearly perpendicular to the West Luzon Arc. Wolfe and Self (1983) identified fault-related lineaments which they thought to have controlled volcanism. Defant et al (1980) called this discordant volcanic zone the Macolod Corridor (Fig. 1-3) and noted that all active volcanoes in the southern West Luzon Arc belong to this zone. Convergence between the South China Basin and the West Luzon Arc was computed by De Boer et al, (1980) to be ENE-WSW ($67^{o} \pm 30^{o}$).

1.3.3. Convergent Margins of Mindanao

Marginal basins in southern Philippines are the Sulu and Celebes Sea Basins. The Sulu Sea Basin seems to have formed as a back-arc or intra-arc basin during Lower to early Middle Miocene as inferred from radiolarian biostratigraphy

overlying the basement (Ocean Drilling Program, 1989). The sediment record indicates progressively rapid deposition of volcanic clays to coarse tuffs to continentally-derived turbidites which suggest eruptions from centres surrounding the basin and shallowing followed by isolation of the basin from deeper waters of the Pacific. At present, the maximum horizontal stress trends NE which is consistent with expected stresses from collision of the Sulu and Palawan ridges during Miocene.

In contrast to the Sulu Sea, the Celebes Sea basin originated in an open ocean environment 42 Ma BP during middle Eocene (Ocean Drilling Program, 1989), in general accord with age estimates from magnetic anomalies by Weissel (1980). The two basins are distinguished from other basins around the Philippines by their relative lack of deep seismicity along their subducted margins. This could either be due to recent subduction along the Sulu Trough and NE Celebes Sea Basin (Weissel, 1983) or because eastward subduction is in its terminal phase (Acharya and Aggarwal, 1980).

Subduction of the Sulu Basin along the Negros Trench has produced the Negros Island Arc system (Fig. 1-3). The arc consists of three main eruption centres which form Negros island. The western Panay Island is the outer subduction ridge and the Iloilo Basin is the forearc basin. To the east of the Negros volcanic arc are Cebu and Bohol islands which probably evolved in a back-arc setting. In summary, the Negros arc has all the morphologic features of an active volcanic chain. This is also supported by sediment accretion where Sulu Basin oceanic crust subducted along southern Negros Trench and suggests underthrusting beneath eastern Negros Arc (Mascle and Biscarat, 1978; Cardwell et al, 1980). However, no active underthrusting focal mechanism solution has been found along the northern Negros Trench .

The Cotabato Trench lies SW of Mindanao where subduction of the Celebes Sea Basin has produced the Cotabato Island Arc (or West Mindanao Arc). Recent earthquakes define a seismic plane and indicate active eastward underthrusting of the Celebes Basin beneath western Mindanao (Stewart and Cohn, 1977). However, seismic activity decreases southward where the trace of the Cotabato Trench becomes obscure and separate from the north Sulawesi Trench (Cardwell et al, 1980).

Other tectonic features in the Mindanao region suggest the continuity of arc systems related to subduction south of latitude 5°N. The East and West Mindanao Volcanic Arcs (Fig. 1-3) appears to be related with the Halmahera and West Sangihe Arcs of the northern Molucca Sea region. The East Mindanao Arc is an east-facing island arc system that bounds the West Philippine Sea Basin. The Philippine Trench in this region has a very small accretionary prism and the reported shallow seismic zone and lack of Quaternary volcanism (Cardwell et al, 1980) indicates recent subduction that is propagating southward (Karig, 1975; Moore and Silver, 1983). Cardwell et al (1980) suggested that the presence of a thick lobe of sediments east of the Philippine Trench was shed from an East Mindanao-Talaud Ridge which predates the Philippine Trench.

The Agusan-Davao Basin separates the Central and East Mindanao Island Arcs (Fig. 1-3). A cross-section across Davao Gulf (Fig. 1-4) in southern Mindanao shows deformed sediments along the western portion of the basin compared with less disturbed onlap of basin fill from the East Mindanao Ridge. Any active convergence between the Central and East Mindanao Arcs must therefore be restricted to E-directed thrusting. The Agusan-Davao Basin probably contains the suture between the two arcs but because the geology of Mindanao is poorly known it has not been identified. Cardwell et al (1980) conjectured that the Agusan-Davao

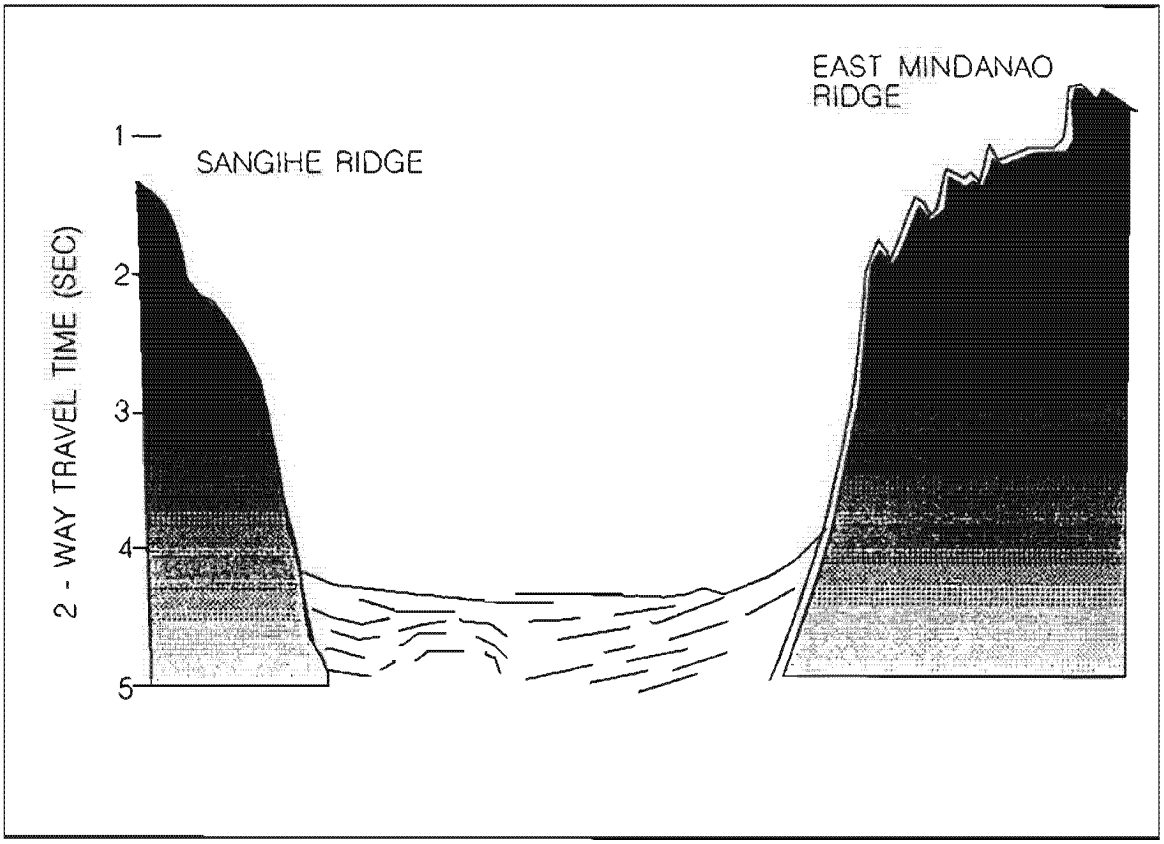

Figure 1-4. Interpretation of seismic profile across Davao Gulf, from about 6 N at Davao Gulf to 5 N. After Cardwell et al (1980).

Basin is the forearc basin for the East Mindanao Arc and that the suture lies just east of the Central Mindanao Volcanic Arc.

1.3.4. Shear Between Eastern and Western Convergent Margins

The Philippine Fault is a 1,200 km linear physiographic feature that occurs between the opposed subduction systems of the Philippines (Fig. 1-3). Stream offsets which cut recent gravels suggest a sinistral sense of motion (Ranneft et al, 1960; Allen, 1962; Rutland, 1968; Moore and Silver, 1983) with inferred large but indeterminate total displacement. An earthquake in 1973 registered a magnitude of 7.3 and a maximum left-lateral displacement of 3.2m (Morante and Allen, 1974). The 16 July 1990 earthquake of Central Luzon had a magnitude of 7.8 and produced similar left-lateral displacements of up to 5.9m. There are many hotsprings along the fault zone in the area of Leyte, Central Philippines and to the east of Davao Gulf in Mindanao (Malicdem and Pena, 1967) but it is not certain whether these large thermal anomalies are due to initiation of volcanism associated with the Philippine Trench or geothermal activity along the Philippine Fault.

Movement of the Philippine Fault amounts to approximately 68 mm/yr (Acharya and Aggarwal, 1980) and is comparable to seismic slip rates for the Alpine Fault of New Zealand (72 mm/yr) and the San Andreas Fault (66 mm/yr) according to Brune (1968). The existence of the Philippine Fault between two opposed subduction systems was originally unclear (Hamilton, 1979) because no trench-trench transform connects the northern Philippine Trench to the southern end of the Manila Trench. However, Acharya and Aggarwal (1980) found that rates of motion of the Philippine Fault are similar to slip rates of the Manila and Philippine Trenches (63.5 and 82 mm/yr respectively) and suggested that movement along the Philippine Fault probably accommodates a shearing component between the Philippine Sea and Eurasian Plates.

The presence of a southern extension of the Philippine Fault was questioned by Hamilton (1979) because of lack of evidence for strike-slip motion in Mindanao. Perhaps thick sediment fill within the Agusan-Davao Basin obscures the trace of the fault. However, occurrence of large-magnitude earthquakes within a linear zone (Rowlett and Kelleher, 1976), geological mapping (Ranneft et al, 1960; Philippine Bureau Mines, 1963) and stream offsets (Moore and Silver, 1983) confirm the presence of the Philippine Fault in Mindanao.

1.4. DEVELOPMENT OF ARC SYSTEMS IN THE PHILIPPINES

The earliest formation in the Philippines occurs in North Palawan and SW Mindoro, which were part of the North Palawan--Reed Bank--Luconia Shoal areas (Fig. 1-5a, 5b) of a proto-SE Asian margin (Taylor and Hayes, 1983). This continental margin was characterised by an Andean-type arc that was active from Middle Jurassic to Cretaceous. NW-directed subduction produced rhyolitic volcanism and granitic plutons along SE China (Allen and Stephens, 1971) that ceased by 85 Ma BP. The significance of the SE Asian continental margin to the tectonic history of the Philippines is that volcanism probably resulted from the early stages of rifting which formed the South China Basin (Taylor and Hayes, 1983) and drove the North Palawan microcontinental block towards the SE.

The West Philippine Basin was probably formed by seafloor spreading when the Pacific Plate motion changed from NNW to WNW 40 Ma BP (Clague and Jarrard, 1973; McDougall, 1979). The change in plate motion caused a Palau-Kyushu transform fault to become a subduction zone, capturing a segment of the Pacific Plate that became the West Philippine Sea Basin (Taylor and Hayes, 1980). The estimated paleomagnetic pole is 26° N, 129° W and an estimated paleolatitude of 4° S (Shih, 1980) which suggests that the West Philippine Basin has undergone a 60° clockwise rotation from its original orientation and has drifted 15° - 20° northward since 35 - 40 Ma BP.

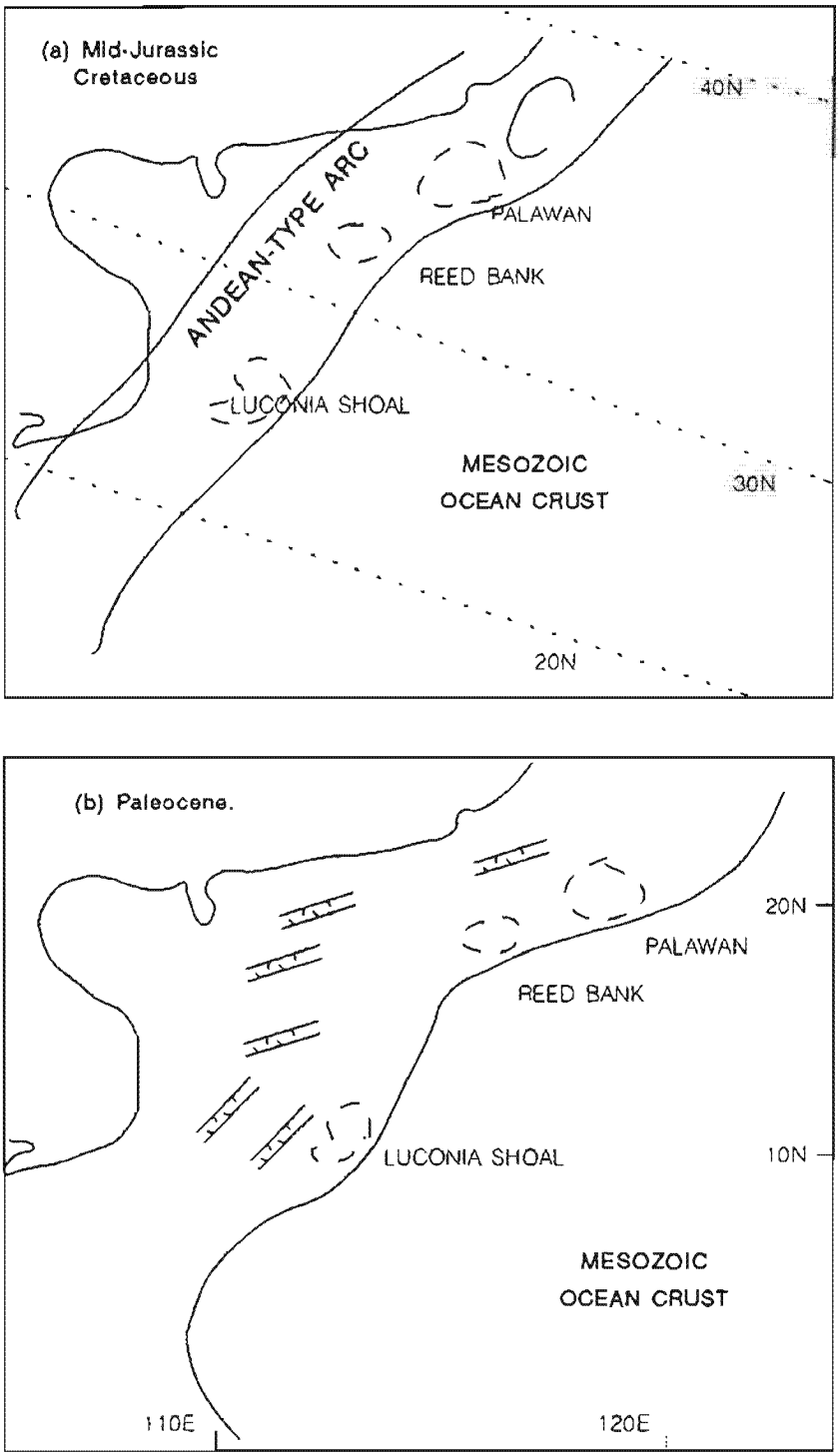

Figure 1-5. Reconstruction of tectonic history of the South China region. After Hayes et al (1983). In (a) NW subduction of Mesozoic crust beneath SE China and SE Vietnam resulted in an Andean-type Arc, producing widespread rhyolitic volcanism and silicic intrusions. Rifting of the SE China margin commenced at this time. In (b) rifting pushed Mesozoic ocean crust SE, along with the North Palawan-Reed Bank block and Luconia Shoal area.

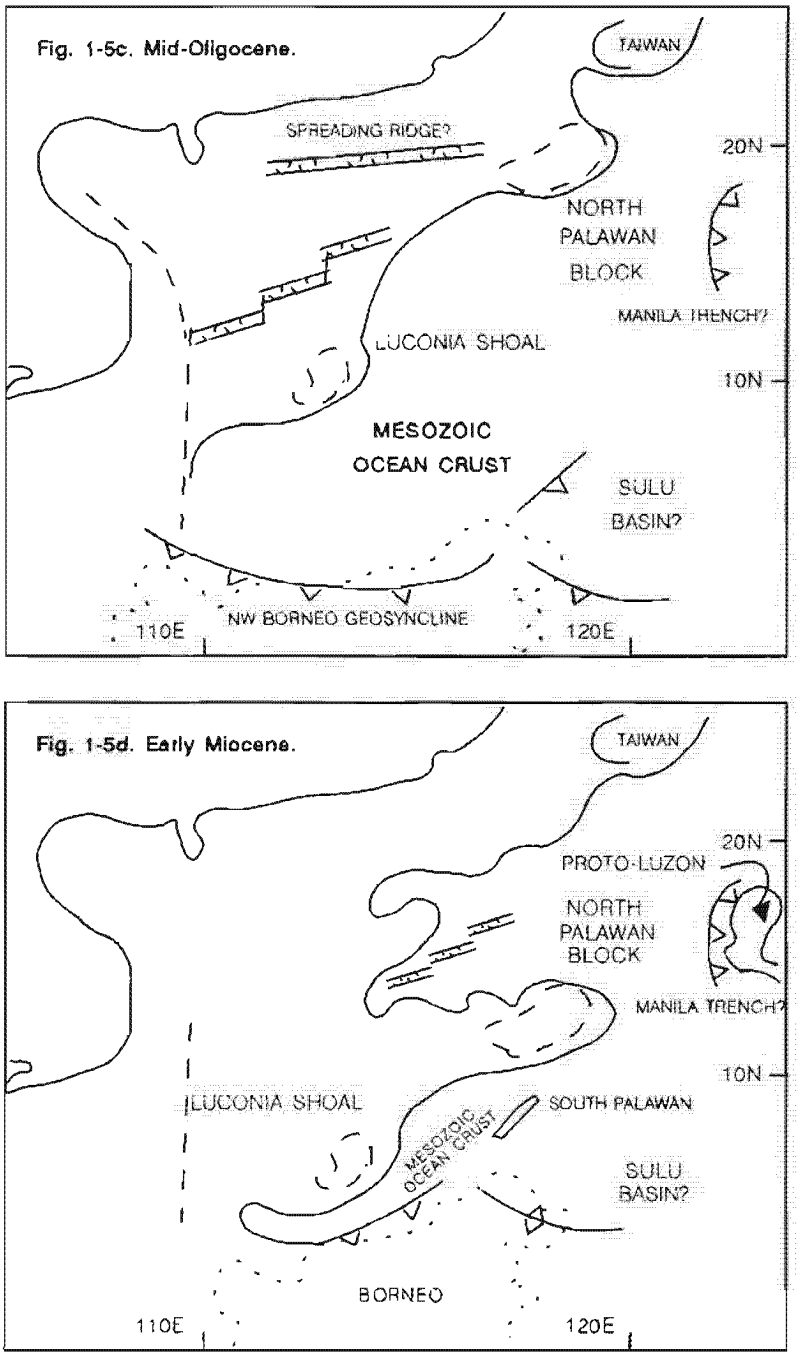

Figure 1-5. In (c) rifting of the SE China margin continued through Eocene and Oligocene. Collision of Mesozoic ocean crust and Borneo terrane in Mid-Oligocene resulted in a south-dipping subduction margin along NW Borneo. This is evidenced by Paleocene melange in NW Borneo. In (d) continued subduction along NW Borneo accommodates opening of the South China Basin.

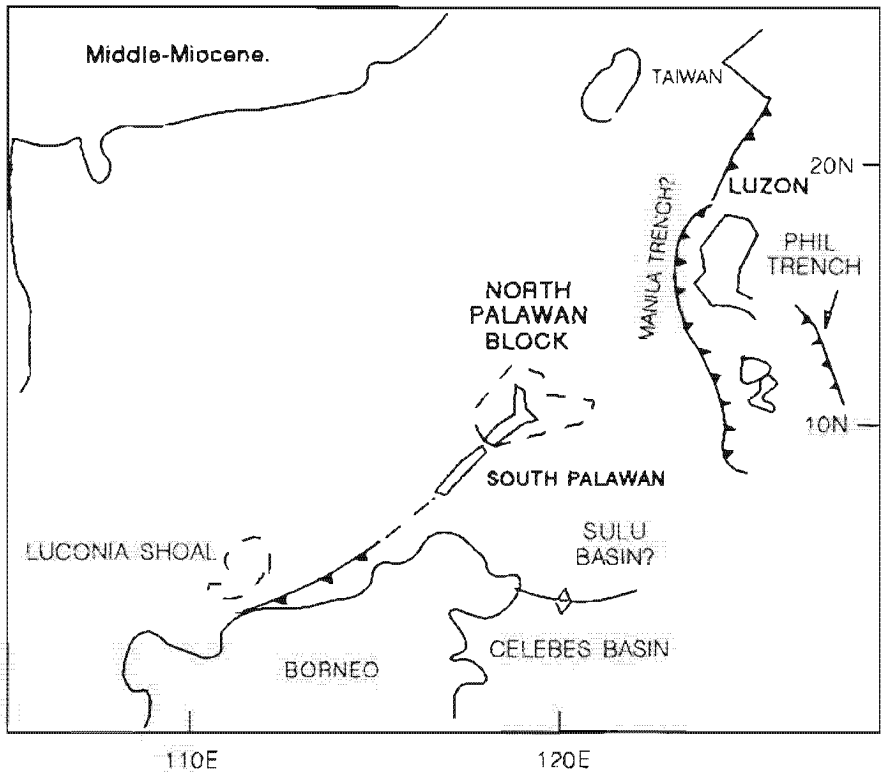

Figure 1-5e. At the end of early Miocene, seafloor spreading in the South China Basin ceased. By Middle Miocene, subduction along Palawan stopped. Collision between the North Palawan-Reed Bank block and South Palawan blocks was also complete. To the NE, subduction of South China Basin crust beneath W Luzon resulted in collision between the Luzon and Taiwan arcs.

1.4.1. EAST LUZON ARC

The formation of a proto-Luzon probably began in the Late Mesozoic as an east-facing intraoceanic island arc which comprised an early Luzon core. Late Cretaceous strata in the southern Sierra Madre Range (Reyes and Ordonez, 1979; Hashimoto, 1980) was interpreted by Karig (1981) as a Cretaceous ophiolite derived from a marginal basin behind the proto-Luzon arc. A regional unconformity found within voluminous turbidites of the South China Basin over earlier Mesozoic crust marks the end of Cretaceous and early Paleocene, presumably as Cretaceous arcs were being eroded. Holloway (1981) suggested this unconformity was due to the onset of rifting along the South China Basin.

Rifting of the South China Basin continued through Eocene. In east Luzon, subduction related to a spreading ridge near the Central Basin Fault (Lewis and Hayes, 1980) caused compression which created the Sierra Madre Range (Fig. 1-3). Magmatic episodes in the Sierra Madre Range produced mafic to ultramafic rocks which represent a subduction complex associated with an E-facing island arc. Eocene and Oligocene granitic plutons in northern Sierra Madre Range may represent the intrusive component of this older magmatic arc (Wolfe, 1981) which extends from Sierra Madre Range to western Bicol Volcanic Arc, Samar Island and perhaps farther south (Balce et al, 1979). The eastward convexity and east-directed thrusts suggest this region to be the relict subduction zone in east Luzon (Karig and Wageman, 1975; Lewis and Hayes, 1980; Hamburger et al, 1983).

Seafloor spreading in the South China Basin formed oceanic crust along an east-west trending spreading ridge by mid-Oligocene (Fig. 1-5c). The spreading centres were probably associated with extrusion of seamounts W of Luzon (Taylor and Hayes, 1983, Fig. 5) or a NE-trending graben structure in the SW of South China Basin. Southward movement of the North Palawan-Reed Bank microcontinental block was probably accommodated by subduction beneath Borneo

(Taylor and Hayes, 1983) which also formed the non-volcanic ridge of South Palawan (Fig. 1-5d). Evidence for Paleogene subduction and the formation of a "Northwest Borneo Geosyncline" as described by Haile (1969) was given by Hamilton (1979) who postulated the NW migration of the Borneo subduction front to the present Palawan Trough. Thus marginal basins around Luzon formed during Eocene-Oligocene, indicating one or more subduction zones.

1.4.2. WEST LUZON ARC

Subduction of the eastern margin of the South China Basin began with initiation of the Manila Trench during mid-Oligocene (Schweller et al, 1983). At this time Luzon was still at about 125°E, SE of its present position and composed of discrete arc segments. Eastward subduction at the Manila Trench produced igneous activity in W Luzon that has been continuous since late Oligocene. Magmatic arcs, now represented by rocks of Luzon Central Cordillera, were also built during this time.

By Lower Miocene, seafloor spreading in the South China Basin had produced an oceanic basin two-thirds of its final size (Taylor and Hayes, 1983), and pushed Mesozoic crust farther SE, subducting along the Borneo - South Palawan margin. The latter is part of the NE Borneo (Sabah) subduction complex of Late Cretaceous-Paleogene and is geologically different from North Palawan. The NE portion of the North Palawan-Reed Bank complex collided with the West Luzon-Sulu Arc system which stopped subduction in the latter and brought the North Palawan and South Palawan segments together (Fig. 1-5e). This collision also coincides with cessation of eastward seafloor spreading in the South China Basin.

The Manila Trench continued to migrate westward and propagated to the north until it collided with Taiwan. To further accommodate the NW movement of the West Philippine Sea Plate, subduction took place along the Ryukyu Trench N of Luzon.

By Middle Miocene Luzon became a single landmass with sedimentary basins filling between the West and East Luzon Arcs (Mineral and Fuels Division, 1976). In SE Luzon volcanic activity at Samar indicated active subduction along the Philippine Trench which took up convergence between the West Philippine Sea and Eurasian Plates. Not all plate movement could be accommodated by the Philippine and Ryukyu Trenches, however, and crustal shortening in NE Luzon occurred.

From Late Miocene to Pleistocene westward migration of the Manila Trench occurred as indicated by a change in forearc deposition from Central Luzon Basin to the West Luzon Trough (Hamburger et al, 1983).

During Pleistocene to Recent, volcanic arcs were formed along two major N-S belts in the Philippines from Luzon to northern Mindanao. This period is also distinguished by paleomagnetic patterns that remain concordant to the present (Fuller et al, 1983).

1.4.3. Tectonic History of Mindanao

The Mindanao region is a collision complex between two arc systems, in contrast to Luzon where no direct evidence of arc-arc collision has been found. Mindanao was probably made up of two discrete intra-oceanic arcs which evolved during Cretaceous to Paleogene and are now the West, and East Mindanao arcs. The West Mindanao Arc is often considered to include all central Mindanao volcanoes (Moore and Silver, 1983; Barnett et al, 1985). However, the CMVA defined in this study is a Neogene-Quaternary arc which most likely evolved separately from either the West and East Mindanao Arcs.

The relatively youthful collision between the West Mindanao and East Mindanao Arcs may explain the lack of deformed sediment infill along the Agusan-Davao Basin collision zone. Miocene basin sediments comprising andesitic tuffs, agglomerate and volcaniclastic sediments overlies Eocene sediments and indicate

that the West Mindanao Arc was active since pre-Miocene. The East Mindanao Arc was probably part of a longer west-facing arc that strectched from Samar to the present SE corner of Mindanao and was active from Cretaceous to mid-Oligocene (Hamilton, 1979; Cardwell et al, 1980). The volcanic sequence is overlain by late Oligocene carbonates, Miocene coal and shales which suggest the cessation of volcanism by late Oligocene.

The West Mindanao and East Mindanao Arcs collided during Miocene. Arc-arc collision was probably diachronous, starting from northern Mindanao, possibly in the latitude of present-day Samar (12^{o}N) and proceeded southward to West Sangihe and Halmahera Arcs in the northern Molucca Sea region (Hamilton, 1979). A reconstruction of the configuration of the convergence between the facing arcs of West and East Mindanao Arcs is shown in Figure 1-6. The collision process probably evolved by progressive closure of the West Sangihe-West Mindanao Arcs by an East Mindanao and Talaud-Halmahera arc system (Moore and Silver, 1983). The configuration of the East Mindanao Arc is still uncertain. Cardwell et al (1980) suggested that the East Mindanao Arc was transformed from a west-facing arc to an east-facing arc system and subsequent westward subduction formed along the southern Philippine Trench. Evidence for a shift from eastward to westward directed subduction along east Mindanao comes from the thick turbidites deposited east of the Philippine Trench which suggest that sediments were being shed by an active west-facing Mindanao ridge prior to the formation of the Philippine Trench. However, the lack of west-directed thrust structures make this interpretation suspect. The tectonic history of the CMVA has been uncertain because of lack of seismicity defining a subduction zone. Cardwell et al (1980) suggested that lithosphere formerly subducting beneath Central Mindanao was detached from the East Mindanao Arc and that sinking of this detached slab may now be responsible for the deep seismicity (~670km) and Quaternary volcanism in Central Mindanao. An alternative interpretation is given in Chapter 5.

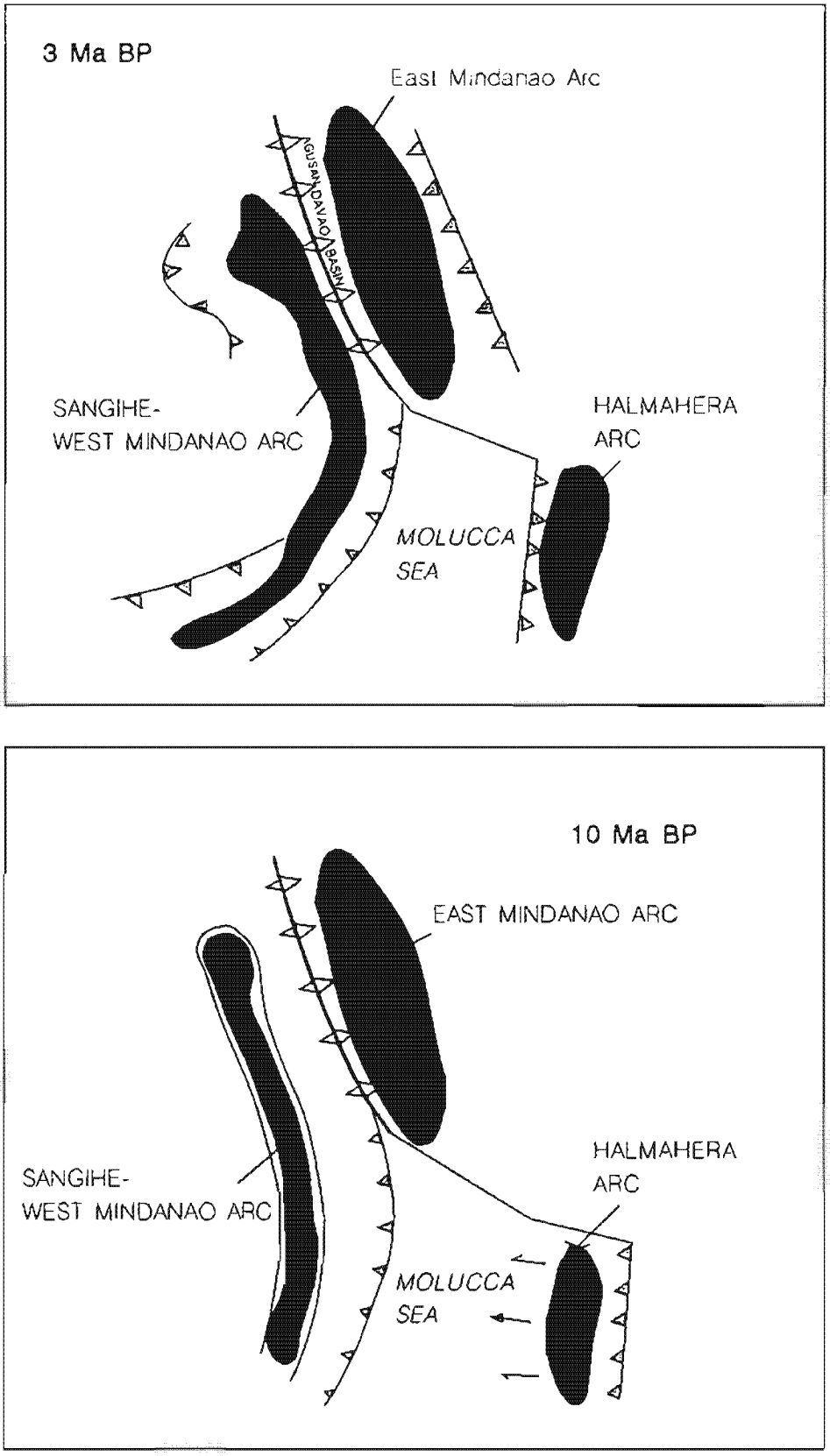

Figure 1-6. Schematic reconstruction of collision between the West and East Mindanao arcs. Modified after Moore and Silver (1983).

Sediments eroded from the West and East Mindanao ridges were deposited into the intervening Agusan-Davao Basin and were subsequently folded during mid-Miocene (Hashimoto, 1980). By mid-Pliocene (3 Ma BP) the Mindanao collision zone was nearly complete. Profiles across the Agusan-Davao Basin show relatively young sediments which are only slightly folded indicating slowing or cessation of convergence between the West and East Mindanao Arcs. Central Mindanao volcanism probably commenced by mid to Upper Pliocene, although large cones of CMVA evolved during Quaternary. Renewed subduction of the NW Celebes Basin took place in western Mindanao along the Cotabato Trench. At present the Philippine and Cotabato Trenches are propagating southward and will probably generate volcanic arcs in western and eastern Mindanao with continued subduction.

1.5. VOLCANISM IN MINDANAO

There are many Quaternary volcanic centres in Mindanao (Fig. 1-7). The Sulu islands form a linear cluster of volcanoes SE of Zamboanga Peninsula, parallel to the Sulu Trench and overlies arc-related greenschist facies metamorphic rocks (Phil. Bur. Mines, 1982). Volcanoes of this chain are largely inactive except for Bud Dajo, a cinder cone that reportedly erupted in 1641 (PHIVOLC, 1982). The NE trend of the Sulu volcanics is continued onshore Mindanao by the Zamboanga Peninsula. Only a few main volcanic centres comprise the Zamboanga Cordillera. The NE Sulu volcanic arc must have been active recently because the Quaternary Mt Butung and Mt Bigong are little eroded. Another young eruption centre in NE Zamboanga Cordillera is the large (900 km^2) Mt Malindang volcanic complex.

The Lanao Volcanics in NW Mindanao form a cluster of domes and cinder cones around Lake Lanao. The most active volcanoes in this region occur south of Lake Lanao where Mt Bita, Mt Ragang and subsidiary centres comprise a chain of volcanoes transverse to the CMVA. Mt Ragang erupted in 1834, January to April 1840, 1 November 1856, 18 February 1858, 1865, December 1871 and 16 January

1. Bud Dajo
2. Mt Bigong-Mt Butung
3. Mt Ampiro-Mt Malindang
4. Mt Bita
5. Mt Ragang
6. Mt Kalatungan
7. Mt Katanglad
8. Mt Musuan
9. Butong
10. Mt Mangaban
11. Mt Pamalihi
12. Mt Balatocan
13. Mt Obulan
14. Hibok-Hibok
15. Mt Paco/Mt Maniayao
16. Mt Leonard
17. Mt Talomo
18. Mt Apo
19. Mt Sibulan
20. Mt Matutum
21. Mt Parker
22. Balut Is.

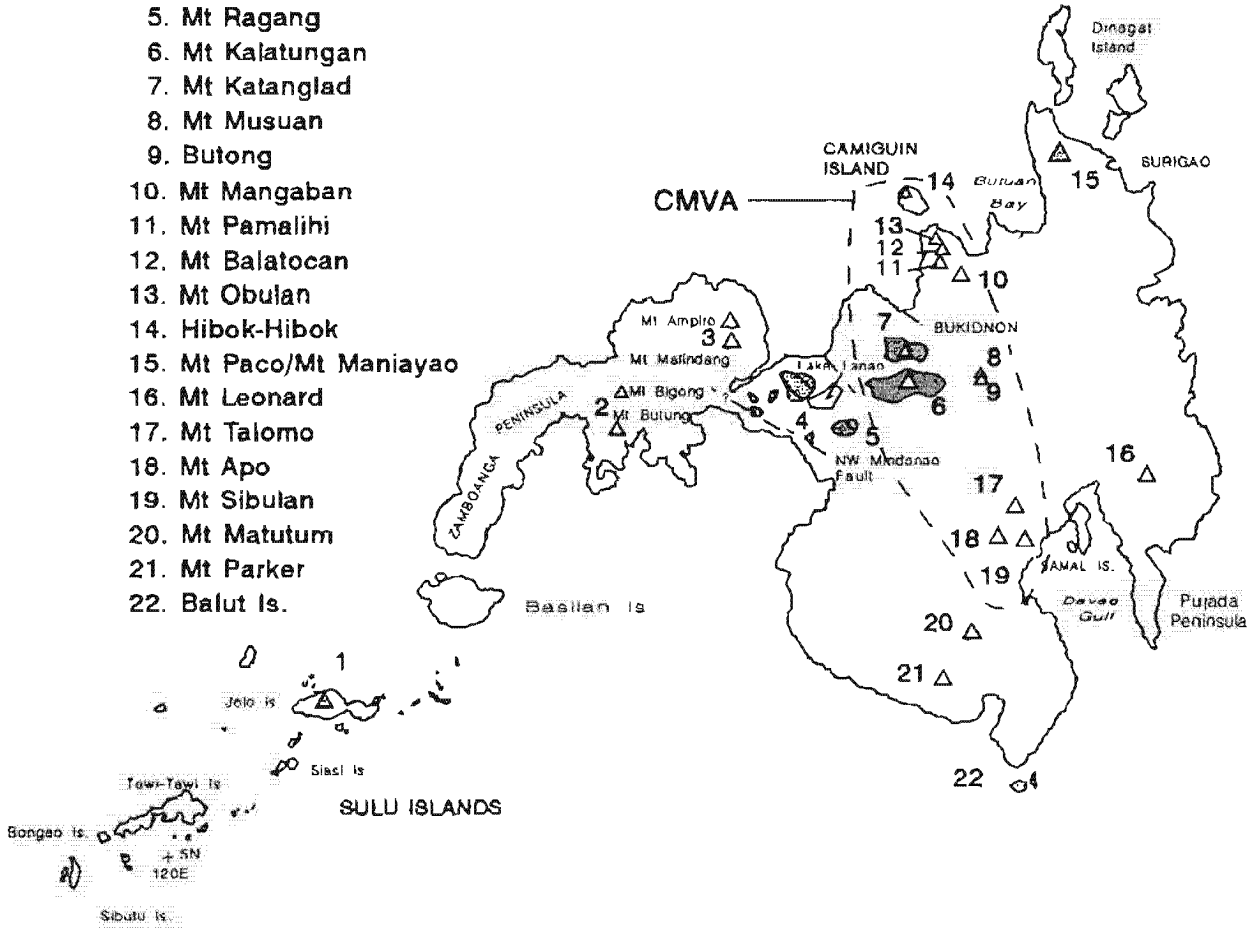

Figure 1-7. Quaternary volcanic centres in Mindanao. Thin dashed field encloses CMVA centres.

to April 1873 (PHIVOLC, 1982). Ashfall from the 1840 eruption reportedly reached 95 km to the west and 480 km NW of Mindanao. The most recent eruption in 1916 produced a thick column of smoke from a fissure. Burnt vegetation and scattered volcanic debris in the SE sector were perhaps caused by a lateral blast in 1915 (PHIVOLC, 1982).

Inactive centres of the Lanao Volcanics predominate north of Lake Lanao. Whether basalts of the Lanao highlands are related to the regional NW trend of western Mindanao is still unclear. Gervasio (1964), however, noted the alignment of volcanic plugs and cones subparallel to the trace of the NW Mindanao Fault (Fig. 1-7).

In eastern Mindanao there are only three main volcanic complexes which have been identified (PHIVOLC, 1982; Barnett et al, 1985), sited at Surigao in the northern Pacific Cordillera and in Davao to the south. In Surigao, Mt Paco and Mt Maniayo along with a cluster of domes occur within a graben formed by the Philippine Fault. In SE Mindanao a large volcanic complex (2,000 km^2) occurs between a graben bound by NW-SE splays of the Philippine Fault. The main volcano is Mt Leonard with a young summit caldera. Pyroclastics of the caldera were carbon-dated at 1800 yr BP and recent activity is manifest by solfataras within the caldera. An intermediate intrusive complex associated with Mt Leonard volcanics outcrops to the south of the caldera and has a K-Ar age of greater than 10 Ma (Barnett et al, 1985).

The scarcity of volcanoes in E Mindanao may be due to the relatively recent subduction of the West Philippine Basin along the southern Philippine Trench. The Wadati-Benioff zone associated with the southern Philippine Trench reaches only to about 150 km deep which probably explains why volcanism has commenced only within the past 100,000 years (Wolfe and Self, 1983). New seismic data (Chapter 5) provides an alternative explanation.

A N-S linear zone of volcanoes compose the CMVA. The arc is comprised of at least three segments: the Misamis, Bukidnon and Davao arc segments. Camiguin Island in the northern Misamis segment is host to Hibok-Hibok Volcano, the most active volcano in Mindanao. Large volcanic complexes forms Misamis Peninsula. Mt Obulan and Mt Balatucan is a pair of coalescing volcanic centres which formed summit calderas. This chain continues southward to another stratovolcano called Mt Pamalihi and ends at Mt Mangaban.

East of Lake Lanao are two E-W trending composite volcanic chains called Mt Katanglad and Mt Kalatungan. The latter volcano is surrounded by smaller domes and cones which penetrate a pyroclastic plateau and thrusted basement complex. One of these small domes, Mt Musuan, reportedly erupted during 1887 and was seismically active during 13 - 16 November 1976.

Another large volcanic field occurs in south-central Mindanao. The largest centre is Mt Apo which forms a complex with Mt Talomo and Mt Sibulan. To the south is Mt Matutum which reportedly erupted on 7 March 1911. Mt Parker is another composite cone but is now inactive. The southernmost emergent part of the Davao arc segment is Balut Island which, like Mt Apo, is geothermally active.

CHAPTER II GEOLOGY

2.1. GENERAL GEOLOGY OF MINDANAO

The geology of Mindanao is complex due to amalgamation of arc terranes. In general, previous geologic studies (e.g. Phil. Bureau Mines, 1982) classified Mindanao into western, central and eastern geologic provinces, in accordance with the regional structure of other Philippine islands to the north. Other studies (Hamilton, 1979; Cardwell et al, 1980; Moore and Silver, 1983) show the tectonic evolution and geologic structure of Mindanao is more related to the region south of Latitude 5°N. This is also indicated by abrupt termination of Mindanao arc terrane south of Bohol Island as shown by crustal sections (Rangin et al, 1989) of the Visayas. This study therefore considers Mindanao as distinct from geologic provinces of Visayas and Luzon.

Mindanao is a group of islands from Latitude 4°30'N - 10°N and Longitude 119°30E - 127°E (Fig. 2-1). There are 3 main physiographic-structural units. The first unit trends N - NNW and comprises the Pacific Cordillera, Mindanao Central Cordillera and Agusan-Davao Basin. The second unit trends NW and includes the Tiruray-Daguma Range and Cotabato Basin. A diffuse zone of volcanoes in central Mindanao are bound by the Agusan-Davao Basin to the east and the Cotabato Basin to the S. Volcanic centres clustered N and W of Lake Lanao are crudely aligned NW and are probably associated with the the NW-trending Mindanao terrane. The third unit encompasses the NE-trending Zamboanga Peninsula and Sulu Islands.

In general, Miocene to Quaternary volcanic centres overlie Cretaceous basement rocks.

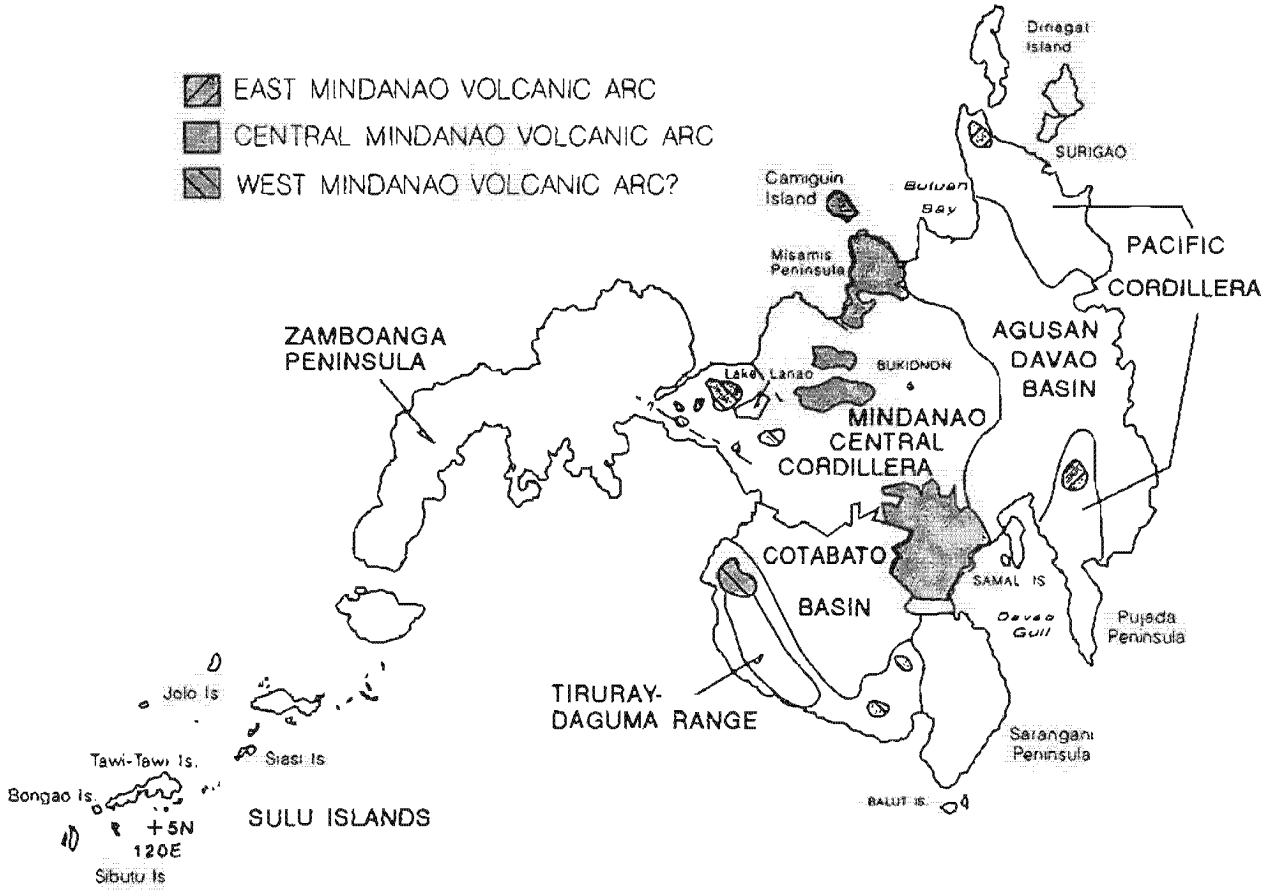

Figure 2-1. Sketch map of Mindanao showing major physiographic units. Volcanic fields of Mindanao are grouped into West, Central and East Mindanao Arcs.

Figure 2-2 shows the general geology of Mindanao. Figure 2-3 gives stratigraphic relationships of key lithologies discussed in text.

2.1.1. Pacific Cordillera

This mountain range spans 400 km from Dinagat Island to the SE tip of Mindanao (Fig. 2-1). Cretaceous greenschist and amphibolite schist are probably the oldest rocks. Late Cretaceous serpentinised peridotites are thrust over the schists (Santos-Ynigo, 1944). A large portion of the Pacific Cordillera is comprised of Cretaceous - Oligocene volcanics (Ranneft et al, 1960; Matsumaru, 1974; Hashimoto, 1981). Hamilton (1979) and Cardwell et al (1980) inferred that these volcanics were part of an East Mindanao Arc that was active from Cretaceous to Oligocene. Late Oligocene limestones and Miocene coals overlying the East Mindanao Arc indicate volcanism ceased by upper Oligocene (Matsumaru, 1974). At present, there are few Quaternary volcanic centres which have been identified in east Mindanao (see Fig. 1-7). It is not clear whether these centres are caused by subduction along the Philippine Trench or volcanic activity along the Philippine fault. Cardwell et al (1980) suggested that these volcanics are not associated with the former because only recent subduction has taken place. Neogene plutons intruding the basement probably represent the precursor of Quaternary volcanism.

2.1.2. Agusan-Davao Basin

This 350-km N-S trending elongated basin separates the Pacific Cordillera from the CMVA (Fig. 2-1). The basin opens out toward Butuan Bay and Davao Gulf to the N and S, respectively. The basin is filled with about 6 km of Eocene to Holocene sediments overlying a basement complex (Ranneft et al, 1960; Cardwell et al, 1980). Discontinuous exposures in NW Agusan indicate basement rocks are serpentinite and peridotite with minor proportions of basalt, gabbro, andesite and their metamorphic equivalents. This assemblage was classified by Ranneft et al (1960) as early Tertiary since Eocene strata overlie the ultramafic sequence

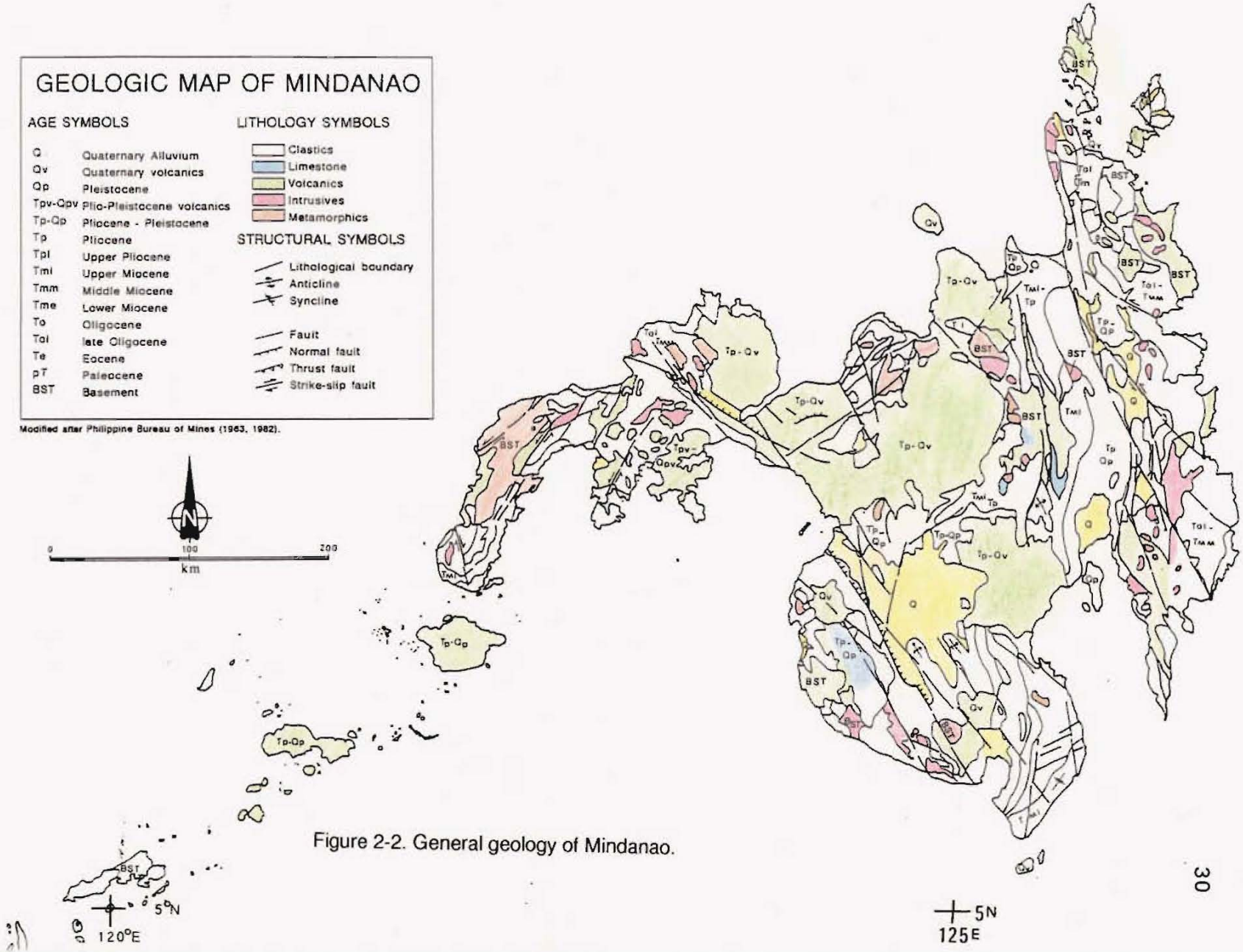

Figure 2-2. General geology of Mindanao.

Figure 2-3a. Stratigraphic sections for eastern Mindanao. Modified after Phil. Bureau Mines, 1982.

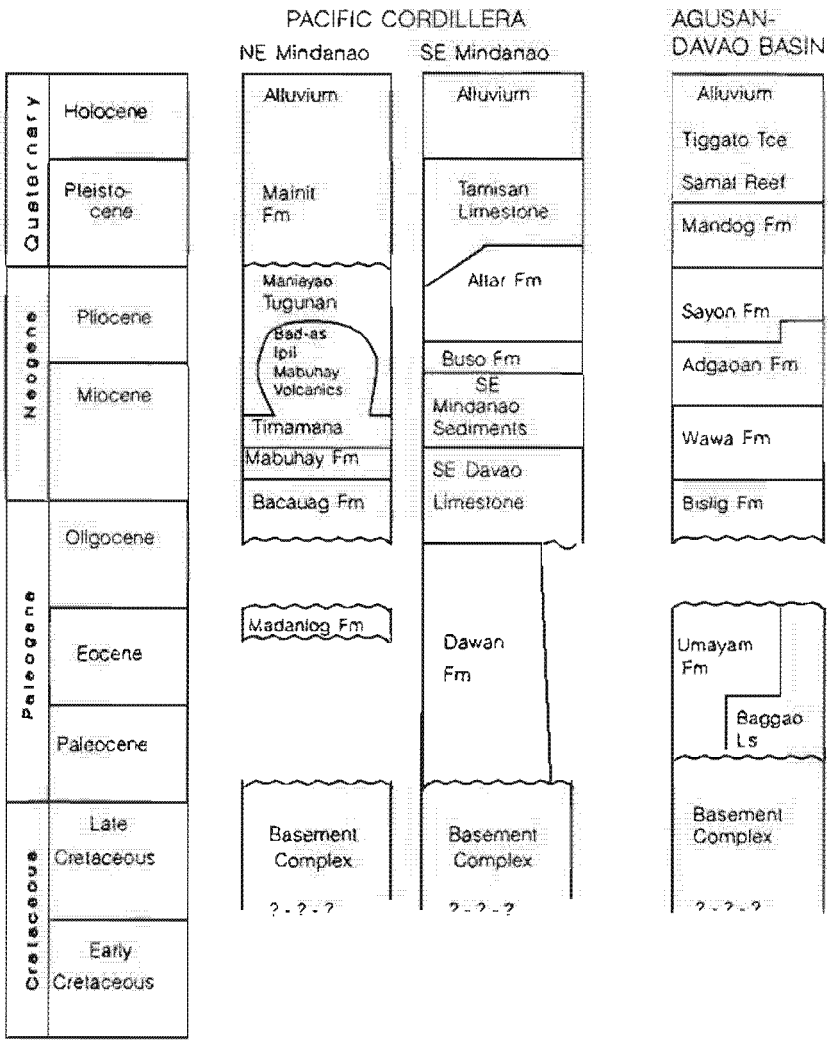

Figure 2-3b. Stratigraphic columns for Central Mindanao. Modified after Phil. Bureau Mines (1982).

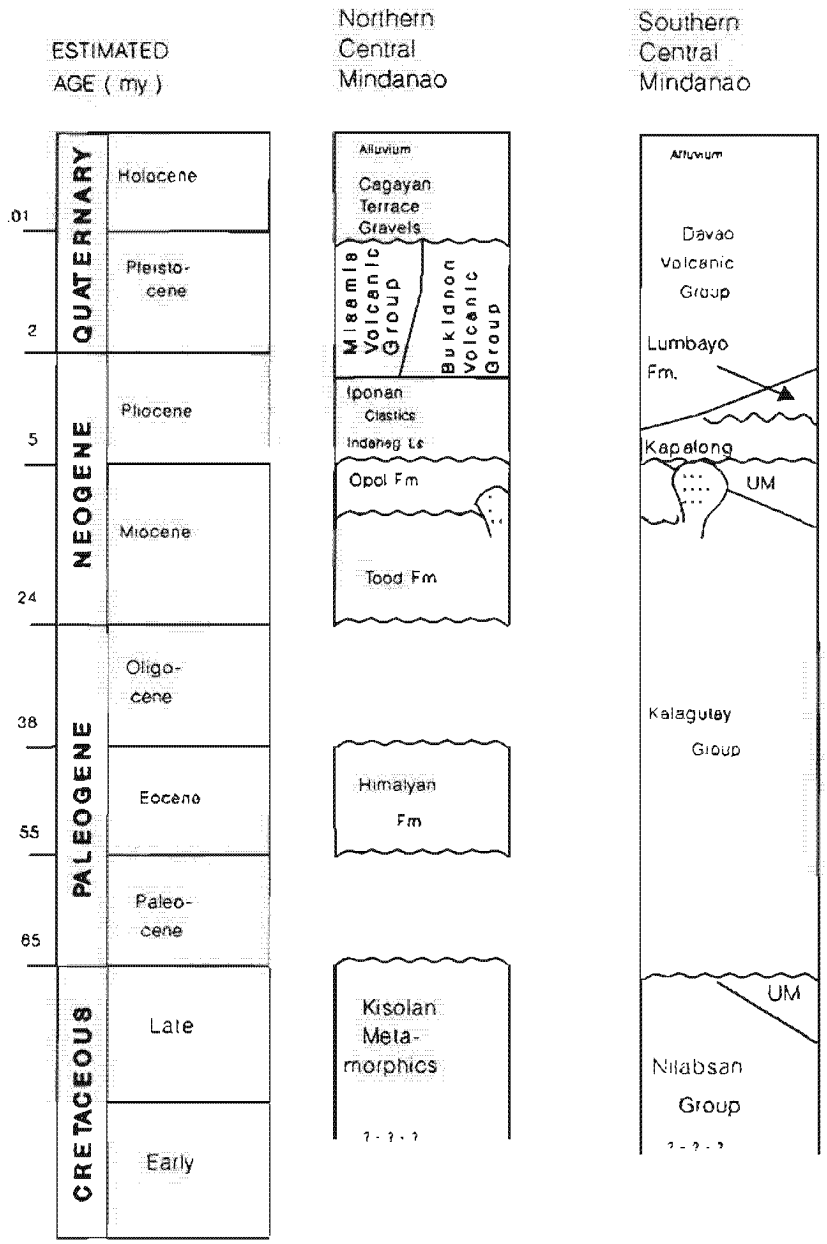

Figure 2-3c. Stratigraphic columns for SW Mindanao. Modified after Phil. Bureau Mines (1982).

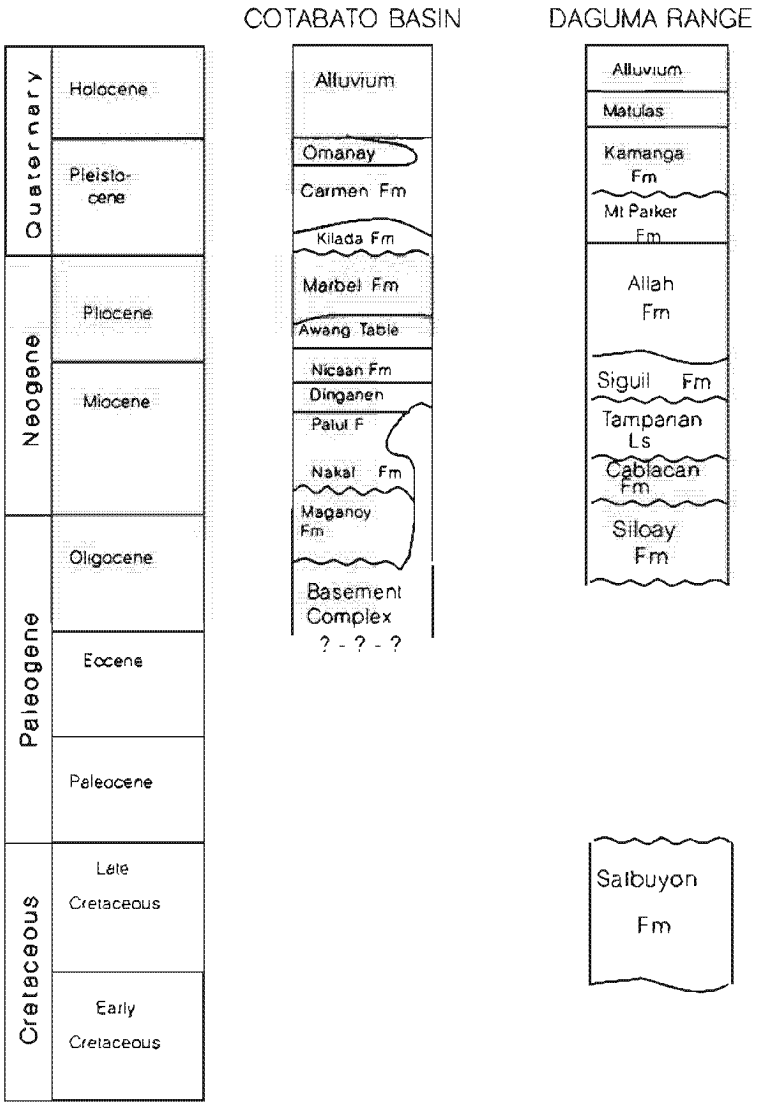

Figure 2-3d. Stratigraphic columns for Zamboanga Peninsula and Sulu Islands.

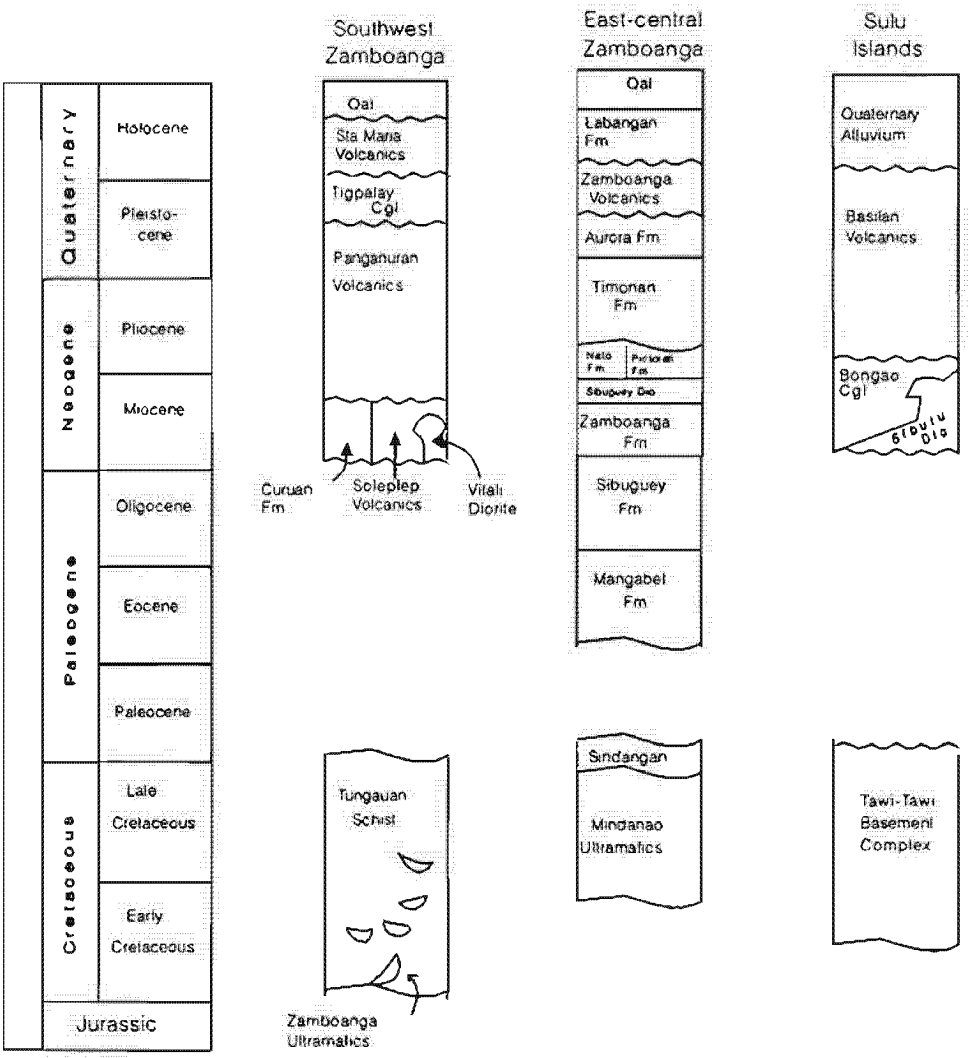

(Fig. 2-3a). Basement rocks probably predate Eocene, however, because pelagic sediments associated with melange in the eastern basin margin (Pujada Peninsula) are Cretaceous (Agusan-Davao Consortium, 1979). Eocene limestone around the margins of the Agusan-Davao Basin led Ranneft et al (1960) to suggest that much of this basin is underlain by limestone. More likely, carbonate deposits represent growth of isolated reefs along shallow margins whereas pelagic sediments fill the basin deep.

An extensive deposit in the Agusan-Davao Basin is the Middle Miocene Wawa Formation (Fig. 2-3a). The sequence is so widely distributed that other sedimentary units which bear similar lithology and age but which occur in different places are included in this unit (Phil. Bureau Mines, 1966). In NE Agusan, carbonates of the Wawa Formation are clearly derived from reef complexes of back-reef and main-reef facies. In NW Agusan, the Wawa Formation occurs as shales and intervening sandstones. Farther south near the boundary between the Agusan-Davao Basin and CMVA, the sandstone-shale beds are disturbed and broken, presumably due to convergence between the East Mindanao Arc and CMVA. Pliocene basic to intermediate volcanics intrude Middle Miocene limestones and sandstones. Further evidence of tectonic disturbance is suggested by the Samal Reef Limestone covering Samal Island in Davao Gulf (Fig. 2-1). These limestones are equivalent to the "raised" reef limestones of Casasola (1956) and indicate carbonate growth on a submerged or tilted platform.

2.1.3. Mindanao Central Cordillera

Central Mindanao is a broad region of uplifted Cretaceous-Paleogene basement intruded by Neogene plutons. Quaternary volcanoes cover most of the range. The oldest rocks in central Mindanao are Cretaceous mica and chlorite schists, slates and ultramafics (Pacis, 1966). These crystalline metamorphics correlate with intensely folded and faulted basement schists and quartzites

described by Ranneft et al (1960) as thrusted rocks in the central part of the range. The earliest volcanics occur as Cretaceous-Early Pelocene basalt and andesite intercalated with mudstone. Middle to Late Miocene gabbro and diorite intrude the basement (Fig. 2-3b).

Previous studies (Hamilton, 1979; Moore and Silver, 1983) consider central Mindanao volcanoes as the northern extension of the Sangihe Arc in the Molucca Sea. Whilst volcanic centres of Tiruray-Daguma Range and volcanoes bordering N, S and W of Lake Lanao can be related to an E-dipping West Mindanao-Sangihe subduction system, other Quaternary volcanoes east of Lake Lanao are more likely associated with a W-dipping subduction system. This is indicated by the W-dipping seismic zone beneath the CMVA (Cardwell et al, 1980). Hence, only Camiguin Island, Mt Obulan, Mt Balatocan, Mt, Pamalihi, Mt Mangaban, Mt Katanglad, Mt Kalatungan, Musuan Volcano, Butong, and the Mt Apo-Sibulan-Talomo complex are included in the CMVA.

2.1.4. Cotabato Basin

This sedimentary basin is situated in SW Mindanao (Fig. 2-1). It is bounded by Mt Apo to the E, the Lanao-Bukidnon highlands to the N, the Tiruray-Daguma Range to the SW and by Mt Matutum and Mt Parker volcanoes to the SE. The basin is underlain by Oligocene or older metamorphosed sediments, ultramafics and volcanics. The earliest basin sediments are late Oligocene - Lower Miocene volcaniclastics and carbonates (Phil. Bureau Mines, 1975). The tuffaceous component in sediments near the northern portion of the basin indicate that volcanic activity commenced during late Oligocene. One possible source of volcaniclastics is a volcanic field NNW of Mt Apo. Early Miocene marine deposition was halted by a period of diorite intrusions (Phil. Bureau Mines, 1982).

Stratigraphy of the basin (Fig. 2-3c) suggests several episodes of deepening and emergence. In general, deepening of the basin occurred during Middle Miocene

as inferred from abrupt facies change, from carbonates to shales. During Late Miocene uplift and erosion occurred and this is indicated by the regressive sequence of pelagic mudstone to sandstone and limestone. The basin progressively shallowed during Pliocene-Pleistocene with development of reefs. Much volcanic sediment was also deposited in the basin, presumably from the Lanao-Bukidnon highlands and from early Mt Apo.

2.1.5. TIRURAY-DAGUMA RANGE

This block forms the SW margin of Cotabato Basin. The basement is composed of Cretaceous-Paleogene metamorphosed sediments and volcanics. Lower Miocene to Middle Miocene sediments are intruded by diorites. Pliocene to Pleistocene andesitic pyroclastics and lavas forms Mt Parker in SE Tiruray-Daguma Range. The northern portion is covered by uplifted Pleistocene reefal limestone and andesite. The period of uplift was probably contemporaneous with en-echelon gravity faults which presently bounds the N Cotabato Basin. Stratigraphy of this unit is summarised in Figure 2-3c.

2.1.6. ZAMBOANGA PENINSULA

The Zamboanga Peninsula is the westernmost landmass of mainland Mindanao. In general, the peninsula is classified into Southwest and East-central terranes (Figure 2-3d). The earliest rocks are probably Upper Jurassic - Cretaceous serpentinised ultramafics, schists, gneiss and quartzites now exposed in SW Zamboanga (Santos-Ynigo, 1953; Paderes and Miranda, 1965). The SW Zamboanga ultramafics correlate with basement rocks (serpentinised peridotites) of East-central Zamboanga. The oldest volcanics are hydrothermally-altered strata of the Sindangan Volcanics. Shale and sandstone intercalate with thin basaltic flows, and together with limestone lenses, overlie the Sindangan Volcanics to form the Mangabel Formation. Biostratigraphy of the limestone suggest this unit formed during Eocene (Phil. Bureau Mines, 1982).

Lower to Middle Miocene metavolcanics, marble and clastics of the Zamboanga Formation are intruded by the Sibuguey Diorite; stocks, dikes and sills apparently related to region-wide mineralisation at the close of Middle Miocene. Upper Miocene shale, sandstone and conglomerate are overlain by Pliocene limestone. The Pliocene also contain pyroclastic beds but more extensive volcanism occurred during Pleistocene when basic to intermediate lava flows and domes (Zamboanga Volcanics) fused SW and East-central Zamboanga to mainland Mindanao.

2.1.7. SULU ISLANDS

The NE-SW trend of the Zamboanga Peninsula continues offshore into a chain of many islands roughly 100km wide by 400km long. The islands, mostly volcanic, forms the Sulu Islands. The Sulu island group is divided into 4 general areas based on lithology. These are i) northern Tawi-Tawi and adjacent islands; ii) southern Tawi-Tawi; iii) Sibutu Islands and iv) Basilan-Jolo-Siasi Islands (Fig. 2-1). The earliest rocks are Cretaceous to early Paleocene serpentinite, basalt and gabbro. This sequence contrasts with contemporaneous silicic and intermediate intrusives of the Semporna and Dent Peninsula of northern Borneo. The southern half of Tawi-Tawi Island is underlain by a Miocene sandstone-conglomerate sequence called the Bongao Conglomerate (Corby et al, 1951). The Basilan-Jolo-Siasi Islands in northern Sulu Islands are principally composed of Pliocene-Pleistocene volcanics (Basilan Volcanics; Fig. 2-3d). These islands are fringed by Recent reefs and poorly sorted gravels and sandstones containing volcanic detritus.

2.2. GEOLOGY OF CENTRAL MINDANAO VOLCANIC ARC (CMVA)

Volcanic rocks in central Mindanao are post-Cretaceous. Although igneous activity persisted throughout the Tertiary, today's larger arc volcanoes developed mainly during the Quaternary. This is evident in many well preserved cones, stratovolcano complexes and active centers in central Mindanao.

In this study, the CMVA is divided into 3 main segments: i) a northern segment includes Camiguin Island, Mt Balatocan, Mt Pamalihi, and Mt Mangaban, ii) a central arc segment which encompasses Mt Katanglad, Mt Kalatungan, Musuan Volcano, Butong and associated smaller volcanoes of the Bukidnon highlands, and iii) a southern segment formed mainly by Mt Apo, Mt Talomo and Mt Sibulan.

The general distribution of volcanic deposits in the CMVA is shown in Fig. 2-4 and in the map at the back pocket of this thesis.

Previously, Pliocene-Quaternary volcanics of the southern (Misamis) and central (Bukidnon) arc segments have been considered as part of the Mambuaya Formation. However, Misamis is separated from Bukidnon by a NW - SE lineament from Tagaloan to north of Malaybalay and by thrust faults (Fig. 2-4) so that the name Mambuaya Formation should apply only to Mt Katanglad volcanics. In southern CMVA, Quaternary volcanic rocks S of Bukidnon were grouped into the Malambo Formation (RP-Japan Project, 1974), but the term `Malambo' is inappropriate since the type locality of Mt Malambo comprises Upper Miocene sediments and volcanics (Fig. 2-4). To simplify stratigraphic classification of the CMVA, this paper proposes the terms Misamis Volcanic Group, Bukidnon Volcanic Group, and Davao Volcanic Group to refer to Pliocene-Quaternary volcanic complexes in the respective arc segments (Fig. 2-3b).

2.2.1. Misamis Volcanic Group

Four main volcanic centres comprise Misamis Volcanic Group (MVG). Mt Mangaban is the southernmost in this NW-SE chain of volcanoes. To the NW is Mt Pamalihi. Mt. Balatocan farther N is a large stratocone with nested summit calderas and coalesces with a northern cone called Mt Obulan. At present, Mt Balatocan is inactive although steam vents and hot springs occur within and around the caldera. Farther NW still is Camiguin Island which represents a volcanic complex built on a

Figure 2-4.

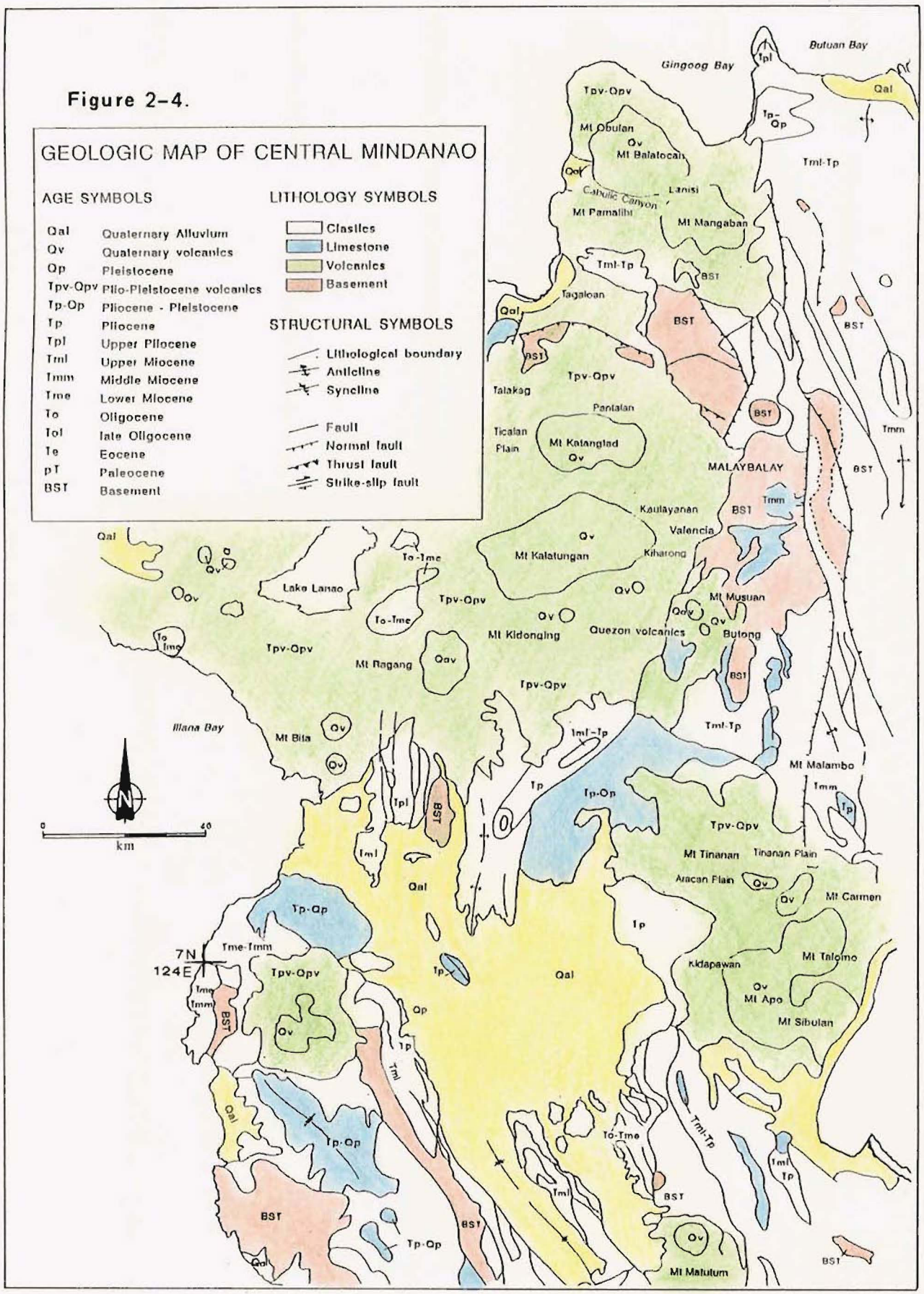
GEOLOGIC MAP OF CENTRAL MINDANAO
AGE SYMBOLS
Qal Quaternary Alluvium
Qv Quaternary volcanics
Qp Pleistocene
Tpv-Qpv Plio-Pleistocene volcanics
Tp-Qp Pliocene - Pleistocene
Tp Pliocene
Tpl Upper Pliocene
Tml Upper Miocene
Tmm Middle Miocene
Tme Lower Miocene
To Oligocene
Tol late Oligocene
Te Eocene
pT Paleocene
BST Basement
LITHOLOGY SYMBOLS
Clastics
Limestone
Volcanics
Basement
STRUCTURAL SYMBOLS
Lithological boundary
Anticline
Syncline
Fault
Normal fault
Thrust fault
Strike-slip fault
Butuan Bay
Gingoog Bay
Mt Obulan
Mt Balatocan
Mt Pamalihi
Mt Mangaban
Lanisi
Cabulig Canyon
Tagaloan
Talakag
Pantalan
Ticalan Plain
Mt Katanglad
MALAYBALAY
Kaulayanan
Valencia
Kihalong
Mt Kalatungan
Lake Lanao
Mt Musuan
Mt Kidonging
Quezon volcanics
Butong
Mt Ragang
Iligan Bay
Mt Bita
Mt Malambo
Mt Tinanan
Tinanan Plain
Aracan Plain
Mt Carmen
Kidapawan
Mt Talomo
Mt Apo
Mt Sibulan
Mt Matutum
7N
124E
0
40
km

submerged platform contiguous with Misamis Peninsula. Recent eruptions make Camiguin Island the youngest of CMVA volcanoes.

Several exposures indicate the basement to be Cretaceous or earlier crystalline metamorphics. Slates, phyllites, and mica schists crop out S of Mt Mangaban and are lithologically similar to basement rocks of the Bukidnon and Davao arc segments. N of Mt Mangaban from Mt Balatocan to Camiguin Island, the Cretaceous metamorphics are absent and the earliest rocks, based on xenoliths, are pre-Pliocene lavas (Phil. Bureau Mines, 1982).

(i) Mt Mangaban

Mt. Mangaban is the oldest centre, as indicated by lack of recent volcanic activity and highly dissected morphology. The earliest products must be Pliocene or earlier lavas because raised coral reefs which correlate with the Pliocene Indahag Limestone (Pacis, 1966), overlie distal lava flows along the west coast of Misamis Peninsula (Fig. 2-3b). The Pliocene lavas which form the walls of Cabulic Canyon probably resulted from extensive volcanism near the present Mt Pamalihi, and these are overlain by volcanic breccias with intercalated lava flows. This sequence is similar for Lanisi to about 900m but at higher elevations, steep-sided lava flows predominate ridges and gully floors. The youngest rocks comprise the Mt Pamalihi cone which probably formed during late Pleistocene - Recent because of similar morphology to other Quaternary volcanoes in MVG.

(ii) Mt Balatocan

Northwest of Mt Mangaban is Mt Balatocan, which together with subsidiary flank cones, covers the greatest area (1,400 Km^2) of Misamis Peninsula. Mt Balatocan has slopes which average 3^o - 5^o from the northern coastline to 500m elevation. From 500m to the peak, the slope greatly increases to 20-30^o with precipitous cliffs and ridges within and around the summit (~2,560m). The more

gentle slopes expose coarse fluvial and lahar deposits near the coast with tuffaceous breccias, pyroclastic flows and intercalated lava flow deposits inland. Near the NW coast is a cluster of plug or lava domes flanked by massive to jointed lava flows. These lava flows have a regular lobate morphology which suggest a young age.

On the southern slopes of Mt Balatocan, the high ridges which form the upper flanks are massive to jointed lava flows mantled by thick volcanic breccias. Several lava domes also occur. Some exposures show vertically jointed lavas beneath thick debris flows and soil.

The caldera in Mt Balatocan is 10 - 12 km wide and is assymetric in plan which indicates a multiple and complex subsidence history. The caldera has a steep rim, from 30° to near vertical, and is floored by a chaotic assemblage of debris flows and dense lava blocks. Subsidiary arcuate scarps along the inner caldera slopes suggest post-caldera avalanches which form the characteristic hummocky surface of the valley floor. Scarps which have produced a bench-like morphology along the southern caldera wall also indicate large-scale subsidence. Several lava domes occur within the caldera and the centrally-located tholoid probably plugs the main vent.

Eruptions within the SE caldera has produced a crater which, because of the absence of lava domes and highly incised morphology, appears to be partially filled with pyroclastic debris. This crater apparently is a young volcanic centre. The crater together with resurgent domes in the central caldera, represent the most recent features of mainland Misamis.

2.2.2. Bukidnon Volcanic Group

Bukidnon Volcanic Group (BVG) volcanoes are situated on an uplifted metamorphic basement that results in the high mean elevation (500m+) of central Mindanao. Cretaceous schists, slates and phyllites sometimes occur as inliers

produced from west-directed thrusts and block faults east of Bukidnon. The basement is covered by Oligocene to Pliocene sediments, patches of Middle Miocene carbonates, and Pliocene to Quaternary clastics and limestone. The most extensive deposits are Pliocene to Recent volcanics.

The main volcanic centres of Bukidnon are Mt Katanglad and Mt Kalatungan. Mt Ragang and Mt Bita SW of Mt Kalatungan and volcanoes bordering Lake Lanao to the N and W are probably related to the West Mindanao-Sangihe Arc (Hamilton, 1979; Cardwell et al, 1980; Moore and Silver, 1983).

(i) Mt Katanglad

The Mt Katanglad complex forms a series of domes and explosion craters which rise to about 2,300m above the Bukidnon 'plateau' (Fig. 2-5a). These eruption centres are roughly aligned E-W so that a fissure probably underlies the main edifice. Deposits of the Katanglad Mountains are part of the Pleistocene Mambuaya Group and were described by the Phil. Bureau Mines (1982) as an assemblage of intercalated agglomerate, tuffaceous sandstone, pebbly sandstone, and conglomerate. This sequence, however, applies only to limited outcrops along the western slopes which is also known as the Ticalan Plain (Fig. 2-4). At Talakag, the main deposits are volcanic conglomerate and fluvial sediments, the conglomerates containing dense lava clasts which were presumably derived from highlands west of the mountain range. In N-central Mt Katanglad , S of Pantalan (Fig. 2-4), streams and gullies are floored by lava flows and debris flows. The lavas also occur as highly vegetated ridges with lava boulders strewn along the top and termini of the flows. In contrast, the broad and gently sloping E sector is a plain floored by pyroclastics. The main deposit consists of tuffs with highly vesicular dark lava bombs 3-4m in diameter. Lava bombs are also found as discrete fragments on the surface, perhaps due to erosion of the matrix.

Figure 2-5. Volcanoes of Bukidnon Volcanic Group. (a) Mt Katanglad, (b) Mt Kalatungan and (c) Musuan.

(ii) Mt Kalatungan

Volcanoes of Mt Kalatungan form an E-W trending volcanic ridge similar in morphology to Mt Katanglad (Fig. 2-5b). It is larger, however, and has domes along the S and E flanks. The 30km ridge is unexplored but an apparent vent in the central ridge appears to be the source area of Recent massive lava flows. These lavas form steep hills to the north and a broad shield south of Mt Kalatungan. Pyroclastic breccias and debris flow deposits cover NW Mt Katanglad (Fig. 2-3). Highly weathered lavas and volcanic breccias comprise SE of Mt Kalatungan. The eastern flanks are built from lava flows which are mantled by thick pyroclastics. From Kaulayanan to Kiharong (Fig. 2-4), the slopes are covered by patchy boulder fields covered with 3 - 5m vesicular to massive blocks and bombs.

To the south is Mt Kidonging, a stratocone with a plug dome which rises to 1,250m (Fig. 2-4). The dome is surrounded by gently sloping lava flows which grade downslope into pyroclastic breccias and fluvial sediments. The lava flows are dammed to the west by deposits from Mt Ragang so the overall flow direction is to the south. SE of Mt Kalatungan is a lava dome (unnamed; 1,128m high) which has a central lava dome with radiating lava flows on its upper to middle slopes, and pyroclastic aprons and debris flows on the lower section. Thick wedges of volcanic breccias comprise the SE flanks of this dome.

Three other Pleistocene - Recent volcanic deposits which may relate to Mt Kalatungan occur in the E -- Quezon volcanics, Butong, and Musuan Volcano (Fig. 2-4). The Quezon volcanics underlie Musuan Volcano and Butong, and are composed of massive to jointed lava flows which are also exposed in the type locality of Quezon River. Butong is a cinder cone with a summit crater lake to the SE of Quezon volcanics. Its slopes are mainly covered by tuffs and lava bombs. Musuan Volcano is a dome and lava flow N of Butong (Fig. 2-5c). The highly symmetrical Musuan dome is made from dense massive lavas with patches of

pumiceous ash. Its lower slopes comprise lava flows (30-50m thick) with minor pyroclastic cover. Musuan Volcano overlies Upper Miocene to Lower Pliocene clastics and is surrounded by Quaternary Alluvium. The smooth, undissected morphology and recent seismic activity suggest this lava dome is the youngest volcanic centre in Bukidnon.

2.2.3. DAVAO VOLCANIC GROUP

Volcanoes of Davao overlie a Cretaceous - Early Paleocene basement complex. The latter is widely exposed as a north-south band of lavas and tuffaceous pyroclastics that border the SE Cotabato Basin. The main volcanic centres in Davao are the Mt Apo-Mt Talomo-Mt Sibulan complex. Several eruptive centres probably occur NW of this complex and a volcanic ridge to the N (related to Mt Tinanan?) was probably the source area (Fig. 2-4) for tuffaceous clasts in Oligocene sediments of Cotabato Basin.

Pyroclastic deposits to the N and NW of Mt Talomo are considered the oldest volcanics in Davao. The Aracan and Tinanan Plains (Fig. 2-4) are composed of Pliocene and younger tuffs and volcanic breccias, with lava flows being more prominent near NW Mt Talomo. Mt Carmen is another Pliocene-Pleistocene volcano N of Mt Talomo. The steep flanks of Mt Carmen are made of dense vertically jointed lavas overlain by blocky debris flows. These grade into extensively reworked pyroclastics in the northern slopes. To the south is the Mt Talomo stratocone. The broad NW slopes are underlain by pyroclastic flows and debris flows near Davao. Above 500m elev, the pyroclastics are overlain by dense massive lavas which are deeply incised by radiating gullies.

Mt Sibulan is a Pleistocene stratovolcano in SE DVG. Its cone is built around a central vent which is breached to the south. Like Mt Talomo, Mt Sibulan is dissected by gullies which are floored by lava flows or pyroclastic deposits. Only

limited pyroclastic aprons occur along the lower flanks which are mainly covered by volcanic breccias and alluvium.

Mt Apo is the largest volcanic center in the DVG and is the highest peak (2,950m+) in the Philippines. Unlike other volcanoes in DVG, the western slopes of Mt Apo, from Kidapawan to its summit are formed mainly by pyroclastic flows and volcanic breccias. These pyroclastic flows typically contain large lava blocks within a hydrothermally-altered tuffaceous matrix. Dense lava flows occur in the NNE near the summit. The peak is a small ridge of agglomerate and blocks which is probably a remnant of a dome. East of the summit, the flanks dip steeply and are covered by large unconsolidated wedges of volcanic blocks. At several points in the upper eastern slopes are steam vents which have mantled surrounding blocks with thick sulfur. The high proportion of pyroclastics at Mt Apo indicate predominance of explosive eruptions. At present, Mt Apo is solfataric and recent activity is evident in the fresh blocky sections near the summit.

2.3. VOLCANIC GEOLOGY OF CAMIGUIN ISLAND

2.3.1. INTRODUCTION

Camiguin Island is the northernmost stratovolcano complex in CMVA (Fig. 2-4). The island comprises many eruptive centres that form a NW-SE volcanic chain nearly parallel to the regional trend of the southern Philippine Fault and the Philippine Trench. The main zone of volcanism is 7 - 10 km wide and geographically continuous with the Misamis Peninsula of northern Mindanao. Volcanic products on Camiguin Island are mainly basic to intermediate lavas, pyroclastic flows and domes which form the rugged 1,580m peak of Mt Mambajao and the 1,200m-high Hibok Hibok - Mt Catarman dome complex. Only the NW end of Camiguin Island has experienced historical volcanic activity (Fig. 2-6).

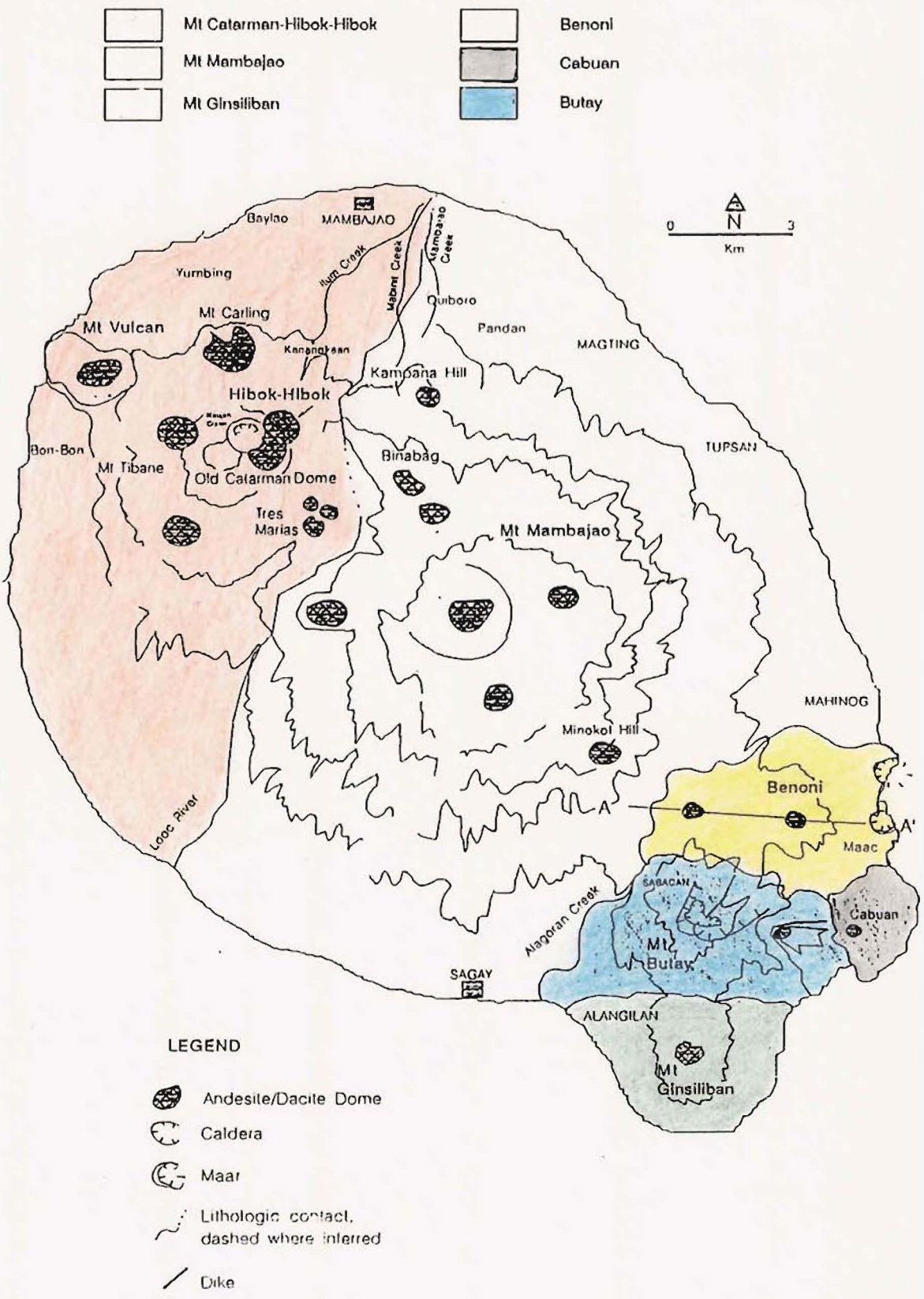

Figure 2-6. Geology of Camiguin Island.

Major eruptions from Camiguin Island, particularly from Hibok-Hibok (literally, to shake) are a major hazard as over 20,000 people live on nearby slopes, pyroclastic plains and lahar-inundated areas. The explosivity and proximity to population centres make Hibok-Hibok one of the most destructive volcanic centres in the Philippines in recent time. Prior to 1948, pyroclastic flows and surges were unknown at Hibok-Hibok. As a result the local community was not prepared for the eruption of 1951, causing the death of over 500 people.

2.3.2. Previous Studies

Camiguin Island was identified as volcanically active when a dome-building episode formed Mt Vulcan in 1871. The first account was by Jagor (1875) who scaled Mt Catarman and reported a crater lake near the summit. Succeeding reports by Maso et al (1903) focused on the progress of volcanic activity, mostly solfataric, in 1897 and 1902. Eruptions were documented by Pelaez (1948) then by Abad (1949) while the general nature of the 1951 eruptions was discussed by Alcaraz et al (1952). Details of the eruption, transport and effects of pyroclastic flows were given by MacDonald and Alcaraz (1956).

It was Renard (1889) who first provided a detailed account of the petrographic characteristics of rock specimens from Mt Vulcan during the expedition of the H.M.S. Challenger to the island in 1875 but it was not until the 1980's that further petrography was undertaken by Crisologo et al (1986) and then by Solidum and de Torres (1986, 1988).

The span of rock types identified and described in earlier surveys are, however, incomplete. While there was a suspicion by previous workers of more evolved rocks than andesite, no such rocks were ever found. Renard (1889) described what he referred to as "granitic fragments" that were incorporated in lavas erupted during the growth of Mt Vulcan dome in 1871. In his report, Renard noted light-coloured inclusions that crumbled like pulverized glass. Microscopically, these

inclusions contained quartz and highly corroded crystals of feldspar, biotite and augite. However, these inclusions are probably xenocrysts, the source of which is at present unknown. On the basis of physiography of recent extrusives, Abad (1949) inferred a relatively high silica content for lavas of Hibok-Hibok, compared to older rocks, but this inference was not substantiated. MacDonald and Alcaraz (1953) identified clasts from pyroclastic flow deposits erupted in 1951 as dacites and found banded varieties to constitute Hibok-Hibok dome.

2.3.3. Stratigraphic Classification

For the purpose of this study, volcanic rocks that form Camiguin Island occur within the Camiguin Volcanic Field, or CVF. Within CVF, large individual volcanoes or many closely-spaced sources of volcanic rocks are identified as volcanic centres following the usage of Fisher and Schmincke (1984) in delineating geographic-volcanic subdivisions.

Relative chronology and stratigraphy of domes, flows and other volcanic units have been deduced on the basis of morphology and field relations as there have been no absolute ages determined at this time. Except for historic deposits there is a lack of chronostratigraphic markers. This can create problems where deposits from adjacent volcanoes do not overlap. As a result names given at this time are informal. Ancient deposits are accorded descriptive or lithologic terms in view of their frequently ambiguous origin. A litho-genetic terminology is applied to modern deposits which have good and numerous exposures, well preserved morphology and accounts of volcanic processes which produced them.

2.3.4. Geology of Pre-Historic Deposits

The geologic map of the Philippines (Phil. Bureau Mines, 1963) classifies Camiguin Island as a "Quaternary Active Volcano". Except for descriptions of recent deposits emplaced since 1871 little else was known about the geology of the island.

This section presents the stratigraphy of the island, relating geologic observations to the history of the island.

The Camiguin Volcanic Field can be subdivided into six major edifice-forming eruptive centres. These are from south to north: 1) Mt Ginsiliban, 2) Butay, 3) Cabuan, 4) Benoni, 5) Mt Mambajao and 6) Mt Catarman and Hibok-Hibok (Fig. 2-6). A schematic column depicts the stratigraphic relationships of these volcanic units (Fig. 2-7).

(i) Basement Rocks

The structure and nature of basement rocks which underlie CVF is unclear, although Lejay (1938) reported strong positive gravity anomalies at the tip of Misamis Peninsula which he postulated to result from basaltic rocks. Abad (1949) conjectured that Camiguin Island was probably built on a basaltic submarine platform which extends from Misamis Peninsula. Alcaraz et al (1952) observed that subaerial distribution of mafic rocks in CVF was limited to the SE portion and hence did not support Lejay's contention that "...heavy materials, ...revealed by samples at the surface, must be in great quantity in the root." Recovery of basaltic samples off the coast of Bon-Bon (Fig. 2-6) in NW CVF and in phreatic beds of Benoni, however, suggest a much more extensive basaltic formation underlying Camiguin.

(ii) Butay volcanics

The oldest volcanic deposits probably occur at Butay volcano, SE CVF. Butay is highly dissected and its flanks are overlain by extrusive rocks from Ginsiliban and Mt Mambajao. The boundary between Butay and Mt Mambajao was earlier defined by the Sagay-Mahinog lineament (Abad, 1949), a general NE trend of river valleys between these towns. The boundary is evident along the Alagoran Creek, east of Sagay and at Barangay (hamlet) Sabacan (Fig. 2-6). The most distinctive feature of Butay is a NE-facing breached crater that resembles an

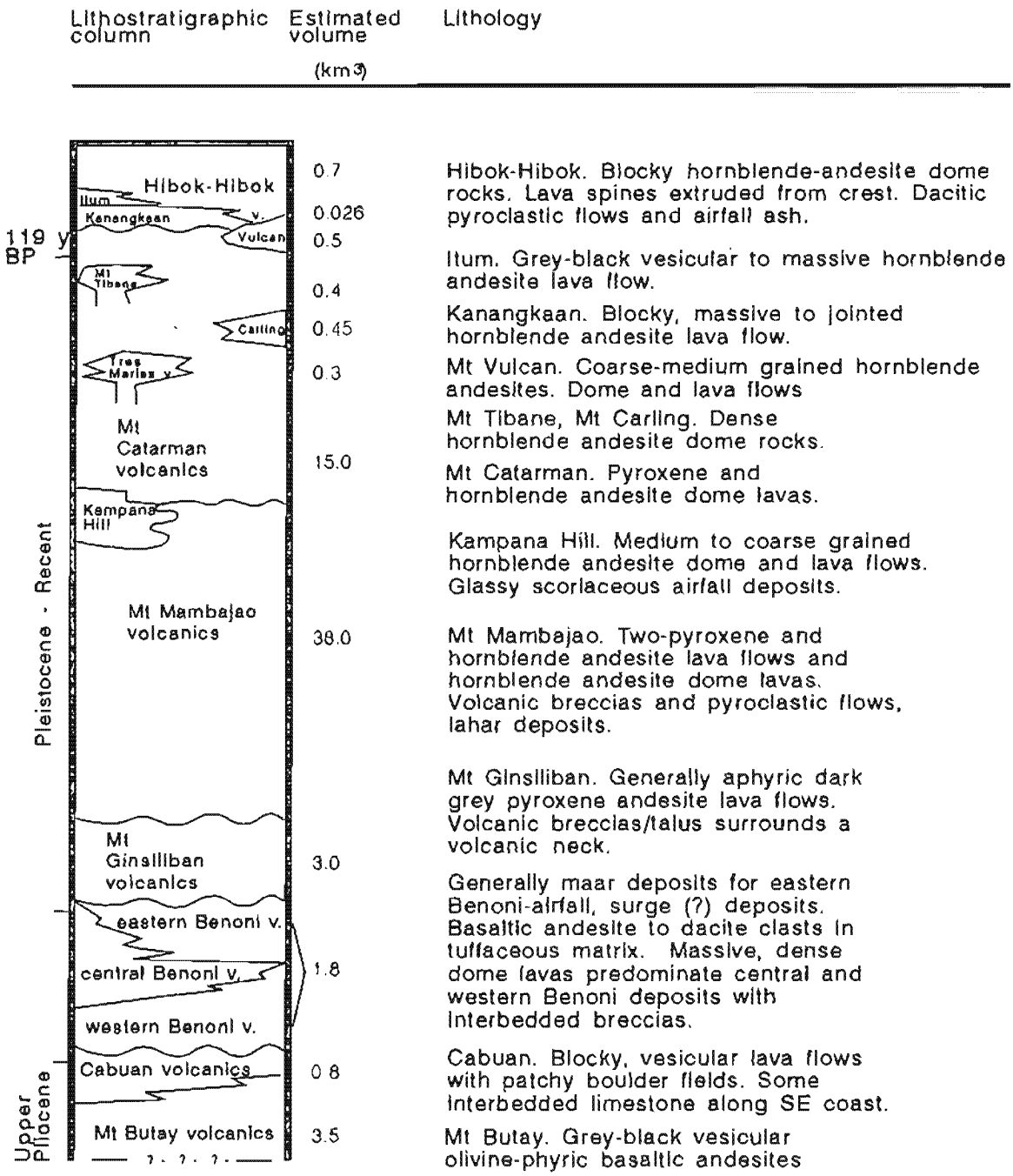

Figure 2-7. Proposed stratigraphic column of Camiguin Island.

explosive amphitheatre. However, erosion probably played a major role in the present morphology, exposing lava ridges which could be radial dikes. ESE of Butay summit is a crater which is probably a parasitic cone. The central cone is now filled by lavas and the southern portion has been breached by a series of short lava flows.

East of Butay is the Cabuan volcanics, which may be divided into a gently sloping northern section and a hilly, irregularly sloping southern section. Outcrops of northern Cabuan exhibit 20m high cliffs of broadly jointed lavas overlain by a veneer of volcanic breccia. To the SE is the 120m peak of Cabuan, with vertically and horizontally jointed grey lava which form near vertical faces along river valleys. The base of these lavas is overlain by volcanic breccia and conglomerate which intercalate with coralline sediments exposed along the SE coast. The occurrence of large bombs and blocks suggests a near-vent source. The proximity of Cabuan makes this the most probable source of volcanic flows and debris found in southern Cabuan.

(iii) Benoni volcanics

In the region between the Butay volcanics and Mahinog, the Benoni volcanics are exposed. These comprise a sequence of pyroclastics and lava flows exposed inland which grade into phreatomagmatic beds and tuff cone deposits along the SE coast (Fig. 2-8). An E-W section depicts three adjacent centres, here referred to as the Western, Central and Eastern Benoni volcanics. Western Benoni volcanics comprise an eroded lava dome surrounded by volcanic breccias and epiclastic debris which interfinger with deposits from Mt Mambajao and Butay. The highly eroded morphology has produced an irregular and hummocky terrain in which several volcaniclastic flows have been dissected into mounds.

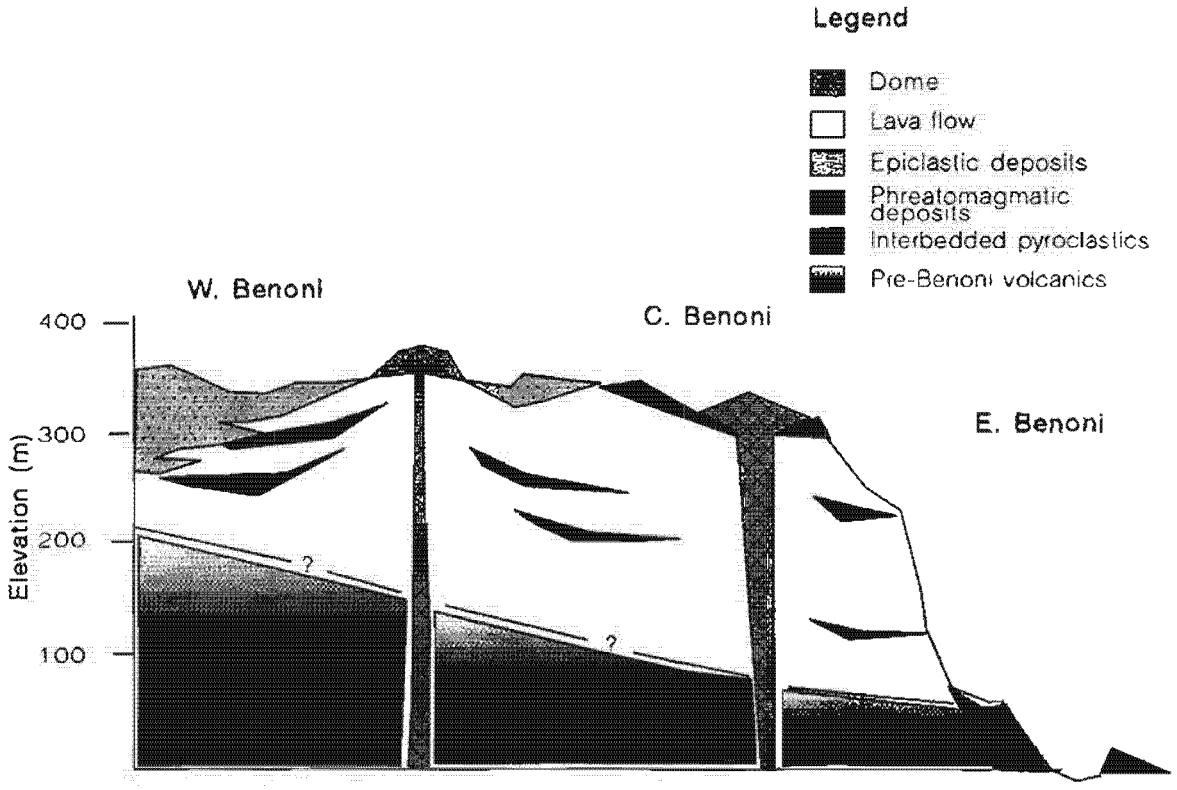

Figure 2-8. Schematic section across Benoni volcanics (line A-A' in Fig. 2-6) showing dome and lava flows inland to maar deposits on the coast.

The Central Benoni volcanics comprise at least two overlapping tuff cones which are now partially buried and filled by lava domes and flows. Short lobes of lava appear to have flowed from these domes and subsequently eroded to form high cliffs along a short segment north of Benoni. Along the shore, steep, vertically-jointed lava is overlain by volcaniclastic beds from Eastern Benoni where 2 tuff cones occur. The southern (Maac) cone is a maar with a vent area now occupied by a shallow lagoon. About 1 km N of Maac is an arcuate wall of shallow dipping pyroclastic beds which were probably erupted from a tuff cone whose eastern section has been eroded by wave action. The vent area for this tuff cone is SE of the present shoreline (Fig 2-6).

Deposits from Western Benoni underlie the Central Benoni volcanics and are therefore inferred to be the earliest. The younger Central and Eastern Benoni volcanics are probably related because of their proximity. The eruptive styles greatly differ, however, and range from effusive dome-building to pyroclastic eruptions probably resulting from several discrete eruptions. Fisher and Schmincke (1984) discussed the formation of maars and noted that in nearly synchronous eruptive centres, vents in the upland areas produce cinder cones with co-magmatic lava flows while associated vents near the coast result in maars or tuff cones.

(iv) Mt Ginsiliban volcanics

Ginsiliban is the southernmost volcano of the CVF (Fig. 2-6) and is an exposed volcanic neck surrounded by a talus apron. Lavas and volcaniclastics of northern Ginsiliban overlie Butay and are therefore younger. The relative stratigraphy between Ginsiliban and deposits from Cabuan and Benoni cannot be determined without absolute dating as these centres do not overlap. However, Ginsiliban is considered the youngest centre in southern CVF because of its well-preserved and simple morphology.

Mt Ginsiliban peak rises to 580m and forms a near vertical column of massive to broadly jointed lava (Fig. 2-9) Between sea level and 400m, the flanks are highly vegetated pyroclastic aprons which grade into debris flow and fluvial deposits near the coast. Lava flows are exposed along river beds SE of Ginsiliban peak.

(v) Mt Mambajao volcanics.

Mt Mambajao occupies 60% of total land area in CVF, making it the largest volcanic centre. The Mt Mambajao volcanic centre has built to a peak of 1,580m and there is a summit caldera 1,500m in diameter with an inner, possibly resurgent tholoid. The caldera wall is breached to the NW which suggests a penultimate paroxysmal eruption. Arcuate detachement scarps cut through deposits within and just outside the NW caldera wall and were probably produced by debris avalanches.

With the exception of Kampana Hill in NW Mt Mambajao, all lava domes occur within 2 km of a central NW-SE axis of the CVF, in general alignment with Hibok-Hibok, Mt Mambajao, Minokol Hill and Butay (Fig. 2-6). The lack of eruptive centres between Mt Mambajao peak and the NE-SW flanks result in regular distribution of volcanic facies from vent deposits (volcanic breccias; Salugsugan, pers. comm., 1989) to distal assemblages of lava flows, volcaniclastic flows and epiclastic debris.

Vertically-jointed lavas crop in the E coast along separate sections of Tupsan and Magting (Fig. 2-6). These lavas form gentle slopes (< 5^{o}) until approximately 200m, where shorter, steep-sided lava flows overlie coastal lavas from an earlier eruptive phase.

Lavas to the N of Mt Mambajao peak form an arcuate ridge which separates an area to the E characterised by highly eroded volcanic breccias, from an area to the west dominated by dome and lava flow deposits. The eastern volcanics predate lavas from the western section.

Figure 2-9. NW view to Camiguin island from Misamis Peninsula. Shown are Mt Ginsiliban (left) and Butay volcanic centres. Line drawing shows general distribution of deposits, from vertically-jointed lavas (volcanic neck) to pyroclastic breccias and debris flows on the flanks of Mt Ginsiliban. Butay volcanics are mainly pyroclastics. Lithological contact indicates Mt Ginsiliban centre is younger than Butay.

The cluster of domes and lava flows NW of Mt Mambajao peak may represent "transitional" volcanics between Mt Mambajao and Mt Catarman. The location of Kampana Hill and Binabag domes (Fig. 2-6) suggest these centres are part of the Mt Mambajao volcanics but compositionally they are similar to intermediate lavas from Mt Catarman. More detailed mapping and absolute dating is necessary to resolve this stratigraphic uncertainty.

SE of Mt Mambajao peak is the lava dome of Minokol Hill (Fig. 2-6). An associated lobe of lava has flowed southward and clearly overlies the NW Butay and Benoni volcanics so that this stage of volcanism (late Mt Mambajao volcanics) is younger than either Butay or Benoni.

(vi) Mt Catarman volcanics.

Mount Catarman is the second largest volcanic centre. Volcanics associated with this cone cover over 70 km^2 of NW CVF (Fig. 2-10). In the SW, Mt Catarman volcanics are separated from Mt Mambajao by the Looc River. Further N, the Mabinit and Mambajao Creeks delineate a zone of interfingering pyroclastic flows, lahars and fluviatile sediments from Mt Catarman with debris flows and epiclastic deposits from Mt Mambajao.

Mt Catarman is a stratocone with several flank domes and 3 summit vents which rise to 1,400m. The NW summit crater is called Naujan, a 100m-wide vegetated pit that is sometimes filled with water. The ephemeral lake was reported to be ebullient (Jagor, 1875) although no historic eruptions have been attributed to this site. The southern dome (Old Mt Catarman dome) is the main summit vent and is composed of blocky lavas.

On the NW flank of Mt Catarman is a circular and flat-topped dome called Mt Carling (Figs. 2-6; 2-10). Streams have incised the northern flank and have deposited a volcaniclastic field to the north. Mt Carling deposits consist mainly of

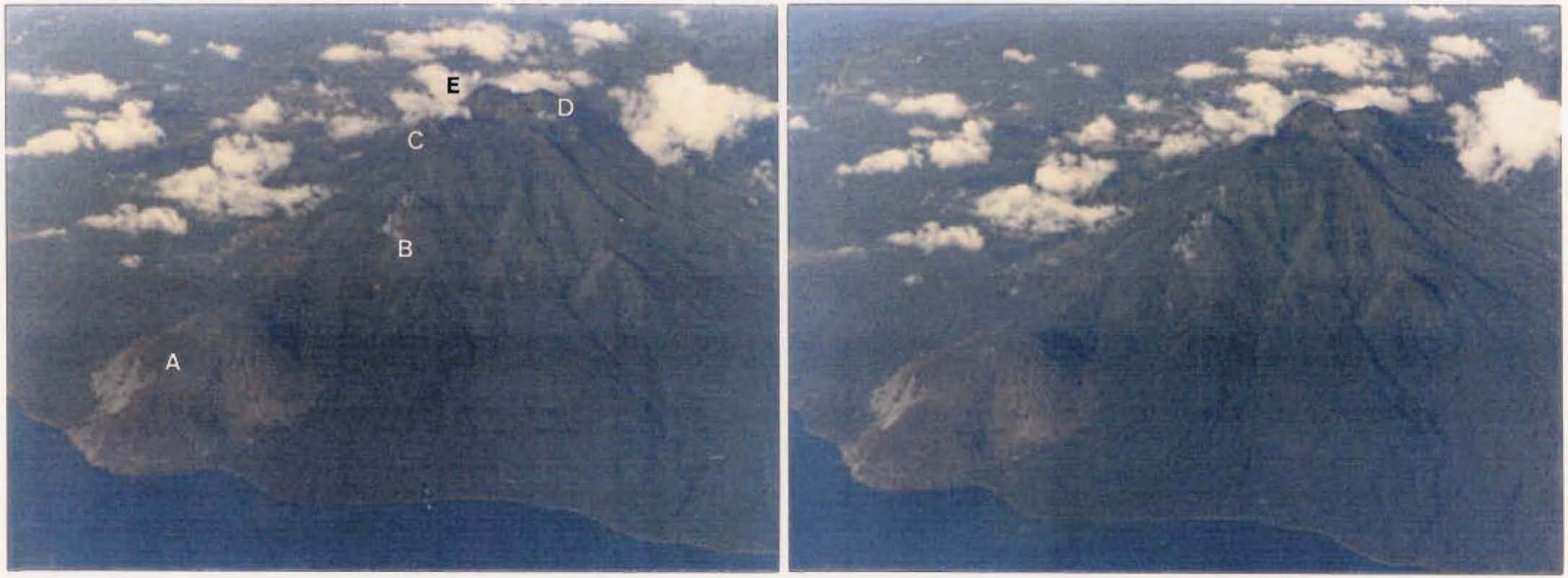

Figure 2-10 Stereo-photograph of NW Camiguin Island showing (a) Mt Vulcan, (b) Tibane dome, (c) Naujan Crater, (d) Old Catarman dome and (e) Hibok-Hibok dome.
Photographs courtesy of R.S. Punongbayan.

massive lavas which intercalate with volcanic breccias, debris flows and tuffaceous beds in the northern flank.

On the NW slope is the prehistoric dome of Mt Tibane (Figs. 2-6; 2-10) which overlie flank lavas from Mt Catarman. Mt Tibane is probably younger than Mt Carling dome because of its less eroded form and well-defined elliptical crater. A lava flow which originates from the base of Mt Tibane represents an early effusive stage while pyroclastic debris which mantle the upper flanks and summit area indicate a late explosive phase.

SE of Old Mt Catarman dome is the thickly vegetated and highly eroded Tres Marias dome. Sections exposed by by recent avalanches of the eastern flank show massive to jointed lavas. Unlike many domes in the CVF, there are no associated co-magmatic lava flows.

Overlying Tres Marias dome is an extensive pyroclastic apron which has aggraded over the SW flank of Mt Catarman. From 600 to 900m, its relatively smooth upwards-concave surface contrasts with adjacent rugged lava ridges. Gullies 100m deep have been cut into a series of volcanic breccias and flows. Below 250m the pyroclastic apron grades into lahar fields and braided channel deposits with very different stream patterns to those that have developed over Mt Mambajao volcanics east of Looc River (Fig. 2-6). Sequences of fluviatile sheet flood deposits, coarse channel deposits and buried vegetation show active sediment transport within the SW Mt Catarman pyroclastic apron, in contrast to ephemeral streams and highly vegetated topography of adjacent western Mt Mambajao. Thus deposits of Mt Catarman are inferred to be younger than western Mt Mambajao deposits. This stratigraphic relationship is consistent with volcanic sequences exposed in northeastern Tres Marias where pyroclastic flows from Mt Catarman overlie lavas from Binabag dome (Mt Mambajao volcanics). Recent

pyroclastic flows and lahars from Hibok-Hibok also overlie fluviatile deposits of northern Mt Mambajao.

2.3.5. Geology Of Recent Deposits

Products of recent eruptions represent only 80 years of volcanic history and were emplaced entirely within northern Mt Catarman volcanics. Figure 2-11 presents the geology of recent volcanic deposits.

(i) Airfall Pyroclastics

Deposition of airfall tephra is highly dependent on wind direction. In northern Mindanao the prevailing winds from November to April are northeasterlies while winds from June to October are the southwesterlies. During May, easterlies (Trade Winds) become prevalent. Thus when pyroclastic eruptions at Hibok-Hibok commenced on 1 September 1948, ash first fell to the NE of Mt Catarman. However, rainfall has washed away pyroclastic units which mantled the upper slopes. Airfall ash erupted during 1948-1953 are therefore only preserved as intervening beds within pyroclastic flow deposits or as thin lenses buried by small post-eruption avalanches.

(ii) Lava Domes

Mt Vulcan was formed from 1871 to 1875, on the NW flank of Mt Catarman (Fig. 2-9). The peak rises to 475m with a 50m-wide summit pit. The slopes of Mt Vulcan are striated due to loose blocks which spall off the upper slopes. The NW profile of the dome is assymetric because lava flowed during the waning phase of eruption, producing a seacliff. During this eruption approximately 1 km^2 of the NW part of Mt Vulcan subsided, probably as a result of magma withdrawal.

NE of Old Mt Catarman Dome is Hibok-Hibok dome (Figs. 2-10; 2-12a). Hibok-Hibok dome represents the last phase of eruption from 1951-1953 and

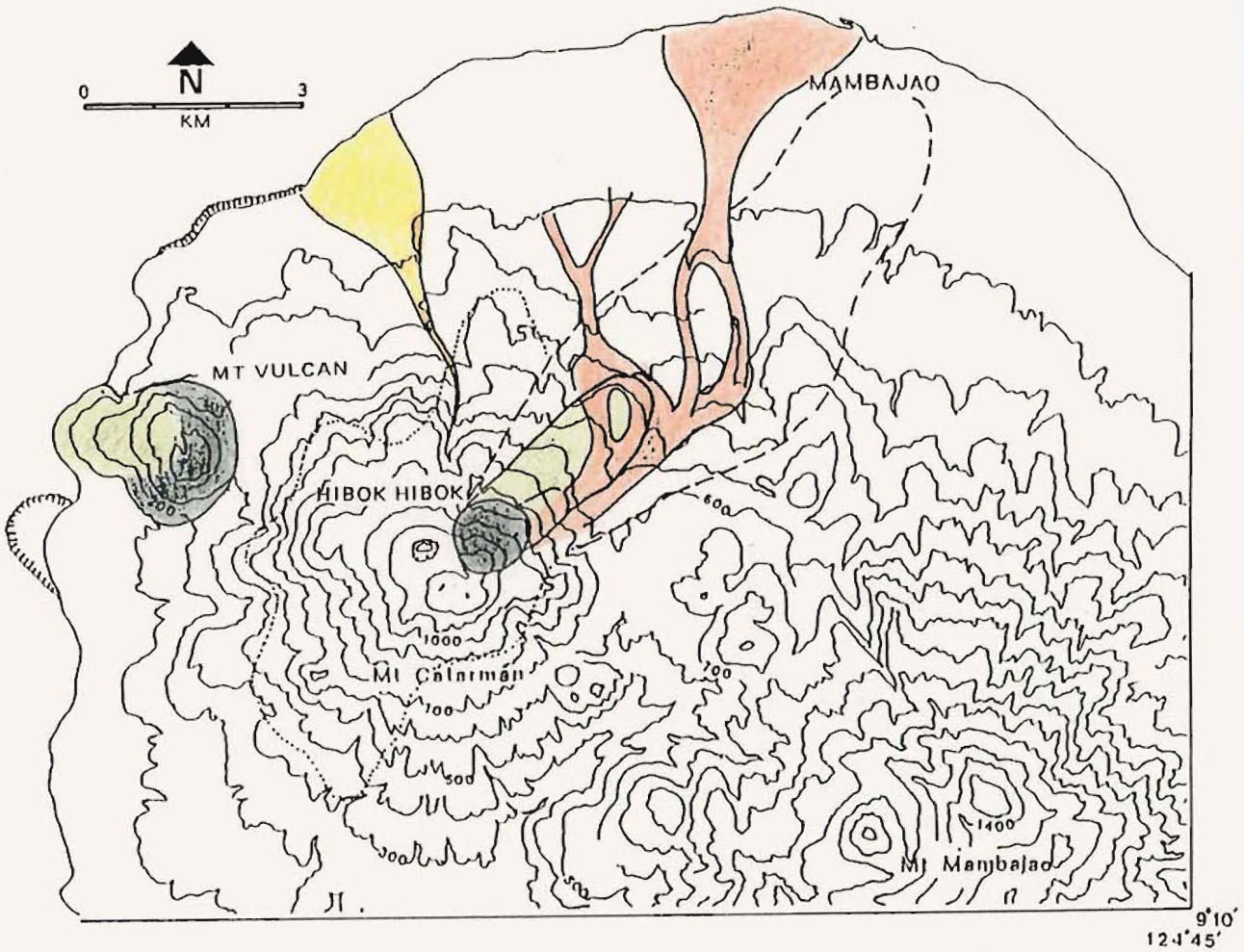

Figure 2-11. Geology of Recent deposits, northern Camiguin Island. Shown are lava domes of Mt Vulcan (1871-1875 activity) and Hibok-Hibok (1948-1953). Dashed field encloses area devastated by a pyroclastic surge on 4 December 1951.

overlies lavas erupted during 1948. Hibok-Hibok peak reaches 1,400m with lava spines vertically-projecting 10-20m above the dome crest. The spines are dense, glassy lavas similar to rocks found on the summit of Hibok-Hibok but contrast to vesicular blocks found at the base of the dome. Flank deposits are composed of loose meter-sized blocks and breadcrust bombs but gullies in the NE expose pyroclastic layers (2m thick) of coarse ash and lapilli.

Prior to extrusion of lavas in 1949, there were several solfataras in the active vent system. Repeated phreatic eruptions from these vents and accompanying earthquakes triggered landslides which resulted in enlargement of the NE flank valleys into a single scarp. When Hibok-Hibok erupted, the avalanche slope refilled with lavas until progressive dome growth overlapped Old Mt Catarman dome.

(iii) Lava Flows

The earliest lava extruded from Hibok-Hibok is the Kanangkaan lava flow (Fig. 2-12b), named after the hamlet which the flow overran. Kanangkaan is a NE-trending steep-sided flow which rises 20-50m above the present Itum valley floor. The top and sides of the flow are mantled by loose blocks. Its upper surface has been eroded to a relatively flat plain by later pyroclastic flows which have also carved longitudinal ridges on the SE margin. Kanangkaan lava flow overlies prehistoric lavas from Mt Catarman and its SE edge has constricted the Itum valley into a narrow (< 20 m) channel. The volume of lava is about 26 x $10^6 m^3$.

The Itum lava flow (Figs. 2-12a & b) was deposited during early and late eruptive phases contemporaneous with dome building and pyroclastic eruptions of Hibok-Hibok in 1951. The Itum lava flow overlies Kanangkaan and is distinguished from surrounding Hibok-Hibok lavas because of its contrasting colour.

Figure 2-12. (a) Panoramic view of Mt Catarman showing Hibok-Hibok dome. Foreground shows the pyroclastic flow deposits of 4 and 6 December 1951 eruptions. (b) view to ESE showing Hibok-Hibok dome and Kanangkaan lava flow. The ridge of this flow, at far left, diverted part of the 4 and 6 December pyroclastic flows to Mambajao Town (towards viewer). Key features: (1) Hibok-Hibok dome; (2) Kanangkaan lava flow; (3) Itum lava flow.

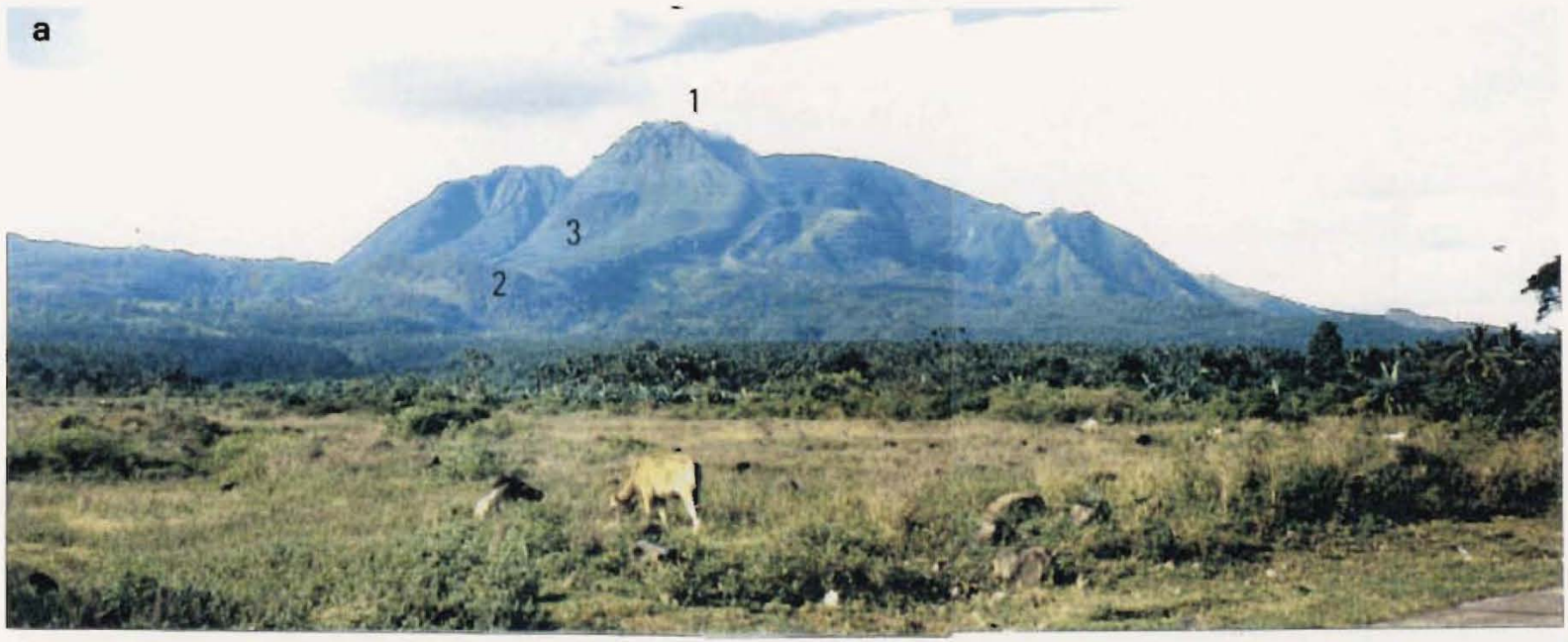
a
1
3
2


b
1
2
3

(iv) Pyroclastic Flows

Quiboro pyroclastic flow deposit. On the lower slopes of Kampana lava ridge is the hamlet of Quiboro, which pyroclastic flows from Hibok-Hibok overwhelmed on 4 December 1951. The outline of the area covered by this flow shortly after eruption is shown in Figure 2-13a with a NE axis leading to Mambajao town. Nearly all the deposits have been eroded and only thin lenses of marginal facies are now found in Quiboro (Fig. 2-13b). The section exposed at the junction of Quiboro and Pandan roads is a local, ponded pyroclastic flow deposit. The outcrop comprises a single bed, 6 - 9cm thick, with 3 - 5cm pumice clasts set in a coarse ash and lapilli matrix. NE of Kampana Hill, at 260m elevation, is a ridge-top facies which consists of a fine-coarse grained, cross laminated ash layer. The layer has a maximum thickness of 8-9cm and pinches out laterally. Thicker deposits occur west of Kampana Hill. Similar lenticular ash deposits are exposed along the roadcut to Itum at 360m elev and represent the eastern limit of the Quiboro pyroclastics.

Mabinit Pyroclastic Flow Deposit. The sequence of massive, poorly sorted and stratified ash beds exposed along Mabinit Creek, Mambajao, Esperanza and Baylao is collectively referred to as the Mabinit Pyroclastic Flow Deposit (Fig. 2-11). This unit was erupted on 6 December 1951. For the first 2 km the flow travelled partly along the narrow Itum Creek, aggrading the valley floor 50-100 m to the level of Kanangkaan lavas. A major portion of the flow drained thru Mabinit Creek and small patches of ash with scour marks occur on the SE Mabinit valley. These indicated the maximum flow level to be approximately 150m above the valley floor (Alcaraz et al, 1952). From an elevation of about 100m to the northern coast, the flow fanned out and reached its maximum runout at Mambajao (Fig. 2-13a) where portions of the basal flow, surge and airfall deposits are now preserved.

Part of the flow spilled over the Kanangkaan lava flow deposit. The diverted flow formed a pyroclastic plain about 1 km^2 over Esperanza and followed 2

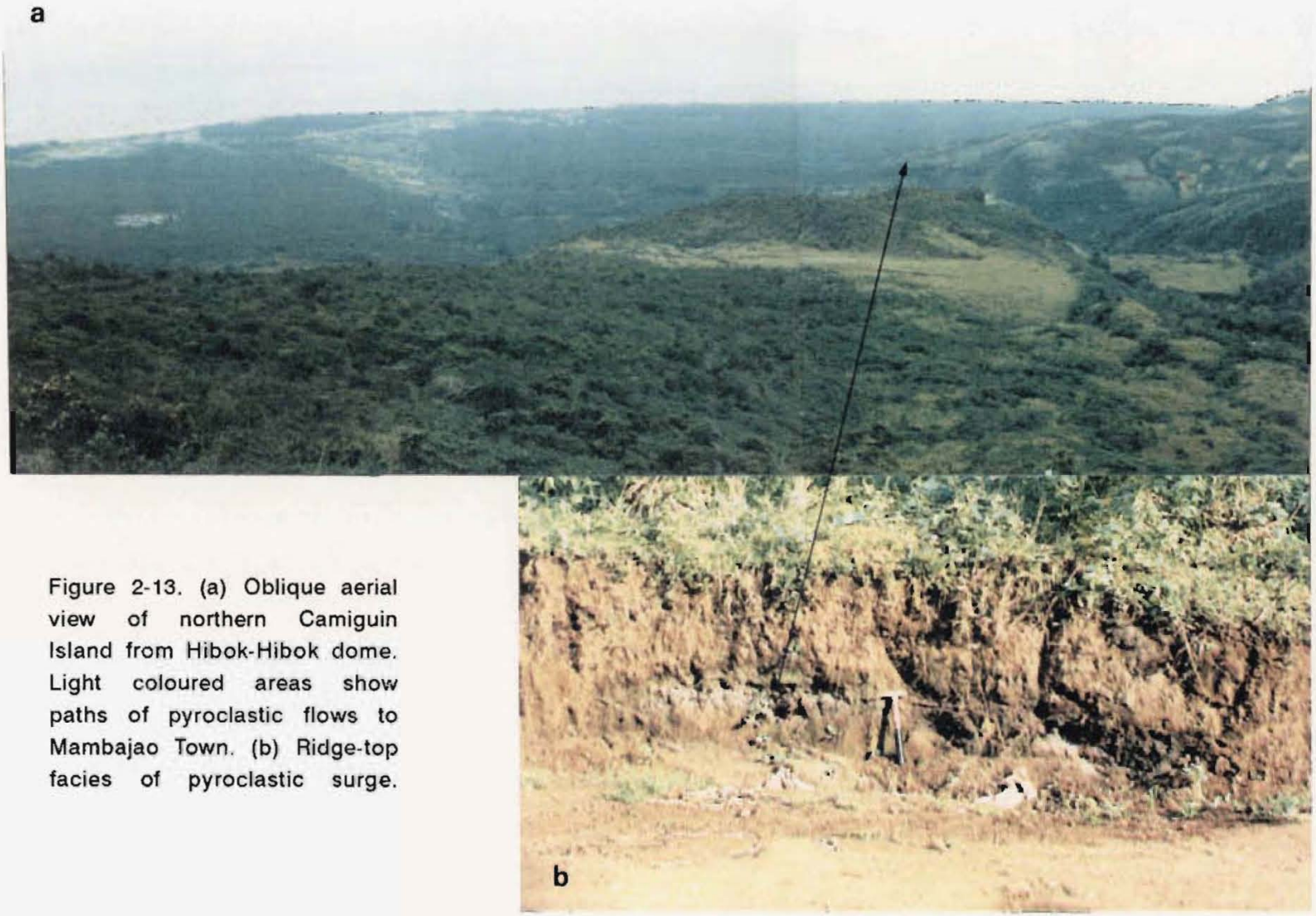

Figure 2-13. (a) Oblique aerial view of northern Camiguin Island from Hibok-Hibok dome. Light coloured areas show paths of pyroclastic flows to Mambajao Town. (b) Ridge-top facies of pyroclastic surge.

tributaries as far north as Baylao, where there are numerous lava blocks 5m in diameter.

(v) Lahars

Debris flows which form the floodplains and river banks N of Mt Catarman are referred to as the Yumbing Lahars. These formed shortly after eruptions in 1948. The deposits are massive, poorly sorted and matrix-supported with heterolithologic blocks averaging about 0.4m across although larger blocks up to 3 m in diameter are found.

2.3.6. Evolution Of Camiguin Island

At first glance it appears that there was a progressive migration of volcanic centres along a NW-SE zone in CVF, beginning from Ginsiliban in the south to the present active site of Hibok-Hibok to the north. In a broad sense, this is correct with the more eroded volcanics of southern CVF representing an early phase of volcanism followed by an intermediate eruptive phase of dome building and lava flows at Mt Mambajao. Mount Catarman and associated volcanic centres of NW CVF represent the latest extrusives and is the site of all historic eruptions. This concept of northward younging of volcanic centres within the CVF is reinforced by an apparent compositional variation within the relative stratigraphy as will be discussed in Chapters 4 and 5.

The progressive migration of volcanism is, however, an oversimplification when looked in detail. For example, some volcanic units found in southern CVF, e.g., Minokol Dome, are younger than domes occurring to the north. Equally in the most recent eruption sequence activity from Mt Vulcan preceded eruptions from Hibok-Hibok. Abad (1949) proposed that the CVF began by formation of Ginsiliban followed by Uhay (Butay), because of the predominant basaltic character of these volcanoes. He further conjectured that volcanism then changed from a north-south

trend to a NW-SE trend represented by alignment of Mt Mambajao, Mt Catarman and Mt Vulcan. Punongbayan (1988) considered the first eruptions formed an early "Camiguin Tanda" (proto-Camiguin) which comprised the NW portion of present-day Camiguin Island. Mt Uhay (Butay) and Ginsiliban later developed as separate centres, still separated from Camiguin Tanda by the sea. Mt Mambajao was then built approximately midway between Camiguin Tanda and Uhay/Ginsiliban, and eventually fused all volcanoes into a single landmass.

The proposed evolutionary model of the CVF given here is based on geologic relations discussed in previous sections.

The Central Mindanao Volcanic Arc (CMVA) is reportedly underlain by a basement complex of basalts, gabbros, andesitic tuffs agglomerates and volcaniclastic sedimentary rocks of Cretaceous to Paleogene (Cassasola, 1956; Metal Mining Agency, 1972). Similar Cretaceous to Paleogene rocks are found north of Camiguin Island at Cebu and Bohol Islands (Phil. Bur. Mines, 1982). It is thus reasonable to assume that a similar Cretaceous to Paleogene basement complex exists beneath the CVF and that this is geographically continuous with the CMVA and co-linear with Bohol.

The onset of volcanism within CVF probably postdates the Miocene-Pliocene volcanoes of central Mindanao because these extinct volcanoes exhibit high degrees of degradation and have developed thick soil profiles that are absent at CVF. Subaerial volcanism began with development of Butay perhaps at the end of Pliocene (Fig. 2-14a). The inital Butay volcanics were volcaniclastic deposits derived from several nestled tuff cones. Volcaniclastic aprons of western Butay represent remnants of extensive pyroclastic eruptions followed by intrusion of radial lava dikes, now exhumed by erosion. The last eruptive phase from Butay produced a cinder cone on the eastern flank which was then breached by lavas that flowed SE.

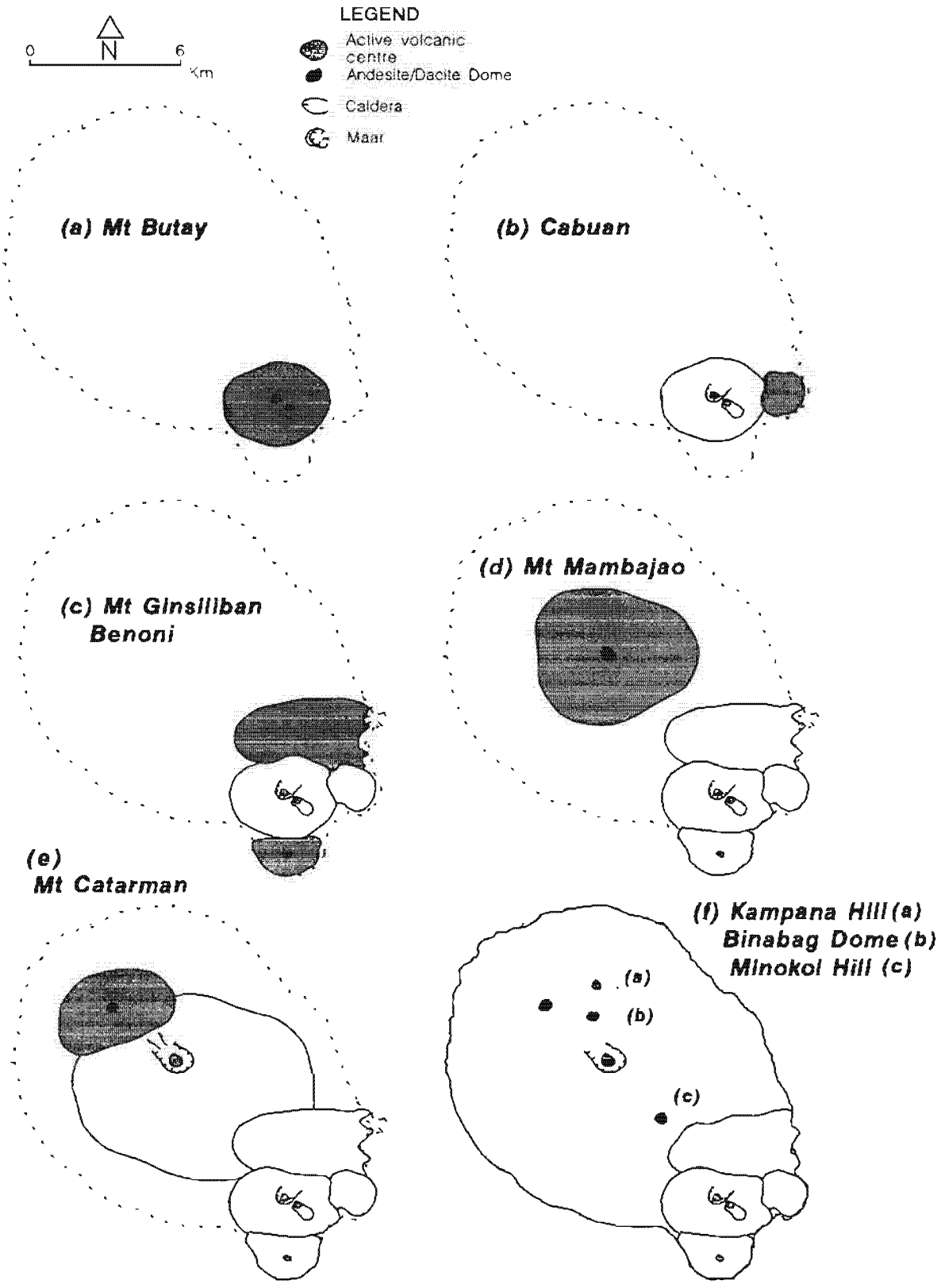

Figure 2-14. Proposed evolution of Camiguin Island showing accretion from prehistoric centres. Final outline of the island was probably achieved mainly from Mt Mambajao and Mt Catarman dome complexes. Labelled centres in (f) are some morphologically young prehistoric domes.

An E-W fissure developed at the eastern base of Mt Butay and extruded the mafic to intermediate lavas of Cabuan (Fig. 2-14b).

After eruption of Cabuan lavas, volcanism shifted north of Butay and produced the pyroclastic breccias of western Benoni (Fig. 2-14c). Pyroclastic flows of Benoni and epiclastic deposits from Butay led to accretion and joining of both centres into a single island. After eruptions at western Benoni ceased, a series of overlapping tuff cones produced the central Benoni volcanics. Extrusion of lavas filled and partially breached the tuff cones and lavas flowed eastward. The last phase of Benoni volcanism was the propagation of volcanic centres farther NE, producing the hydroclastic beds of eastern Benoni. Subsequent wave action breached the NW rim of Maac and extensively eroded the Benoni maar where only the NW rim and flank deposits remain.

Approximately 2 km south of Butay peak, the andesitic Mt Ginsiliban volcano was formed and built a stratocone over 600m high. Central vent eruptions persisted such that deposits produced a near circular cone 1.5 km in diameter. To the north, pyroclastic breccias bridged the gap between Mt Ginsiliban and Butay.

The last phase of Mt Ginsiliban volcanism was extrusion of andesitic lavas which flowed westward to Alangilan (SW Mt Ginsiliban; Fig. 2-6) and aggraded the Mt Ginsiliban-Butay paleovalley to nearly 200m elev. A period of erosion followed which exposed the Ginsiliban volcanic neck, reducing peak elevation to below 600m and built a talus apron that overlaps Butay to the N.

By the close of Mt Ginsiliban volcanism, SE CVF comprised Butay, Cabuan, Benoni and Mt Ginsiliban volcanoes with Butay at the approximate geometric centre. The role of Butay as the major volcano of early CVF is evident in the distribution of other vents which are all situated approximately 2 km from Butay summit.

A major shift in volcanism occurred with eruptions at Mt Mambajao (Fig. 2-14d) which probably continued until late Pleistocene. The early Mt Mambajao lavas were voluminous which spread to within a few km of the present NE and SW Mt Mambajao shoreline, and perhaps annexed SE Camiguin Island. An extended phase of edifice-forming eruptions followed, primarily by extrusion of thick, stubby lava flows, domes and interbedded pyroclastics. A cluster of domes formed Mt Mambajao peak which grew to about 1,800m and 2,000m in diameter. The summit was destroyed by late-stage pyroclastic eruptions, forming a NW-facing amphitheatre, accompanied by a debris avalanche depositing volcanic breccias on the NW flank. Soon afterward, a resurgent dome plugged the central summit vent. Subsequent eruptions involved dome-building episodes and the earliest flank dome was built to west of Mt Mambajao peak.

During late Pleistocene, eruptions on the lower NW slope of Mt Mambajao began to form early Mt Catarman volcano (Fig. 2-14e). The earliest lavas were probably more fluid than subsequent extrusions because relatively thin, early lava flows occur at the present SW Mt Catarman shoreline. A predominant cone-building phase followed with extrusion of intermediate lavas from a central vent and valley-filling breccias.

The earliest adventive dome was Tres Marias and an unnamed dome on the SW flank. To the north Mt Carling was extruded. These domes differ from others because of the lack of co-magmatic lava flows, such as that extruded at Mt Tibane and Mt Vulcan. Formation of flank domes were accompanied by ground subsidence and debris avalanches, which resulted in a major flank depression SW of Mt Catarman. This valley was rapidly filled by avalanche deposits. Summit activity from Mt Catarman rebuilt the southern flank and deposited thick sequences of pyroclastic beds which overlapped SW Mt Mambajao volcanics.

Recurrent volcanism at Mt Mambajao formed the domes of Mt Binabag and Kampana Hill (Fig. 2-14f). Lavas from the NW Mt Mambajao domes overlapped flows from Mt Catarman and extended the northern Mt Mambajao shoreline. The last eruptive phase of Mt Mambajao was the extrusion of Minokol Hill in the SE flank, nearly opposite Mt Binabag dome.

Late prehistoric activity of Mt Catarman was eruption of pyroclastic flows from the summit, perhaps during the Holocene. The flows descended the eastern flank and traversed lava ridges of Binabag dome. Earthquake-triggered avalanches from Mt Mambajao buried pyroclastic flows which are now exposed by a valley incised by the Looc River in SW Camiguin Island.

CHAPTER III PETROGRAPHY AND MINERALOGY

3.1. INTRODUCTION

The main lava types within the CMVA are poorly known despite several decades of geologic mapping. Recent interest as a result of geothermal exploration and volcanic eruptions has shed some light on CMVA lavas, but efforts have been few and localised. The purpose of this chapter is to identify major lava groups and magma types within the CMVA. The fundamental chemistry of these magma types is reflected in the modal mineralogy and chemistry of their erupted products and provides a basis for classification.

In general, mineral studies on arc volcanoes have focused on high-pressure phase relations (e.g. Kinzler and Grove, 1992; Foden and Green, 1992) to define source region chemistry and on relatively low-pressure phase relations (e.g. Shi, 1992) to explain basalt evolution. As most geochemical variations in both approaches involve mineral-liquid fractionations (Mitropoulos and Tarney, 1992) this chapter examines the mineral chemistry of CMVA lavas to assess whether the observed mineral assemblages crystallised in equilibrium with their melts, and to determine some conditions of crystallisation (see Appendix 5). Variations in mineral analyses from basalt to andesite, and andesite to dacite, are also examined to determine some changes in phenocryst chemistry associated with fractionation.

3.2. SAMPLE LOCATION AND ANALYTICAL METHODS

99 rocks were chosen for detailed petrography and 90 of these were analysed for major and trace elements. Their locations are shown in Appendix 1. A subset of 17 rock sections was chosen for microprobe analysis. Tables of petrographic descriptions and mineral chemistry are given in Appendices 2 and 3, respectively.

Electron microprobe analyses were undertaken at the Geology Department of Otago University, Dunedin, using a JEOL 8600 Superprobe fitted with 2 dispersive spectrometers. The machine used an accelerating voltage of 15kv and a probe current of 20 nA. A beam diameter of ~1 micron was used for most spot analyses. Because nearly all samples are highly charged with microlites a diffused beam (to analyse groundmass) was rarely used. The standards used are mostly synthetic pure oxides plus synthetic $CaSiO_3$ for Ca, Amelia albite for Na and St Gottard adularia for K. On-line data reduction (Kawachi and Trinder, unpubl.) was by ZAF method (Sweatman and Long, 1969) but various constants were upgraded. Fluorescent correction was used for characteristic X-rays, but not for continuous X-rays, as the latter was very small and can be safely ignored. The lower limits of detection (LLD, wt%) were: SiO_2, 0.07; Al_2O_3, 0.05; TiO_2, 0.07; FeO, 0.12; MnO, 0.10; MgO, 0.05; Na_2O, 0.08; K_2O, 0.03; Cr_2O_3, 0.10;, NiO, 0.18.

3.3. CLASSIFICATION

Basaltic rocks from island arcs are usually characterised by having plagioclase more calcic than An_{50} (Wilkinson, 1967): quartz and alkali feldspar are absent with augite as the main ferromagnesian mineral. However, because phyric basalts in this study are few and because andesites frequently have plagioclase in the bytownite-labradorite range, classification and nomenclature of volcanic rocks of the CMVA follows the scheme of Le Maitre (1989). The procedure is to make a general classification using the QAPF diagram if modal data permits, followed by chemical classification.

In general, two types of andesite are recognised in the CMVA. Pyroxene andesites usually have clinopyroxene ± orthopyroxene > 5 vol%, with clinopyroxene as the dominant pyroxene. Hornblende andesite usually has amphibole > 4 vol% with general Px_{total}/Hb ratios < 0.5. These two types may be further subdivided by the occurrence of olivine (up to 7.0 vol%). The modal contents of ferromagnesian

phases used to differentiate pyroxene andesite from hornblende andesite are only approximate, however, as these two types grade into another.

There is also a gradual modal transition to distinguish dacite from andesite. Useful criteria, although not universal, are the presence of quartz and generally coarser texture. Dacites also tend to have plagioclase "phenocrysts" with a higher degree of resorption and glassy matrices. Some samples with these characterisitics are therefore classified as dacitic although whole-rock SiO_2 contents fall slightly below 63 wt%.

3.4. GENERAL TEXTURES AND MODAL ANALYSES

CMVA lavas are aphyric or porphyritic with the latter observed in 74% of the samples. Very fine grained varieties are frequently restricted to basalts and some basaltic andesites. Most rocks exhibit an intergranular or pilotaxitic groundmass.

Total phenocryst contents (Table 3-1) vary from 15 - 64 vol%, although the majority of samples contain 40 - 50 vol% phenocrysts. A general distribution of frequent mafic phenocrysts with increasing SiO_2 is shown in Figure 3-1. These generally decrease in the SiO_2-rich compositions. There are a wide range of phenocryst sizes with the coarsest specimens occuring in the SiO_2-rich andesites and dacites of northern Camiguin Island and Mt Apo. In general, there is a weak positive correlation between SiO_2 and maximum phenocryst sizes (Fig. 3-2).

3.4.1. BASALTS

All CMVA basalt samples are grey-black massive to vesicular lava flows from Pliocene-Recent vents. Basalts have a common phase assemblage of olivine + plagioclase + clinopyroxene $\pm$ magnetite, with rare occurrence of Cr-spinel and orthopyroxene from some lavas at Butay, southern Camiguin Island.

Texturally, basic rocks are divisible into aphyric or very fine grained (< 1.0mm average crystal size; 15.0 - 25.0 vol% by occurrence), fine to medium-grained

TABLE 3-1. Modal data for CMVA lavas, arranged according to volcanic centre, north to south.
Data obtained from Appendix 2; p 264a

Rock Name	Volcanic Centre	Ol (Vol %)	Plag	Hb	Cpx	Opx	Mt	Bio	Total	Texture
1. Hb andesite	Mt Vulcan	1.1	28.5	6.8	4.3	0.1	3.5		44.2	lava dome, mg, glomeroporphyritic
2. Hb andesite	Mt Catarman	0.7	22.3	8.2	4.4	2.5	4.3	2.0	44.4	lf, fg, glomero, pilotaxitic
3. Hb andesite	Hibok-Hibok	0.1	24.7	8.4	3.2		4.0		40.4	lava dome, lf, pf and bc, fmg, glomero, pilotaxitic
4. Px andesite	Hibok-Hibok	1.1	27.0	0.1	7.0	5.0	4.5		44.7	lf, fmg, porphyritic, pilotaxitic
5. Px andesite	Mt Mambajao	1.1	26.0	2.1	5.5	4.3	2.9		41.8	lf, fmg, porphyritic, pilotaxitic
6. Dacite, Type 1	Butay		7.0		3.0		5.0		15.0	lf, mg, porphyritic. pilotaxitic
7. Basalt	Butay	5.0	32.7		7.7	1.5	6.0		52.8	lf, fmg, porphyritic, pilotaxitic
8. Px andesite	Cabuan	4.8	15.0		8.0		4.0		31.8	lf, vfg, px specks
9. Px andesite	Benoni	6.0	35.2	0.3	5.2		4.1		50.8	lf, flat ves, vfg, ol + px grains
10.Px andesite	Mt Ginsiliban		25.3		3.5	6.3	3.0		38.1	lf, aphyric
11.Ol basalt	Mt Balatocan	7.0	10.0		10.0		1.0		28.0	lf, fg, equigranular
12. Basalt	Mt Balatocan	1.0	25.0		3.0		2.0		31.0	lf, mcg, ophitic, porphyritic, glassy gm
13. Basalt	Mt Balatocan	1.0	29.0		8.0		2.0		40.0	lf, fmg, porphyritic, holox gm
14. Px andesite	Mt Balatocan	0.0	8.0		2.0	1.0	4.0		15.0	lf, fmg, porphyritic, pilotaxitic
15. Basalt	Mt Kalatungam	6.0	38.0		3.7		2.0		49.7	lava bomb, mg, porphyritic, cryptoxtalline gm
16. Dacite, Type 1	Mt Katanglad	0.1	8.3		4.8		3.0		16.2	lf, fg, porphyritic, pilotaxitic
17. Basalt	Butong	7.0	38.0		4.0		0.1		49.1	lava dome, fmg, porphyritic
18. Hb andesite	Musuan		15.0	8.0	8.0	1.7	4.0		36.7	lf, fmg, porphyritic
19. Bas px andesite	Quezon	3.2	19.8		7.0		3.6		33.6	lf, fmg, porphyritic, pilotaxitic
20. Px andesite	Mt Apo	2.4	19.7		7.6		3.1		32.8	lf, fmg, porphyritic, glassy gm
21. Px andesite	Mt Apo	2.0	15.0		3.0		4.0		24.0	pf, mcg, glomerophyric, pilotaxitic
22. Hb andesite	Mt Apo		28.9	7.6	3.2		6.4	2.5	48.6	lf, fmg, porphyritic, intergranular
23. Dacite, Type 2	Mt Apo		40.0	12.2	4.0		2.0	5.8	64.0	lf, mcg, glomeroporphyritic, pilotaxitic

Mineral and rock names are abbreviated as: Ol, olivine; Plag, plagioclase; Hb, hornblende; Cpx, clinopyroxene Opx, orthopyroxene, Mt, titanomagnetite; Bio, biotite. Textures coded as vfg, very fine grained; fg, fine-grained; fmg, fine to medium grained; mcg, medium to coarse grained. First column under texture gives rock type, i.e., lf, lava flow; pf, pyroclastic flow deposit.

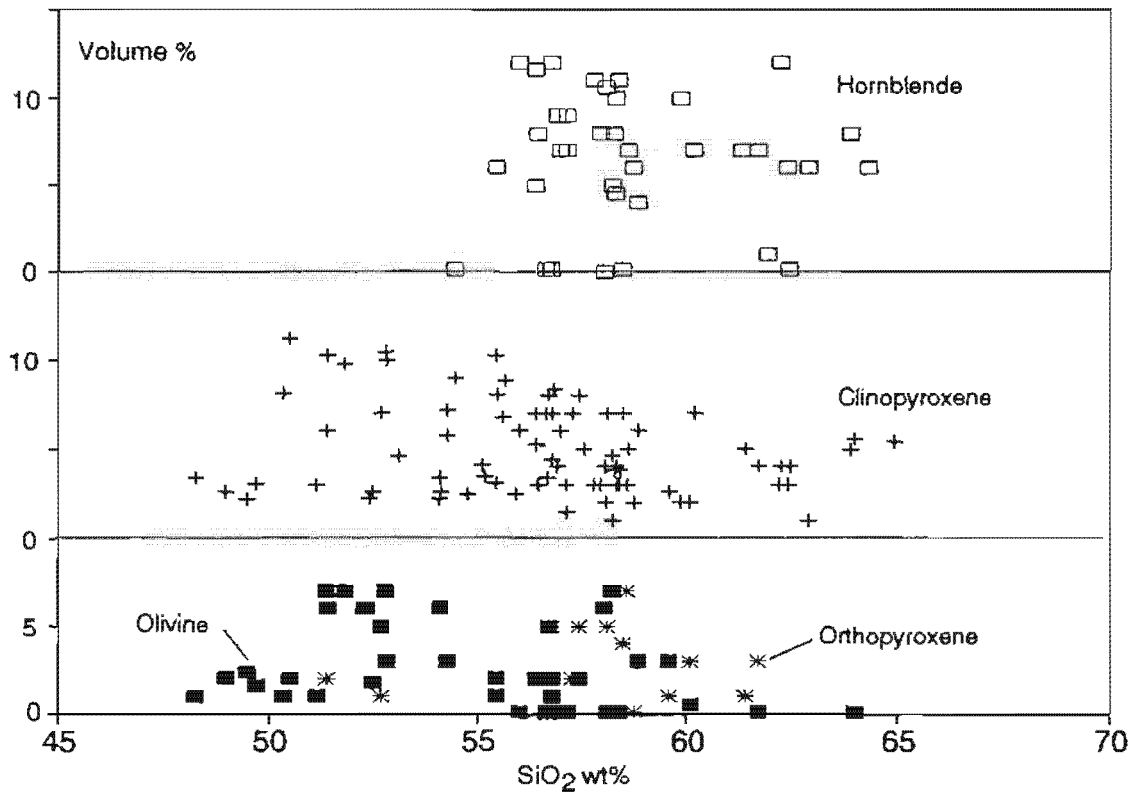

Figure 3-1. General distribution of common mafic phenocrysts.

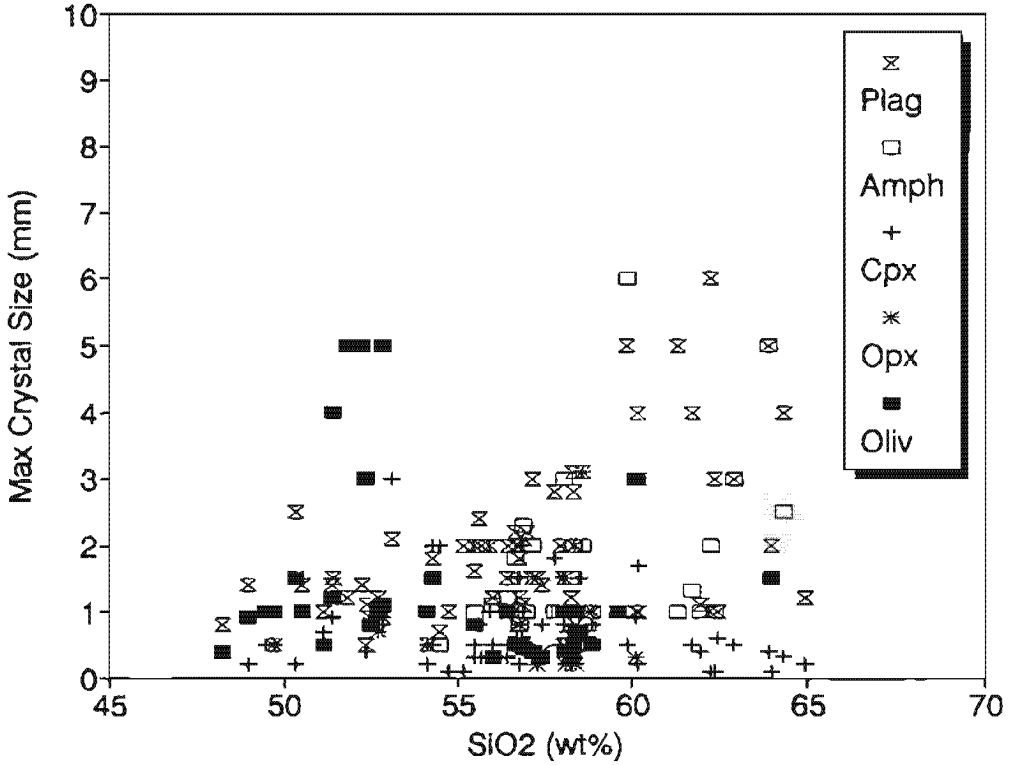

Figure 3-2. Maximum crystal size for most common phenocrysts vs SiO2 content. Plotted are modal data from Appendix 2.

(1.0 - 5.0mm; 41.7 vol%) and medium or sometimes coarse grained varieties (>5.0mm; 33.3 vol%). The fine grained basalts typically contain ≤ 0.5mm grains of olivine (5 vol%), clinopyroxene (~15%) interspersed in microlitic plagioclase (Fig. 3-3a). In contrast, fine to medium grained variants contain plagioclase (2-3mm long) and subophitic clinopyroxene (Fig. 3-3b). Groundmass textures vary due to dominance of acicular to tabular plagioclase and grade from intergranular to intersertal. In the medium and sometimes coarse grained basic rocks (Fig. 3-3c), calcic plagioclase occurs as euhedral glomerocrysts (up to 6mm long) and sometimes as inclusions in 6 - 7mm dia clinopyroxene and olivine. The groundmass often comprises microlitic plagioclase with little glassy matrix.

As expected, the incidence of mafic minerals is most frequent in basalts which have high modal olivine (7 vol%) and clinopyroxenee (15 vol%) and absence of amphibole and mica. Olivine occurs both as phenocrysts and in the groundmass, a feature not observed in acid andesites and dacites. Groundmass olivine forms 0.2 - 0.5mm granules but in relatively magnesian basalts (e.g. sample BAL4), olivine occurs as large phenocrysts (3 - 5mm) with clinopyroxene as an intergranular phase. Most olivines are altered along their edges, and in phyric varieties, are rimmed by small grains of clinopyroxene and magnetite. Olivine phenocrysts may be enclosed by clinopyroxene but generally do not have reaction rims.

Clinopyroxene occurs as small pale-green to colourless phenocrysts or granules in the groundmass. The ubiquity of clinopyroxene and lack of disequilibrium features in phenocrysts suggest a wide stability range similar to that of plagioclase. In contrast, orthopyroxene is scarce. Its corroded appearance suggest this mineral to be a relict or xenocrystic phase.

Plagioclase is always the most abundant phase. Average crystal sizes are 2 - 3mm for phenocrysts, 0.3 - 0.8mm for microphenocrysts and < 0.3mm for microlites. Zoning is very frequent and consists of various combinations of normal, reverse, continuous and oscillatory. However, plagioclase in the labradorite-

Figure 3-3. Microphotographs of basaltic rocks. Examples of fine-grained (a) and fine-medium grained lavas (b) from southern Camiguin Island. (c) Medium-coarse grained basalt from Mt Balatocan. Minerals identified as: Ol, olivine; Pl, plagioclase and Cp, clinopyroxene. Other phases (where appropriate) are: Op, orthopyroxene; Mt, magnetite; and Hb, hornblende. Crossed polars.

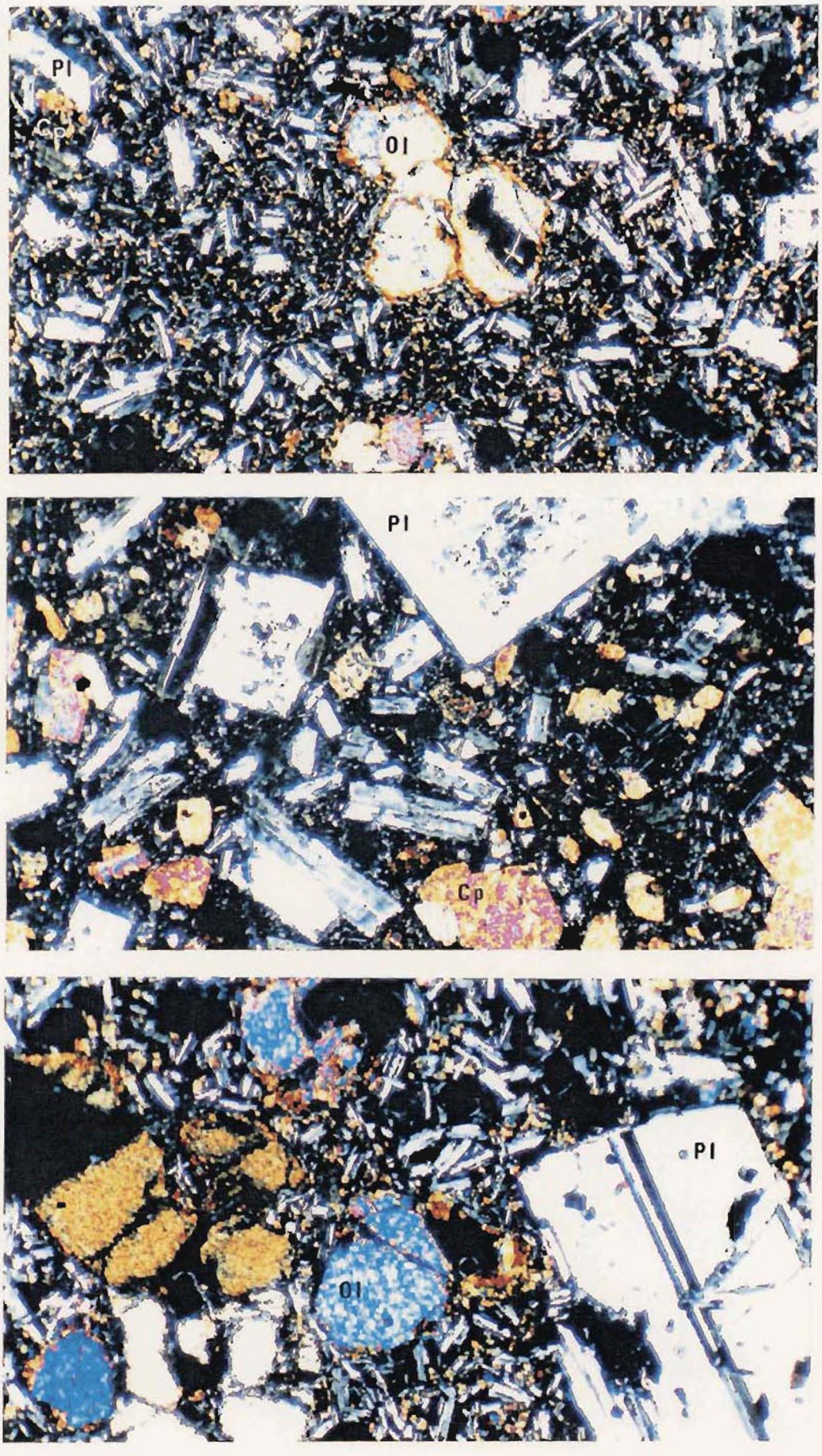
Pl
Cp
Ol
Pl
Cp
Pl
Ol
0 1 2 3 mm

bytownite range tend to have less complex zoning and exhibit euhedral outlines compared with more sodic plagioclase.

Melt inclusions also distinguish calcic from sodic plagioclase in basalts. Glassy inclusions in calcic plagioclase are generally uniformly distributed within each crystal. In andesites and dacites, plagioclase is often zoned within the core or forms thin discrete bands. Some melt inclusions in calcic plagioclase have angular cavities which suggest non-resorption or reaction between entrapped melt and crystal. This feature suggests calcic plagioclase to be in equilibrium with the host liquid (Watson, 1976). Most other inclusions are probably secondary in origin (Roedder, 1984) because they form at the end of fractures which extend to the rim of the mineral.

3.4.2. ANDESITES

Intermediate lavas are found in each major volcanic centre in CMVA. Their wide distribution and frequent occurrence suggest andesite is the main lava type. In general, basaltic andesites have similar mineralogy to basalts with plagioclase and clinopyroxene the most abundant. A mineral common to both lava types is olivine, which persists throughout the andesite range, although this mineral rarely occurs above 1.0 vol% in SiO_2-rich hornblende andesites. The main petrographic difference between basic and intermediate rocks is the appearance of amphibole, and in limited cases, occurrence of orthopyroxene and sometimes quartz.

Of the two types of andesite, pyroxene andesite is commonly associated with basalt whereas hornblende andesite grades into dacite. The gradual transition between these andesites is evident in many suites. For example, andesites of eastern Mt Mambajao are chiefly two-pyroxene andesites with amphibole becoming more important in late Pleistocene flows to the north (e.g. Kampana Hill). Similarly, prehistoric Mt Catarman lavas are mostly pyroxene andesites with amphibole a conspicuous phase in Recent late-stage domes (Hibok-Hibok). Pyroxene and hornblende andesite are often phenocryst-rich (65 vol% average), vesicular grey

lavas. These rocks are highly glomerophyric, fine to coarse-grained with intergranular to pilotaxitic groundmass.

Pyroxene andesites are typified by plagioclase (7 - 43 vol%), olivine (up to 6 vol%) and clinopyroxene (up to 8 vol%) set in a glassy matrix of plagioclase microlites and augite granules (Fig. 3-4a). Occasionally, intergranular to subophitic groundmasses are observed with increasing phenocryst content.

Plagioclase is commonly euhedral in basaltic andesites but calcic plagioclase in silicic andesites are frequently corroded (Fig. 3-4b). The modal occurrence of plagioclase is usually high and can account for 88% of total phenocrysts. As in basalts, plagioclase distribution in phenocryst-rich andesites is polymodal and can be classified into 3 size subpopulations: phenocrysts (> 0.5mm), microphenocrysts (0.1- 0.5mm), and groundmass plagioclase (< 0.1mm). Large plagioclases (> 2.0mm) are conspicuous because of their highly resorbed and sometimes embayed margins and complex zoning. These disequilibrium features are observed in both types of andesite but are predominant in the more SiO_2-rich hornblende andesite which are common in Hibok-Hibok and Mt Apo. Frequently, phenocrysts are mantled by clear "equilibrium" plagioclase with compositions (An_{37-15}) similar to groundmass feldspars. The latter plagioclase are either weakly zoned or unzoned.

In pyroxene andesites, clinopyroxene is the dominant pyroxene (except in Mt. Ginsiliban, southern Camiguin Island) and occurs extensively as augite phenocrysts and granules. Nearly colorless orthopyroxene may coexist as phenocrysts but usually appear as a microphenocryst (Fig. 3-4c) or as small granules surrounding olivine.

The amphiboles present are the reddish-brown variety oxyhornblende, or in less oxidised samples, appear as strongly pleochroic dark olive-brown crystals which occur as poorly terminated columnar-tabular phenocrysts (Fig. 3-4d). The amphiboles are mostly rimmed by opaque phases or by aggregates of fine grained

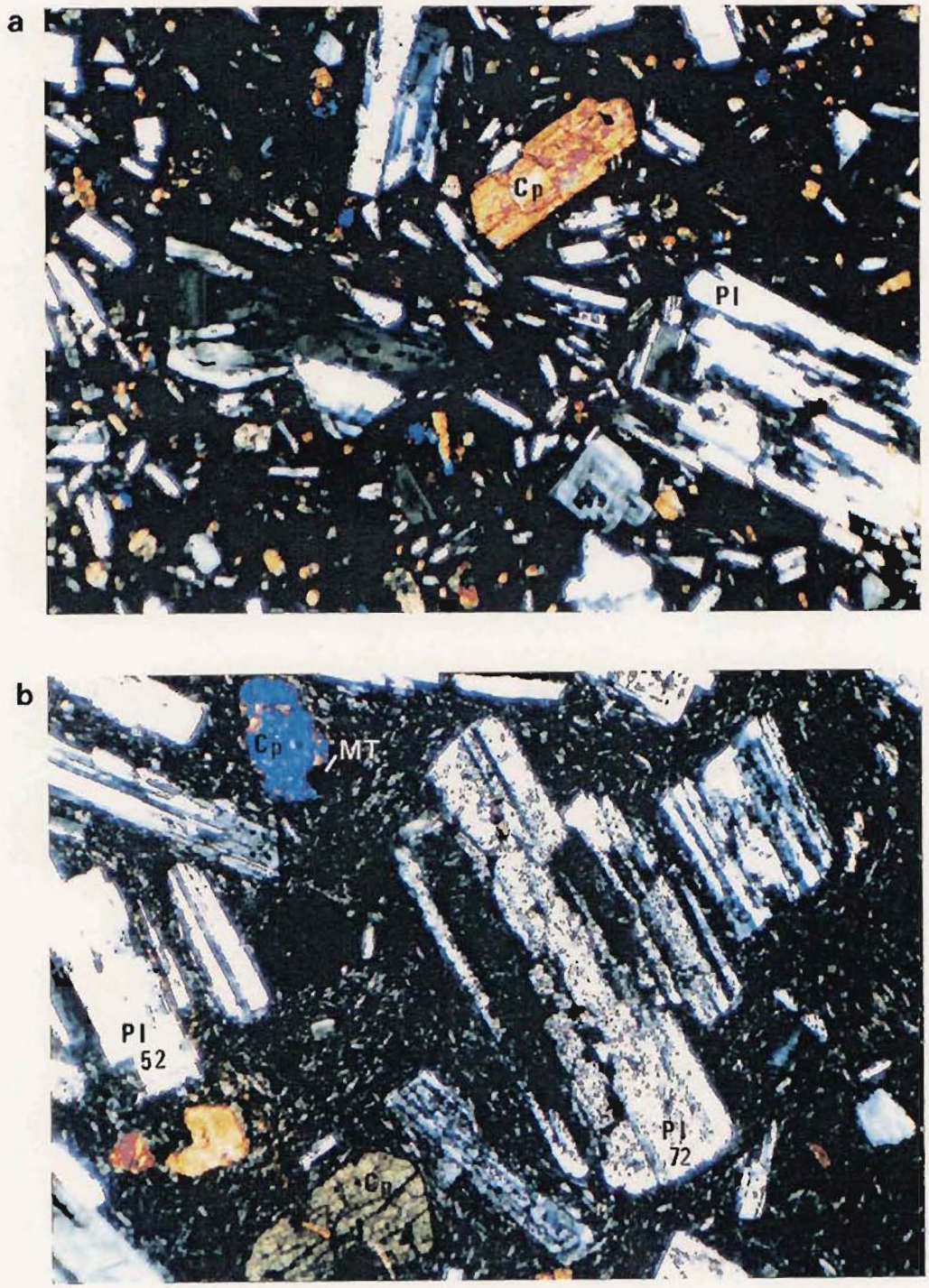

Figure 3-4. Microphotographs of representative basaltic andesites. (a) Fine-grained pyroxene (augite, above centre) andesite from Mt Mambajao. (b) Fine to medium-grained andesite from Mt Apo showing calcic plagioclase phenocryst (An72), andesine micro-phenocryst (An52), augite and Ti-magnetite. Magnification in both views is 10x. Crossed polars.

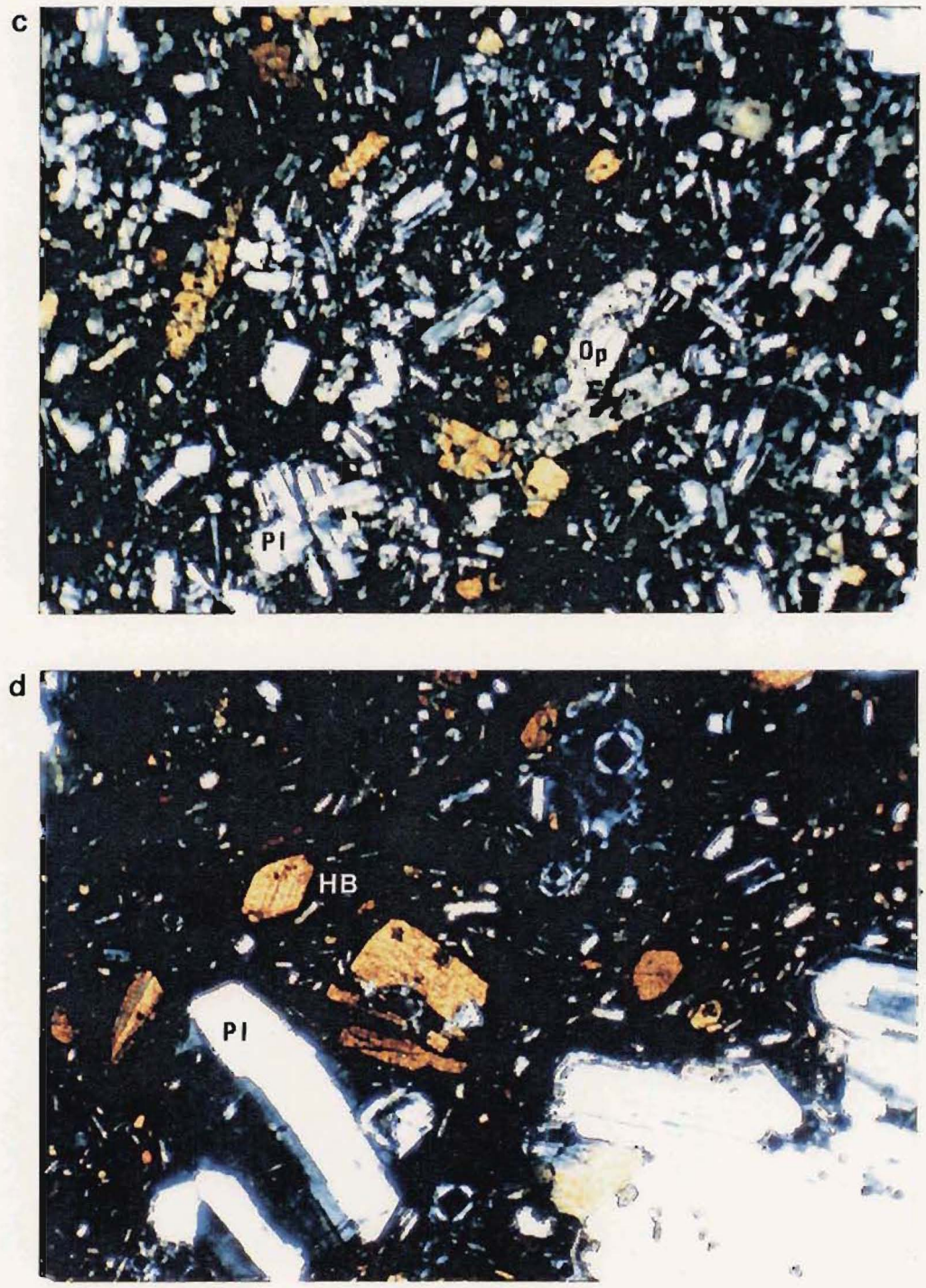

Figure 3-4. continued. (c) Fine-grained 2-pyroxene andesite from Mt Ginsiliban, Camiguin Island. (d) Typical hornblende andesite from Hibok-Hibok, Camiguin Island. Magnification in both views is 10x. Crossed polars.

plagioclase, clinopyroxene and magnetite. Minute inclusions of plagioclase and clinopyroxene are common within the core. Modal hornblende varies between 5 - 10 vol%; the mineral occurring significantly only in the andesites of Hibok-Hibok, Mt Vulcan, northern Mt Mambajao, Musuan and Mt Apo. Hornblende occurs in subordinate amounts in pyroxene andesites of Mt Catarman, eastern Mt Mambajao and Mt Balatocan. Rarely, resorbed hornblendes, extensively pseudomorphed by opacite, are found in basalts of Cabuan but their absence in Mt Ginsiliban illustrates the antipathetic relationship between amphibole and orthopyroxene.

3.4.3. DACITES

Rocks of this group are mainly found as late-stage pyroclastic flows and domes in Camiguin Island, Mt Katanglad and Mt Apo. Dacites are typically porphyritic and pilotaxitic but exhibit a wide range of textures and mineral assemblages which differ from site to site. Petrographically, two types of dacite are recognized. Type 1 dacite lavas (erupted from Mt Katanglad and southern Camiguin Island) are fine grained and have relatively low phenocryst contents (Fig. 3-5a). Type 2 dacite is the more widely occurring type and is distinguished by having hornblende as the main mafic constituent (Fig. 3-5b). The first type has an anhydrous assemblage of plagioclase, clinopyroxene, magnetite and rare resorbed olivine. The plagioclase occurs as sporadic microphenocrysts (8.3 vol%), usually < 0.3mm and zoned with a resorbed core and an euhedral mantle. An intermediate concentric dusty zone frequently occurs between the core and mantle. The rest of the plagioclase are dispersed in the groundmass and are pilotaxitic. The clinopyroxene in Type 1 dacites is either subhedral microphenocryts (4.8 vol%) or occurs as granules in the matrix. Unlike the plagioclases, most clinopyroxenes have clear interiors and do not exhibit reaction rims. Trace amounts of amphibole may occur but these are always extensively replaced by an opaque mineral.

Type 2 dacites are highly porphyritic and have the coarsest components, with plagioclase and amphibole glomerocrysts up to 8mm long in hand specimens.

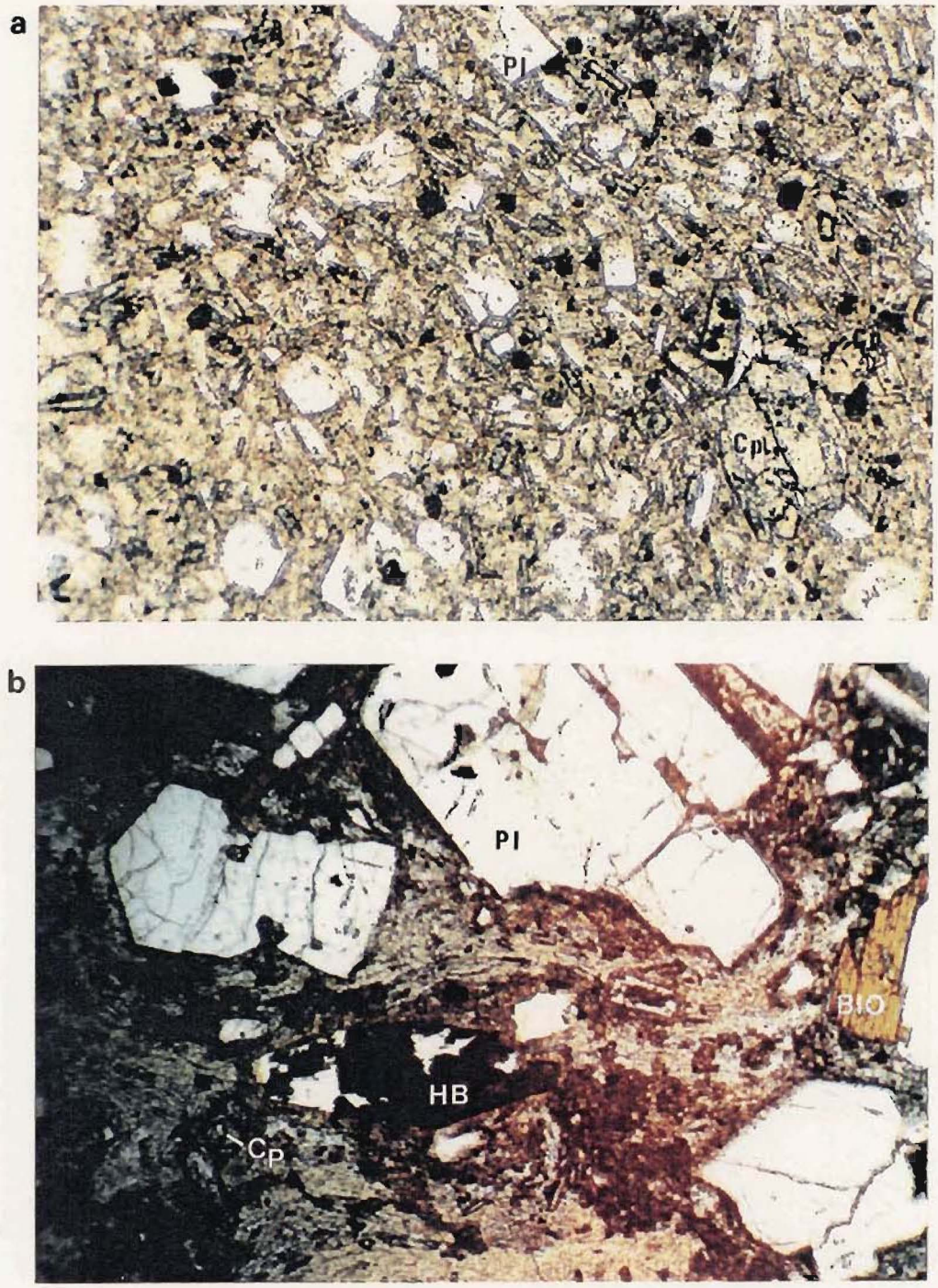

Figure 3-5. (a) Microphotographs of representative Type 1 dacite from Mt Katanglad showing plagioclase (An46-50) and augite granules in hypocrystalline matrix containing microlitic feldspar (An31). (b) Type 2 dacite from Mt Apo composed of andesine phenocrysts (An39-41), euhedral magnesiohornblende, biotite and intergranular diopside in glassy, pilotaxitic groundmass. Magnification in both views is 10x. Uncrossed polars.

Plagioclase phenocrysts exhibit complex zoning, tiny inclusions of magnetite and sometimes, fritted textures, in contrast to clear microphenocrysts. Groundmass plagioclase are often flow-aligned near the rims of phenocrysts but crystal-rich dacites usually result in intergranular groundmasses. Hornblende phenocrysts, commonly rimmed by opacite in andesite and wholly resorbed in Type 1 dacite, appear clear and euhedral in Type 2 dacite. These may enclose minute plagioclase laths. Augite is a significant phase in dacite while orthopyroxene is absent as a phenocryst and is found only as a mantle on some quartz granules. The latter generally occurs as a xenocryst in basic rocks in Camiguin Island or as a secondary interstitial mineral.

3.5. PETROGRAPHY OF CRYSTAL CLOTS AND LITHIC INCLUSIONS

Many andesites and some dacites from CMVA contain crystal aggregates which are texturally distinct from phenocryst assemblages. Such aggregates range from minute specks of mono-mineralic clusters to heterogenous meter-sized lava blocks and bombs. More often, crystalline aggregates occur as medium-grained enclaves < 5cm in dia and are best described as crystal clots or lithic inclusions. Four types of xenolith can be recognised:

(i) Medium to coarse grained clusters of subhedral plagioclase, clinopyroxene and magnetite (Fig. 3-6aCAB55). Plagioclase has a similar composition to phenocrystic plagioclase;

(ii) Relict phases (e.g., plagioclase and/or hornblende) extensively pseudomorphed by clinopyroxene + plagioclase (Fig. 3-6b). The plagioclase is generally more calcic than plagioclase phenocrysts;

(iii) Resorbed olivine (Fig. 3-6c). With more advanced resorption, olivine becomes extensively replaced by plagioclase + clinopyroxene + orthopyroxene. Opaque oxides increase in abundance, occurring in the core and rim. With complete replacement, only a pseudomorph remains and,

(iv) An aggregate of calcic plagioclase and amphibole forming a nearly holocrystalline open framework (Fig. 3-7a). The plagioclase is normally zoned and similar to bytownites in basalts and usually more calcic than phenocrystic plagioclase. Amphiboles lack opacite rims (Fig. 3-7b) commonly found in andesite domes and flows. In other inclusions, the crystal assemblage is similar, chemically and morphologically to the enclosing assemblage (Fig. 3-7c).

Figure 3-6. Microphotographs of crystal xenoliths. (a) Example of plagioclase-pyroxene cluster in basaltic pyroxene andesite from Cabuan volcanic centre, Camiguin Island. (b) Hornblende core replaced by plagioclase-augite-magnetite in pyroxene andesite, Mt Apo. (c) Resorbed olivine (Fo_{80}) in Type 1 dacite, Mt Katanglad.

a

b

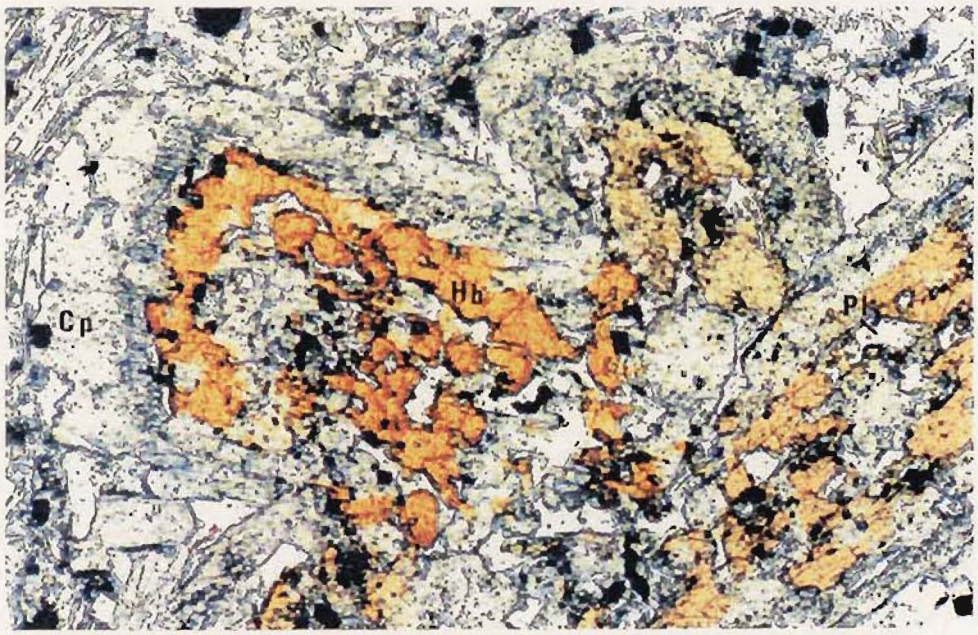

c

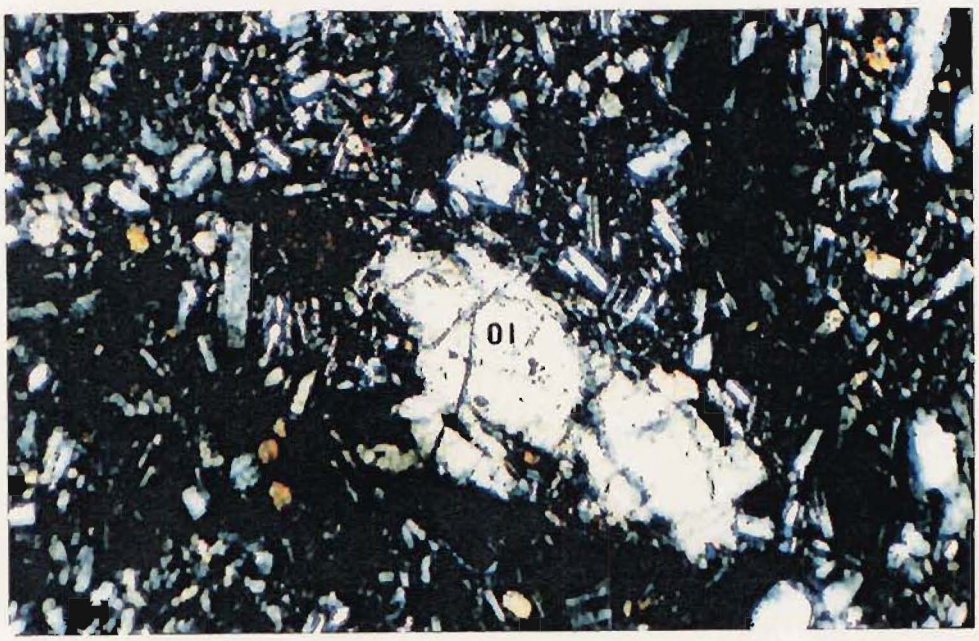

Type (i) xenoliths could be a relict of deep-seated processes, i.e., refractory phases brought from the zone of partial melting (Flood et al, 1977) or cumulate material disrupted and entrained during eruption (Arculus and Wills, 1980). The granular assemblage of plagioclase + clinopyroxene could represent cognate crystals which have nucleated on the walls of a shallow subvolcanic magma chamber and entrained during eruption. This is generally supported by the composition of plagioclase which is within the range of observed phenocryst compositions.

Reaction of early-formed crystals with the host magma could result in Type (ii) xenocrysts. Resorbed amphibole presumably crystallised at a higher P-T environment from phenocrystic amphibole which usually appear to have formed relatively late in andesite. Stewart (1975) suggested that rapid ascent from shallow reservoirs may result in breakdown of amphiboles into an anhedral assemblage of plagioclase + clinopyroxene + magnetite due to decreasing fH_2O in the magma chamber. In this study, however, not all amphiboles which exhibit extensive breakdown and replacement textures produce the medium-coarse grained fabrics observed in Type (i) xenoliths. More likely, oxidation and dehydrogenation occurs during extrusion (Garcia and Jacobson, 1979) forming opacite rims on amphiboles.

In Type (iii) xenoliths, an assimilation reaction is implied. If crystalline material which formed early in the reaction series is added to a more evolved melt, the magma will react with the more refractory phases by dissolving the included crystals while concurrently crystallising the liquidus phases. An included crystal may be prevented from further reaction with the surrounding melt by mantling of liquidus phases (Dowty, 1980). Some glomerophyric clusters of plagioclase + clinopyroxene + magnetite (Fig. 3-6a) were proposed by Conrad and Kay (198) to represent extended crystallisation of liquidus phases due to inclusion of early-formed crystals. Some magnesian olivine grains in acid andesite and dacite have simple

Figure 3-7. Microphotographs of inclusions. (a) Crystal-rich inclusion of calcic plagioclase (An_{85}) and bladed amphibole (basaltic composition, sample HIB37). (b) Section across inclusion (left half) and host rock. Included rock is unoxidised with calcic plagioclase (An_{73} vs. An_{62}) and Mg-rich amphibole. (c) Hornblende and andesite inclusion (left half). Compositions of included feldspar and hornblende are similar to host rock. Magnification in all views is 10x. Crossed polars.

a

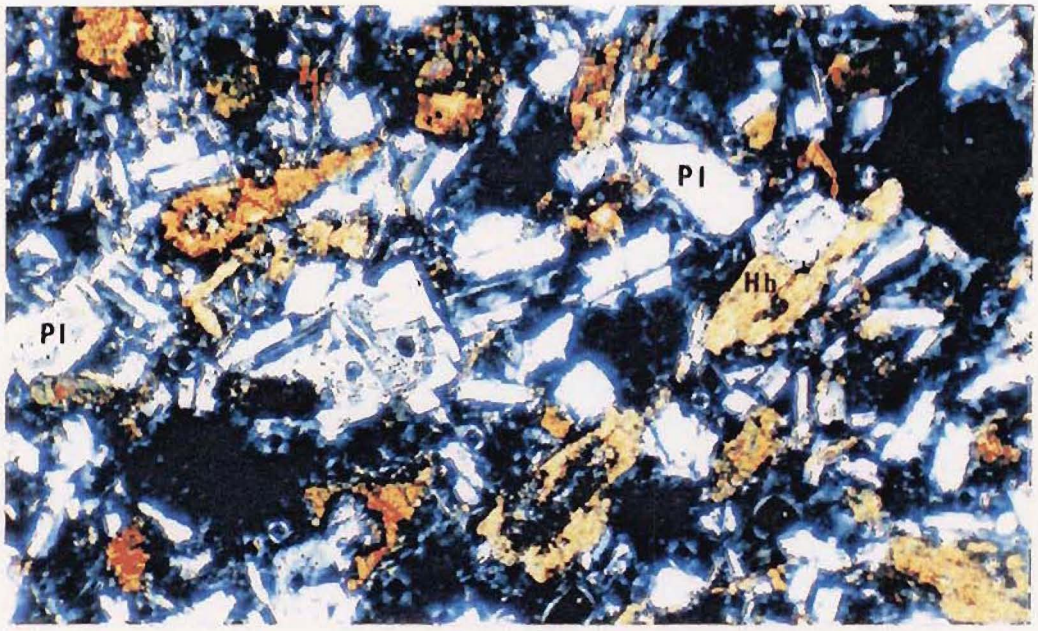

b

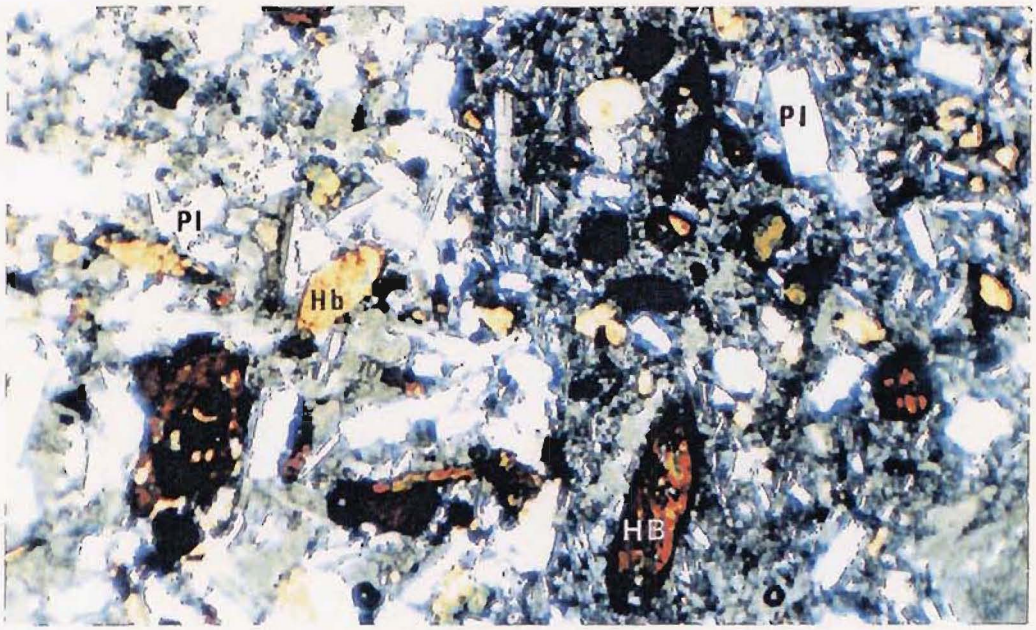

c

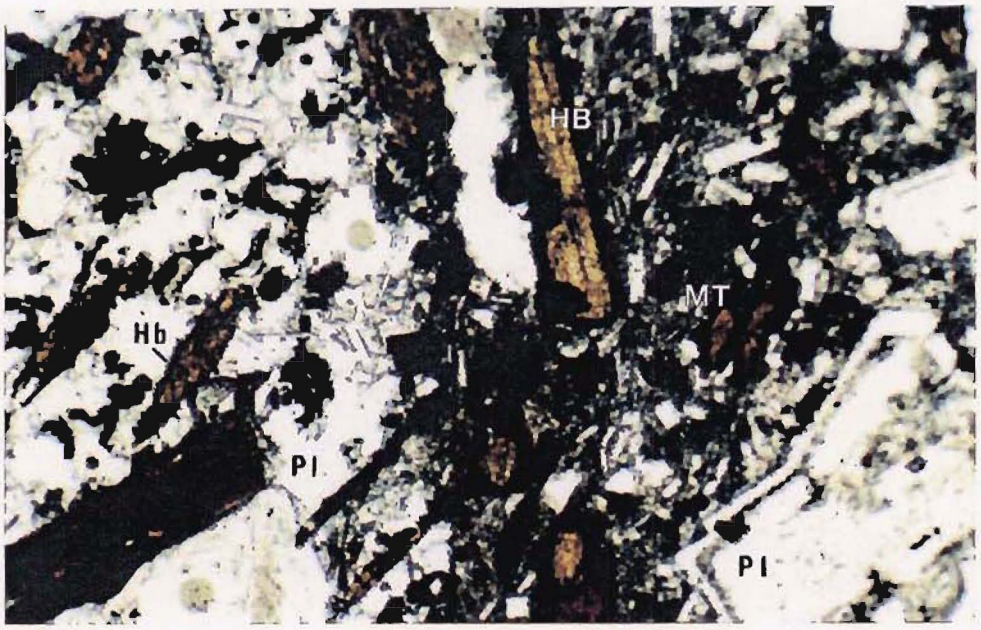

orthopyroxene rims. Such minerals are probably cognate and persisted in relatively SiO_2-rich liquids because of pyroxene mantling.

The lack of opacite mantles on some amphiboles which form an aggregate together with plagioclase (Type (iv) xenoliths) is strong evidence that these inclusions originate at depth probably from the walls of magma chambers (*in situ* crystallisation). These inclusions contrast sharply from the surrounding glassy, porphyritic lava. The interface between the two rock types is sharp and there is no pronounced reaction (Fig. 3-6b) or mixing textures (i.e., banding). This suggests a simple mechanical inclusion during eruption.

3.6. CHEMISTRY OF PHENOCRYST ASSEMBLAGES

3.6.1. FELDSPAR

Plagioclase is the only feldspar in the lavas from CMVA except for occasional sanidine crystals found in pyroclastic flows of Camiguin Island. Plagioclase compositions vary between An_{31-84} and become more Na-rich with increasing SiO_2 wt% (Fig. 3-8a). Some Fe and Mg occurs in the plagioclases (Fig. 3-8b). Both elements generally decrease with lower An contents, in agreement with general relations concluded by Ribbe and Smith (1966). This trend probably reflects adjustment of feldspar to lower temperatures or because of direct crystallisation at lower temperatures which results in lower Fe content (Sen, 1960; Corlett and Ribbe, 1967). All plagioclase have low Or (Fig. 3-9) although normative feldspathic components of many host rocks plot within the 2-feldspar field. K is therefore concentrated in the groundmass, relatively enriched in some microlites or taken up by mica in SiO_2-rich lavas.

Interestingly, the most An-rich plagioclases do not occur in basalt (labradorite to bytownite, An_{50-78}) but are found in basaltic andesites and SiO_2-rich andesites (bytownite, An_{78-84}). The highest An component was analysed from a normally-zoned plagioclase (anal# N31M4 and N31R47, Table A3-1c, Appendix 3-2; bulk rock

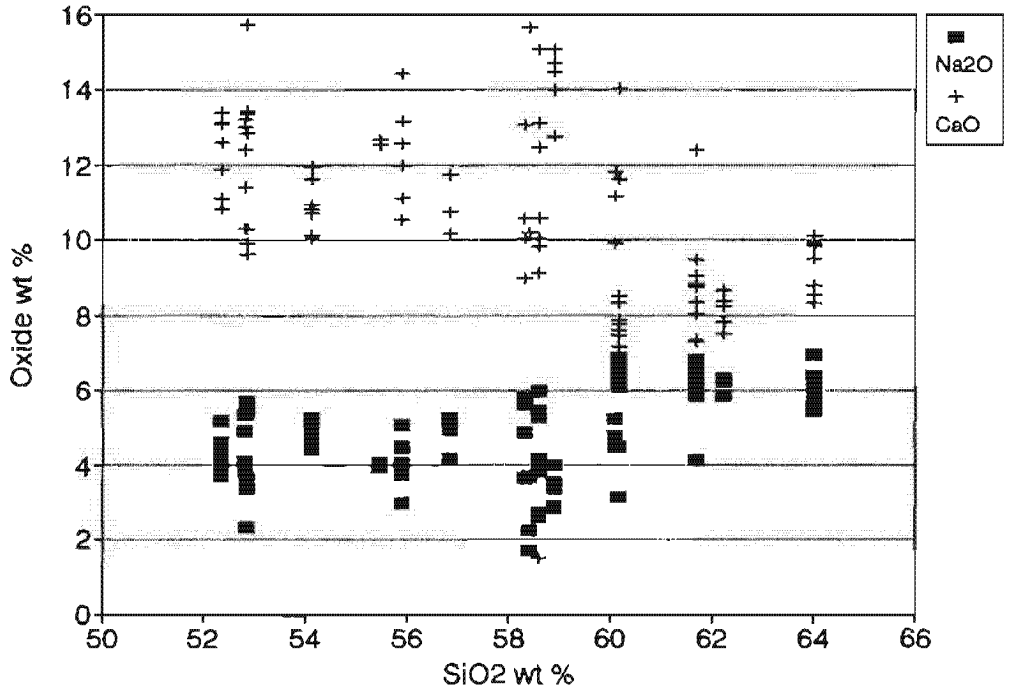

Figure 3-8a. Variation of Na2O and CaO with SiO2 in CMVA plagioclases.

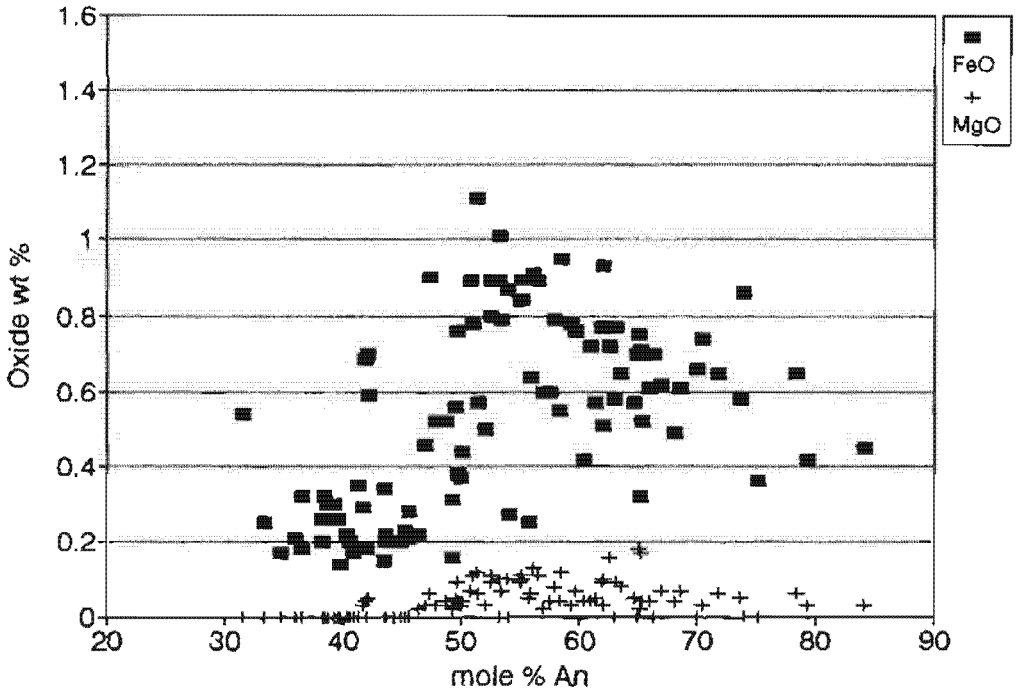

Figure 3-8b. Variation of FeO and MgO with An in CMVA plagioclases.

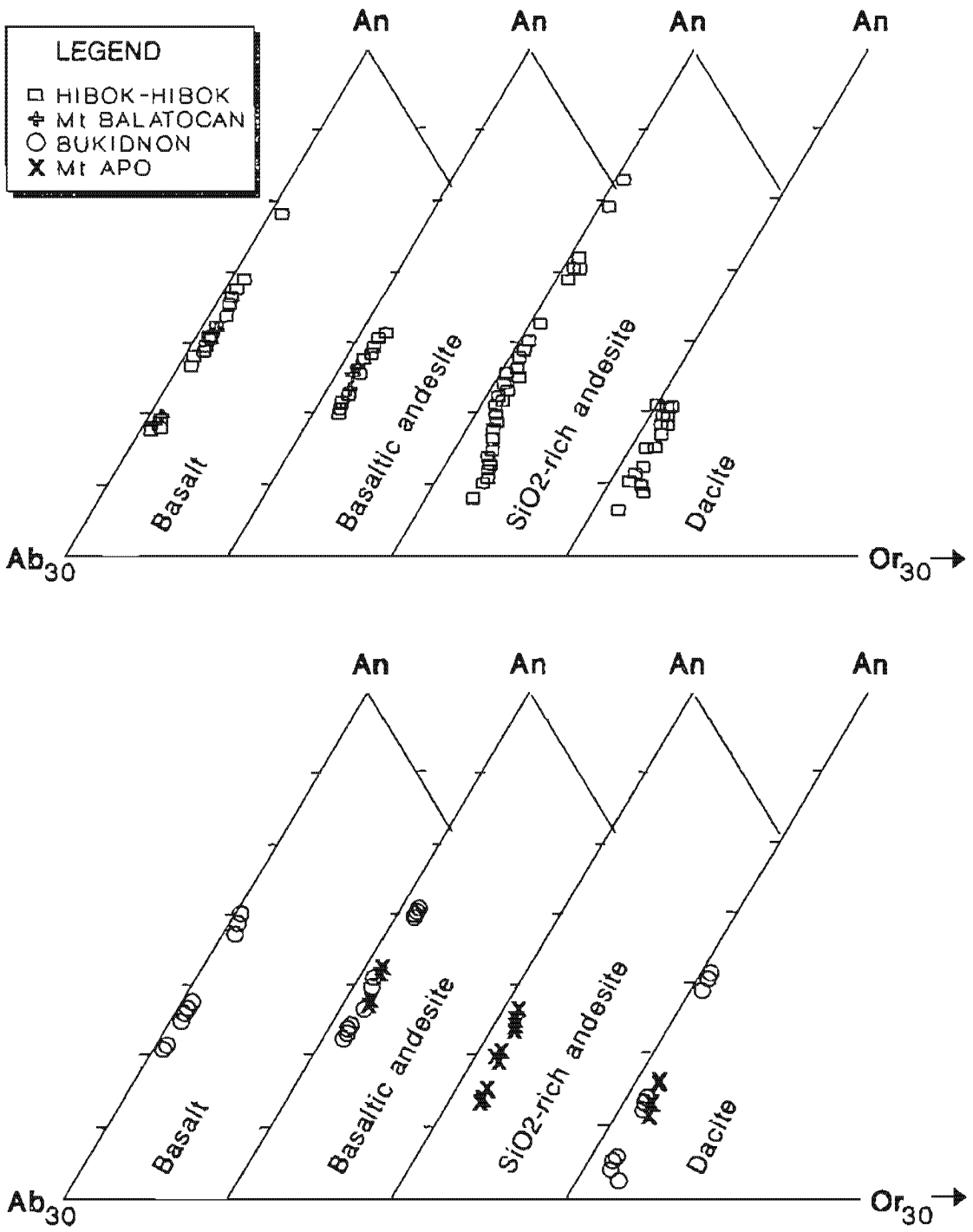

Figure 3-9. Ab-An-Or ternary diagram showing plagioclase compositions for representative rocks of the CMVA. Samples plotted are compositions from combined analyses listed in Appendix 3-2, Tables A3-1a to A3-1d.

sample BEN31, analysis 42, Appendix 4-2). This crystal may have formed early in the cooling history of Benoni magmas, and later entrained by more evolved liquids. The plagioclase in dacites consistently plot within the andesine range (An_{31-50}).

There are 2 main types of plagioclase; (i) euhedral and (ii) anhedral:

(i) Euhedral plagioclase generally have clear cores and rims (Fig. 3-10a). These generally exhibit normal zoning or slight variations in An content and have outer margins which are similar to groundmass feldspars. Euhedral plagioclase also display resorbed cores and clear rims (Fig. 3-10b) but are usually normally zoned. These resorption features are generally absent in basalts and dacites.

(ii) Anhedral plagioclase is common in some basaltic andesites and SiO_2-rich andesites. The core may be either clear (Fig. 3-10c) or show varying degrees of dissolution. The zoning in anhedral or rounded plagioclases vary considerably but the incidence of reversely zoned crystals are greater than in euhedral plagioclases.

Euhedral plagioclase with either clear, homogenous interiors or normal zoning suggest these crystals are phenocrysts. In basaltic andesites and dacites, clear plagioclase in the intermediate size range (0.3 - 0.8mm, 1- 3mm) also exhibit the least variation in core to rim compositions. The restricted sizes of clear plagioclase in these rocks could result from a discrete episode of near-equilibrium crystallisation at constant growth rates and little undercooling. Deviation from near-equilibrium crystallisation is often attributed to increased degrees of undercooling. In experiments by Lofgren (1972) and Smith and Lofgren (1979), rapidly undercooled samples exhibit reversely zoned crystals with rims containing abundant glass inclusions. Such a mechanism appears to be viable for reverse zoning in some plagioclases of CMVA lavas, where other crystals are co-precipitating, since crystallisation of another component in the melt could increase the cooling interval (Hort and Spohn, 1991).

If undercooling is a significant process involved in plagioclase crystallisation, some driving force is required to maintain this cooling interval since depletion of the melt in the crystallising component drives the residual melt composition path back to the liquidus which therefore reduces the undercooling. Decrease in water, perhaps by eruption, will promote cooling and increase plagioclase crystallisation (Swanson, 1977; Huppert and Worster, 1985).

Figure 3-10. Microphotographs of (a) euhedral plagioclase (An_{39-43}) phenocryst in Type 2 dacite, Mt Apo and (b) rounded calcic plagioclase (An_{62}) in SiO_2-rich andesite, Camiguin Island. The average plagioclase composition in this sample is An_{46}. (c) Resorbed cores in subhedral plagioclase (An_{51} rim, similar to clear plagioclase microphenocryst at left).

a

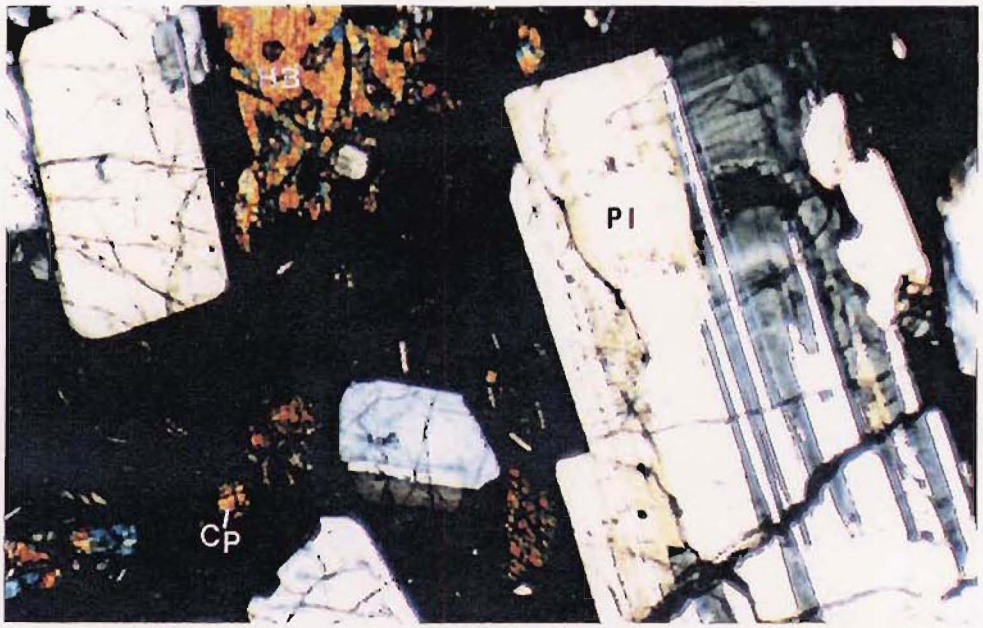

b

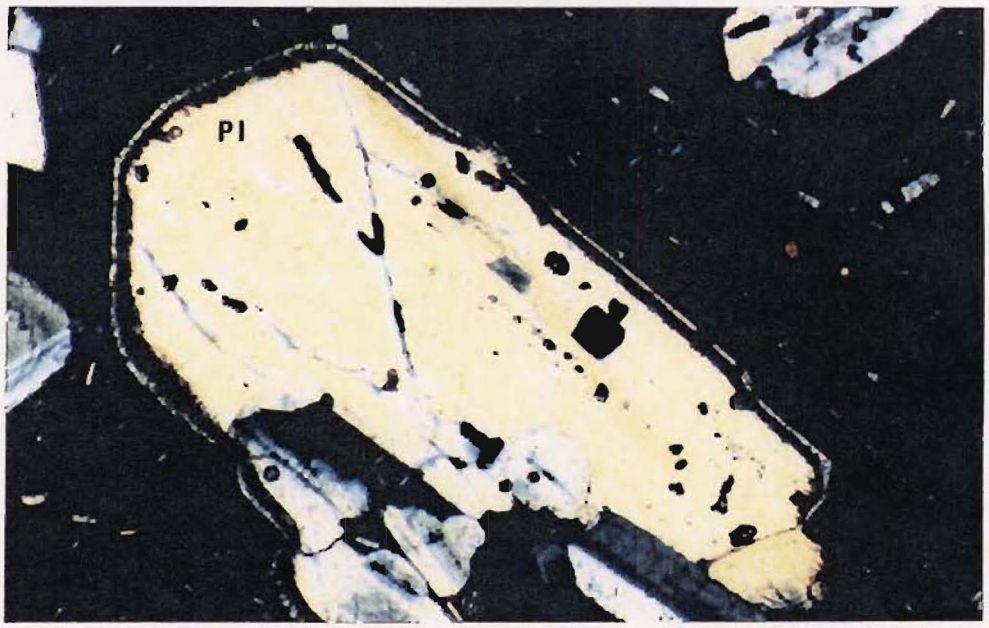

c

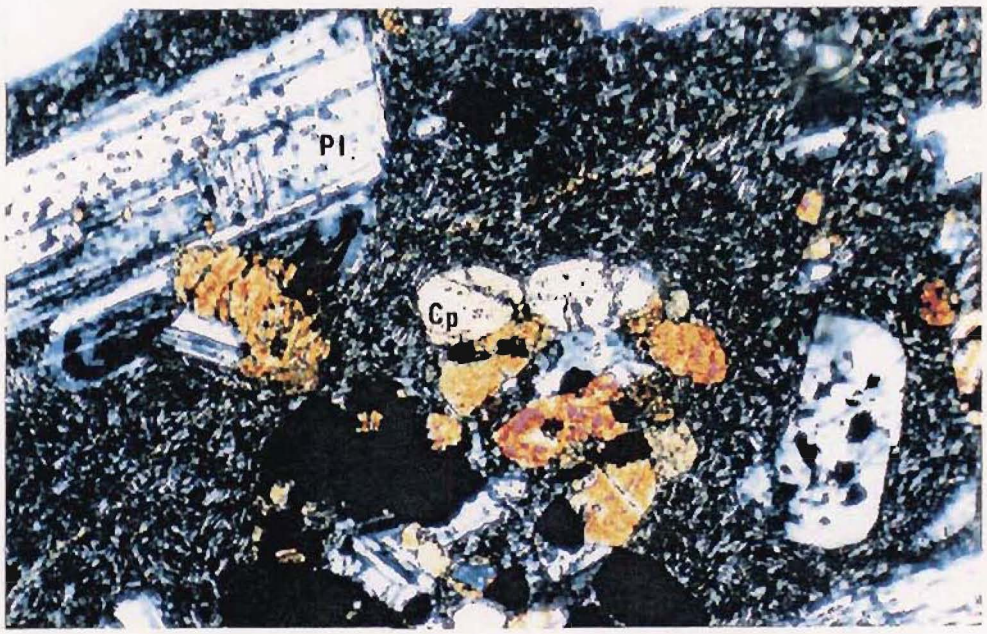

Anhedral plagioclase, which abound in the SiO_2-rich andesites, can be explained by dissolution of early formed crystals or by reaction of melt with entrained plagioclase xenocrysts. Clear crystals with resorbed rims and weakly zoned interiors have been experimentally produced by Tsuchiyama (1985) and resulted from simple dissolution of plagioclase when run temperatures exceeded the plagioclase liquidus. Whether dissolution or overgrowth textures occur depends on relative compositions of melt and crystal. Crystal-melt reactions involving solid solutions have been discussed by Lofgren and Norris (1981), Kuo and Kirkpatrick (1982) and Tsuchiyama (1985). During assimilation of plagioclase xenocrysts, plagioclase more sodic than that in equilibrium with the melt will be resorbed producing rounded (anhedral) margins. However, relatively calcic plagioclase will be little affected and an overgrowth of sodic feldspar will form. Similar resorption textures can result from mixing of magmas with differing compositions as explained by Kuo and Kirkpatrick (1982).

Mixing and assimilation can also produce inclusion-rich concentric intermediate zones in andesites and dacites. Randomly oriented crystals show that these dusty zones are three-dimensional networks of plagioclase and melt often surrounding a clear and rounded core. The An-content of these dusty zones is slightly higher (~5 mol%) than the cores. These are attributed by Bentor (1951) and MacDonald and Katsura (1965) to incomplete resorption of earlier crystals (core) which break down into a more calcic feldspar and glass.

The compositions of groundmass feldspars overlap with those of microphenocrysts although the most calcic microlites are consistently more sodic than the most calcic phenocrysts. Nearly all plagioclase except microlites have optically distinct Na-rich outer rims (5 - 50 μm) which suggest rapid post-eruption cooling.

3.6.2. Olivine

Magnesium-rich olivines occur mainly in basalts and basaltic andesites and trace amounts are found in some SiO_2-rich andesites and dacites (Fig. 3-11). The

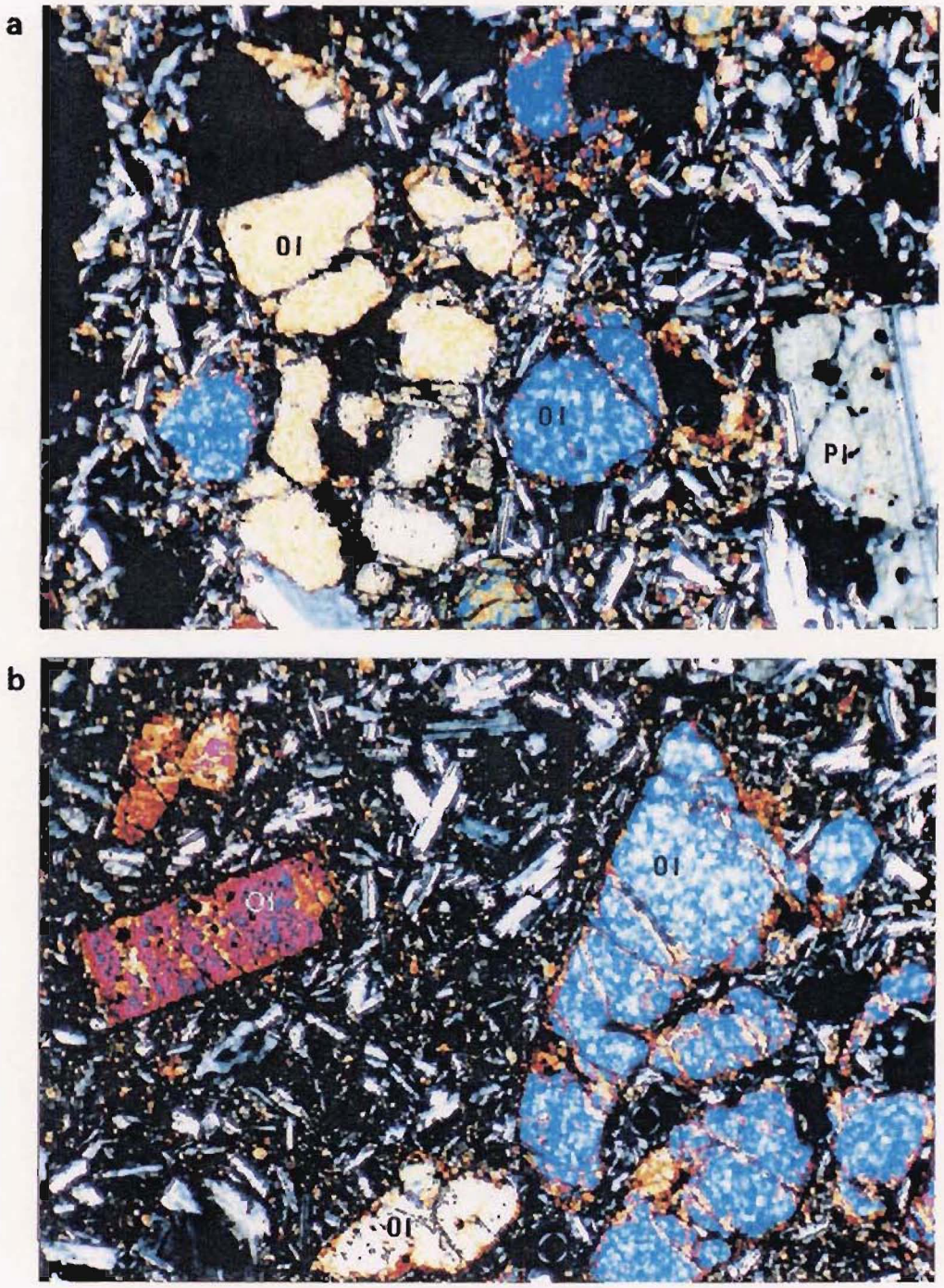

Figure 3-11. Microphotographs of olivines in basalts. (a) Olivine (Fo77) glomerocryst from lava flows of Mt Balatocan and (b) olivine crystals (Fo82-79) from pyroclastic flows of Butong, Bukidnon.

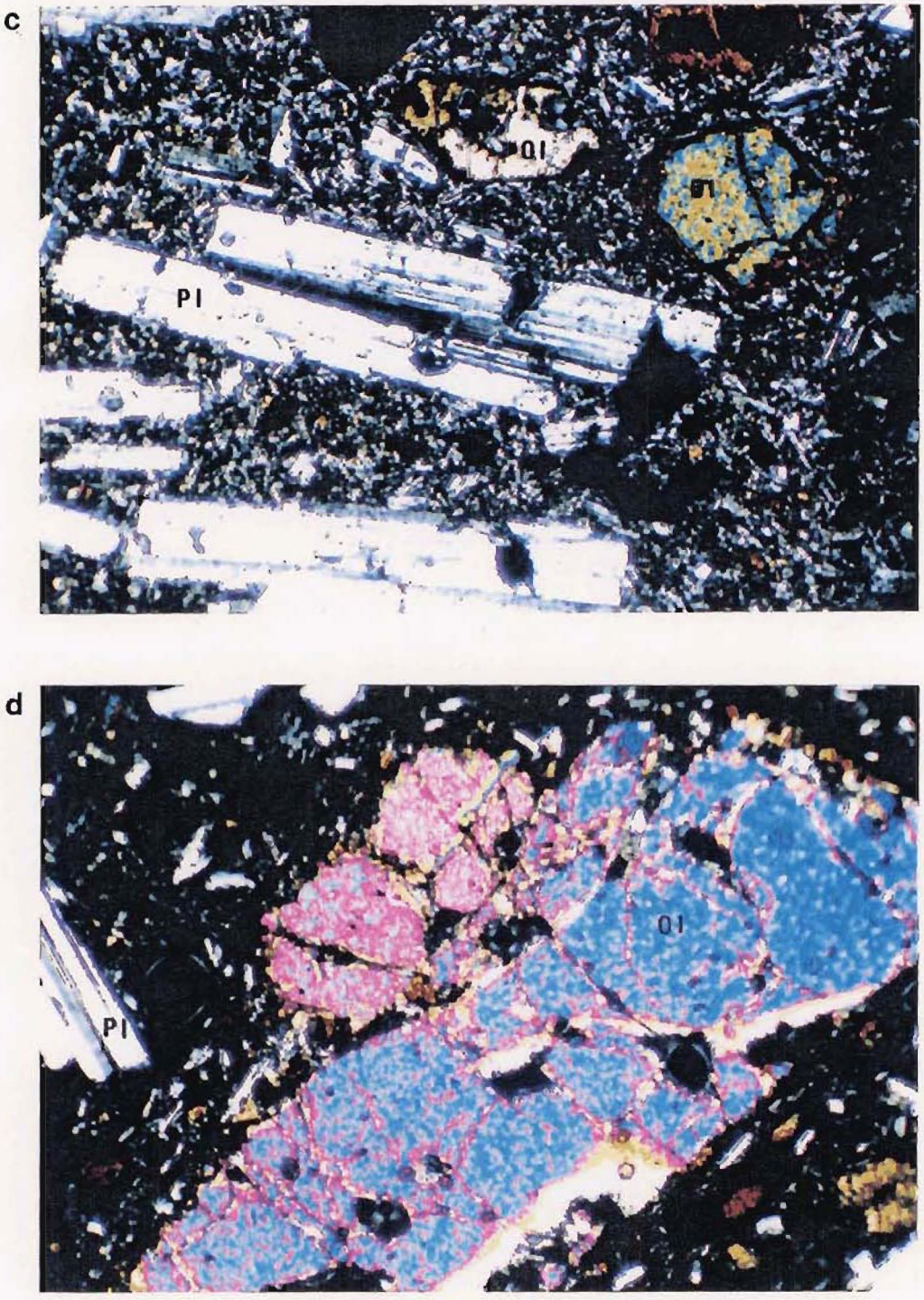

Figure 3-11. continued. (c) Olivine phenocrysts (Fo72-76) in basaltic andesite, Mt Kalatungan. (d) Olivine phenocryst (Fo81-84) in SiO2-rich andesite, Hibok-Hibok. Magnification in both views is 10x.

stability of olivine throughout the crystallisation of basaltic liquids is indicated by abundance of clear forsteritic olivine as subhedral phenocrysts and as groundmass crystals (Fig. 3-11a and 3-11b). In basaltic andesites (Fig. 3-11c) there are fewer olivine phenocryst or microphenocryst while in SiO_2-rich andesite and dacite crystals are sporadic and appear xenocrystic: discrete broken and anhedral crystals showing dissolution (Fig 3-6c). Occasional subhedral olivine megacrysts also occur in SiO_2-rich andesite (Fig. 3-11d).

(i) Mg-Fe Variations

Olivines range from Fo_{84} to Fo_{72} (Table A3-2, Appendix 3-2). The compositional spectrum for each lava type is limited, however, with overlaps occurring from basalt to andesite and andesite to dacite (Fig. 3-23). In general, olivines from basalts exhibit the widest Fo variation with increasing Fa components towards basaltic andesites and dacite. A qualitative appraisal to determine whether or not olivines in acid andesites are in equilibrium with the host rock is shown in Figure 3-12. Comparison of the MgO/FeO ratio (1.29) of a representative SiO_2-rich andesite bulk composition (analysis no. 5, Table 3-2) with equilibrium olivine compositions in Figure 3-12 suggest that olivines in some SiO_2-rich lavas may have equilibrated with the liquids (Fo_{81-84} observed, Fo_{81-83} estimated). Basaltic olivines have MgO/FeO ratios close to estimated values (Fo_{82} and Fo_{85-87}, respectively) but olivines from basaltic andesites appear to be Fe-enriched compared to equilibrium olivines. However, this condition cannot be rigorously evaluated because of uncertainties in the Fe_2O_3/FeO ratios of the magma (roughly assumed to be 0.3) and the assumption of K_D=0.30. Also, equilibrium conditions using partition coefficients for minor elements in olivine suggest the olivines in silicic lavas are xenocrystic. One consistent feature borne out by MgO/FeO ratios of bulk rocks is that the equilibrium temperatures decrease from basalt to andesite to dacite and thus suggest that olivine may not be the first crystallising phase in the more evolved melts. The occurrence of olivines in acid andesites and dacites is not unusual, since in more evolved liquids, increased concentrations of monovalent

Table 3-2. Selected whole rock analyses (mole %) which contain modal olivine.

Location	Bal	But	Kal	Apo	Cam
Analysis #	1	2	3	4	5
Lab #	23259	23264	23261	23269	21839
SiO2	55.24	55.67	59.57	61.49	63.90
TiO2	0.67	0.90	0.83	0.75	0.50
Al2O3	9.50	10.39	10.98	11.15	11.29
Fe2O3	0.84	0.91	0.72	0.66	0.58
FeO	6.23	6.75	5.38	4.91	4.30
MnO	0.15	0.14	0.13	0.10	0.16
MgO	12.05	11.81	7.63	5.84	5.54
CaO	11.70	9.80	8.66	8.46	8.57
Na2O	3.12	3.25	3.87	3.91	3.98
K2O	0.42	0.32	1.94	2.56	1.03
P2O5	0.07	0.07	0.28	0.15	0.13
Total	100	100	100	100	100
MgO/FeO (1)	1.94	1.75	1.26	1.19	1.29
MgO/FeO (2)	1.02	1.40	1.15	0.77	1.30
FeO/MgO (3)	0.29	0.21	0.26	0.39	0.23
MnO/FeO (4)	0.024	0.019	0.014	0.77	0.012
MnO/FeO (5)	0.027	0.021	0.021	1.19	0.037

(1) Actual values
(2) Calculated values using KD=0.3 (Roeder,1974)
(3) FeO/MgO for olivine
(4) Calculated values using KD=1.4 (Roeder, 1974)
(5) Actual values
Abbreviations: Cam, Camiguin Island; Bal, Mt Balatocan, But, Butong; Apo, Mt Apo; Kal, Mt Kaltungan.

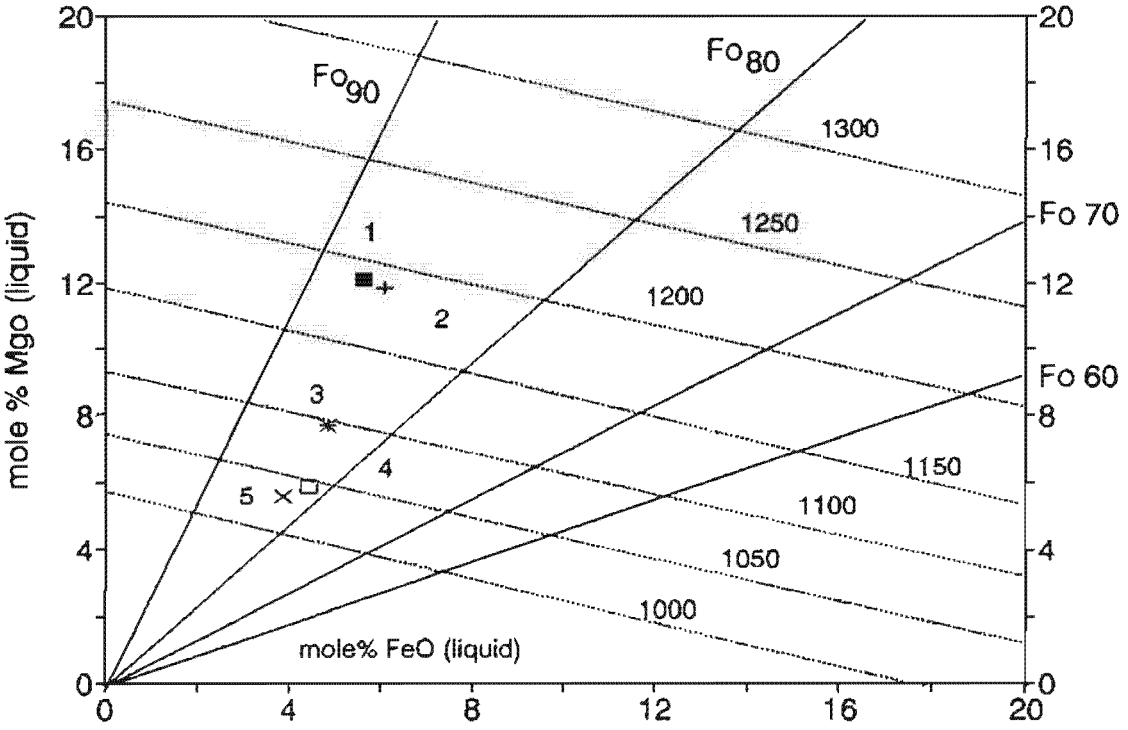

Figure 3-12. MgO-FeO relations in olivine assuming equilibrium with host liquid at 1 atm (after Roeder and Emslie, 1970). Points are selected CMVA bulk compositions (Table 3-2).

cations reduce linking of SiO_4^- tetrahedra and expands the stability of olivine (Kushiro, 1975).

(ii) Ca, Mn and Ni Contents

Of the minor elements present in olivine, Ca is most important because it is significantly partitioned in other rock-forming silicates. Figure 3-13a shows that Ca (0.12 - 0.22 wt%) generally increases with decreasing MgO. The concentrations are within the range commonly observed for olivines in extrusive environments (Simkin and Smith, 1970).

One important feature of Ca is that its concentration in olivine can vary linearly with the concentration of Ca in the coexisting melt. This dependence was found by Watson (1979) to apply to the system Na_2O-CaO-MgO-Al_2O_3-SiO_2 at 1 atm in the range 1,250°C - 1,450°C. Thus this relation can be applied to basaltic liquids to further test whether or not olivine equilibrated with the host rock. Application of Watson's equation: Wt% Ca_{ol} = 0.0275 Wt% Ca_{liquid} to basaltic compositions in Table 3 - 2 (using analyses 1 and 2) gives higher calculated CaO values (0.22 vs 0.28 wt%, in analysis 1; and 0.18 vs 0.27 wt%, in analysis 2). If the discrepancies are truly significant, the low actual CaO wt% in basaltic olivines are likely caused by coprecipitation of clinopyroxene and calcic plagioclase. Manganese behaves similarly to Ca in olivines, showing negative correlation with MgO (Fig. 3-13b) whereas Ni shows a positive trend (Fig. 3-13c).

(iii) Alteration

Two types of alteration are observed. The most common type occurs as thin brown mantles around the rims or along cracks in olivine (Fig. 3-11c), corresponding to Type 1 "Iddingsite" of Baker and Haggerty (1967). This kind of alteration occurs at relatively low temperatures (< 140°C) under oxidising conditions.

The other type of alteration occurs in olivine clusters (Fig. 3-3c) showing partial alteration of olivine. Breakdown of olivine into a magnetite (± pyroxene) assemblage was ascribed by Haggerty and Baker (1967) to high-temperature oxidising conditions. The equant grains of magnetite suggest oxidation close to

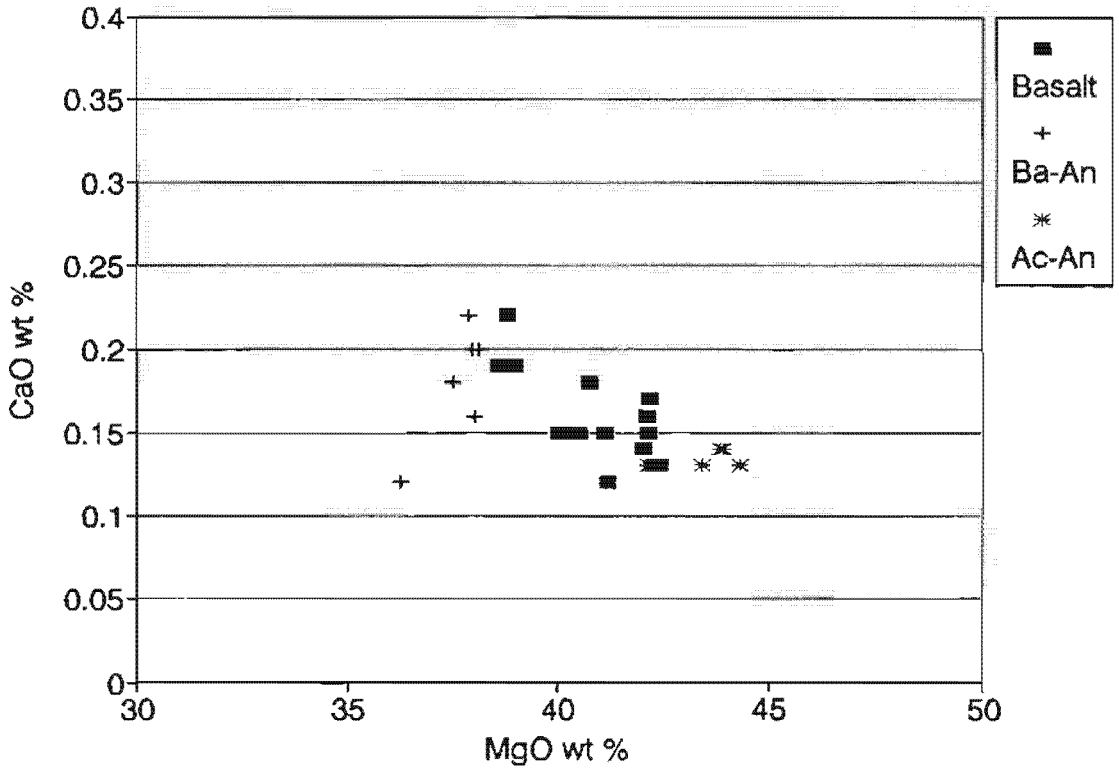

Figure 3-13a. CaO variation with MgO in selected olivines.

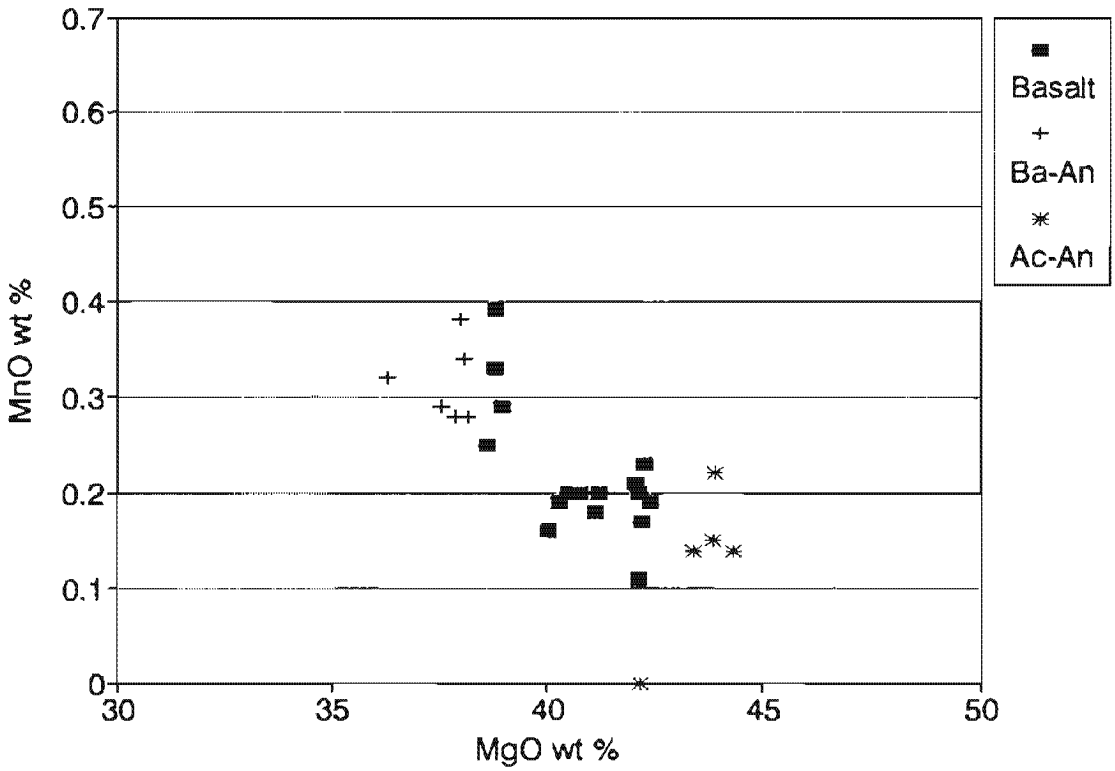

Figure 3-13b. MnO distribution with changing MgO in selected olivines of CMVA lavas.

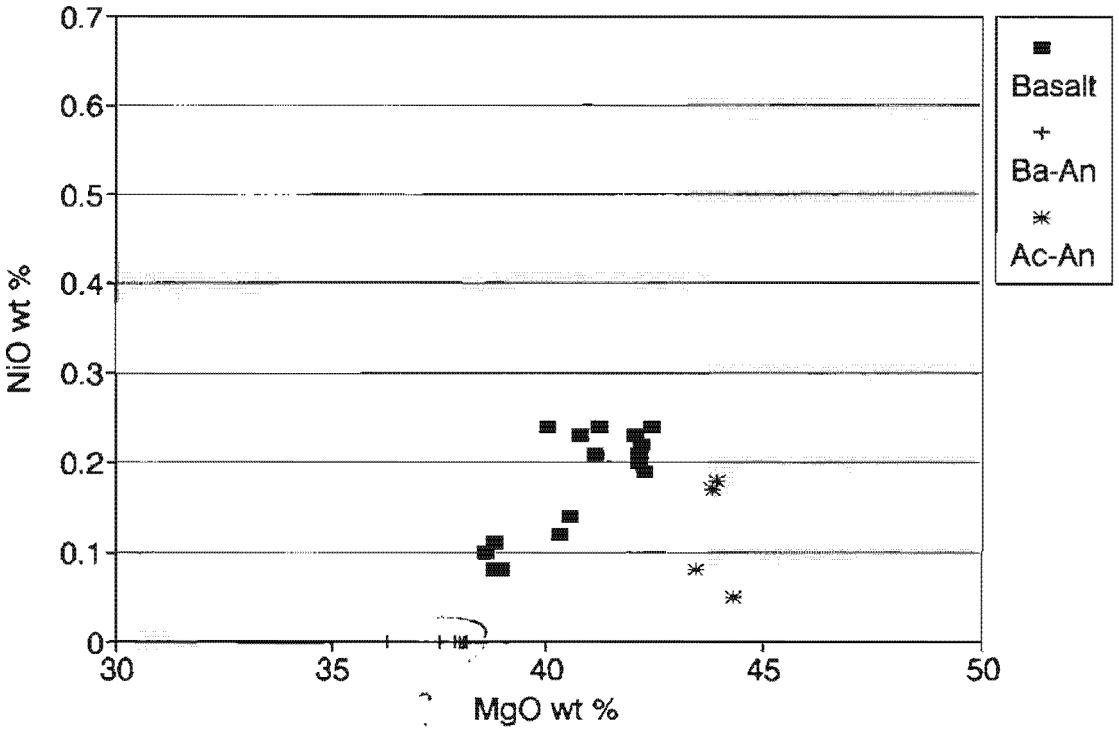

Figure 3-13c. Plot of NiO concentrations with MgO in selected olivines. NiO contents decreases linearly with decreasing MgO from basalt to basaltic andesite, in contrast to SiO2-rich andesite.

1,000°C (Champness, 1970) and their random distribution may be due to homogenous nucleation (Putnis, 1979). In other olivines the margins are intruded by vermicular opaques similar to high-temperature alteration products described by Goode (1974).

3.6.3. PYROXENES

The most widely occurring mafic phase is pyroxene. Their abundance in CMVA lavas makes pyroxene an important geochemical discriminant for petrogenesis since pyroxene compositions reflect bulk rock chemistry and crystallisation order (Poldevaart and Hess, 1951), oxygen fugacity and cooling rate (Grove and Bence, 1977). Variations in pyroxene chemistry also relate to magmatic affinity, as demonstrated by Si-Al relations (Kushiro, 1960; Le Bas, 1962), Si-Ti distribution (Verhoogen, 1962) and compositional variations of non-quadrilateral components such as Na, Ti, Cr, Mn and K (Nisbet and Pearce, 1977). Pyroxene compositions from plutonic and volcanic environments are chemically similar and thus aid comparison between pyroxenes gathered from differing tectonic settings with variable modes of emplacement. In addition, pyroxenes are highly resistant to post-magmatic dissolution making it possible to classify the parentage of highly altered rocks (Mevel and Velde, 1976).

Only those pyroxene analyses where oxides sum to 100 $\pm$ 2 wt% and the charge equation [$^{(iv)}Al + {}^{(vi)}Fe^{3+} + {}^{(vi)}Cr^{2+} + 2Ti^{4+} = {}^{(iv)}Al + Mn$] balances to 0.02 or better are quoted. Pyroxene formulae were derived by calculating to 4 cations and 6 oxygens (Vieten and Hamm, 1978). The distribution of cations follows the convention of Bown (1964; p.190) and procedures from Morimoto (1989) where the T site is summed to 2.000 using Si and Al. In this study, Al^{3+} is always sufficient to fill the tetrahedral sites so that Fe^{3+} (as calculated from charge balance) along with excess Al^{3+}, Ti, Mg^{2+} and some Fe^{2+} are allocated into the M1 site. The rest of the Fe^{2+} is added to Mn^{2+}, Ca^{2+} and Na^{+} to fill the M2 site. The sum of M2 cations must be near 1.000 otherwise the analysis is rejected.

Two types of pyroxenes are recognised in CMVA. Calcic pyroxene is the most abundant and, with exception of some mafic inclusions, occurs in all samples as phenocrysts or in the groundmass. Calcic-poor pyroxenes are only encountered in the acid andesites of southern and central Camiguin Island. Representative microprobe analyses of pyroxenes are given in Table A3-3, Appendix 3-2.

(i) Si-Al-Ti and Minor Element Compositions

Kushiro (1960) has shown that Si^{+4} and Al^{+3} are antipathetic (Fig. 3-14) and the high SiO_2 and low Al_2O_3 are characteristic of pyroxenes from subalkaline lavas (Le Bas, 1962). The same relations are observed for Ti (Fig. 3-15). The plots also show that Al_2O_3/SiO_2 and TiO_2/SiO_2 ratios generally decrease with more evolved lavas. These results are in accord with the findings of Murata (1960); Ramberg (1952) for non-alkaline rocks which typically have low $Al^{(IV)}$ contents (Fig. 3-16), since Fe/Mg ratios of phenocrystic pyroxene have no apparent trend. The proportion of Al which enters 4-fold coordination is generally 40% - 55% of total Al. This is less than that observed for tetrahedral substitution by Al in alkaline and tholeiitic rocks (Schweitzer et al 1979; Fig. 9, p.509). However, the low $Al^{(iv)}$ contents may also reflect the saturation of other melt components (Carmichael et al, 1970), notably Si, rather than low total Al. In fact, Al is always adequate to fill the tetrahedral vacancies.

The plot of [Ca + Na] vs Ti clearly shows the subalkaline nature of these pyroxenes, having overall low Ti (Fig. 3-17). However, this diagram cannot separate pyroxenes of orogenic calcalkaline lavas from those of tholeiitic affinities since Ti is relatively scarce in both magma types. A discriminant between these types is the plot of total Al and Ti (Fig. 3-18) using the field boundaries of Letterier et al (1982), which indicates the calcalkaline nature of pyroxenes in basalts and basaltic andesites. A peculiarity of this diagram (which was intended for basalts) is the low Ti/Al ratios in SiO_2-rich andesites and dacites. This is most likely caused by decreased crystallisation intervals between pyroxenes and Fe-Ti oxides.

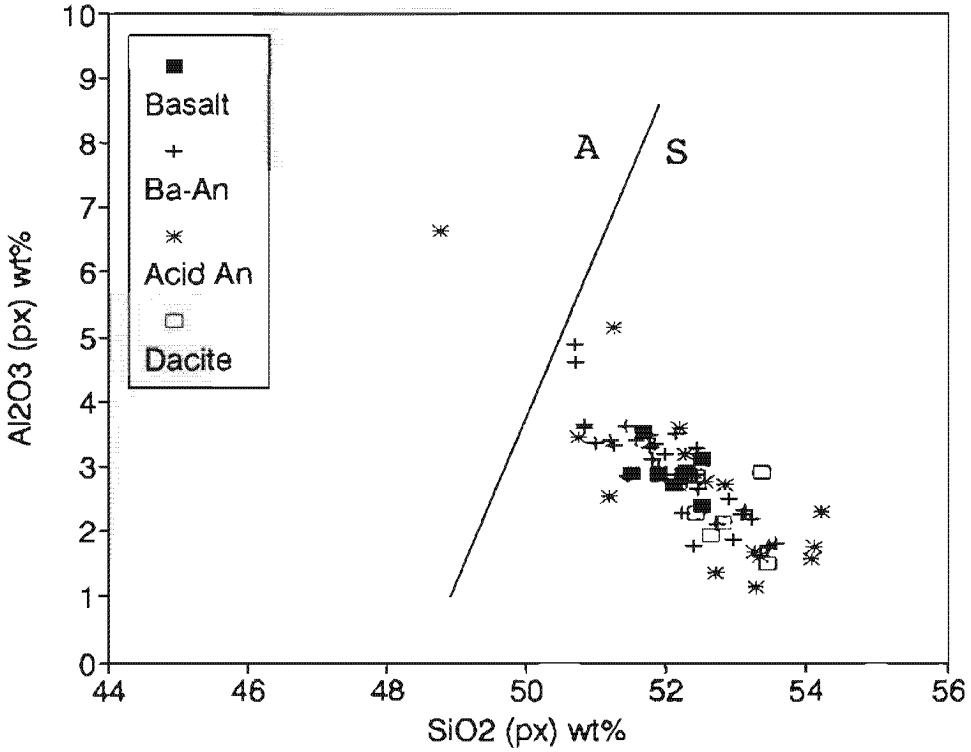

Figure 3-14. Variation of Al2O3 with SiO2 in pyroxenes of the CMVA. S = subalkali and A = alkali fields of Nisbet and Pearce (1977).

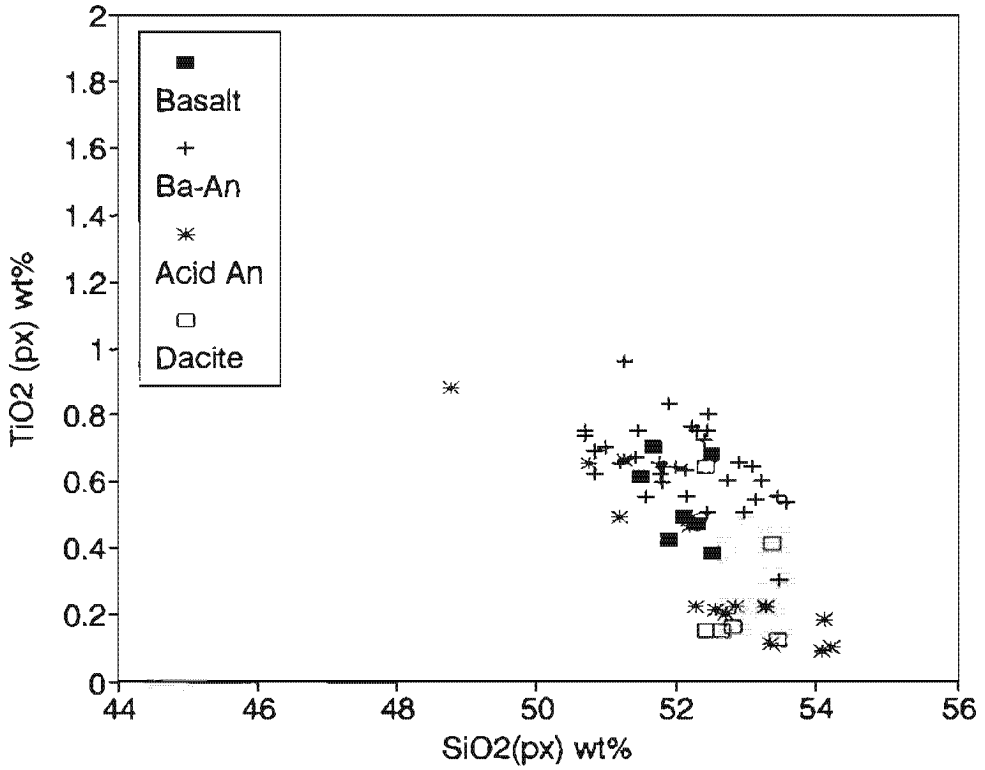

Figure 3-15. Variation of TiO2 with SiO2 in pyroxenes of the CMVA.

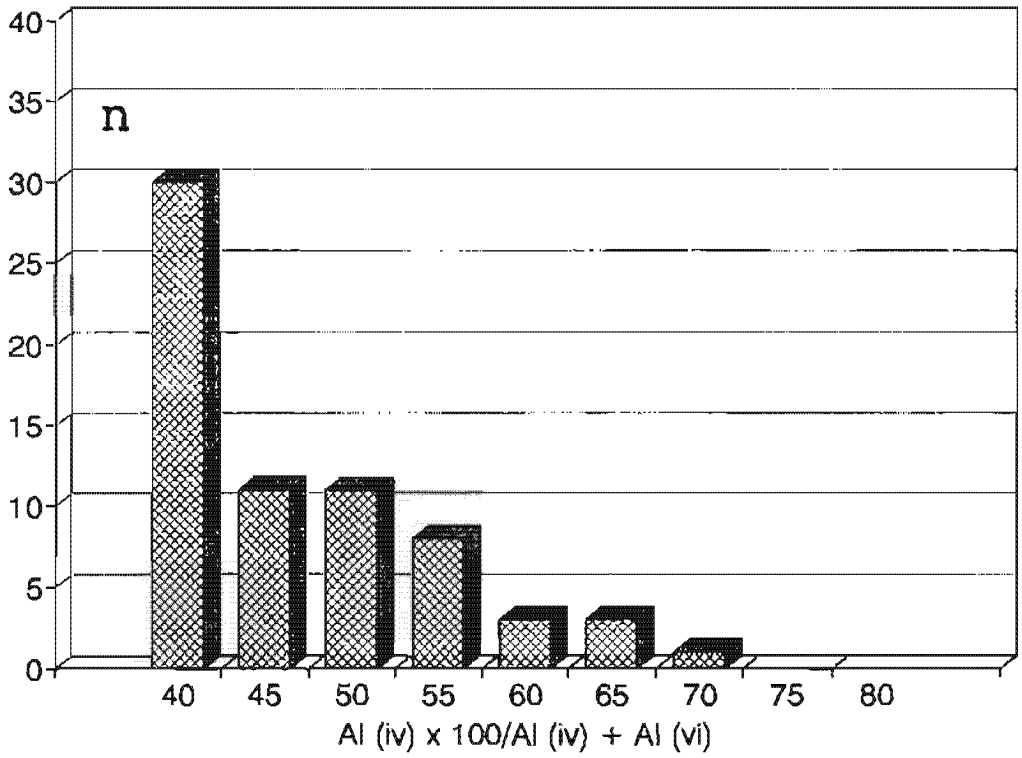

Figure 3-16. Frequency distribution of tetrahedrally-coordinated Al in pyroxenes of Central Mindanao.

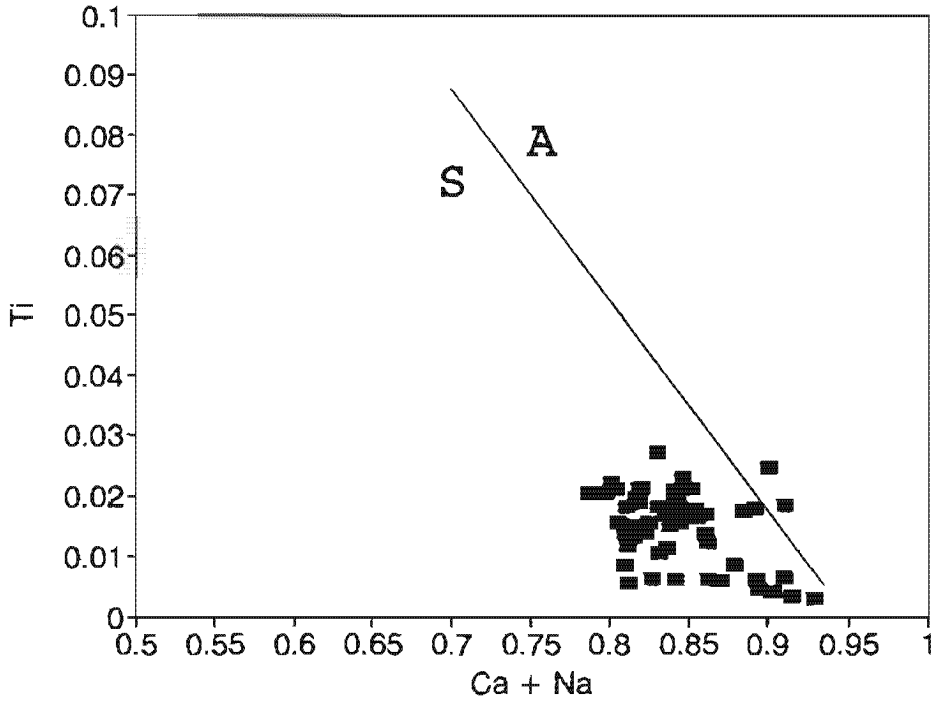

Figure 3-17. Discriminant diagram for clinopyroxene phenocrysts from the CMVA. Field boundaries S = subalkaline and A = alkaline from Letterier et al (1982).

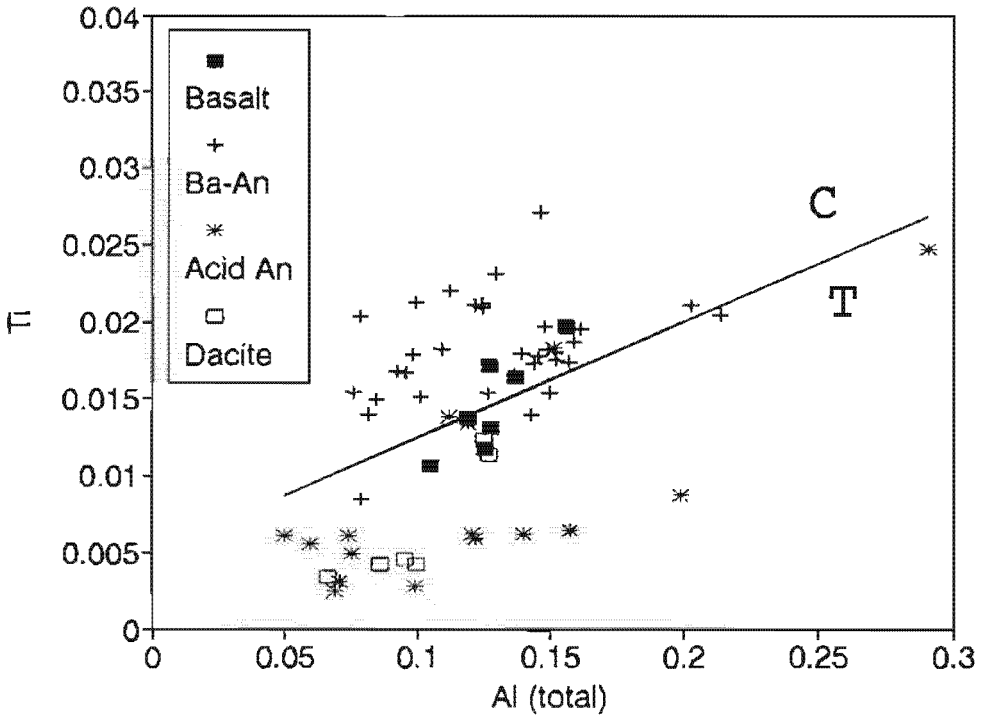

Figure 3-18. Discriminant diagram for pyroxenes of Central Mindanao showing the calcalkaline affinity of mafic (basalt- and basaltic lavas). Boundary relations between C=calcalk-aline and T=tholeiitic fields after Letterier et al (1982).

Plots of selected cations vs. Fe^{2+}/Fe^{2+} + Mg (atomic %) as a measure of differentiation further support the calc-alkalic nature of the lavas. The $Al^{(iv)}$ and Mn contents do not show any significant trends (Fig. 3-19 and Fig. 3-20).

(ii) Ca-Mg-Fe Relations

Calcium occurs constantly within a restricted range as opposed to scattered patterns in alkaline and tholeiitic suites reported by Schweitzer et al (1979). Two subgroups are delineated by Ca contents: basalts and basaltic andesites with flat Ca trends with respect to $Fe^{2+}/(Fe^{2+}$ + Mg) ratios and slightly enriched Ca in SiO_2-rich andesites and dacites. Calcium-rich clinopyroxenes approaching salite compositions for the latter subgroup suggest relatively high H_20 contents (Conrad and Kay, 1984), consistent with appearance of hydrous mafic minerals in SiO_2-rich lavas. Finally, clinopyroxene Mg numbers decrease within a limited range of increasing bulk rock FeO/MgO ratios (Fig. 3-21). This tendency distinguishes pyroxenes from calcalkaline rocks from more Fe-enriched differentiated tholeiitic and alkaline suites (Gill, 1981; Kay and Kay,1985, Fig.5b, p.284).

Calcic Pyroxenes. The Ca-rich pyroxenes of Central Mindanao are mainly augites which generally show uniform compositions in the Ca-Mg-Fe quadrilateral (Fig. 3-22). The augites grade into salites (diopside, Morimoto, 1989) and the Ca component ranges from $Wo_{40.6}$-$Wo_{47.8}$. The limited compositional spectrum is also indicated by optically continuous crystals with rare sector zoning. Core to rim divisions are only occasionally observed and concentric mantles, where present, are generally < 0.1mm thick. Compositional differences between core-mid-rim analyses are slight (with the exception of H15m70, analysis 42, Table A3-3c, Appendix 3-2) and this is also true for phenocrysts and xenocrysts. To evaluate major element variations, calcic pyroxenes are grouped into their host lava types; basalt, basaltic andesite, SiO_2-rich andesite and dacite.

Clinopyroxene compositions in basalt are shown in Figure 3-23. The tight data set reveals two clusters: one defines a relatively magnesian pyroxene group

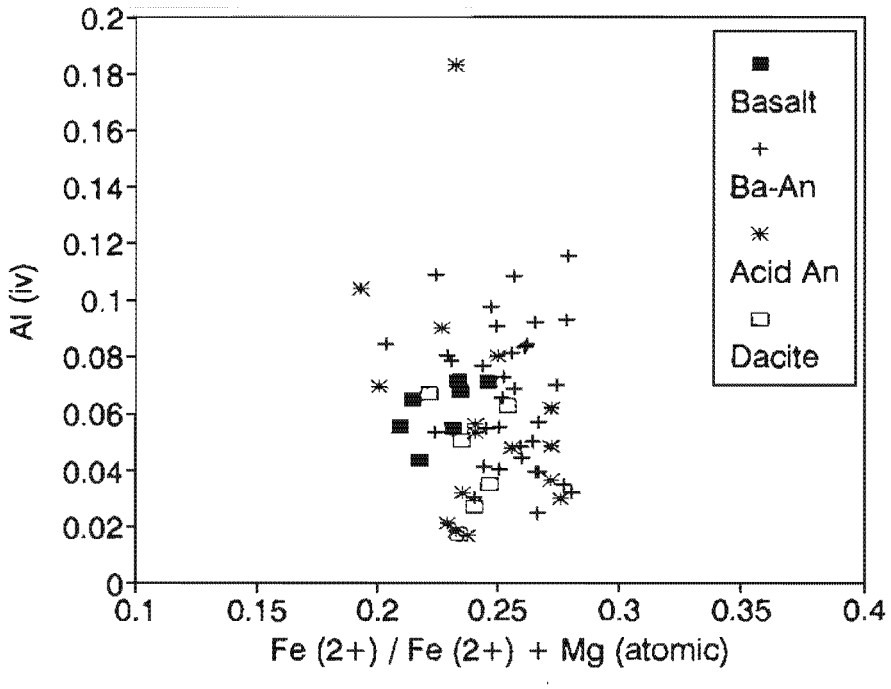

Figure 3-19. Distribution of tetrahedrally coordinated Al with Fe/Fe+Mg. Poor correlation shows that Al substitution (and Si contents) do not follow the trend of decreasing Al (iv) with differentiation.

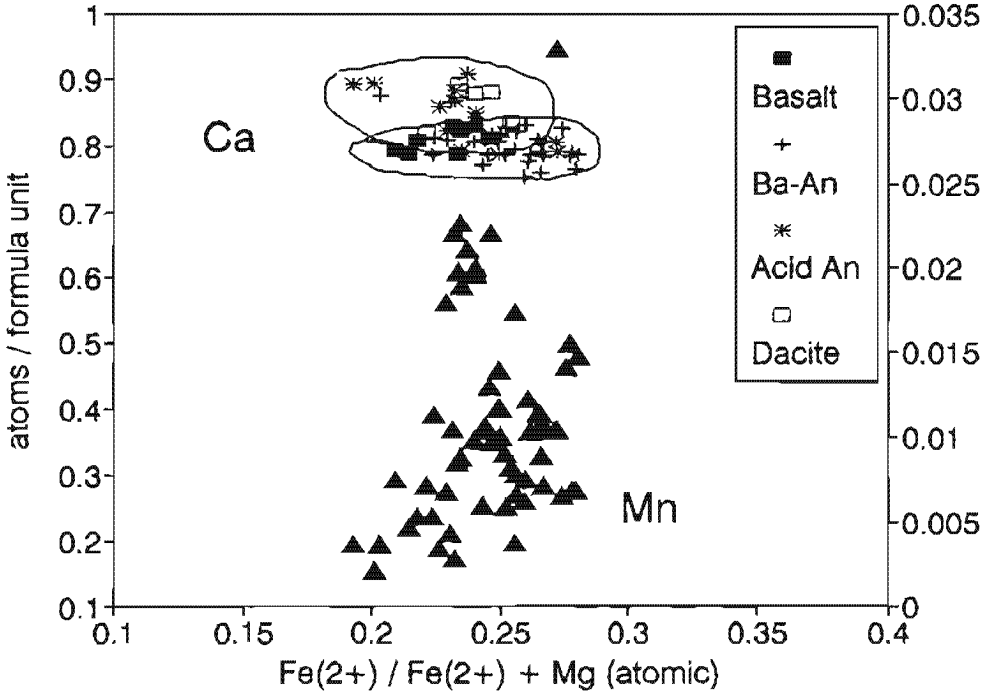

Figure 3-20. Ca and Mn (right scale) variations in pyroxenes from basalts to dacites. Higher average Ca contents occur in lavas with bulk rock SiO2 wt% > 57.

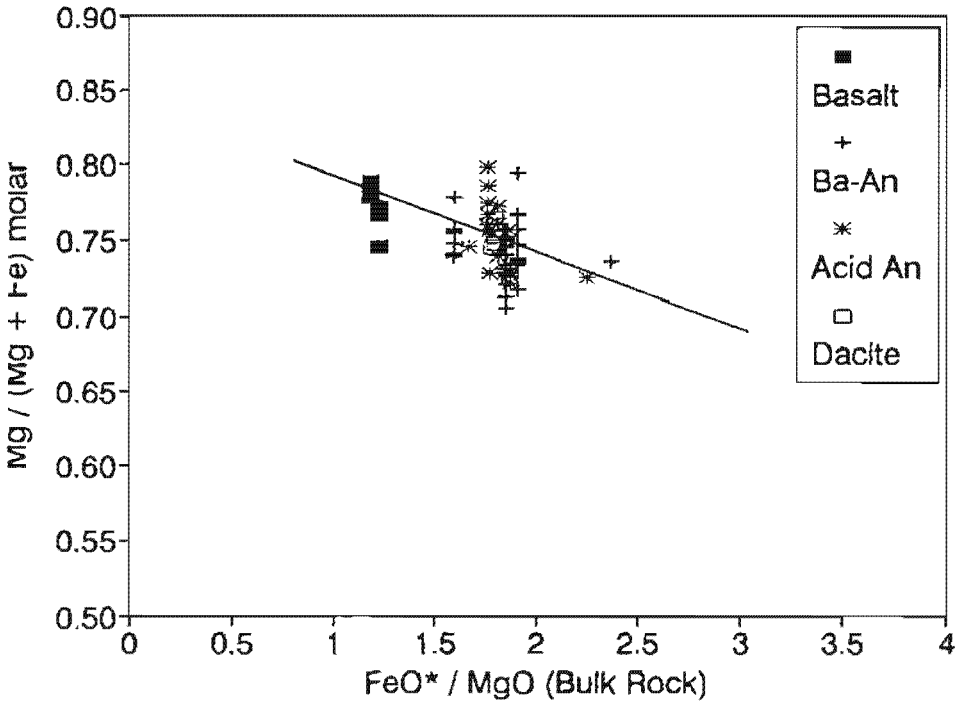

Figure 3-21. Negative correlation of Mg# (px) with Fe/Mg ratios (shown by trendline). Basalts distinguished by high Mg# and low Fe/Mg ratios but more evolved lavas show limited Fe enrichment.

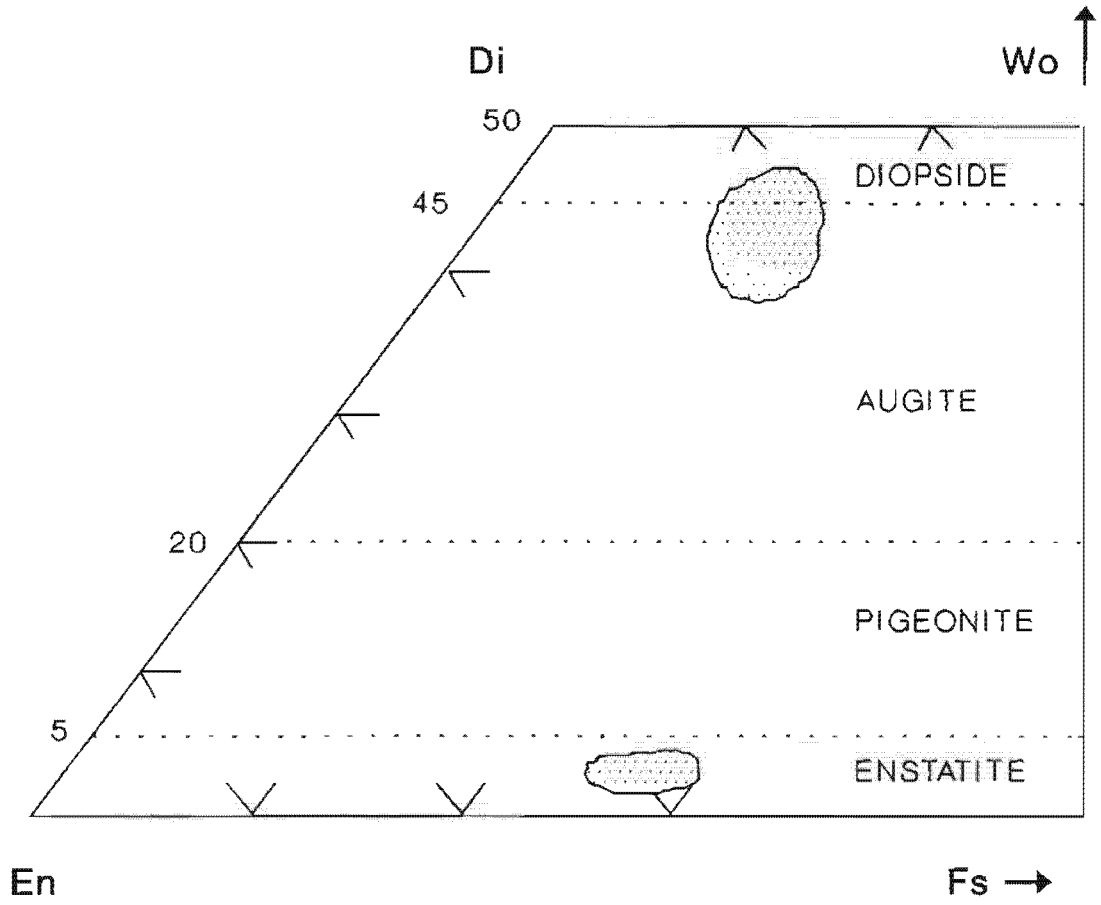

Figure 3-22. Compositional fields of pyroxenes from the CMVA. Data from Appendix 3-2, Tables A3-3a to A3-3d. Pyroxene classification after Morimoto (1989).

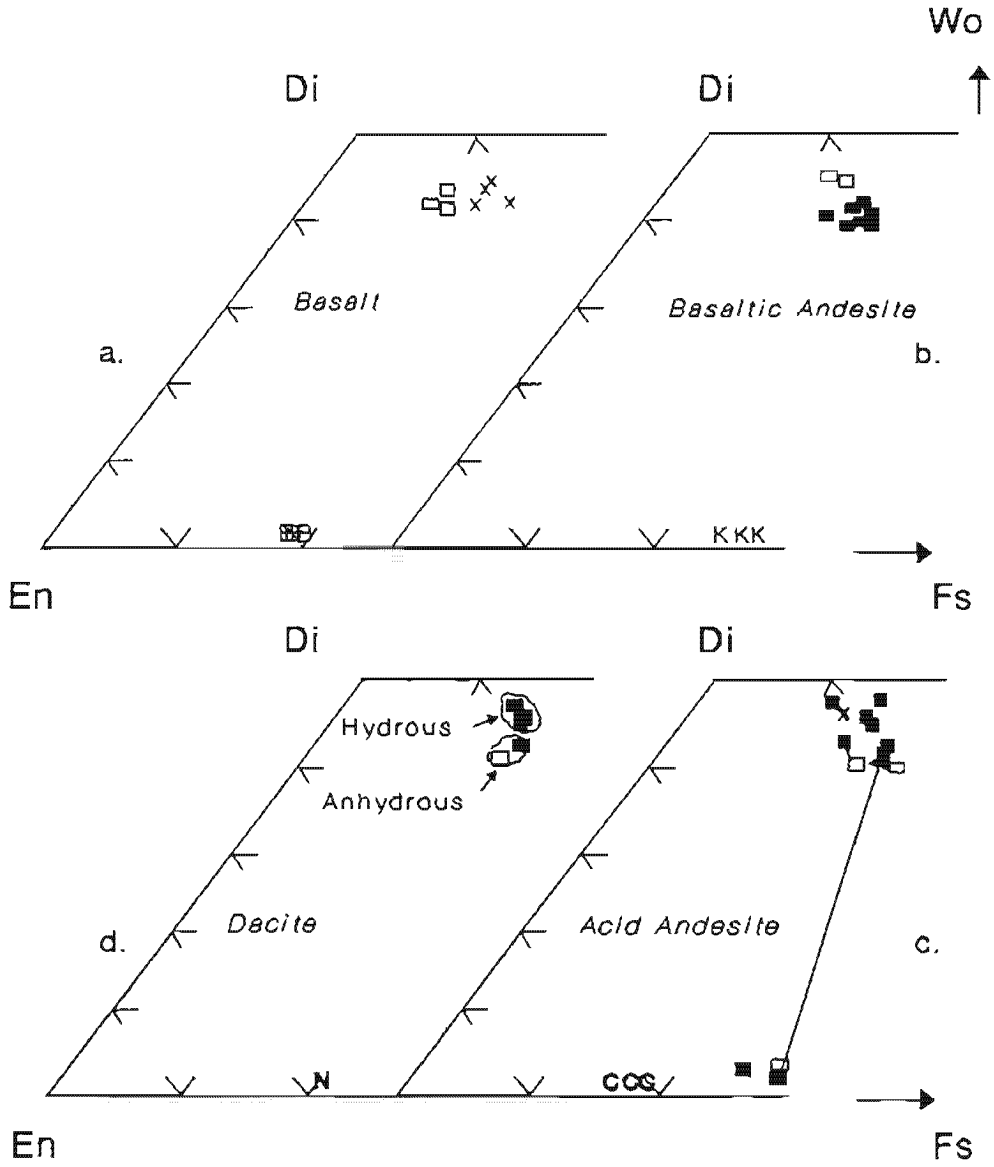

Figure 3-23. Distribution of quadrilateral components in pyroxenes among CMVA lavas. Filled symbols: cores, open symbols:rims, X:xenocrysts. Tieline connects co-existing augite-enstatite. Coexisting olivines = letter symbols, B:Butong, K & N: Katanglad, C:Camiguin Island.

($Ca_{41}Mg_{46}Fe_{13}$; Fig. 3-24a) from megacrysts in lava bombs of northern Mindanao, and another a cluster of less magnesian phenocrysts ($Ca_{44}Mg_{43}Fe_{13}$; Fig. 3-24b) of Butay, Camiguin Island. Only a slight decrease in Wo component (~1 mol%) occurs toward the rims, where it approaches groundmass compositions.

Clinopyroxenes from basaltic andesites display greater compositional spread than basalts. In the former, a large incidence of reverse zoning is observed with augite cores ($Ca_{41-43}Mg_{43}Fe_{16-14}$) and Ca-enriched rims ($Ca_{46}Mg_{43-42}Fe_{11-12}$) (Fig. 3-23b). The rims could represent compositions coexisting with Fe-oxides. Reverse zoning of this kind was suggested by experiments on pyroxene crystallisation at increased P_{H2O} and fO_2 (Helz, 1973) where the crystals progressively become depleted in Fe at a given temperature and richer in the Wo component than pyroxenes from anhydrous phase assemblages.

The SiO_2-rich andesites come closest to exhibiting a "normal" pyroxene crystallisation trend with an increase in Fe and Mn and decrease in Ca from core to rim or groundmass (Fig. 3-23c). However, these trends become less defined in lavas dominated by amphibole. The fractionation of hydrous minerals as a stable phase assemblage in acid andesites probably suppresses Fe-enrichment. The stability of amphiboles suggest high H_20 fugacities in SiO_2-rich intermediate rocks and this is thought to depress the pyroxene liquidus to a temperature below the pigeonite-orthopyroxene inversion (Best and Mercy, 1967). In addition, the groundmass augite is Ca-enriched relative to pyroxene rims. This increase in Ca contents in late crystallising pyroxenes is probably caused by cessation of crystallisation of calcic plagioclase and decrease in temperature in the more evolved lavas, preventing replacement of Ca by either Mg or Fe.

Clinopyroxenes from dacites are depleted in the Fs component by about 2 mol% relative to andesite (analyses number 34 vs 47, Tables A3-3b and A3-3c, Appendix 3-2). The difference is probably caused by the increased occurrence in dacite of amphibole and biotite into which Fe is preferentially partitioned. As shown

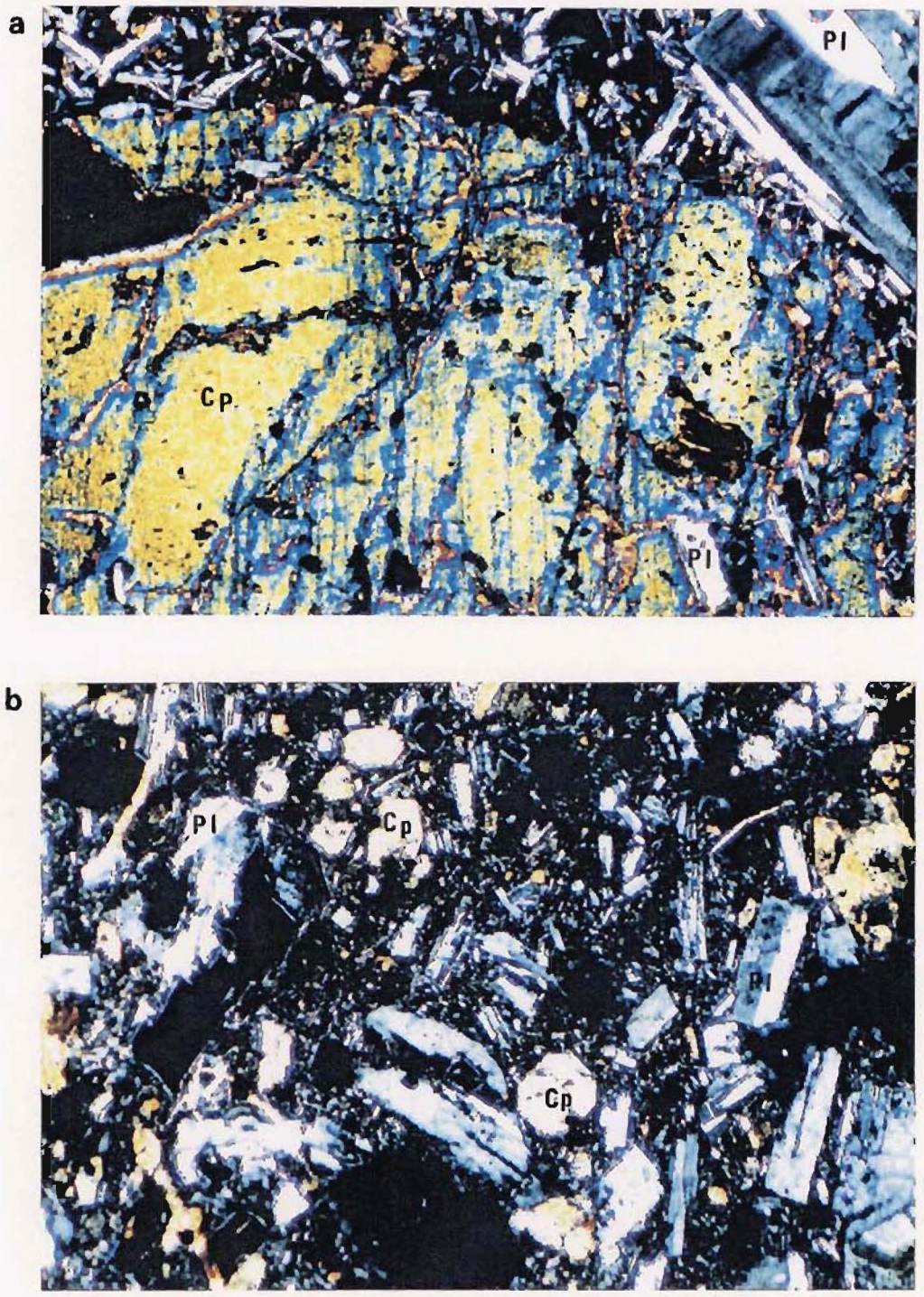

Figure 3-24. Microphotographs of pyroxenes in basalts. (a) Augite megacryst from Mt Balatocan lava flow. (b) Augite grains in fine-grained basalt flow, Camiguin Island. Magnification in both views is 10x.

in Fig. 3-23d, Fe contents of pyroxene cores in Type 2 dacite are about 1 mol% less than those in the anhydrous dacite. Besides limiting Fe-enrichment in pyroxenes, increased P_{H2O} and fO_2 in Type 2 dacites restricts the stability field of pyroxenes (Helz, 1973). This relationship probably explains decreased pyroxene modes in hornblende-rich dacites as well as the presence of subhedral-granular diopside (Fig. 3-25a), in contrast to relatively abundant and subhedral augite in anhydrous andesite and dacite (Fig. 3-5a; Fig. 3-25b).

Orthopyroxenes. This mineral occurs as elongate prismatic phenocrysts in lavas of central and southern Camiguin Island (Fig. 3-25c, d). Modal orthopyroxene is dominant or subordinate to coexisting clinopyroxene in Mt Mambajao whereas orthopyroxene is always more abundant than clinopyroxene in Mt Ginsiliban (Fig. 3-25d; Table 3-1). The occurrence of orthopyroxene seems limited to silicic andesites with bulk rock SiO_2 from 57.55 - 61.40 wt%. Within this range, the highest modes were observed in rocks with SiO_2 > 58 wt%.

Representative microprobe analyses of orthopyroxene and coexisting clinopyroxene are given in Table A3-3d, Appendix 3-2. The Ca-poor pyroxenes plot within the bronzite field (enstatite; Morimoto, 1989). Pigeonite and subcalcic augite are absent. Slight variations in elemental abundances among orthopyroxene in terms of Si, Ti, Mn and Na are insignificant because discrepancies are near the limits of detection.

3.6.4. Spinel

The main opaque phases are titanomagnetites (or magnetite) and rarely, Cr-spinel. While magnetite consistently occurs in nearly all specimens from basalts to dacites, Cr-spinel was only observed as discrete inclusions in olivine from relatively Mg-rich lavas of Butay.

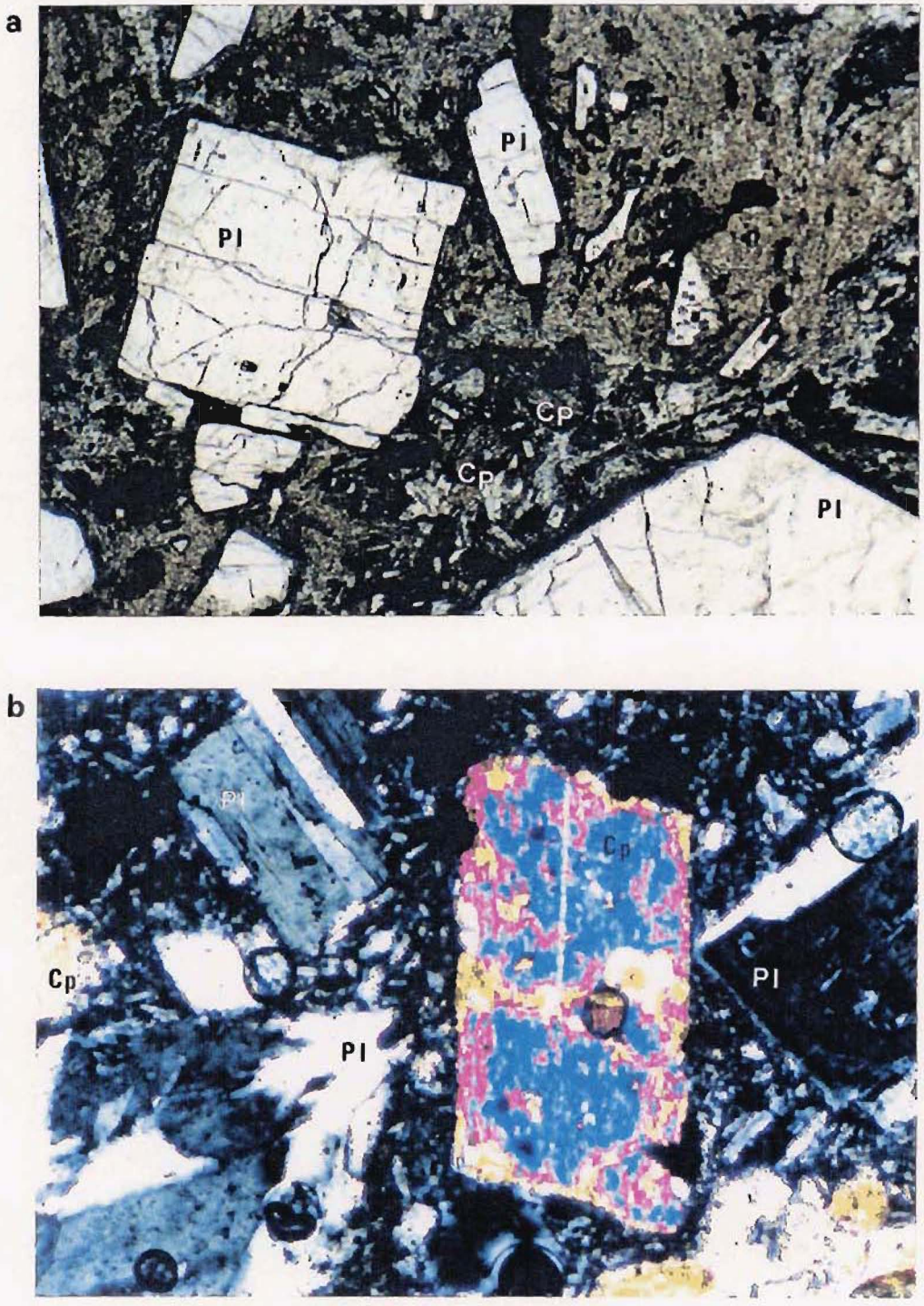

Figure 3-25. Microphotographs of pyroxenes in SiO2-rich compositions.
(a) Granular diopside [below centre] from Type 2 dacite, Mt Apo. Uncrossed polars. Magnification is 10x. (b) Augite in pyroxene andesite, Camiguin Island. Crossed polars. Magnification is 40x.

Figure 3-25. continued. Microphotographs of pyroxenes. (c) Co-existing augite [left] and enstatite [just off extinction] in 2-pyroxene andesite, Mt Mambajao. (d) Enstatite [left] and augite in fine grained SiO_2-rich andesite, Mt Ginsiliban. Magnification in both views is 40x. Crossed polars.

(i) Cr-Spinel

Several aspects of Cr-spinel chemistry (analyses 1 and 2, Table A3-4a, Appendix 3-2) suggest these crystals formed *in situ* and not as xenocrysts from a peridotitic or picritic source. Comparison with spinels from alpine peridotites examined by Loney et al (1971) show that Butay spinels have similar (Cr/Cr + Al) but lower Mg/Mg + Fe2+ ratios. Values for the latter ratios are lower than in Cr-spinels from oceanic basalts (Sigurdsson and Schilling, 1976). Also, the Fe3+/Cr + Al + Fe3+ ratios are higher (0.227 vs. .037, 4 oxygen basis) and the Al lower than in spinels examined from sea-floor basalts and from the laboratory-synthesized basalts described by Fisk and Bence (1980). It would appear then that relatively low values for Mg# and Al are caused by olivine and plagioclase crystallisation. If the liquidus phases at the time of spinel crystallisation are spinel + olivine + pyroxene + plagioclase, then progressive crystallisation will result in increased Fe (and lower Mg) with constant Cr# as suggested by Henderson (1975). Crystallisation trends of spinels from Mt Butong cannot be evaluated because these crystals display no chemical zoning and do not coexist with magnetite.

(ii) Magnetite

Magnetite is generally a late precipitating phase but sometimes forms inclusions in pyroxene and plagioclase. Usp ranges from 16 - 45 mole% (Table A3-4a to A3-4c, analyses 3 - 27, Appendix 3-2) which is similar to calc-alkaline suites from the Aleutians (Brophy, 1986), Sarigan island in the Marianas (Usp_{40-20}, Meijer and Reagan, 1981) and Tonga (Usp_{26-18}, Ewart et al, 1973). A schematic distribution of magnetite with Usp components is shown in Figure 3-26. It is obvious that among Central Mindanao lavas, early-formed phenocryst magnetite is stable only in basalts. In groundmass magnetite, Usp increases with increasing SiO_2. In lavas with relatively high fO_2 (spinels coexisting with biotite and amphibole), the spinels are low in TiO_2 (Carmichael, 1967).

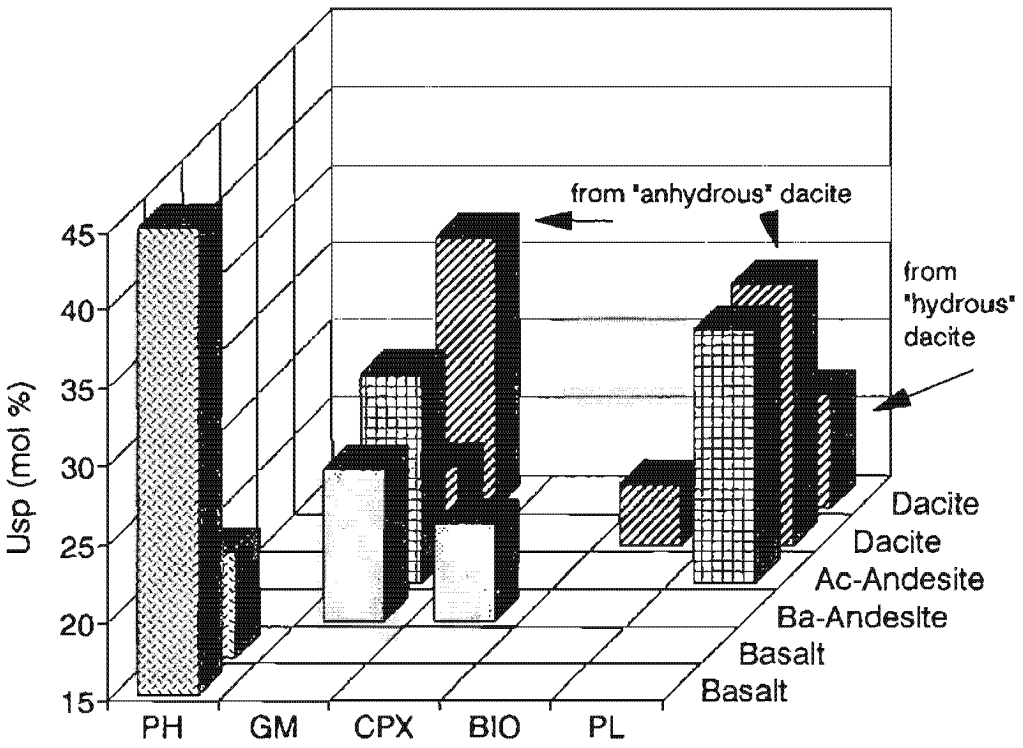

Figure 3-26. Distribution graph of Ti-magnetites in CMVA lavas.
Symbols: PH, phenocryst; GM, groundmass; CPX, clinopyroxene; BIO, biotite; PL, plagioclase.

Mg variation is significant (0.9 - 3.0 wt%). The higher Mg values (>2.0 wt%) indicating magnetite is in equilibrium with olivine in basaltic lavas as suggested by Frost and Lindsley (1991). Spinels with lower Mg contents have probably lost Mg due to cation exchange on cooling. An even greater variabiliy is reflected in minor elements: Al_2O_3 changes from 1.0 - 3.7 wt% and MnO is usually present in abundances of 0.3 - 1.0 wt%. These compositions, however, are within observed ranges of calc-alkaline lavas.

3.6.5. AMPHIBOLE

Amphiboles from andesite and dacite from Mt. Apo and Camiguin Island were analysed. Andesite from Mt Musuan also contain amphiboles but these are highly oxidised and replaced by opaque oxides and are therefore unsuitable for microprobe analysis. In all cases, amphiboles (or relic amphibole structure) were only found in lavas with at least 55 wt% SiO_2.

Optically, the low extinction angles ($Z \wedge C \approx 0$ in most cases), red-olive brown pleochroism and variable 2Vx (~50^o - 80^o) suggest a classification into oxyhornblende or kaersutitic compositions. The presence of significant ferric iron in the amphibole structure, as implied by optical descriptions, presents a limitation to classification from microprobe results because the A-site occupancy varies with ferric iron contents. The effect of variations in ferric iron is readily seen in Figure 3-27a where all Fe is assumed to be FeO and in Figure 3-27b with Fe recalculated to FeO + Fe_2O_3. Entry of ferric iron increases tetrahedral Al and minimises A-site atoms. Thus in Figure 3-29a, 25% of the analyses would be classified as edenite or edenitic hornblende instead of magnesium hornblende (Fig. 3-27b). Petrographic observations suggest the latter name is preferred.

Site allocation followed in this study calculates an analysis on the basis of 46 + Ti (Ti=Ti atoms in cell) charges and adjusting Fe^{2+}/Fe^{3+} to reduce the cation

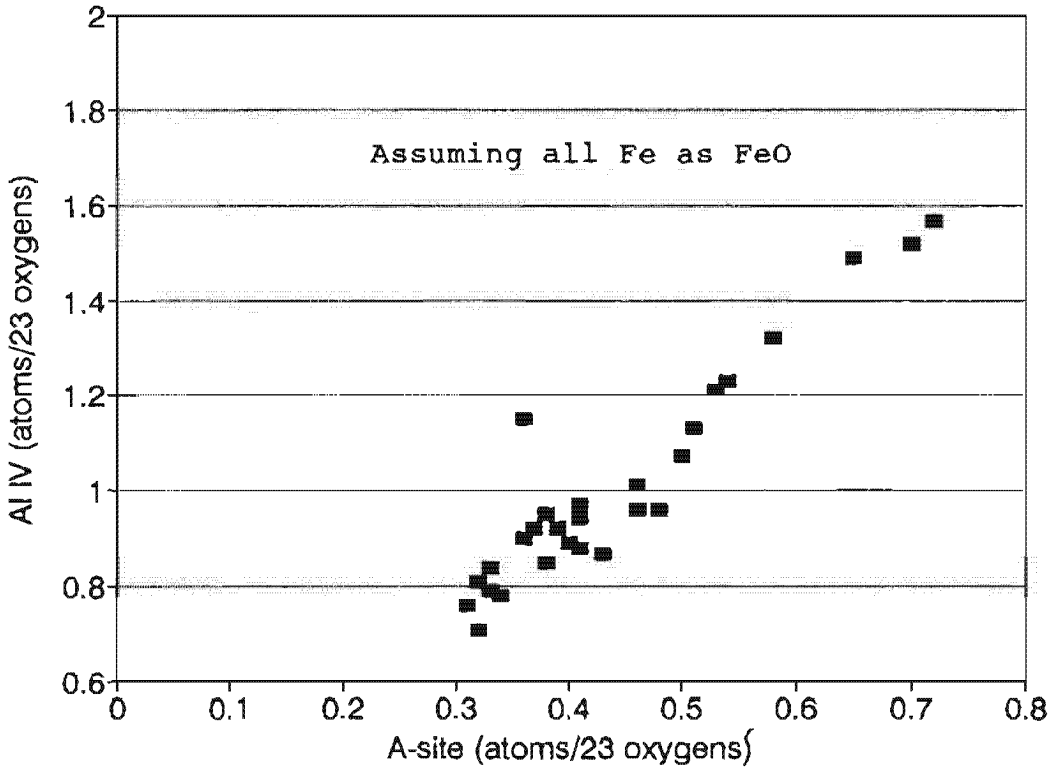

Figure 3-27a. Effect of ferric iron on tetrahedral Al and A-site atoms in amphibole. (compare to Figure 3-27b)

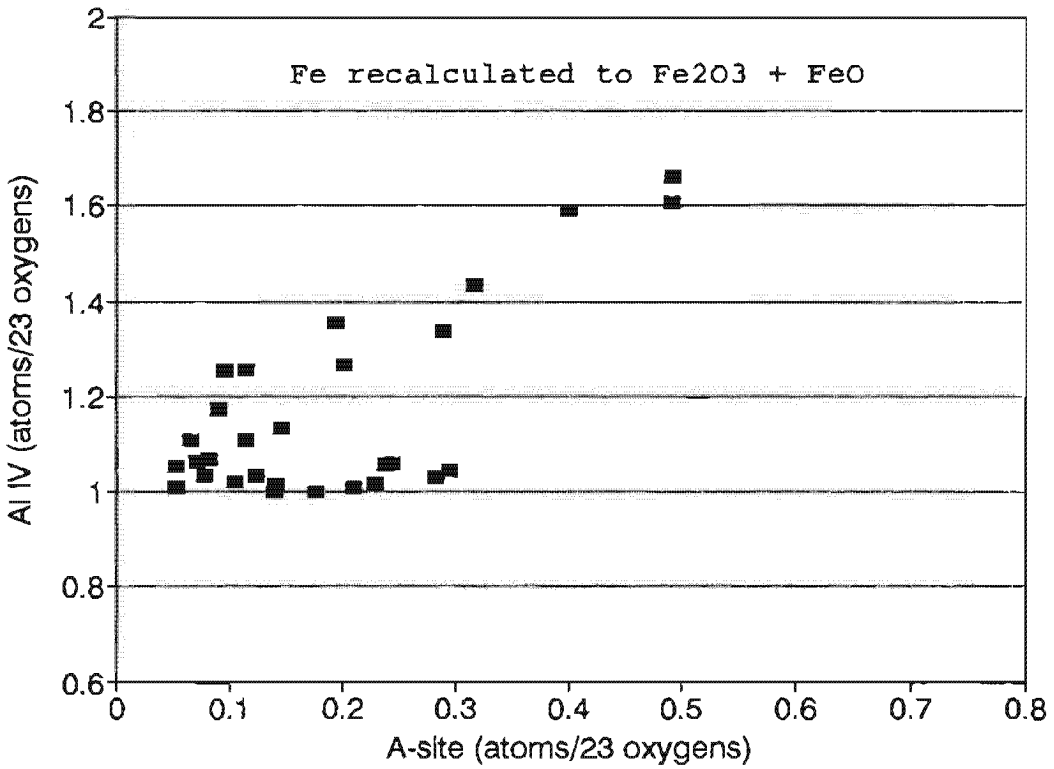

Figure 3-27b. Effect of entry of ferric iron on Al and A-site atoms in amphibole.

sum to 13 for cases in which Na + Ca exceeds 1.34, assuming crystal chemical limits outlined by Robinson et al (1982). Although alternative schemes are possible (normalising to differing cation sums) the chosen method allows Na to be distributed between the A and B sites, as Jaffe et al (1978) suggests for calcic amphiboles. An algorithm using this scheme with assignment to endmembers (in mol%) based on the classification of Leake (1978) is fully discussed by Currie (1991). Results of the recalculation are given in Tables A3-5a and A3-5b, Appendix 3-2.

All the amphiboles are calcic, with magnesium-ferri hornblende (Fig. 3-28) occurring at Mt Apo and Camiguin Island. In the latter, lower Si (6.733-6.340 atoms per formula unit [pfu]) contents results in compositions close to tschermakitic or barroisitic endmembers. In all cases $Al^{(IV)}$ is always sufficient to fill the T site and the minimum value of 1.000 (silicic hornblendes) suggest crystallisation above subsolidus conditions, by analogy with experimentally produced igneous hornblendes (Helz, 1982). Figure 3-29 shows $Al^{(IV)}$ plotted against Ti content. The general slope approaches that of Ti-Tschermakite substitution ($Al^{(IV)}$:Ti=2:1) for andesites whereas flat trends distinguish dacites. Overall Ti contents are low (0.1 - 0.2 atoms pfu). Holloway and Burnham (1972) suggest that Ti in amphibole is strongly dependent on fO_2 and observed low Ti content where hornblendes crystallised at the Hematite-Magnetite buffer.

Amphibole compositions along with analyses from coexisting Ca-rich pyroxenes are projected onto the SiO_2-FeO-Na_2O+K_2O and MgO-FeO-Na_2O+K_2O planes (Fig. 3-30). Amphiboles are always less magnesian than augites (Fig. 3-30a) as shown by lower Mg/Mg+Fe (0.72 - 0.81 vs. 0.76 - 0.82 for andesites; 0.75-0.76 vs 0.76 - 0.77 for dacites), but the difference becomes less apparent in dacites. Amphiboles are also strongly undersaturated, relative to pyroxenes (Fig. 3-30b). Thus fractionation of hornblendes limits Fe enrichment in intermediate to dacitic melts. Relative to andesites, hornblendes from dacites generally have lower total Fe

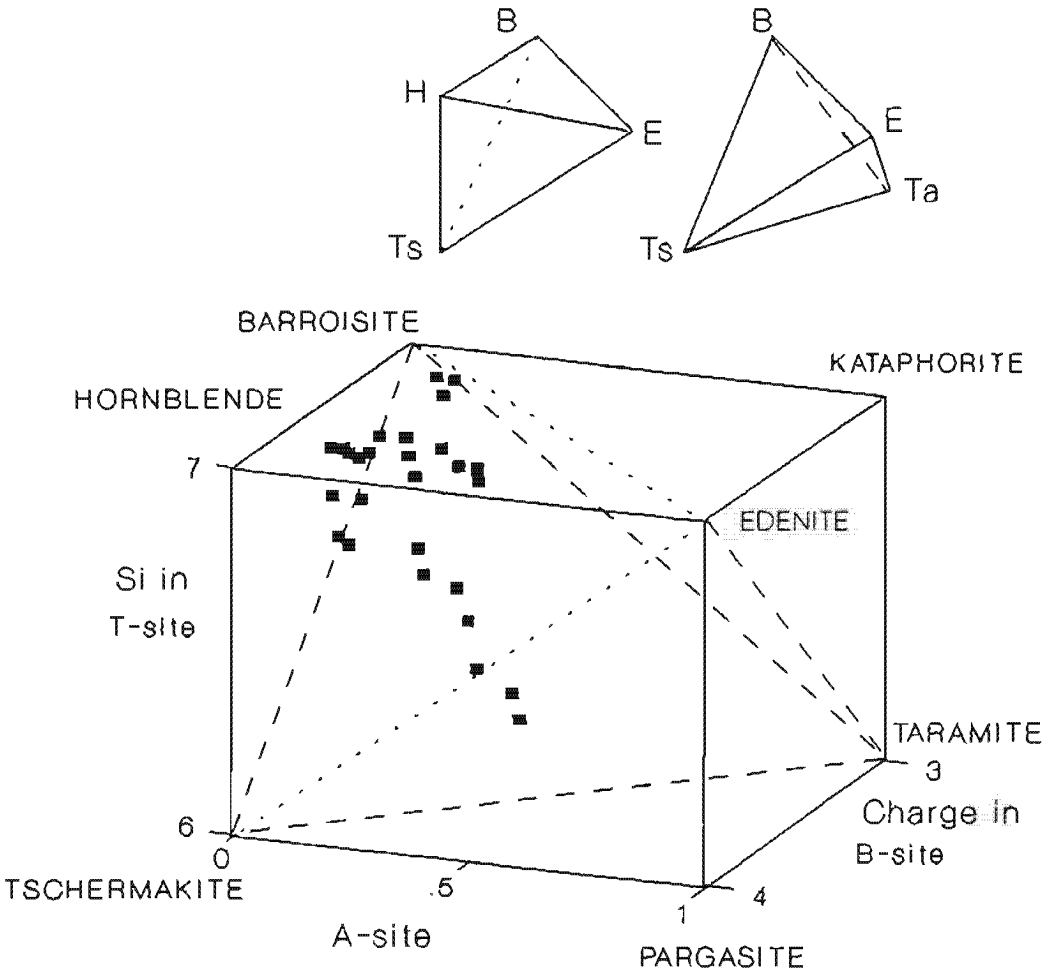

Figure 3-28. Plot of A, B(charge) and T site occupancies in amphibole composition space for Mt Apo and Camiguin Island lavas. Analyses plotted are from Tables A3-5a to b, Appendix 3-2.

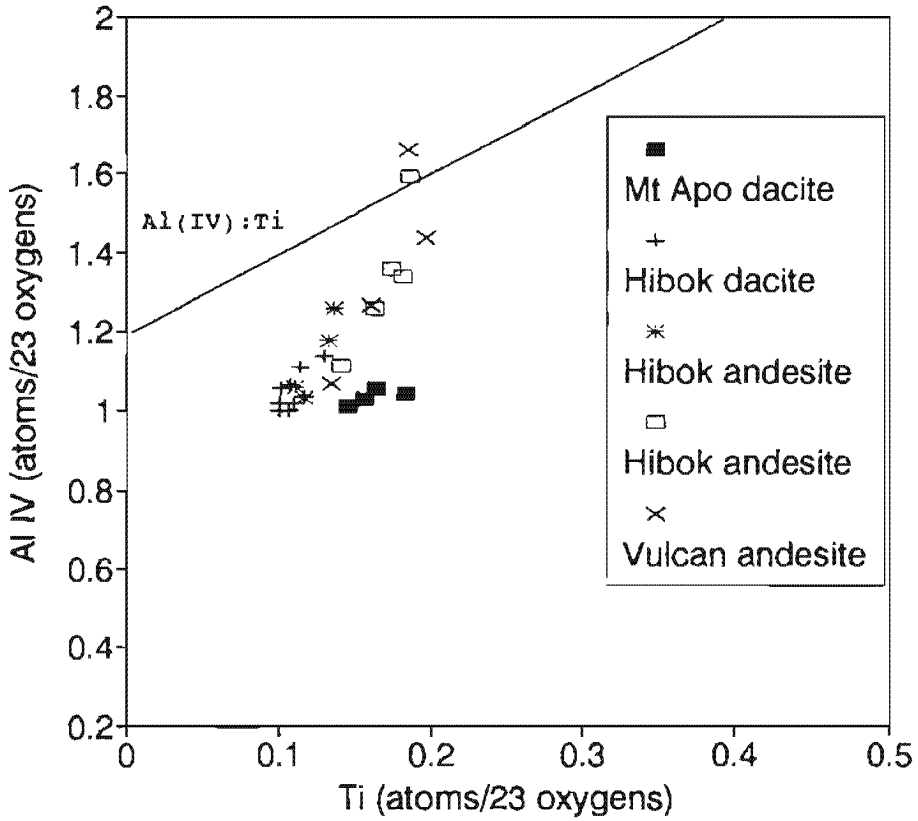

Figure 3-29. Al(IV) - Ti distribution in amphiboles of SiO2-rich lavas.

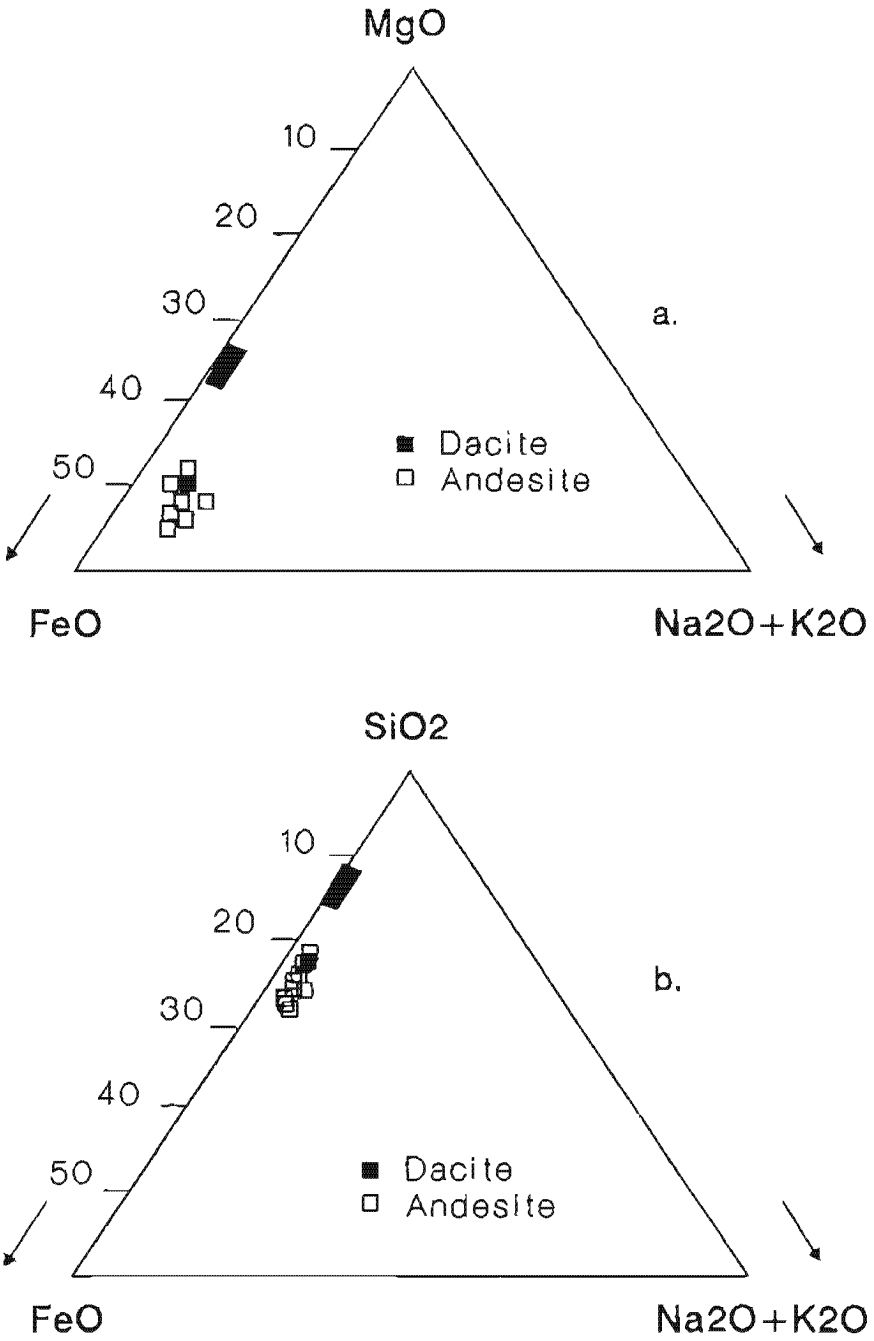

Figure 3-30. Oxide variation diagrams for hornblende (squares) and co-existing clinopyroxene (filled bars). Selected data from Appendix 3-2.

(Fig. 3-30a), a reflection of low Fe contents in the host rocks, during the late-stage crystallisation sequence.

CHAPTER IV GEOCHEMISTRY

4.1. INTRODUCTION

Previous studies (Phil. Bureau Mines, 1982; Datuin, 1982) suggest a broad volcanic region in eastern Philippines, from SE Luzon to central Mindanao, comprises a tholeiitic-calcalkaline-alkaline progression (Fig. 4-1). However, it is unlikely that a simple compositional variation occurs across a collision complex of two mature facing arcs. There are also few chemical analyses in previous studies to characterise the CMVA. An intriguing concept presented by Uyeda and McCabe (1982) relates central Mindanao volcanics to back-arc spreading but as in previous studies, no geochemical data in support of this idea was presented. To provide geochemical constraints on the source and evolution of the CMVA, this chapter presents new major and trace element compositions.

4.2. SAMPLE PREPARATION AND ANALYTICAL METHODS

Fused glass disks for major element analysis were made following the general methods of Norrish and Hutton (1969), Harvey et al (1973) and Schroeder et al (1980). Specimens were broken down into chips using a hydraulic crusher with tungsten carbide jaws. About 400 gm of material was then transferred to a tungsten carbide swing mill and ground into approximately B.S. 240 mesh. Dried powder samples, each about 0.30 gm, were mixed with Lithium tetraborate-Lithium carbonate-Lanthanum oxide flux and ammonium nitrate oxidant in Pt/Au crucibles and then fused in an electric furnace at 1,000^{o}C for 15-20 minutes. After careful weighing to determine loss on ignition, each melt was poured into an aluminium platten and pressed to form a bead. Trace elements were measured on 50mm diameter pressed powder pellets using approximately 15 gm of rock powder mixed with 20-25 drops of polyvinyl alcohol binder. Each mixture was formed into a disk

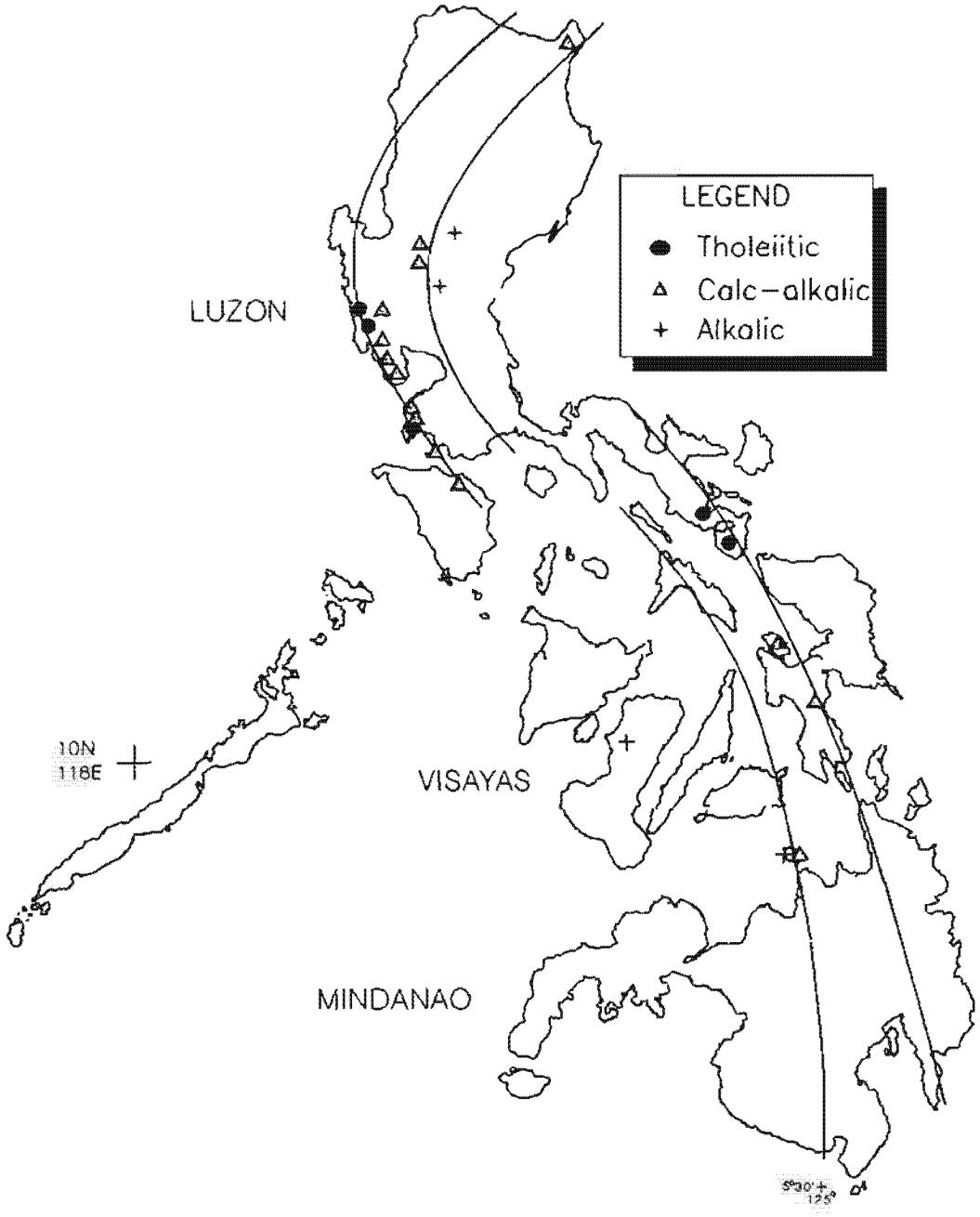

Figure 4-1. Outline map of the Philippines showing proposed zonation of tholeiitic-calcalkalic-alkalic suites by Datuin (1982).

using a pneumatic steel die and then transferred into an oven at 60°C until dry. The glass beads and powder pellets were stored in polyvinyl sachets and placed in a dessicator prior to analysis.

Major and trace element concentrations were determined at the University of Canterbury geochemistry laboratory using a Philips PW 1400 X-ray spectrometer. Analyses of rock standards for major elements using Sc and Cr tubes are listed in Appendix 4-1. Trace elements V, Cr, Ni, Zn, Sr, Zr, Nb, Ba, La, Ce, Nd and Ga, Pb, Rb, Sr, Th Y were analysed using Au and Mo tubes. Mass absorption corrections were made using Compton and Rayleigh tube lines.

4.3. CLASSIFICATION

The total alkali-silica diagram (TAS) in Figure 4-2 initially classifies CMVA lavas into subalkaline and alkaline compositions. The subalkaline group clearly displays the main characteristics of calk-alkaline (CA) island arc volcanics. These are generally Q and hy normative (Table 4-1; Appendix 4-2) with no pronounced Fe-enrichment (Fig. 4-3).

Samples which plot within the alkaline field, mainly from Mt Balatocan lavas, are not appropriately classified by TAS because their modal and normative mineralogies suggest subalkaline compositions. Using the cpx-ol-ne'-Q tetrahedron (Fig. 4-4), nearly all CMVA lavas are subalkaline. Normative classification is probably more accurate than TAS because more components are considered.

High-alkali Mt Balatocan samples also have relatively high FeO* and FeO*/MgO ratios (Fig. 4-5) suggesting a tholeiitic (TH) affinity. However, in the classification of Irvine and Barager (1971), all samples plot within the calcalkaline field (Fig. 4-3). In Miyashiro's (1974) CA-TH discriminant diagram, some Mt Balatocan samples occur within the CA field.

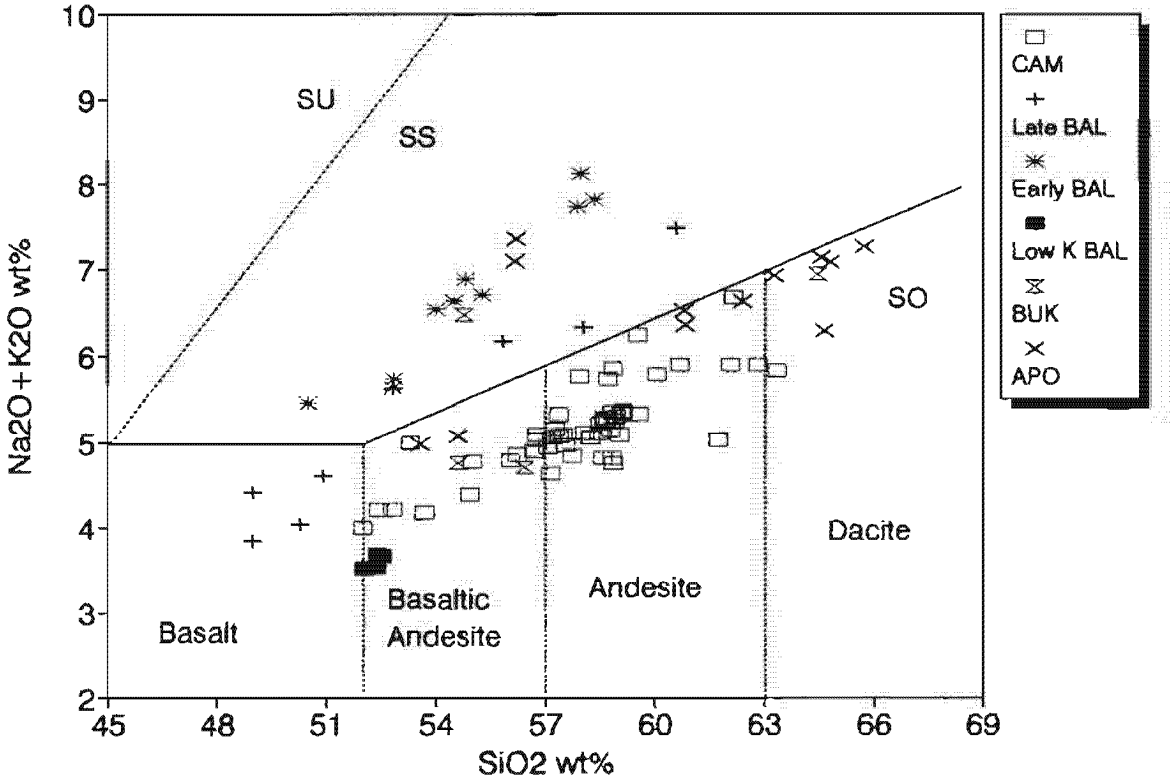

Figure 4-2. Total alkali-silica diagram (TAS) for CMVA lavas. Abbreviations: CAM, Camiguin Island; BAL, Mt Balatocan; BUK, Bukdnon volcanoes; APO, Mt Apo. Fields defining SU, SS and SO (silica undersaturated, silica saturated and silica oversaturated) are from Le Maitre (1989).

Table 4-1. Representative and average analyses of CMVA lavas.

	CAMIGUIN ISLAND			MT BALATOCAN						BUKIDNON					MT APO		
				Late			Early										
Analysis #	36		45	54		59	60		69	75	77	76	78	79	80		89
Code	A	B	C	A	B	C	A	B	C	BUT6	QUE7	KAL8	MUS15	KAT9	A	B	C
SiO2 wt%	52.03	58.02	63.38	48.98	52.96	60.60	50.52	54.91	58.35	52.40	54.63	54.79	56.47	64.48	53.58	60.59	64.85
TiO2	0.83	0.63	0.89	0.91	0.83	0.50	0.82	0.93	0.99	1.12	0.84	1.01	0.75	0.58	0.83	0.67	0.51
Al2O3	18.53	17.84	19.32	19.01	18.91	18.71	20.95	18.45	17.05	16.60	16.60	17.14	16.97	16.97	19.05	17.28	16.28
Fe2O3	2.13	1.53	2.13	2.37	1.89	1.11	1.82	1.85	1.74	2.28	1.69	1.77	1.65	0.94	2.13	1.36	1.00
FeO	7.08	5.08	7.08	7.92	6.30	3.69	6.06	6.17	5.81	7.60	5.64	5.91	5.53	3.11	7.13	4.53	3.34
MnO	0.14	0.14	0.21	0.19	0.16	0.13	0.16	0.17	0.18	0.16	0.13	0.14	0.14	0.09	0.19	0.13	0.10
MgO	5.72	3.73	6.06	5.63	4.04	1.67	3.51	2.89	2.01	7.46	7.81	4.71	6.16	2.20	4.15	2.74	1.87
CaO	9.32	7.59	9.69	10.91	9.39	5.75	10.28	7.38	5.45	8.61	7.68	7.43	7.35	4.42	7.56	6.00	4.79
Na2O	3.03	3.64	4.71	2.86	3.16	3.63	2.97	3.95	4.67	3.15	3.45	3.68	3.32	4.12	3.34	3.51	3.67
K2O	0.97	1.52	2.83	0.99	2.03	3.86	2.48	2.77	3.15	0.47	1.30	2.79	1.39	2.82	1.65	2.93	3.42
P2O5	0.22	0.28	0.43	0.23	0.33	0.36	0.42	0.51	0.59	0.15	0.24	0.62	0.27	0.26	0.40	0.26	0.18
*FeO**	8.88	2.19	3.04	10.13	7.94	4.61	7.68	7.78	7.34	9.64	7.12	7.42	6.92	3.92	8.87	5.68	4.20
Mg#	0.59	0.57	0.60	0.56	0.53	0.45	0.51	0.46	0.38	0.65	0.71	0.59	0.67	0.56	0.51	0.52	0.50
Q	0.51	8.32	16.92	0	2.44	9.48	0	1.76	4.86	1.98	1.65	1.02	6.41	16.29	3.1	11.48	17.11
or	5.67	8.90	16.55	5.91	11.84	22.4	14.6	16.26	18.56	2.78	7.62	16.31	8.1	16.55	9.57	17.06	20.03
ab	25.3	30.59	39.69	24.2	26.51	30.21	25.05	33.21	39.09	26.65	29.02	30.72	27.67	34.61	28.69	29.47	30.8
an	33.65	27.62	33.65	35.78	31.00	22.96	36.37	24.30	16.4	29.71	25.79	21.75	26.93	19.32	31.87	22.44	17.69
C	0	0.00	0.00	0	0.00	0	0	0.00	0	0	0	0	0	0	0	0.00	0
di	8.64	6.51	12.38	13.66	10.70	2.3	9.59	7.23	5.51	9.66	8.4	8.66	5.86	0.62	2.15	4.29	3.86
hy	19.85	12.98	19.85	5.05	6.61	7.03	0.11	9.19	8.39	22.08	21.37	13.48	18.33	8.3	17.12	9.53	6.3
ol	0	0.25	12.90	8.26	3.72	0	7.76	0.78	0	0	0	0	0	0	0	0.00	0
mt	3.04	2.19	3.04	4.89	3.84	2.23	3.71	3.76	3.55	4.66	3.44	3.58	3.34	1.9	4.28	2.75	2.03
il	1.56	1.18	1.67	1.82	1.57	0.93	1.56	1.76	1.9	2.13	1.58	1.9	1.41	1.1	1.6	1.26	0.97
ap	0.51	0.64	1.00	0.53	0.74	0.81	0.97	1.18	1.39	0.35	0.56	1.41	0.63	0.6	0.93	0.60	0.42

Analyses recalculated to 100%, anhydrous. FeO calculated assuming Fe2O3/FeO=0.3. Original analyses given in Appendix 4. CIPW norms in wt%.
Cation norms used in ne'-ol-Q projection (Figure 4-4). Samples listed according to volcanic centre, north-south. Sample numbers, when given, refer to original analyses in Appendix 4.
Codes: A = most SiO2-poor in series; B = average composition in series; C = highest SiO2 sample in series. When field codes are given, these refer to individual analyses.

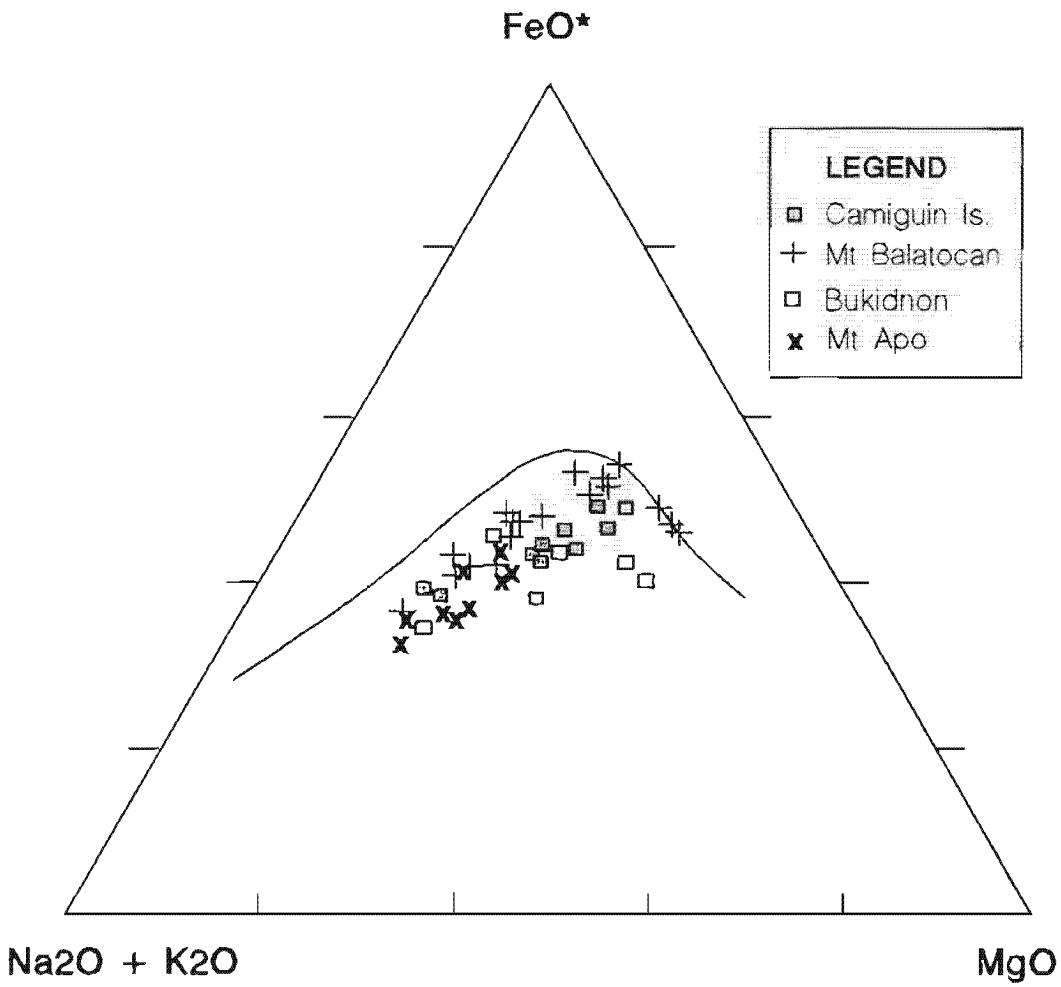

Figure 4-3. AFM plot of representative CMVA lavas showing general CA trend. Mt Balatocan lavas exhibit the highest FeO*/MgO ratios but plot within the CA field of Irvine and Barager (1971).

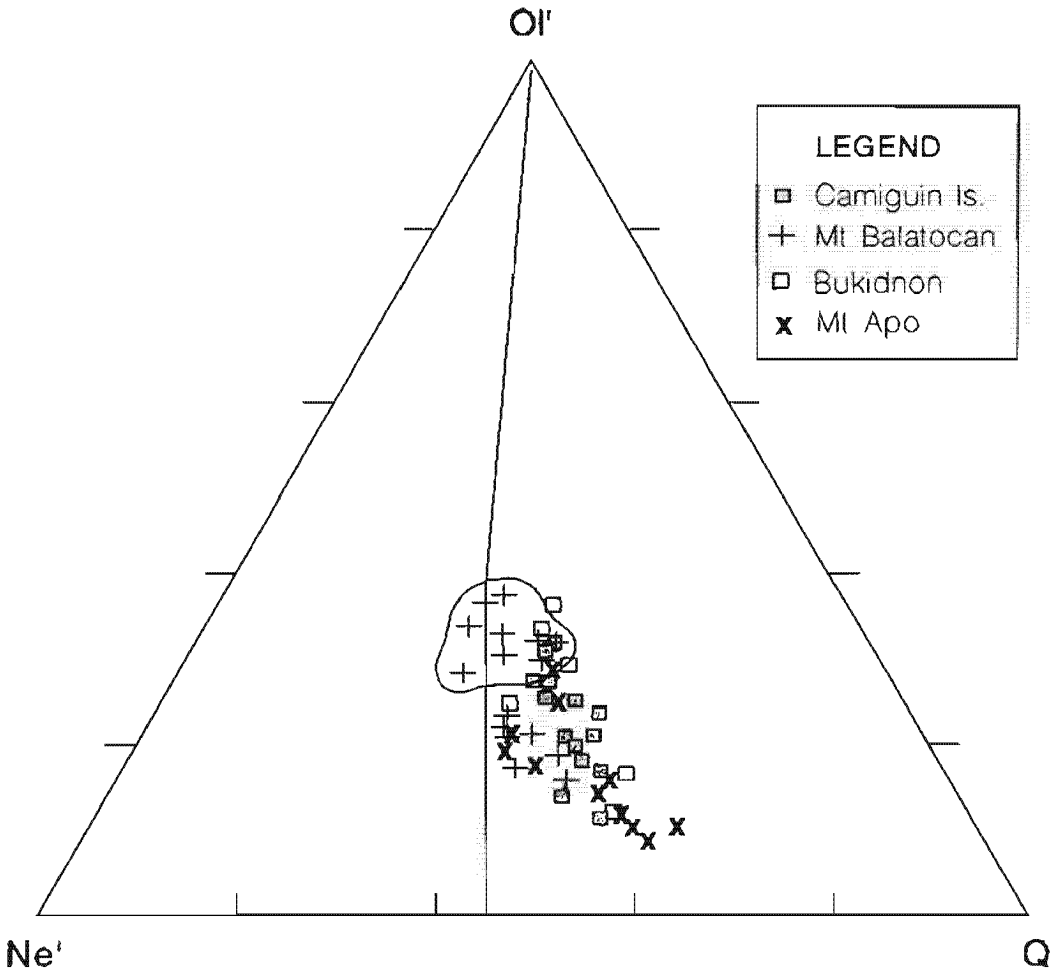

Figure 4-4. Projection of CMVA lavas onto basal triangle ne'-ol-Q of the cpx-ol-ne'-Q tetrahedron. Dividing plane between SiO2-undersaturated (Ne') and SiO2-oversaturated fields are taken from Irvine and Barager (1971). Enclosed samples are from high-K early Mt Balatocan.

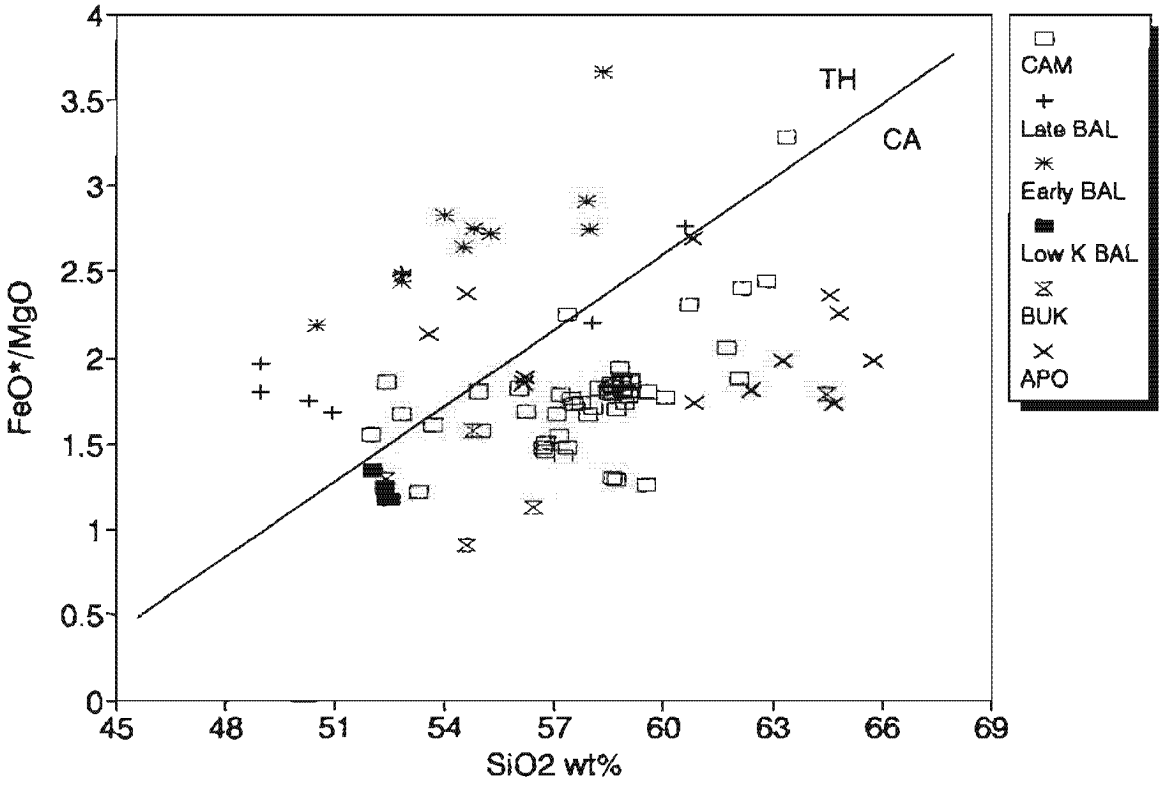

Figure 4-5. Discrimination of high FeO*/MgO ratios for CMVA lavas. Mt Balatocan samples have generally higher FeO*/MgO ratios than for other volcanoes. Dividing line between TH (tholeiitic) and CA (calcalkaline) fields is derived from Miyashiro (1974).

Figure 4-6 also shows that high total alkali contents in Mt Balatocan lavas are achieved by a high and increasing proportion of normative Or. This leads to the preferred classification of CMVA lavas summarised by the K_2O-SiO_2 diagram (Fig. 4-7). A majority of these samples plots as medium-K CA basalts, andesites and dacites with few samples occurring as high-K CA lavas. Mt Balatocan lavas can be further distinguished on the basis of stratigraphy. Lavas which form an early to mid-Quaternary formation, designated informally as *early* Mt Balatocan, consistently plot as high-K CA basalt to andesite. Overlying late Quaternary and Recent lavas which form Mt Balatocan proper are here called *late* Mt Balatocan lavas, and are classified as medium to high-K CA basalt and andesite.

4.4. GEOCHEMISTRY OF CMVA LAVAS

This section discusses the main regional chemical variations based on analyses recast to 100%, anhydrous basis. Table 4-1 gives representative chemical analyses of each major volcanic centre. Appendix 4-2 gives original whole-rock compositions.

4.4.1. MAJOR ELEMENTS

(i) K_2O and Na_2O

The alkalis show positive correlation with SiO_2. As shown by comparison of Figures 4-8 and 4-9, the rate of increase in K_2O is greater than Na_2O for most of the CMVA, except early Mt Balatocan. K_2O also more readily discriminates between lavas from different volcanic centres. Variations in K_2O content are reflected not only by oxide abundances but also by different slopes defined by trendlines (i.e. different K_2O-SiO_2 ratios). These differences are not as apparent in terms of Na_2O since nearly all samples except for Mt Balatocan lavas exhibit low Na_2O-SiO_2 gradients. This leads to a general increase in K_2O/Na_2O ratios with increasing K_2O, from average values of 0.42 (Camiguin Island) to 0.67 (Mt Balatocan) to 0.87 (Mt Apo).

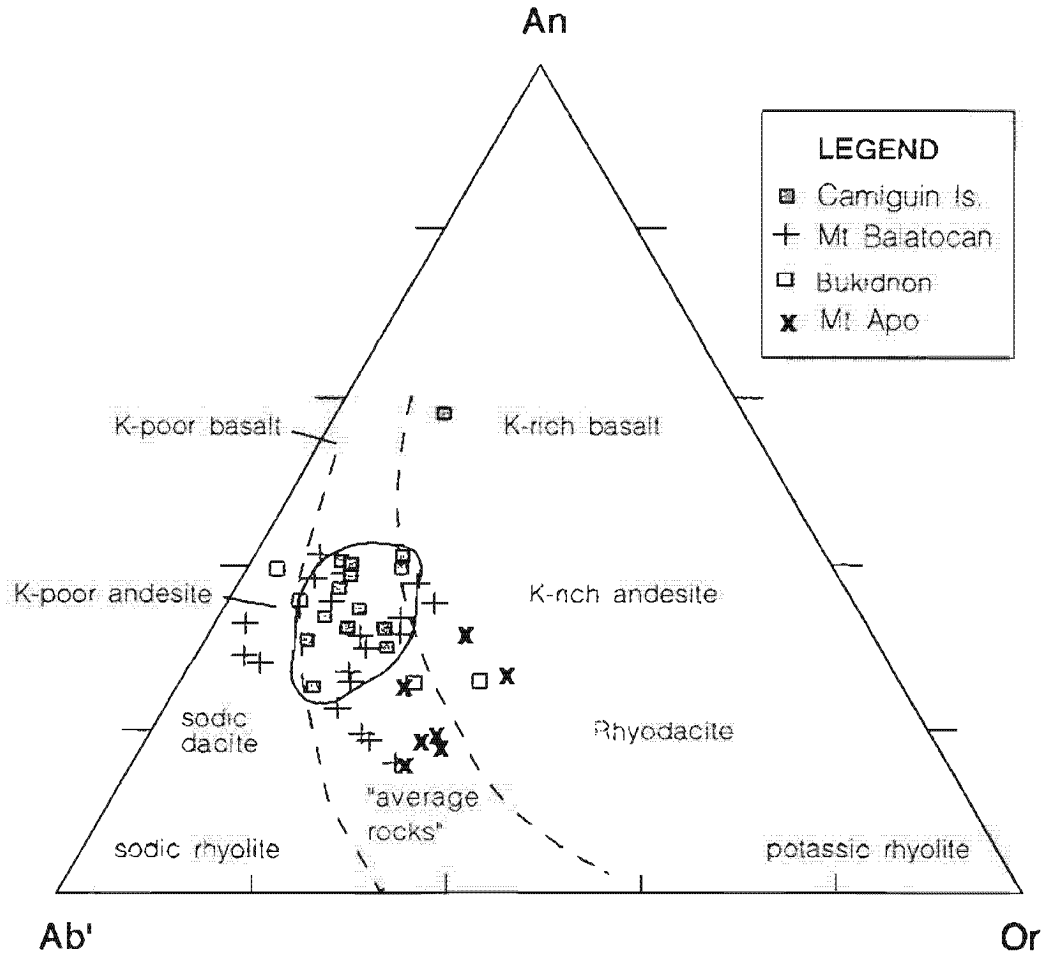

Figure 4-6. Distribution of CMVA lavas with respect to normative Ab, An and Or. Mt Balatocan samples show a trend from K-poor andesite to K-rich andesite. Mt Apo also exhibit increased K contents from andesite to dacite. Solid line field encloses Camiguin Island lavas which plot within the "average rocks" field. Field names and boundaries (dashed curves) are from Irvine and Barager (1971).

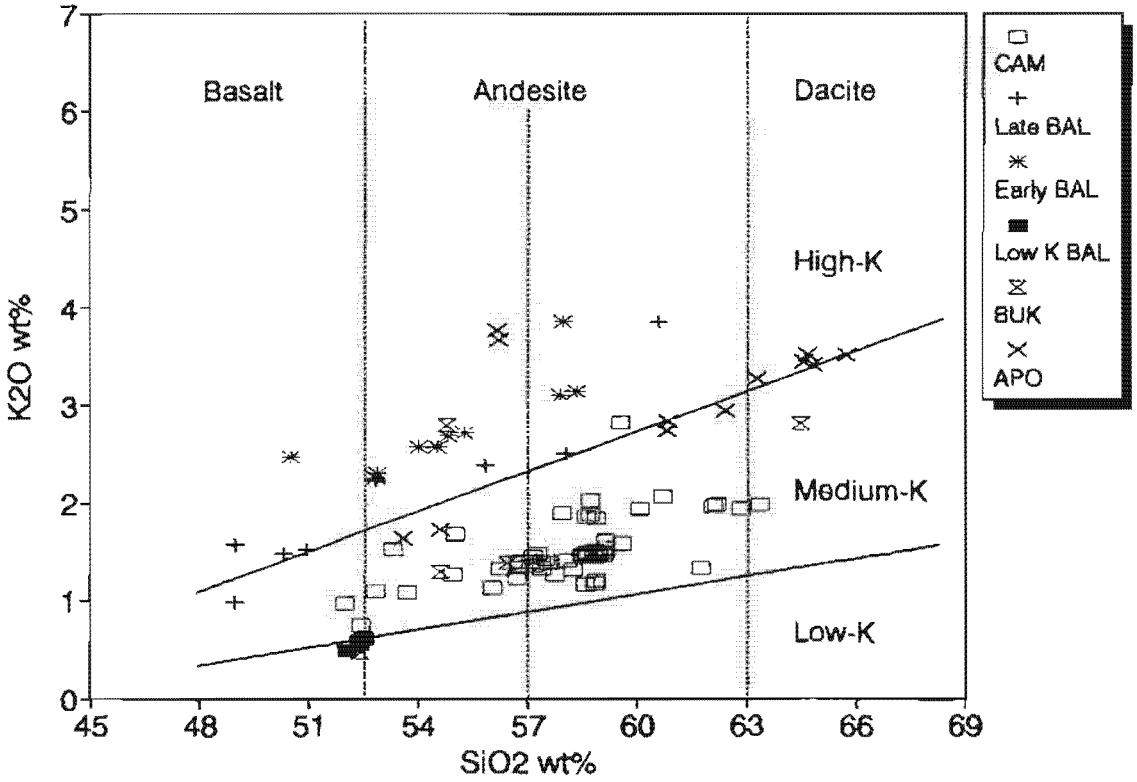

Figure 4-7. Variation of K_2O with SiO_2 showing predominantly medium-K andesites in CMVA. Mt Balatocan lavas typically plot within high-K fields and have characteristics of either calcalkaline or tholeiitic suites. Field boundaries after Le Maitre (1989) and Le Bas (1991). Abbreviations as in Figure 4-2.

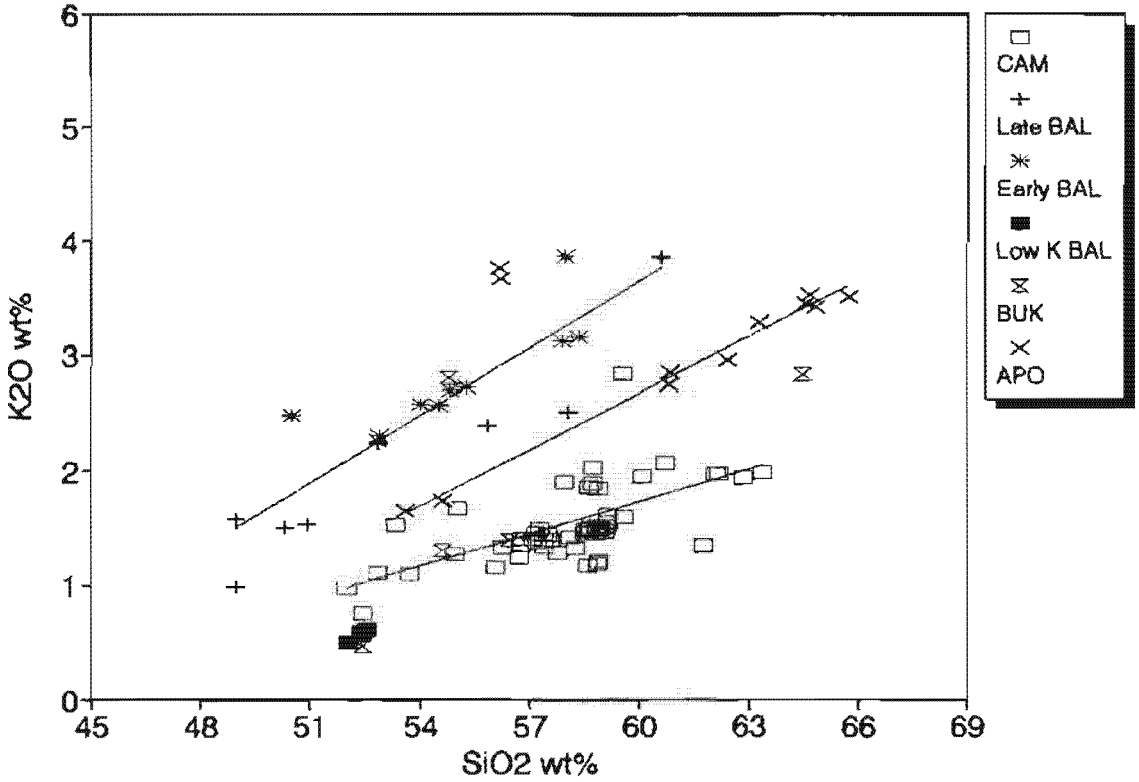

Figure 4-8. Grouping of CMVA lavas defined by different K_2O-SiO_2 distributions. Trendlines are simple linear regressions of each lava group. Low-K Mt Balatocan samples are not included in the trendline as they are not considered comagmatic with the rest of the Mt Balatocan group. Abbreviations as in Figure 4-2.

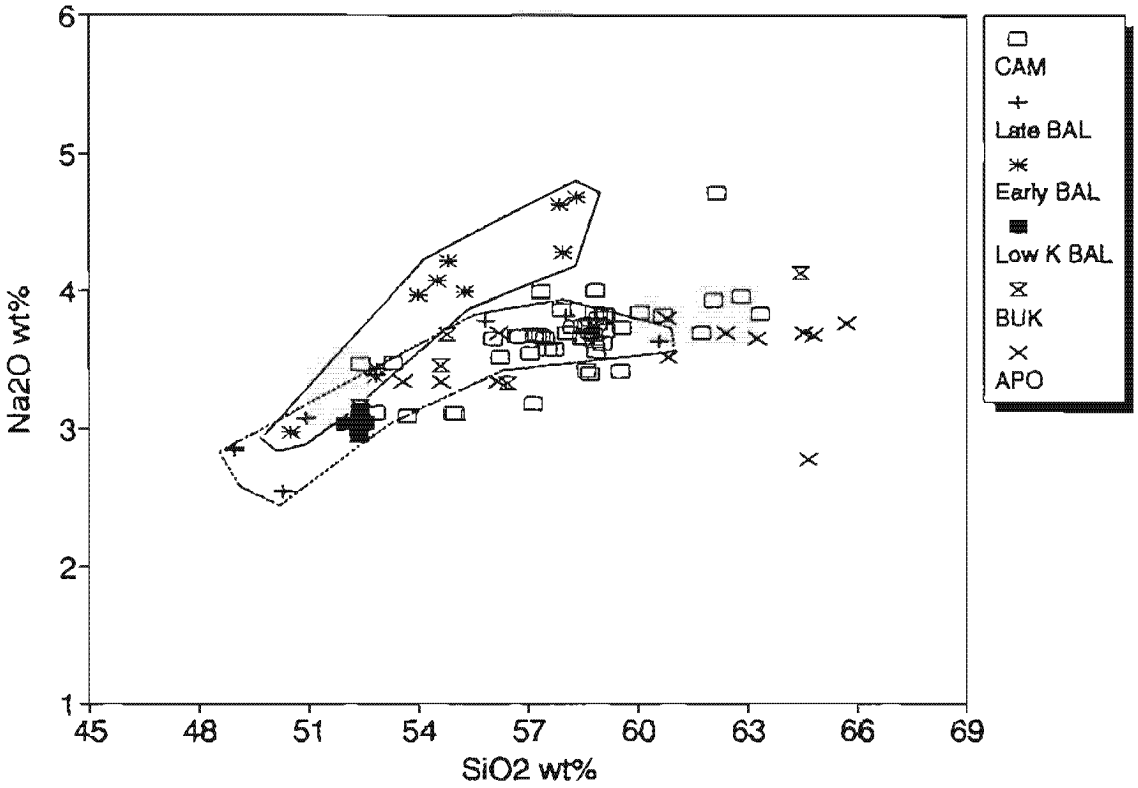

Figure 4-9. Na_2O concentrations in CMVA lavas. Na_2O trends increases slightly across the majority of suites, except for early Mt Balatocan samples (enclosed by solid line) which show enrichment comparable to K_2O. Initial enrichment is also observed for late Mt Balatocan lavas (dotted line field). Abbreviations as in Figure 4-2.

(ii) FeO*, MgO and TiO_2.

Total Fe (as FeO^*) ranges from 10.1 - 3.7 wt% and shows strong linear relationship with SiO_2 (Fig. 4-10). Plots of SiO_2-FeO^* for each major volcano shows two trends. The main CA suite exhibits a linear decrease in FeO^* throughout the compositional range. A second trend, demonstrated by early Mt Balatocan lavas (Fig. 4-11), shows FeO^* increases to a maximum at about 54.5 wt% SiO_2 and then decreases to parallel the main CA sequence.

MgO contents, of each volcanic centre, vary more than any other major oxide (Fig. 4-12). Although K_2O displays the same degree of variation (1 - 2 wt%) between different volcanic centres, scattered patterns of MgO show significant differences within groups of related lavas. Large differences in MgO contents of basalts probably reflect inhomogeneous starting compositions or indicate accumulation of olivine. Some phenocryst-rich basalts indicate early fractionation of olivine (± spinel) and clinopyroxene to account for relatively low Mg numbers (Mg#).

TiO_2 has trends similar to FeO^* and MgO (Fig. 4-13). All lavas show decreasing concentrations with respect to SiO_2 (CA trend) except for early Mt Balatocan lavas which increase between 51 - 58 wt% SiO_2. Delayed fractionation of magnetite probably accounts for the initial increase in TiO_2 and FeO* and may suggest a tholeiitic trend. However, sample 23248 (Appendix 4-2) which occurs in the same suite exhibits the typical CA trend.

(iii) CaO, Al_2O_3, P_2O_5 and MnO.

CaO generally decreases with SiO_2 (Fig. 4-14) showing significant differences between CA suites. Most lavas exhibit a strong linear trend with SiO_2, probably caused by fractionating calcic-plagioclase and high-Ca clinopyroxene. High-K early Mt Balatocan andesites are relatively depleted in CaO compared to other andesites at similar SiO_2 levels, although there is no modal correspondence (Table 3-1) to indicate this relationship.

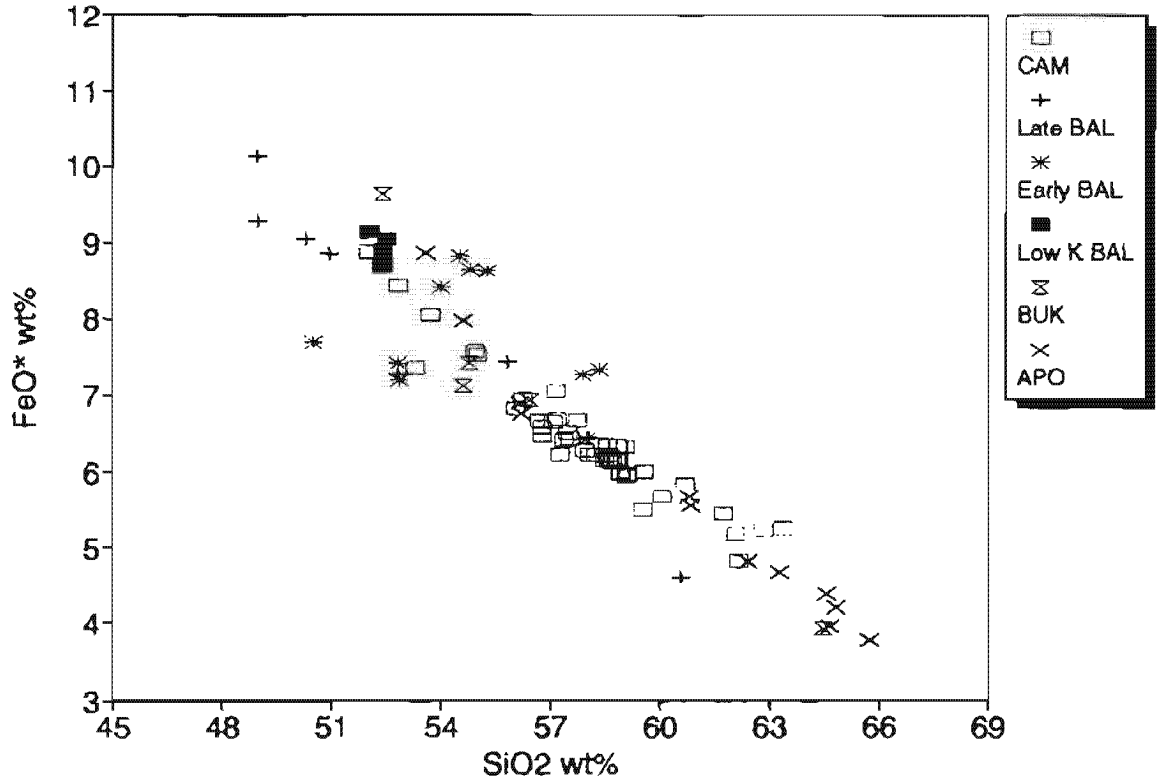

Figure 4-10. Variation of total Fe (as FeO*) in CMVA lavas, showing good linear relationship with SiO2. Early Mt Balatocan samples exhibit an initial increase in FeO*.

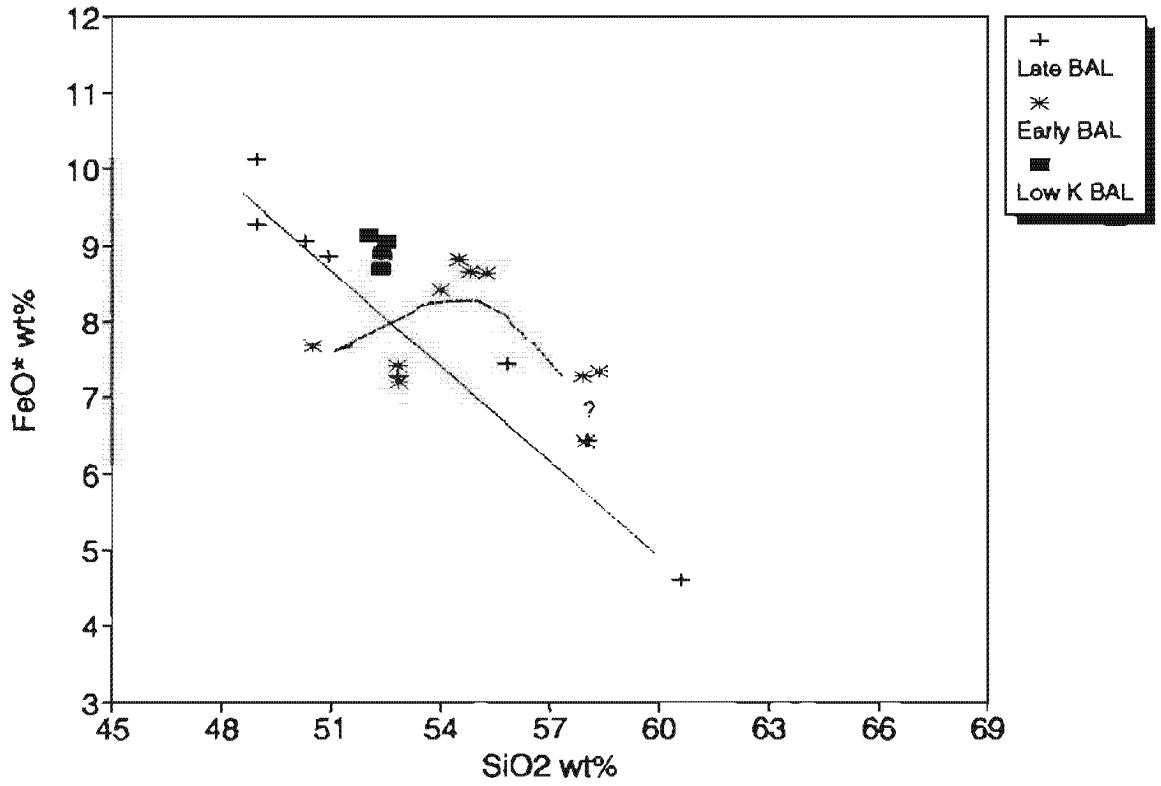

Figure 4-11. Same data as in Fig. 4-10 but showing only Mt Balatocan samples. Early "BAL" subset shows a moderate enrichment trend.

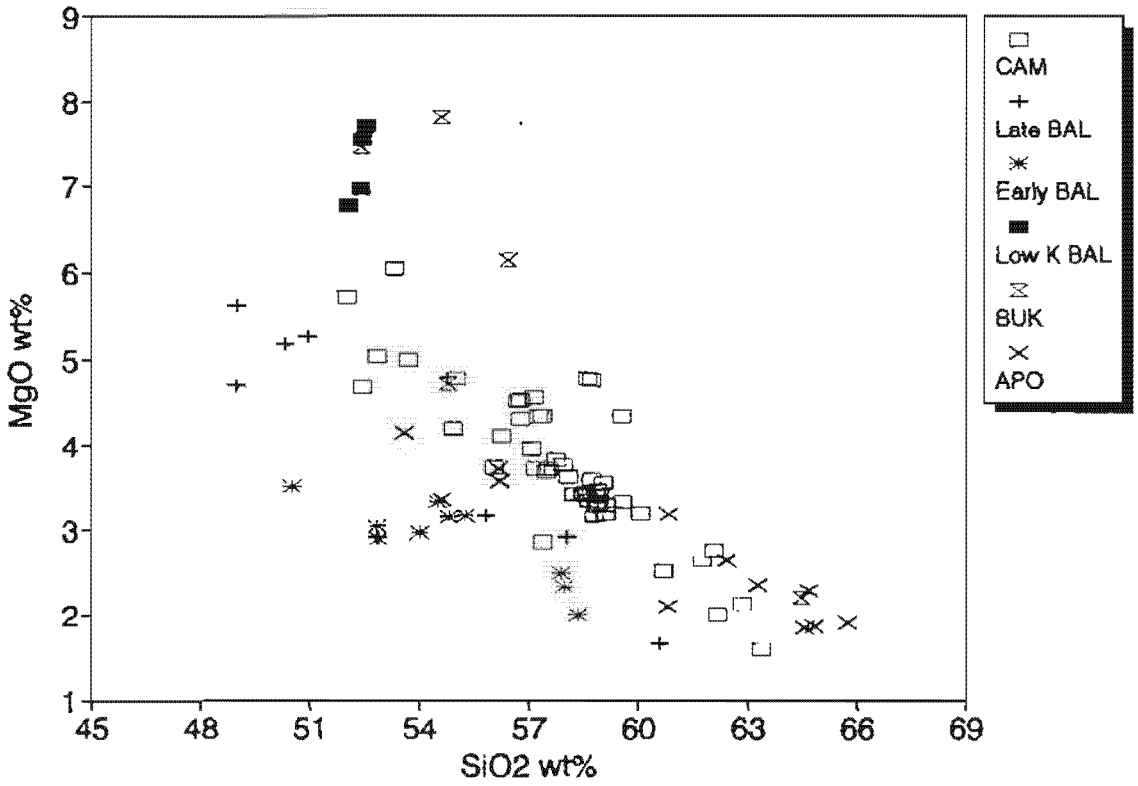

Figure 4-12. Change in MgO concentrations with SiO_2. Except for early Mt Balatocan and some Bukidnon lavas, MgO steadily decreases with increasing SiO_2. Some Bukidnon lavas (e.g. hornblende andesite, sample MUS15) have higher than usual MgO, probably reflecting olivine accumulation. Abbreviations as in Figure 4-2.

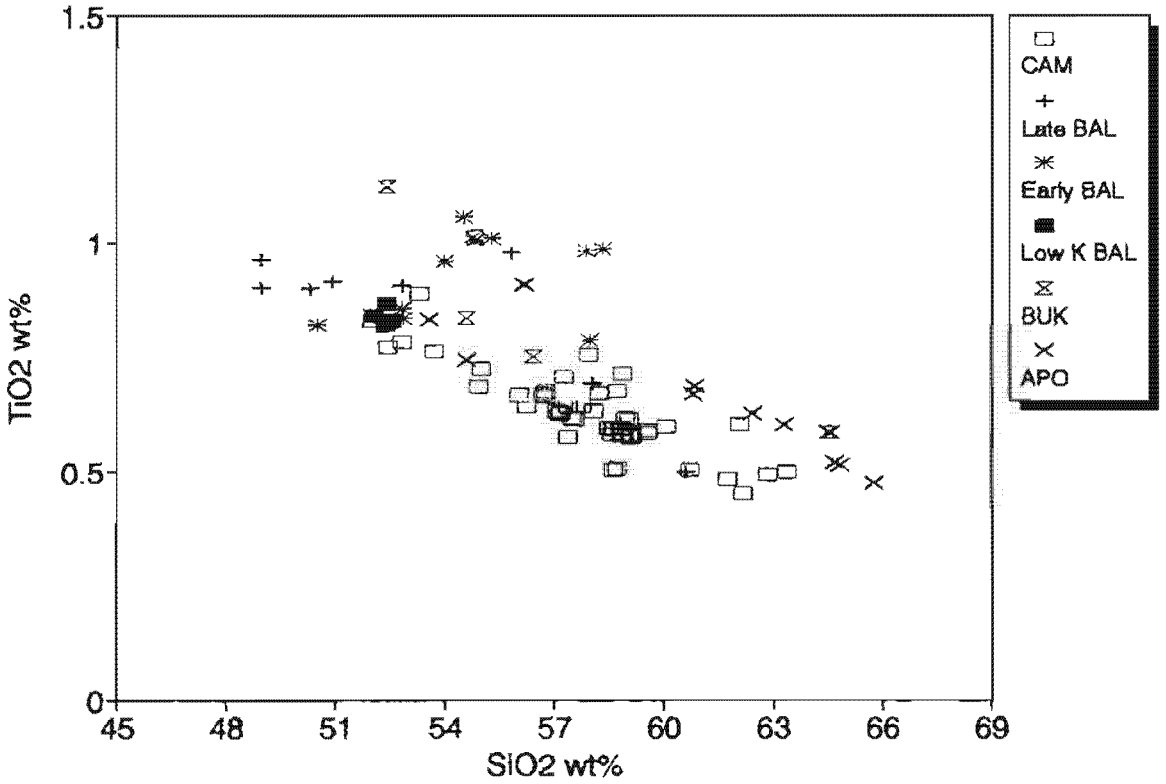

Figure 4-13. TiO_2 vs SiO_2 for CMVA lavas. Moderate increase in TiO_2 characterise most basaltic andesites from early Mt Balatocan lavas. The high FeO*, FeO*/MgO ratios and TiO_2 relative to other CA lavas of early Mt Balatocan samples may indicate delayed fractionation of Fe-Ti oxide phases. Abbreviations as in Figure 4-2.

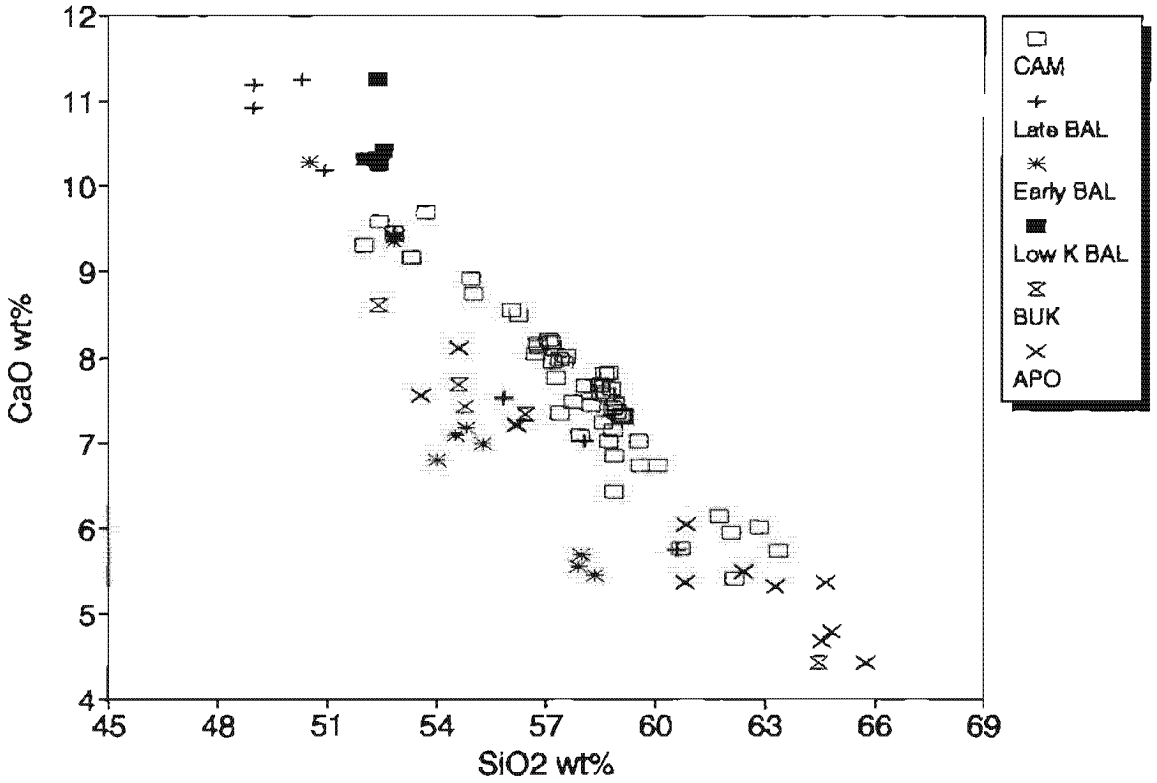

Figure 4-14.

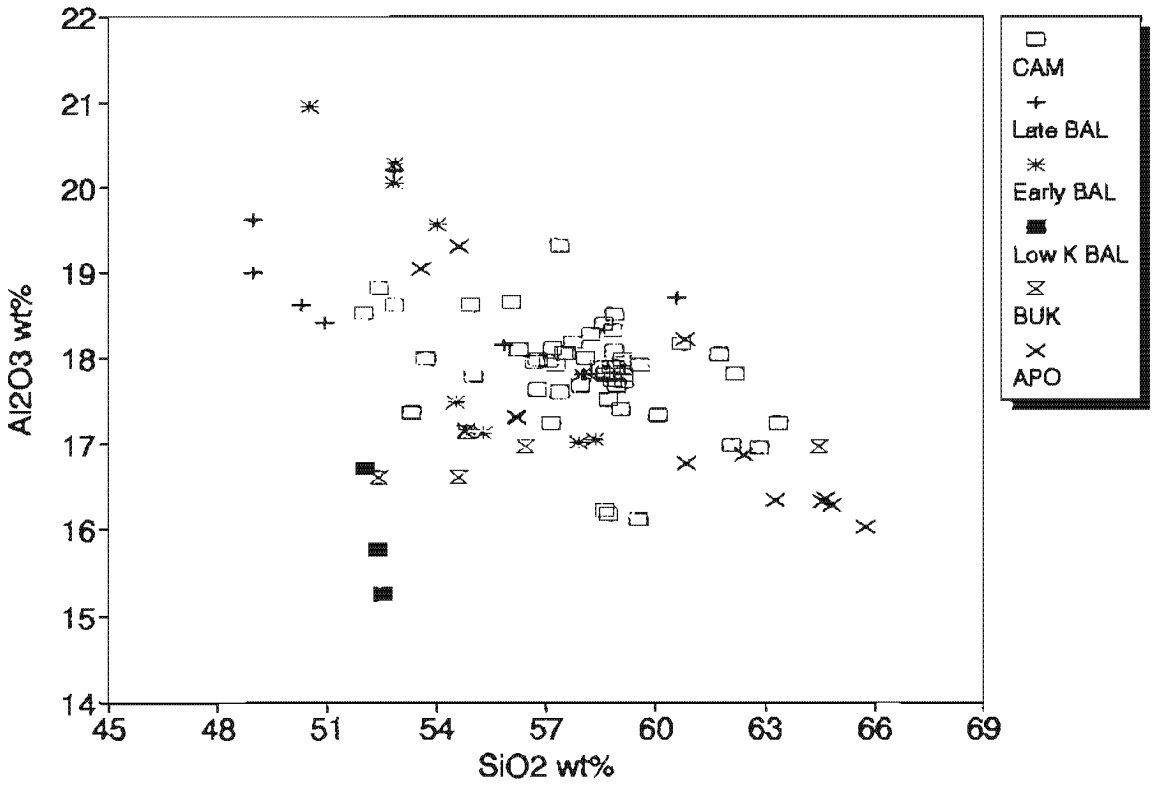

Figure 4-15. Al2O3 vs SiO2. Variable modal plagioclase contents (Table 3-1) probably accounts for most of the Al2O3 range.

Al_2O_3 also decreases with increasing differentiation (Fig. 4-15) but with greater intra-suite variations than CaO. Pronounced scatter in Al_2O_3 contents may also be attributed to plagioclase accumulation but there is no rigorous way to quantify this process. Plagioclase accumulation tends to increase CaO and reduces MgO and K_2O but this effect is not always apparent because Ca is significantly apportioned to other phases. Lack of plagioclase accumulation is, however, evident in some Mt Balatocan basalts which have low modal plagioclase (Table 3-1) and relatively low Al_2O_3 (15.2 - 16.7 wt%).

Two contrasting trends in P_2O_5 contents (0.15 - 0.62 wt%) are apparent in CMVA lavas. The dominant CA suites display relatively flat trends with small but significant intra-suite variations (0.2 - 0.3 wt%). In Camiguin Island, the greatest difference occurs between 57.0 - 58.5 wt% SiO_2 (Fig. 4-16) and then decreases steadily in dacites. This inflection probably marks crystallisation of apatite.

In early Mt Balatocan lavas, P_2O_5 correlates positively with SiO_2. From about 50.5 - 57.8 wt% SiO_2, P_2O_5 increases from 0.4 - 0.6 wt%, similar to the TH trend described by Anderson and Gottfried (1971). Sample 23248 is again the exception with a P_2O_5 content similar to some Camiguin Island CA samples. Late Mt Balatocan lavas have relatively constant P_2O_5 contents typical of other CA CMVA lavas.

MnO has overall low concentrations (0.1 - 0.22 wt%). MnO correlates negatively with SiO_2 and exhibits 2 distribution trends (Fig. 4-17). Firstly, MnO steadily decreases in basaltic and dacitic compositions (<53 and >62 wt% SiO_2). This is perhaps due to incorporation of Mn in olivine in basalts and in pyroxene of some SiO_2-rich andesites and most dacites (see Tables A3-2a and A3-35c, Appendix 3-2). The second type of distribution shows considerable scatter in andesites presumably because of large variations in either pyroxene and magnetite,

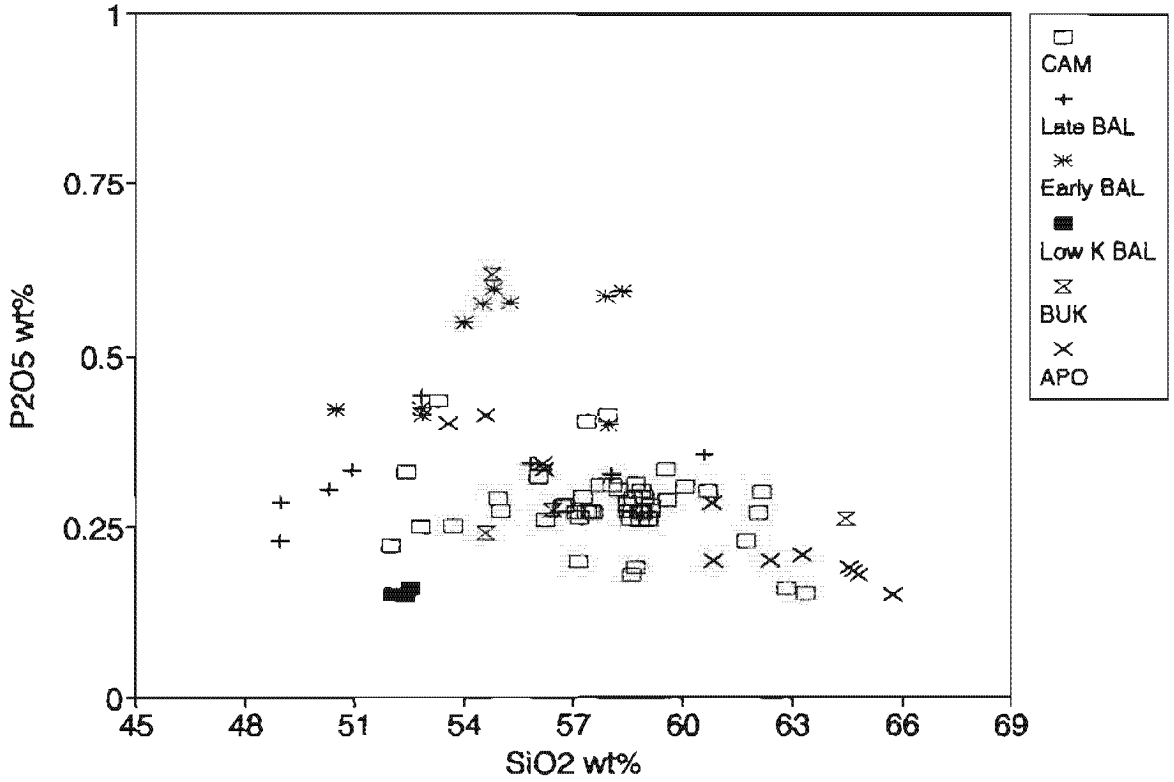

Figure 4-16. P_2O_5 varies little and generally decreases in concentration with increasing SiO_2 in most suites. Early Mt Balatocan lavas show a contrasting trend. Abbreviations as in Figure 4-2.

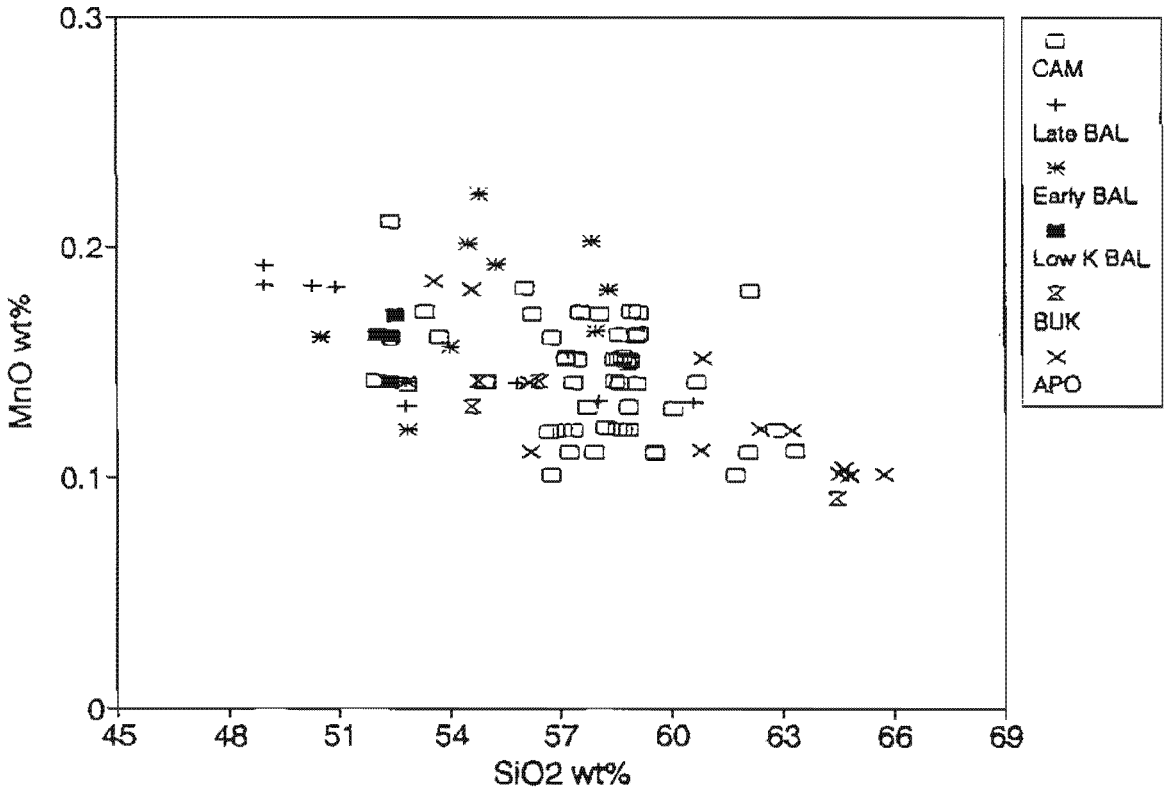

Figure 4-17. MnO vs SiO_2. Abbreviations as in Figure 4-2.

and entry of amphibole. Prolonged crystallisation of plagioclase would also increase Mn in andesites.

4.4.2. TRACE ELEMENTS

(i) Ba, Rb and Sr

These large ion lithophile elements (LILE) show the characteristic variations with SiO_2. All suites show positive linear correlation of Ba with fractionation and generally shows an increase of 200 ppm per 5 wt% increase in SiO_2 (Fig 4-18a). In contrast, Rb contents discriminate between suites (Fig. 4-18b) and mimics K distribution. Low to medium-K CA basalts and andesites of Camiguin Island and Bukidnon volcanoes have the lowest Rb concentrations. This pattern is continued by medium to high-K CA SiO_2-rich andesites and dacites of Mt Apo. High-K CA basalts and andesites from Mt Balatocan have the highest Rb contents.

Sr behaves differently from either Ba or Rb, exhibiting a crude negative correlation with SiO_2 (Fig. 4-19). Extremes in Sr concentration may reflect modal proportions of plagioclase which peaks in low to medium-K CA basalts and andesites of Camiguin Island and reaches a minimum in medium to high-K dacites of Mt Apo. Low Sr contents are characteristic of basic lavas from Mt Balatocan and Mt Balatocan, perhaps reflecting early plagioclase fractionation or lack of plagioclase accumulation.

(ii) Zr, Y and Nb

These high field strength elements (HFSE) exhibit highly variable concentrations among CMVA lavas. In general, there is irregular variation of these elements with differentiation even for lavas erupted from the same vent (Fig. 4-20). Zr appears to act as an incompatible element from basalts to andesites but this is most apparent only for Camiguin Island and Mt Balatocan. Slight curvature in the SiO_2-Zr distribution of some andesites suggests fractionation of Zr-bearing phases, such as amphibole or possibly Ti-magnetite and clinopyroxene. In SiO_2-rich

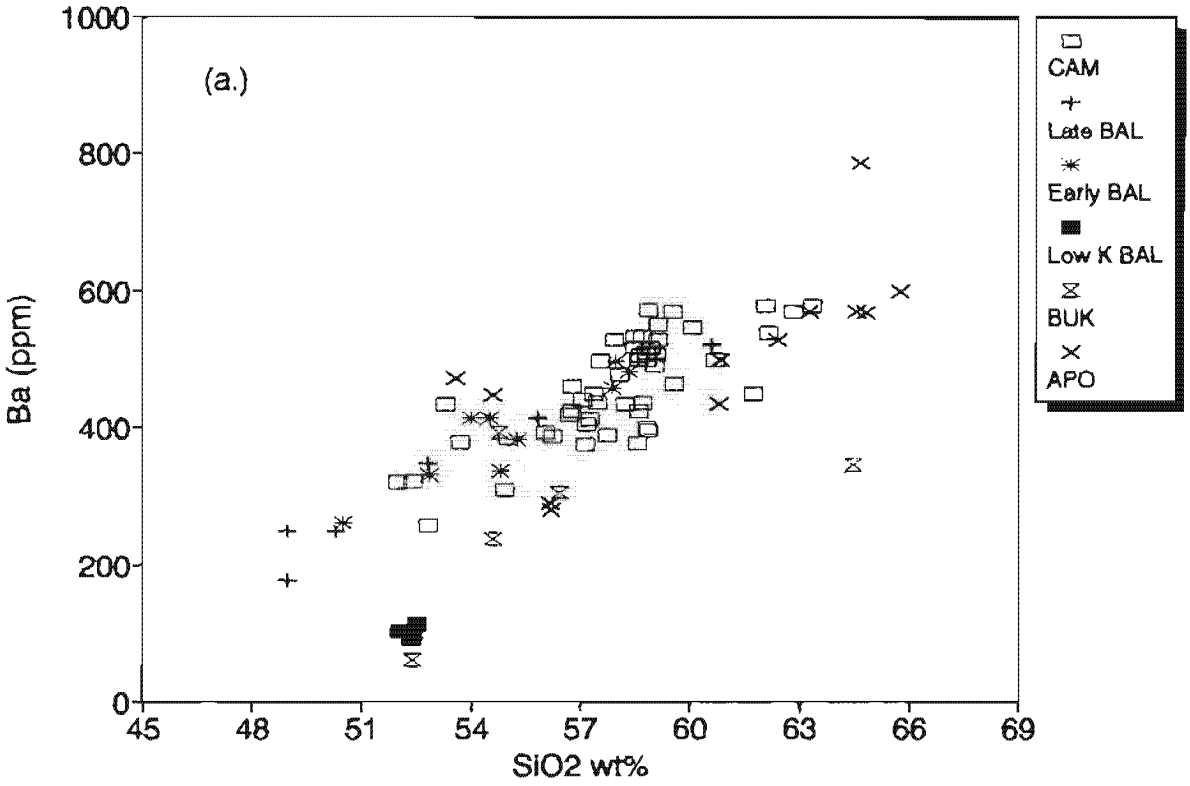

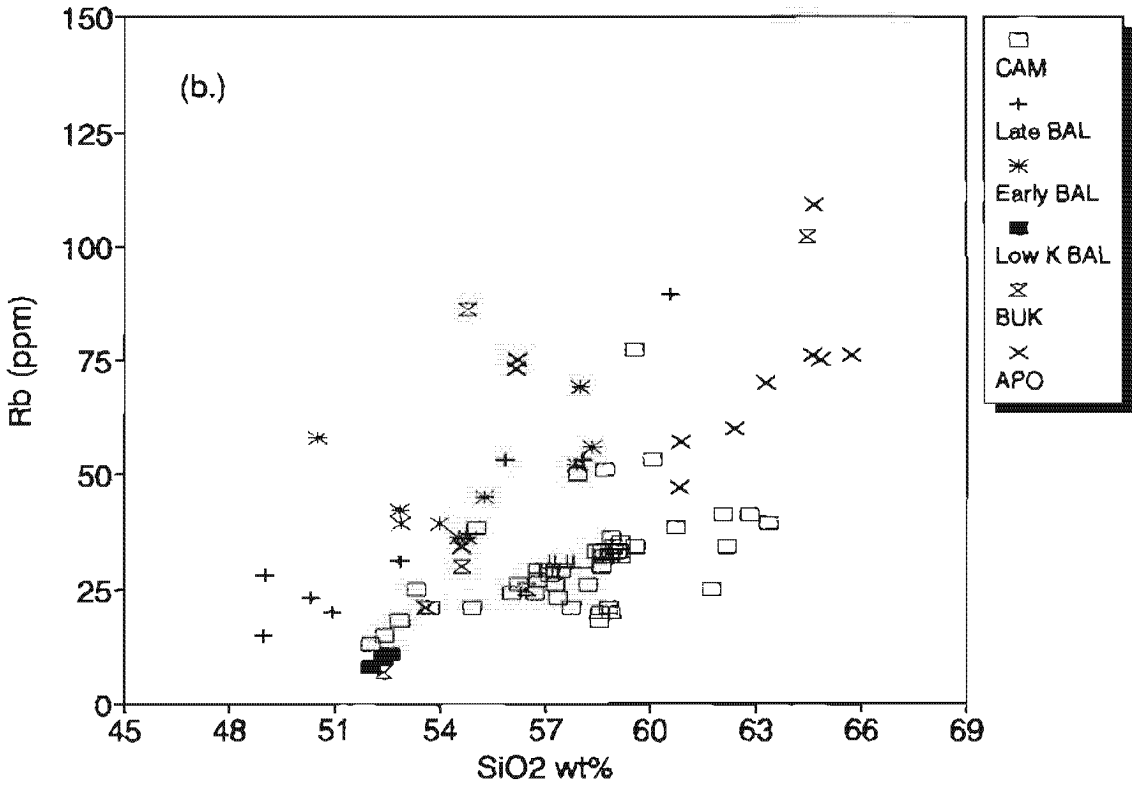

Figure 4-18. Distribution of Ba (a) and Rb (b) in CMVA lavas, showing positive correlation with SiO2.

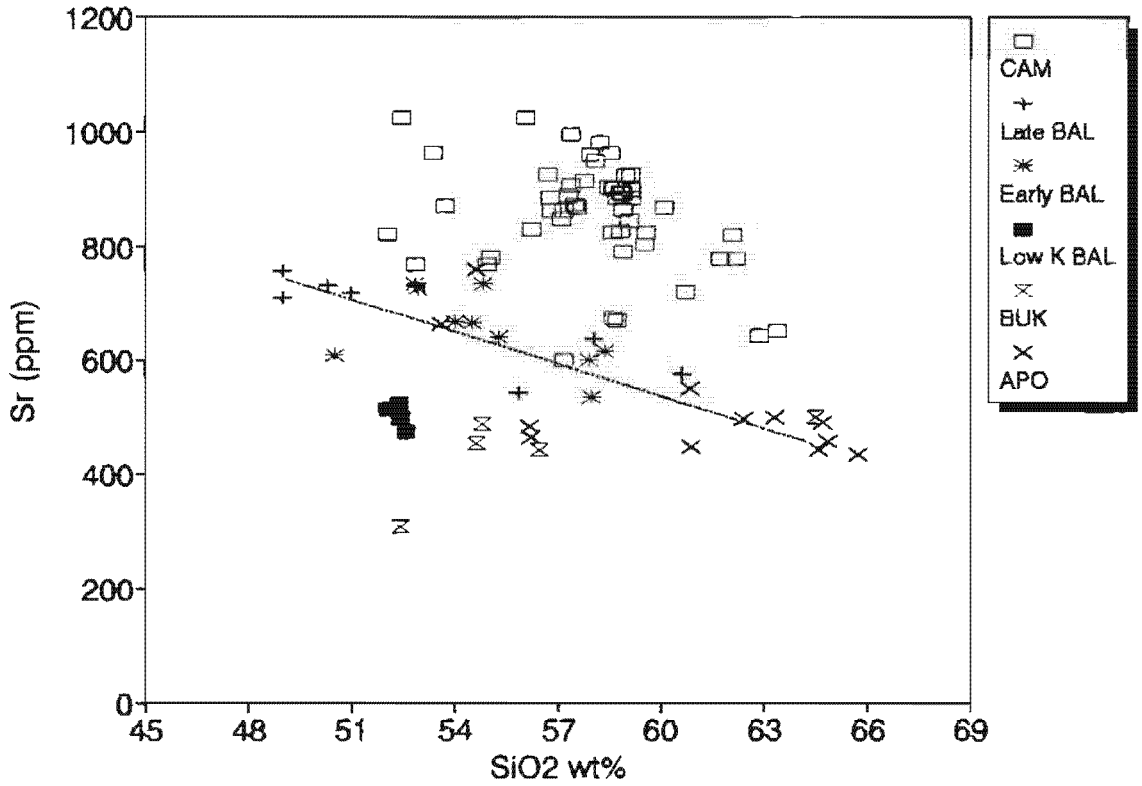

Figure 4-19. Variable Sr distribution in CMVA lavas. The general decreasing concentration in Mt Balatocan and Mt Apo is shown by the dotted line and is also crudely displayed by Camiguin Island lavas. Increasing Sr in andesites is exhibited by Bukidnon volcanoes. Abbreviations as in Figure 4-2.

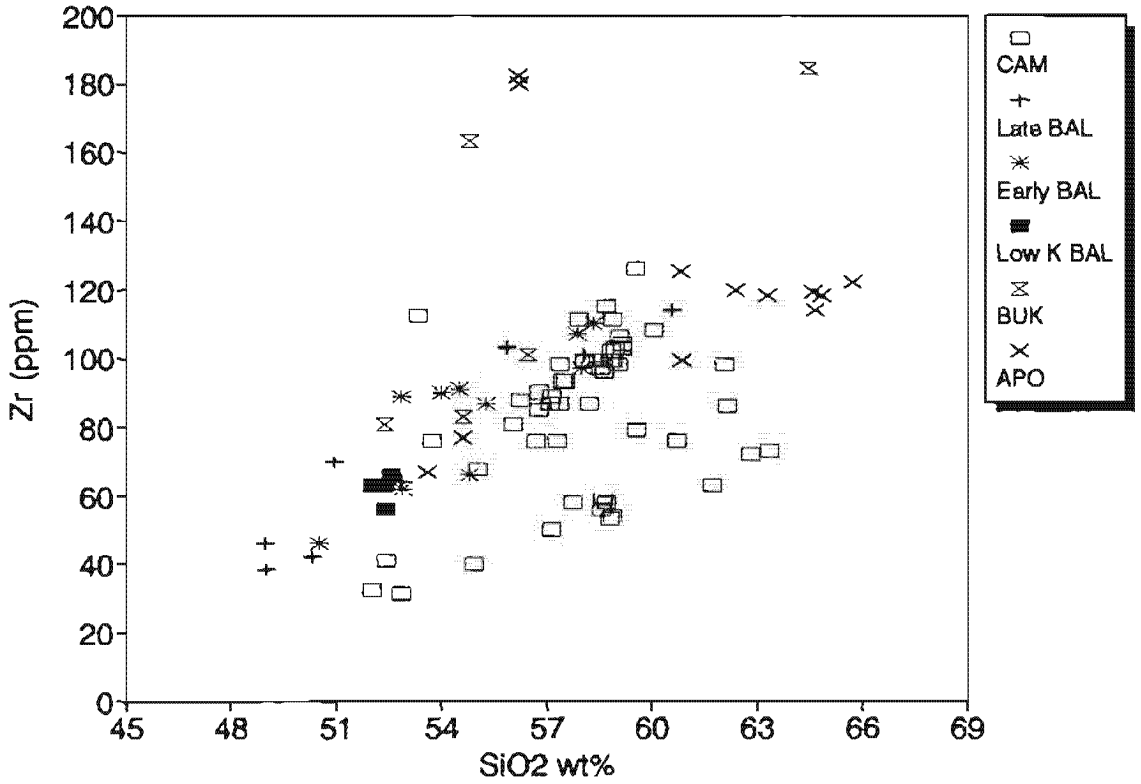

Figure 4-20. Zr concentration vs SiO_2 in CMVA lavas. Mt Apo lavas have decreasing Zr probably due to amphibole fractionation. High Zr concentration is shown by anhydrous Type 1 dacite from Mt Katanglad. Relatively constant Zr or scattered abundances distinguish other suites. Abbreviations as in Figure 4-2.

andesites and dacites of Mt Apo, flat trends of Zr is probably correlated with amphibole fractionation.

Zr, as an incompatible element in either Camiguin Island or Mt Balatocan, can be used as a differentiation index for other trace elements. Y effectively discriminates between early and late suites of Mt Balatocan lavas (Fig. 4-21). In the early lava suite of Mt Balatocan, Y is consistently incompatible whereas Y behaves compatibly in late Mt Balatocan samples. Similarly, Hibok-Hibok basic andesites show slight Y-enrichment trends in contrast to the overall decreasing abundances of other Camiguin Island lavas.

(iii) Ni, Cr and V

Ni and Cr concentrations generally decrease with SiO_2 (Gill, 1981) but in CMVA, this relationship is not clear. Their variation with differentiation is better shown with respect to MgO (Fig. 4-22). It is evident that whereas basalts have relatively high Ni and Cr contents (114 and 216 ppm), the highest concentrations occur in basic andesites (162 and 280 ppm). This trend, observed in Bukidnon lavas, is probably caused either by olivine and clinopyroxene accumulation or delayed fractionation of these minerals in basic andesites. However, there is no petrographic evidence of accumulation or mafic inclusions in these lavas. The usual trend is a continuous decrease in Ni and Cr from CA basalts to dacites with rapid decline in concentrations between 8 - 4 wt% MgO. This progressive trend perhaps reflects olivine (± spinel) and clinopyroxene-dominated fractionation in basalts and clinopyroxene fractionation in andesites and dacites. In Mt Balatocan, the two suites cannot be related by a fractionation trend because late Mt Balatocan samples have generally higher Cr and Ni than the early Mt Balatocan subset. There are also significant differences in Ni and Cr distributions between early Mt Balatocan and other CMVA lavas. For a given MgO level, Ni and Cr contents are lower in early Mt Balatocan samples than other CA suites.

Vanadium contents in each major centre show good linear relationship with SiO_2 (Fig. 4-23). Variation in V is mainly controlled by mafic phases (except olivine)

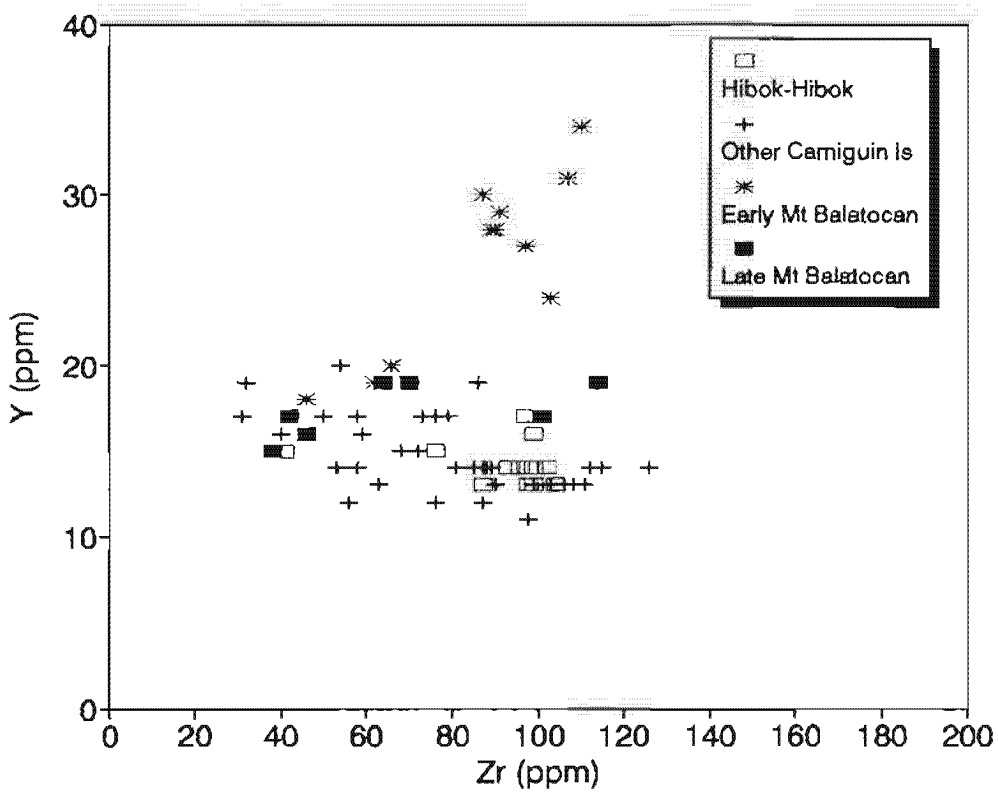

Figure 4-21. Y vs Zr diagram for northern CMVA lavas. Y increases with Zr in early Mt Balatocan and in Hibok-Hibok samples, in contrast to other lavas.

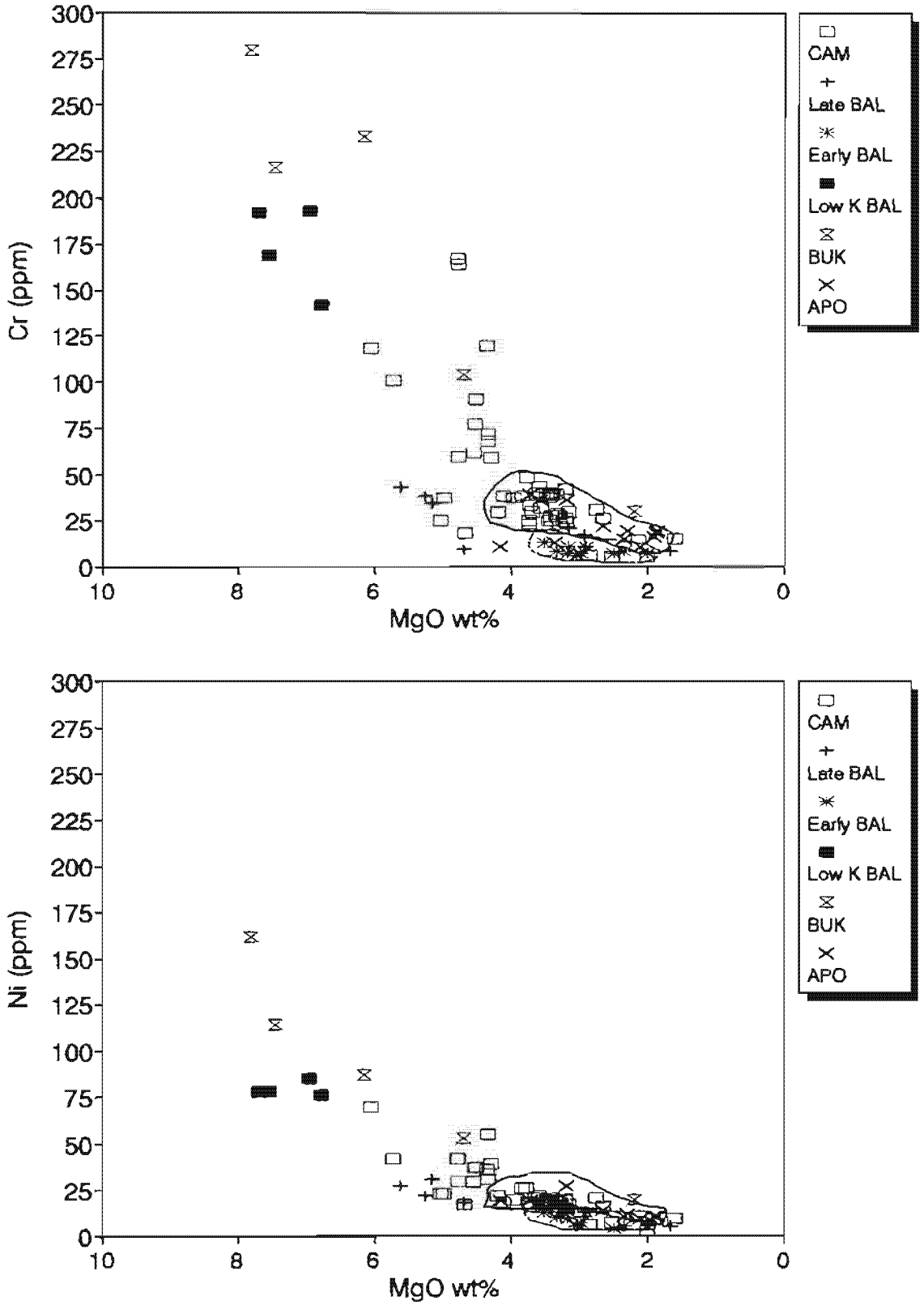

Figure 4-22. Variation in Cr (a) and Ni (b) with MgO in CMVA lavas. Samples enclosed by dotted line define early Mt Balatocan lavas, showing depressed Cr and Ni contents relative to other suites. Solid line fields define the majority of andesite and dacite.

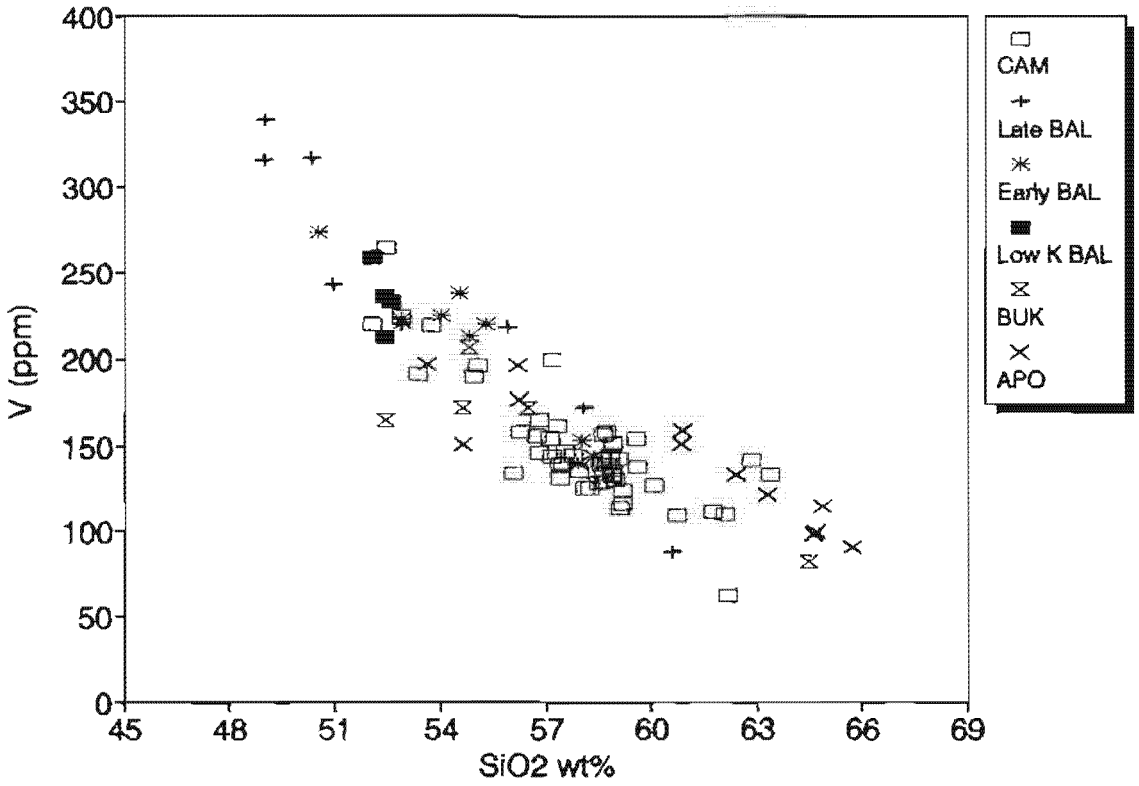
400
350
300
250
200
150
100
50
0
V (ppm)
45
48
51
54
57
60
63
66
69
SiO2 wt%
CAM
Late BAL
Early BAL
Low K BAL
BUK
APO

Figure 4-23.

as indicated by high distribution coefficients of V in clinopyroxene, amphibole and Ti-magnetite (Irving, 1978; Gill, 1978) relative to other trace elements. However, the steady decrease in V over the compositional range does not reflect changes in modal proportions of clinopyroxene, amphibole and magnetite. The V-SiO_2 trend also does not discriminate between clinopyroxene or amphibole-dominated lavas as would be expected in basalts and andesites. Fractionation of magnetite is not apparent (or is steady) because there are no inflections in V distribution. An alternative cause may be late crystallisation of magnetite when increased viscosity prevents separation. The complex behaviour of V and other trace elements may also be related to varying distribution coefficients as magmas differentiate (Berman, 1981).

4.5. CHEMICAL VARIATIONS OF CAMIGUIN ISLAND VOLCANOES

Among the many volcanic fields in the CMVA, Camiguin Island is ideal for geochemical study because of its recent eruptions and relatively simple geology. There are 5 main chemical units corresponding to the major volcanic centres in Camiguin Island. These units, in order of decreasing inferred age, are Benoni-Mt Butay, Mt Ginsiliban, Mt Mambajao, Mt Vulcan and Hibok-Hibok. Representative analyses of each unit are given in Table 4-2.

4.5.1. MAJOR ELEMENTS

Camiguin Island lavas are mainly medium-K CA basalts, andesites and dacites (Fig. 4-24). Mt Ginsiliban andesites and a Hibok-Hibok basalt plot near the low to medium-K boundary whereas a Mt Mambajao andesite occurs near the medium to high-K boundary. Trends for FeO, MgO, CaO and TiO_2 show good linear relationship with SiO_2. Al_2O_3 exhibits significant scatter most likely due to variable proportions of high-Ca clinopyroxene and plagioclase. Na_2O and P_2O_5 have distributions similar to but have flatter trends than K_2O.

The main distinctions shown by Harker diagrams are the wide compositional SiO_2 range of Benoni - Butay samples, from 52.03 to 63.38 wt% SiO_2, compared

Table 4-2. Representative analyses of Camiguin Island lavas.

	Hibok-Hibok			*Mt Vulcan*	*Mambajao*	*Mt Butay*			*Mt Ginsiliban*		
Analysis #	1		25			36		45	47		52
Code	A	B	C	B	B	A	B	C	A	B	C
SiO2 wt%	52.43	57.67	62.09	57.74	58.45	52.03	57.89	63.38	57.75	59.23	61.74
TiO2	0.77	0.63	0.60	0.63	0.67	0.83	0.62	0.89	0.64	0.58	0.48
Al2O3	18.82	17.95	16.99	17.94	17.50	18.53	17.54	18.63	18.18	18.22	18.03
Fe2O3	2.07	1.54	1.23	1.51	1.47	2.13	1.58	2.13	1.58	1.47	1.30
FeO	6.88	5.13	4.10	5.02	4.89	7.08	5.26	7.08	5.26	4.89	4.31
MnO	0.21	0.15	0.11	0.17	0.12	0.14	0.15	0.18	0.13	0.12	0.10
MgO	4.69	3.74	2.76	3.72	3.75	5.72	3.95	6.06	3.83	3.35	2.64
CaO	9.58	7.84	5.96	7.85	7.11	9.32	7.60	9.45	7.49	6.94	6.13
Na2O	3.46	3.65	3.92	3.73	3.73	3.03	3.55	4.71	3.56	3.63	3.69
K2O	0.75	1.43	1.97	1.38	2.00	0.97	1.64	2.07	1.27	1.29	1.34
P2O5	0.33	0.28	0.27	0.30	0.33	0.22	0.24	0.43	0.31	0.27	0.23
Mg#	0.55	0.54	0.55	0.57	0.58	0.59	0.55	0.40	0.46	0.50	0.52
Q	0.8	7.86	13.96	7.74	7.74	0.51	7.95	16.92	8.94	11.44	15.84
or	4.43	8.36	11.58	8.10	11.68	5.67	9.60	12.12	7.51	7.63	7.86
ab	29.19	30.64	33	31.31	31.22	25.3	29.73	39.69	30.04	30.65	31.05
an	33.46	28.17	22.77	27.88	24.85	33.65	26.84	33.65	29.76	29.48	28.52
C	0	0.00	0	0.00	0.00	0	0.00	0.00	0	0.00	0
di	9.64	7.04	3.98	7.23	6.49	8.64	7.30	12.38	4.29	2.51	0.19
hy	16.87	12.58	10.54	12.83	12.86	19.85	13.52	19.85	14.91	14.10	12.66
ol	0	0.52	0	0.00	0.00	0	0.00	0.00	0	0.00	0
mt	2.99	2.21	1.77	2.17	2.10	3.04	2.27	3.04	2.28	2.12	1.87
il	1.46	1.20	1.14	1.19	1.26	1.56	1.16	1.67	1.22	1.10	0.91
ap	0.76	0.65	0.63	0.68	0.75	0.51	0.56	1.00	0.72	0.63	0.53

Explanation as in Table 4-1.

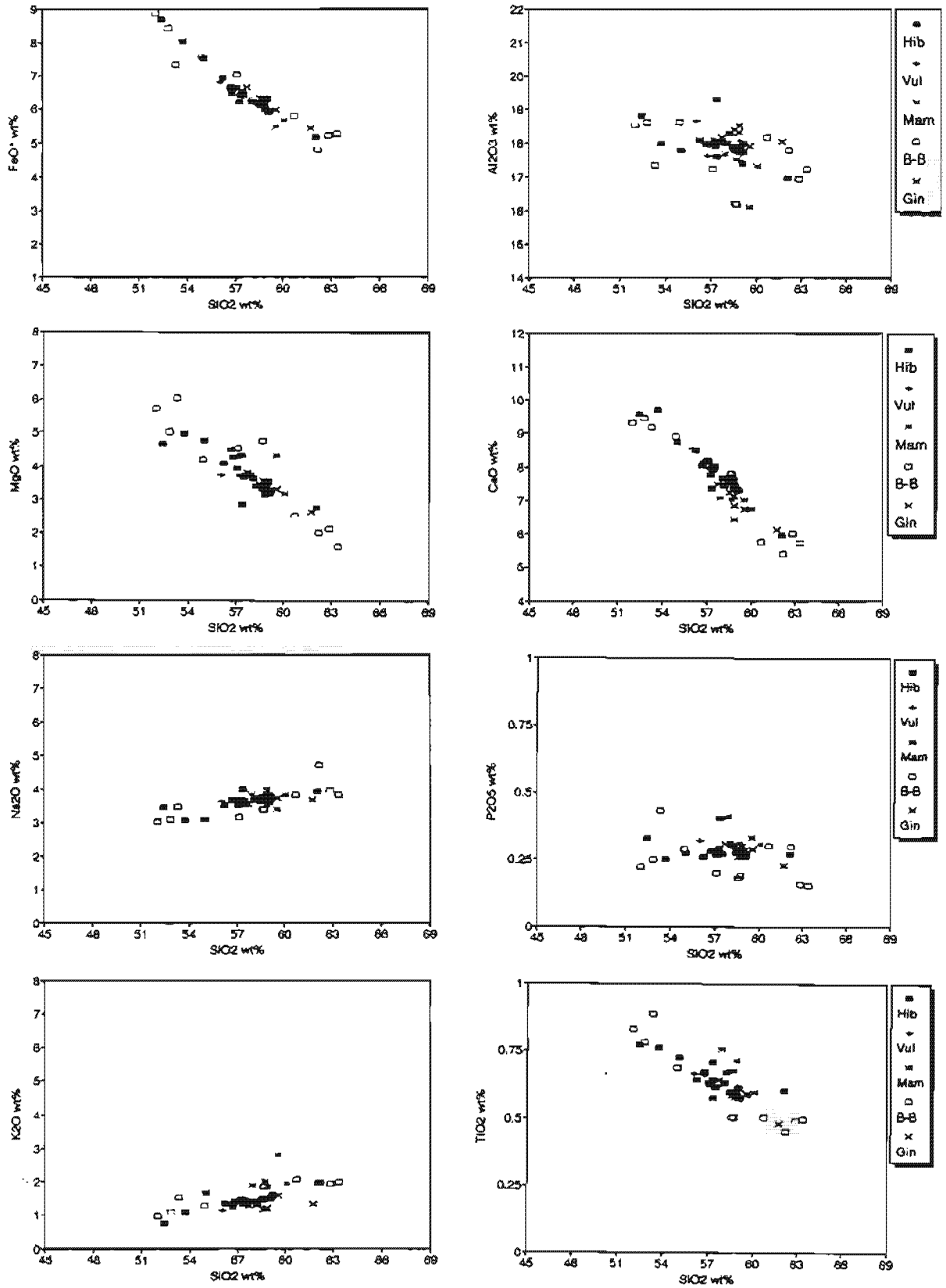

Figure 4-24. Major element distribution of Camiguin Island lavas.

with other units although there is a relative sparsity of compositions in the 56-60 wt% SiO_2 range. Despite a deliberate search for mafic compositions at Hibok-Hibok no basaltic samples were found from this volcano except as mafic inclusions (analysis 2, Appendix 4-2) in lavas erupted in 1948. The main compositions of Hibok-Hibok, Mt Vulcan, Mt Mambajao and Mt Ginsiliban are clustered from 56.25 to about 60 wt% SiO_2. Mt Vulcan and Hibok-Hibok occur within the same complex and have very similar major element contents. Mt Mambajao has slightly higher alkali, MgO, TiO_2 and P_2O_5 contents but are again similar to Hibok-Hibok lavas in other major oxide contents. Mt Ginsiliban samples also have major element patterns similar to Hibok-Hibok but this seems non-diagnostic, given the wide spacing and different relative ages (see Chapter 2).

4.5.2. Trace Elements

The distributions of Ba and Rb (Fig. 4-25) generally show good positive correlation with SiO_2. Rb departs from linearity in the case of Mt Mambajao pyroxene andesites and behaves very similarly to K_2O. The high K_2O and Rb of Mt Mambajao andesites suggest the lack of amphibole or other Rb-rich phase, consistent with predominant fractionation by clinopyroxene which has a very low K_{Rb} (Shimuzu and Allegre, 1978; Ewart and Hawkesworth, 1987). Interestingly, the lowest K_2O and Rb concentrations at similar SiO_2 levels occur in Mt Ginsiliban pyroxene andesites and not from Hibok-Hibok hornblende andesites. This could reflect, in part, the lower state of differentiation of Mt Ginsiliban with respect to K_2O and Rb. Sr exhibits significant scatter within Camiguin Island lavas. A general decrease in Sr is evident in all volcanoes with the lowest concentrations occurring at Benoni- Butay.

Discrimination and grouping of Camiguin Island lavas are evident in element plots versus Zr. This has not been obvious for comparisons between other CMVA lavas presumably due to pooling of unrelated compositions. A survey of Zr fractionation effects in a wide variety of geological settings (Bradshaw, 1992) shows that Zr behaves as an incompatible element until at least 67 wt% SiO_2. This is

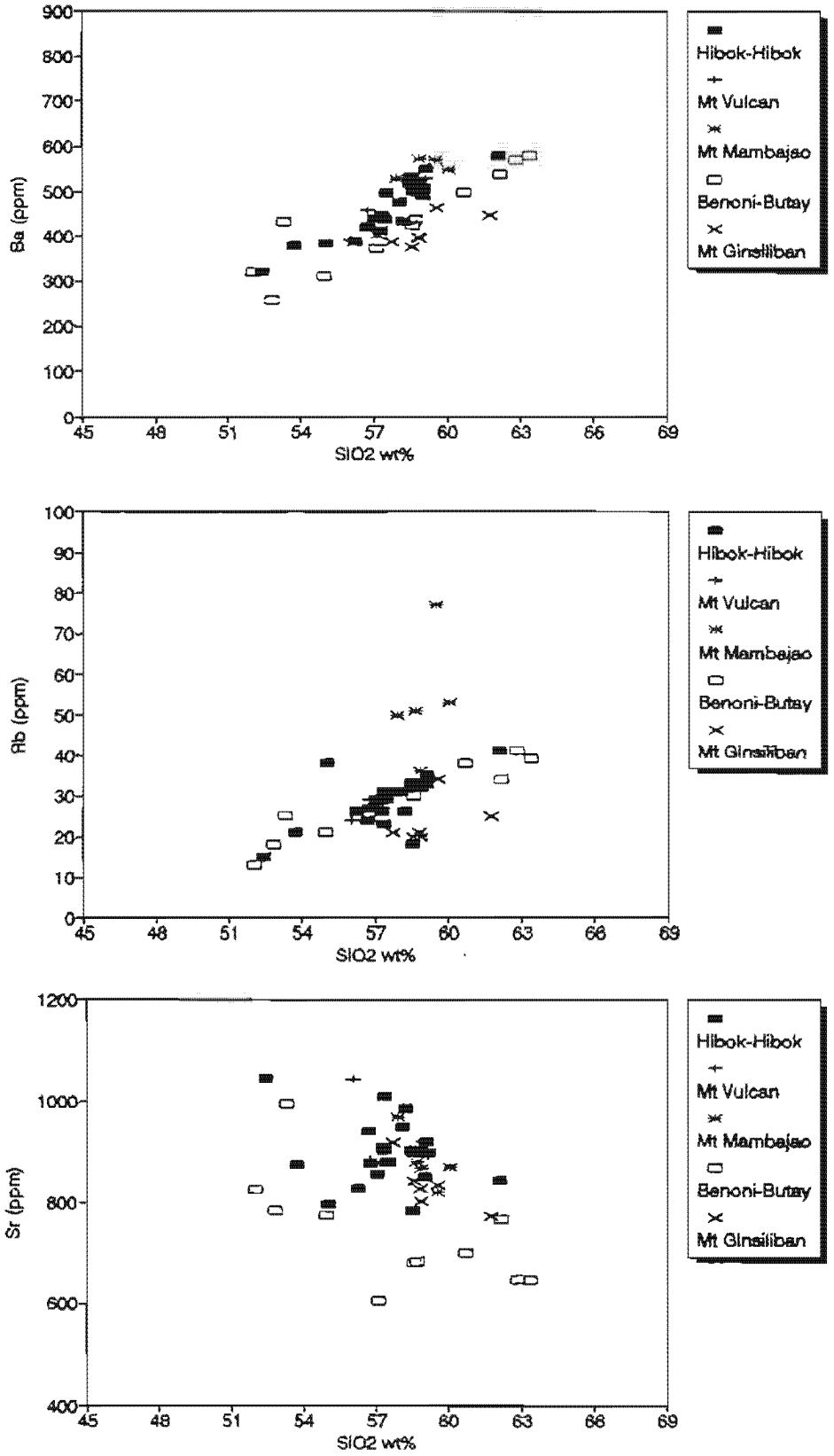

Figure 4-25. Variation of Ba, Rb and Sr with SiO2 for Camiguin Island lavas.

apparent in Figure 4-26a where samples from Benoni, Butay and Hibok-Hibok represent two lava groups with different Zr differentiation trends. This plot also shows the affinity of Mt Ginsiliban lavas to Benoni-Mt Butay rather than to Hibok-Hibok. Mt Mambajao and Mt Vulcan have similar Zr trends to Hibok-Hibok samples. This grouping is consistent with clustering and age relationships of these volcanoes.

Variations in Y and Nb content from basic to acid compositions are shown in Figures 4-26b and 4-26c. Yttrium and Nb show good linear correlation with Zr and reflect the grouping observed by Y and Nb versus SiO_2. For mafic rocks Y contents are fairly constant, the largest variation occurring in Mt Ginsiliban (12 - 20 ppm). There is a slight decrease in Y for intermediate and acid magmas possibly due to crystallisation of amphibole, and to a lesser degree of clinopyroxene, based on partition coefficients given by Pearce and Norry (1979). In contrast Nb increases consistently with Zr, compatible with the observation that olivine, plagioclase and clinopyroxene are the main liquidus phases. Departure in Nb distribution is shown by an andesite from Hibok-Hibok (sample CAM16, analysis 16, Appendix 4-2) which has lower Nb (5 ppm) than other Hibok-Hibok lavas (average 8 ppm) at the same Zr content. This cannot be caused solely by larger-than-normal amphibole fractionation since Zr increases progressively and because of very similar distribution coefficients of Zr and Nb in the crystallising phases. Fractionation of magnetite is probably responsible for depleted Nb contents relative to Zr.

The abundance of Cr and Ni (Fig. 4-27) are lower than other CMVA lavas, the highest concentration in mafic rocks being 118 ppm. Higher Cr occurs in a SiO_2-rich andesite (sample BEN31, analysis 42, Appendix 4-2) perhaps due to accumulation of clinopyroxene. Although there is considerable scatter in the Cr-Zr distribution, there is rapid decrease in Cr with increasing Zr. This trend is more apparent in Cr versus MgO and considering strong partition of Cr in mafic phases, is a good indication of fractionation of mafic phases.

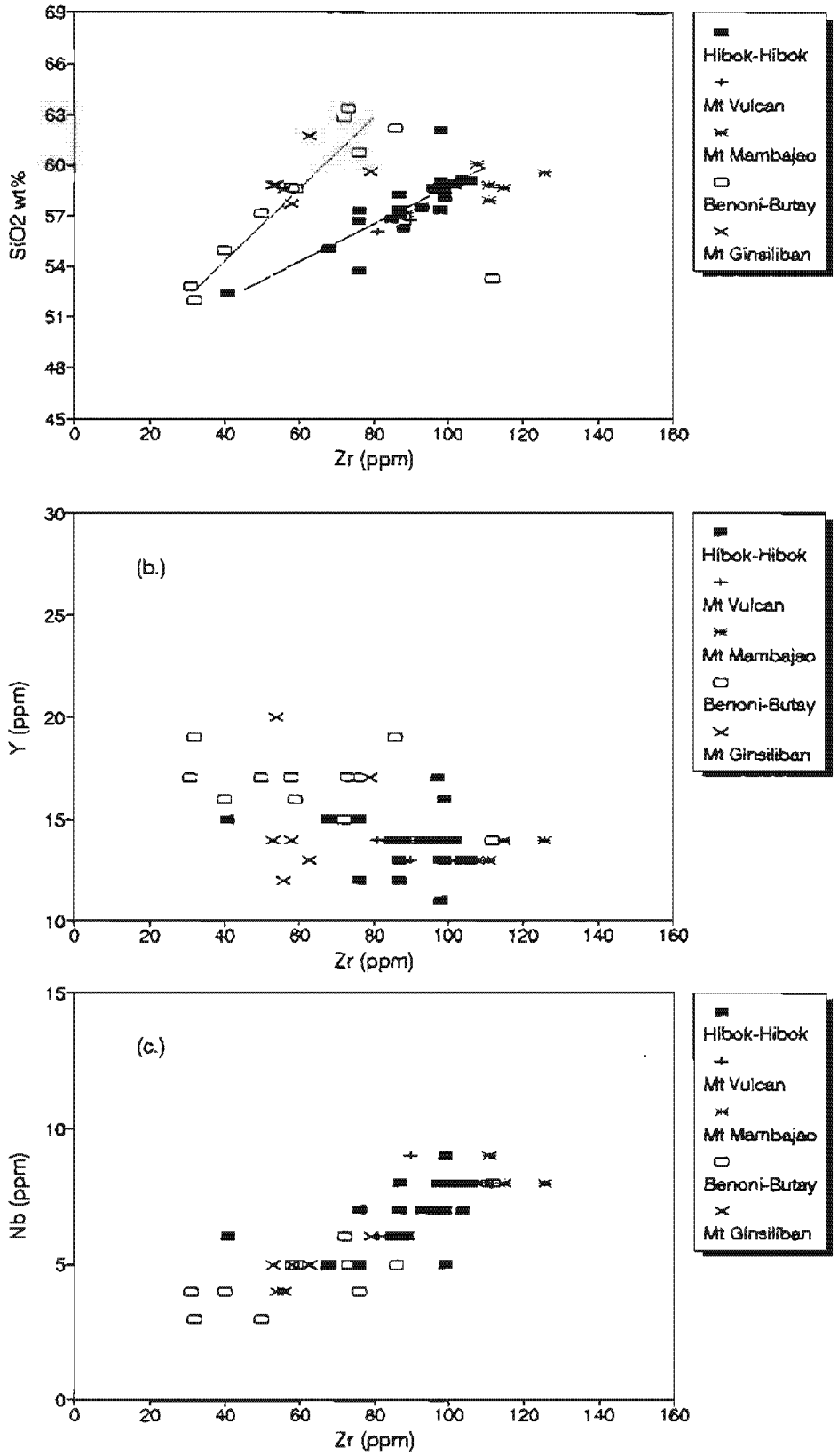

Figure 4-26. Variation of Nb and Y using Zr as a fractionation index for Camiguin Island lavas. Dotted lines in (a) are two Zr fractionation trends

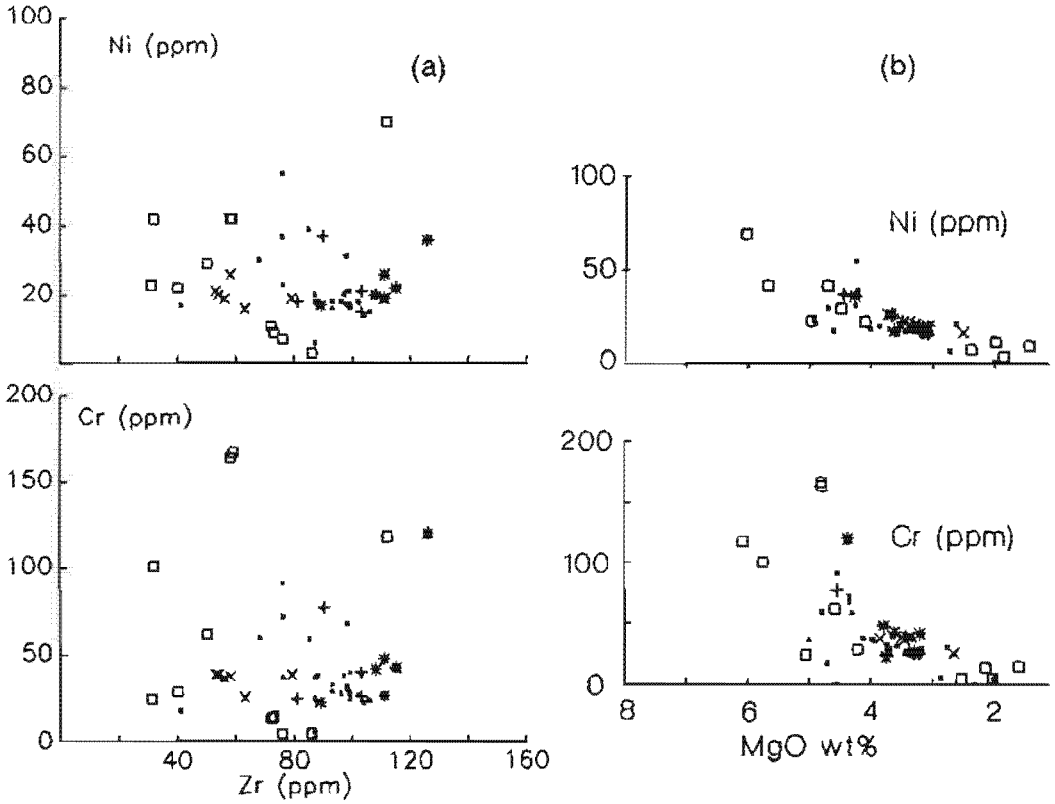

Figure 4-27. Cr and Ni distribution in Camiguin Island lavas using (a) Zr and (b) MgO as differentiation indices. Symbols as in Figure 4-24.

The high Cr in sample BEN31, if significant, suggests that this sample cannot be derived by fractional crystallisation of more primitive Benoni-Butay lavas. Ni also reproduces the same distribution with MgO, and as with Cr, shows rapid decay with respect to Zr. In general, Cr and Ni compositions for Mt Ginsiliban are within the trends observed at Benoni-Mt Butay while Cr and Ni contents from Mt Vulcan lavas are similar to Hibok-Hibok.

4.6. COMPARISON OF MAJOR AND TRACE ELEMENT CHARACTERISTICS BETWEEN THE CMVA AND LAVAS FROM OTHER TECTONIC SETTINGS.

4.6.1. MAJOR ELEMENTS

In basalts, high FeO^* contents are within the observed range (6 - 15 wt%) for Island Arc Basalts (IAB). The high range of FeO^* are in fact similar to primitive parental IAB (8 - 10 wt%) and similar to Mid-Oceanic Ridge Basalt (MORB) glasses examined by Perfit et al (1980).

MgO abundances in basalts (3.5 - 7.8 wt%) are typical of IAB but are lower than MORB (generally 5 - 11 wt%; Melson et al, 1976) or Oceanic Island Basalt (OIB: 13-21 wt%, Flower, 1991). Mg numbers (Mg#) are generally in the range of 50 - 65 and, therefore, suggest that CMVA basalts are not primary melts from the mantle wedge.

TiO_2 content varies from 1.12 - 0.45 wt% which are within limits commonly observed in IAB (1.2 - 0.5 wt%). For comparison, MORB and OIB are relatively enriched in TiO_2 (2.5 - 1.5 wt%, Bence et al, 1979; Bence et al, 1980).

4.6.2. TRACE ELEMENTS

The rate of increase in Ba shown by CMVA lavas (Fig. 4-18a) is higher than in more primitive island arcs such as the Marianas (110 ppm over the same SiO_2 interval; Chow et al, 1980). The range in Sr contents observed in CMVA basalts (310

- 1044 ppm) is substantially higher than MORB (about 100 ppm; Ando, 1975; Baker, 1978).

Ratios of the K group trace elements further indicate some characteristics of original CMVA lavas. Using only basaltic compositions (< 53 wt% SiO_2) to reduce the effects of fractional crystallisation, the plot of K_2O/Rb vs K_2O (Fig. 4-28a) suggest CMVA lavas to be chemically intermediate between MORB and Alkaline Olivine Basalt (AOB). Compared with intra-oceanic arc basalts (Marianas), some CMVA lavas have lower Ba/Sr ratios (Fig. 4-28b), reflecting overall high and variable modal plagioclase. The lowest Ba/Sr ratios are indicative of relatively unfractionated CMVA basalts, similar to average MORB. However, the majority of CMVA basalts have high Sr (feldspar accumulation?) and low Rb/Sr ratios (Fig. 4-29) which are characteristic of more fractionated CA lavas.

Nb behaves differently from Y, showing an overall positive correlation with Zr (Fig. 4-30). The abundance of Nb is low (3-10 ppm). Zr/Nb ratios of CMVA basalts (7 - 14, Appendix 4-2) are significantly less than Normal-MORB (N-MORB: > 30; Erlank and Kable, 1976; Sun and McDonough, 1989) but overlap ratios for Enriched-type MORB and Ocean Island Basalt (E-MORB and OIB: 4 - 15, BVSP, 1981; Weaver et al, 1987). Zr/Y ratios (Fig. 4-31) are generally higher than chondritic (about 2.8, Tarney et al, 1979). Similarities in Zr/Nb and Zr/Y ratios between CMVA basalts and E-MORB probably reflect the mantle source ratios of magmas which gave rise to CMVA basalts.

Compared with basalts from MORB and OIB, Ni and Cr contents from CMVA lavas are lower, which is characteristic of IABs. Wilkinson (1980) has shown that IAB have Ni and Cr concentrations comparable with MORB glasses which suggest that the most primitive IAB, represented by Mt Balatocan and Bukidnon (Mg# = 65 and 71 respectively), have undergone fractionation and therefore represent derivative melts.

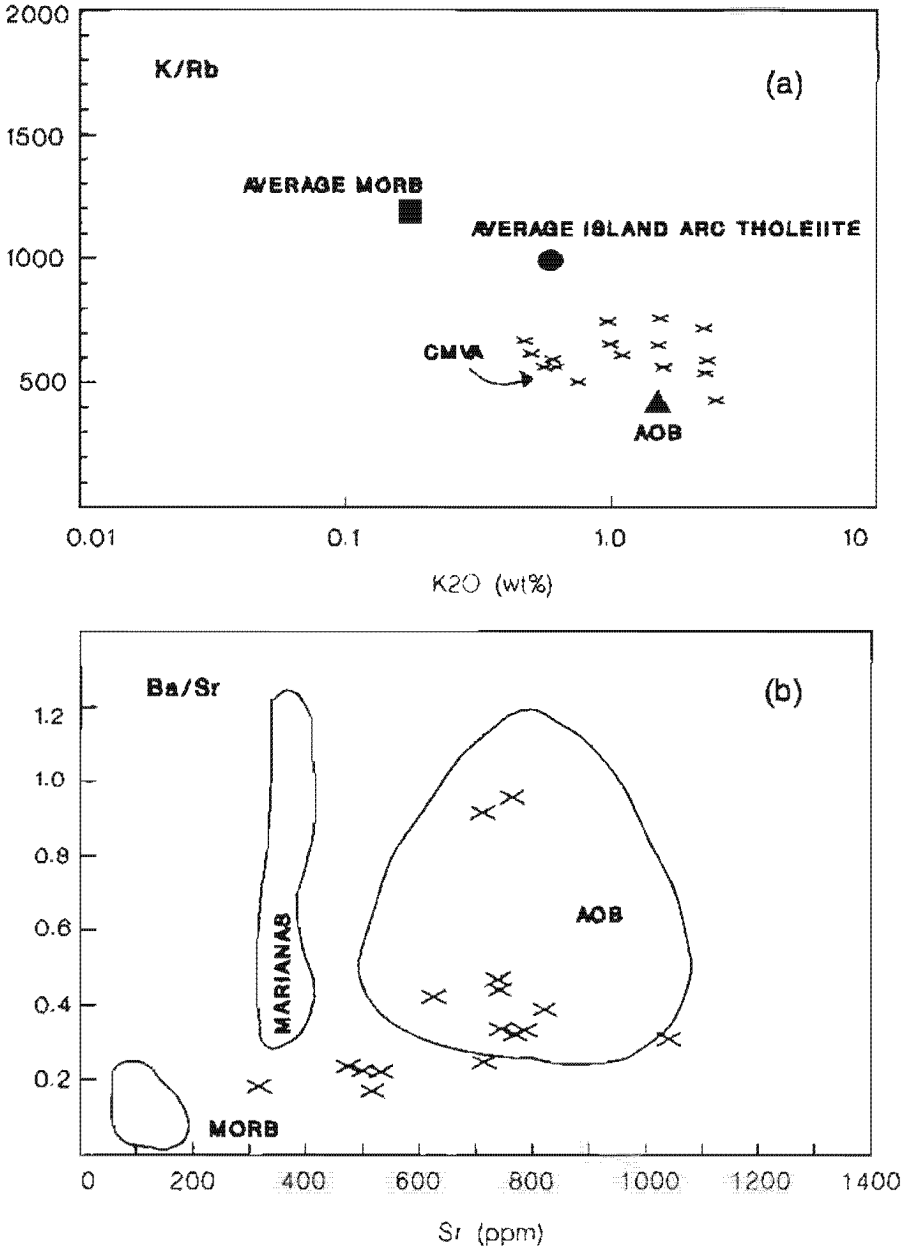

Figure 4-28. Selected K-group trace element ratios of CMVA basalts compared with average Mid-Oceanic Ridge Basalt (MORB), Island Arc Tholeiitic basalt (IATH) and Alkaline Olivine Basalt (AOB). Data for MORB, IATH and AOB after Chow et al (1980).

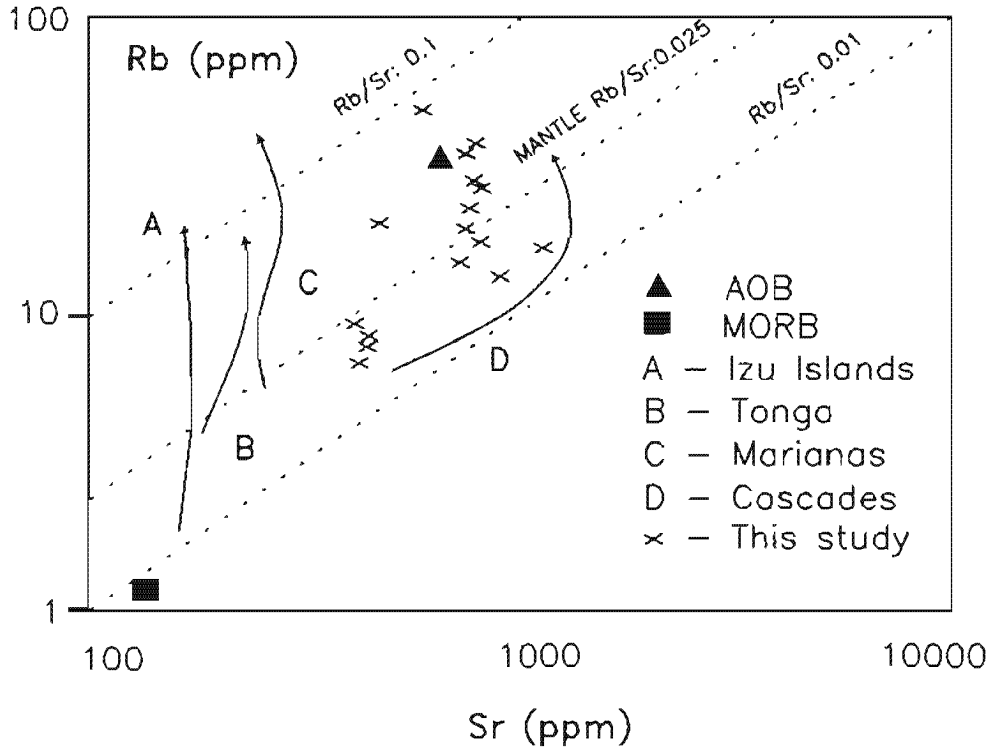

Figure 4-29. Rb/Sr ratios of CMVA lavas compared with other island arc basalts of the Pacific region. Data sources: A, Matsuda et al (1977); B, Ewart et al (1973); C, Chow et al (1960) and D, Peterman et al (1970).

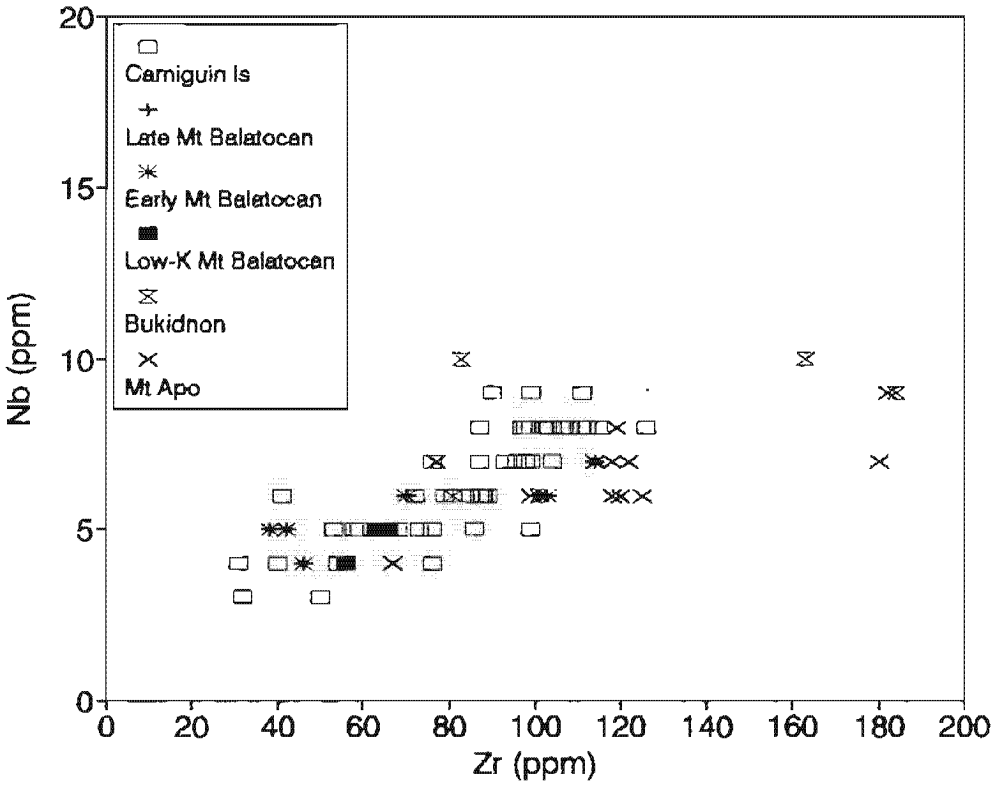

Figure 4-30. Nb vs Zr diagram of CMVA lavas.

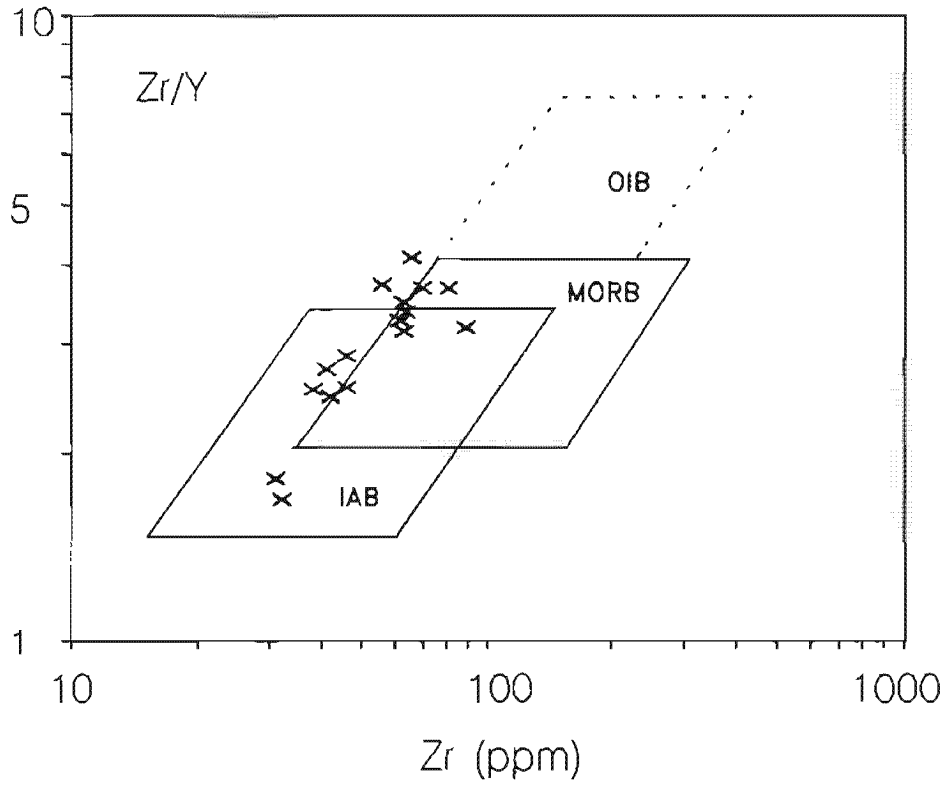

Figure 4-31. Variation of Zr/Y ratios with Zr for CMVA basalts. Field boundaries for some general lava types are from Pearce and Norry (1979).

In summary, trace element patterns with respect to MORB sources are shown in Figures 4-32a and b. All CMVA samples exhibit the characteristic depletion of Zr, Ti, Y and to a lesser extent, of Ce relative to N-MORB. The LILE (Rb, Ba, Th, K_2O) and Pb show the distinctive enrichment. Although Nb is depleted relative to LILE, it is somewhat higher than more primitive IAB (sample / N-MORB < 1.0) represented by the Marianas (Woodhead, 1989), Vanuatu (Gorton, 1977) and an "average" IAB (McCulloch and Gamble, 1991). Nb and other HFSE concentrations, however, are similar to some IABs from Indonesia (Vukadinovic and Nicholls, 1989). In Camiguin Island, trace element patterns are near-identical (Figure 4-32b). In general all CMVA basalts show similar trace element distributions along the length of the arc probably reflecting a homogeneous source region. This source region, based on HFSE (Zr/Nb ratios), indicate an E-MORB/OIB-type mantle wedge.

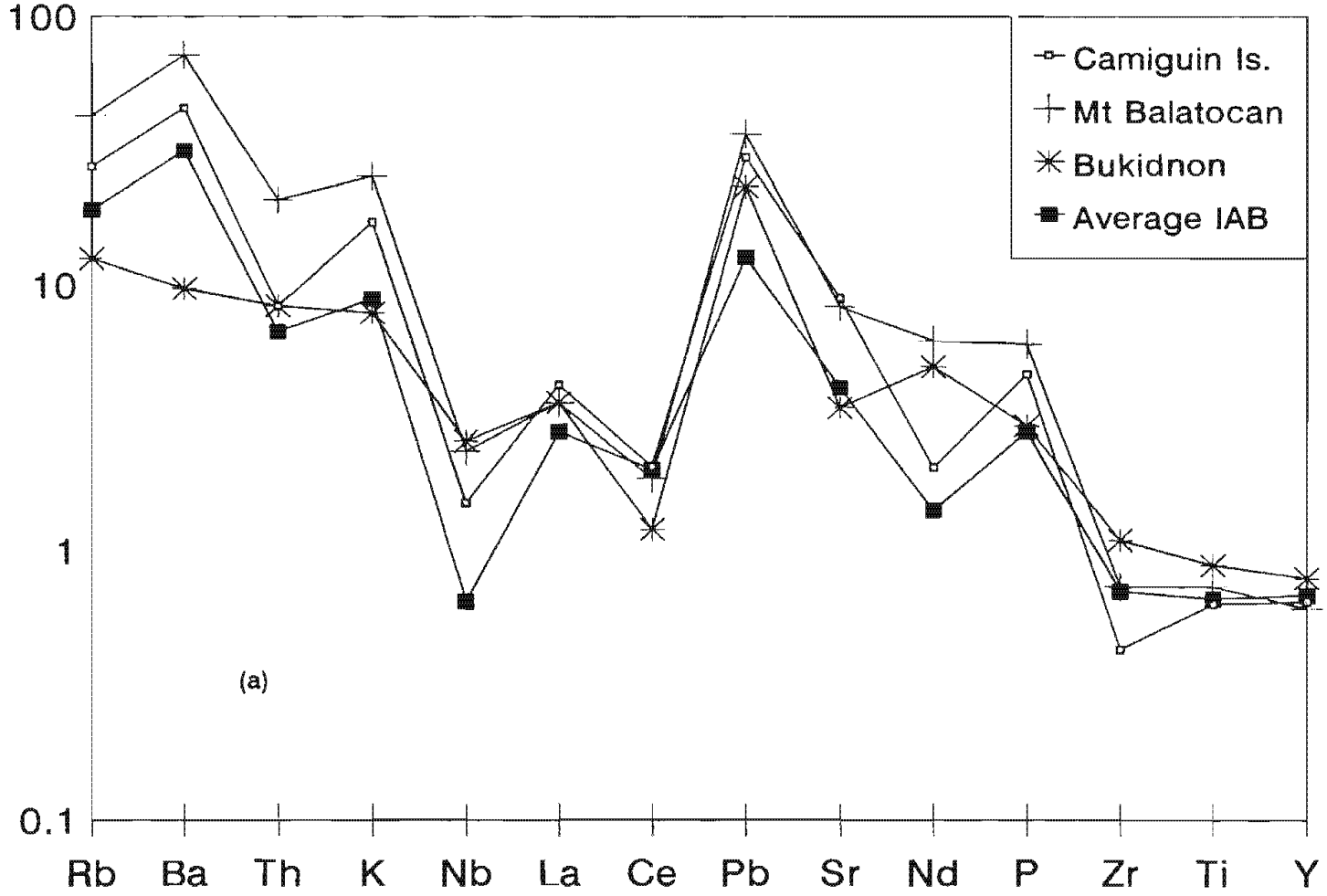

Figure 4-32. N-MORB normalised element abundance diagrams for (a) CMVA and an average IAB (McCulloch and Gamble, 1991) and (b) Camiguin Island basalts [next page]. N-MORB normalisation factors after Sun and McDonough (1989).

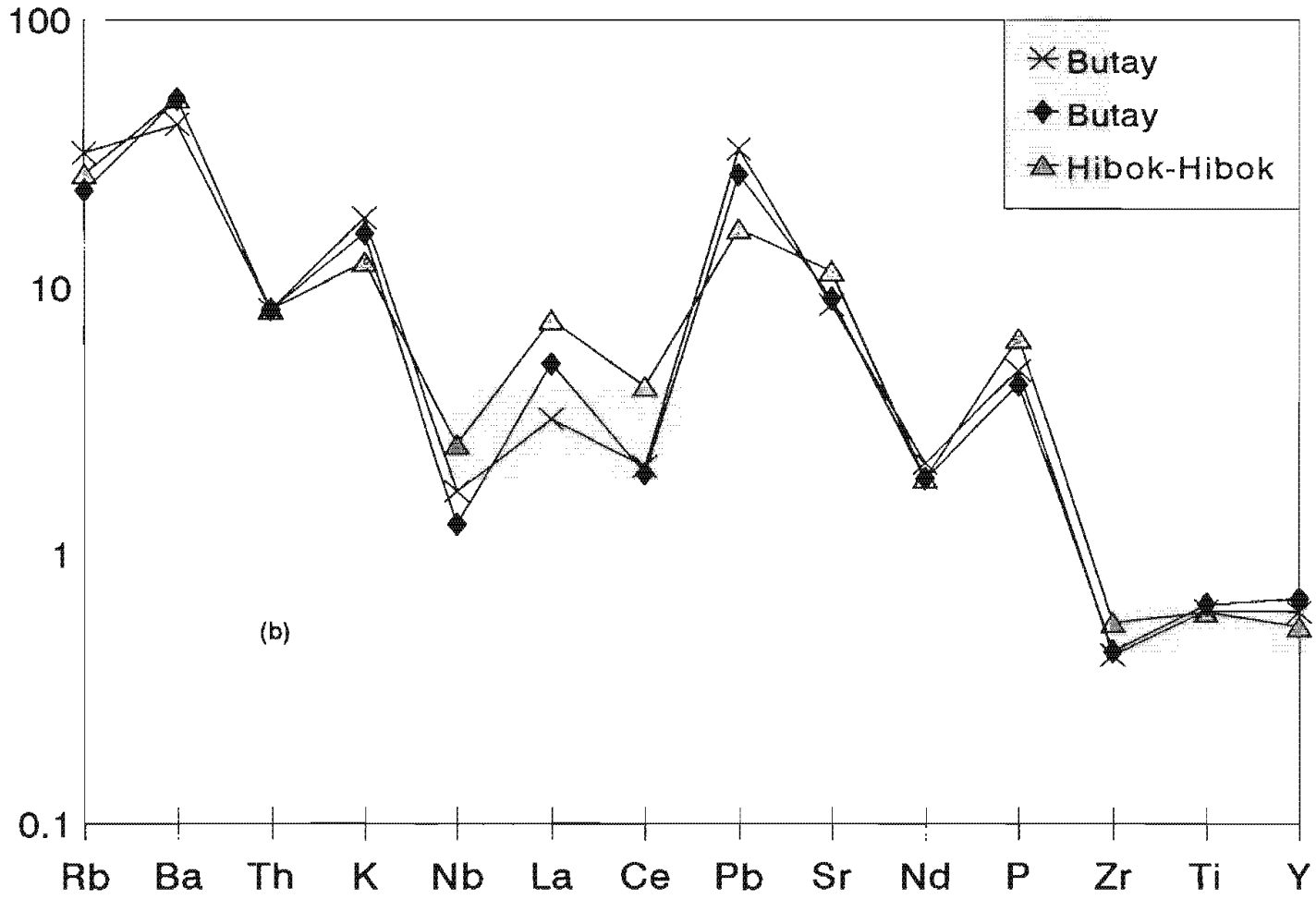

Figure 4-32. continued.

CHAPTER V PETROGENESIS

5.1. INTRODUCTION

The high LILE/HFSE ratios of predominantly calc-alkaline lavas in the CMVA indicate a subduction-related setting. Other geochemical features exhibited by CMVA basalts are their low Zr/Nb ratios (E-MORB, OIB-type affinity) relative to N-MORB and slightly higher trace element contents than average IAB (see Fig. 4-32). In subduction-related lavas, the 2 latter features suggest a mantle wedge enriched in trace element contents compared with N-MORB (Morris and Hart, 1983). In general, high LILE concentrations relative to HFSE in island arcs are attributed to mass transfer of K, Rb, Sr and Ba and other LILE from subducted lithosphere to mantle wedge and/or preferential retention of HFSE-bearing phases (e.g. titanite, perovskite, etc.) during magma generation (McCulloch and Gamble, 1991). Enrichment in highly incompatible trace element contents may also be caused by small degrees of partial melts. To approximate the source mantle compositions for CMVA lavas, it is therefore necessary to estimate primitive compositions from basalt analyses, and from pressure (therefore depth) and partial melting calculations. As fractionation of LILE relative to HFSE is not readily explained by partial melting of source mantle (Ellam and Hawkesworth, 1988) it is also necessary to evaluate the relative importance of subducted lithosphere-derived components (mobile LILE) and possible incorporation of sediment into the mantle wedge.

Basalt-andesite-dacite associations in each major volcanic field of the CMVA probably point to common differentiation processes. Variations in geology, modal mineralogy and geochemistry as discussed in Chapters 2, 3 and 4 suggest an interplay of differentiation processes (e.g. fractional crystallisation, assimilation and magma mixing). The roles of these processes in selected volcanic suites are therefore evaluated to explain the range of observed rock compositions.

5.2. GEODYNAMIC CONSTRAINTS

In the past, the presence of subducted slab beneath central Mindanao has been uncertain because of discontinuities between shallow and deep foci earthquakes (Fig. 5-1). Cardwell et al (1980) and Moore and Silver (1983) suggested that central Mindanao volcanism resulted from a detached slab (presumably from lithosphere subducting west of the present Philippine Trench) that sank to about 600 - 700 km. The difficulty in associating Central Mindanao volcanism with the Philippine Trench was the large arc-trench gap (~300 km) together with inferred dip of subduction (~45^{o}) suggesting a depth to a postulated subducted slab of about 300 km (Fig. 5-1). However, Figure 5-1 refers to a NNE trending west-Mindanao volcanic zone NW and S of Lake Lanao (e.g. Mts Bita and Ragang, Fig. 2-3) which Cardwell et al (1980) and Moore and Silver (1983) suggest was once part of a Sangihe–West Mindanao arc. It is probable that these West Mindanao volcanoes are not part of the CMVA. The CMVA forms a N-S volcanic cluster parallel to the Philippine Trench. When these volcanoes are plotted on the crustal section in Figure 5-1, the inferred arc-trench gap between the CMVA and Philippine Trench is approximately 200 - 220 km and a depth to the top of a seismic zone of < 200 Km. It is possible that the angle of subduction at shallower levels is less than 45^{o} (24^{o}, Cardwell et al, 1980) so that the top of subducted slab is 150 - 200 km. New seismic data (PHIVOLCS, 1992) define a more or less continuous inclined seismic zone, to around the 670 km phase transformation boundary (Fig. 5-2). There are still seismic gaps between 400 - 500 km depths but this is probably due to the limited time interval of data collection. A decrease in seismicity and a steepening of subducted lithosphere is apparent from southern to northern Mindanao (6^{o}N - 9^{o}N). Although more critical asessment of these earthquakes is required to further define the subduction zone, the presence of a subducted slab beneath the CMVA is now considered probable. As the CMVA overlies the mantle wedge region, CMVA lavas are clearly subduction-related and processes occurring within the supra-subduction zone can be considered.

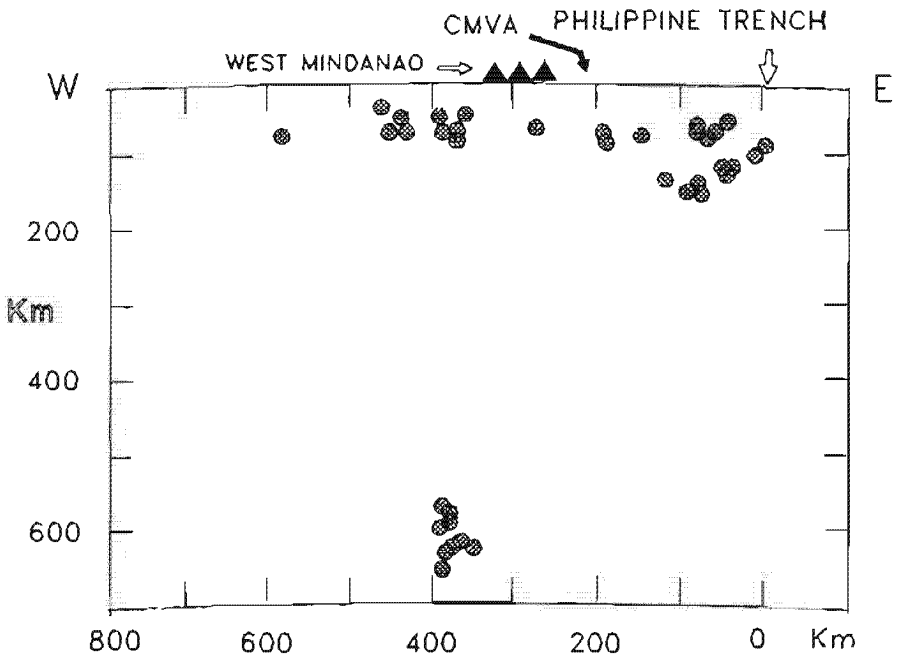

Figure 5-1. West-east vertical crustal section (approximately across Latitude 7°30'N) of southern Mindanao showing hypocenters. The CMVA is plotted next to west-Mindanao volcanoes of section D, Figure 5 of Cardwell et al (1980).

a.

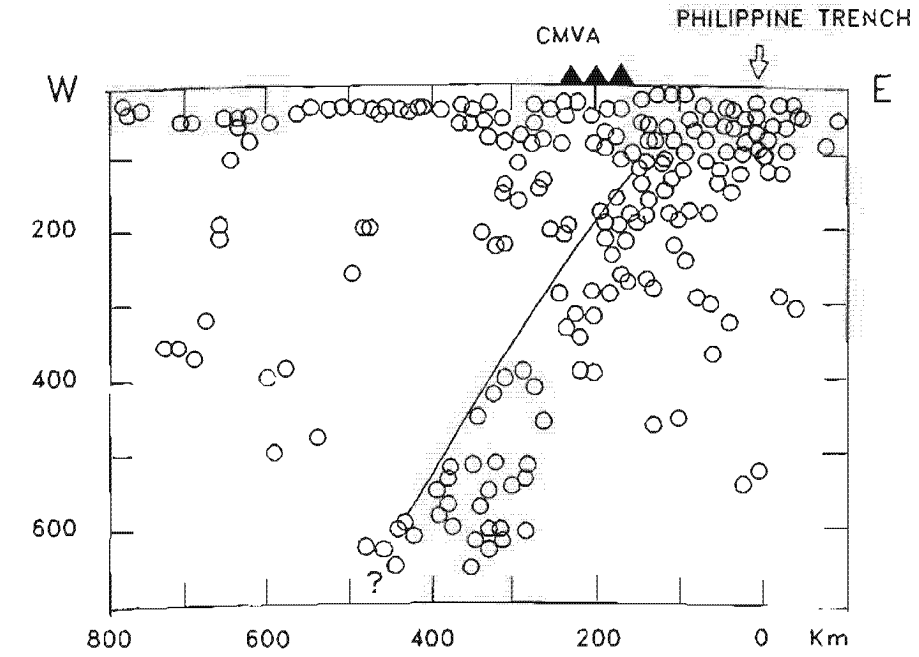
PHILIPPINE TRENCH
CMVA
W
E
200
400
600
?
800
600
400
200
0
Km

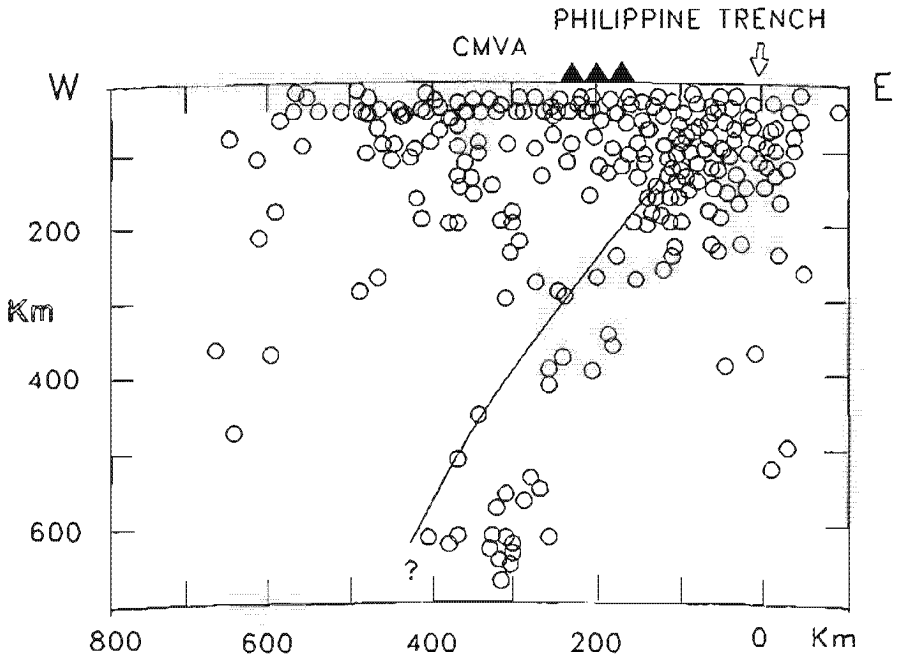
PHILIPPINE TRENCH
CMVA
W
E
200
Km
400
600
?
800
600
400
200
0
Km

b.

c.

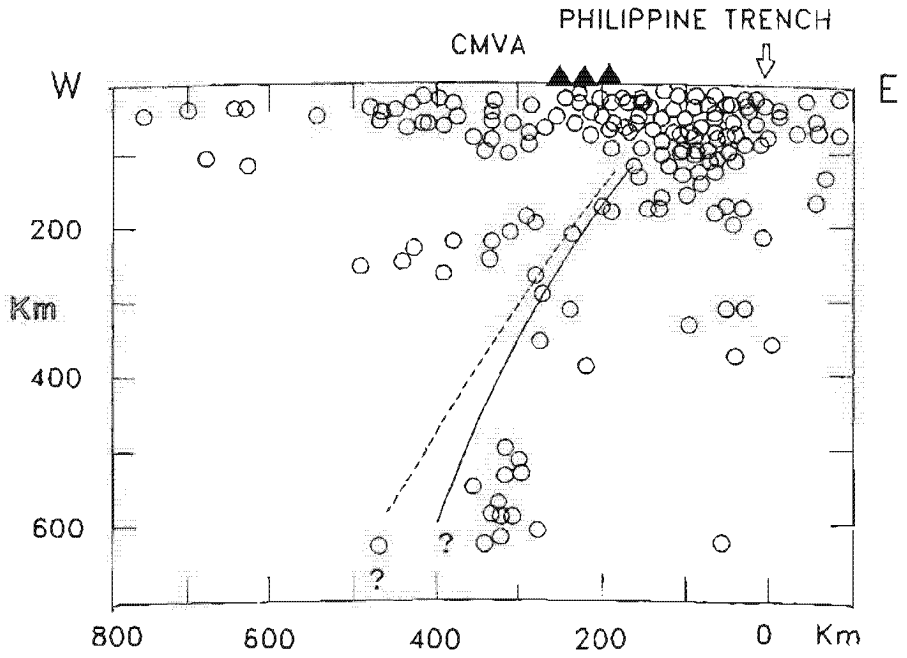

Figure 5-2. Crustal sections similar to Figure 5-1, using hypocenters located by the Philippine Institute of Volcanology and Seismology (unpublished data, PHIVOLCS). Earthquake data selected from over 4,000 events of Magnitude > 2.0. Hsu (1971) noted then that the Philippine seismic network could only accurately locate events of Magnitude ≥ 5.5. Additional seismographs since then have made the network more capable. As pointed out by Cardwell et al (1980) mislocated hypocenters can increase the apparent thickness of the seismic zone by tens of kilometers but on a regional scale, as shown above, the overall configuration of the seismic zone should not be grossly affected. **a.** section along Lat 6^{O}N. The thin sloping line is the inferred top of inclined seismic zone. **b.** section along Lat 7^{O}N. **c.** section along Lat 9^{O}N. Dashed line is the inferred top of inclined seismic zone in section **a.**

5.3. SOURCE REGION CHARACTERISTICS

5.3.1. PRESSURE (P), TEMPERATURE (T) AND αSiO_2

As discussed by Ringwood (1975), initiation of melt generation beneath arcs is likely to occur at temperatures at or above the oceanic geotherm. Magmas which are postulated to be partial melts must have equilibrated with mantle peridotite at pressure-temperature conditions at or above the pyrolite solidus. To determine the source conditions of CMVA magmas, pressure (P_{TOTAL}), temperature and silica activity (αSiO_2) of selected basalts were calculated (see Appendix 5) using thermodynamic methods similar to the approach of Barton and Wyers (1991). This gives an approximate depth at which phases start to crystallise. The results indicate a maximum depth of equilibration between crystal and melt of approximately 15 - 17 km (5.5 kbar) for the least differentiated lava (sample BUT6, Table 5-1). Applying the αSiO_2 of selected basalts to the petrogenetic grid of DePaolo (1981) returns a similar (6 kbar) pressure estimate (Fig. 5-3). Comparison of equilibrium pressure derived for CMVA basalt BUT6 with recent peridotite melting experiments show that, CMVA basalts equilibrated with their associated melts at lower pressure. At 8 kbar the experimental melt in equilibrium with a spinel lherzolite is an olivine tholeiite, and at 15 - 20 kbar, the equilibrium melt is an alkaline olivine basalt (Takahashi and Kushiro, 1983). Fujii and Scarfe (1985) similarly concluded that melts in equilibrium with a spinel peridotite at 10 kbar have magnesian MORB-like compositions. In terms of pressure - temperature conditions, the least differentiated CMVA basalts must therefore be derivatives of more primitive melts.

Table 5-1. Crystallising conditions of CMVA lavas.

Sample No.	Location	Lava Type	T °C	P_{Total} kbar	P_{H2O} kbar	X_{H2O} mol%	H_2O wt_i%	H_2O wt_p%
BUT51	Camiguin Is.	Basalt	1,118	2.7	0.8	0.052	1.3	-
HIB15	Camiguin Is.	Hb And	1,100	2.7	1.0	0.061	1.6	2.5
HIB20	Camiguin Is.	Hb And	1,064	2.0	1.0	0.067	1.7	3.5
HIB46	Camiguin Is.	Dacite	1,053	1.76	1.1	0.075	1.9	3.0
BAL4	Mt Balatocan	Basalt	1,090	4.6	0.75	0.040	1.0	1.4
BUT6	Bukidnon	Basalt	1,161	5.5	0.75	0.038	0.9	1.8
APO6	Mt Apo	Dacite	1,051	1.6	1.5	0.100	2.8	7.8

Sample numbers refer to compositions in Appendix 4-2. Geothermometry and geobarometry calculations explained in Appendix 5. Values for H_2O columns are initial followed by pre-eruption wt% H_2O content. The calculated αSiO_2 (-log units) are: H51, -0.36; BAL4, -0.33; BUT6, -0.35.

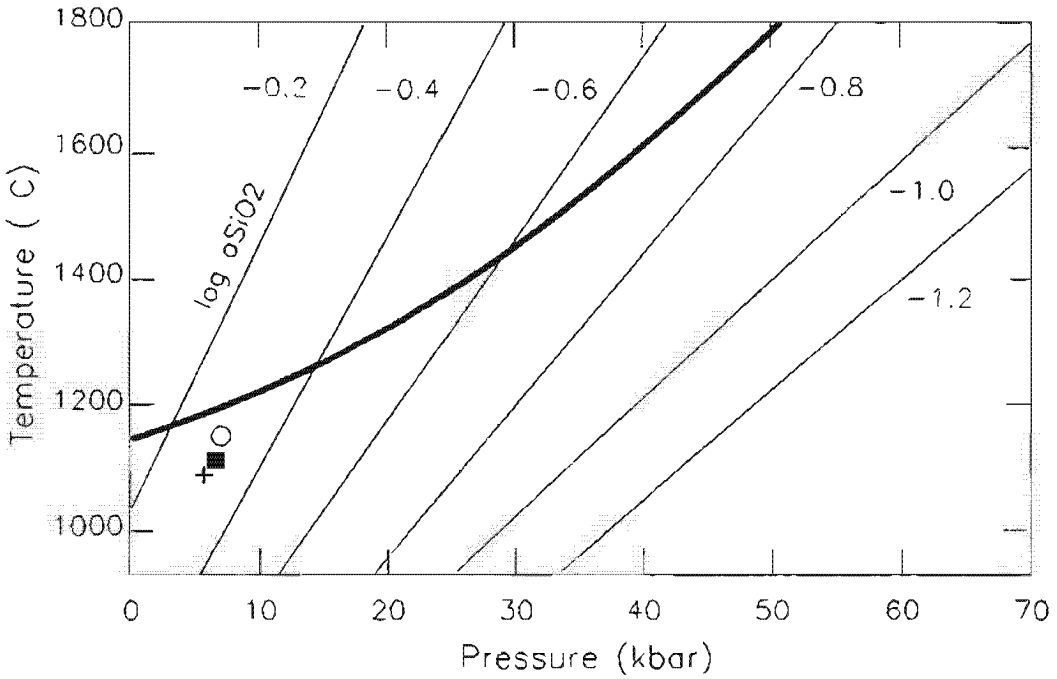

Figure 5-3. Petrogenetic grid of DePaolo (1981), for anhydrous conditions. The pressure of equilibration between melt and crystals can be determined given temperature (from olivine and plagioclase geothermometry) and from αSiO_2, as calculated in Appendix 5. Legend: O is from Bukidnon, + is from Mt Balatocan, ■ is from Camiguin Island. The thick line is the P-T curve for pyrolite solidus.

5.3.2. PRIMITIVE COMPOSITIONS

If CMVA basalts are derivative melts, it is important to know the original conditions and compositions of partial melts so that a realistic petrogenetic model for the CMVA may be obtained. Generally, model mantle compositions may be simplified by assuming that the MORB-type mantle source is uniform in mineralogy, consisting of olivine, two pyroxenes and an aluminous phase (Kinzler and Grove, 1992). This is supported by αSiO_2 values of CMVA basalts which suggest a main magma type geochemically between olivine tholeiite and alkaline olivine basalt (Fig. 5-4), occurring within the spinel peridotite stability field. If the primitive source composition is better defined, other conditions of parental CMVA magmas such as segregation depth of partial melts from source rock and degree of partial melting can be inferred.

Liquids considered to be primitive, generated by partial melting of upper mantle peridotite are those resembling magnesian MORBs (Mg# > 68), generally with low incompatible elements and high concentrations of V, Cr and Ni (Frey et al, 1978; BVSP, 1981; Fujii and Scarfe, 1985; Crawford et al, 1987; Gust and Perfit, 1987). The compositions shown in Table 5-2 and Appendix 4-2 indicate that no sampled CMVA basalt can represent a primary melt. All CMVA basalts have lower Mg#, Cr and Ni contents than primitive MORB.

Examination of variation in Cr, Ni and V gives an idea of which type of ferromagnesian phases fractionated. Figures 4-22 and 4-23 show rapid decline in Cr and Ni but less change in V for selected CMVA basalts. The variation in V of Mt Balatocan basalts is probably due to differences in modal clinopyroxene and suggests pyroxene accumulation in some samples. Magnetite is mostly a groundmass phase so this mineral does not appear to affect early V concentrations. Changes in V contents within Bukidnon volcanoes appear to be small (7 ppm from basalt to basaltic andesite). The fall in Cr content is assumed to be due to fractionation of Cr-spinel, which is a phenocryst in BUT6 olivine basalt.

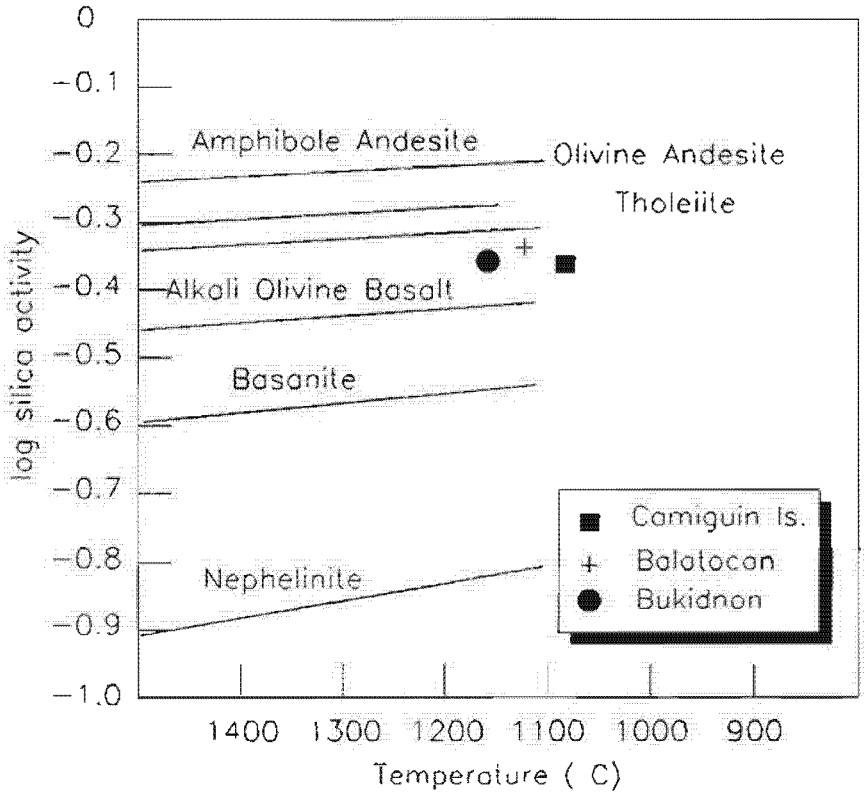

Figure 5-4. Plot of selected CMVA basalts (as in Fig. 5-3) in terms of αSiO_2 with temperature. Field boundaries of major lava types are taken from Ghiorso and Carmichael (1980).

Table 5-2. Examples of primitive MORB compositions and selected CMVA basalts.

Sample	1	2	3	4	5	6
Oxide (wt%)						
SiO_2	49.76	48.81	47.54	52.01	52.54	52.84
TiO_2	1.44	0.73	0.61	1.10	0.83	0.88
Al_2O_3	16.20	16.13	13.81	16.58	15.25	17.20
FeO	8.93	8.89	9.75	9.27	9.03	7.35
MnO	0.17	0.16	0.21	0.16	0.17	0.17
MgO	9.43	10.15	10.87	7.45	7.71	6.00
CaO	10.48	11.65	12.62	8.59	10.40	9.09
Na_2O	3.22	2.13	1.30	3.16	3.04	3.44
K_2O	0.24	0.07	0.41	0.46	0.62	1.51
P_2O_5	0.13	-	0.22	0.15	0.16	0.43
Mg#	0.68	0.71	0.69	0.65	0.66	0.65
Trace Elements (ppm)						
Sample	1	2	3	4	5	6
V	206	na	262	165	233	191
Cr	437	290	329	216	192	118
Ni	227	138	87	114	78	70

Major elements: Sample 1 is an E-MORB from le Roex et al (1985), analysis V39-26, Table 2; Sample 2 from Flower (1991), basalt no.2, Table 7.1; Sample 3 from Defant et al (1991), sample 120, Table 1a; Samples 4, 5 and 6 are CMVA basalts, analyses 75, 74 and 38, Appendix 4-2. Trace elements: data source same as for majors except: sample 2 is N-MORB average from Sun and McDonough (1989). Fe as total FeO. Mg# = Mg^{2+} / Fe^{2+} + Mg^{2+}. na = not available.

These observations suggest that the main fractionating phase is olivine (± Cr-spinel). A CMVA basalt parent can be therefore modelled as having a higher Mg# than the least differentiated basalt in a particular suite. This has been taken into account by addition of liquidus olivine into selected CMVA basalts until the major element compositions is in equilibrium with Fo_{88} similar to the approach by Hoffman et al (1984). As noted by Ormerod et al (1991), changes in trace element abundances using this correction method are small and should have no effect on trace element ratios. Assuming olivine-dominated fractionation from a parent magma, concentrations for selected incompatible elements from the analysed basalts are little affected and can be used to infer source magma characteristics.

The corrected analyses suggest possible *parental* CMVA magma compositions (Table 5-3). The amount of olivine added is 3 - 10 wt%, suggesting only small to moderate amounts of olivine fractionated from a partial melt to produce the CMVA derivative magmas. The corrected analyses have similarities with some representative primary MORB compositions in terms of SiO_2, TiO_2, Al_2O_3, FeO, MnO, MgO, and P_2O_5 at similar Mg#s (columns C and D). However, significant differences occur with respect to CaO, Na_2O and K_2O. These may be explained in several ways. If the low CaO level is an inherent feature, then more parental magmas must have even lower CaO because olivine fractionation increases both CaO and Al_2O_3 in derivative liquids. Thus assuming equilibrium with olivine + clinopyroxene + orthopyroxene residues, CaO and Al_2O_3 concentrations at a given degree of partial melting decreases with increasing pressure due to increasing MgO and FeO caused by contraction of the olivine phase volume (Falloon and Green, 1988). Some low CaO and Al_2O_3 primitive lavas (8.8 -9.7 wt% CaO, 10.1 - 10.9 wt% Al_2O_3, Mg# 0.75 - 0.78) also occur in the Tonga arc. Falloon and Green (1987) suggested these result from relatively high degrees of partial melting (> 25 %). Alternatively, low CaO and Al_2O_3 in CMVA basalts may be due to clinopyroxene and/or plagioclase fractionation but this is presumably volumetrically less important than olivine fractionation. Also, low plagioclase modes in CMVA basalt

Table 5-3. Corrected major element abundances.

	Camiguin		Mt Balatocan		Bukidnon		MORB	
Sample	4		5		6			
Wt % ol added	10		3		6			
Oxide	A	B	A	B	A	B	C	D
SiO_2	52.14	48.13	52.56	51.35	52.40	49.98	48.26	50.48
TiO_2	0.83	0.75	0.83	0.81	1.12	1.05	0.89	0.87
Al_2O_3	18.51	16.79	15.26	14.81	16.60	15.63	16.80	15.33
FeO	8.88	10.66	9.04	9.51	9.64	10.63	9.32	8.36
MnO	0.14	0.13	0.17	0.16	0.16	0.15	0.17	0.15
MgO	5.73	10.32	7.71	9.13	7.46	10.26	10.48	10.72
CaO	9.34	8.45	10.40	10.09	8.61	8.11	11.23	11.84
Na_2O	3.03	2.74	3.04	2.95	3.15	2.97	2.40	1.88
K_2O	0.97	0.88	0.62	0.60	0.47	0.44	0.03	0.17
P_2O_5	0.22	0.20	0.16	0.16	0.15	0.14	0.06	0.09
Mg#	0.59	0.69	0.66	0.71	0.64	0.68	0.68	0.69
Fo (E)	0.83	0.88	0.87	0.88	0.85	0.88	0.88	0.88

Correction by adding liquidus olivine to analyses in column A in 0.1 wt % increments following the method of Hoffman (1984). Calculations used $K_D=(FeO/MgO)_{MAGMA}$= 0.3 and $(Fe_2O_3/FeO)_{MAGMA}$= 0.3 (Roeder, 1974) until liquid is in equilibrium with Fo_{88} (column B), comparable to primitive MORB compositions given in columns C (sample CH21-D20-29, BVSP, 1981) and D (sample P2, most primitive olivine basalt, le Roex et al, 1981). Mg# = molar Mg / Mg + Fe^{2+}). Fo (E) is the olivine composition in equilibrium with liquid.

(mainly groundmass phases) do not suggest volumetrically significant early feldspar separation. Only small changes in Na_2O and K_2O contents are caused by olivine fractionation so the relatively high Na_2O and K_2O, compared with primitive MORB, suggest an enriched source. As the K_2O contents of corrected CMVA basalts are even higher than E-MORB signature (0.10 - 0.30 wt% at Mg# > 65; le Roex, 1987) it suggests either slab contribution or later (crustal?) contamination.

5.3.3. LIL-Element Enrichment

Arc basalts in the northern Philippines have been modelled in terms of a depleted mantle source (Defant et al, 1991b). However, some studies (Morris and Hart, 1983; Stern, 1981) suggest an OIB-type mantle to account for arc source geochemistry. This study proposes a slightly enriched mantle source to explain the relatively high Nb/Zr and Nb/Ce ratios. Other studies of basalts in the western Pacific also display E-type MORB characteristics, indicating that enriched mantle in the Philippine region is not unusual. For example, ocean floor basalts of the Shikoku Basin have E-MORB rather than N-MORB affinity (Wood et al, 1980). Similarly, Ikeda and Yuasa (1989) suggests an E-MORB geochemical reservoir for the southern part of the Izu-Bonin arc. However, an E-MORB, OIB-like mantle cannot be responsible for highly decoupled LILE/HFSE distributions. In OIBs, a deep mantle plume accounts for enrichment (Le Roex, 1987) but in convergent settings where the magma source is restricted to the mantle wedge, the subducted slab is a source of high K and other LILE concentrations. Most petrogenetic studies of arc magmas (e.g. Hawkesworth and Ellam, 1988; Zindler and Hart, 1986) therefore assume that HFSE contents are a primary feature of the mantle before subduction (mantle-derived component) and LILE concentrations are introduced by subduction (slab-derived component). The slab-derived component is LILE-rich but HFSE-depleted thus providing enrichment of K, Ba, Rb, and Pb whilst preserving HFSE mantle concentrations. To apply this model to CMVA lavas, evidence for slab (crust and/or sediment) involvement must be ascertained.

The role of subducted crust in arc magmas is usually evaluated using Sr, Nd, Th and Pb isotopes. Alternatively, crustal involvement may be qualitatively assessed for slab-derived flux by comparing variations in LILE to HFSE. An example is shown by the plot of Ba vs. Nb for CMVA basalts as well as other island arcs (Fig. 5-5). Also shown is the field of Ba/Nb ratios for MORB, generally considered an inherent feature of the mantle (Hawkesworth et al, 1991). The Ba/Nb ratios for MORB suggests similar bulk distribution coefficients for Ba and Nb. In contrast, the IAB field is consistently displaced towards higher Ba, possibly indicating slab-derived Ba. A better defined trend is shown by CMVA data whose uniform Nb concentrations (3 - 6 ppm) indicate this element is mantle-derived, considering low solubility in hydrous fluids. In contrast, Ba varies considerably (103 - 657 ppm). Because Ba has a low distribution coefficient (see Table A5-2, Appendix 5) the high Ba contents may be caused by small degrees of partial melting but this condition is unlikely as shown by partial melting calculations. The preferred interpretation is that variable and high Ba and K_2O contents are a direct contribution from the subducted slab.

The extent of contribution of a slab-derived component to the source region is still uncertain because of lack of isotope measurements. In general, radiogenic isotope data in other IABs indicate a smaller slab-derived component than suggested by their respective trace element contents (Hawkesworth and Ellam, 1988; Hawkesworth et al, 1991).

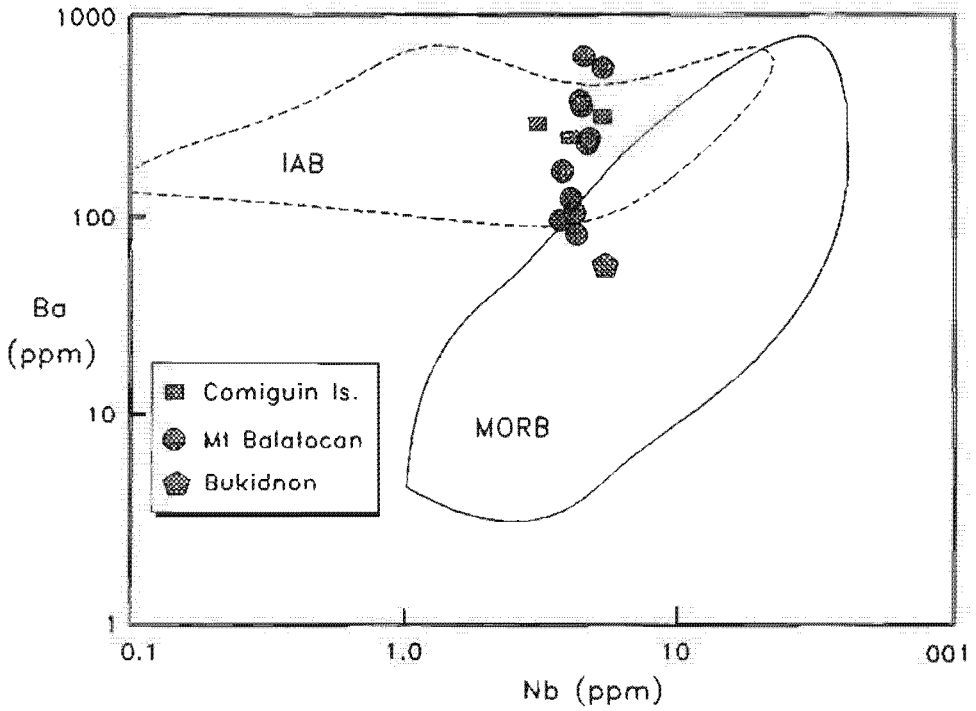

Figure 5-5. Plot of Ba vs. Nb for CMVA basalts showing that variation in Ba/Nb ratios is achieved by variation in Ba. Also shown are fields for IAB and MORB, after Hawkesworth et al, 1991.

McDermott and Hawkesworth (1991) noted their average IAB data have lower Rb/Sr ratios (0.03) than average continental crust (0.12, Taylor and McLennan, 1985) possibly indicating low crustal influence. CMVA basalts consistently have lower Rb/Sr ratios (0.015 - 0.026) than the average IAB data compiled by McDermott and Hawkesworth (1991) and indicates, at least, a similar or smaller fraction of slab-derived component than observed for other arcs.

Compelling evidence for incorporation of sediment in arc magmas is the presence of the cosmogenic isotope ^{10}Be in lavas (Morris and Tera, 1989; Morris et al, 1990). ^{10}Be is short-lived, traceable to 1.5 Ma so it is detected only in sediments. However, ^{10}Be measurements for the CMVA are not available. An alternative although less convincing evidence for sediment subduction is a negative Ce anomaly in REE patterns of IABs (Woodhead, 1989). Inspection of spider-diagrams of Figure 4-32 shows the differential behaviour of Ce compared with La and could indicate sediment involvement, although lack of other REE data (Sm - Lu) precludes better evaluation of the anomaly.

5.4. PARTIAL MELTING CONDITIONS

Generation and separation of partial melts from mantle material is usually modelled in terms of either batch or fractional melting. In equilibrium batch melting, the partial melt stays with the residue until melting is complete. The bulk composition of the system (melt + residue) remains constant. Equilibrium between melt and solid is assumed and the pressure associated with melt formation is the pressure of segregation. In fractional melting, the melt separates from the mantle in small increments which separate as soon as they are produced, preventing equilibrium between melt and residue. A variant of fractional melting is continuous melting or near-fractional melting, where small melt fractions are continuously, but not completely removed from the residue as melting proceeds. In the last two processes, the bulk composition of the system changes constantly during melting and the pressure related with a magma formed by aggregating each small melt fraction at a shallower depth will reflect the range in pressures of each melt fraction.

Recent models of partial melting favour polybaric, near-fractional melting conditions (McKenzie, 1984). Experiments on basalt melts demonstrate the ability of small melt fractions to escape from an olivine matrix (Riley and Kohlstedt, 1992). Trace element studies (Allegre and Condomines, 1982) also suggest that MORB is derived by small degrees of melting (< 1 %) and that large volumes of melt cannot remain in contact with their associated residue because of the potential for low viscosity basaltic melts to migrate (McKenzie, 1985). However, studies on fluid dynamic effects show that melt compositions cannot be very sensitive to fluid mechanics of the melting process (McKenzie and Bickle, 1988) so that qualitatively, aggregate melts produced by fractional melting are very similar to those modeled from equilibrium batch melting (Miller et al, 1992).

Partial melting experiments on various peridotite compositions (Jaques and Green, 1980; Stolper, 1980; Takahashi and Kushiro, 1983; Takahashi, 1986; Falloon et al, 1988) have led to establishment of a melting grid based on the CIPW molecular basalt tetrahedron. The projection from Di can be used to infer the depth of segregation for a primitive magma composition because the movement with changing pressure of the assemblage olivine + orthopyroxene ± clinopyroxene + liquid cotectic is well defined in the range 8 - 35 kbar (Falloon and Green, 1988). Results for the inferred CMVA primitive compositions suggest a depth of origin (segregation) between 10 and 15 kbar (Fig. 5-6).

To infer source chemistry and degrees of partial melting the equilibrium batch melting equation for trace elements (Shaw, 1970; Arth, 1976; Hanson and Langmuir, 1978) was solved for CMVA magmas. The choice of source mineralogy was constrained mainly by inferred depth of origin. It is assumed that garnet is not a significant phase controlling partial melt compositions because Zr/Y ratios are relatively constant with increasing Zr through basaltic compositions (see Fig. 4-31).

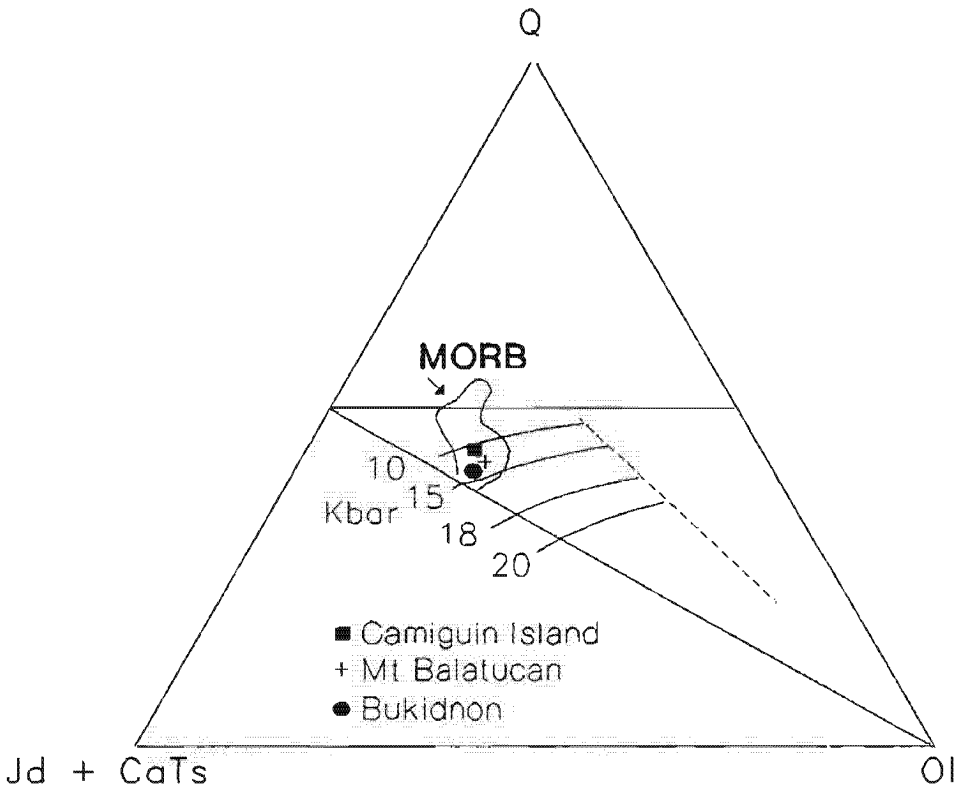

Figure 5-6. Composition of CMVA basalts, corrected for olivine fractionation, plotted in the CIPW molecular normative basalt tetrahedron. The projection is from diopside (Di) onto the base jadeite + Ca-Tschermak's molecule (Jd + CaTs) - Quartz (Q) - Olivine (Ol). CMVA basalts plot witin fields defined for compositions in equilibrium with peridotite partial melts at 10 - 15 kbar. Enclosed field shows primitive MORB glasses. Data for MORB and 15 - 20 kbar cotectic from Falloon and Green (1988). 10 kbar cotectic from Falloon and Green (1987). Procedure for projection is from Green (1970): Jd + CaTs = Ab + An + Ne; Qz = Ab + An + Hy + Qz - Ne; Ol = Ol + Hy. Normalised to 100%.

However, fractionation between the light and heavy rare earth elements should be evaluated in future studies.

The results given in Table 5-4 show the trace element abundances of the source assuming $D_P = 0$, similar to the approach of Arculus and Johnson (1978) and using a P source mantle value of 0.02 (Ringwood, 1974; Hoffman, 1988). The inferred degree of melting is 10 - 14%. Note that estimated K_2O source abundances are higher than enriched mantle so that to relate derived K_2O values of 0.063 - 0.076 wt% to the mantle value of 0.030 wt% (enriched source; Johnson, 1990) requires a degree of melting of < 5%. The moderate to high degrees of melting required for low CaO/Al_2O3 ratios in Table 5-3 favours the higher degrees of melting. Also, even if an enriched mantle source is responsible for high K_2O levels, absolute abundances of HFSE should also be high for magmas derived by relatively small partial melts. This is not the case for Zr and Nb, which are about 3 times and an order of magnitude lower respectively, than magmas derived by low degrees of melting of an enriched source (le Roex et al, 1992). Calculated values for Nb in the source for mainland CMVA (0.64 - 0.68 ppm; for sample BAL4 and BUT6) is higher than mantle (0.61 ppm; Hoffman, 1988) so that the presence of a residual titanate phase (titanite, perovskite, rutile) in the source region is unlikely. It has been suggested that increased Nb may be caused by higher - level fractionation processes (McCulloch and Gamble, 1991) and/or smaller degrees of partial melting (Plank and Langmuir, 1988; Hawkesworth and Ellam, 1989). The former process could account for relative enrichment in the CMVA if it is supposed that crust beneath Camiguin Island is thinner, as inferred from its oceanic setting, than crust beneath the central part of the arc (Bukidnon Volcanic Group). The lower calculated Nb content in the source region of Camiguin Island basalt may therefore indicate a smaller extent of fractionation than mainland CMVA basalts. However, inferred source Nb concentrations increases from Camiguin Island to Mt Balatocan to Bukidnon, indicating Nb contents are a feature of the source mantle.

Table 5-4. Inferred source chemistry of CMVA basalts

	Camiguin		Mt Balatocan		Bukidnon	
Analysis #	36		74		75	
% melt	10		12.5		14.3	
	Cl	Co	Cl	Co	Cl	Co
K (wt%)	0.75	0.076	0.57	0.072	0.44	0.063
Zr (ppm)	32.00	4.10	66.00	10.06	81.00	13.76
Nb	3.00	0.31	5.00	0.64	6.00	0.88
Ba	320.00	32.98	114.00	14.59	61.00	8.90
Rb	13.00	1.40	11.00	1.45	7.00	1.05
Sr	824.00	102.54	476.00	70.81	306.00	50.88
La	13.00	1.35	7.00	0.90	9.00	1.32
Ce	15.00	1.61	5.00	0.66	9.00	1.35
Nd	14.00	1.63	38.00	5.35	36.00	5.71
Y	19.00	6.56	16.00	5.82	22.00	8.29
Rb/Sr	0.016	0.014	0.023	0.020	0.023	0.021
K/Ba	23.438	23.044	50.00	49.35	72.131	70.79
K/Rb	576.92	542.86	518.18	496.55	628.57	600.00
K/Nb	2500.00	2451.61	1140.00	1125.00	733.33	715.90
Ce/Nb	5.00	5.19	1.00	1.03	1.50	1.53
Ba/Nb	106.67	106.39	22.80	22.80	10.17	10.11

Elemental abundances calculated assuming batch equilibrium melting Cl/Co = 1/[D + F(1-D)]. Partition coefficients based on Table A5-2. Source mineralogy assumed from spinel peridotite mantle: ol=0.55, opx=0.25, cpx=0.18, Sp=0.02 (le Roex, 1992). P was assumed to be incompatible, D=0. Cl=concentration of element in initial liquid; Co=calculated concentration of element in source.

Further evidence on the source region composition may be inferred from the graph of Ce/Nb vs. Ba/Nb ratios (Fig. 5-7), showing distinct fields for N-MORB, E-MORB, OIB and continental crust. Sample BUT6 from Bukidnon plots between primordial MORB (Sun E-M) and OIB, with a Ba/Ce ratio consistent with subduction-related lavas/continental crust. Some inferences are: 1) the low Ce/Nb, high Ba/Nb ratio for BUT6 is an inherent feature of the source, consistent with $D_{Ba} < D_{Nb} < D_{Ce}$ (i.e. relative extraction is the inverse of this sequence), and 2) to account for high Ce/Nb and Ba/Nb ratios displayed by Camiguin Island (Table 5-3), an enrichment process must be invoked. As Ba/Nb ratios of CMVA basalts and other IABs are higher than MORB in general, this enrichment must come from a slab-derived component. A depletion in Nb could produce the same result, as suggested by Ryerson and Watson (1987), but this is not indicated by Nb concentrations, which are higher than N-MORB levels.

5.5. DIFFERENTIATION PROCESSES

5.5.1. FRACTIONAL CRYSTALLISATION

Chemical diversity within a comagmatic suite is usually explained in terms of fractional crystallisation in magma chambers. A main premise is that fractional crystallisation follows the Rayleigh law (Allegre et al, 1977), meaning the immediate removal of crystals from melt as they form. This process results in a continuous variation of residual liquids (the liquid line of descent). Eruptions which tap a magma chamber at various stages of its liquid line of descent ideally produce the general basalt-andesite-dacite-rhyolite association of orogenic settings.

Fractional crystallisation was frequently visualised by gravitative crystal settling on a chamber-wide scale (Cox et al, 1979) due to homogeneous nucleation. This process was proposed to account for layered intrusions (Irvine, 1980) and occurrence of large volumes of residual liquids through compaction of cumulates (McKenzie, 1984; Sparks et al 1985).

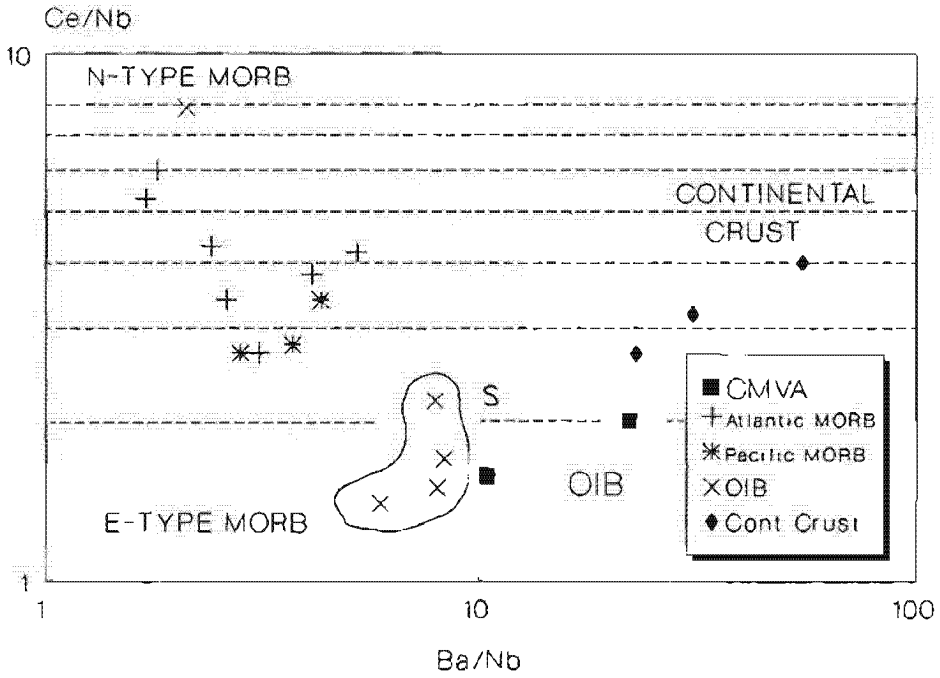

Figure 5-7. Plot of Ce/Nb vs. Ba/Nb ratios for 2 representative CMVA basalts showing affinity with E-type MORB/OIB and continental crust. MORB data from Saunders et al (1988), Hofmann et al (1986). OIB data from Weaver et al (1987), Palacz and Saunders (1986). Continental crust (bulk) data from Weaver and Tarney (1984). Data for S (E-MORB) after Sun (1980) and Sun and McDonough (1989).

Other studies (Chen and Turner, 1980; Nilson et al, 1985) favour crystallisation along the margins of a magma chamber where thermal and chemical contrasts between wallrock and magma are considerable. Such conditions may result in *in situ* crystallisation (Langmuir, 1989) which forms a crystal mush layer (or solidification zone) between dominantly liquid interior and solid chamber walls.

One major effect of *in situ* crystallisation is fractionation of phases below the liquidus of the main magma body and this produces crystals and residual liquids which normally appear late in the crystallising sequence. Modeling of *in situ* crystallisation using natural magma compositions (Nielsen, 1991) showed that whereas homogeneous crystallisation is confined to the cotectic, in situ crystallisation is not. For example, the solidification zone may be saturated with Ti-magnetite assuming a high % of crystallisation (as found in gabbros) but at the same time liquids erupted from the main magma chamber may be saturated only with olivine (common in basalt flows). A consequence of this process is suppression of Ti-enrichment in subsequent lavas because magnetite is being crystallised in the solidification zone. Similarly, Ca or P enrichment in a magma chamber, usually caused by homogenous crystallisation, could be suppressed if augite or apatite respectively were crystallising in the solidification zone and residual liquids re-enter the main magma chamber. If these liquids are erupted, their compositions could reflect the Ca or P suppression without evidence of either augite or apatite in the liquidus.

If evolved melts resulting from *in situ* crystallisation ascend fast enough to prevent thermal and chemical re-equilibration with the main liquidus phases, a compositionally stratified magma chamber will result, with SiO_2-rich andesite and dacite overlying denser mafic magma. The manner in which residual melt escapes quickly enough to form a stratified chamber is still uncertain. Recent modeling (Bedard et al, 1992) suggest residual melts may rapidly evacuate a solidification zone by intra-cumulate channels which are formed by residual liquids themselves. The above experiment also supports the notion of compositional zoning resulting

from a thermally convecting lower zone overlain by a relatively stagnant evolved upper layer.

If homogeneous crystallisation or *in situ* fractionation are dominant processes in the evolution of magma chambers, some evidence should be observed to relate the above processes to comagmatic rocks. Fractional crystallisation paths are usually identified by curved trends in whole-rock oxide and element variation diagrams, resulting from crystallisation and separation of various minerals. Some general trends are continuously decreasing MgO, CaO, TiO_2 and increasing K_2O, Na_2O, Ba and Rb with increasing SiO_2. The trend of certain elements early in the differentiation history allows identification of early fractionating phases. For example, rapid fall in Ni and Cr with decreasing MgO and of V with increasing SiO_2 indicate early crystallisation of olivine and clinopyroxene. More subtle but significant characteristics are displayed by mineral chemistry. A general decrease in TiO_2/SiO_2 ratios, Ca and increase in Fe and Mn of zoned clinopyroxenes record a "normal" pyroxene crystallisation trend. MgO/FeO ratios of olivines should agree with calculated MgO/FeO values of bulk rocks (assuming appropriate K_D). Overall, crystallisation temperatures decrease from mafic to silicic compositions as the cotectic evolves to lower temperatures.

5.5.2. Magma Mixing

Magma mixing is usually envisaged as involving two chemically distinct magmas derived from different sources and is petrographically and chemically documented by compositional banding, disequilibrium mineral assemblages and presence of xenoliths (Michael, 1989; Gourgaud and Thouret, 1990). However, magma mixing may occur for magmas derived from a common source (Russell, 1991). In the latter, mixing may be caused by 1) intrusion of basaltic magma into a more fractionated magma chamber (Nixon, 1988) or 2) as an internal differentiation process caused by convection of a once compositionally stratified magma chamber (Brophy, 1987). In the first case, mixing may be due to chamber replenishment, and mixing occurs as an essentially open chemical system. This results in buffering of

major elements while increasing incompatible element contents. In the second example, the magma chamber is relatively a closed system, with basaltic and SiO_2-rich endmembers exhibiting *initial* crystal fractionation features overprinted by a mixing signature, usually identified by *linear* trends in variation diagrams.

Mixing in magma chambers need not occur in a large scale. If residual liquids from *in situ* crystallisation are somehow incorporated back into the main magma body, a mixing effect may be induced. Sparks (1989) inferred that such mixing produces disequilibrium as more evolved residual liquids from the chamber walls are heated and attempt to re-equilibrate with liquidus crystals. Similarly, more evolved crystals derived from *in situ* crystallisation, if swept toward the chamber interior (perhaps by turbulent convection, brecciation etc.), are likely to be in disequilibrium with more primitive melts and may be subjected to melting or resorption. This may be one reason why disequilibrium features (e.g. reverse, oscillatory zoning, sieved plagioclase, etc.) attributed to magma mixing are also common in magmatic systems modelled by crystal fractionation alone as there may be a small mixing component.

5.6. REGIONAL DISCUSSION OF 'BEST-FIT' PROCESSES

Any differentiation process used to explain the evolution of central Mindanao volcanoes must take into account that andesites and dacites dominate large cones of this volcanic arc. An origin of calcalkaline andesite by hydrous fusion of eclogite (Yoder and Tilley, 1962) or lherzolite (Kushiro, 1972) is now largely discounted because of geochemical dissimilarities between proposed and observed compositions (Mysen et al, 1974; Gill, 1974; Green, 1976; Crawford et al, 1987). Although some studies still propose melting of subducted slab to produce andesite-dacite suites (Defant et al, 1991a), these models are appropriate only to special cases (e.g. subduction of relatively hot crust in Central America). The majority of

1991; Defant et al, 1991; Miller, 1992; Price et al, 1992; Singer, 1992; and many others) agree that crystal fractionation, magma mixing and assimilation, are the dominant processes in orogenic andesite genesis. Because petrographic and chemical evidence also suggest some of these processes are responsible for the range of CMVA compositions, this section investigates in detail the role of various differentiation mechanisms.

5.6.1. HIBOK-HIBOK

(i) Fractional crystallisation

Mass balance calculations (Bryan et al, 1969) were made on samples from Hibok-Hibok which range from andesite to dacite. No basalts or basaltic andesite flows are associated with the specific rock suite chosen from Hibok-Hibok so basaltic andesite enclaves occuring in andesite lava flows were used as starting compositions. The use of basaltic andesite enclaves in petrogenetic modelling may be questioned. Vukadinovic and Nicholls (1989) excluded basaltic enclaves from their studies because these enclaves displayed anomalous incompatible element characteristics, compared with the rest of their samples. They inferred possible interaction between mafic enclaves with acidic host rock while in predominantly liquid states resulting in element-element interchange between two transient liquids, as discussed by Ryerson and Hess (1978). These conditions are considered unlikely at Hibok-Hibok enclaves because 1) the contact between inclusions and host rock is sharp which does not suggest reaction and 2) major and trace element concentrations (sample HIB37, analysis 2, Appendix 4-2) are similar to other basaltic rocks of Camiguin Island (cf sample KAN23, analysis 1, Appendix 4-2). Differences between these rocks are mainly in Cr, Ni and Sr which may reflect various amounts of fractionated olivine and accumulation of plagioclase. Similarities in trace elements are emphasised by Figure 5-8. Thus basaltic andesite enclaves appear to be mechanically-entrained fragments of an early mafic pulse of Hibok-Hibok which have not been remelted by a more evolved magma.

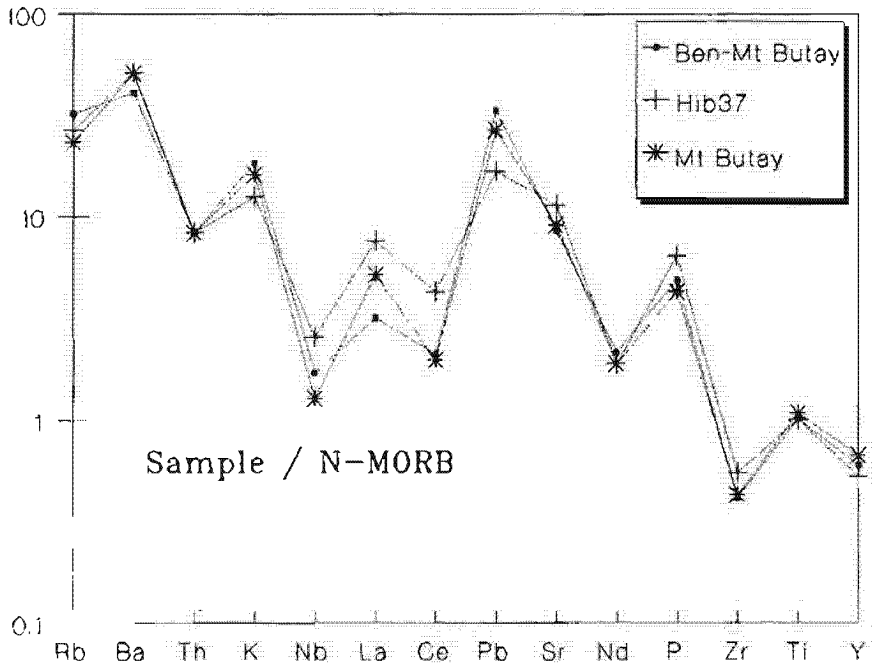

Figure 5-8. N-MORB normalised element plot of Camiguin Island mafic lavas. Sample Hib37 is a basaltic inclusion with generally similar trace element contents with other basalts. Normalisation factors from Sun and McDonough (1989).

Results of least squares mixing calculations are given in Table 5-5. Trace elements were calculated using mineral partition coefficients from Table A5-2 (Appendix 5) and F values derived from major element calculations.

A number of possibilities occur for fractionating differing mineral proportions from the parent magma to yield the desired daughter compositions but the calculations presented here have ΣR^2 values < 1.0. Defant and Nielsen (1990) conclude that high arbitrary ΣR^2 values (e.g., 1.2, Wyers and Barton, 1986) are not indicative of crystal fractionation but suggest other processes such as magma mixing or assimilation.

A simple two-stage model was selected to demonstrate crystal fractionation from i) basaltic andesite to SiO_2-rich andesite and ii) SiO_2-rich andesite to dacite. Mineral compositions of proposed parent rocks were used as fractionating assemblages (see Table 5-5 and Appendix 3-2). The first stage involves predominant separation of plagioclase (An_{67}) and Ca-rich pyroxene ($Ca_{43}Mg_{42}Fe_{15}$) with lower proportions of olivine (Fo_{82}) and magnetite (Usp_{23}). Stage two mimics disappearance of olivine from the liquidus, continued fractionation of plagioclase (An_{49}), Ca-rich pyroxene ($Ca_{41}Mg_{44}Fe_{15}$), magnetite (Usp_{24}) and appearance of amphibole. Major element calculations produce acceptable ΣR^2 values and a reasonable amount of crystallisation (34 - 42%). Calculated trace element concentrations are generally close to the observed daughter for Rb, Sr, V and Zr while misfits occur for Ba, Cr and Ni. Relatively large residuals for Ba probably result from uncertainties in bulk partition coefficient D_{Ba} while Cr and Ni are strongly constrained by low starting concentrations. An alternative mass balance calculation relating andesite sample HIB15 to the same daughter composition results in a better match between calculated and observed oxide concentrations (ΣR^2=0.107). However, the first set of mass balance mix is the the most consistent in terms of combined major and trace element data and adequately supports crystal fractionation as the dominant differentiation process in Hibok-Hibok.

Table 5-5a Mass balance calculations to demonstrate fractional crystallisation of Hibok-Hibok (Camiguin Island) lavas.

Stage 1: Basaltic andesite ⇒ SiO_2-rich Andesite

	Parent	Daughter			Phase removed			
	Bas-and	Andesite			0.040	0.291	0.268	0.086
Anal #	21864	21843			H294	H1R339	H51398	H51238
Sample	HIB37	HIB12	Calc	Resid	Ol	Pl	Cp	Mt
SiO_2	53.83	57.57	53.83	0.00	39.87	52.06	51.52	0.12
TiO_2	0.76	0.62	0.73	0.03	0	0.06	0.61	8.37
Al_2O_3	18.03	18.08	18.01	0.01	0	29.19	2.88	4.73
FeO	8.08	6.57	8.09	0.01	16.77	0.62	8.73	77.59
MnO	0.16	0.16	0.16	0.00	0.14	0	0.41	0.46
MgO	5.00	3.69	5.00	0.00	43.44	0.07	14.20	3.06
CaO	9.71	7.94	9.71	0.00	0.13	13.42	20.28	0
Na_2O	3.09	3.65	3.14	-0.03	0	3.56	0.47	0
K_2O	1.09	1.44	0.95	0.07	0	.020	0	0
P_2O_5	0.25	0.27	0.18	0.07	-	-	-	-

ΣR^2= 0.036 F = 0.66 %Crystallised = 34

Trace Elements

	D	Calc	Obs	Resid	Daughter
Rb	0.02	19	21	2	29
Ba	0.09	301	380	79	441
Sr	1.04	899	876	-23	882
V	2.01	216	220	5	142
Cr	3.05	69	37	-32	29
Ni	1.78	22	23	1	16
Zr	0.05	63	76	13	94

Abbreviations: Anal #–whole rock or mineral analyses given in Appendix 4-2 and 3-2. Calc is the calculated daughter composition. Resid are residuals. Mineral fractionated Ol= olivine, Pl=plagioclase, Cp=clinopyroxene and Mt=magnetite. F is the fraction of liquid remaining. D is the bulk distribution coefficient of selected trace elements calculated from partition coefficients given in Table A5-2, Appendix 5. All calculations used algorithms in PETMIN (Eby, 1990), an integration of IGPET (Carr, 1987) and MINFILE (Afifi and Essene, 1988) programs. Weighting factors for oxides are SiO_2, 0.50; TiO_2, 1.00; Al_2O_3, 0.60; FeO, 1.00; MnO, 0.50; MgO, 0.50; CaO, 1.00; Na_2O, 0.5; K_2O, 0.50; P_2O_5, 0.50. These are default values in PETMIN, except for Na_2O, K_{2O} and P_2O_5 which were adjusted accordingly. Dashed fields: not determined.

Table 5-5b. continued.

Stage 2: SiO_2-rich Andesite ⇒ SiO_2-rich Andesite

	Parent Andesite	Daughter Andesite			Phase removed 0.404	0.198	0.058	0.029
Anal #	21843	21869			H51368	15638	C1510	H02589
Sample	HIB12	CAT46	Calc	Resid	Pl	Hb	Cp	Mt
SiO_2	57.57	62.17	57.59	-0.01	58.12	43.70	52.73	0.06
TiO_2	0.62	0.60	0.71	-0.10	0	1.70	.020	8.59
Al_2O_3	18.08	17.01	18.00	0.04	26.68	11.81	1.35	1.56
FeO	6.57	5.21	6.57	0.01	0.16	13.85	8.88	83.52
MnO	0.16	0.11	0.13	0.02	0	0.27	0.60	0.59
MgO	3.69	2.76	3.69	0.01	0.03	12.68	15.43	1.04
CaO	7.94	5.96	7.95	0.00	9.81	11.33	19.83	0.02
Na_2O	3.65	3.93	3.93	-0.14	5.47	2.29	0.27	0
K_2O	1.44	1.97	1.25	-0.09	0.21	0.47	0	0
P_2O_5	0.27	0.27	0.16	0.06	-	-	-	-

ΣR^2= 0.042 F = 0.58 %Crystallised = 42

Trace Elements

	D	Calc	Obs	Resid	Daughter
Rb	0.03	24	29	5	41
Ba	0.15	367	441	74	582
Sr	1.14	894	882	-11	826
V	2.62	267	142	-126	111
Cr	9.52	1	29	28	31
Ni	2.68	53	16	-37	21
Zr	0.05	59	94	35	99

Abbreviations as in Table 5-5a.

Further evidence for crystal fractionation at Hibok-Hibok lavas are shown by Pearce Element Ratio (PER) plots (Russell and Nicholls, 1989). If K is assumed incompatible throughout the crystallisation sequence, this element may be considered conserved and used as a common denominator. Figure 5-9 is a PER plot of a comagmatic suite from Hibok-Hibok lava flows and domes erupted in 1948-1951. This graph shows that predominant fractionation of olivine + plagioclase + clinopyroxene strongly controls the compositional variation of lavas, shown by a slope close to 1.0. This assemblage is consistent with the main fractionating phases required by mass balance, and shows the minor role of magnetite, which petrography indicates to be a late crystallising phase. However, fractionation of olivine and plagioclase also produces a slope close to unity so this assemblage cannot be rejected in the differentiation sequence. By contrast, segregation of olivine + clinopyroxene, or either of plagioclase or olivine alone cannot reproduce observed fractionation trends.

(ii) Role of Amphibole

In andesites and dacites which lack the complete phenocryst assemblage olivine + plagioclase + clinopyroxene, amphibole can be used to infer the equilibrium pressure of crystallisation. One-atmosphere experiments (Grove et al, 1982, 1983) define a possible reaction between olivine + clinopyroxene + plagioclase + liquid to form amphibole at elevated H_2O pressures. Continued cotectic crystallisation of these minerals at low pressure leads to elimination of olivine, crystallisation of magnetite and orthopyroxene to drive liquid to rhyolitic compositions (Grove and Donnelly-Nolan, 1986). However, experimental studies (e.g. Helz, 1973) show that amphibole can crystallise from the reaction olivine + clinopyroxene + liquid in basaltic systems at higher pressure. A crystallisation path towards calcalkaline andesites may result from clinopyroxene ± olivine fractionation from a basaltic liquid at 5 - 10 kbar, forming amphibole in equilibrium with basaltic andesite (53 - 54 wt% SiO_2, Foden and Green, 1992). In their melting experiments, Foden and Green (1992)

inferred a reaction boundary in which clinopyroxene reacts with liquid to form amphibole + liquid. This reaction may explain 1) formation of hornblende andesites from Hibok-Hibok at the expense of clinopyroxene and 2) the relatively high crystallisation pressure (P_{TOTAL} ~2.7 kbar, 1100°C) estimate for hornblende andesite (sample HIB15, Table 5-1). Hibok-Hibok dacites evolved at approximately P_{TOTAL} ~1.7kbar (1,053°C). The first observation of amphibole at Hibok-Hibok occurs at 55 wt% SiO_2 (see Ch. 3) and may indicate a pressure of origin similar to SiO_2-rich hornblende andesites.

The above results indicate magma genesis was polybaric and may reflect existence of magma chambers at different subcrustal levels beneath Camiguin Island. A simple interpretation of the equilibrium pressure data is location of a magma chamber in the lower crustal region (8 - 10 km) and another at about ~5 km. The depths of magma reservoirs probably vary and in one instance may be very shallow, as indicated by subsidence NW of Camiguin Island during dome extrusion of Mt Vulcan from 1871-1875.

5.6.2. Butay, Benoni and Mt Ginsiliban

Lavas from southern Camiguin Island also have a wide compositional range (SiO_2 = 52.84 - 62.85 wt%). Previous studies (e.g. Abad, 1949; Alcaraz, 1950; Alcaraz, 1952) and this study proposes that these three volcanic centres represent a distinct phase of Camiguin Island volcanism. Their close spatial occurrence and major element properties suggest a common petrogenesis. Mt Butay, the oldest centre, is built largely from basaltic andesites whereas Benoni volcanics are composed of SiO_2-rich andesite-dacite pyroclastics. Mt Ginsiliban lavas consistently plot between the above compositions, from 57.55 - 61.4 wt% SiO_2.

Assuming a similar source, could these volcanic centres be related by a common fractionation process (i.e. represent different segments of a liquid line of descent) or represent some mixing mechanism? Evidence for either case may be

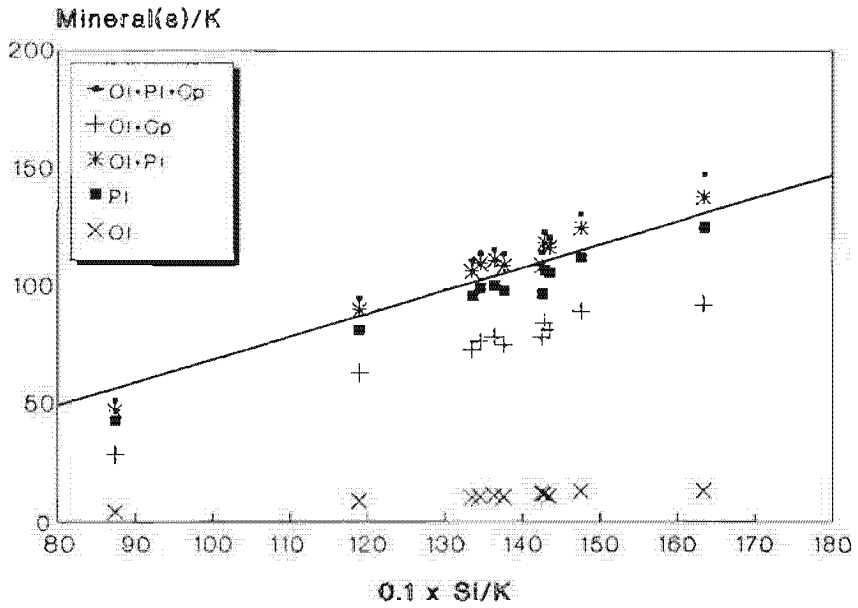

Figure 5-9. Pearce element ratio plot of a comagmatic calcalkaline suite from Hibok-Hibok. The line shown has a slope of 1.0.

acquired from intermediate compositions. Mt Ginsiliban SiO_2-rich andesites are unusual in that these are invariably microphyric to aphyric, dominated by crystals of augite and hypersthene, with few plagioclase phenocrysts.

Most of these crystals have ragged edges and mottled texture (see Fig. 3-27c) which is in contrast to clear and euhedral pyroxenes of other CMVA volcanoes. Two pyroxene geothermometry of Mt Ginsiliban andesites also yields lower temperature (~ 977^{o}C) than other andesites at similar SiO_2 levels or even dacites (1,064 - 1,100^{o}C, ~1,050^{o}C, respectively).

A possible explanation of disequilibrium features described above is mixing between Mt Butay basaltic andesite and Benoni SiO_2-rich andesite and dacite to produce Mt Ginsiliban compositions. This is supported by paucity of compositions intermediate between Butay and Benoni volcanics (Fig. 5-10a). The majority of intermediate compositions are represented by Mt Ginsiliban (Fig. 5-10b). However, compositional gaps are not as well defined with changing SiO_2 (Fig. 5-10c). The nearly linear variation of major oxides and trace elements with SiO_2 may also indicate an effect of mixing rather than fractionation.

Least-squares mixing calculations (Table 5-6) show that a basaltic andesite from Mt Butay and a dacite from Benoni can be combined in 2.1:1.0 proportions to produce SiO_2-rich andesites of Mt Ginsiliban (ΣR^2=0.39). In principle, trace element concentrations plot correctly, forming a co-linear trend between Benoni and Mt Butay compositions (Fig. 5-10c, d).

A strong argument against a mixing hypothesis between southern Camiguin Island volcanoes is the unusual aphyric andesite of Mt Ginsiliban lavas. Usually, hybrid lavas derived from two compositionally different magmas display distinct petrographic characteristics such as compositional banding, reaction rims around minerals, xenoliths, etc., none of which is observed at Mt Ginsiliban.

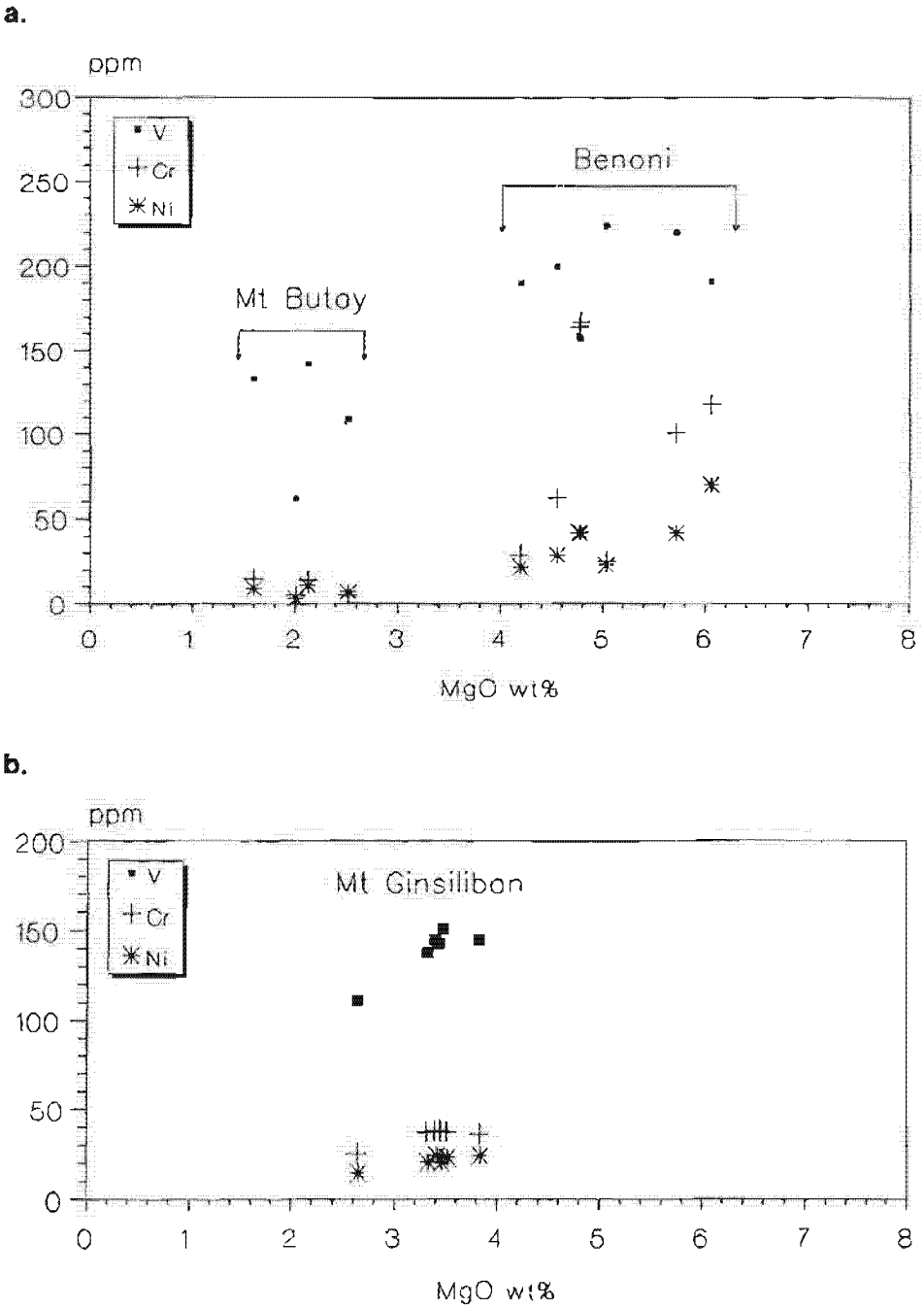

Figure 5-10. Variation of V, Cr and Ni for southern Camiguin Island volcanoes. Samples from each centre were separated for clarity. a) Basaltic andesites occur at Mt Butay whereas SiO_2-rich compositions generally occur at Benoni. b) Intermediate compositions dominate Mt Ginsiliban.

c.

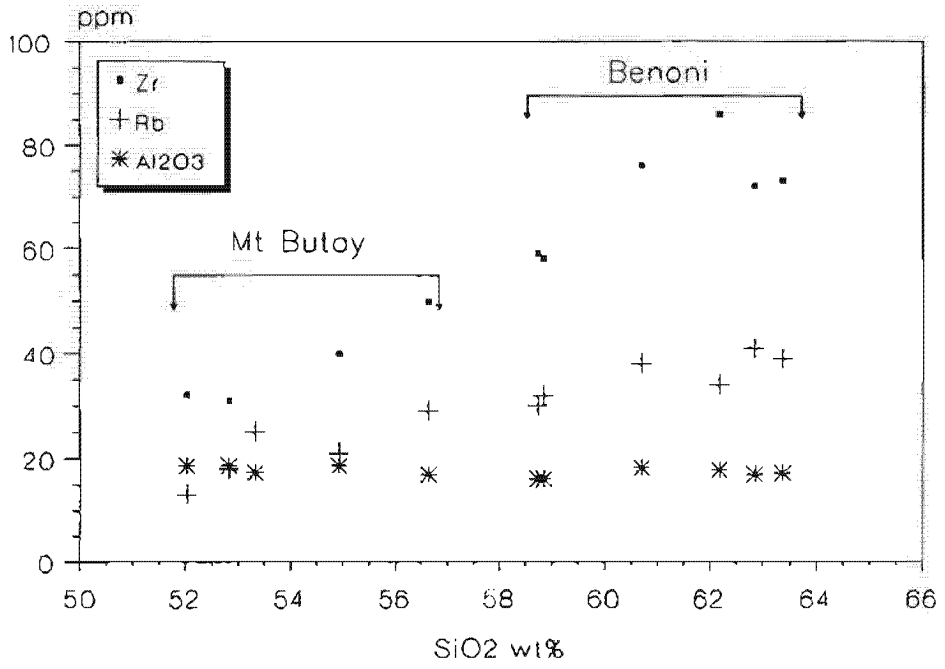

d.

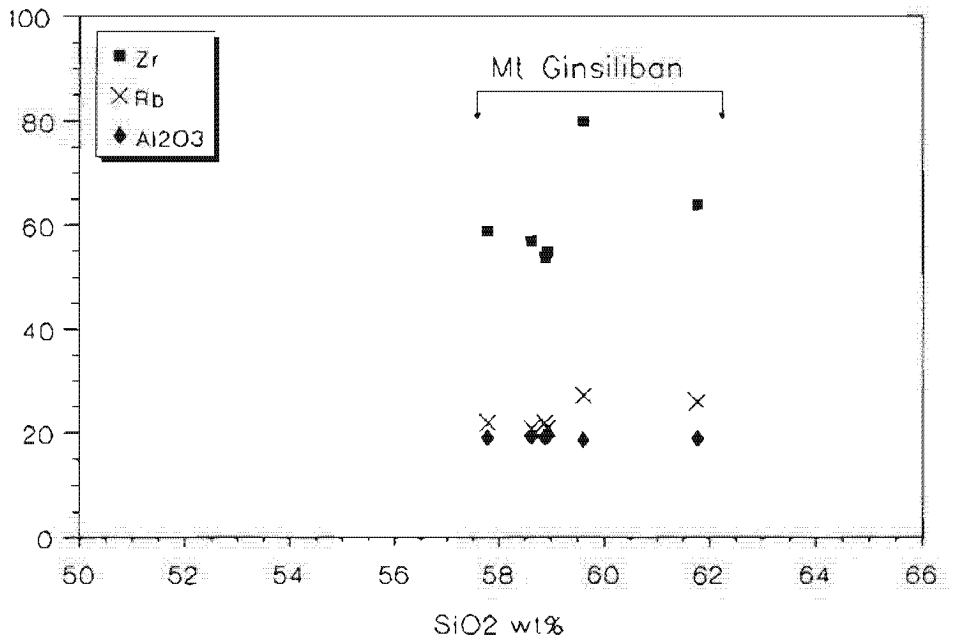

Figure 5-10c and d. Same samples as in Fig. 5-10a and b but showing variation of Zr, Rb and Al_2O_3 with SiO_2.

Table 5-6 . Least squares mass balance calculation for possible magma mixing of Benoni-Butay lavas to produce Mt Ginsiliban compositions. Oxides in wt%, trace elements in ppm.

Sample	BUT51	BEN30	CAM275	CALC	DIFF
SiO_2	53.42	62.93	59.66	59.86	-0.10
TiO2	0.89	0.49	0.59	0.62	-0.03
Al_2O_3	17.39	16.98	17.93	17.09	0.50
FeO	7.44	5.26	6.01	5.94	0.07
MnO	0.17	0.12	0.11	0.14	-0.01
MgO	6.07	2.14	3.33	3.37	-0.02
CaO	9.19	6.02	6.75	7.01	-0.26
Na_2O	3.48	3.96	3.73	3.80	-0.08
K_2O	1.53	1.95	1.60	1.81	-0.21
P_2O_5	0.43	0.16	0.29	0.25	0.04

Mixing proportion: Basaltic andesite: Dacite ⇒ 2.1:1.0 $\Sigma R^2 = 0.39$

Element	Calculated	Observed	Residual	BUT51	BEN30
Rb	36	34	-2	25	41
Ba	531	465	-66	432	570
Sr	744	829	84	961	641
V	158	139	-20	191	142
Cr	46	39	-7	118	14
Ni	29	19	-10	70	11
Zr	85	79	-6	112	72

Abbreviations as in Table 5-5a.

The only way to reconcile Mt Ginsiliban petrography is for complete blending to have taken place but this is unlikely because then, hybrid magmas should have very narrow compositions, in contrast to Figures 5-10b and d. The unusual texture of Mt Ginsiliban SiO_2-rich andesite are better accounted for by *in situ* crystal fractionation. It was demonstrated by Nielsen and DeLong (1992) that *in situ* crystal fractionation would produce aphyric evolved compositions. Such a mechanism might also explain the apparent lack of plagioclase phenocrysts which are common in other CMVA andesites, if it is assumed that the majority of plagioclase and other early phenocrysts have crystallised along the chamber walls and a major fraction of erupted material were residual liquids.

5.6.3. BUKIDNON

Three lava types occur in close proximity at Bukidnon. Butong Hill is a basaltic cinder cone which is among the least differentiated in the CMVA (low SiO_2 and K_2O, Mg# = 0.65). Sample BUT6 from this centre is therefore the starting composition. About 5 km north is Musuan Volcano, a small andesite dome. Musuan lavas are unusual in that these have higher MgO, Cr and Ni (sample MUS15. Appendix 4A) than other andesites at similar SiO_2 levels, but still more evolved than Butong Hill basalts so that a differentiation trend may be inferred. This is tested by simple crystal fractionation (Table 5-7a). The major element solution is acceptable (ΣR^2 = 0.128) but the trace element fit is poor. A simple fractional crystallisation scheme between these lavas is therefore unlikely.

An alternative parent lava is a basaltic andesite from Quezon River volcanics (sample QUE7), which underlies Butong Hill and Musuan Volcano. QUE7 has high MgO (Mg# = 0.71, SiO_2 = 54.72 wt%), which could better explain the high MgO contents of Musuan lavas. Table 5-7b shows a more reasonable fit for major (ΣR^2 = 0.044) and trace elements, and indicates fractional crystallisation is possible between QUE7 and MUS15.

Table 5-7a. Mass balance calculation to model possible fractional crystallisation between basaltic andesite to andesite from Bukidnon.

	Parent	Daughter			Phase removed			
	Bas-and	Andesite			0.102	0.415	0.165	0.078
Anal #	23264	23262			B6583	T6MC6	B6357	B6108
Sample	BUT6	MUS15	Calc	Resid	Ol	Pl	Cp	Mt
SiO_2	52.57	56.56	52.57	0.00	40.16	53.39	51.26	0.09
TiO_2	1.11	0.75	0.88	0.23	0	0.04	0.96	7.80
Al_2O_3	16.76	17.00	16.77	-0.01	0	29.27	3.32	4.74
FeO	9.37	7.03	9.39	-0.02	16.28	0.70	8.76	77.97
MnO	0.16	0.14	0.13	0.03	0.19	0	0.12	0.32
MgO	7.53	6.17	7.52	0.01	42.43	0	14.32	2.67
CaO	8.68	7.37	8.69	-0.01	0.13	13.10	19.83	0.07
Na_2O	3.16	3.32	2.90	0.15	0	3.87	0.48	0
K_2O	0.46	1.39	0.92	-0.23	0	0.07	0	0
P_2O_5	0.15	0.27	0.18	-0.01	0	0	0	0

ΣR^2= 0.128 F = 0.65 %Crystallised = 35

Trace Elements

	D	Calc	Obs	Resid	Daughter
Rb	0.02	17	7	10	25
Ba	0.08	209	61	-147	305
Sr	0.95	439	306	-129	441
V	2.40	319	165	-152	172
Cr	3.10	67	218	170	233
Ni	2.59	174	114	-59	87
Zr	0.04	68	81	14	101

Abbreviations as in Table 5-5a.

Table 5-7b.

	Parent	Daughter			Phase removed			
	Bas-and	Andesite			0.057	0.095	0.030	0.002
Anal #	23263	23262			Q6108	QMC0	QC175	Q2702
Sample	QUE7	MUS15	Calc	Resid	Ol	Pl	Cp	Mt
SiO_2	54.72	56.56	54.73	-0.01	39.45	53.24	52.23	0.09
TiO_2	0.84	0.75	0.66	-0.18	0	0.05	0.76	8.91
Al_2O_3	16.62	17.00	16.67	-0.02	0	29.20	2.27	2.36
FeO	7.18	7.03	7.20	-0.02	17.08	0.66	0.081	81.53
MnO	0.13	0.14	0.13	0.00	0.11	0	8.65	0.42
MgO	7.82	6.17	7.81	0.01	42.15	0	14.96	1.88
CaO	7.69	7.37	7.65	0.04	0.15	13.12	19.68	0.04
Na_2O	3.46	3.32	3.59	-0.06	0	3.77	0.49	0
K_2O	1.30	1.39	1.15	0.07	0	0.07	0	0
P_2O_5	0.24	0.27	0.23	0.01	-	-	-	-

ΣR^2= 0.044 F = 0.81 %Crystallised = 19

Trace Elements

	D	Calc	Obs	Resid	Daughter
Rb	0.02	21	30	9	25
Ba	0.08	256	238	-18	305
Sr	0.96	443	454	11	441
V	0.41	156	172	16	172
Cr	3.80	297	280	-17	233
Ni	5.29	146	162	16	87
Zr	0.03	84	83	-1	101

Abbreviations as in Table 5-5a.

5.6.4. MT APO

The proportion of mafic to silicic products provides a significant constraint on probable differentiation processes involved in the formation of the Mt Apo volcanics and strongly indicates the extent to which these processes have taken place. Throughout an 800 m vertical section only SiO_2-rich andesite-dacite pyroclastic ejecta were found (Fig. 5-11a). Some basaltic andesite boulders also enclose SiO_2-rich andesite (Fig. 5-11b) but are not found as lava flows.

The only nearby basaltic andesite lava flows outcrop along SE Mt Apo and are unlikely to be related to the section studied. A speculation of differentiation processes at Mt Apo could therefore involve fractionation of basaltic andesite to form SiO_2-rich andesite and/or assimilation of more evolved lavas into basaltic andesite to form a range of intermediate to SiO_2-rich lavas. Although the basaltic andesite host as shown in Fig. 5-11b are apparently younger than SiO_2-rich andesite enclaves, the reverse could occur. For example, magmas from the lower portion of a compositionally zoned chamber may entrain more evolved magmas, the latter derived from sidewall crystallisation. These basaltic andesite hosts (MAR samples, Appendix 4-2) may be therefore considered 'parental' to more evolved compositions.

The occurrence of compositionally contrasting lavas at Mt Apo initially suggest a contamination or assimilation process so an assimilation plus fractional crystallisation (AFC) calculation (DePaolo, 1981) was applied to selected Mt Apo lavas using a medium-K basaltic andesite parent (sample MAR5), a medium-high K andesite daughter (sample APO2), a high-K dacite (sample APO6) as contaminant and a 2 or 3-phase (plagioclase + clinopyroxene $\pm$ olivine) crystallising assemblage. Even the best results were unsuccessful, providing R values (mass assimilated/mass crystallised) > 3 (above limits for R values involving assimilation of granitic material by mafic magmas, as calculated by Grove et al, 1988) despite good major element (ΣR^2 = 0.027) and trace element fits. To produce the observed andesite-dacite composition by AFC, a large amount of SiO_2-rich material must be assimilated, more than imposed by the heat budget of a crystallising basic magma (Grove et al, 1988).

Figure 5-11a. SiO_2-rich andesite block dislodged from pyroclastic matrix at ~900m elev, along roadcut WSW of Mt Apo peak.

Figure 5-11b. Basaltic andesite boulder with sub-rounded SiO_2-rich andesite enclaves, at ~850m elev, Marbel River, Mt Apo.

It is therefore most unlikely the voluminous silicic ejecta can be derived *primarily* by AFC processes using the observed compositions. This does not, however, invalidate AFC as a differentiation process at Mt Apo because field evidence suggests such assimilation occurred. As shown in Fig. 5-11b, most of the enclaves are subrounded indicating some assimilation. The AFC model given above probably fails because it assumes complete assimilation. Clearly this was not the case.

An alternative to AFC processes is simple crystal fractionation. A simple two-step mass balance calculation (Tables 5-8a and 5-8b) tests the possibility of deriving SiO_2-rich hornblende andesite and dacite from basaltic andesite. The results are reasonable for the first step but marginal for the second (ΣR^2 = 0.066, 0.129), requiring olivine + plagioclase + amphibole in the first stage and plagioclase + hornblende + magnetite and minor clinopyroxene in the second stage. The high residuals for trace elements do not indicate simple crystal fractionation. This condition is reflected by poor fits for Ba, Sr and V, showing only a small increase in Ba and slight decrease in Sr, which are inconsistent with the calculated bulk partition coefficients (D_{Ba}, D_{Sr}, Table 5-8a). Suppressed enrichment of incompatible trace elements may be caused by *in situ* crystallisation whereas compatible elements may not decrease as expected if accumulation or buffering takes place.

The proposed differentiation trend can be demonstrated by plotting Mt Apo compositions on the CMAS pseudoternary projection of Baker and Eggler (1983), assuming the analyses represent liquid compositions. The proposed fractionation path depicts a magma multiply saturated with olivine + plagioclase + clinpopyroxene + magnetite. The compositional trend in Fig. 5-12 follows a curve towards the normative quartz + orthoclase apex, as expected for fractional crystallisation of the liquidus phases. However, a trend based on simple binary mixing of basaltic andesite and dacitic endmember compositions is also possible. Similar differentiation trends for calc-alkaline andesite - dacite involving fractionation, assimilation and mixing were concluded by Grove et al (1982).

Table 5-8a. Mass balance calculation to derive SiO_2-rich hornblende andesite from basaltic andesite at Mt Apo.

Stage 1: Basaltic andesite ⇒ Hornblende Andesite

	Parent	Daughter			Phase removed			
	Bas-and	Hb-Andesite			0.040	0.407	0.048	0.051
Anal #	23271	23273			AT2248	T4C645	AT4639	M3444
Sample	MAR6	APO2	Calc	Resid	Ol	Pl	Cp	Mt
SiO_2	54.91	62.69	54.91	0.00	38.64	55.68	51.84	0.10
TiO_2	0.74	0.60	0.90	-0.16	0	0.04	0.64	9.72
Al_2O_3	19.27	16.78	19.26	0.01	0	27.67	3.34	3.79
FeO	7.99	4.84	7.97	0.02	25.33	0.65	6.82	77.97
MnO	0.18	0.11	0.23	-0.05	0.29	0	0.12	0.55
MgO	3.35	2.66	3.37	-0.02	36.28	0.06	14.79	2.62
CaO	8.09	5.47	8.08	0.01	0.12	11.17	22.11	0.02
Na_2O	3.33	3.71	3.50	-0.08	0	4.48	0.22	0
K_2O	1.73	2.94	1.59	0.07	0	0.63	0	0
P_2O_5	0.41	0.20	0.09	0.16	-	-	-	-

ΣR^2= 0.066 F = 0.45 %Crystallised = 55

Trace Elements

	D	Calc	Obs	Resid	Daughter
Rb	0.02	28	34	6	60
Ba	0.11	265	446	181	527
Sr	1.37	672	759	87	496
V	1.97	292	151	-141	133
Cr	1.78	41	13	-28	22
Ni	1.48	21	19	-2	14
Zr	0.02	56	77	21	120

Abbreviations as in Table 5-5a.

Table 5-8b. Mass balance calculation to derive dacite from SiO_2-rich hornblende andesite at Mt Apo.

Stage 2: Hornblende andesite ⇒ Dacite

	Parent	Daughter			Phase removed			
	Hb-And	Dacite			0.154	0.076	0.004	0.012
Anal #	23273	23272			A3C489	A2674C	A24924	A29644
Sample	APO2	APO1	Calc	Resid	Pl	Hb	Cp	Mt
SiO_2	62.48	65.80	62.61	-0.05	60.10	48.22	53.27	0.09
TiO_2	0.63	0.48	0.59	0.04	0.03	1.51	0.22	9.09
Al_2O_3	16.89	16.04	16.52	0.19	25.18	7.07	1.69	4.33
FeO	4.88	3.82	4.89	-0.01	0.32	12.79	7.64	77.39
MnO	0.12	0.10	0.12	0.00	0.00	0.42	0.70	0.61
MgO	2.66	1.91	2.65	0.01	0.00	14.44	14.16	2.75
CaO	5.50	4.43	5.46	0.04	7.75	10.99	21.76	0.00
Na_2O	3.69	3.76	3.93	-0.24	6.45	1.47	0.36	0.00
K_2O	2.95	3.52	2.80	0.15	0.64	0.72	0.00	0.00
P_2O_5	0.20	0.15	0.11	0.09	-	-	-	-

ΣR^2= 0.129 F = 0.75 %Crystallised = 25

Trace Elements

	D	Calc	Obs	Resid	Daughter
Rb	0.03	58	60	2	76
Ba	0.11	471	527	56	600
Sr	2.44	658	496	-162	430
V	2.82	155	133	-22	91
Cr	9.89	206	22	-184	16
Ni	2.82	19	14	-5	11
Zr	0.04	94	120	26	122

Abbreviations as in Table 5-5a.

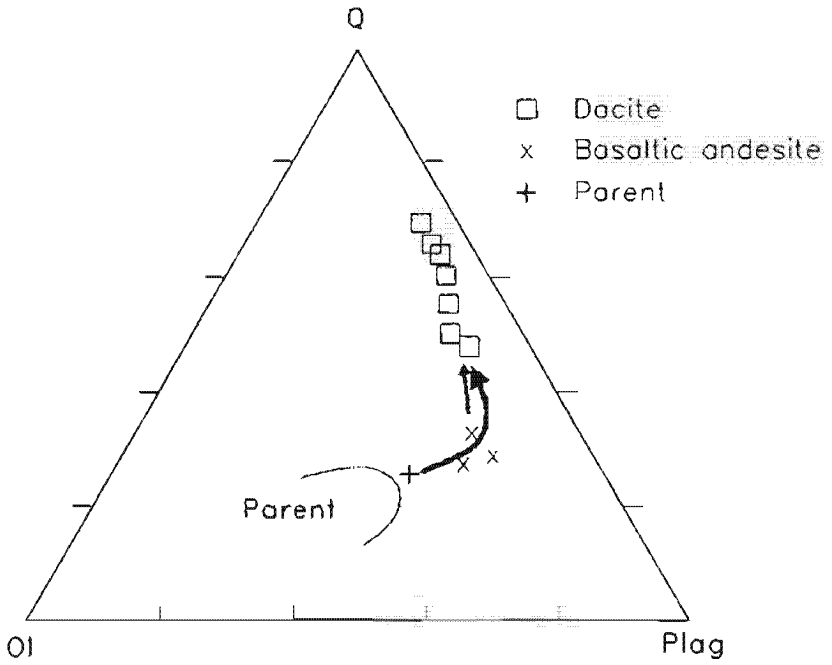

Figure 5-12. Composition of Mt Apo volcanics projected on the pseudoternary Olivine (Ol) - Quartz (Q) - Plagioclase (Pl). Differentiation from basaltic andesite to dacite may be caused by a crystal fractionation trend shown by the thick curve. However, a simple mixing path between basaltic andesite and dacite (short straight arrow) is also possible. Parent composition (+) is taken from BUT6, and a speculative parental field is partially outlined by an arc. FeO + Fe_2O_3 used in the projection was calculated from the technique of Sack et al (1980).

In summary, it appears that differentiation at Mt Apo cannot be modelled using a unique process and it is more likely that a complex combination of crystal fractionation (i.e. *in situ* crystallisation), AFC and perhaps magma mixing were responsible for producing the observed compositions. The lack of basaltic lava flows at Mt Apo is enigmatic and precludes more detailed investigation on source chemistry. Sparks et al (1977) suggested that a large proportion of basic magmas is never erupted because of its higher density than SiO_2-rich magmas. This study proposes a model in which a magma chamber occurs at depth (3 - 5 km) based on pressure estimates of hornblende phenocrysts in Mt Apo dacites. Basaltic magmas supplied to this chamber evolve by crystal fractionation and the chamber becomes compositionally zoned. Only more evolved magmas reach the surface to form thick pyroclastic sequences. Perhaps during large eruptions, deeper portions of the chamber are tapped, allowing basaltic andesite to reach the surface.

5.7. MODEL OF GEOCHEMICAL EVOLUTION

Early models of magma genesis in subduction zones (Nicholls and Ringwood, 1973; Ringwood, 1975) envisaged subsolidus dehydration of amphibolite followed by migration of fluid into overlying mantle. The hydrated peridotite rises as a diapir and melts at shallower levels, where partial melts segregate. This model was questioned by subsequent studies (e.g. Wyllie, 1978; Tatsumi et al, 1983) in that temperatures in the mantle above the main sources of fluids derived from subducted ocean crust are too low for hydrous melting to occur. Even if melting occurs, the main source of fluids must originate at pressures > 35 kbar but this condition contradicts estimates which show that subducted crust dehydrates at shallower depths (Anderson, 1978; Tatsumi, 1986).

Models of arc petrogenesis should therefore be consistent with the following conditions: i) the main source of hydrous fluids is derived from amphibole (or other hydrous phases) in subducted ocean crust at 25 kbar and ii) partial melts apparently rise from regions overlying the subducted slab at 35 kbar which corresponds to the

restricted depth range of the Wadati-Benioff zone below the volcanic front (e.g., 124 $\pm$ 38 km, Gill, 1981; 112 $\pm$ 19 km, Tatsumi et al, 1983).

In the model of Tatsumi (1986), amphibole in the subducted slab dehydrates at 20 - 25 kbar and releases fluids into overlying mantle. As temperatures in the hydrated mantle at this depth are too low to form melts, amphibole is re-formed. Tatsumi (1986) reasoned that amphibole in a peridotite system is more stable than amphibole in a basalt system at high pressures. Mantle convection then drags hydrated mantle to greater depths where amphibole breaks down at 35 kbar, releasing hydrous fluids (Fig. 5-13). This is similar to slab-induced convection models (e.g., Saunders et al, 1991; Tarney et al, 1991) to initiate melting in mantle wedge.

More recent theory (Davies and Stevenson, 1992) builds on Tatsumi's (1986) model and suggests that repeated amphibole breakdown and recrystallisation results in overall lateral transport of water away from the subducted slab (Fig. 5-14). Mitropoulos and Tarney (1992) suggests that magmas not as depleted in incompatible trace elements as N-MORB may be caused by variable slab-derived flux into mantle wedge. Both concepts may explain the variable depths to inferred top of subducted lithosphere beneath CMVA centres.

Synthesis of petrologic and geochemical data suggests the following evolutionary scheme for the CMVA. Melting is initiated by H_2O-rich fluids derived from hydrous phases of the subducted slab (Tatsumi et al, 1986) and fluxed into overlying peridotite at ~35 kbar. Partial melting of a slightly enriched mantle wedge occurs at about 10 - 15 kbar, within the spinel peridotite field. The resulting primary melt is enriched with as much as twice the K_2O content of E-MORB type mantle (0.07 vs. 0.03 wt%). It is assumed that the high LILE component of the inferred source is derived from subducted slab.

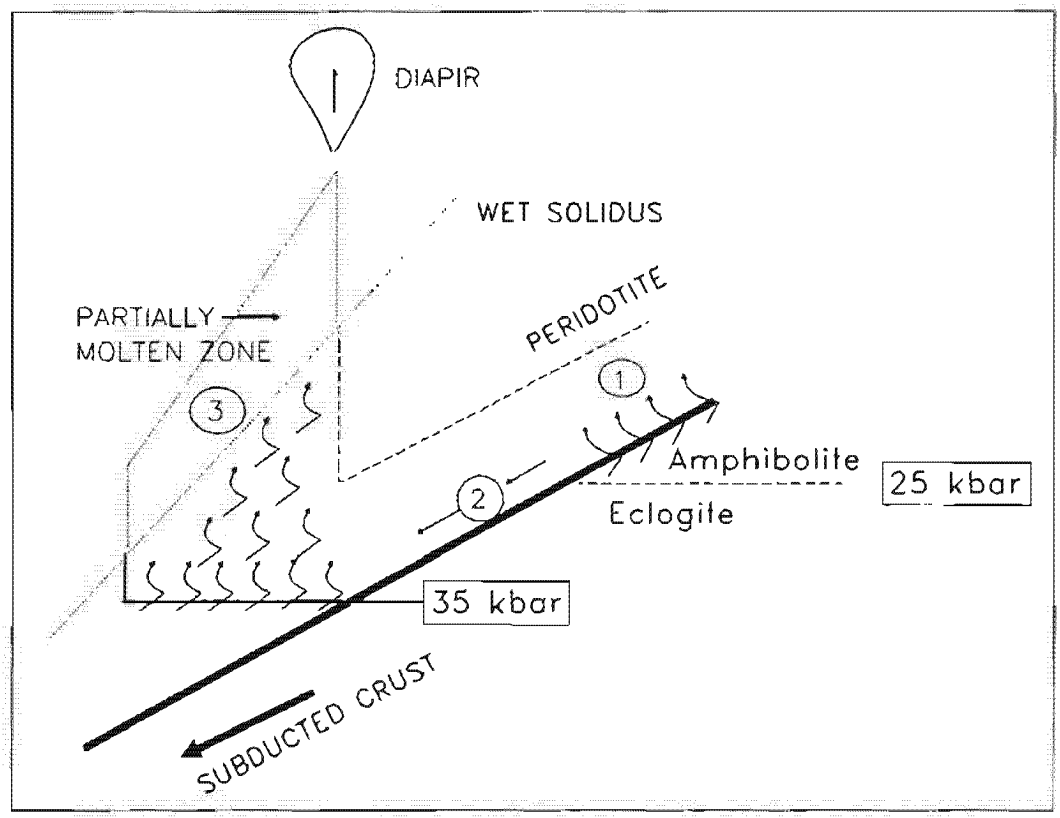

Figure 5-13. Schematic diagram of dehydration of amphibole from subducted slab and fluxing of overlying peridotite mantle. In **(1)** amphibole in subducted slab becomes unstable at about 25 kbar, releasing aqueous fluids into overlying peridotite. Mantle amphibole stable at high pressure is formed. **(2)** mantle convection drags amphibolitised mantle to 35 kbar where amphibole breaks down, releasing LILE-rich hydrous fluids. At **(3)** rising hydrated peridotite crosses peridotite wet solidus, where partial melts form. After Tatsumi (1986).

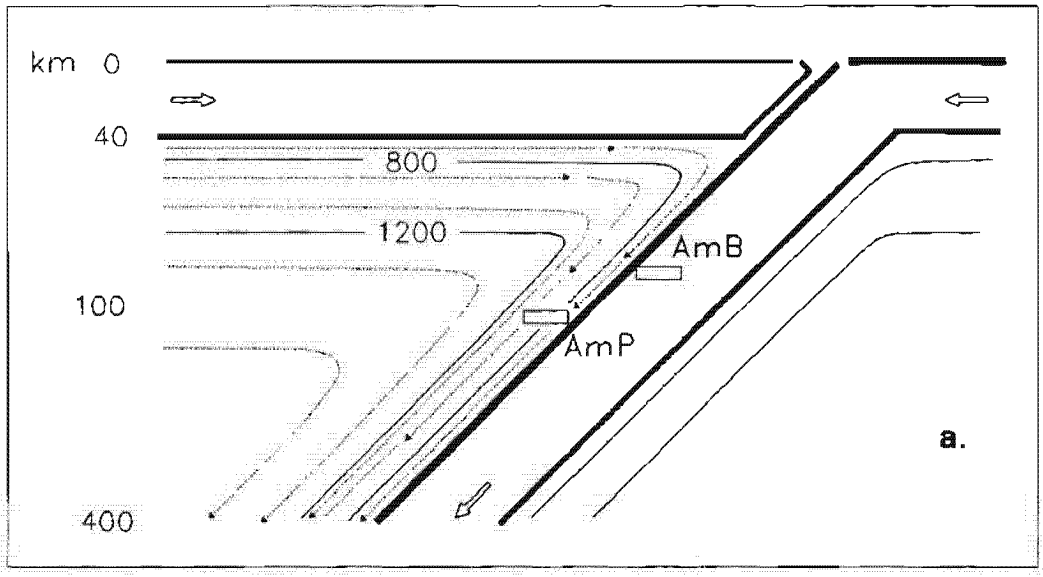

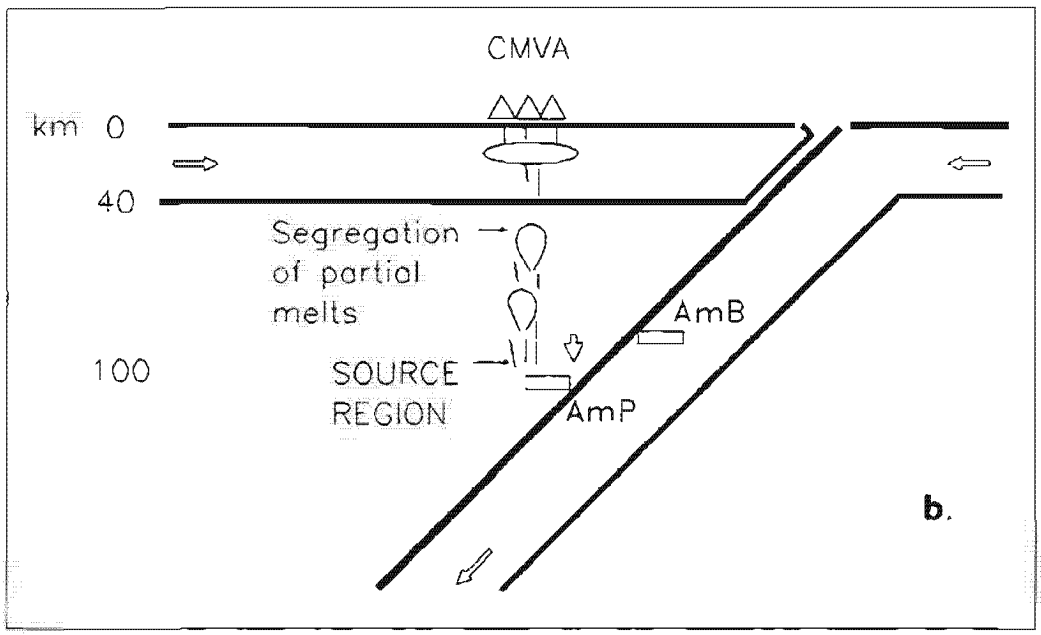

Fig. 5-14. Schematic diagram of subduction zone beneath CMVA. **(a)** Melt flow in mantle wedge region shown by dotted lines, direction by arrowheads (after Peacock, 1991; Davies and Stevenson, 1992). Numbered contours corresponds to temperature. Horizontal bars are the breakdown limits of amphibole in basalt crust (AmB) and mantle wedge peridotite (AmP). **(b)** diagram for CMVA incorporating ideas from Tatsumi (1986), Davies and Bickle (1991) and Davies and Stevenson (1992). Induced mantle wedge flow and amphibole stability (AmB and AmP) as in Fig. 5-14a. Small inverted arrow is the point of origin of hydrous fluids following Tatsumi's model. The preferred source region is perhaps farther from the slab (left-end of AmP bar), possibly resulting in relatively distant location of volcanic front from the trenchline. Thickness of crust is for illustration purposes only as this is at present unknown.

Diapiric movement of primary melt is accompanied by crystallisation of olivine (±Cr-spinel), followed by clinopyroxene and plagioclase. This assemblage equilibrates with the melt at ~5.5 and 2.7 kbar for Bukidnon and Camiguin Island respectively. Melt compositions at this stage are slightly olivine or nepheline normative to Di-normative tholeiites. As magma ascends farther, it cools, becomes more dense and ponds at the lower crust where olivine + clinopyroxene + liquid react out to form amphibole, and the magma evolves to basaltic andesite compositions (Fig. 5-15). These basalt - basaltic andesite magma chambers becomes staging areas for discrete melts which migrate to shallower levels and differentiate.

The main differentiation process in shallower levels is fractional crystallisation of plagioclase + olivine + clinopyroxene + magnetite or plagioclase + clinopyroxene + magnetite + amphibole (+/- orthopyroxene), resulting in SiO_2-rich andesite, dacite and increased P_{H2O}. Extensive fractional crystallisation and establishment of long-lived shallow magma chambers (e.g. prolonged lava extrusion at Hibok-Hibok; dome complexes) results in dominantly andesitic compositions and ubiquitous disequilibrium features: reverse, oscillatory zoned phenocrysts. These features suggest that at some stage the magma chamber was chemically zoned (Fig. 5-16a to c).

Early tapping of the upper portion of a chemically zoned magma chamber will result in predominantly andesitic - dacitic ejecta. In time, chemical zoning in chambers become less pronounced and the proportion of SiO_2-rich to basaltic lavas increase. If the deeper chamber interior is sampled then more basaltic melts will be erupted. However, predominance of andesites and dacites in the CMVA suggest otherwise.

Many volcanic centers in the CMVA are presently inactive and comprise large stratovolcanic complexes of intermediate lavas. The foregoing observations suggest that this arc is at a mature stage of its chemical evolution and in time should produce increasingly SiO_2-rich lavas. In a predominant suite of andesites and dacites, eruption of more mafic ejecta could indicate intrusion of a new batch of magma.

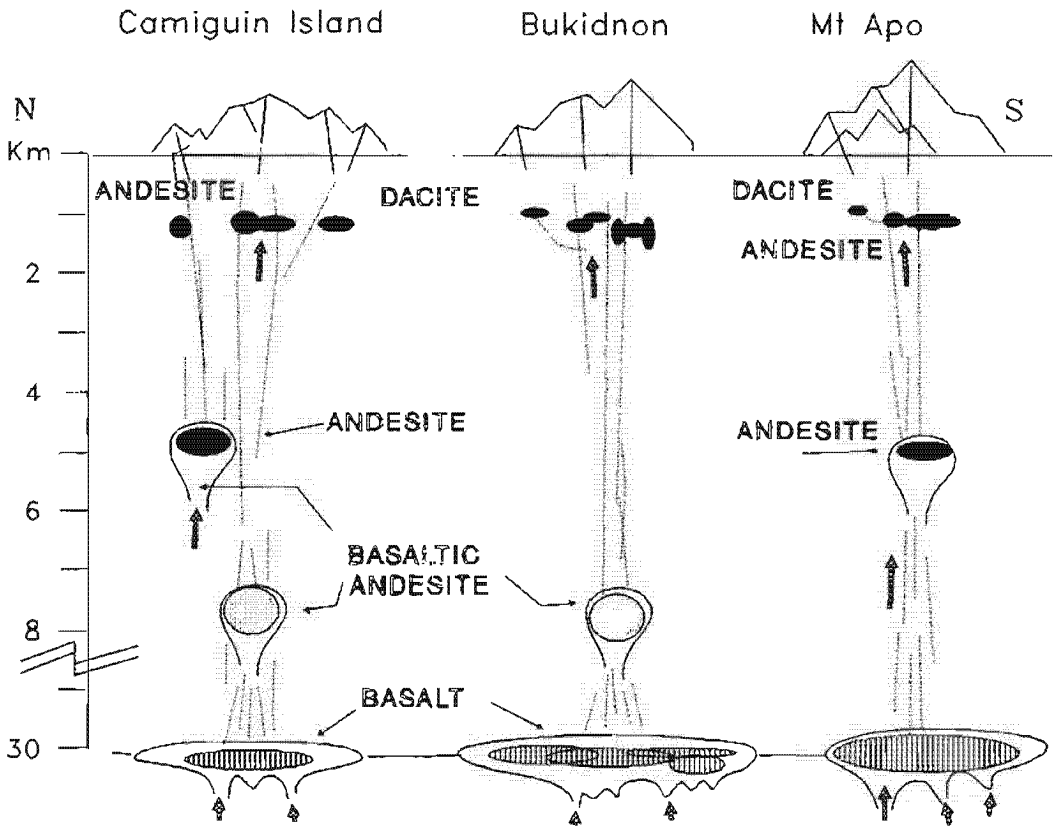

Figure 5-15. Cartoon showing inferred varying depths to magma chambers beneath CMVA. Primary melts which segregate at depth collects at the base of the crust. Individual diapirs rise, establish magma chambers, differentiate and erupt to form the CMVA. Eruption probably draws from subvolcanic chambers. Bukidnon basalt is the least differentiated and possibly equilibrated at about 15 - 20 km. Camiguin Island and Mt Apo probably differentiated at shallower levels as inferred from lower equilibration pressure of andesite and dacite.

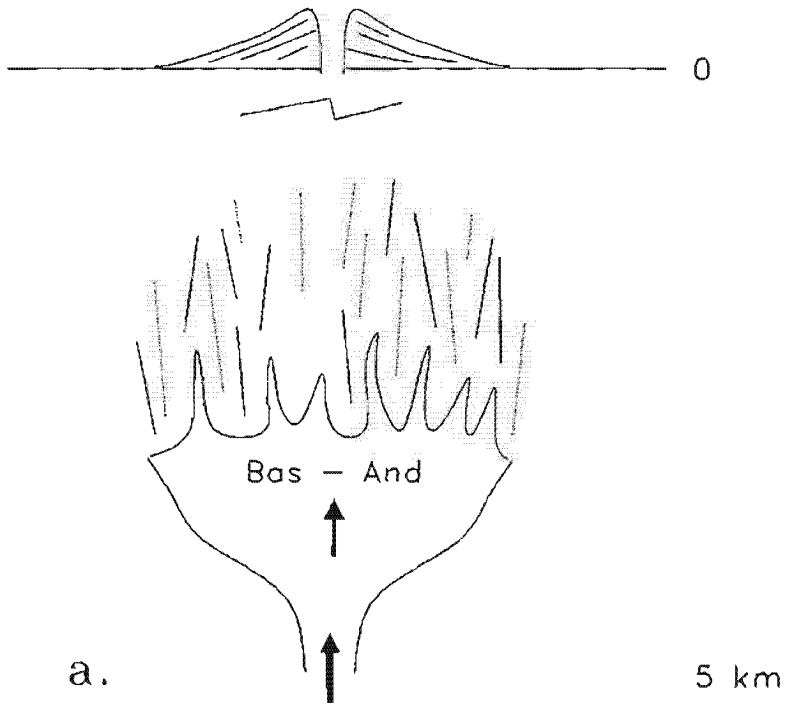
0
Bas – And
a.
5 km

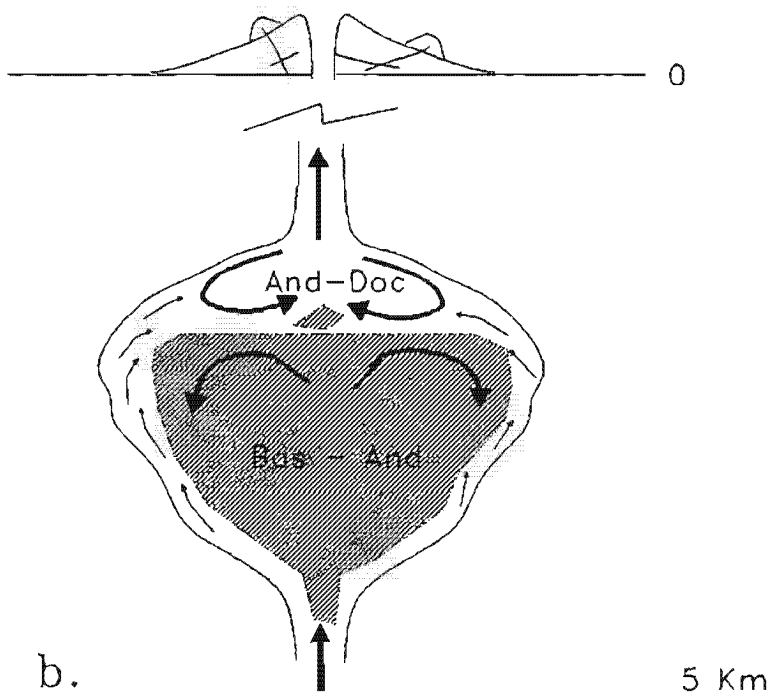
0
And–Doc
Bas – And
b.
5 Km

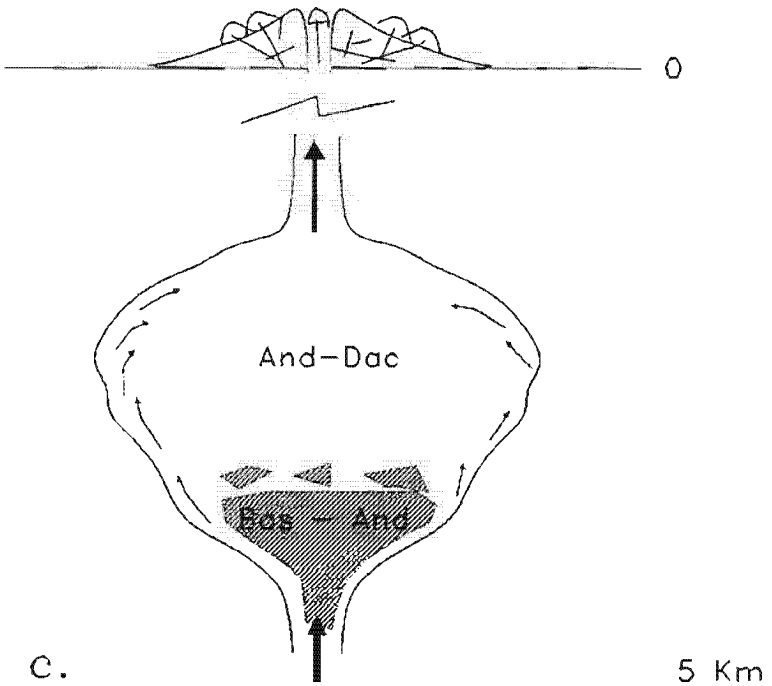

Figure 5-16. Highly schematic summary of inferred magma chamber processes at shallow levels (< 5 km). **a**. early magma chamber dominated by basalt - basaltic andesite, first eruptions are the least differentiated. Convection possibly caused by eruption, and crystallisation occurs along chamber walls and conduit. **b**. Pooling of evolved liquids at upper levels results in a compositionally zoned chamber. Initial eruptions of shallow chamber probably produces evolved, aphyric lavas (e.g. Mt Ginsiliban). In time, mixing of underlying mafic and SiO_2-rich lavas possibly occurs. **c**. mature stage of chamber evolution, predominated by andesite - dacite magma resulting in dome complexes.

CHAPTER VI SUMMARY AND CONCLUSIONS

6.1. TECTONIC ASSOCIATION

Assessment of regional setting and seismic data for the southern Philippines shows that Neogene-Quaternary centres of the CMVA occur 150-200 km above a west-dipping Wadati-Benioff zone. Based on present-day seismicity, subduction along the Philippine Trench probably produced the CMVA. In contrast, West Mindanao centres occurring in the Tiruray-Daguma Range and NW and S of Lake Lanao overlie the deeper portion of the Philippine Trench seismic zone (~670km) and therefore cannot be associated with west-dipping subduction. West Mindanao Arc volcanoes probably evolved from an east-dipping subduction system (West Sangihe-West Mindanao Arc).

6.2. VOLCANIC GEOLOGY

Field and stratigraphic relations indicate CMVA centres can be subdivided into 3 arc segments. The Misamis arc segment includes Camiguin Island, Mt Obulan, Mt Balatocan, Mt Pamalihi and Mt Mangaban. Volcanoes of the Bukidnon arc segment are Mt Katanglad, Mt Kalatungan, Musuan, and Butong. The southernmost Davao arc segment includes Mt Apo, Mt Talomo and Mt Sibulan. CMVA volcanoes are Quaternary centres overlying Pliocene and earlier strata. All have built volcanic landforms typical of andesite volcanism: lava domes, steep-sided blocky lava flows and pyroclastic ejecta. All 3 arc segments are volcanically and seismically active.

The most active volcanic field in the CMVA is Camiguin Island. Stratigraphy shows 6 major volcanic centres at Camiguin Island: 1) predominantly pyroclastics of

Butay, 2) domes, and pyroclastics of Cabuan, 3) lava flows and phreatomagmatic deposits of Benoni, 4) "aphyric" lavas of Mt Ginsiliban, 5) the dome and stratovolcano complex of Mt Mambajao and 6) the dome and stratovolcano complex of Mt Catarman/Hibok-Hibok. Synthesis of geologic data suggests Camiguin Island volcanism commenced with prehistoric eruptions at Butay followed by eruptions from Cabuan, Benoni, Mt Ginsiliban, Mt Mambajao, Mt Catarman and finally by recent activity which formed Mt Vulcan and Hibok-Hibok. This sequence suggests a general NW progression of volcanism.

6.3. PETROLOGY AND GEOCHEMISTRY

CMVA lavas are usually crystal-rich with a main phenocryst assemblage of olivine (Fo_{84-72}) + clinopyroxene (mainly augite with some diopside) + plagioclase (An_{84-31}). Plagioclase, magnesium-ferri hornblende and subordinate augite plus magnetite typify SiO_2-rich andesite and dacite. Two types of andesite occur extensively: pyroxene and hornblende andesite. In the former, augite is dominant whereas enstatite occurs mainly in aphyric lavas of Mt Ginsiliban and fine-medium grained lavas of Mt Mambajao. Amphibole is a significant phase in SiO_2-rich pyroclastic flows, lava flows and late stage domes. Two types of dacite are also recognised. Type 1 dacite is composed of a fine-grained anhydrous assemblage of plagioclase + augite $\pm$ resorbed olivine. These are found only at Mt Katanglad and southern Camiguin Island. Type 2 dacite occurs frequently in northern Camiguin Island and Mt Apo and is distinguished by diopside and amphibole.

Regional geochemistry shows the main lava types of the CMVA are medium-K calc-alkaline (CA) basalt, andesite and dacite with few occurrences of low and high-K CA lavas. These are generally Q and Hy-normative with no pronounced Fe-enrichment. Some high-K Mt Balatocan lavas representing an early eruptive phase are distinguished from other CA samples by their relatively high FeO^*/MgO ratios, and generally increasing TiO_2, Na_2O and P_2O_5 with increasing SiO_2.

In general, trace element distributions are similar for all suites, with the exception of i) lower Ni and Cr contents for a given MgO level and ii) incompatible behaviour of Y with increasing Zr in early Mt Balatocan lavas relative to other CA CMVA lavas .

Detailed major element chemistry of Camiguin Island shows that lavas from the earliest centres (ie Benoni-Butay) have the widest compositional range (52 - 63 wt% SiO_2) whereas lavas from Mt Mambajao, Mt Vulcan and Hibok-Hibok generally occur within 56 - 60 wt% SiO_2. Trace element relations using element-Zr plots suggest that Mt Mambajao, Mt Vulcan and Hibok-Hibok have similar fractionation trends and therefore belong to one chemical group whereas Benoni-Butay and Mt Ginsiliban lavas form another chemical association. This grouping is supported by fractionation trends for Cr and Ni with MgO which define affinity of Mt Ginsiliban compositions to Benoni-Butay lavas. Similarly, Mt Vulcan and Mt Mambajao lavas show chemical trends comparable with lavas of Hibok-Hibok centre.

CMVA lavas have major and trace element concentrations similar to other island arc basalts (IAB) but have generally lower TiO_2, MgO, Cr and Ni relative to Mid-Oceanic Ridge Basalts (MORB). The main chemical feature relating CMVA lavas to a subduction setting is the characteristic depletion of high field strength elements (HFSE) relative to large ion lithophile elements (LILE). The slightly higher HFSE concentrations of CMVA lavas relative to Normal-type MORB (N-MORB) and average IAB, combined with low Zr/Nb ratios (7-14) indicate an enriched-type MORB (E-MORB) / Ocean Island Basalt (OIB) type of mantle wedge.

6.4. PETROGENESIS

6.4.1. Source Region Characteristics and Partial Melting Conditions

The lower Mg#, Cr and Ni contents of CMVA basalt and basaltic andesite relative to magnesian MORB and products of peridotite melting experiments show

that CMVA compositions are derivative melts of a more primitive magma. Correcting for olivine (± spinel) fractionation, an approximate CMVA parental basalt composition is obtained. Corrected major element analyses are similar to representative primary MORB compositions except for CaO, Na_2O and K_2O. Low CaO may be related to increasing MgO and FeO at increasing pressure. High K_2O and Na_2O levels in proposed CMVA parental basalts may be due to a slab-derived component or later crustal contamination. Qualitative assessment of slab-derived influence on source region compositions may be accomplished by comparing variations in LILE to HFSE. In particular, high and variable Ba/Nb ratios relative to MORB are achieved by variable Ba, and indicate, a direct contribution from subducted slab. The amount of slab-derived component incorporated into the CMVA source region is probably low, based on low Rb/Sr ratios of CMVA basalts relative to Rb/Sr ratios of continental crust.

The depth range of CMVA source magmas is derived from a melting grid based on the CIPW normative basalt tetrahedron. Results for projecting selected CMVA compositions from the Di apex suggest a segregation depth between 10 and 15 kbar, within the spinel peridotite field. Partial melting calculations assuming equilibrium batch melting indicate moderate degrees of melting (10 - 14%). The inferred CMVA source region chemistry shows higher Nb levels than mantle (0.64 to 0.68 ppm vs 0.61) so that the presence of a HFSE-retaining phase is unlikely.

6.4.2. Differentiation Processes

The general range of compositions of comagmatic suites in each arc segment can be modelled by fractional crystallisation. Recent theories and experiments suggest crystal fractionation proceeds in the manner of *in situ* crystallisation. Mass balance calculations demonstrate the possibility of deriving SiO_2-rich andesite by fractionating olivine, plagioclase, clinopyroxene and magnetite from basaltic andesite at Hibok-Hibok. Dacite may be derived from the former by

fractionating plagioclase, hornblende, clinopyroxene and magnetite. For southern Camiguin Island volcanoes, magma mixing between Butay basaltic andesite and Benoni SiO_2-rich andesite/dacite may account for Mt Ginsiliban andesites. Alternatively, in situ crystallisation may be invoked to account for SiO_2-rich "aphyric" lavas of Mt Ginsiliban.

Least squares mixing calculations also suggest crystal fractionation of olivine + plagioclase + clinopyroxene + magnetite from either Butong or Quezon Volcanics basaltic andesite to obtain Musuan SiO_2-rich andesite.

At Mt Apo, hornblende andesite may be derived from basaltic andesite by fractionating olivine, plagioclase, clinopyroxene and magnetite. Further fractionation of plagioclase, hornblende, clinopyroxene and magnetite probably results in dacite. However, marginal trace element fits and occurrence of subrounded SiO_2-rich andesite enclaves in basaltic andesite suggest a complex combination of assimilation, fractional crystallisation and magma mixing.

6.4.3. Geochemical Evolution

Melt generation is probably initiated by fluxing of mantle peridotite by H_2O-rich fluids derived from a subducted slab at around 35 kbar. Partial melts segregate from the zone of melting at 10 - 15 kbar. The resultant melts are LIL-element enriched, presumably from a slab-derived component. The initial phases to crystallise are olivine (± Cr-spinel), clinopyroxene and calcic plagioclase. The calculated equilibrium pressures of crystallisation for Butong and Camiguin Island basalt and basaltic andesite range from 2.7 - 5.5 kbar. This suggests a polybaric crystallisation history. One theory is that primitive magma ascends, cools and ponds near the base of the crust and initially differentiates to basaltic andesite. Discrete basalt-basaltic andesite magmas migrate to shallower levels, establish magma chambers and further differentiate to andesitic compositions. Eruptions probably draw from shallow subvolcanic chambers as evidenced by shallow seismicity and local subsidence during prolonged extrusion of SiO_2-rich andesite and dacite.

ACKNOWLEDGEMENTS

I thank Professor J.W. Cole and Dr. S.D. Weaver for supervising this study. I also thank Dr. Y. Kawachi and Dr. T. Reay for use of a JEOL 8600 Superprobe microanalyser at the Department of Geology, University of Otago. Canterbury University department staff S. Brown, D. Jones, K. Swanson, A. Downing, K. Holder, S. Alpers and R. Spiers provided various help on geology equipment.

I thank Dr. R.S. Punongbayan for endorsing a study leave from the Philippine Institute of Volcanology and Seismology (PHIVOLCS) and for supporting a geological study on Camiguin Island and central Mindanao. I also acknowledge partial funding of field expenses from UNESCO-ROSTSEA through Dr. S.T. Malling. Dr. M. Camacho (University of Southern Philippines) graciously provided a hospitable place in Davao. I especially thank J. Bautista for providing logistical support in Cagayan de Oro and in rock sampling at Musuan Volcano. Study at Canterbury University was made possible by a fees scholarship, awarded by the New Zealand Ministry of External Relations and Trade, 1990-1991, and New Zealand Vice-Chancellor's Committee, 1992. Partial funding for thesis preparation was provided by the Mason Trust, 1991-1992.

I greatly appreciate the expert assistance of PHIVOLCS staff : B. Bautista, L. Bautista and T. Rasdas for providing seismic data for the Mindanao region; D. Labininay for rock sampling at Mt Balatocan; Ting and R. Macaspac for sample preparation; L. Ramos and library staff for sending key reference material and to L. Salugsugan and the staff of Hibok-Hibok Volcano Observatory for their constant assistance in Camiguin Island.

I thank my parents, Onofre and Aurora, for their support and encouragement.

Finally, I am most grateful to my wife, Tati Joan Carmela, for her tremendous support, patience and understanding.

REFERENCES

Abad, L.F. (1949) The geology and volcanism of Camiguin Island, Philippines. Phil. Bur. Mines, Unpublished report. 24p.

Acharya, H.K. (1980) Seismic slip on the Philippine Fault and its tectonic implications. *Geology*, 8: 40-42.

Acharya, H.K. and Aggarwal, Y.P. (1980) Seismicity and tectonics of the Philippine Islands. *J. Geophys. Res.*, 85: 3239-3250.

Afifi, A.M. and Essene, E.J. (1988) MINFILE: a microcomputer program for storage and manipulation of chemical data on minerals. *Am. Mineral.*, 73: 446-448.

Agusan-Davao Consortium (1979) Agusan - Davao Basin evaluation report. Unpublished report, 35p.

Alcaraz, A., Abad, L.F., and Quema, J.C. (1952) Hibok-Hibok Volcano, Philippine Islands, and its activity since 1948. *The Volcano Lett. Parts 1 & 2, U.S. Geol. Surv.*, 516: 1-6.

Alcaraz, A., Abarquez, R., Abad, L., Quema, J. and Teves, J. (1950) A Preliminary Report on the Recent Eruptions of Hibok-Hibok Volcano, Camiguin Island, Philippines. *Bull. Volcanologique*. Serie II, Tome XII: 215-225.

Allegre, C.J., Treuil, M., Minster, J.F., Minster, B. and Albarede, F. (1977) Systematic use of trace element in igneous process, Part I: Fractional crystallization processes in volcanic suites. *Contrib. Mineral. Petrol.*, 60: 57-75.

Allegre, C.J. and Condomines, M. (1982) Basalt genesis and mantle structure studied through Th-isotope geochemistry. *Nature*, 299: 21-24.

Allen, C.R. (1962) Circum-Pacific faulting in the Philippines-Taiwan region, *Jour. Geophys. Res.*, 67: 4795-4811.

Allen, P.M. and Stephens, E.A. (1971) Report on the geological survey of Hongkong. Hongkong Government Printer, Hongkong. 107p.

Anderson, A.T. and Gottfried, D. (1971) Contrasting behaviour of P, Ti and Nb in a differentiated high-alumina olivine tholeiite and a calc-alkaline andesite suite. *Geol. Soc. Am. Bull.*, 82: 1929-1942.

Anderson, R.N., DeLong, S.E. and Schwarz, W.M. (1978) Thermal model for subduction with dehydration in the downgoing slab. *Jour. Geol.*, 86: 731-739.

Ando, S. (1975) Minor element geochemistry of the rocks from Mashu volcano, eastern Hokkaido. *J. Fac. Sci. Hokkaido Univ.*, Ser. IV, 16: 553-566.

Andrews, J.E. (1980) Morphologic evidence for reorientation of sea-floor spreading in the West Philippine Basin. *Geology*, 8: 140-143.

Aramaki, S. and Ui, T. (1982) Japan. In: Thorpe, R.S. (ed) Andesites: Orogenic andesites and related rocks. John Wiley & Sons, New York, 259-292.

Arculus, R.J. and Wills, K.J.A. (1980) The petrology of plutonic blocks and inclusions from the Lesser Antilles island arc. *J. Petrol.*, 21: 743-799.

Arth, J.G. (1976) Behaviour of trace elements during magmatic processes - a summary of theoretical models and their applications. *J. Res. U.S. Geol. Surv.*, 4: 41-47.

Askren, D.R.R., Whitney, J.A. and Roden, M.F. (1991) Petrology and geochemistry of the Huerto Andesite, San Juan volcanic field, Colorado. *Contrib. Mineral. Petrol.*, 107: 373-386.

Bailey, J.C., Frolova, T.I. and Burikova, I.A. (1989) Mineralogy, geochemistry and petrogenesis of Kurile island-arc basalts. *Contrib. Mineral. Petrol.*, 102: 265-280.

Baker, P.E. (1978) The South Sandwich Islands: III. Petrology of the volcanic rocks. *Br. Antarct. Surv. Sci. Report* No.93.

Baker, I. and Haggerty, E. (1967) The alteration of olivine in basaltic and associated lavas, Part II: Intermediate and low temperature alteration. *Contrib. Mineral. Petrol.*, 16: 258-273.

Baker, D.R. and Eggler, D.H. (1983) Fractionation paths of Atka (Aleutians) high-alumina basalts: I. Constraints from phase relations. *J. Volcanol. Geotherm. Res.*, 18: 387-404.

Baker, D.R. and Eggler, D.H. (1987) Compositions of anhydrous and hydrous melts coexisting with plagioclase, augite, and olivine or low-Ca pyroxene from 1 atm to 8 kbar: Application to the Aleutian volcanic center of Atka. *Am. Mineral.*, 72: 12-28.

Baker, I. and Haggerty, E. (1967) The alteration of olivine in basaltic and associated lavas, Part II: Intermediate and low temperature alteration. *Contrib. Mineral. Petrol.*, 16: 258-273.

Balce, G.R., Magpantay, A.L., and Zanoria, A.S. (1979) Tectonic scenarios of the Philippines and northern Indonesian region, paper presented at Ad Hoc Working Group Meeting on the geology and tectonics of Eastern Indonesia, ESCAP-CCOP-IOC-SEATAR, Bandung, Indonesia, July 9-14,1979.

Barnett, P.R., Delfin, F.G. and Espanola, O.S. (1985) Geothermal exploration in the Southern Philippines. *Phil. Geologist.*, 39 (3): 44-53.

Barton, M. and Wyers, G.P. (1991) Estimates of P, T, P_{H2O} and fO_2 for lavas from Patmos (Greece) and implications for magmatic evolution. *J. Volcanol. Geotherm. Res.*, 47: 265-297.

Basaltic Volcanism Study Project (1981) Basaltic Volcanism on the Terrestrial Planets. Pergammon Press, New York. 1286p.

Bedard, J.H., Kerr, R.C. and Hallworth, M.A. (1992) Porous sidewall and sloping floor crystallization experiments using a reactive mush: implications for the self-channelization of residual melts in cumulates. *Earth Planet. Sci. Lett.*, 111: 319-329.

Ben-Avraham, Z. and Uyeda, S. (1973) The evolution of the China Basin and the Mesozoic paleogeography of Borneo. *Earth Planet. Sci. Lett.*, 18: 365-376.

Bence, A.E., Baylis, D.M., Bender, J.F. and Grove, T.L. (1979) Controls on the major and minor element chemistry of mid-ocean ridge basalts and glasses. In: Talwani, M., Harrison, C.G. and Hayes, D.E. (eds) Deep Drilling Results in the Atlantic Ocean: Ocean Crust. Am. Geophys. Union, Washington, D.C., p. 331-341.

Bence, A.E., Grove, T.L. and Papike, J.J. (1980) Basalts as probes of planetary interiors: constraints on the chemistry and mineralogy of their source regions. *Precambrian Res.*, 10: 249-279.

Bender, B.F., Hodges, F.N. and Bence, A.E. (1978) Petrogenesis of basalts from the Project Famous area: experimental study from 0 to 15 kbar. *Earth Planet. Sci. Lett.*, 41: 277-302.

Bentor, Y.K. (1951) On the formation of cloudy zones in plagioclases. *Schweiz. Mineral. Petrol. Mitt.*, 31: 535-552.

Berman, R.G. (1981) Differentiation of of calc-alkaline magmas: evidence from the Coquihalla volcanic complex., British Colombia. *J. Volcanol. Geotherm. Res.*, 9: 151-179.

Best, M.G. and Mercy, E.L.P. (1967) Composition of crystallization of mafic minerals in the Guadalupe igneous complex. *Am. Mineral.*, 52: 436-424.

Blundy, J.D. and Holland, J.B. (1990) Calcic amphibole equilibria and a new amphibole-plagioclase geothermometer. *Contrib. Mineral. Petrol.*, 104: 208-224.

Bown, M.G. (1964) Recalculation of pyroxene analyses. *Am. Mineral.*, 49: 190-194.

Bradshaw, T.K. (1992) The adaptation of Pearce element ratio diagrams to complex high silica systems. *Contrib. Mineral. Petrol.*, 109: 450-458.

Brophy, J.G. (1986) The Cold Bay volcanic center, Aleutian volcanic arc I: Implications for the origin of high-aluminium arc basalt. *Contrib. Mineral. Petrol.*, 93: 368-380.

Brophy, J.G. (1987) The Cold Bay Volcanic Center, Aleutian Volcanic arc. *Contrib. Mineral. Petrol.*, 97: 378-388.

Brown, G.M., Vincent, E.A. and Brown, P.E. (1957) Pyroxenes from the early and middle stages of fractionation of the Skaergaard intrusion, East Greenland. *Min. Mag.*, 31: 511-543.

Brune, J.N. (1968) Seismic moment, seismicity, and rate of slip along major fault zones. *J. Geophys. Res.*, 73: 777-784.

Bryan, W.B., Finger, L.W. and Chayes, F. (1969) Estimating proportions in petrographic mixing equations by least squares approximation. *Science*, 163: 926-927.

Burnham, C.W. and Davis, N.F. (1974) The role of H_2O in silicate melts: II. Thermodynamic and phase relations in the system $NaALSI_3O8$-H_2O to 10 kilobars, 700°C to 1000°C. *Am. Jour. Sci.*, 274: 902-940.

Cardwell, R.K., Isaaks, B.L. and Karig, D.E. (1980). The spatial distribution of earthquakes, focal mechanism solutions and subducted lithosphere in the Philippine and Northeastern Indonesian islands. In Hayes, D.E (ed) The tectonic and geologic evolution of Southeast Asian seas and islands, Part 1, Geophysical Monograph 23. American Geophysical Union. p. 1-35.

Carmichael, I.S.E. (1967) The iron-titanium oxides of salic volcanic rocks and their associated ferromagnesian silicates. *Contrib. Mineral. Petrol.* 14: 36-44.

Carmichael, I.S.E., Nicholls, J. and Smith, A.L. (1970) Silica activity in igneous rocks. *Am. Mineral.*, 55: 246-263.

Carr, M.J. (1987) IGPET2 computer program. In: Rock, N.M.S. Progress in 1988-1990 with computer applications in the "hard-rock" arena: geochemistry, mineralogy, petrology and volcanology. *Comput. Geosci.*, 19: 1067-1090.

Casasola, A.G. (1956) Petroleum and geological field investigation of Western Davao. Phil. Bur. Mines, 13p.

Cawthorn, R.G. (1976) Melting relations in part of the system CaO-MgO-Al_2O_3-SiO_2-Na_2O-H_2O under 5 kb pressure. *J. Petrol.*, 17: 44-72.

Champness, P.E. (1970) Nucleation and growth of iron oxides in olivines, $(Mg,Fe)2SiO4$. *Mineral. Mag.*, 37: 790-800.

Chen, C.F. and Turner, J.F. (1980) Crystallization in a double-diffusive convective system. *J. Geophys. Res.*, 85: 2573-2593.

Chow, T.J, Stern, R.J. and Dixon, T.H. (1980) Absolute and relative abundances of K, Rb, Sr and Ba in Circum-Pacific island arc magmas , with special reference to the Marianas. *Chem. Geol.*, 28: 111-121.

Clague, D.A. and Jarrard, R.D. (1973) Tertiary Pacific plate motion deduced from the Hawaii-Emperor chain. *Geol. Soc. Am. Bull.*, 84: 1134-1154.

Commission on Volcanology, Philippines (1981) Catalogue of volcanoes and geothermal areas in the Philippines. Unpublished report.

Conrad, W.K. and Kay, R.W. (1984) Ultramafic and mafic inclusions from Adak Island: crystallization history and implications for the nature of primary magmas and crustal evolution in the Aleutian arc. *J. Petrol.*, 25: 88-125.

Corby, G.W. et al (1951) Geology and oil possibilities of the Philippines. Republic of the Philippines Dept. of Agriculture and Natural Resources Tech. Bull., 21: 536p.

Corlett, M. and Ribbe, P.H. (1967) Electron probe microanalysis of minor elements in plagioclase feldspars. SMPM 47: 317-332.

Cox, K.G., Bell, J.D. and Pankhurst, R.J. (1979) The interpretation of igneous rocks. George Allen and Unwin, London, 450 p.

Crawford, A.J., Falloon, T.J. and Eggins, S. (1987) The origin of island arc high-alumina basalts. *Contrib. Mineral. Petrol.*, 97: 417-430.

Crisologo, E. (1986) Progress report on the geology of Camiguin Island. Phil. Inst. Volcanol. Unpublished report.

Currie, K.L. (1991) A simple quantitative calculation of mol fractions of amphibole end-members. *Can. Mineral.*, 29: 287-299.

Datuin, R. (1982) An insight on quaternary volcanoes & volcanic rocks of the Philippines. *J. Geol. Soc. Phil.*, 36: 1-11.

Davies, J.H. and Bickle, M.J. (1991) A physical model for the volume and composition of melt produced by hydrous fluxing above subduction zones. *Philos. Trans. R. Soc. Lond.* A, 335: 355-364.

Davies, J.H. and Stevenson, D.J. (1992) Physical model of source region of subduction zone magmatism. *J. Geophys. Res.*, 97: 2037-2070.

DeBoer, J., Odom, L.A., Ragland, P.C., Snider, F.G. and Tilford, N.R. (1980) The Bataan orogene: eastward subduction, tectonic rotations and volcanism in the western Pacific (Philippines). *Tectonophysics.*, 67: 251-282.

Defant, M.J., Jacques, D., Maury, R.C., de Boer, J.Z. (1989) Geochemistry and tectonic setting of the Luzon Arc, Philippines. *Geol. Soc. Am. Bull.* 101: 663-672.

Defant, M.J. and Nielsen, R.L. (1990) Interpretation of open system petrogenetic processes: phase equilibria constraints on magma evolution. *Geochim. Cosmochim. Acta*, 54: 87-102.

Defant, M.J. Clark, L.F., Stewart, R.H., Drummond, M.S., de Boer, J.Z., Maury, R.C., Bellon, B., Jackson, T.E. and Restrepo, J.F. (1991a) Andesite and dacite genesis via contrasting processes: the geology and geochemistry of El Valle Volcano, Panama. *Contrib. Mineral. Petrol.*, 106: 309-324.

Defant, M.J., Maury, R.C., Ripley, E.M., Feigenson, M.D. and Jacques, D. (1991b) An example of island-arc petrogenesis: geochemistry and petrology of the southern Luzon Arc, Philippines. *J. Petrol.*, 32: 455-500.

Defant, M.J., Richerson, P.M., De Boer, J.Z., Stewart, R.H., Maury, R.C., Bellon, H, Drummond, M.S., Feigenson, M.D. and Jackson, T.E. (1991c) Dacite genesis via both slab melting and differentiation: petrogenesis of La Yeguada Volcanic Complex, Panama. *J. Petrol.*, 32, Part 5: 1101-1142.

DePaolo, D.J. (1979) Estimation of depth of origin of basic magmas: A modified thermodynamic approach and a comparison with experimental melting studies. *Contrib. Mineral. Petrol.*, 69: 265-278.

DePaolo, D.J. (1981) Trace element and isotopic effects of combined wallrock assimilation and fractional crystallisation. *Earth Planet. Sci. Lett.*, 53: 189-202.

Divis, A.F. (1980) The petrology and tectonics of Recent volcanism in the Central Philippine Islands. In Hayes, D.E (ed) The tectonic and geologic evolution of Southeast Asian seas and islands, Part 1, Geophysical Monograph 23. American Geophysical Union. p. 127-144.

Dowty, E. (1980) Synneusis reconsidered. *Contrib. Mineral. Petrol.*, 74: 75-84.

Draper, D.S. (1991) Late Cenozoic bimodal magmatism in the northern Basin and Range Province of southeastern Oregon. *J. Volcanol. Geotherm. Res.*, 47: 299-328.

Eby, N. (1990) PETMIN. Unpublished computer program for geochemistry.

Ellam, R.M. (1992) Lithospheric thickness as a control on basalt geochemistry. *Geology*, 20: 153-156.

Ellam, R.M. and Hawkesworth, C.J. (1988) Elemental and isotopic variations in subduction related basalts: evidence for a three component model. *Contrib. Mineral. Petrol.*, 98: 72-80.

Elthon, D. (1983) Isomolar and isostructural pseudo-liquidus phase diagrams for oceanic basalts. *Am. Mineral.*, 68: 508-511.

Erlank, A.J. and Kable, E.J.D. (1976) The significance of incompatible trace elements in Mid-Atlantic Ridge basalts from 45^{0}N with particular reference to Zr/Nb. *Contrib. Mineral. Petrol.*, 54: 281-291.

Evans, B.W. and Frost, B.R. (1975) Chrome-spinel in progressive metamorphism - a preliminary analysis. *Geochim. Cosmochim. Acta*, 39: 959-972.

Ewart, A., Bryan, W.B. and Gill, J.B. (1973) Mineralogy and geochemistry of the younger islands of Tonga ,S.W. Pacific. *J. Petrol.*, 14: 429-465.

Ewart, A. (1979) A review of the mineralogy and chemistry of Tertiary-Recent dacitic, latitic, rhyolitic and related salic volcanic rocks. In: F. Baker (ed), Trondhjemites, Dacites and Related rocks. Elsevier, Amsterdam, p.13-21.

Ewart, A. and Hawkesworth, C.J. (1987) The Pelistocene-Recent Tonga-Kermadec arc lavas:interpretation in light of new isotopic and rare earth data in terms of a depleted mantle source. *J. Petrol.*, 28: 495-530.

Fabries, J. (1979) Spinel-olivine geothermometry in peridotites from ultramafic complexes. *Contrib. Mineral. Petrol.*, 69: 329-336.

Falloon, T.J., Hatton, C.J. and Harris, K.L. (1988) Anhydrous partial melting of a fertile and depleted peridotite from 2 - 30 kb and application to basalt petrogenesis. *J. Petrol.*, Special Lithosphere Issue.

Falloon, T.J. and Green, D.H. (1987) Anhydrous partial melting of MORB pyrolite and other peridotite compositions at 10 kb: implications for the origin of primitive MORB glasses. *Contrib. Mineral. Petrol.*, 37: 181-219.

Falloon, T.J. and Green, D.H. (1988) Anhydrous partial melting of peridotite from 8 to 35kb and the petrogenesis of MORB. *J. Petrol.*, Special Lithosphere Issue: 379-414.

Fisher, R.V. and Schminke, H.V. (1984) Pyroclastic rocks. Springer-Verlag. 472p.

Fisk, M.R. and Bence, A.E. (1980) Experimental crystallization of Cr-Spinel in FAMOUS basalt 527-1-1. *Earth Planet. Sci. Lett.*, 48: 111-123.

Flood,R.H.,Vernon,R.H.,Shaw,S.E.and Chapell, B.B. (1977) Origin of pyroxene-plagioclase aggregates in a rhyodacite. *Contrib. Mineral. Petrol.*, 60: 299-306.

Flower, M. (1991) Magmatic processes in oceanic ridge and intraplate settings. In: Floyd, P.A. Oceanic Basalts. Blackie, New York, 1991. p.116-147.

Foden, J.D. (1983) The petrology of the calcalkaline lavas of Rindjani volcano, East Sunda Arc: a model for island arc petrogenesis. *J. Petrol.*, 24: 98-130.

Foden, J.D. and Green, D.H. (1992) Possible role of amphibole in the origin of andesite: some experimental and natural evidence. *Contrib. Mineral. Petrol.*, 109: 479-493.

Frey, F.A., Green, D.H. and Roy, S.D. (1978) Integrated models of basalt petrogenesis: a study of quartz tholeiites to olivine melilites from southeastern Australia utilizing geochemical and experimental petrology data. *J. Petrol.*, 19: 463-518.

Froelich, H.A. and Melendres, M. (1960) Summary and geology of Cotabato. Unpublished manuscripts.

Frost, B.R. and Lindsley, D.H. (1991) Occurrence of Iron-titanium oxides in igneous rocks. In Lindsley, D.H., ed., Oxide Minerals: Petrologic and Magnetic significance, Reviews in Mineralogy 25, Min. Soc. Am., Michigan, p.433-468.

Fujii, T. and Scarfe, C.M. (1985) Composition of liquids coexisting with spinel lherzolite at 10 kbar and the genesis of MORBs. *Contrib. Mineral. Petrol.*, 90: 18-28.

Fuller, M., McCabe, R., Williams, I.S., Almasco, J., Encina, R.Y., Zanoria, A.S. and Wolfe, J.A. (1983) Paleomagnetism of Luzon. In Hayes, D.E (ed) The tectonic and geologic evolution of Southeast Asian seas and islands, Part 2, Geophysical Monograph 27. American Geophysical Union. p.79-94.

Garcia, M.O. and Jacobson, S.S. (1979) Crystal clots, amphibole fractionation and the evolution of calc-alkaline magmas. *Contrib. Mineral. Petrol.*, 69: 319-327.

Gasparik, T. and Lindsley, D.H. (1980) Phase equilibria at high pressure of pyroxenes containing monovalent and trivalent ions. Reviews in Mineralogy 7, Pyroxenes. Mineral. Soc. Am., p. 309-339.

Gervasio, F.C. (1964) A study of the tectonics of the Philippine Archipelago. *Phil. Geol.*, 20 (2): 51-75.

Gervasio, F.C. (1966). Age and nature of orogenesis of the Philippines. *Phil. Geol.*, 20: 121-140.

Ghiorso, M.S. and Carmichael, I.S.E. (1980) A regular solution model for met-aluminous silicate liquids: application to geothermometry, immiscibility, and the source regions of basic magmas. *Contrib. Mineral. Petrol.*, 71: 323-342.

Ghiorso, M.S., Carmichael, I.S.E., Rivers, M.L. and Sack, R.O. (1983) The Gibbs Free Energy of mixing of natural silicate liquids; an expanded regular solution approximation for the calculation of magmatic intensive variables. *Contrib. Mineral. Petrol.*, 84: 107-145.

Gill, J.B. (1974) Role of underthrust oceanic crust in the genesis of a Fijian calc-alkaline suite. *Contrib. Mineral. Petrol.*, 43: 29-45.

Gill, J.B. (1978) Role of trace element partitioning coefficients in models of andesite genesis. *Geochim. Cosmochim. Acta.*, 42: 709-724.

Gill, J.B. (1981) Orogenic andesites and plate tectonics. Springer Verlag. 390 p.

Glazner, A.F. (1984) Activities of olivine and plagioclase components in silicate melts and their application to geothermometry. *Contrib. Mineral. Petrol.*, 88: 260-268.

Goode, A.D.T. (1974) Oxidation of natural olivines. *Nature* , 248: 500-501.

Gorton, M.P. (1977) The geochemistry and origin of Quaternary volcanism in the New Hebrides. *Geochim. Cosmochim. Acta*, 41: 1257-1270.

Gourgaud, A. and Thouret, J. (1990) Magma mixing and petrogenesis of the 13 November 1985 eruptive products at Nevado del Ruiz (Colombia). *J. Volcanol. Geotherm. Res.*, 41: 79-96.

Green, D.H. (1970) The origin of basaltic and nephelinitic magmas. *Trans. Leicester Lit. Phil. Soc.* 64: 28-54.

Green, D.H. (1976) Experimental testing of "equilibrium" partial melting of peridotite under water-saturated, high pressure conditions. *Can. Mineral.*, 14: 255-268.

Grove, T.L. and Bence, A.E. (1977) Experimental study of pyroxene-liquid interaction in quartz-normative basalt 15597. Proc. Lunar Sci. Conf. 8th. 1549-1579.

Grove, T.L., Gerlach, D.C. and Sando, T.W. (1982) Origin of calc-alkaline series lavas at Medicine Lake Volcano by fractionation, assimilation and mixing. *Contrib. Mineral. Petrol.*, 80: 160-182.

Grove, T.L. and Bryan, W.B. (1983) Fractionation of pyroxene-phyric MORB at low pressure: an experimental study. *Contrib. Mineral. Petrol.*, 84: 293-309.

Grove, T.L. and Donnely-Nolan, J.M. (1986) The evolution of young silicic lavas at Medicine Lake Volcano, California: implications for the origin of compositional gaps in calc-alkaline series lavas. *Contrib. Mineral. Petrol.*, 92: 281-302.

Grove, T.L. and Kinzler, R.J. (1986) Petrogenesis of andesites. In *Annual Review of Earth and Planetary Sciences*, 14: 417-454.

Gust, D.A. and Perfit, M.R. (1987) Phase relations of a high-Mg basalt from the Aleutian island arc : implications for primary island arc basalts and high-Al basalts. *Contrib. Mineral. Petrol.*, 97: 7-18.

Haggerty, E. and Baker, I. (1967) The alteration of olivine in basaltic and associated lavas, Part I: High temperature alteration. *Contrib. Mineral. Petrol.* 16: 233-257.

Haile, N.S. (1969) Geosynclinal theory and the organisational pattern of the Northwest Borneo Geosyncline. Quart. *J. Geol Soc. London*, 124: 171-194.

Hamburger, M.W., Cardwell, R.K. and Isacks, B. (1983) Seismotectonics of the northern Philippine island arc. In Hayes, D.E (ed) The tectonic and geologic evolution of Southeast Asian seas and islands, Part 2, Geophysical Monograph 27. American Geophysical Union. p.1-22.

Hamilton, W. (1979) Tectonics of the Indonesian Region. Prof. Paper 1078, U.S. Geol Surv., Reston, Va., 345p.

Hanson, G.N. and Langmuir, C.H. (1978) Modeling of major elements in mantle-melt systems using trace element approaches. *Geochim. Cosmochim. Acta*, 42: 725-741.

Harvey, P.K., Taylor, D.M., Hendry, R.D. and Bancroft, F. (1973) An accurate fusion method for the analysis of rocks and chemically related materials by X-ray fluorescence spectrometry. X.R.S., 2: 33-44.

Hashimoto, W. (1980) Geologic development of the Philippines. *Contrib. Geol. Paleontol. Southeast Asia*, 217: 83-190.

Haston, R., Fuller, M. & Schmidtke, E. (1988) Paleomagnetic results from Palau, West Carolina Islands: A constraint on Philippine Sea Plate Motion. *Geology*, 16: 654-657.

Hawkesworth, C.J. and Ellam, R.M. (1989) Chemical fluxes and wedge replenishment rates along destructive plate margins. *Geology*, 17: 46-49.

Hawkesworth, C.J., Hergt, J.M., Ellam, R.M. and McDermott, F. (1991) Element fluxes associated with subduction related magmatism. *Phil. Trans. R. Soc. Lond.* A, 335: 393-405.

Hawkins, J.W. and Evans, C.A. (1983) Geology of the Zambales Range, Luzon, Philippine Islands: ophiolite derived from an island arc-back arc basin pair. In Hayes, D.E (ed) The tectonic and geologic evolution of Southeast Asian seas and islands, Part 2, Geophysical Monograph 27. American Geophysical Union. p.95-123.

Helz, R.T. (1973) Phase relations of basalts in their melting range at P_{H2O} = 5 kb as a function of oxygen fugacity. *J. Petrology*, 14: 249-302.

Helz, R.T. (1976) Phase relations of basalts in their melting ranges at P H_2O = 5 kb. Part II. Melt compositions. *J. Petrol.*, 17:139-193.

Helz, R.T. (1982) Phase relations and compositions of amphiboles produced in studies of the melting behaviour of rocks. In Veblen, D.R., Ribbe, P.H. (eds.) Amphiboles: petrology and experimental phase relations, Reviews in Mineralogy 9B, Min. Soc. Am., Michigan, p. 279-348.

Henderson, P. (1975) Reaction trends shown by Cr-Spinels of the Rhum layered intrusion *Geochim. Cosmochim. Acta*, 39:1035-1044.

Henderson, P. (1982) Inorganic Geochemistry. Pergammon Press, Oxford. 353p.

Herzberg, C.T. (1978) Pyroxene geothermometry and geobarometry: experimental and thermodynamic evaluation of some subsolidus phase relations in involving pyroxenes in the system CaO-MgO-Al_2O_3-SiO_2. *Geochim. Cosmochim. Acta*, 42: 945-957.

Hess, H.H. (1941) Pyroxenes of common mafic magmas, part 2. *Am. Mineral.* 26: 573-594.

Hoffer, J.M. (1966) Compositional variations of plagioclase feldspars from a basaltic flow. *Am. Mineral.*, 51: 807-813.

Hoffman, A.W., Feigenson, M.D. and Raczek, I. (1984) Case studies in the origin of basalt III:. Petrogenesis of the Mauna Ulu eruption, Kilauea, 1969-1971. *Contrib. Mineral. Petrol.*, 88: 24-35.

Hoffman, A.W., Jochum, K.P., Saufert, M. and White, W.M. (1986) Nb and Pb in oceanic basalts: new constraints on mantle evolution. *Earth. Planet. Sci. Lett.*, 79: 33-45.

Hoffman, A.W. (1988) Chemical differentiation of the Earth: the relationship between mantle, continental crust and oceanic crust. *Earth. Planet. Sci. Lett.* 90: 297-314.

Holloway, N.H. (1981) The stratigraphic and tectonic relationship of Reed Bank, north Palawan and Mindoro to the Asian mainland and its significance in the evolution of the South China Sea. *Bull. Geol. Soc. Malaysia*, 6: 16-86.

Holloway and Burnham (1972) Melting relations of Ba with Equilibrium H2O Pressure less than Total pressure. *J. Petrol.*, 13: 1-30.

Hort, M. and Spohn, T. (1991) Crystallization calculations for a binary melt cooling at constant rates of heat removal: implications for the crystallization of magma bodies. *Earth. Planet. Sci. Lett.*, 107: 463-474.

Hsu, M.T. (1971) Seismicity of Taiwan. *Int. Inst. Seismol. Earthquake Eng. Bull.*, 8: 41-160.

Huppert, H.E. and Worster, M.G. (1985) Dynamic solidification of a binary melt, *Nature* , 314: 703-707.

Ikeda, Y. and Yuasa, M. (1989) Volcanism in nascent back-arc basins behind the Shichito Ridge and adjacent area in the Izu-Ogasawara arc, northeast Pacific: evidence for mixing between E-Type MORB and island arc magmas at the initiation of back-arc rifting. *Contrib. Mineral. Petrol.*, 101: 377-393.

Irvine, T.N. and Barager, W.R.A. (1971) A guide to chemical classification of the common volcanic rocks. *Can. Jour. Earth Sci.*, 8: 523-548.

Irvine, T.N. (1980) Physics of magmatic processes. Hargraves, R.B. (ed.) Princeton University Press, New Jersey. p. 325-383.

Irving, A. J. (1978) A review of experimental studies of crustal/liquid trace element partitioning. *Geochim. Cosmochim. Acta*, 42: 743-770.

Ito, E. and Stern, R.J. (1985) Oxygen and strontium isotopic investigations of subduction zone volcanism: the case of the Volcano Arc and Marianas Island Arc. *Earth Planet. Sci. Lett.*, 76: 312-320.

Jacques, A.L. and Green, D.H. (1980) Anhydrous melting of peridotite at 0-15 kbar pressure and the genesis of tholeiitic basalts. *Contrib. Mineral. Petrol.*, 73: 287-310.

Jaffe, H.W., Robinson, P. and Tracy, R.J. (1978) Orthoferrosilite and other Fe-rich pyroxenes in microperthite gneiss of the Mount Marcy area, Adirondack Mountains, *Am. Mineral.* 63: 1116-1136.

Johnson, R.W and Arculus, R.J. (1978) Volcanic rocks of the Witu Islands, PNG: the origin of magmas above the deepest part of the New Britain Benioff zone. *Bull. Volcanol.*, 41: 609-655.

Johnson, K.T.M., Dick, H.J.B. and Shimuzu, N. (1990) Melting in the oceanic upper mantle: an ion microprobe study of diopsides in abyssal peridotites. *J. Geophys. Res.*, 95: 2661-2678.

Johnson, M.C. and Rutherford, M.J. (1988) Experimental calibration of an Aluminum-in-Hornblende geobarometer applicable to calc-alkaline rocks. EOS, 69: 1511.

Karig, D.E. (1971) Origin and development of marginal basins in the western Pacific. *J. Geophys. Res.*, 76: 2543-2561.

Karig, D.E. (1973) Plate convergence between the Philippines and the Ryukyu Islands. *Mar. Geol.*, 14: 153-168.

Karig, D.E. (1975) Basin genesis in the Philippine Sea. In: Initial Report of the Deep Sea Drilling Project, 31, Karig. D.E. et al (eds), U.S. Government Printing Office, Washington D.C. p. 857-879.

Karig, D.E. and Wageman, J.M. (1975) Structure and sediment distribution in the northwest corner of the West Philippine Basin. *Initial Rep. Deep-Sea Drilling Proj.*, 31: 615-620.

Karig, D.E. (1981) Northward propagating subduction along eastern Luzon, Philippine Islands . Abstract, AGU Fall Meeting.

Karig, D.E., Sarewitz, D.R. & Haeck, G.D. (1986) Role of strike-slip faulting in the evolution of allocthonous terranes in the Philippines. *Geology*, 14: 852-855.

Kay, R.W. and Hubbard, N.J. (1978) Trace elements in ocean ridge basalts. *Earth Planet. Sci. Lett.*, 38: 95-116.

Kay, S.M. and Kay, R.W. (1985) Aleutian tholeiitic and calc-alkaline magma series I: the mafic phenocrysts. *Contrib. Mineral. Petrol.*, 90: 276-290.

Kelemen, P.B., Johnson, R.T.M., Kinzler, R.J., and Irving, A.J. (1990) High field strength element depletions in arc basalts due to mantle-magma interaction. *Nature*, 345: 521-524.

Kerrick, D.M. and Darken, L.S. (1975) Statistical thermodynamic models for ideal oxide and silicate solid solutions and application to plagioclase. *Geochim. Cosmochim. Acta*, 39: 1431-1442.

Kinzler, R.J. and Grove, T.L. (1992) Primary magmas of mid-ocean ridge basalts 2. Applications. *J. Geophys. Res.*, 97: 6907-6926.

Kirkpatrick, R.J., Klein, L., Uhlman, D.R. and Hays, J.F. (1979) Rates and processes of crystal growth in the system anorthite-albite. *J. Geophys. Res.*, 84: 3671-3676.

Kouchi, A. and Sunagawa, I. (1989) A model for mixing basaltic and dacitic magmas as deduced from experimental data. *Contrib. Mineral. Petrol.*, 89: 17-25.

Kudo, A.M. and Weill, D.F. (1970) An igneous plagioclase thermometer. *Contrib. Mineral. Petrol.*, 25: 52-65.

Kuo, L. and Kirkpatrick, R.J. (1982) Pre-eruption history of phyric basalts from DSDP Legs 45 and 46: evidence from morphology and zoning patterns in plagioclase. *Contrib. Mineral. Petrol.* 79: 13-27.

Kushiro, I. (1960) Si-Al relations in clinopyroxenes from igneous rocks. *Am. Jour. Sci.* 258: 548-554.

Kushiro, I. (1972) Effect of water on the composition of magmas formed at high pressures. *J. Petrol.*, 13: 311-334.

Kushiro, I. (1975) On the nature of silicate melt and its significance in magma genesis: regularities in the shift of the liquidus boundaries involving olivine, pyroxene and silica minerals. *Am. Jour. Sci.*, 275: 411-431.

Langmuir, C.H. (1989) Geochemical consequences of in situ crystallization. *Nature*, 340: 199-205.

Le Bas, M.J. (1962) The role of aluminum in igneous clinopyroxenes with relation to their parentage. *Am. Jour. Sci.* , 660: 267-288.

Le Maitre (ed), R.W., Bateman, P., Dudek, A., Keller, J. et al (1989) A classification of Igneous rocks and Glossary of Terms: Recommendations of the International Union of Geological Sciences Subcommission on the Systematics of Igneous Rocks. Blackwell Scientific Publications, Oxford.

le Roex, A.P., Erlank, A.J. and Needham, H.D. (1981) Geochemical and mineralogical evidence for the occurrence of at least three distinct magma types in the 'FAMOUS' region. *Contrib. Mineral. Petrol.*, 77: 24-37.

le Roex, A.P., Dick, H.J.B., Reid, A.M., Frey, F.A., Erlank, A.J. and Hart, S.R. (1985) Petrology and geochemistry of basalts from the American-Antarctic Ridge, Southern Ocean: implications for the westward influence of the Bouvet mantle plume. *Contrib. Mineral. Petrol.*, 90: 367-380.

le Roex, A.P. (1987) Source regions of mid-ocean ridge basalts: evidence for enrichment processes. In: Menzies, M.A., Hawkesworth, C.J. (eds), Mantle metasomatism. Academic Press, London, p. 389-419.

le Roex, A.P., Dick, H.J.B. and Watkins, R.T. (1992) Petrogenesis of anomalous K-enriched MORB from the southwest Indian Ridge: 11°53'E to 14°38'E. *Contrib. Mineral. Petrol.*, 110: 253-268.

Leake, B.E. (1978) Nomenclature of Amphiboles. *Can. Mineral.* , 16: 501-520.

Lejay, P.S.J. (1938) The general characteristics of gravity in the Philippines. *Phil. Univ. Nat. and Appl. Sci. Bull.* , 6, 4: 223-290.

Letterier, J.,Maury, R.C.,Thonon, P.,Girard, D. and Marchal, M. (1982) Clinopyroxene composition as a method of identification of the magmatic affinities of paleovolcanic series. *Earth Planet. Sci .Lett.*, 59: 139-154.

Lewis, S.D. and Hayes, D.E. (1980) Northward-propagating subduction along eastern Luzon, Philippine Islands (abstract). *EOS. Trans. Amer. Geophys.Union*, 61: 1105.

Lewis, S.D. and Hayes, D.E. (1983) The tectonics of northward propagating subduction along eastern Luzon, Philippine islands. In Hayes, D.E (ed) The tectonic and geologic evolution of Southeast Asian seas and islands, Part 2, Geophysical Monograph 27. American Geophysical Union. p.57-78.

Lofgren, G.E. (1972) Temperature induced zoning in synthetic plagioclase feldspar. In: MacKenzie, W.S., Zussman, J. (eds) The Feldspars. Manchester University Press, Manchester, England, p. 362-375.

Lofgren, G.E. (1974) An experimental study of plagioclase crystal morphology: isothermal crystallisation. *Am. Jour. Sci.*, 274: 243-273.

Lofgren, G.E. and Norris, P.N. (1981) Experimental duplication of plagioclase sieve and overgrowth textures. *Geol. Soc. Amer. Abstracts with Programs*, 13: 498.

Loney, R.A., Himmelberg, G.R. and Coleman, R.G. (1971) Structure and petrology of the alpine type peridotite at Burro Mountain, California, USA. *J. Petrol.*, 12: 245-309.

Luhr, J.F. and Carmichael, I.S.E. (1980) The Colima volcanic complex, Mexico I. Post caldera andesites from Volcan Colima. *Contrib. Mineral. Petrol.*, 71: 343-372.

Luhr, J.F. and Carmicihael, I.S.E. (1985) Jorullo Volcano, Michoacan, Mexico (1759-1774): The earliest stages of fractionation in calk-alkaline magmas. *Contrib. Mineral. Petrol.*, 90: 142-161.

Maaloe, S. (1976) The zoned plagioclase of the Skaergaard intrusion. East Greenland. *J. Petrol.*, 17: 398-419.

MacDonald, G.A. and Alcaraz, A. (1956) Nuees Ardentes of the 1948-1953 eruption of Hibok-Hibok. *Bull. Volcanol.*, 18: 169-178.

MacDonald, G.A. and Katsura, T. (1965) Eruption of Lassen Peak, Cascade Range, California, in 1915: example of mixed magmas. *Bull. Geol. Soc. Am.* 76: 475-482.

Malicdem, D.G and Pena, R. (1967) Geology of copper-gold deposits of the Masara Mine area, Mabini, Davao. *Phil. Geol.*, 21: 16.

Mascle, A. and Biscarrat, P.A. (1979) The Sulu Sea: A marginal basin in Southeast Asia. In Watkins, J. et al (eds), Geological and geophysical investigations of continental margins, *Am. Assoc. Petrol. Geol. Memoir* 19: 373-381.

Maso, M. and Saderra, S.J. (1903) Volcanoes and seismic centers of the Philippine Archipelago. Census of the Philippine islands, p.184-254.

Matsumaru, K. (1974) Larger Foraminifera from east Mindanao, Philippines. *Geol. Paleontol. Southeast Asia*, 14: 101-115.

McCabe, R., Almasco, J. & Diegor, W. (1982) Geologic and paleomagnetic evidence for a possible Miocene collision in western Panay, central Philippines. *Geology*, 10: 325-329.

McCallum, I.S. and Charette, M.P. (1978) Zr and Nb partition coefficients: implications for the genesis of Mare basalts, KREEP and sea floor basalts. *Geochim. Cosmochim. Acta.*, 42: 859-869.

McCulloch, M.T. and Gamble, J.A. (1991) Geochemical and geodynamical constraints on subduction zone magmatism. *Earth Planet. Sci. Lett.*, 102: 358-374.

McDermott, F. and Hawkesworth, C.J. (1991) Th, Pb and Sr isotope variations in young arc volcanics and oceanic sediments. *Earth Planet. Sci. Lett.*

McDougall, I. (1979) Age of shield-building volcanism of Kauai, linear migration of volcanism in the Hawaiian Island chain. *Earth Planet. Sci. Lett.*, 46: 31-42.

McKenzie, D. (1984) The generation and compaction of partially molten rock. *J. Petrol.*, 25: 713-765

McKenzie, D. (1985) The extraction of magma from the crust and mantle. *Earth Planet. Sci. Lett.*, 74: 81-91.

McKenzie, D. and Bickle, M.J. (1988) The volume and composition of melt generated by extension of the lithosphere. *J. Petrol.*, 29: 625-629.

Meijer, A. and Reagan, M. (1981) Petrology and geochemistry of the Island of Sarigan in the Mariana Arc: Calc-alkaline volcanism in an oceanic setting. *Contrib. Mineral. Petrol.* 77: 337-354.

Melson, W.G., Vallier, T.L., Wright, T.L., Byerly, G. and Nelen, J. (1976) Chemical diversity of abyssal volcanic glass erupted along PAcific, Atlantic, and Indian Ocean sea floor spreading centers. *Monogr. Am. Geophys. Union*, 19: 351-368.

Metal Mining Agency (1972) Report of geological survey of eastern Mindanao in the first phase. Overseas Tech. Coop. Assoc., Tokyo.

Mevel, C . and Velde, D. (1976) Clinopyroxenes in Mesozoic pillow lavas from the French Alps: influence of ccoling rate on compositional trends. *Earth Planet Sci. Lett.*, 32: 158-164.

Michael, P.J. (1989) Intrusion of basaltic magma into crystallizing granitic magma chamber: Cordillera del Paine In the southernmost Andes, Chile. In: Continental Magmatism, IAVCEI General Assembly, New Mexico Bureau Mines Mineral Res., Bull. 131: 189.

Michael, P.J. and Bonatti, E. (1985) Peridotite compositions from the North Atlantic: regional and tectonic variations and implications for partial melting. *Earth Planet. Sci. Lett.*, 73: 91-104.

Miller, D.M., Langmuir, C.H., Goldstein, S.L. and Franks, A.L. (1992) The importance of parental magma composition to calc-alkaline and tholeiitic evolution: evidence from Umnak Island in the Aleutians. *J. Geophys. Res.*, 97: 321-343.

Mineral and Fuels Division, Bureau of Mines, Manila, The Philippines (1976) A review of oil exploration and stratigraphy of sedimentary basins of the Philippines. *Tech. Bull. U. N. Econ. Soc. Comm. Asia Pac., Comm. Co-ord. St. Prospec. Miner. Resourc. South Pac. Offshore Areas*, 10: 55-102.

Mitropoulos, P. and Tarney, J. (1992) Significance of mineral composition variations in the Aegean island arc. *J. Volcanol. Geotherm. Res.*, 51: 283-303.

Miyashiro, A. (1974) Volcanic rock series in island arcs and active continental margins. *Am. Jour. Sci.*, 274: 321-355.

Moore, G.F. & Silver, E.A. (1983) Collision processes in the Northern Molluca Sea. In Hayes, D.E (ed) The tectonic and geologic evolution of Southeast Asian seas and islands, Part 2, Geophysical Monograph 27. American Geophysical Union. p.360-372.

Morante, E.M. and Allen, C.R. (1974) Displacement on the Philippine Fault during the Ragay Gulf earthquake of March 17, 1973 (abstract). *Geol. Soc. Amer. Abstr. with Programs*, 5: 744-745.

Morimoto, N. (1989) Nomenclature of pyroxenes. *Can. Mineral.* 27: 143-156.

Morrice, M.G. and Gill, J.B. (1986) Spatial patterns in the mineralogy of island-arc magma series: Sangihe arc, Indonesia. *J. Volcanol. Geotherm. Res.*, 29: 311-353.

Morrice, M.G., Jezek, P.A., Gill, J.B., Whitford, D.J. and Monoarfa, M. (1983) An introduction to the Sangihe arc: volcanism accompanying arc-arc collision in the Molluca Sea, Indonesia. *J. Volcanol. Geotherm. Res.*, 19: 135-165.

Morris, J.D. and Hart, S.R. (1983) Isotopic and incompatible element constraints on the genesis of island arc volcanics from Cold Bay and Amark Island, Aleutians and implications for mantle structure. *Geochim. Cosmochim. Acta*, 47: 2015-2030.

Morris, J.D. and Tera, F. (1989) ^{10}Be and ^{9}Be in mineral separates and whole rocks from volcanic arcs: implication for sediment subduction. *Geochim. Cosmochim. Acta*, 53: 3197-3206.

Morris, J.D., Leeman, W.P. and Tera, F. (1990) The subducted component in island arc lavas: constraints from Be isotopes and B-Be systematics. *Nature*, 344: 31-36.

Muir, I.D. and Tilley, C.E. (1958) The compositions of coexisting pyroxenes in metamorphic assemblages. *Geol. Mag.* 95: 403-408.

Murata, K.J. (1960) A new method of plotting chemical analyses of basaltic rocks. *Am. Jour. Sci.*, 258: 247-252.

Mysen, B.O., Kushiro, I. Nicholls, I.A. and Ringwood,A.E. (1974) A possible mantle origin for andesite magmas: discussion and replies. *Earth Planet. Sci. Lett.*, 21: 221-229.

Nakamura, Y. and Kushiro, I. (1970) Compositional relations of coexisting orthopyroxene, pigeonite and augite in a tholeiitic andesite from Hakone Volcano. *Contrib. Mineral. Petrol.*, 26: 265-275.

Nicholls, I.A. and Ringwood, A.E. (1973) Effect of water on olivine stability in tholeiites and production of silica-saturated magmas in the island-arc environment. *J. Geol.*, 81: 1665-1688.

Nicholls, J. (1977) The activities of components in natural silicate melts. In: Fraser, D.G. (ed) Thermodynamics in Geology 30, Proceedings of the NATO Advanced Study Institute, Oxford, p. 327-348.

Nicholls, J. (1980) A simple thermodynamic model for estimating the solubility of H_2O in magmas. *Contrib. Mineral. Petrol.*, 74: 211-220.

Nicholls, J., Carmichael, I.S.E. and Stormer, J. (1971) Silica activity and P_{total} in igneous rocks. *Contrib. Mineral. Petrol.*, 33: 1-20.

Nicholls, J. and Carmichael, I.S.E. (1972) The equilibration temperature and pressure of various lava types with spinel and garnet peridotite. Am. Mineral., 57: 941-959.

Nielsen, R.L. (1986) Simulation of igneous differentiation processes. In: *Ann. Rev. Earth Planet. Sci.*, 14: 65-105.

Nielsen, R.L. (1991) Simulation of igneous differentiation processes. In: Nicholls, J. and Russel, J.K (eds) Modern methods of igneous petrology: understanding magmatic processes, Reviews in Mineralogy 24, Min. Soc. Am., Michigan, p. 65-106.

Nielsen, R.L. and DeLong, S.E (1992) A numerical approach to boundary layer fractionation: application to differentiation in natural magma systems. *Contrib. Mineral. Petrol.*, 110: 355-369.

Nilson, R.H., McBirney, A.R. and Baker, B.H. (1985) Liquid fractionation. Part II: fluid dynamics and quantitative implications for magmatic systems. *J. Volcanol. Geotherm. Res.*, 24: 25-54.

Nisbet, E.G. and Pearce, J.A. (1977) Clinopyroxene composition in mafic lavas from different tectonic settings. *Contrib. Mineral. Petrol.* 63: 149-160.

Nixon, G.T. (1988) Petrology of the younger andesites and dacites of Iztaccihautl Volcano, Mexico: II. Chemical stratigraphy, magma mixing and the composition of basaltic magma influx. *J. Petrol.*, 29: 265-303.

Norrish, K. and Hutton, J.T. (1969) An accurate X-ray spectograph method for the analysis of a wide range of geological samples. *Geochim. Cosmochim. Acta*, 33: 431-453.

Ocean Drilling Program (1989) Origins of marginal basins. *Nature*, 338: 380-381.

Ormerod, D.S., Rogers, N.W. and Hawkesworth, C.J. (1991) Melting in the lithospheric mantle: Inverse modelling of alkali-olivine basalts from Big Pine Volcanic Field, California. *Contrib. Mineral. Petrol.*, 108: 305-317.

Pacis, M.G. (1966) Report on the geology of parts of the province of Misamis Oriental, Bukidnon and Lanao del Norte. Philippine Bureau of Mines. Unpublished report.

Paderes, A.E. and Miranda, F.E. (1965) Geology of the Vitali and Anungan quadrangles, Zamboanga Peninsula. Philippine Bureau of Mines. Unpublished. report.

Palacz, Z.A. and Saunders, A.D. (1986) Coupled trace element and isotope enrichment in the Cook-Austral-Samoa Islands, southwest Pacific. *Earth Planet. Sci. Lett.*, 79: 270-280.

Peacock, S.M. (1991) Numerical simulations of subduction zone pressure-temperature-time paths: constraints on fluid production and arc magmatism. *Philos. Trans. R. Soc. Lond.* A, 335: 341-353.

Pearce, J.A. and Norry, M.J. (1979) Petrogenetic implications of Ti, Zr, Y, and Nb variations in volcanic rocks. *Contrib. Mineral. Petrol.*, 69: 33-47.

Pelaez, V.R. (1948) The Volcanic Activity of Catarman and Hibok-Hibok, Camiguin Island, Mindanao, of September, 1948. Eigth Pacific Science Congress. 88-108.

Perfit, M.R., Gust, D.A., Bence, A.E., Arculus, R.J. and Taylor, S.R. (1980) Chemical characteristics for mantle sources. *Chem. Geol.*, 30: 227-256.

Philippine Bureau of Mines (1963) Geological map of the Philippines, scale 1:1,000,000, 9 sheets. Manila.

Philippine Bureau of Mines and Geosciences (1982) Geology and Mineral resources of the Philippines (I): Geology, Manila. 406p.

Philippine Bureau of Mines, Petroleum Division (1966) A review and assessment of oil exploration in the Philippines, 1. 193p.

Philippine Bureau of Mines and Geosciences, Petroleum Division (1975) A review and assessment of oil exploration in the Philippines, 2. 95p.

Philippine Geodetic & Geophysical Institute. A preliminary report on the recent eruptions of Hibok-Hibok Volcano, Camiguin Island, Philippines. *Bull. Volcanol.*, 12: 215-225.

Philippine Institute of Volcanology (1982) Volcanoes and geothermal areas in Mindanao, Quezon City: 24p.

Philippine Institute of Volcanology and Seismology (1992) Unpublished seismic data.

Pittman E.D. (1963) Use of zoned plagioclase as an indicator of provenance. *J. Sed. Petrol.*, 33: 380-386.

Plank, T. and Langmuir, C.H. (1988) An evaluation of the global variations in the major element chemistry of arc basalts. *Earth Planet. Sci. Lett.*, 90: 349-370.

Poldevaart, A. and Hess, H.H. (1951) Pyroxenes in the crystallization of of basaltic magma. *J. Geol.* 59: 472-489.

Powell, R. (1977) Activity-composition relationships for crystalline solutions. In: Fraser, D.G. (ed) Thermodynamics in Geology 30, Proceedings of the NATO Advanced Study Institute, Oxford, p. 57-65.

Price, R.C., McCulloch, M.T., Smith, I.E.M. and Stewart, R.B. (1992) Pb-Nd-Sr isotopic compositions and trace element characteristics of young volcanic rocks from Egmont Volcano and comparisons with basalts and andesites from Taupo Volcanic Zone, New Zealand. *Geochim. Cosmochim. Acta*, 56: 941-953.

Pringle, G.J., Trembath, L.T., Parjari Jr., G.E. (1974) Crystallisation history of a zoned plagioclase. *Mineral. Mag.*, 39: 867-877.

Prinzhofer, A. and Allegre, C.J. (1985) Residual peridotites and mechanisms of partial melting. *Earth Planet. Sci. Lett.*, 74: 251-265.

Punongbayan, R.S. (1988) Proposed evolution of Camiguin Island. In: Volcanoes of Camiguin Island. Quezon City, p.22.

Putnis, A. (1979) Electron petrography of high temperature oxidation in olivine from Rhum layered intrusion. *Mineral Mag.*, 43: 293-296.

Ramberg, H. (1952) Chemical bonds and the distribution of cations in silicates. *J. Geol.*, 60: 331-335.

Rangin, C., Muller, C. and Porth, H. (1989) Neogene dynamic evolution of the Visayan Region. In Porth, H. and Daniels, C.H. (eds). On the geology and hydrocarbon prospects of the Visayas Basin, Philippines. *Geologisches Jahrbuch, Reihe B*, 70: 7-27

Ranken, B., Cardwell, R.K., and Karig, D.E. (1984) Kinematics of the Philippine Sea Plate. *Tectonics*, 3: 555-575.

Ranneft, T.S.M., Hopkins, R.M., Froelich, A.J. and Gwinn, J.W. (1960) Reconnaissance geology and oil possibilities of Mindanao. *AAPG Bull.*, 44 (5): 529-569.

Renard, A. (1889) Report on the Rock Specimens collected on Ocean Islands during the voyage of the HMS Challenger, during the years 1873-1876, 180p.

Republic of the Philippines-Government of Japan Project (1974) Report on the geological survey of eastern Mindanao, Phase III. Unpublished report.

Reyes, M.V. and Ordonez, E.P. (1979) Philippine Cretaceous smaller foraminifera. *J. Geol. Soc. Phil., 24: 1-67.*

Ribbe, P.H. and Smith, J.V. (1966) X-Ray emission microanalyses of rock forming minerals. IV: plagioclase feldspars. *J. Geol.* 74: 217-233.

Riley, G.N.and Kohlstedt, D.L. (1992) Melt migration in silicate melt-olivine systems. *Earth Planet. Sci. Lett.*, In press.

Ringwood, A.E. (1974) Petrological evolution of island arc systems. *Geol. Soc. London J.* , 130: 183-204.

Ringwood, A.E. (1975) Composition and petrology of the earth's mantle. McGraw-Hill, New York.

Robinson, P. (1982) General review of metamorphic amphibole compositions. In Veblen, D.R., Ribbe, P.H., eds., Amphiboles: petrology and experimental phase relations, Reviews in Mineralogy 9B, Min. Soc. Am., Michigan, p.3-22.

Roedder, E. (1984) Fluid inclusions. Mineral. Soc. Am. Rev. Mineral. 12: 644.

Roeder, D. (1977) Philippine arc system-collision or flipped subduction zones? *Geology*, 5: 203-206.

Roeder, P.L. (1974) Activity of iron and olivine solubility in basaltic liquids. *Earth Planet. Sci. Lett.*, 23: 397-410.

Roeder, P.L. and Emslie, R.F. (1970) Olivine-liquid equilibrium. *Contrib. Mineral. Petrol.*, 29: 275-289.

Rowlett, H. and Kelleher, J. (1976) Evolving seismic and tectonic patterns along the Western Margin of the Philippine Sea Plate. *J. Geophys. Res.*, 81: 3518-3524.

Russell, J.K. (1991) Magma mixing processes: insights and constraints from thermodynamic calculations. In: Nicholls, J. and Russel, J.K eds., Modern methods of igneous petrology: understanding magmatic processes, Reviews in Mineralogy 24, Min. Soc. Am., Michigan, p. 153-187.

Russell, J.K. and Nicholls, J. (1989) Analysis of petrologic hypothesis with Pearce Element Ratios. *Contrib. Mineral. Petrol.*, 99: 25-35.

Rutland, R.W. (1968) A tectonic study of part of the Philippine fault zone. *Geol. Soc. Lond.*, 123: 293-327.

Ryerson, F.J. and Hess (1978) Implications of liquid-liquid distribution coefficients to mineral-liquid partitioning. *Geochim. Cosmochim. Acta*, 42: 915-919.

Ryerson, F.J. and Watson, E.B. (1987) Rutile saturation in magmas: implications for Ti-Nb-Ta depletion in island arc basalts. *Earth Planet. Sci. Lett.*, 86: 225-239.

Sack, R.O., Carmichael, I.S.E., Rivers, M. and Ghiorso, M.S. (1980) Ferric-ferrous equilibria in natural silicate liquids at 1 bar. *Contrib. Mineral. Petrol.*, 75: 369-376.

Sakuyama, M. (1981) Petrological study of the Myoko and Kurohime volcanoes, Japan: crystallization sequence and evidence for magma mixing. *J. Petrol.*, 22: 553-583.

Santos-Ynigo, L.M. (1944) Geology of the Surigao Gold District. Phil. Bur. Mines, unpublished report.

Santos-Ynigo, L.M. (1953) Geology of southern Zamboanga Province. *Phil. Geol.*, 7 (2): 45-64.

Saunders, A.D., Norry, M.J. and Tarney, J. (1988) Origin of MORB and chemically-depleted mantle reservoirs: trace element constraints. *J. Petrol.*, Special Lithosphere Issue: 415-445.

Saunders, A.D., Norry, M.J. and Tarney, J. (1991) Fluid influence on the trace element compositions of subduction zone magmas. *Phil. Trans. R. Soc. Lond. A*, 335: 377-392.

Schroeder, B., Thompson, G., Sulanowska, M.and Ludden, J.N. (1980) Analysis of geologic materials using an automated X-ray fluorescence system. *X.R.S.*, 9: 198-205.

Schweitzer, E.L., Papike,J.J. and Bence, A.E. (1979) Statistical analysis of clinopyroxenes from deep-sea basalts. *Am.Mineral.*, 64: 501-513.

Schweller, W.J. and Karig, D.E. (1979) Constraints on the origin and emplacement of the Zambales ophiolite, Luzon, Philippines (abstract). *Geol. Soc. Amer. Abstr. with Programs*, 11: 512-513.

Schweller, W.J. Karig, D.E. and Bachman, S.B. (1983) Original setting and emplacement history of the Zambales ophiolite, Luzon, Philippines, from stratigraphic evidence. In Hayes, D.E (ed) The tectonic and geologic evolution of Southeast Asian seas and islands, Part 2, Geophysical Monograph 27. American Geophysical Union. p.124-138.

Sen, S.K. (1960) Some aspects of of the distribution of barium, strontium, iron and titanium in plagioclase feldspars. *J. Geol.*, 68: 638-665.

Seno, T. and Kurita, K. (1978) Focal mechanisms and tectonics in the Taiwan-Philippine region. *J. Phys. Earth*, 26, suppl.: S249-S263.

Seno, T. (1977) The instantaneous rotation vector of the Philippine Sea Plate relative to the Eurasian Plate. *Tectonophysics* 42: 709-776.

Shaw, D.M. (1970) Trace element fractionation during anatexis. *Geochim Cosmo. Acta*, 34: 237-243.

Shi, P. (1992) Basalt evolution at low pressure: implications from an experimental study in the system CaO-FeO-MgO-Al_2O_3-SiO_2. *Contrib. Mineral. Petrol.*, 110: 139-153.

Shih, T. (1980) Marine magnetic anomalies from the western Philippine Sea: implications for the evolution of marginal basins. In Hayes, D.E (ed) The tectonic and geologic evolution of Southeast Asian seas and islands, Geophysical Monograph 23. American Geophysical Union. p.49-76.

Shimuzu, N. and Allegre, C.J. (1978) Geochemistry of transition elements in garnet lherzolite nodules in kimberlites. *Contrib. Mineral. Petrol.*, 67: 41-50.

Sigurdsson, H. and Schilling, J.G. (1976) Spinels in Mid-Atlantic Ridge basalts: chemistry and occurrence. *EPSL*, 29: 7-20.

Simkin, T. and Smith, J.V. (1970) Minor-element distribution in olivine. *J. Geol.* 78: 304-325.

Singer, B.S., Myers, J.D. and Frost, C.D. (1992) Mid-Pleistocene lavas from the Seguam volcanic center, central Aleutian arc: closed system fractional crystallization of a basalt to rhyodacite eruptive suite. *Contrib. Mineral. Petrol.*, 110: 87-112.

Smith, R.K. and Lofgren, G.E. (1979) The Physico-chemical and crystal growth kinetics necessary for zonal development in plagioclase. *Geol. Soc. Amer. Abstr. with Programs*, 7: 520.

Solidum, R.U. and de Torres, C. (1986) Preliminary report on the petrography of rocks from Hibok-Hibok Volcano. Phil. Inst. Volcanol. Volcanol. Seismol. Unpublished report. 8p.

Solidum, R.U. (1988) Reconnaissance geologic survey of Mt. Balatocan, Misamis Oriental. Phil. Inst. Volcanol. Seismol. Unpublished report., 4p.

Sparks, R.S.J. (1989) *In situ* differentiation in magma. *Nature*, 340: 187.

Sparks, R.S.J. and Huppert, H.E. (1984) Density changes during the fractional crystallization of basaltic magmas: implications for the evolution of layered intrusions. *Contrib. Mineral. Petrol.*, 85: 300-309.

Sparks, R.S.J., Huppert, H.E., Kerr, R.C., McKenzie, D.P. and Tait, S.R. (1985) Post cumulus processes in layered intrusions. *Geol. Mag.*, 122: 555-568.

Sparks, R.S.J., Siggurdsson, H. and Wilson, L. (1977) Magma mixing: a mechanism for triggering acid explosive eruption. *Nature*, 267: 315-318.

Spulber, S.D. and Rutherford, M.J. (1983) The origin of rhyolite and plagiogranite in oceanic crust: an experimental study. *J. Petrol.*, 24:1-25.

Stern, R.J. (1981) A common mantle source for western Pacific island arc and "hot spot" magmas- Implications for layering in the upper mantle. Carnegie Inst. Washington Yearb., 81: 455-462.

Stewart, D.C. (1975) Crystal clots in calc-alkaline andesites as breakdown products of high-Al amphiboles. *Contrib. Mineral. Petrol.*, 53: 195-204.

Stewart, G.S and Cohn, S.N. (1977) The August 16, 1976, Mindanao, Philippine earthquake (M=7.8) - evidence for a subduction zone south of Mindanao (abstract). *Eos. Trans. AGU*, 58: 1194.

Stolper, E. (1980) A phase diagram and for mid-ocean ridge basalts: preliminary results and implications for petrogenesis. *Contrib. Mineral. Petrol.*, 74: 3-27.

Sun, S.S. (1980) Pb-isotope study of young volcanic rocks from MORB, ocean islands and island arcs. *Phil.Trans. R. Soc. London.*, A297: 409-45.

Sun, S.S. and McDonough, W.F. (1989) Chemical and isotopic systematics of ocean basalts: implications for mantle composition and processes. In: Saunders, A.D. and Norry, M.J. (eds) Magmatism in theOcean Basins, Geol. Soc. London Spec. Publ., 42: 313-345.

Swanson, S.E. (1977) Relations of nucleation and crystal growth rate to the development of granitic textures. *Am. Mineral.* 62: 966-978.

Sweatman, T.R. and Long, J.V.P. (1969) Quantitative Electron-probe micro-analysis of rock-forming minerals. *Jour. Petrol.*, 10: 332-379.

Takahashi, E. and Kushiro, I. (1983) Melting of a dry peridotite at high pressures and basalt magma genesis. *Am. Mineral.*, 68: 859-879.

Takahashi, E. (1986) Melting of a dry peridotite KLB-1 up to 14Gpa: Implications on the origin of peridotite upper mantle. *J. Geophys. Res.*, 91: 9367-82.

Tamaki, K. and Honza, E. (1991) Global tectonics and formation of marginal basins: role of the western Pacific. *Episodes* 14(3): 224-230.

Tarney, J., Saunders, A.D., Weaver, S.D., Donnellan, N.C.B. and Hendry, G.L. (1979) Minor element geochemistry of basalts from Leg 49. In: Luyendyk, B.P., Cann, J.R. et al (eds) Initial Reports of the Deep Sea Drilling Project 49, p.660-685.

Tarney, J., Pickering, K.T., Knipe, R.J. and Dewey,, J.F. (1991) Preface to behaviour and influence of fluids in subduction zones. The Royal Society London, 195 p.

Tatsumi, Y., Sakuyama, M., Fukuyama, H. and Kushiro, I. (1983) Generation of arc basalt magmas and thermal structures of the mantle wedge in subduction zones. *J. Geophys. Res.*, 88: 5815-5825.

Tatsumi, Y. (1986) Formation of volcanic front in subduction zones. *Geophys. Res. Lett.*, 13: 717-720.

Tatsumi, Y., Hamilton, D.L. and Nesbitt, R.W. (1986) Chemical characteristics of fluid phase released from a subducted lithosphere and origin of arc magmas: evidece from high-pressure experiments and natural rocks. *J. Volcanol. Geotherm. Res.*, 29: 293- 309.

Tatsumi, Y., Murasaki, M., Arsadi, E.M. and Nohda, S. (1991) Geochemistry of Quaternary lavas from NE Sulawesi: transfer of subduction components into the mantle wedge. *Contrib. Mineral. Petrol.*, 107: 137-149.

Tatsumi, Y., Murasaki, M. and Nohda, S. (1992) Across-arc variation of lava chemistry in the Izu-Bonin Arc: identification of subduction components. *J. Volcanol. Geotherm. Res.*, 49: 179-190.

Taylor, B. and Hayes, D.E. (1980) The tectonic evolution of the South China Basin. In Hayes, D.E (ed) The tectonic and geologic evolution of Southeast Asian seas and islands, Geophysical Monograph 23. American Geophysical Union. p.89-104.

Taylor, B. and Hayes, D.E. (1983) Origin and history of the South China Basin. In Hayes, D.E (ed) The tectonic and geologic evolution of Southeast Asian seas and islands, Part 2, Geophysical Monograph 27. American Geophysical Union. p.23-56.

Taylor, S.R. and McLennan, S.M. (1985) The continental crust: its composition and evolution. Oxford, Blackwell, 1985. 312p.

Tsuchiyama, A. (1985) Dissolution kinetics of plagioclase in melt of the system dopside-albite-anorthite, and origin of dusty plagioclase in andesites. *Contrib. Mineral. Petrol.*, 89: 1-16.

Turner, F.J. and Verhoogen, J. (1951) Igneous and Metamophic Petrology. McGraw Hill, New York. 602p.

Turner, J.S., Huppert, H.E. and Sparks, R.S.J. (1983) An experimental investigation of volatile exsolution in evolving magma chambers. *J. Volcanol. Geotherm. Res.*, 16: 263-277.

Uyeda, S. and McCabe, R. (1982) A possible mechanism of episodic sea-floor spreading of the Philippine Sea. In: Balce, G.R. & Zanoria, A.S. (eds), 1982, Geology & Tectonics of the Luzon-Marianas Region. Proceedings of the CCOP-IOC SEATAR Workshop, Philippines, 21-28 Nov.1981.

Verhoogen, B.J. (1962) Distribution of titanium between silicates and oxides in igneous rocks. *Am. Jour. Sci.*, 260: 211-220.

Vieten, K. and Hamm, H.M. (1978) Additional notes "On the calculation of the crystal chemical formula of clinopyroxenes and their contents of Fe^{3+} from microprobe analyses. *Neues Jahrb. Mineral.*, Monatsh, 71-83.

Vukadinovic, D. and Nicholls, I.A. (1989) The petrogenesis of island arc basalts from Gunung Slamet volcano, Indonesia: Trace element and Sr^{87}/Sr^{86} constraints. *Geochim. Cosmochim. Acta*, 53: 2349-2363.

Walker, D., Shibata, T. and DeLong, S.E. (1979) Abyssal tholeiites from the Oceanographer Fracture Zone. II. Phase equilibria and Mixing. *Contrib. Mineral. Petrol.*, 70: 111-126.

Watson, E.B. (1976) Glass inclusions as samples of early magmatic liquid: determinative method and application to a south Atlantic basalt. *J. Volcanol. Geotherm. Res.*, 1: 73-84.

Watson, E.B. (1979) Calcium content of forsterite coexisting with silicate liquid in the system Na2O-CaO-MgO-Al2O3-SiO2. *Am. Mineral.*, 64: 824-829.

Weaver, B.L. and Tarney, J. (1984) Estimating the composition of the continental crust: an empirical approach. *Nature*, 310: 575-577.

Weaver, B.L., Wood, D.A., Tarney, J. and Joron, J.L. (1987) Geochemistry of ocean island basalts from the South Atlantic: Ascension, Bouvet, St. Helena, Gough and Tristan de Cunha. In: Fitton, J.G. and Upton, B.G. J. (eds) Alkaline Igneous Rocks, Geol. Soc. London Spec. Publ. 30, p.253-267.

Weissel, J.K. (1980) Evidence for Eocene oceanic crust in the Celebes Basin. In Hayes, D.E (ed) The tectonic and geologic evolution of Southeast Asian seas and islands, Part 1, Geophysical Monograph 23. American Geophysical Union. p.37-47.

Wiebe, R.A. (1968) Plagioclase stratigraphy: a record of magma conditions and events in a granitic stock. *Am. Jour. Sci.*, 266: 690-703.

Wilkinson, J.F.G (1967) The petrography of basaltic rocks. In Hess, H.H. and Poldevaart, A. (eds) Basalts, The Poldevaart treatise on rocks of basaltic compositions, Vol. 1. p.163-214.

Wilkinson, J.F.G. (1980) The genesis of mid-ocean ridge basalt. Earth Sci. Rev.

Wilkinson, J.F.G. (1991) Mauna Loan and Kilauean Tholeiites with low 'Ferromagnesian-Fractionated' 100 Mg/(mg + Fe^{2+}) ratios: Primary liquids from the Upper Mantle? *J. Petrol.*, 32: 863-907.

Willis, B. (1944) Philippine earthquakes and structure. *Bull. Seismol. Soc. Am.*, 34: 69-81.

Wolfe, J.A. (1981) Philippine geochronology. *J. Geol. Soc. Phil.*, 35: 1-30.

Wolfe, J.A. (1983) Origin of the Phillppines by accumulation of allochthons. *Phil. Geol.*, Jul-Sep: 17-33.

Wolfe, J.A. and Self, S. (1983) Structural Lineaments and Neogene Volcanism in Southwestern Luzon. In: The tectonic and Geologic Evolution of Southeast Asian seas and islands, Part 2 Geophysical Monograph Series, 27: 157-172.

Wood, B.J. (1976) Mixing properties of Tschermakitic clinopyroxenes. *Am. Mineral.*, 61: 599-602.

Wood, D.A., Joron, J.L., Marsh, N.G., Tarney, J. and Treuil, M. (1980) Major and trace element variations in basalts from the North Philippine Sea drilled during Deep Sea Drilling Project Leg 58: a comparative study of back-arc-basin basalts with lava series from Japan and mid-oceanic ridges. *Init. Rep. DSDP*, 58: 873-894.

Woodhead, J.D. (1989) Geochemistry of the Marianas arc, Western Pacific: source composition and and process. *Chem. Geol.*, 76: 1-24.

Wyers, G.P. and Barton, M. (1986) Petrology and evolution of transitional alkaline-subalkaline lavas from Patmos, Dodecanesos, Greece: evidence for fractional crystallization, magma mixing and assimilation. *Contrib. Mineral. Petrol.*, 93: 297-311.

Wyllie, P.J. (1978) Water and magma generation at subduction zones. *Bull. Volcanol.*, 41: 360 - 377.

Yoder, H.S. Jr., Tilley, C.E. (1962) Origin of basalt magmas: An experimental study of natural and synthetic rock systems. *J. Petrol.*, 3: 342-532.

Zindler, A. and Hart, S. (1986) Chemical geodynamics. In Ann. Rev. Earth Planet. Sci., 14: 493-571.

Appendix 1. Sample location map.

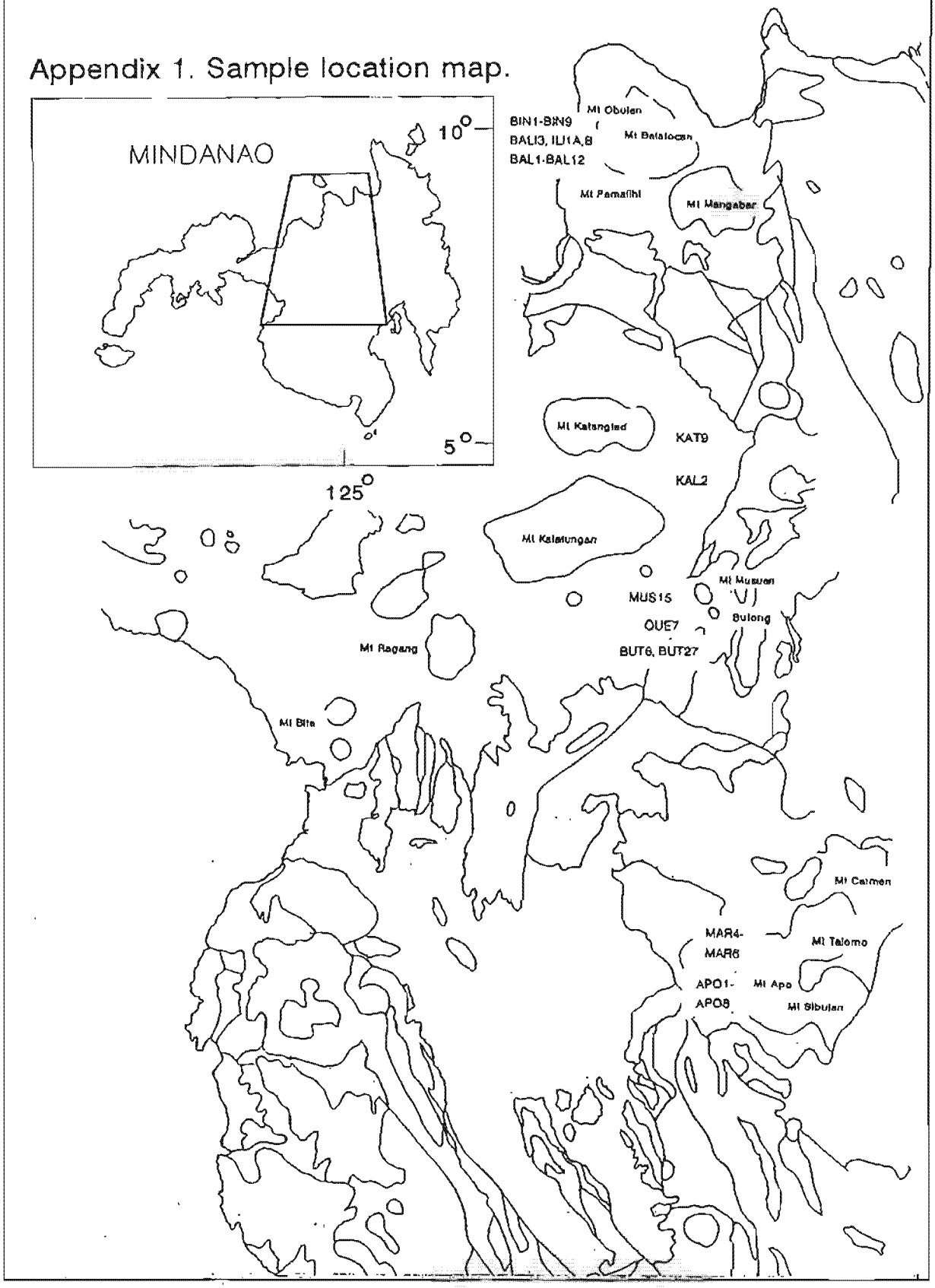

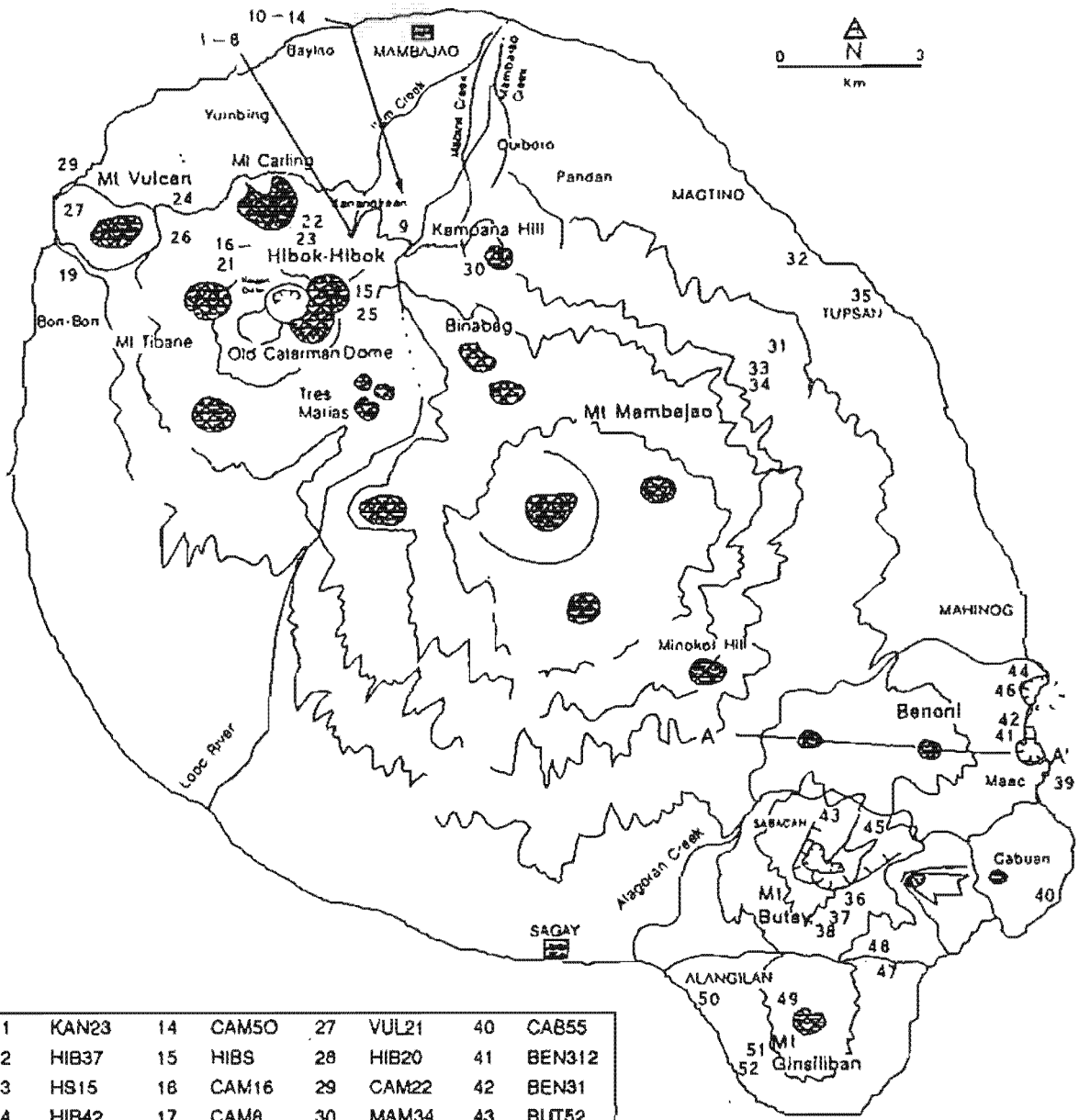

1	KAN23	14	CAM5O	27	VUL21	40	CAB55
2	HIB37	15	HIB5	28	HIB20	41	BEN312
3	HS15	16	CAM16	29	CAM22	42	BEN31
4	HIB42	17	CAM8	30	MAM34	43	BUT52
5	CA782	18	HIB4	31	MAM47	44	BEN315
6	HIB41	19	CAM14	32	MAM33	45	BUT54
7	CAM24	20	CAM7	33	MAM48	46	BEN30
8	HIB40	21	CAM17	34	MAM57	47	GIN53
9	CAM10	22	HIBB	35	MAM32	48	GIN56
10	HIB12	23	HIB15	36	BUT28	49	GIN27
11	HIB5	24	CAM58	37	BUT1	50	GIN265
12	HIB3	25	CAT46	38	BUT51	51	CAM275
13	HIB25	26	VUL50	39	BEN29	52	GIN26

Appendix 1. continued. Location of Camiguin Island samples.
Numbers are analyses numbers given in Appendix 4.

Appendix 2. Petrographic analyses

Lab No.	Sample No.	Rock Name	Ol	Plag	Hb	Cpx	Op	Mt	Bi	Qz	Total	Maximum Phenocryst Size (mm) Ol	Plag	Hb	Cpx	Opx	Mt	Bio	Qz	Texture
						(vol%)														
21856	Ben29	px and		35.0	0.1	9.0		4.0			48.1		0.7	0.5	2.0					pf clast, fmg, subophitic
21858	Ben31	px and	6.0	35.0		4.0		4.0			49.0	1.0	0.5		1.5					pf clast, porphyritic
21859	Ben31/2	px and		32.0		3.8		5.3			41.1	1.0	0.8		0.6		0.1			pf/surge clast, fg
21860	Ben31/5	px-hb and		30.0	1.0	0.1		3.0			34.1		1.1	1.0	0.4					bc, por, pilotaxitic
21857	Ben30	px and		40.0	0.1	4.0		7.0			51.1		1.0		0.6					lf, fmg, porphyritic
21855	But28	ol bas	7.0	40.0		6.0	2				55.0	1.2	1.4		0.9					bomb, fmg, pilotaxitic
21830	But1	bas and	5.0	35.0		7.0	1	7.0			55.0	1.0	1.2		1.0	0.7	0.3			lf, vfg, px specks
21874	But51	bas and	3.0	23.0		10.0		5.0			41.0	1.1	0.9		0.8		0.1			lf, fmg, ol and px specks
21875	But52	px and		7.0		7.0		4.0			18.0		1.0		1.7					lf, fg, ophitic, glomerophyric
21877	But54	px and		7.0		3.0		5.0			15.0		1.0							lf, mg, porphyritic. pilotaxitic
21878	Cab55	px and	5.0	15.0		8.0		4.0			32.0	0.5	0.8		1.5					lf, flat ves, vfg, ol + px grains
21872	Cat49	bas	1.0	23.0		3.0		7.0			35.0	0.5	1.0		0.7		0.4			lf, vesicular, porphyritic
21885	Cat8/2	hb and		24.8	11.6	5.2		4.7			46.3		1.5		1.0		0.5			lf, fmg, porphyritic
21848	Cat19	hb and		30.0	8.0	3.0		3.0			44.0		2.0	1.2	0.5					lf, fmg, glomerophyric
21850	Cat24	px and	1.0	18.0				3.0			22.0		1.2		0.2					lf, fg, glomerophyric, pilotax
21851	Cat25	px and		18.0		7.0	2	5.0			32.0		1.5		0.4	0.2	0.2			lf, fmg, glomerophyric
21869	Cat46	hb and	0.1	20.0	7.0	4.0	3	2.0	2	0.1	36.2		4.0	1.3	0.5				0.1	pf clast, mg, glomerophyric
21876	Gin53	px and		25.0		5.0	10	4.0			44.0	NA								lf, aphyric
21879	Gin56	px and		30.0		1.0	7				38.1				0.2					lf, vfg, px granules
21854	Gin27	px and		23.0		3.0	7	2.0			58.0	NA								lf, aphyric, dark grey
21853	Gin26/5	px and									0.0	NA								lf, vfg
21852	Gin26	px and		23.0		5.0	1				29.1	NA								lf, vfg
none	Hib9	hb and		21.9	9.1	3.8		1.9			36.7									lf, mg, glomerophyric
none	Hib11	hb and		22.8	10.5	3.1		1.6			38.0									lf, mg, glomerophyric, pilotaxitic
21864	Hib37	hb and		38.2	6.5	4.6		4.1			53.4		2.0	4.0	0.5		0.3			lf, fmg, glomerphyric

Abbreviations: Ol, olivine; Plag, plagioclase; Hb, hornblende; Cpx, clinopyroxene; Opx, orthopyroxene; Mt, magnetite; Bio, biotite; Qz, quartz.
Rock names: bas, basalt; bas and, basaltic andesite; and, andesite; dac, dacite. Texture: first column gives deposit type, lf= lava flow; pf= pyroclastic flow, and domes. Next terms gives textures: vfg= very fine grained; fg= fine grained; mg=medium grained; fmg= fine to medium grained; mcg= medium to coarse grained. and cg= coarse grained. Lab No. is the geochemistry laboratory number, Canterbury University. NA= not applicable.

Appendix 2. Petrographic analyses

Lab No.	Sample No.	Rock Name	Ol	Plag	Hb	Cpx (vol%)	Opx	Mt	Bio	Qz	Total	Maximum Phenocryst Size (mm) Ol	Plag	Hb	Cpx	Opx	Mt	Bio	Qz	Texture
none	Hib45	hb and		30.0	7.0	0.1		5.0			42.1		2.4	2.5	0.3		0.4			dome, fmg, glomero, hypox gm
21867	Hib42	hb and	0.1	22.0	12.0	6.0		5.0			45.1	0.3	1.2	1.1	0.5		0.2			lf, fmg, porphyritic
21866	Hib41	px and	0.1	26.0	0.1	7.0		5.0		0.1	38.3	0.5	2.2	1.8	0.5					lf, fmg, porphyritic
21842	Cam10	hb and	0.1	27.9	12.0	4.4		3.7			48.1		2.0	0.8	0.5				0.3	lf, fmg, glomerophyric
21865	Hib40	px and	2.0	28.0	0.1	7.0	5	4.0			46.1	0.5	1.8	0.5	1.5	0.8				lf, fmg, glomerophyric
21843	Hib12	hb and		23.0	9.0	4.0					36.0	0.5	2.1	2.3	1.0					lf, fmg, glomerophyric
21836	Hib5	hb and	0.1	28.0	7.0	6.0		3.0			44.1		2.2	1.0	0.5					pf clast, fg, porphyritic, felty gm
21831	HibB	hb and	0.1	24.0	9.0	3.0		4.0			40.1	0.4	3.0	2.0	0.3					lf, fmg, glomerophyric, pilotax
21834	Hib3	hb and	0.1	15.0	7.0	1.5		2.0			25.6		1.5	2.0	0.3		0.2			pf clast, glomerophyric, pilotax
21833	HibA	hb and		26.0	11.0	3.0		3.0			43.0		2.8	1.0	1.8		0.3			dome, fmg, glomerophyric, pilotax
21846	Cam16	hb and		29.0	8.0	3.0		3.0			43.0		2.0	1.0	0.5		0.5			dome, mg, porphyritic
21838	Cam8	hb and		36.7	10.6	2.0		5.5			54.8		1.5	3.0	0.8					pf clast, mg, glomerophyric
21835	Hib4	hb and	0.1	15.0	5.0	0.1		2.0			22.2	0.3	1.2	1.0	0.2					pf clast, fg, porphyritic
21844	Cam14	hb and		24.0	8.0	3.8					35.8		3.1	2.0	0.4					lf, fmg, glomerophyric, pilotax,
21837	Cam7	hb and	0.1	22.0	4.5	3.0		6.0			35.6	0.5	2.8	2.0	0.3					bc, mg, glomeroporphyritic
21847	Cam17	hb and	0.1	28.0	11.0	3.0		4.0			46.1		2.0	1.0	0.4	0.2	0.3			lf, mg, glomeroporphyritic
21845	Hib15	hb and		23.0	7.0	5.0					35.0		3.1	2.0	3.1		0.3			dome, mg, glomerophyric
21868	Hib44	hb and		26.0	7.0	0.1		6.0			39.1		5.0	1.0						dome, mg, glomerporphyritic
21882	Cam58	hb and	0.1	26.0	7.0	3.0		4.0			40.1	0.2	1.9		1.6		0.2			lf, fmg, porphyritic
21870	Mam47	px and	2.0	33.0		8.0	5	5.0			53.0	0.3	1.4		0.8	0.4	0.5			lf, fg, porphyritic
21862	Mam33	px and	0.1	27.0		7.0	5	0.1			39.2	0.4	1.0		1.0	0.2	0.1			lf, fmg, pilotaxitic
21863	Mam34	hb and	0.1	25.0		6.8		2.1			34.0	0.2	1.8	3.5	0.7		0.5			lf, fmg, porphyritic
21871	Mam48	px and		29.0	0.1	7.0	4	3.0			43.1	0.7			1.5	0.6				lf, fmg, porphyritic, pilotaxitic
21880	Mam57	px and	3.0	15.0	4.0	6.0		2.0			30.0	0.5	1.0	1.0	0.8					lf, fmg, pilotaxitic
21861	Mam32	px and	0.5	26.0		2.0	3	3.0			34.5	3.0	1.0		0.9	0.3				lf, fg, glomerophyric

Abbreviations: Ol, olivine; Plag, plagioclase; Hb, hornblende; Cpx, clinopyroxene; Opx, orthopyroxene; Mt, magnetite; Bio, biotite; Qz, quartz.
Rock names: bas, basalt; bas and, basaltic andesite; and, andesite; dac, dacite. Texture: first column gives deposit type, lf= lava flow; pf= pyroclastic flow, and dome. Next terms gives textures: vfg= very fine grained; fg= fine grained; mg=medium grained; fmg= fine to medium grained; mcg= medium to coarse grained. and cg= coarse grained. Lab No. is the geochemistry laboratory number, Canterbury University. NA= not applicable.

Appendix 2. Petrographic analyses

Lab No.	Sample No.	Rock Name	Ol	Plag	Hb	Cpx	Opx	Mt	Total	Maximum Phenocryst Size (mm) Ol	Plag	Hb	Cpx	Mt	Texture
						(vol%)									
21884	HS15	hb and		30.4	7.0	3.8		2.1	43.3		1.3	1.8	0.5		lf, fmg, porphyritic
21873	Vul50	hb and		38.0	6.0	8.0		7.0	59.0		0.8	1.0	0.3		dome, fmg, hypoxtalline
21840	Vul21	hb-px and	2.0	26.0	5.0	7.0		2.0	42.0	1.0	1.0	1.0	0.3		dome, mg, porphyritic
21839	Hib20	hb and	0.1	35.0	10.0	4.0		2.0	51.1	1.0	2.0	1.5	0.5	0.5	dome, mg, glomeroporphyritic
21841	Cam22	hb and		15.0	6.0	2.0	0.1	3.0	26.1		1.0	0.8	0.6		lf, fg, seriate
23236	Bal1	bas	2.4	24.2		2.2			28.8	1.0	1.0		0.5		lf, fg, hypoxtalline
23237	Bal2	bas	2.1	16.4		2.6			21.1	0.9	1.4		0.2		lf, fg, hypoxtalline
23238	Bal3	bas	1.6	18.5		3.1			23.2	1.0	0.5		0.5		lf, fg, hypoxtalline
23239	Bal4	bas	1.8	18.8		2.6			23.2	0.8	0.9		0.8		lf, fg, hypoxtalline
23240	Bal9	bas	1.0	24.1		3.4		2	30.5	0.4	0.8		0.4		lf, fmg, porphyritic, holox gm
23241	Bal10	px and		29.5		8.3		3	40.8		1.1		0.6	0.1	lf, fmg, porphyritic, glassy gm
23242	Bal11	bas	2.0	30.2		11.2		4	47.4	1.0	1.4		1.0	0.2	lf, fmg, subhed plag, subophitic, intergranular cpx
23243	Bal12	px and	3.0	8.9		2.6	1	4	19.5	1.0	1.0				lf, fmg, porphyritic, pilotaxitic
23244	Bin1A	bas	1.0	28.7		8.1		2	39.8	1.5	2.5		0.2		lf, mg, hypox gm, xeno incl.
23245	Bin1B	bas and		19.5		2.5			22.0		1.0		0.1		lf, fg, hypox gm, inclusion-rich plag
23246	Bin2A	bas and		27.6		2.2		4	33.8						lf, mcg, porphyritic
23247	Bin2B	bas and		29.6		2.3			31.9		1.1		0.4		lf, fg, pophyritic, microlitic gm
23248	Bin3	px and		6.8		3.4	0	5	15.2		2.0		0.6	0.1	lf, fg, porphyritic, pilotaxitic
23249	Bin4	px and								NA					lf, aphyric, pilotaxitic, skeletal plag
23250	Bin5	px and								NA					lf, aphyric, phenocryt-free, skeletal plag
23251	Bin6	bas and		5.3		2.6			7.9		0.5		0.5		lf, fg, phenocryst poor,pilotaxitic
23252	Bin7	px and		15.4		3.5		3	21.9		2.0		0.1		lf, fmg, phenocryst poor, incl-rich plag, cpx in gm
23253	Bin8	px and		2.9		4.1			7.0						lf, fg, vesicular, phenocryst poor
23254	Bin9	bas and								NA					lf, fg, phenocryst poor
23255	Lum1	px and	1.0	34.7		10.2		5	50.9	0.8	2.0				lf, fmg, poikilitic px, hypox gm
none	Lum2	px and	3.0	29.8		6.7		4	43.5	1.0	1.0		0.2	0.1	lf, fg, vesicular

Abbreviations: Ol, olivine; Plag, plagioclase; Hb, hornblende; Cpx, clinopyroxene; Opx, orthopyroxene; Mt, magnetite; Bio, biotite; Qz, quartz.
Rock names: bas, basalt; bas and, basaltic andesite; and, andesite; dac, dacite. Texture: first column gives deposit type, lf= lava flow; pf= pyroclastic flow, and dome. Next terms gives textures: vfg= very fine grained; fg= fine grained; mg=medium grained; fmg= fine to medium grained; mcg= medium to coarse grained, and cg= coarse grained. Lab No. is the geochemistry laboratory number, Canterbury University. NA= not applicable.

Appendix 2. Petrographic analyses

Lab No.	Sample No.	Rock Name	Ol	Plag	Hb	Cpx	Opx	Mt	Bio	Total	Maximum Phenocryst Size (mm)							Texture
						(vol%)					Ol	Plag	Hb	Cpx	Opx	Mt	Bio	
23256	Bal1A	ol bas	7.0	10.8		9.8				27.6	5.0	1.2		>5				lf, mcg, ophitic, glassy gm
23257	Bal1B	ol bas	6.0	8.2		10.2				24.4	4.0	1.5		>5				lf, mcg, ophitic, glassy gm
23258	Bali3	ol bas	6.0	21.6		15.6		5		48.2	5.0	1.4		>5				lf, mcg, ophitic, glassy gm
23259	Bal4	ol bas	7.0	10.4		10.4		1		28.8	5.0	1.0		>5				lf, mcg, ophitic, porphyritic, glassy gm
23260	Kat9	dac	0.1	28.6		5.5		3		37.2	1.5	2.0		0.1				lf, fmg, sieve plag, pilotaxitic
23261	Kal8	ol bas and	6.0	38.4		3.4		2		49.8	1.0	1.0		0.2		0.1		bomb, mg, porphyritic, cryptoxtalline gm
23262	Mus15	hb and		15.6		8.8		4		28.4		2.0	2.0	0.3		0.2		dome, fmg, porphyritic
23263	Que7	ba px and	3.0	16.2		5.7		1		25.9	1.5	1.8		0.5		0.1		lf, fmg, porphyritic
23264	But6	ol bas	6.0	38.5		15.4		10		69.9	3.0	0.5		0.4		0.1		lf, fg, granular
23265	But27	px and	7.0	38.2		4.6		0.1		49.9		1.0		0.7				lf, fg, porphyritic, pilotaxitic
23266	Mar1	ba px and	2.0	15.2		3.1		4		24.3		1.6		0.5				lf, fmg, porphyritic, glassy gm
23268	Mar3	1bas an		15		2.5		0.1		17.6		2.0		1.0		0.1		lf, fmg, vesicular, porphyritic
23269	Mar4	1bas an		28		6.7		0.5		35.2		2.4		0.8		0.2		lf, fmg, hypox gm
23270	Mar5	1bas an		25		4.6		1		30.6		2.1		3.0				lf, fmg, hypox gm, pilotaxitic
23271	Mar6	1bas an		22		7.1		1		30.1		1.5		2.0				incl, fmg, clear plag with mt incl, intergranular px
23272	Apo1	3dac		18		5.4		0.4		23.8		1.2		0.2				lf, mcg, vesicular, pilotaxitic
23273	Apo2	3dac		31	6	3		4	3	47.0		3.0	1.0	0.1		0.1	2.0	lf, mg, glomeroporphyritic, pilotaxitic
23274	Apo3	2hb and		25	7	<1		1		33.0		4.0	3.0	0.2		0.2		lf, mg, glomeroporphyritic
23275	Apo4	2hb and		22	6	1		1		30.0		3.0	3.0	0.5		0.1		lf, mg, glomeroporphyritic, pilotaxitic
23276	Apo5	3dac		18	6	<1		1		25.0		4.0	2.5	0.3		0.1		lf, mg, porphyritic, glassy gm
23277	Apo6	3dac		40	12	4		2	6	64.0		6.0	2.0	0.1		0.8	1.2	lf, mcg, glomeroporphyritic, pilotaxitic
23278	Apo7	2hb and		28	10	2		3		43.0		5.0	6.0	0.5		0.5		lf, mcg, glomeroporphyritic, pilotaxitic
23279	Apo8	3dac		33	8	5		2		48.0		5.0	5.0	0.4		0.2		lf, mcg, glomeroporphyritic, pilotaxitic

Abbreviations: Ol, olivine; Plag, plagioclase; Hb, hornblende; Cpx, clinopyroxene; Opx, orthopyroxene; Mt, magnetite; Bio, biotite; Qz, quartz.
Rock names: bas, basalt; bas and, basaltic andesite; and, andesite; dac, dacite. Texture: first column gives deposit type, lf= lava flow; pf= pyroclastic flow, and dome. Next terms gives textures: vfg= very fine grained; fg= fine grained; mg=medium grained; fmg= fine to medium grained; mcg= medium to coarse grained. and cg= coarse grained. Lab No. is the geochemistry laboratory number, Canterbury University. NA= not applicable.

Table 3-1 was constructed from a combination of averaged and individual petrographic analyses from Appendix 2.

1. Hb andesite. Vulcan

	Mineral	Avg	Samples averaged
	Ol	1.1	21840, 21839
	Plag	28.5	21873,21840,21839,21841
	Hb	6.8	21873,21840,21839,21841
	Cpx	4.3	21840,21839,21841
	Opx	0.1	21841 only
	Mt	3.5	21873,21840,21839,21841
2. Hb andesite. Mt Catarman	Ol	0.7	21872,21850,21869
	Plag	22.3	21872,21885,21848,21850,21851,21869
	Hb	6.2	21885,21848,21869
	Cpx	4.4	21782,21885,21848,21851,21869
	Opx	2.5	21851,21869
	Mt	4.3	21872,21885,21848,21850,21851,21869
	Bio	2.9	21869
3. Hb andesite. Hibok-Hibok	Ol	0.1	21867,21842,21836,21831, 21834,21835,21837,21847,21882
	Plag	24.7	21867,21842,21843,21836,21831,21834 ,21833,21846,21838, 21835,21844,2183,
7,21847,21845,21868,21882			
	Hb and Cpx		as per Plag
	Mt	4.0	21867,21842,21836,21831,21834,21833,
21846,			21838,21835,21837,21847, 21882
4. Px andesite. Hibok-Hibok	Ol	1.1	21866,21865
	Plag	27	21866,21865
	Hb	0.1	21866,21865
	Cpx	7.1	21866,21865
	Opx	5.2	21866,21865
	Mt	3.5	21866,21865
5. Px andesite. Mt Mambajao.	Ol	1.1	21870,21862,21880,21861
	Plag	26	21870,21862,21871,21880,21861
	Opx	4.3	21870,21862,21871,21861
	Mt	2.9	21870,21862,21871,21880,21861
6. Dacite, Type 1. Butay			21877
7. Basalt, Butay	Ol	5.0	21855,21830,21874
	Plag	32.7	21855,21830,21874
	Cpx	7.7	21855,21830,21874
	Opx	1.5	21855,21830
	Mt	6.0	21830,21874
8. Px andesite. Cabuan			21878
9. Px andesite. Benoni	Ol	1.5	21858
	Plag	30.0	21856,21858,21859, 21857
	Cpx	3.2	21856,21858,21859, 21857
	Mt	5.1	21856,21858,21859,21857
10. Px andesite. Mt Ginsiliban			21876,21879,21854,21852
11. Ol Basalt. Mt Balatocan - analysis 23259			
12. Basalt. Mt Balatocan - analysis 23240			
13. Basalt. Mt Balatocan - analysis 23242			
14. Basalt. Mt Balatocan - analysis 23244			
15. Px andesite. Mt Balatocan -			23248,23252,23253
16. Basalt. Mt Kalatungan			23261
17. Dacite, Type 1. Mt Katanglad - all from 23260			
18. Basalt. Butong - from 23264			
19. Hb andesite. Musuan - from 23262.			
20. Apo samples.Px andesite, 23266; Hb andesite, 23278, 23275, 23274, Dacite, Type 2, 23277			

Appendix 3-1. Index to mineral analyses.

Rock Type	Volcanic centre	Volcanic Group	Sample No	Lab. No.
Basalt	Butay	Misamis	BUT51	21874
Basalt	Mt Balatocan	Misamis	BAL4	23259
Basalt	Butong	Bukidnon	BUT6	23264
Basaltic andesite	Hibok-Hibok	Misamis	HIB37	21864
Basaltic andesite	Mt Balatocan	Misamis	BAL10	23241
Basaltic andesite	Mt Kalatungan	Bukidnon	KAL8	23261
Basaltic andesite	Quezon volcanics	Bukidnon	QUE7	23263
Basaltic andesite	Mt Apo	Apo	MAR6	23271
SiO2-rich andesite	Hibok-Hibok	Misamis	HIB20	21839
SiO2-rich andesite	Hibok-Hibok	Misamis	HIB12	21843
SiO2-rich andesite	Hibok-Hibok	Misamis	HIB15	21845
SiO2-rich andesite	Mt Mambajao	Misamis	MAM32	21861
SiO2-rich andesite	Mt Ginsiliban	Misamis	CAM275	21852
SiO2-rich andesite	Mt Apo	Apo	APO2	23273
Dacite	Hibok-Hibok	Misamis	CAT46	21869
Dacite	Mt Katanglad	Bukidnon	KAT9	23260
Dacite	Mt Apo	Apo	APO6	23277

Appendix 3-2. Microprobe analyses.

Table A3-1a. Microprobe analyses of plagioclase in basalts.

Location	Mt Balatocan						Camiguin Island							Butong						Quezon	
Sample #	I46305	409861	4C1026	4R0996	410943	4MC10	H1C338	H1M339	H1R339	H13252	B1C368	B1M368	B1R369	T6C663	T6M663	T6R663	T6C631	T6R630	T6MC6	QMC0	QMC1
Xtal Type	(C	R)	(C	R)	(C)	(GM)	(C	M	C	R)	(C	M	R)	(C	M	R)	(C	M	R)	(GM)	(GM)
SiO2	51.41	53.47	53.29	54.53	52.93	55.87	56.42	56.49	52.06	48.67	52.67	53.09	56.42	55.11	53.39	52.65	53.57	54.57	53.24	55.59	54.42
TiO2	0.04	0.03	0.06	0.05	0.02	0.05	0.02	0	0.06	0	0	0	0.07	0.06	0.04	0.04	0.07	0.05	0.05	0.07	0.09
Al2O3	29.92	27.81	28.16	27.03	28.35	26.13	26.56	26.57	29.19	31.59	29.61	29.47	25.83	28.02	29.27	29.5	28.73	27.98	29.2	27.25	27.98
Fe2O3	0	0	0	0	0	0	0	0	0	0	0	0	0	0	0	0	0	0	0	0	0
FeO	0.61	0.72	0.75	0.91	0.71	1.11	0.56	0.38	0.62	0.65	0.49	0.52	0.9	0.6	0.7	0.7	0.58	0.72	0.66	0.89	0.78
MnO	0	0	0	0	0	0	0	0	0	0	0	0.02	0	0	0	0	0.02	0	0	0	0
MgO	0.15	0.16	0.18	0.13	0.17	0.12	0.05	0.04	0.07	0.06	0.04	0.04	0.06	0.02	0	0	0	0.04	0	0	0.03
CaO	14.08	12.4	13	11.4	13.21	10.32	10.32	9.89	13.42	15.72	13.36	12.83	9.61	11.14	13.1	13.4	12.6	11.9	13.12	10.86	11.89
Na2O	3.31	4.11	3.87	4.91	3.88	5.35	5.57	5.43	3.56	2.35	3.38	3.65	5.68	4.61	3.87	3.72	4.03	4.16	3.77	5.17	4.47
K2O	0.05	0.12	0.11	0.16	0.13	0.24	0.43	0.21	0.2	0.09	0.15	0.2	0.43	0.08	0.07	0.06	0.09	0.1	0.07	0.18	0.08
Total	99.57	98.82	99.42	99.12	99.4	99.19	99.93	99.01	99.18	99.13	99.7	99.82	99	99.64	100.44	100.07	99.69	99.54	100.11	100.01	99.74
Number of cations on the basis of 8 oxygens																					
Si+4	2.35	2.45	2.43	2.49	2.42	2.55	2.55	2.56	2.39	2.25	2.4	2.41	2.57	2.49	2.41	2.39	2.43	2.48	2.41	2.51	2.47
Ti+4	0	0	0	0	0	0	0	0	0	0	0	0	0	0	0	0	0	0	0	0	0
Al+3	1.61	1.5	1.52	1.46	1.53	1.4	1.41	1.42	1.58	1.72	1.59	1.58	1.39	1.49	1.56	1.58	1.54	1.5	1.56	1.45	1.5
Fe+2	0.02	0.03	0.03	0.03	0.03	0.04	0.02	0.01	0.02	0.03	0.02	0.02	0.03	0.02	0.03	0.03	0.02	0.03	0.03	0.03	0.03
Mn+2	0	0	0	0	0	0	0	0	0	0	0	0	0	0	0	0	0	0	0	0	0
Mg+2	0.01	0.01	0.01	0.01	0.01	0.01	0	0	0	0	0	0	0	0	0	0	0	0	0	0	0
Ca+2	0.69	0.61	0.64	0.56	0.65	0.5	0.5	0.48	0.66	0.78	0.65	0.62	0.47	0.54	0.63	0.65	0.61	0.58	0.64	0.53	0.58
Na+1	0.29	0.37	0.34	0.44	0.34	0.47	0.49	0.48	0.32	0.21	0.3	0.32	0.5	0.4	0.34	0.33	0.36	0.37	0.33	0.45	0.39
K	0	0.01	0.01	0.01	0.01	0.01	0.02	0.01	0.01	0.01	0.01	0.01	0.03	0	0	0	0.01	0.01	0	0.01	0
TOTAL	4.99	4.98	4.98	5	4.99	4.99	5	4.97	4.98	5	4.96	4.97	5	4.96	4.98	4.98	4.97	4.96	4.97	4.99	4.98
An	70.3	62.5	65.0	56.1	65.2	51.3	49.5	49.7	66.9	78.4	68.1	65.3	47.3	57	64.9	66.3	63	60.9	5.5	53.2	59.3
Ab	29.5	36.8	34.4	43.0	34.0	47.3	48.0	49.1	31.9	21.1	31.0	33.5	50.2	42.6	34.7	33.3	36.5	38.5	34.1	45.8	40.2
Or	0.3	0.7	0.6	0.9	0.8	1.4	2.4	1.2	1.2	0.5	0.9	1.2	2.5	0.5	0.4	0.4	0.5	0.6	0.4	1	0.5

Tables 1a-d. Representative microprobe analyses of plagioclase from Central Mindanao. Crystal types are phenocrysts, otherwise these are specified as 'GM' = groundmass feldspars, 'MP' = microphenocryst or 'X' = xenocryst. Parentheses group individual analytical points of 'C' = core, 'M' = mid or 'R' = rim.

Appendix 3-2. Microprobe analyses.

Table A3-1b. Representative microprobe analyses of plagioclase in basaltic andesites.

Location	Mt. Kalatungan											Mt. Apo						Mt Balatocan	
Sample No.	K2C395	K24091	2C3851	K2R374	K2C429	2M4203	K2R412	2C3622	2M3672	2R3612	K23751	T4m63	T4C645	T4M64	T4R648	T4C659	4R6534	1R0844	120660
Xtal Type	(C	R)	(C	R)	(C	M	R)	(C	M	R)	(GM)	(GM)	(C	M	R)	(C	R)	(C	R)
SiO2	54.92	55.82	55.87	55.36	56.01	55.93	57.12	54.79	55.37	54.68	54.67	54.22	55.56	53.8	53.38	51.45	56.81	53.22	52.89
TiO2	0.09	0.06	0.08	0.09	0.08	0.08	0.03	0.08	0.08	0.09	0.08	0.09	0.04	0.05	0	0.04	0.05	0.08	0.04
Al2O3	27.17	27.27	26.62	26.61	27.03	25.93	26.35	27.05	26.49	27.49	27.08	28.11	27.61	28.81	29	30.59	26.53	28.6	28.38
Fe2O3	0	0	0	0	0	0	0	0	0	0	0	0	0	0	0	0	0	0	0
FeO	0.89	0.87	0.78	0.84	0.84	0.8	0.76	0.89	0.89	0.95	1.01	0.79	0.64	0.57	0.57	0.65	0.57	0.77	0.77
MnO	0	0	0	0	0	0	0	0	0	0	0	0	0	0	0.04	0	0	0	0
MgO	0.11	0.1	0.11	0.1	0.09	0.09	0.09	0.11	0.11	0.12	0.1	0.08	0.06	0.05	0.05	0.06	0.06	0.09	0.09
CaO	10.85	10.82	10.13	10.97	10.96	10.71	10.04	11.64	10.72	11.96	10.72	12.01	11.14	12.55	13.19	14.41	10.54	12.53	12.68
Na2O	4.55	4.75	5	4.58	4.61	4.97	5.23	4.67	5.07	4.44	4.85	4.51	4.47	4.09	3.76	2.98	5.07	4.08	3.94
K2O	0.63	0.64	0.71	0.62	0.62	0.68	0.74	0.54	0.57	0.51	0.66	0.54	0.63	0.44	0.36	0.24	0.74	0.33	0.3
Total	99.21	100.33	99.3	99.17	100.24	99.19	100.36	99.77	99.3	100.24	99.17	100.35	100.15	100.36	100.35	100.42	100.37	99.7	99.09
Number of cations on the basis of 8 oxygens																			
Si+4	2.51	2.52	0.62	2.53	2.53	2.55	2.57	2.49	2.53	2.48	2.5	2.46	2.51	2.43	2.42	2.34	2.56	2.43	2.43
Ti+4	0	0	0.01	0	0	0	0	0	0	0	0	0	0	0	0	0	0	0	0
Al+3	1.46	1.45	3.31	1.43	1.44	1.39	1.4	1.45	1.42	1.47	1.46	1.5	1.47	1.54	1.55	1.64	1.41	1.54	1.53
Fe+2	0.03	0.03	0.07	0.03	0.03	0.03	0.03	0.03	0.03	0.04	0.04	0.03	0.02	0.02	0.02	0.02	0.02	0.03	0.03
Mn+2	0	0	0	0	0	0	0	0	0	0	0	0	0	0	0	0	0	0	0
Mg+2	0.01	0.01	0.02	0.01	0.01	0.01	0.01	0.01	0.01	0.01	0.01	0.01	0	0	0	0	0	0.01	0.01
Ca+2	0.53	0.52	1.14	0.54	0.53	0.52	0.48	0.57	0.52	0.58	0.53	0.58	0.54	0.61	0.64	0.7	0.51	0.61	0.62
Na+1	0.4	0.42	1.02	0.41	0.4	0.44	0.46	0.41	0.45	0.39	0.43	0.4	0.39	0.36	0.33	0.26	0.44	0.36	0.35
K	0.04	0.04	0.1	0.04	0.04	0.04	0.04	0.03	0.03	0.03	0.04	0.03	0.04	0.03	0.02	0.01	0.04	0.02	0.02
TOTAL	4.98	4.98	6.28	4.98	4.97	4.99	4.98	5	5	4.99	5	5	4.97	4.99	4.98	4.98	4.98	4.99	4.99
An	55.1	53.9	51.0	55.2	55.0	52.5	49.6	56.5	52.5	58.4	53.2	57.9	55.9	61.4	64.7	71.8	51.4	61.9	63.1
Ab	41.2	42.3	44.8	41.2	41.4	43.6	46.1	40.5	44.3	38.7	43.0	39.0	40.3	36.0	33.2	26.7	44.4	36.1	35.1
Or	3.8	3.8	4.2	3.7	3.7	3.9	4.3	3.1	3.3	2.9	3.8	3.1	3.7	2.5	2.1	1.4	4.3	1.9	1.8

Explanation and symbols as in Table A3-1a.

Appendix 3-2. Microprobe analyses.

Table A3-1c. Representative microprobe analyses of plagioclase in SiO2-rich andesites.

Location	Camiguin Island										
Sample #	20C419	20M419	20R420	20MC43	15C712	15M713	15R713	15MC67	32C048	32R045	2MC055
Xtal Type	(C	M	R)	(GM)	(C	M	R)	(GM)	(C	R)	(GM)
SiO2	57.25	56.58	58.95	52.82	58.12	58.54	57.66	56.32	55.66	57.55	54.09
TiO2	0.03	0.03	0	0	0	0	0	0	0	0.02	0
Al2O3	26.95	27.65	26.27	28.94	26.68	26.36	26.08	27.28	27.97	26.85	28.12
Fe2O3	0	0	0	0	0	0	0	0	0	0	0
FeO	0.31	0.27	0.28	0.61	0.16	0.23	0.21	0.5	0.25	0.37	0.55
MnO	0	0	0	0	0	0	0.04	0	0	0	0.03
MgO	0.02	0	0	0.04	0.03	0	0	0.03	0.05	0.03	0.04
CaO	10.05	10.61	8.99	13.07	9.81	9.15	10.07	10.59	11.18	9.91	11.82
Na2O	5.62	4.87	5.77	3.67	5.47	6	5.97	5.28	4.79	5.24	4.51
K2O	0.18	0.18	0.23	0.12	0.21	0.21	0.23	0.23	0.24	0.39	0.29
Total	100.41	100.19	100.49	99.27	100.48	100.49	100.26	100.23	100.14	100.36	99.45
Number of cations on the basis of 8 oxygens											
Si+4	2.56	2.54	2.62	2.41	2.59	2.61	2.59	2.53	2.5	2.57	2.46
Ti+4	0	0	0	0	0	0	0	0	0	0	0
Al+3	1.42	1.46	1.38	1.56	1.4	1.38	1.38	1.45	1.48	1.42	1.51
Fe+2	0.01	0.01	0.01	0.02	0.01	0.01	0.01	0.02	0.01	0.01	0.02
Mn+2	0	0	0	0	0	0	0	0	0	0	0
Mg+2	0	0	0	0	0	0	0	0	0	0	0
Ca+2	0.48	0.51	0.43	0.64	0.47	0.44	0.48	0.51	0.54	0.47	0.58
Na+1	0.49	0.42	0.5	0.33	0.47	0.52	0.52	0.46	0.42	0.45	0.4
K	0.01	0.01	0.01	0.01	0.01	0.01	0.01	0.01	0.01	0.02	0.02
TOTAL	4.98	4.95	4.95	4.97	4.95	4.97	4.99	4.98	4.97	4.96	4.99
An	49.3	54	45.6	65.9	49.3	45.2	45.6	52.0	55.7	50	58.3
Ab	49.7	44.9	53	33.4	49.5	53.6	51.1	46.7	42.9	47.7	40.0
Or	1	1.1	1.4	0.7	1.3	1.2	1.3	1.3	1.4	2.3	1.7

Explanation and symbols as in Table A3-1.

Appendix 3-2. Microprobe analyses.

Table A3-1c. Representative microprobe analyses of plagioclase in SiO2-rich andesites.

Location	Camiguin Island														
Sample #	15MCC6	15M678	15R678	15GLAS	65C161	65R156	188132	186133	MCR161	10C109	10M114	10R114	N31M4	n31R47	31mC3
Xtal Type	(C/GM	M/GM	R/GM)	GLASS	(C/MP	R/MP)	(C	R)	(GM)	(C	M	R)	(C	R)	(MP)
SiO2	53.44	51.02	54.41	78.06	51.22	53.08	51.26	50.06	51.94	55.06	54.63	55.5	48.48	49.56	55.81
TiO2	0	0	0.03	0.27	0	0	0.05	0.04	0	0.06	0.07	0.03	0	0.03	0
Al2O3	29.5	31.13	28.73	13.27	30.61	28.84	29.6	30.07	30.23	26.96	27.7	27.25	32.18	31.34	29.32
Fe2O3	0	0	0	0	0	0	0	0	0	0	0	0	0	0	0
FeO	0.32	0.36	0.51	1.26	0.58	0.65	0.66	0.86	0.61	0.79	0.76	0.89	0.45	0.42	0.42
MnO	0	0	0	0.04	0	0.06	0	0.03	0	0	0	0	0	0	0
MgO	0.02	0	0.03	0.18	0.05	0.08	0	0	0.07	0.07	0.07	0.07	0.03	0.03	0.04
CaO	13.13	15.05	12.48	1.49	14.7	12.75	14.47	15.07	13.98	10.77	11.76	10.18	16.32	15.65	10.21
Na2O	3.84	2.71	4.16	2.59	2.86	3.99	3.37	2.89	3.52	4.96	4.2	5.23	1.69	2.24	3.69
K2O	0.1	0.06	0.06	3.23	0.1	0.14	0.08	0.08	0.09	0.42	0.33	0.4	0.03	0.04	0.04
Total	100.35	100.33	100.41	100.39	100.12	99.59	99.49	99.1	100.44	99.09	99.52	99.55	99.18	99.31	99.53
Number of cations on the basis of 8 oxygens															
Si+4	2.41	2.32	2.45	3.33	2.33	2.42	2.35	2.31	2.36	2.51	2.48	2.52	2.24	2.28	2.5
Ti+4	0	0	0	0.01	0	0	0	0	0	0	0	0	0	0	0
Al+3	1.57	1.67	1.53	0.67	1.64	1.55	1.6	1.64	1.62	1.45	1.48	1.46	1.75	1.7	1.55
Fe+2	0.01	0.01	0.02	0.04	0.02	0.02	0.03	0.03	0.02	0.03	0.03	0.03	0.02	0.02	0.02
Mn+2	0	0	0	0	0	0	0	0	0	0	0	0	0	0	0
Mg+2	0	0	0	0.01	0	0.01	0	0	0	0	0	0	0	0	0
Ca+2	0.64	0.73	0.6	0.07	0.72	0.62	0.71	0.75	0.68	0.53	0.57	0.49	0.81	0.77	0.49
Na+1	0.34	0.24	0.36	0.21	0.25	0.35	0.3	0.26	0.31	0.44	0.37	0.46	0.15	0.2	0.32
K	0.01	0	0	0.18	0.01	0.01	0	0	0.01	0.02	0.02	0.02	0	0	0
TOTAL	4.97	4.97	4.97	4.52	4.98	4.99	5	5	4.99	4.99	4.97	4.99	4.97	4.97	4.88
An	65.1	75.14	61.98	16.9	73.6	63.5	70	73.9	68.5	53.4	59.7	50.8	84.1	79.3	60.4
Ab	34.4	24.48	37.4	45.6	25.8	35.7	29.5	25.6	31.0	44.1	38.3	46.8	15.7	20.5	39.3
Or	0.6	0.38	0.61	37.4	0.6	0.8	0.5	0.5	0.5	2.5	2	2.4	0.2	0.2	0.3

Explanation and symbols as in Table A3-1a.

Appendix 3-2. Microprobe analyses.

Table A3-1c. Representative microprobe analyses of plagioclase in SiO2-rich andesites.

Location	Mt. Apo										
Sample #	A3C489	A3M493	3R4984	3C3555	A3M366	A33685	3X3514	A3X352	341963	342463	342236
Xtal Type	(C	M	R)	(C	M	R)	(X)	(X)	(C	M	R)
SiO2	60.1	59.12	59.76	58.99	61.39	60.88	55.32	51.78	60.85	60.14	59.73
TiO2	0.03	0	0	0.03	0	0.02	0	0.04	0	0	0.02
Al2O3	25.18	25.49	25.17	26.25	24.36	24.82	27.82	30.35	25.38	25.3	25.4
Fe2O3	0	0	0	0	0	0	0	0	0	0	0
FeO	0.32	0.35	0.32	0.26	0.25	0.21	0.6	0.74	0.26	0.3	0.29
MnO	0	0	0	0	0	0	0	0	0	0	0
MgO	0	0	0	0	0	0	0.04	0.03	0	0	0.03
CaO	7.75	8.52	7.61	7.87	6.57	7.16	11.64	14.02	7.49	7.62	8.32
Na2O	6.45	6.34	6.83	6.24	6.86	6.55	4.51	3.15	6.2	6.26	6.11
K2O	0.64	0.55	0.73	0.61	0.77	0.75	0.41	0.17	0.76	0.61	0.54
Total	100.47	100.37	100.42	100.25	100.2	100.39	100.34	100.28	100.94	100.23	100.44
Number of cations on the basis of 8 oxygens											
Si+4	2.67	2.64	2.66	2.63	2.72	2.7	2.49	2.35	2.68	2.67	2.66
Ti+4	0	0	0	0	0	0	0	0	0	0	0
Al+3	1.32	1.34	1.32	1.38	1.27	1.3	1.48	1.62	1.32	1.33	1.33
Fe+2	0.01	0.01	0.01	0.01	0.01	0.01	0.02	0.03	0.01	0.01	0.01
Mn+2	0	0	0	0	0	0	0	0	0	0	0
Mg+2	0	0	0	0	0	0	0	0	0	0	0
Ca+2	0.37	0.41	0.36	0.38	0.31	0.34	0.56	0.68	0.35	0.36	0.4
Na+1	0.56	0.55	0.59	0.54	0.59	0.56	0.39	0.28	0.53	0.54	0.53
K	0.04	0.03	0.04	0.03	0.04	0.04	0.02	0.01	0.04	0.03	0.03
TOTAL	4.96	4.98	4.99	4.97	4.95	4.95	4.98	4.98	4.94	4.95	4.96
An	38.4	41.3	36.5	39.6	33.3	36	57.5	70.4	38.2	38.7	41.7
Ab	57.8	55.6	59.3	56.8	62.4	59.5	40.1	28.6	57.2	57.6	55.1
Or	3.8	3.2	4.2	3.7	4.6	4.5	2.4	1	4.6	3.7	3.2

Explanation and symbols as in Table A3-1.

Appendix 3-2. Microprobe analyses.

Table A3-1d. Representative microprobe analyses of plagioclase in dacites.

Location	Camiguin Island											
Sample #	46C119	46M120	46R121	46C150	46R153	46C184	46M183	46R183	6MCX1	H46112	H46M1	H46R1
Xtal Type	(C	M	R)	(C/MP	R/MP)	(C	M	R)	(X/GM)	(GM)	(C	R)
SiO2	58.81	59.32	59.53	57.97	59.15	58.43	58.29	60.22	53.73	61.49	59.07	61.24
TiO2	0	0	0	0.02	0	0	0.02	0.02	0.07	0.02	0	0.03
Al2O3	26.41	25.78	25.22	26.5	25.93	25.52	26.45	25.1	28.51	24.54	25.97	25.08
Fe2O3	0	0	0	0	0	0	0	0	0	0	0	0
FeO	0.2	0.18	0.22	0.22	0.2	0.22	0.2	0.18	0.93	0.17	0.15	0.14
MnO	0	0	0	0.02	0	0	0	0.03	0.03	0.03	0	0
MgO	0	0	0	0.02	0	0	0	0	0.1	0	0	0
CaO	8.84	8.35	8.03	9.46	8.75	8.8	9.05	7.34	12.38	6.48	8.74	7.31
Na2O	5.96	6.16	6.37	5.9	6.08	6.11	5.96	6.81	4.15	6.49	6.07	5.86
K2O	0.28	0.33	0.33	0.24	0.28	0.29	0.27	0.36	0.15	0.39	0.29	0.39
Total	100.5	100.12	99.7	100.35	100.39	99.37	100.24	100.06	100.05	99.61	100.29	100.05
Number of cations on the basis of 8 oxygens												
Si+4	2.62	2.64	2.66	2.59	2.63	2.63	2.6	2.68	2.44	2.73	2.63	2.71
Ti+4	0	0	0	0	0	0	0	0	0	0	0	0
Al+3	1.38	1.35	1.33	1.4	1.36	1.35	1.39	1.32	1.52	1.29	1.36	1.31
Fe+2	0.01	0.01	0.01	0.01	0.01	0.01	0.01	0.01	0.04	0.01	0.01	0.01
Mn+2	0	0	0	0	0	0	0	0	0	0	0	0
Mg+2	0	0	0	0	0	0	0	0	0.01	0	0	0
Ca+2	0.42	0.4	0.38	0.45	0.42	0.42	0.43	0.35	0.6	0.31	0.42	0.35
Na+1	0.51	0.53	0.55	0.51	0.52	0.53	0.52	0.59	0.37	0.56	0.52	0.5
K	0.02	0.02	0.02	0.01	0.02	0.02	0.02	0.02	0.01	0.02	0.02	0.02
TOTAL	4.96	4.95	4.96	4.97	4.96	4.97	4.97	4.96	4.98	4.92	4.96	4.9
An	44.3	42	40.3	46.4	43.6	43.6	44.9	36.5	62	34.7	43.5	39.8
Ab	54	56	57.8	52.2	54.8	54.7	53.5	61.3	37.2	62.8	54.7	57.7
Or	1.7	2	2	1.4	1.7	1.7	1.6	2.1	0.9	2.5	1.7	2.5

Explanation and symbols as in Table A3-1a.

Table A3-1d. continued. Representative microprobe analyses of plagioclase in dacites.

Location	Mt. Katanglad								Mt. Apo				
Sample #	T9C437	T9M442	T9R440	T9C371	T9M37	T9R374	9MCR4	9MC634	A6C718	A6M70	A6R703	A6C658	A6R656
Xtal Type	(C	M	R)	(C	M	R)	(GM)	(GM)	(C	M	R)	(C	R)
SiO2	56.77	56.95	56.61	57.94	58.28	58.53	62.08	56.87	59.47	59.71	60.43	58.39	59.26
TiO2	0.03	0.04	0.05	0.06	0.03	0.07	0.06	0	0	0	0.03	0	0.03
Al2O3	26.42	26.66	27.11	25.59	25.44	25.5	23.43	25.98	25.51	25.58	24.67	25.45	25.21
Fe2O3	0	0	0	0	0	0	0	0	0	0	0	0	0
FeO	0.46	0.44	0.52	0.59	0.7	0.69	0.54	0.52	0.17	0.2	0.2	0.34	0.3
MnO	0	0	0	0	0.04	0	0.03	0.03	0	0	0	0	0.03
MgO	0.03	0.04	0.04	0.05	0.05	0.04	0	0.03	0	0	0	0	0
CaO	9.51	9.92	10.12	8.79	8.54	8.32	6.26	9.85	8.37	8.24	7.52	8.65	7.83
Na2O	5.67	5.46	5.67	6.38	6.2	6.05	6.95	5.72	6.33	6.27	6.25	5.84	6.34
K2O	0.46	0.03	0.39	0.51	0.54	0.55	0.88	0.39	0.55	0.61	0.72	0.56	0.57
Total	99.35	99.54	100.51	99.91	99.82	99.75	100.23	99.39	100.4	100.61	99.82	99.23	99.57
Number of cations on the basis of 8 oxygens													
Si+4	2.57	2.57	2.54	2.61	2.62	2.63	2.76	2.58	2.65	2.65	2.7	2.63	2.66
Ti+4	0	0	0	0	0	0	0	0	0	0	0	0	0
Al+3	1.41	1.42	1.43	1.36	1.35	1.35	1.23	1.39	1.34	1.34	1.3	1.35	1.33
Fe+2	0.02	0.02	0.02	0.02	0.03	0.03	0.02	0.02	0.01	0.01	0.01	0.01	0.01
Mn+2	0	0	0	0	0	0	0	0	0	0	0	0	0
Mg+2	0	0	0	0	0	0	0	0	0	0	0	0	0
Ca+2	0.46	0.48	0.49	0.42	0.41	0.4	0.3	0.48	0.4	0.39	0.36	0.42	0.38
Na+1	0.5	0.48	0.49	0.56	0.54	0.53	0.6	0.5	0.55	0.54	0.54	0.51	0.55
K	0.03	0	0.02	0.03	0.03	0.03	0.05	0.02	0.03	0.03	0.04	0.03	0.03
TOTAL	4.99	4.96	5	5	4.99	4.97	4.95	4.99	4.97	4.97	4.94	4.96	4.97
An	46.9	50.1	48.7	42.2	42.1	41.9	31.5	47.8	40.9	40.6	38.2	43.5	39.2
Ab	50.4	49.7	49.1	54.9	54.8	54.8	63.2	50	55.9	55.9	57.4	53.1	57.4
Or	2.7	0.2	2.2	2.9	3.1	3.3	5.3	2.2	3.2	3.6	4.4	3.4	3.4

Explanation and symbols as in Table A3-1a.

Appendix 3-2. Microprobe analyses.

Table A3-2a. Selected microprobe analyses of olivines from basalts.

Location	Mt Belatocan				Butong											Hibok-Hibok	
Analysis #	1	2	3	4	5	6	7	8	9	10	11	12	13	14	15	16	17
Sample #	I4511	I4493	I4548	I4615	B6491	B6496	B6108	B6452	B6571	B6575	B6583	B6653	B6570	B6556	B6512	H294	H9x615
XTAL TYPE	(P)	(P)	(P)	(P)	(MP)	(MP)	(P)	(P)	(P)	(P)	C)	(C)	(C)	(C)	(C)	(C)	(C)
SiO2	39.47	38.91	39.28	39.19	39.56	39.48	39.45	39.53	40.3	40.08	40.16	40.11	39.46	39.87	39.89	39.87	39.44
TiO2	0	0	0	0	0	0	0	0	-	-	0	0	0	0	0.05	0	-
Al2O3	0	0	0	0	0	0	0	0	0	0	0	0	0	0	0	0	0
Cr2O3	0	0	0	0	-	-	-	0	0	-	-	-	0	-	-	0	0
Fe2O3	0	0	0	0	0	0	0	0	0	0	0	0	0	0	0	0	0
FeO	20.62	20.9	20.27	20.76	16.8	17.96	17.08	19.22	16.09	16.59	16.28	16.37	18.39	17.31	17.66	16.77	18.87
MnO	0.33	0.29	0.39	0.25	0.23	0.2	0.11	0.2	0.21	0.17	0.19	0.2	0.2	0.16	0.18	0.14	0.19
NiO	0.08	0.08	0.11	0.1	0.19	0.24	0.2	0.14	0.23	0.22	0.24	0.21	0.23	0.24	0.21	-	-
MgO	38.8	38.96	38.8	38.6	42.28	41.23	42.15	40.53	42.06	42.2	42.43	42.14	40.79	40.04	41.13	43.44	40.3
CaO	0.22	0.19	0.22	0.19	0.13	0.12	0.15	0.15	0.14	0.17	0.13	0.16	0.18	0.15	0.15	0.13	0.15
Na2O	0	0	0.02	0	0	0.03	0	0	0	0	0	0	0	0	0.02	0	0
K2O	0	0	0	0	0	0	0	0	0	0	0	0	0	0	0	0	0
Total	99.52	99.33	99.09	99.09	99.19	99.26	99.14	99.77	99.03	99.43	99.43	99.19	99.25	97.77	99.29	100.35	98.95
Number of Cations on the basis of 4 Oxygens																	
Si	1.021	1.011	1.020	1.019	1.009	1.012	1.009	1.014	1.025	1.018	1.018	1.020	1.014	1.033	1.020	1.047	1.017
Ti	0	0	0	0	0	0	0	0	0	0	0	0	0	0	0	0	0
Al	0	0	0	0	0	0	0	0	0	0	0	0	0	0	0	0	0
Fe+2	0.446	0.454	0.440	0.452	0.358	0.385	0.365	0.412	0.342	0.352	0.345	0.348	0.395	0.375	0.378	0.352	0.407
Mn	0.007	0.006	0.009	0.006	0.005	0.004	0.007	0.004	0.005	0.004	0.004	0.004	0.004	0.004	0.004	0.003	0.004
Ni	0.002	0.002	0.002	0.002	0.004	0.005	0.004	0.003	0.005	0.004	0.005	0.004	0.005	0.005	0.004	0.002	0.002
Mg	1.496	1.510	1.502	1.497	1.608	1.576	1.606	1.549	1.594	1.598	1.604	1.598	1.563	1.546	1.568	1.625	1.549
Ca	0.006	0.005	0.006	0.005	0.004	0.003	0.004	0.004	0.004	0.005	0.004	0.004	0.005	0.004	0.004	0.003	0.004
Na	0.000	0.000	0.001	0.000	0.000	0.001	0.000	0.000	0.000	0.000	0.000	0.000	0.000	0.000	0.001	0.000	0.000
Total	2.979	2.989	2.980	2.981	2.990	2.988	2.991	2.986	2.975	2.982	2.981	2.980	2.986	2.967	2.980	3.039	2.983
Fo (x100)	77	77	77	77	82	80	81	79	82	82	82	82	80	80	81	82	79

Appendix 3-2. Microprobe analyses.

Table A3-2b. Selected microprobe analyses of olivines from basaltic andesites and dacites.

Location	Mt Apo						Camiguin Island			
Analysis #	18	19	20	21	22	23	24	25	26	27
Sample #	A2132	A2238	A2327	A2209	A2201	A2248	H296	H20293	H2298	038629
Xtal Type	(C)	(C)	(C)	(C)	(C)	(C)	[M	C]	(C)	(C)
SiO2	38.57	38.34	38.91	39.06	38.72	38.64	40.85	39.65	40.23	39.92
TiO2	0	0	0	0	-	0	0	0	0	0
Al2O3	0	0	0	0	0	0	0	0	0	0
Cr2O3	0	0	0	0	0	0	0	0	0	-
Fe2O3	0	0	0	0	0	0	0	0	0	0
FeO	22.53	22.6	22.35	21.86	22.57	25.33	17.1	15.55	15.06	15.24
MnO	0.29	0.28	0.28	0.34	0.38	0.32	0	0.22	0.15	0.14
NiO	0	0	0	0	0	0	0.2	0.18	0.17	-
MgO	37.54	37.88	38.15	38.07	37.98	36.28	42.17	43.93	43.86	44.32
CaO	0.18	0.22	0.2	0.16	0.2	0.12	0.13	0.14	0.14	0.13
Na2O	0	0.02	0	0	0	0	-	0	0	0
K2O	0	0	0	0	0	0	0	0	0	0
Total	99.11	99.34	99.89	99.49	99.85	100.69	100.45	99.67	99.61	99.75
Number of Cations on the basis of 4 Oxygens										
Si	1.012	1.005	1.011	1.017	1.009	1.014	1.072	1.041	1.056	1.048
Ti	0	0	0	0	0	0	0	0	0	0
Al	0	0.001	0.001	0	0	0	0	0	0	0
Fe2	0.495	0.495	0.486	0.476	0.492	0.554	0.362	0.325	0.317	0.317
Mn	0.006	0.006	0.006	0.007	0.008	0.007	0.000	0.005	0.003	0.003
Ni	0.000	0.000	0.000	0.000	0.000	0.000	0.004	0.004	0.003	0.001
Mg	1.469	1.480	1.478	1.478	1.475	1.414	1.574	1.634	1.644	1.642
Ca	0.005	0.006	0.006	0.004	0.006	0.003	0.003	0.004	0.004	0.003
Na	0	0.001	0.000	0.000	0.000	0.000	0.001	0.000	0.000	0.000
Total	2.988	2.995	2.988	2.983	2.991	2.993	3.022	3.038	3.031	3.040
Fo (x100)	75	75	75	76	75	72	81	83	84	84

Appendix 3-2. Microprobe analyses.

Table A3-3a. Representative microprobe analyses of pyroxenes from basalt (analyses 1-3) and basaltic andesites.

Location	Mt Balatocan			Hibok					Mt Butay			Quezon					
Analysis #	1	2	3	4	5	6	7	8	9	10	11	12	13	14	15	16	17
Sample #	I4062	I4047x	I4043	51398	51C371	HC068	HR071	H3462x	BU146	BR371x	513723	Q2196	QC175	Q2193	Q2R10	Q2C163	Q2R167
Xtal Type	(C)	(C)	(C)	(C)	(C)	(C	R)	(C)	(C)	R)	(GM)	(C)	(C	(C	R)	(C	R)
SiO2 wt%	52.53	52.3	51.9	51.52	52.12	50.71	52.15	51.43	50.71	51.53	51.69	51.22	52.23	52.16	51.58	50.84	50.84
TiO2	0.38	0.47	0.42	0.61	0.49	0.73	0.63	0.67	0.75	0.58	0.7	0.65	0.76	0.55	0.55	0.69	0.62
Al2O3	2.39	2.91	2.85	2.88	2.7	4.88	3.49	3.63	4.61	3.1	3.54	3.39	2.27	2.87	3.41	3.65	3.58
Cr2O3	0	0	0	0	0	0	0	0	0	0	0	0	0	0	0	0	0
Fe2O3	0	0	0.13	0.52	0	0.25	0	0.65	0.1	0	0	0.76	0.09	0	0.51	0.49	2.32
FeO	7.61	7.35	7.61	8.26	7.8	9.61	8.5	9.61	8.42	7.85	8	8.47	8.65	8.48	9.11	8.82	7.25
MnO	0.17	0.24	0.15	0.41	0.33	0.22	0.19	0.22	0.21	0.28	0.27	0.37	0.33	0.37	0.39	0.36	0.36
NiO	0.05	0	0.04	0	0	0	0	0	0	0	0	0	0	0	0	0	0
MgO	15.35	15.58	15.63	14.2	14.52	13.91	14.15	13.98	13.69	14.38	14.76	14.32	14.96	14.26	14.48	13.71	14.07
CaO	20.28	19.93	19.74	20.28	20.76	19.26	20.94	19.9	20.55	20.47	19.73	20.17	19.68	20.53	19.51	20.17	20.41
Na2O	0.31	0.3	0.32	0.47	0.42	0.43	0.35	0.4	0.42	0.45	0.39	0.35	0.49	0.35	0.4	0.42	0.54
K2O	0	0	0	0	0	0	0	0	0	0	0	0	0	0	0	0	0
Total	99.07	99.08	98.79	99.15	99.14	99.99	100.4	100.48	99.46	98.64	99.08	99.7	99.46	99.57	99.94	99.15	99.99
Number of cations on the basis of 6 oxygens.																	
Si	1.957	1.944	1.935	1.929	1.945	1.885	1.928	1.907	1.891	1.932	1.929	1.909	1.945	1.945	1.917	1.908	1.891
Ti	0.011	0.013	0.012	0.017	0.014	0.020	0.018	0.019	0.021	0.016	0.020	0.018	0.021	0.015	0.015	0.019	0.017
Al(iv)	0.043	0.056	0.065	0.071	0.055	0.115	0.072	0.093	0.109	0.068	0.071	0.091	0.055	0.055	0.083	0.092	0.109
Al(vi)	0.061	0.072	0.061	0.056	0.064	0.098	0.080	0.066	0.094	0.069	0.084	0.058	0.045	0.071	0.067	0.070	0.048
Cr	0.000	0.000	0.000	0.000	0.000	0.000	0.000	0.000	0.000	0.000	0.000	0.000	0.000	0.000	0.000	0.000	0.000
Fe3+	0.000	0.000	0.004	0.015	0.000	0.007	0.000	0.018	0.003	0.000	0.000	0.021	0.003	0.000	0.014	0.014	0.065
Fe2+	0.237	0.229	0.237	0.259	0.243	0.299	0.263	0.298	0.263	0.246	0.250	0.264	0.269	0.264	0.283	0.277	0.226
Mn	0.005	0.008	0.005	0.013	0.010	0.007	0.006	0.007	0.007	0.009	0.009	0.012	0.010	0.012	0.012	0.011	0.011
Ni	0.001	0.000	0.001	0.000	0.000	0.000	0.000	0.000	0.000	0.000	0.000	0.000	0.000	0.000	0.000	0.000	0.000
Mg	0.852	0.863	0.869	0.793	0.808	0.771	0.780	0.773	0.761	0.804	0.821	0.796	0.831	0.793	0.802	0.767	0.780
Ca	0.809	0.794	0.789	0.814	0.830	0.767	0.829	0.791	0.821	0.822	0.789	0.806	0.785	0.820	0.777	0.811	0.813
Na	0.022	0.022	0.023	0.034	0.030	0.031	0.025	0.029	0.030	0.033	0.028	0.025	0.035	0.025	0.029	0.031	0.039
K	0	0	0	0	0	0	0	0	0	0	0	0	0	0	0	0	0
# Oxy	6.01	6.01	6.00	6.00	6.00	6.00	6.01	6.00	6.00	6.01	6.01	6.00	6.00	6.01	6.00	6.00	6.00
Charge	0.02	0.02	0.00	0.00	0.01	0.00	0.02	0.00	0.00	0.02	0.02	0.00	0.00	0.02	0.00	0.00	0.00
Wo	42.5	41.9	41.4	43.0	43.9	41.5	44.2	41.9	44.3	43.7	42.2	42.4	41.4	43.4	41.1	43.1	42.9
En	44.8	45.6	45.7	41.9	42.7	41.7	41.5	41.0	41.0	42.7	44.0	41.9	43.8	42.0	42.5	40.8	41.2
Fs	12.7	12.5	12.9	15.1	13.4	16.9	14.3	17.1	14.7	13.6	13.8	15.6	14.9	14.6	16.4	16.1	15.9
F/F+M	0.22	0.21	0.21	0.25	0.23	0.28	0.25	0.28	0.26	0.23	0.23	0.25	0.24	0.25	0.26	0.27	0.22
Mg#	0.78	0.79	0.79	0.75	0.77	0.72	0.75	0.72	0.74	0.77	0.77	0.75	0.76	0.75	0.74	0.73	0.78

Table A3-3b. Representative microprobe analyses of pyroxenes from basaltic andesites.

Location	Butong					Mt Apo													Mt Balatocan					
Analysis #	16	19	20	21	22	23	24	25	26	27	28	29	30	31	32	33	34	35	36	37	38	39	40	41
Sample #	B2C369	B2R367	B2M372	B2R368	B6357	AT4686	AT4686x	AT4675	AT4651x	AT4C633	AT4R637	AT4C64	AT4639	AT4C47x	AT4728x	AT4733x	T2C045	T2R04x	BLC046	BLMM04	BL2R03	T2149	LU1138	BL100
Xtal Type	(C	R)	M	R)	(C)	(C)	(C)	(C)	(C)	(C	R)	(C)	(C)	(C	R)	(C)	(C	R)	(C	M	R)	(M)	(C)	(C)
SiO2	52.14	51.47	52.12	51.91	51.26	52.46	52.46	52.74	52.98	52.65	51.78	52.66	51.64	52.32	53.14	52.64	50.89	51.77	52.16	52.01	51.82	52.47	52.1	51.2
TiO2	0.75	0.75	0.78	0.63	0.96	0.53	0.75	0.6	0.5	0.6	0.62	0.54	0.64	0.65	0.55	0.64	0.7	0.65	0.5	0.64	0.59	0.3	0.72	0.49
Al2O3	2.76	2.63	2.54	2.97	3.32	1.9	2.85	2.11	1.86	2.19	3.29	2.32	3.34	2.49	1.73	2.25	3.36	3.46	3.26	3.16	3.11	1.76	1.77	2.53
Cr2O3	0	0	0	0	0	0	0	0	0	0	0	0	0	0	0	0	0	0	0	0	0	0	0	0
Fe2O3	0	0.71	0	0.78	0	0	0	0	0	0	0	0	0.1	0	0	0	1.15	0.2	0	0	0	0	0	1.5
FeO	7.79	8.57	8.17	7.79	8.76	8.28	8.16	8.95	8.93	8.53	7.63	8.43	8.73	8.14	8.39	8.63	8.26	8.2	8.83	8.73	9.33	8.93	8.67	8.66
MnO	0.17	0.19	0.2	0.22	0.12	0.31	0.23	0.24	0.47	0.34	0.14	0.34	0.12	0.33	0.36	0.32	0.31	0.33	0.29	0.25	0.21	0.49	0.28	0.44
NiO	0	0	0	0	0	0	0	0	0	0	0	0	0	0	0	0	0	0	0	0	0	0	0	0
MgO	15.15	14.95	14.88	14.72	14.32	14.71	14.13	14.29	14.28	14.81	14.29	14.54	14.79	14.27	14.53	14.52	14.15	14.55	14.72	14.21	13.85	14.53	14.99	14.6
CaO	19.64	19.26	19.8	20.43	19.63	20.02	20.29	20.95	19.8	20.38	21.77	19.72	22.11	20.29	19.85	20.48	20.47	19.82	19.78	20.68	20.72	19.56	18.86	19.62
Na2O	0.46	0.48	0.65	0.51	0.48	0.46	0.5	0.39	0.48	0.37	0.27	0.45	0.22	0.34	0.48	0.41	0.34	0.35	0.35	0.31	0.32	0.35	0.38	0.3
K2O	0	0	0	0.01	0	0	0	0	0	0	0	0	0	0	0	0	0	0	0	0.01	0	0	0	0
Total	98.86	99.19	98.94	100.15	99.05	99.69	100.37	100.27	100.3	100.07	99.79	100.2	99.69	99.83	100.03	100.09	99.74	100.35	99.89	100.02	99.95	99.41	98.75	99.34
Number of cations on the basis of 6 oxygens.																								
Si	1.947	1.923	1.952	1.920	1.919	1.970	1.943	1.956	1.968	1.959	1.922	1.960	1.916	1.950	1.975	1.960	1.903	1.916	1.935	1.932	1.930	1.965	1.960	1.920
Ti	0.021	0.021	0.022	0.023	0.027	0.015	0.021	0.017	0.014	0.017	0.017	0.015	0.018	0.018	0.015	0.018	0.020	0.018	0.014	0.018	0.017	0.008	0.020	0.014
Al(iv)	0.053	0.077	0.048	0.080	0.081	0.030	0.057	0.044	0.032	0.041	0.078	0.040	0.084	0.050	0.025	0.040	0.097	0.084	0.065	0.068	0.070	0.035	0.040	0.080
Al(vi)	0.068	0.048	0.064	0.050	0.065	0.054	0.067	0.048	0.049	0.054	0.066	0.062	0.061	0.059	0.051	0.058	0.050	0.068	0.078	0.071	0.067	0.044	0.039	0.032
Cr	0.000	0.000	0.000	0.000	0.000	0.000	0.000	0.000	0.000	0.000	0.000	0.000	0.000	0.000	0.000	0.000	0.000	0.000	0.000	0.000	0.000	0.000	0.000	0.000
Fe3+	0.000	0.020	0.000	0.021	0.000	0.000	0.000	0.000	0.000	0.000	0.000	0.000	0.003	0.000	0.000	0.000	0.032	0.006	0.000	0.000	0.000	0.000	0.000	0.042
Fe2+	0.243	0.268	0.257	0.241	0.274	0.260	0.264	0.278	0.306	0.264	0.237	0.292	0.208	0.285	0.292	0.268	0.256	0.265	0.274	0.271	0.291	0.311	0.304	0.272
Mn	0.005	0.006	0.006	0.007	0.004	0.010	0.007	0.008	0.015	0.011	0.004	0.011	0.004	0.010	0.011	0.010	0.010	0.010	0.009	0.008	0.007	0.016	0.009	0.014
Ni	0.000	0.000	0.000	0.000	0.000	0.000	0.000	0.000	0.000	0.000	0.000	0.000	0.000	0.000	0.000	0.000	0.000	0.000	0.000	0.000	0.000	0.000	0.000	0.000
Mg	0.843	0.833	0.819	0.812	0.799	0.823	0.780	0.780	0.791	0.818	0.791	0.804	0.815	0.783	0.805	0.803	0.787	0.803	0.814	0.787	0.769	0.811	0.841	0.816
Ca	0.786	0.771	0.754	0.810	0.785	0.805	0.805	0.832	0.788	0.809	0.866	0.764	0.876	0.810	0.791	0.814	0.818	0.786	0.786	0.823	0.827	0.785	0.760	0.788
Na	0.033	0.033	0.047	0.037	0.035	0.033	0.036	0.026	0.035	0.027	0.019	0.032	0.016	0.025	0.035	0.029	0.025	0.025	0.025	0.022	0.023	0.025	0.028	0.022
K	0	0	0	0	0	0	0	0	0	0	0	0	0	0	0	0	0	0	0	0	0	0	0	0
# Oxy	6.01	6.00	6.01	6.00	6.00	6.01	6.01	6.00	6.01	6.01	6.00	6.01	6.00	6.01	6.01	6.01	6.00	6.00	6.01	6.01	6.00	6.01	6.01	6.00
Charge	0.02	0.00	0.02	0.00	0.00	0.02	0.02	0.01	0.01	0.01	0.00	0.02	0.00	0.02	0.02	0.02	0.00	0.00	0.02	0.02	0.01	0.02	0.02	0.00
Wo	41.6	40.6	40.4	42.8	42.5	42.4	42.9	43.6	41.4	42.5	45.6	41.4	46.0	42.7	41.6	43.0	43.0	41.8	41.7	43.6	43.7	40.8	39.7	40.8
En	44.9	43.9	43.9	42.9	42.7	43.4	41.8	41.4	41.8	43.0	41.7	42.5	42.8	41.8	42.4	42.4	41.3	42.5	43.2	41.7	40.6	42.2	43.9	42.2
Fs	13.2	15.5	15.7	14.2	14.8	14.2	15.5	14.9	17.0	14.5	12.7	16.0	11.3	15.6	16.0	14.7	15.7	15.9	15.0	14.8	15.7	17.0	16.4	17.0
F/F+M	0.22	0.24	0.26	0.23	0.26	0.24	0.27	0.26	0.28	0.24	0.23	0.27	0.20	0.26	0.27	0.25	0.25	0.26	0.25	0.26	0.27	0.28	0.27	0.25
Mg#	0.78	0.76	0.74	0.77	0.74	0.76	0.73	0.74	0.72	0.76	0.77	0.73	0.80	0.74	0.73	0.75	0.75	0.74	0.75	0.74	0.73	0.72	0.73	0.75

Appendix 3-2. Microprobe analyses.

Table A3-3c. Representative microprobe analyses of pyroxenes from SiO2-rich andesites and dacites.

Location	Hibok-Hibok, Camiguin Island						Mt Katanglad		Mt Apo					
Analysis #	41	42	43	44	45	46	47	48	49	50	51	52	53	54
Sample #	H15C10	H15M70	H15R70	0380mp	20449p	0409mp	KT9419	KT9386	A34924	A34444	A67093	A67103	A66244	733267
Xtal Type	(C	M	R)	(MP)	(C)	(MP)	(C)	(C)	(C)	(C)	(C)	(C)	(C)	(C)
SiO2	52.73	48.77	53.3	50.76	51.86	51.05	51.8	52.38	53.27	53.36	53.46	52.65	52.44	52.12
TiO2	0.2	0.88	0.22	0.65	0.23	0.31	0.44	0.41	0.22	0.11	0.12	0.15	0.15	0.16
Al2O3	1.35	6.63	1.14	3.44	3.59	4.52	2.84	2.91	1.69	1.61	1.51	1.94	2.27	2.14
Cr2O3	0	0	0	0	0	0	0	0	0	0	0	0	0	0
Fe2O3	0.46	1.5	0	1.36	0	0	0	0	0	0	0	0	0.55	0
FeO	8.46	6.88	8.16	6.06	6.4	7.23	8.57	7.78	7.64	7.57	7.63	7.71	7.59	7.97
MnO	0.6	0.09	0.57	0.12	0.07	0.11	0.26	0.23	0.7	0.67	0.63	0.9	0.72	0.69
NiO	0	0	0	0	0.02	0	0	0.03	0	0	0	0	0	0
MgO	15.43	12.75	15.39	14.23	14.29	13.86	14.11	15.34	14.16	13.66	14.04	13.69	13.88	13.66
CaO	19.83	22.16	20.71	22.3	22.4	21.44	20.85	20.69	21.76	22.8	22.48	21.9	22.12	21.78
Na2O	0.27	0.22	0.26	0.25	0.23	0.27	0.37	0.26	0.36	0.3	0.3	0.32	0.31	0.2
K2O	0	0	0	0	0	0	0	0	0	0	0	0	0	0
Total	99.34	99.88	99.75	99.18	99.09	98.79	99.24	100.03	99.8	100.08	100.17	99.26	100.04	98.72
Number of cations on the basis of 6 oxygens.														
Si	1.968	1.817	1.979	1.896	1.931	1.910	1.937	1.933	1.982	1.983	1.983	1.973	1.950	1.965
Ti	0.006	0.025	0.006	0.018	0.006	0.009	0.012	0.011	0.006	0.003	0.003	0.004	0.004	0.005
Al(iv)	0.032	0.183	0.021	0.104	0.069	0.090	0.063	0.067	0.018	0.017	0.017	0.027	0.050	0.035
Al(vi)	0.027	0.108	0.028	0.047	0.088	0.109	0.062	0.060	0.056	0.054	0.049	0.058	0.049	0.060
Cr	0.000	0.000	0.000	0.000	0.000	0.000	0.000	0.000	0.000	0.000	0.000	0.000	0.000	0.000
Fe3+	0.013	0.042	0.000	0.038	0.000	0.000	0.000	0.000	0.000	0.000	0.000	0.000	0.015	0.000
Fe2+	0.264	0.214	0.253	0.189	0.199	0.226	0.268	0.240	0.238	0.235	0.237	0.242	0.236	0.251
Mn	0.019	0.003	0.018	0.004	0.002	0.003	0.008	0.007	0.022	0.021	0.020	0.029	0.023	0.022
Ni	0.000	0.000	0.000	0.000	0.001	0.000	0.000	0.001	0.000	0.000	0.000	0.000	0.000	0.000
Mg	0.859	0.708	0.852	0.792	0.793	0.773	0.787	0.844	0.785	0.757	0.776	0.765	0.769	0.768
Ca	0.793	0.684	0.824	0.892	0.894	0.860	0.835	0.818	0.867	0.908	0.893	0.879	0.881	0.880
Na	0.020	0.016	0.019	0.018	0.017	0.020	0.027	0.019	0.026	0.022	0.022	0.023	0.022	0.015
K	0	0	0	0	0	0	0	0	0	0	0	0	0	0
# Oxy	6.00	6.00	6.00	6.00	6.01	6.01	6.01	6.01	6.01	6.01	6.01	6.01	6.00	6.01
Charge	0.00	0.00	0.00	0.00	0.02	0.02	0.02	0.02	0.02	0.02	0.02	0.02	0.00	0.02
Wo	40.7	47.8	42.3	46.6	47.3	46.2	44.0	42.8	45.4	47.3	46.4	45.9	45.8	45.8
En	44.1	38.2	43.8	41.4	42.0	41.5	41.4	44.2	41.1	39.4	40.3	40.0	40.0	40.0
Fs	15.2	14.0	13.9	12.1	10.7	12.3	14.6	13.0	13.6	13.3	13.3	14.1	14.2	14.2
F/F+M	0.24	0.23	0.23	0.19	0.20	0.23	0.25	0.22	0.23	0.24	0.23	0.24	0.23	0.25
Mg#	0.76	0.77	0.77	0.81	0.80	0.77	0.75	0.78	0.77	0.76	0.77	0.76	0.77	0.75

Appendix 3-2. Microprobe analyses.

Table A3-3d. Representative microprobe analyses of 2-pyroxene andesites (Camiguin Island).

Location	Mt. Mambajao			Mt. Ginsiliban			
Analysis #	55	56	57	58	59	60	61
Sample #	M3c22x	M3r212	M3208x	GC0682	GR063x	GC114x	GR114
Xtal Type	(C X	R)	(C)	(C	R)	(C	R)
SiO2	51.89	51.93	53.08	53.22	54.12	52.18	52.14
TiO2	0.22	0.21	0.09	0.1	0.18	0.48	0.22
Al2O3	3.17	2.76	1.58	2.29	1.76	2.71	2.73
Cr2O3	0	0	0	0	0	0	0
Fe2O3	0	0	0	0	0	0.05	0
FeO	7.89	7.95	16.67	15.58	16.93	9.66	9.42
MnO	0.62	0.63	1.05	0.56	0.46	0.33	0.33
NiO	0	0	0	0	0	0	0
MgO	13.98	14.07	25.01	25.44	24.94	14.5	14.15
CaO	21	21.17	0.92	1.54	1.64	19.87	20.07
Na2O	0.28	0.28	0.02	0	0.04	0.33	0.31
K2O	0	0	0	0	0	0	0
Total	99.05	99	98.42	98.73	100.07	100.1	99.37
Cations							
Si	1.943	1.946	1.963	1.952	1.970	1.938	1.951
Ti	0.006	0.006	0.003	0.003	0.005	0.013	0.006
Al(iv)	0.057	0.054	0.037	0.048	0.030	0.062	0.049
Al(vi)	0.083	0.068	0.032	0.051	0.045	0.057	0.072
Cr	0.000	0.000	0.000	0.000	0.000	0.000	0.000
Fe3+	0.000	0.000	0.000	0.000	0.000	0.001	0.000
Fe2+	0.247	0.249	0.516	0.478	0.515	0.300	0.295
Mn	0.020	0.020	0.033	0.017	0.014	0.010	0.010
Ni	0.000	0.000	0.000	0.000	0.000	0.000	0.000
Mg	0.781	0.786	1.379	1.391	1.353	0.803	0.789
Ca	0.843	0.850	0.036	0.061	0.064	0.791	0.805
Na	0.020	0.020	0.001	0.000	0.003	0.024	0.022
K	0	0	0	0	0	0	0
# Oxy	6.01	6.01	6.01	6.01	6.01	6.00	6.01
Charge	0.02	0.02	0.02	0.02	0.02	0.00	0.02
Wo	44.6	44.6	1.9	3.1	3.3	41.5	42.4
En	41.3	41.3	70.2	71.5	69.5	42.1	41.6
Fs	14.1	14.1	27.9	25.4	27.2	16.4	16.1
F/F+M	0.24	0.24	0.27	0.26	0.28	0.27	0.27
Mg#	0.76	0.76	0.73	0.74	0.72	0.73	0.73

Table A3-4a. Representative analyses of spinels from basalt and basaltic andesites.

Location	HIB	HIB	BUT	BUT	BUT	BAL	QUE	APO	APO	APO	APO
Analysis #	4	5	6	1	2	3	7	8	9	10	11
Sample #	H51238	H51264	B6108	B6562	B6615	I4590	Q2702	T4505	M3444	T4494	T4496
SPINEL	TMT	TMT	TMT	CRS	CRS	TMT	TMT	TMT	TMT	TMT	TMT
XTAL TYPE	PH	PH	GM	OL	OL	PH	GM	CP	CP	CP	PH
Oxide Wt %											
SiO2	0.12	0.06	0.09	0.2	0.06	0.12	0.09	0.07	0.1	0.1	0.09
Al2O3	4.73	2.51	4.74	19.18	18.48	1.5	2.36	2.06	3.79	3.44	4.33
TiO2	8.37	7.77	7.8	1.29	1.34	16.06	8.91	14.7	9.72	7.67	9.09
FeO	77.59	80.62	77.97	37.5	37.17	76	81.53	77.08	77.97	81.42	77.39
MnO	0.46	0.52	0.32	0.03	0.06	0.46	0.42	0.72	0.55	0.42	0.61
MgO	3.06	2.48	2.67	10.63	8.93	1.82	1.88	1.96	2.62	2.19	2.75
CaO	0	0.03	0.07	0.01	0	0.03	0.04	0.03	0.02	0	0
Cr2O3	0.07	0.12	1.44	29.55	31.58	0.11	0.77	0.08	0.11	0.07	0.04
V2O3	0	0	0	0	0	0	0	0	0	0	0
ZnO	0	0	0	0	0	0	0	0	0	0	0
Total	94.4	94.11	95.1	98.39	97.62	96.1	96	96.7	94.88	95.31	94.3
Recalculated Analyses											
FeO	34.198	34.085	34.576	20.183	21.977	42.834	36.661	41.474	35.960	35.090	35.065
Fe2O3	48.223	51.717	48.226	19.245	16.884	36.859	49.864	39.570	46.688	51.488	47.038
Total	99.231	99.291	99.932	99.918	99.312	99.793	100.996	100.664	99.558	100.469	99.003
Mt	76.90	78.22	78.57			55.05	75.32	59.34	73.08	78.79	74.77
Usp	23.10	21.78	21.43			44.95	24.68	40.66	26.92	21.21	25.23
Number of cations on the basis of 4 oxygens											
Si	0.004	0.002	0.003	0.006	0.002	0.004	0.003	0.003	0.004	0.004	0.003
Al	0.204	0.110	0.204	0.733	0.708	0.066	0.102	0.089	0.164	0.149	0.188
Ti	0.230	0.218	0.214	0.031	0.033	0.448	0.246	0.406	0.269	0.212	0.252
Fe3+	1.329	1.449	1.324	0.440	0.413	1.030	1.379	1.094	1.291	1.422	1.304
Fe2+	1.047	1.061	1.055	0.576	0.597	1.330	1.127	1.274	1.105	1.077	1.080
Mn	0.014	0.016	0.010	0.001	0.002	0.014	0.013	0.022	0.017	0.013	0.019
Mg	0.167	0.138	0.145	0.451	0.433	0.101	0.103	0.107	0.144	0.120	0.151
Ca	0.000	0.001	0.003	0.000	0.000	0.001	0.002	0.001	0.001	0.000	0.000
Cr	0.002	0.004	0.042	0.757	0.812	0.003	0.022	0.002	0.003	0.002	0.001
V3+	0.000	0.000	0.000	0.000	0.000	0.000	0.000	0.000	0.000	0.000	0.000
Zn	0.000	0.000	0.000	0.000	0.000	0.000	0.000	0.000	0.000	0.000	0.000
Total	2.998	2.999	2.998	2.997	2.999	2.998	2.998	2.999	2.998	2.998	2.999

Abbreviations

Location: BUT=Mt Butong, LAN=Lanao, CAM=Camiguin Island, KAL=Mt Kalatungan, TAL=Mt Talomo
KAT=Mt Katanglad, APO=Mt Apo

SPINEL: CRS=Cr-Spinel, TMT=Titanomagnetite

XTAL TYPE: OL=Olivine, CP=Clinopyroxene, PL=Plagioclase, BIO=Biotite
PH=Phenocryst, GM=Groundmass spinel

Table A3-4b. Representative analyses of spinels from SiO2-rich andesites.

Location	BAL	CAM	CAM	CAM	CAM	CAM	APO	APO
Analysis #	12	13	14	15	16	17	18	19
Sample #	B10223	H20202	H20420	H02589	H26533	B31471	A3459	A3438
SPINEL	TMT	TMT	TMT	TMT	TMT	TMT	TMT	TMT
XTAL TYPE	CP	MP	PL	MP	MP	MP	PL	MP
Oxide Wt %								
SiO2	0.06	0.1	0.08	0.06	0	0.08	0.07	0.04
Al2O3	3.51	1.05	1.31	1.56	1.85	2.66	1.28	1.08
TiO2	9.42	9.86	10.99	8.59	9.32	8.14	8.24	8.36
FeO	78.32	80.87	80.5	83.52	80.22	80.7	84.64	84.38
MnO	0.48	0.37	0.39	0.59	0.9	0.41	0.56	0.69
MgO	1.94	1.3	1.47	1.04	1.03	1.33	1.01	1.29
CaO	0.01	0.03	0.02	0.02	0	0.03	0.01	0.08
Cr2O3	0.18	0.09	0.07	0.1	0.04	0.03	0.11	0.07
V2O3	0	0	0	0	0	0	0	0
ZnO	0	0	0	0	0	0	0	0
Total	93.92	93.67	94.83	95.48	93.36	93.38	95.92	95.99
Recalculated Analyses								
FeO	36.471	37.483	38.623	37.255	36.967	36.038	36.811	36.281
Fe2O3	46.509	48.218	46.539	51.417	48.069	49.635	52.043	52.343
Total	98.580	98.501	99.493	100.631	98.176	98.353	100.134	100.234
Mt	73.49	71.71	68.90	75.86	73.25	76.79	76.92	76.65
Usp	26.51	28.29	31.10	24.14	26.75	23.21	23.08	23.35
Number of cations on the basis of 4 (O)								
Si	0.002	0.004	0.003	0.002	0.000	0.003	0.003	0.001
Al	0.155	0.047	0.058	0.069	0.083	0.119	0.056	0.047
Ti	0.265	0.282	0.311	0.241	0.268	0.232	0.230	0.233
Fe3+	1.308	1.382	1.316	1.444	1.380	1.414	1.477	1.482
Fe2+	1.140	1.194	1.214	1.163	1.180	1.141	1.155	1.136
Mn	0.015	0.012	0.012	0.019	0.029	0.013	0.018	0.022
Mg	0.108	0.074	0.082	0.058	0.059	0.075	0.056	0.071
Ca	0.000	0.001	0.001	0.001	0.000	0.001	0.000	0.003
Cr	0.005	0.003	0.002	0.003	0.001	0.001	0.003	0.002
V3+	0.000	0.000	0.000	0.000	0.000	0.000	0.000	0.000
Zn	0.000	0.000	0.000	0.000	0.000	0.000	0.000	0.000
Total	2.999	2.998	2.998	2.999	3.000	2.998	2.999	2.999

Abbreviations as in Table A3-4a.

Table A3-4c. Representative analyses of spinels from dacites.

Location	CAM	KAT	KAT	KAT	APO	APO	APO	APO
Analysis	20	21	22	23	24	25	26	27
Sample #	H46186	K9504	K9264	K9509	A6350	A6172	A6260	A6260b
SPINEL	TMT	TMT	TMT	TMT	TMT	TMT	TMT	TMT
XTAL TYP	MP	MP	MP	PL	MP	BIO	PL	PL
Oxide Wt %								
SiO2	0.04	0.07	0.06	0.07	0.04	0	0.06	0.06
Al2O3	1.27	2.56	2.61	1.57	1.6	2.1	1.61	1.6
TiO2	7.1	11.5	8.06	11.16	6.42	6.68	7.87	5.76
FeO	85.37	78.78	79.53	79.36	84.38	82.96	83.11	84.69
MnO	0.58	0.54	0.54	0.53	0.71	0.71	0.75	0.68
MgO	0.87	1.4	3.61	1.55	0.98	1.39	1.19	1.18
CaO	0	0.04	0.03	0.04	0.02	0.01	0.11	0.03
Cr2O3	0.01	0.27	0.12	0.21	0.11	0.27	0.09	0.06
V2O3	0	0	0	0	0	0	0	0
ZnO	0	0	0	0	0	0	0	0
Total	95.24	95.16	94.56	94.49	94.26	94.12	94.79	94.06
Recalculated Analyses								
FeO	35.812	39.277	32.760	38.407	34.951	34.596	35.912	34.021
Fe2O3	53.964	99.558	51.978	45.513	54.933	53.749	52.454	56.311
Total	99.647	99.558	99.768	99.050	99.764	99.505	100.045	99.702
Mt	79.98	67.70	77.71	68.36	81.77	81.10	77.78	83.64
Usp	20.02	32.30	22.29	31.64	18.23	18.90	22.22	16.36
Number of cations on the basis of 4 (O)								
Si	0.001	0.003	0.002	0.003	0.002	0.000	0.002	0.002
Al	0.056	0.113	0.113	0.070	0.071	0.093	0.071	0.071
Ti	0.200	0.323	0.223	0.316	0.182	0.189	0.222	0.163
Fe3+	1.542	1.232	1.436	1.289	1.560	1.521	1.480	1.598
Fe2+	1.132	1.225	1.006	1.209	1.103	1.088	1.126	1.073
Mn	0.018	0.017	0.017	0.017	0.023	0.023	0.024	0.022
Mg	0.049	0.078	0.198	0.087	0.055	0.078	0.067	0.066
Ca	0.000	0.002	0.001	0.002	0.001	0.000	0.004	0.001
Cr	0.000	0.008	0.003	0.006	0.003	0.008	0.003	0.002
V3+	0.000	0.000	0.000	0.000	0.000	0.000	0.000	0.000
Zn	0.000	0.000	0.000	0.000	0.000	0.000	0.000	0.000
Total	2.999	2.999	2.999	2.999	2.999	3.000	2.999	2.999

Abbreviations as in Table A3-4a.

Appendix 3-2. Microprobe analyses.

Table A3-5a. Representative microprobe analyses of amphiboles from andesites.

Location	CAM	CAM	CAM	CAM	CAM	CAM	CAM	CAM	CAM	CAM	CAM	CAM	CAM	CAM
Analysis #	15	16	17	18	19	20	21	22	23	24	25	26	27	28
Sample#	H26108	H26010	H26103	H26500	H20R444	H20348	H20445	H20350	H20437	H15638	H15538	H15643	H15461	BN3147
Xtal Type	PH	PH	PH	PH	PH	PH	PH	PH	PH	PH	PH	PH	PH	PH
Oxide (wt%)														
SiO2	48.18	48.40	47.53	47.34	47.89	46.48	46.09	43.80	46.23	43.70	45.97	46.78	48.51	43.95
TiO2	1.02	1.08	1.23	1.27	1.30	1.49	1.61	1.69	1.68	1.70	1.83	1.49	1.26	1.90
Al2O3	7.26	7.32	7.64	7.93	7.65	9.78	9.15	11.20	9.30	11.81	10.02	8.59	7.23	11.12
FeO	13.64	12.76	13.30	12.79	12.82	12.78	13.74	14.25	14.32	13.85	13.40	13.87	13.29	12.36
MnO	0.63	0.41	0.52	0.39	0.61	0.54	0.55	0.48	0.45	0.27	0.30	0.60	0.58	0.19
MgO	13.94	14.38	14.41	15.14	14.25	12.97	13.51	12.24	13.01	12.68	13.70	13.54	14.34	13.66
CaO	11.82	11.12	10.86	10.97	10.61	10.87	10.44	11.15	10.96	11.33	11.14	10.71	10.67	11.38
Na2O	1.23	1.22	1.21	1.30	1.51	1.31	1.83	1.98	1.86	2.29	1.97	1.76	1.44	2.24
K2O	0.41	0.37	0.45	0.34	0.31	0.31	0.38	0.48	0.42	0.47	0.37	0.32	0.27	0.46
H2O	2.04	2.05	1.96	1.97	2.04	2.02	2.03	2.02	2.05	2.04	2.06	2.04	2.06	2.04
Total	100.17	99.11	99.11	99.44	98.99	98.55	99.33	99.29	100.28	100.14	100.76	99.70	99.65	99.30
Number of cations on the basis of 23 oxygens.														
Si	6.942	6.968	6.827	6.745	6.890	6.743	6.644	6.409	6.662	6.340	6.564	6.733	6.933	6.395
Al IV	1.058	1.032	1.173	1.255	1.110	1.257	1.356	1.591	1.338	1.660	1.436	1.267	1.067	1.605
Al VI	0.175	0.210	0.121	0.077	0.187	0.415	0.199	0.341	0.242	0.359	0.251	0.191	0.151	0.302
Fe3	0.634	0.780	1.147	1.264	0.937	0.757	1.051	0.760	0.780	0.704	0.809	0.942	0.966	0.643
Ti	0.111	0.117	0.133	0.136	0.141	0.163	0.175	0.186	0.182	0.185	0.197	0.161	0.135	0.208
FM	4.081	3.893	3.600	3.523	3.736	3.665	3.576	3.714	3.796	3.752	3.744	3.706	3.748	3.848
Ca	1.825	1.715	1.671	1.675	1.635	1.690	1.612	1.748	1.692	1.761	1.704	1.652	1.634	1.774
Na	0.175	0.285	0.329	0.325	0.365	0.310	0.388	0.252	0.308	0.239	0.296	0.348	0.366	0.226
Na	0.168	0.056	0.008	0.034	0.057	0.058	0.124	0.310	0.212	0.405	0.250	0.143	0.033	0.406
K	0.075	0.068	0.082	0.062	0.057	0.057	0.070	0.090	0.077	0.087	0.067	0.059	0.049	0.085
Total	15.244	15.124	15.091	15.096	15.115	15.115	15.195	15.401	15.289	15.492	15.318	15.202	15.082	15.492
Mg/Mg+Fe2	0.734	0.793	0.857	0.913	0.818	0.765	0.812	0.719	0.736	0.731	0.779	0.784	0.815	0.770
Endmembers														
hornblende	0.523	0.560	0.408	0.324	0.411	0.317	0.063		0.066	0.043		0.183	0.485	
barroisite	0.175	0.285	0.329	0.325	0.365	0.310	0.388	0.131	0.308	0.465	0.271	0.348	0.366	0.065
tschermakite	0.058	0.032	0.173	0.255	0.110	0.257	0.356	0.470	0.338	0.296	0.411	0.267	0.067	0.444
edenite	0.244	0.124	0.091	0.096	0.113	0.115	0.194	0.278	0.289		0.293	0.202	0.082	0.330
taramite								0.121		0.196	0.024			0.161
anthophyllite														
gedrite														
Na-anthophyllite														

Abbreviations: APO , Mt. Apo; CAM, Camiguin Island. Xtal Type: C, Core; R, Rim, PH, Phenocryst

Appendix 3-2. Microprobe analyses.

Table A3-5b. Representative microprobe analyses of amphiboles from dacites.

Location	APO	APO	APO	APO	CAM	CAM	CAM	CAM	CAM	CAM	CAM	CAM	CAM	CAM
Analysis #	1	2	3	4	5	6	7	8	9	10	11	12	13	14
Sample#	A6630C	A6630R	A6672R	A2674C	H46C12	H4R12	H4GR2	H46GM2	H461271	H46155	H46C0	H46R03	H46A1	H46B10
Xtal Type	[C	R]	[R	C]	[C	R]	[R G	C]	PH	PH	[C	R]	PH	PH
Oxide (wt%)														
SiO2	47.75	47.89	47.46	48.22	48.44	48.17	48.14	48.05	48.05	48.35	48.11	48.04	48.41	48.80
TiO2	1.32	1.68	1.42	1.51	1.08	1.00	1.01	1.21	1.39	0.92	0.92	1.06	0.98	0.94
Al2O3	6.50	6.49	6.68	7.07	7.18	7.30	7.09	6.76	6.85	6.85	6.86	7.72	7.08	7.62
FeO	12.65	12.68	12.54	12.79	13.40	13.62	12.97	12.73	13.26	13.29	12.72	13.73	13.67	13.00
MnO	0.43	0.38	0.44	0.42	0.59	0.39	0.42	0.41	0.49	0.68	0.56	0.43	0.52	0.48
MgO	14.39	14.60	14.25	14.44	14.07	14.11	14.23	15.55	13.91	14.08	14.48	13.98	13.78	14.46
CaO	11.24	11.38	11.10	10.99	10.94	10.94	11.00	11.28	11.17	10.93	10.99	10.62	11.06	10.88
Na2O	1.15	1.46	1.46	1.47	1.19	1.09	1.17	1.25	1.19	1.43	1.41	1.23	1.25	1.13
K2O	0.65	0.61	0.64	0.72	0.33	0.39	0.37	0.41	0.35	0.43	0.67	0.36	0.41	0.29
H2O	2.04	2.04	2.06	2.05	2.05	2.04	2.05	2.01	2.05	2.03	2.00	2.04	1.96	2.00
Total	98.12	99.21	98.05	99.68	99.27	99.05	98.45	99.66	98.71	98.99	98.72	99.21	99.12	99.60
Number of cations on the basis of 23 oxygens.														
Si	6.991	6.957	6.971	6.945	6.966	6.936	6.979	6.857	6.986	7.000	6.981	6.891	7.000	6.947
Al IV	1.009	1.043	1.029	1.055	1.034	1.064	1.021	1.137	1.014	1.000	1.019	1.109	1.000	1.053
Al VI	0.112	0.068	0.128	0.145	0.183	0.175	0.190	0.000	0.160	0.169	0.155	0.197	0.206	0.225
Fe3	0.641	0.566	0.540	0.681	0.887	0.962	0.814	1.101	0.681	0.800	0.790	1.059	0.838	1.045
Ti	0.145	0.184	0.157	0.164	0.117	0.108	0.110	0.130	0.152	0.100	0.100	0.114	0.107	0.101
FM	4.101	4.183	4.175	4.011	3.813	3.747	3.886	3.769	4.007	3.931	3.955	3.604	3.849	3.601
Ca	1.763	1.771	1.747	1.696	1.686	1.688	1.709	1.725	1.740	1.695	1.709	1.632	1.713	1.659
Na	0.237	0.229	0.253	0.304	0.314	0.304	0.291	0.275	0.260	0.305	0.291	0.342	0.287	0.312
Na	0.089	0.182	0.163	0.106	0.017	0.000	0.037	0.070	0.076	0.097	0.105	0.000	0.064	0.000
K	0.121	0.113	0.120	0.132	0.061	0.072	0.068	0.075	0.065	0.079	0.124	0.066	0.076	0.053
Total	15.209	15.296	15.283	15.239	15.078	15.056	15.105	15.139	15.141	15.176	15.229	15.014	15.140	14.996
Mg/Mg+Fe2	0.786	0.756	0.747	0.773	0.791	0.807	0.792	0.876	0.753	0.773	0.792	0.824	0.772	0.845
Endmembers														
hornblende	0.543	0.432	0.435	0.402	0.574	0.557	0.582	0.436	0.586	0.519	0.461	0.474	0.574	0.570
barroisite	0.237	0.229	0.253	0.304	0.314	0.304	0.291	0.275	0.260	0.305	0.291	0.342	0.287	0.312
tschermakite	0.009	0.043	0.029	0.055	0.034	0.063	0.021	0.143	0.014	0.176	0.019	0.106	0.139	0.052
edenite	0.211	0.295	0.283	0.239	0.078	0.071	0.106	0.145	0.140		0.229	0.065		0.052
taramite														
anthophyllite						0.002						0.005		0.006
gedrite						0.002						0.007		0.007
Na-anthophyllite												0.001		0.001

Abbreviations: APO , Mt Apo; CAM, Camiguin Island. Xtal Type: C, Core; R, Rim, PH, Phenocryst

APPENDIX 4 MAJOR AND TRACE ELEMENT DATA

Appendix 4-1. List of rock standards for major element analyses[1].

	LVT	Lvt-1	Lvt-2	AR	Ar-1	Ar-2	BAS	Bas-1	Bas-2
SiO_2	61.02	60.54	61.26	76.46	76.41	75.58	48.10	47.94	48.04
TiO_2	0.30	0.30	0.30	0.05	0.06	0.06	2.19	2.19	2.17
Al_2O_3	18.03	18.08	17.94	12.96	12.97	12.84	14.90	14.79	14.93
Fe_2O_3	4.97	4.94	4.97	1.14	1.13	1.14	11.80	11.82	11.75
MnO	0.16	0.13	0.14	0.02	0.01	0.01	0.17	0.18	0.16
MgO	0.54	0.55	0.57	0.08	0.08	0.10	7.33	7.31	7.33
CaO	1.37	1.36	1.37	0.15	0.15	0.15	10.25	10.24	10.19
Na_2O	6.10	6.23	5.88	3.85	3.69	3.62	3.31	3.20	3.57
K_2O	5.68	5.68	5.64	4.38	4.35	4.32	1.17	1.21	1.21
P_2O_5	0.04	0.04	0.04	0.02	0.02	0.03	0.51	0.49	0.51
LOI	1.66	2.12	1.58	0.85	0.70	1.33	-0.49	-0.17	-0.06
Total	99.87	99.97	99.72	99.69	99.55	99.15	99.24	99.20	99.80

[1]Entries under LVT, AR and BAS are recommended results for laboratory standards (S.D. Weaver, 1989). Acceptable values are: Totals, 99.5 ± 1.0. Laboratory standards should give values close to SiO_2 ± 0.5%; Al_2O_3, ± 0.15%; LOI, ± 0.25% (actual). Operating conditions: fused beads were irradiated for major elements using Sc and Cr tubes (3 Kw, 50 Kv, 50mA); pressed powder pellets analysed by Au tube at 60 Kv, 45 mA and Mo tube at 90 Kv, 30 mA.

Appendix 4-2. Whole-rock analyses of CMVA lavas.

Lab. #	21849	21864	21884	21867	21885	21866	21850	21865
Sample #	KAN23	HIB37	HS15	HIB42	CAT82	HIB41	CAM24	HIB40
Analysis #	1	2	3	4	5	6	7	8
SiO2 wt%	52.23	53.51	54.62	56.01	56.40	56.65	56.78	56.79
TiO2	0.77	0.76	0.72	0.64	0.67	0.70	0.57	0.67
Al2O3	18.75	17.92	17.65	18.01	17.85	17.70	19.12	17.98
Fe2O3	9.67	8.93	8.36	7.71	7.18	6.90	7.14	7.40
MnO	0.21	0.16	0.14	0.17	0.10	0.11	0.14	0.12
MgO	4.67	4.97	4.74	4.09	4.27	4.29	2.83	4.52
CaO	9.54	9.65	8.67	8.46	8.08	7.68	7.28	8.06
Na2O	3.45	3.07	3.08	3.50	3.64	3.62	3.95	3.67
K2O	0.75	1.08	1.66	1.33	1.40	1.47	1.32	1.24
P2O5	0.33	0.25	0.27	0.26	0.28	0.29	0.40	0.28
LOI	-0.03	0.20	0.07	-0.51	-0.20	-0.10	0.40	-0.40
Total	100.34	100.50	99.98	99.67	99.67	99.31	99.93	100.33
CIPW norm								
Q	0.8	3.09	4.16	5.78	5.88	6.67	7.35	6.08
or	4.43	6.38	9.81	7.86	8.27	8.69	7.8	7.33
ab	29.19	25.98	26.06	29.62	30.8	30.63	33.42	31.05
an	53.41	55.14	53.04	49.91	47.83	47.49	47.75	48.23
di	9.64	11.72	9.67	8.84	8.19	6.93	2.45	7.54
hy	16.87	15.73	15.54	13.78	13.79	14.12	13.19	15.02
ol	-	-	-	-	-	-	-	-
mt	2.99	2.75	2.58	2.38	2.22	2.13	2.2	2.28
il	1.46	1.44	1.37	1.22	1.27	1.33	1.08	1.27
ap	0.76	0.58	0.63	0.6	0.65	0.67	0.93	0.65
Cr ppm	18	37	60	38	59	72	6	91
Ni	17	23	30	18	39	55	6	37
Rb	15	21	38	26	27	26	23	24
Ba	322	378	384	387	423	411	447	419
Sr	1025	871	780	830	863	888	995	924
La	19	15	15	17	16	16	19	16
Ce	32	32	30	41	33	32	42	36
Nd	14	29	10	11	13	12	17	24
Y	15	15	15	14	14	12	14	12
Zr	41	76	68	88	85	76	87	76
Nb	6	5	5	6	6	7	8	5
Pb	5	5	8	8	7	8	7	9
Th	1	1	2	1	2	3	1	2
V	265	219	196	158	165	162	131	156
Ga	21	19	18	22	22	21	23	19
Zn	86	68	63	74	69	67	88	72
K/Rb	415	427	365	426	433	475	481	428
K/Ba	19	2372	36	29	28	30	25	25
Rb/Sr	0.0	0.0	0.0	0.0	0.0	0.0	0.0	0.0
Rb/Ba	0.0	5.6	0.1	0.1	0.1	0.1	0.1	0.1
Ba/Sr	0.3	0.0	0.5	0.5	0.5	0.5	0.4	0.5
Zr/Nb	6.8	15.2	13.6	14.7	14.2	10.9	10.9	15.2
Zr/Y	2.7	5.1	4.5	6.3	6.1	6.3	6.2	6.3
FeO*/MgO	1.86	1.62	1.59	1.70	1.51	1.45	2.27	1.47
Mg# (x100)	55	58	59	57	60	61	50	61

Total Fe as Fe2O3. CIPW norms calculated using Fe2O3/FeO = 0.3.

Appendix 4-2. Whole-rock analyses of CMVA lavas.

Lab. #	21842	21843	21836	21834	21851	21881	21832	21846
Sample #	CAM10	HIB12	HIB5	HIB3	HIB25	CAM50J	HIBS	CAM16
Analysis #	9	10	11	12	13	14	15	16
SiO2 wt%	56.79	56.89	56.98	57.14	57.27	57.80	57.83	57.94
TiO2	0.63	0.61	0.64	0.61	0.66	0.63	0.59	0.59
Al2O3	17.88	17.87	17.48	17.15	17.97	17.90	17.63	17.71
Fe2O3	7.37	7.22	7.11	7.15	6.91	6.91	6.83	6.88
MnO	0.12	0.15	0.12	0.17	0.12	0.17	0.14	0.15
MgO	3.94	3.65	4.31	3.70	3.36	3.62	3.38	3.41
CaO	8.16	7.85	7.93	7.97	7.32	7.63	7.51	7.61
Na2O	3.52	3.61	3.65	3.55	3.67	3.67	3.70	3.62
K2O	1.40	1.42	1.38	1.38	1.30	1.41	1.46	1.44
P2O5	0.27	0.27	0.27	0.27	0.30	0.31	0.27	0.28
LOI	-0.30	0.16	0.16	0.81	0.70	-0.07	0.67	0.27
Total	99.78	99.70	100.03	99.90	99.58	99.98	100.01	99.90
CIPW norm								
Q	7.09	7.49	6.78	7.94	9.17	8.62	8.97	9.31
or	8.27	8.39	8.16	8.16	7.68	8.33	8.63	8.51
ab	29.79	30.55	30.89	30.04	31.05	31.05	31.31	30.63
an	49.21	48.15	46.86	49.02	48.05	47.6	46.48	47.6
di	8.09	7.25	8.44	7.3	4.63	6.26	6.83	6.66
hy	13.31	12.93	13.78	12.99	13	13	12.03	12.25
ol	-	-	-	-	-	-	-	-
mt	2.28	2.22	2.19	2.2	2.13	2.13	2.1	2.12
il	1.2	1.16	1.22	1.16	1.25	1.2	1.12	1.12
ap	0.63	0.63	0.63	0.63	0.7	0.72	0.63	0.65
Cr ppm	37	29	68	33	25	40	38	25
Ni	20	16	31	18	18	21	20	17
Rb	29	29	31	31	26	31	18	33
Ba	440	436	448	496	434	476	532	517
Sr	847	872	905	868	979	949	961	902
La	19	19	20	21	18	19	22	20
Ce	38	31	39	31	36	34	29	36
Nd	17	20	13	25	18	13	26	25
Y	13	14	14	14	12	13	17	14
Zr	87	93	98	93	87	99	97	99
Nb	7	7	8	7	6	9	8	5
Pb	7	9	9	9	7	10	10	8
Th	2	1	3	3	1	3	1	1
V	155	140	139	147	125	125	139	128
Ga	19	18	20	21	19	20	18	20
Zn	67	69	68	69	71	65	61	67
K/Rb	403	411	372	372	422	380	683	365
K/Ba	27	27	26	23	25	25	23	23
Rb/Sr	0.0	0.0	0.0	0.0	0.0	0.0	0.0	0.0
Rb/Ba	0.1	0.1	0.1	0.1	0.1	0.1	0.0	0.1
Ba/Sr	0.5	0.5	0.5	0.6	0.4	0.5	0.6	0.6
Zr/Nb	12.4	13.3	12.3	13.3	14.5	11.0	12.1	19.8
Zr/Y	6.7	6.6	7.0	6.6	7.3	7.6	5.7	7.1
FeO*/MgO	1.68	1.78	1.48	1.74	1.85	1.72	1.82	1.82
Mg# (x100)	57	56	60	57	55	57	55	55

Total Fe as Fe2O3. CIPW norms calculated using Fe2O3/FeO = 0.3.

Appendix 4-2. Whole-rock analyses of CMVA lavas.

Lab. #	21838	21835	21844	21837	21847	21831	21845	21882
Sample #	CAM8	HIB4	CAM14	CAM7	CAM17	HIBB	HIB15	CAM58
Analysis #	17	18	19	20	21	22	23	24
SiO2 wt%	58.06	58.24	58.28	58.31	58.38	58.51	58.59	58.71
TiO2	0.59	0.57	0.59	0.59	0.59	0.61	0.58	0.57
Al2O3	17.63	17.46	17.70	17.58	17.77	17.24	17.79	17.86
Fe2O3	6.81	6.60	6.81	6.81	6.82	7.03	6.66	6.58
MnO	0.15	0.16	0.14	0.15	0.15	0.16	0.15	0.14
MgO	3.38	3.24	3.33	3.28	3.14	3.53	3.31	3.17
CaO	7.50	7.20	7.52	7.35	7.59	7.26	7.42	7.28
Na2O	3.70	3.65	3.73	3.80	3.65	3.58	3.74	3.80
K2O	1.48	1.59	1.49	1.50	1.45	1.46	1.48	1.50
P2O5	0.27	0.27	0.29	0.27	0.27	0.26	0.27	0.26
LOI	0.43	0.33	-0.03	0.40	-0.03	0.26	0.20	-0.03
Total	100.00	99.31	99.85	100.04	99.78	99.90	100.19	99.84
CIPW norm								
Q	9.14	9.93	9.24	9.21	9.98	10.39	9.65	9.76
or	8.75	9.4	8.81	8.86	8.57	8.63	8.75	8.86
ab	31.31	30.89	31.56	32.15	30.89	30.29	31.65	32.15
an	46.42	46.24	46.25	45.16	47.39	46.81	46.39	45.87
di	6.84	6.08	6.79	6.76	6.65	6.29	6.3	5.9
hy	12.03	11.87	11.91	11.75	11.51	0	11.96	11.71
ol	-	-	-	-	-	12.9	-	-
mt	2.1	2.03	2.1	2.09	2.1	2.16	2.06	2.03
il	1.12	1.08	1.12	1.12	1.12	1.16	1.1	1.08
ap	0.63	0.63	0.67	0.63	0.63	0.6	0.63	0.6
Cr ppm	27	23	28	27	29	32	28	24
Ni	17	14	18	18	17	17	16	15
Rb	33	35	32	33	32	33	32	33
Ba	499	550	505	497	508	490	515	506
Sr	900	883	902	894	893	845	891	923
La	19	24	24	22	19	19	21	20
Ce	41	37	34	36	39	35	30	35
Nd	12	25	24	13	25	22	22	13
Y	16	13	14	14	14	13	13	13
Zr	99	104	96	102	99	98	99	106
Nb	8	7	7	8	8	7	7	8
Pb	10	11	9	9	7	9	8	12
Th	3	1	3	2	1	2	1	1
V	134	116	129	133	139	143	132	113
Ga	21	19	20	21	18	23	21	21
Zn	71	62	65	68	66	70	65	64
K/Rb	375	382	389	380	379	370	387	380
K/Ba	25	24	25	25	24	25	24	25
Rb/Sr	0.0	0.0	0.0	0.0	0.0	0.0	0.0	0.0
Rb/Ba	0.1	0.1	0.1	0.1	0.1	0.1	0.1	0.1
Ba/Sr	0.6	0.6	0.6	0.6	0.6	0.6	0.6	0.5
Zr/Nb	12.4	14.9	13.7	12.8	12.4	14.0	14.1	13.3
Zr/Y	6.2	8.0	6.9	7.3	7.1	7.5	7.6	8.2
FeO*/MgO	1.81	1.83	1.84	1.87	1.95	1.79	1.81	1.87
Mg# (x100)	56	55	55	55	54	56	56	55

Total Fe as Fe2O3. CIPW norms calculated using Fe2O3/FeO = 0.3.

Appendix 4-2. Whole-rock analyses of CMVA lavas.

Lab. #	21869	21873	21840	21839	21841	21863	21870	21862
Sample #	CAT46	VUL50	VUL21	HIB20	CAM22	MAM34	MAM47	MAM33
Analysis #	25	26	27	28	29	30	31	32
SiO2 wt%	61.70	55.47	56.41	58.31	58.73	56.35	57.42	58.09
TiO2	0.60	0.66	0.66	0.61	0.58	0.62	0.75	0.67
Al2O3	16.88	18.46	17.52	17.49	17.67	17.85	17.52	17.33
Fe2O3	5.75	7.57	7.31	6.62	6.62	7.41	6.98	6.79
MnO	0.11	0.18	0.16	0.17	0.17	0.15	0.11	0.12
MgO	2.74	3.70	4.50	3.39	3.18	3.68	3.74	3.56
CaO	5.92	8.46	8.11	7.30	7.25	7.84	7.03	6.95
Na2O	3.90	3.61	3.65	3.75	3.79	3.63	3.82	3.66
K2O	1.96	1.13	1.34	1.48	1.53	1.35	1.88	2.01
P2O5	0.27	0.32	0.28	0.29	0.28	0.26	0.41	0.31
LOI	0.23	0.47	-0.20	-0.13	0.23	-0.33	0.10	0.97
Total	100.06	100.03	99.74	99.28	100.03	98.81	99.76	100.46
CIPW norm								
Q	13.96	5.83	5.73	9.56	9.85	6.95	6.94	8.33
or	11.58	6.68	7.92	8.75	9.04	7.98	11.11	11.88
ab	33	30.55	30.89	31.73	32.07	30.72	32.32	30.97
an	40.82	50.23	47.07	45.53	45.42	48.06	43.72	44.59
di	3.98	7.45	8.93	6.41	6.14	7.21	5.81	6.18
hy	10.54	13.3	14.28	12.05	11.7	13.21	13.3	12.59
ol	-	-	-	-	-	-	-	-
mt	1.77	2.33	2.25	2.04	2.04	2.29	2.15	2.09
il	1.14	1.25	1.25	1.16	1.1	1.18	1.42	1.27
ap	0.63	0.74	0.65	0.67	0.65	0.6	0.95	0.72
Cr ppm	31	25	77	40	26	23	48	43
Ni	21	18	37	21	15	17	26	22
Rb	41	24	29	34	32	28	50	51
Ba	578	392	458	517	528	404	528	533
Sr	820	1024	883	922	897	862	960	884
La	20	18	21	22	24	17	22	22
Ce	36	44	29	41	37	35	40	45
Nd	21	21	18	21	19	22	25	19
Y	11	14	13	13	13	14	13	14
Zr	98	81	90	103	103	89	111	115
Nb	8	6	9	8	8	8	8	8
Pb	11	5	8	9	10	8	11	10
Th	3	2	1	4	1	1	1	3
V	110	134	146	130	124	144	135	139
Ga	17	20	20	18	20	21	20	20
Zn	55	71	69	67	64	71	57	68
K/Rb	399	394	386	366	399	406	315	330
K/Ba	28	24	24	24	24	28	30	32
Rb/Sr	0.1	0.0	0.0	0.0	0.0	0.0	0.1	0.1
Rb/Ba	0.1	0.1	0.1	0.1	0.1	0.1	0.1	0.1
Ba/Sr	0.7	0.4	0.5	0.6	0.6	0.5	0.6	0.6
Zr/Nb	12.3	13.5	10.0	12.9	12.9	14.8	13.9	14.4
Zr/Y	8.9	5.8	6.9	7.9	7.9	6.4	8.5	8.2
FeO*/MgO	1.89	1.84	1.46	1.76	1.87	1.81	1.68	1.72
Mg# (x100)	55	55	61	56	55	56	57	57

Total Fe as Fe2O3. CIPW norms calculated using Fe2O3/FeO = 0.3.

Appendix 4-2. Whole-rock analyses of CMVA lavas.

Lab. #	21871	21880	21861	21855	21830	21874	21856	21878
Sample #	MAM48	MAM57	MAM32	BUT28	BUT1	BUT51	BEN29	CAB55
Analysis #	33	34	35	36	37	38	39	40
SiO2 wt%	58.50	58.86	60.09	51.37	52.68	52.84	54.46	56.71
TiO2	0.71	0.58	0.60	0.82	0.78	0.88	0.68	0.62
Al2O3	17.95	15.93	17.34	18.29	18.57	17.20	18.46	17.10
Fe2O3	6.83	6.10	6.29	9.87	9.38	8.17	8.41	7.84
MnO	0.12	0.11	0.13	0.14	0.14	0.17	0.14	0.15
MgO	3.26	4.30	3.20	5.65	5.02	6.00	4.16	4.53
CaO	6.39	6.95	6.75	9.20	9.42	9.09	8.84	8.11
Na2O	3.97	3.37	3.84	2.99	3.10	3.44	3.08	3.15
K2O	1.84	2.80	1.95	0.96	1.10	1.51	1.26	1.44
P2O5	0.30	0.33	0.31	0.22	0.25	0.43	0.29	0.20
LOI	-0.30	0.00	-0.03	-0.13	-0.46	-0.17	0.17	0.07
Total	99.57	99.33	100.47	99.38	99.98	99.56	99.95	99.92
CIPW norm								
Q	8.46	8.03	10.59	0.51	1.63	0	5.45	7.93
or	10.87	16.55	11.52	5.67	6.5	8.92	7.45	8.51
ab	33.59	28.52	32.49	25.3	26.23	29.11	26.06	26.65
an	43.37	41.31	42.81	57.08	56.09	48.15	55.74	51.47
di	3.3	9.96	5.87	8.64	9.51	12.38	7.51	8.72
hy	13.23	11.97	11.42	19.85	17.38	15.05	15.26	15.09
ol	-	-	-	-	-	-	-	-
mt	2.1	1.88	1.94	3.04	2.89	2.52	2.6	2.42
il	1.35	1.1	1.14	1.56	1.48	1.67	1.29	1.18
ap	0.7	0.76	0.72	0.51	0.58	1	0.67	0.46
Cr ppm	27	120	42	101	25	118	29	62
Ni	19	36	20	42	23	70	22	29
Rb	36	77	53	13	18	25	21	29
Ba	571	569	547	320	258	432	310	374
Sr	864	803	866	822	768	961	768	597
La	22	23	23	13	8	24	10	11
Ce	41	42	44	15	16	45	17	20
Nd	22	23	21	14	16	21	16	15
Y	13	14	13	19	17	14	16	17
Zr	111	126	108	32	31	112	40	50
Nb	9	8	8	3	4	8	4	3
Pb	15	11	12	8	10	9	8	10
Th	3	1	2	1	1	2	1	1
V	136	154	127	220	224	191	190	200
Ga	20	18	21	23	18	20	21	16
Zn	63	58	63	76	66	66	69	68
K/Rb	427	305	305	619	507	505	502	415
K/Ba	27	41	30	25	35	29	34	32
Rb/Sr	0.0	0.1	0.1	0.0	0.0	0.0	0.0	0.0
Rb/Ba	0.1	0.1	0.1	0.0	0.1	0.1	0.1	0.1
Ba/Sr	0.7	0.7	0.6	0.4	0.3	0.4	0.4	0.6
Zr/Nb	12.3	15.8	13.5	10.7	7.8	14.0	10.0	16.7
Zr/Y	8.5	9.0	8.3	1.7	1.8	8.0	2.5	2.9
FeO*/MgO	1.89	1.28	1.77	1.57	1.68	1.23	1.82	1.56
Mg# (x100)	55	64	56	59	57	65	55	59

Total Fe as Fe2O3. CIPW norms calculated using Fe2O3/FeO = 0.3.

Appendix 4-2. Whole-rock analyses of CMVA lavas.

Lab. #	21859	21858	21875	21860	21877	21857	21876	21879
Sample #	BEN312	BEN31	BUT52	BEN315	BUT54	BEN30	GIN53	GIN56
Analysis #	41	42	43	44	45	46	47	48
SiO2 wt%	57.83	58.04	60.19	61.94	62.20	62.44	57.55	58.25
TiO2	0.50	0.50	0.50	0.45	0.49	0.49	0.64	0.58
Al2O3	15.94	16.07	18.01	17.73	16.91	16.85	18.12	18.29
Fe2O3	6.81	6.91	6.46	5.36	5.84	5.80	7.40	7.05
MnO	0.15	0.16	0.14	0.18	0.11	0.12	0.13	0.12
MgO	4.70	4.74	2.50	2.00	1.57	2.12	3.82	3.42
CaO	7.70	7.74	5.71	5.39	5.62	5.97	7.46	7.21
Na2O	3.34	3.38	3.79	4.69	3.76	3.93	3.55	3.63
K2O	1.86	1.84	2.05	1.97	1.95	1.93	1.27	1.16
P2O5	0.19	0.18	0.30	0.30	0.15	0.16	0.31	0.26
LOI	0.57	0.73	0.34	-0.10	0.53	0.20	-0.07	-0.27
Total	99.59	100.29	99.99	99.91	99.13	100.01	100.18	99.70
CIPW norm								
Q	8.08	7.91	12.19	11.58	16.92	15.27	8.94	10.44
or	10.99	10.87	12.12	11.64	11.52	11.41	7.51	6.86
ab	28.26	28.6	32.07	39.69	31.82	33.25	30.04	30.72
an	44.88	44.83	44.85	35.15	42.49	40.5	49.77	49.57
di	11.36	11.39	0.24	2.72	2.85	4.93	4.29	3.2
hy	13.29	13.51	12.82	9.26	8.45	8.77	14.91	14.15
ol	-	-	-	-	-	-	-	-
mt	2.1	2.13	1.99	1.65	1.8	1.78	2.28	2.17
il	0.95	0.95	0.95	0.85	0.93	0.93	1.22	1.1
ap	0.44	0.42	0.7	0.7	0.35	0.37	0.72	0.6
Cr ppm	164	167	5	5	15	14	38	37
Ni	42	42	7	3	9	11	26	19
Rb	32	30	38	34	39	41	21	20
Ba	436	424	498	537	578	570	388	377
Sr	668	672	720	778	650	641	913	825
La	14	11	12	14	17	13	12	10
Ce	21	24	21	33	26	26	22	24
Nd	10	12	17	17	15	16	12	15
Y	17	16	17	19	17	15	14	12
Zr	58	59	76	86	73	72	58	56
Nb	5	5	4	5	5	6	5	4
Pb	12	13	12	16	12	13	8	12
Th	1	1	1	1	1	2	1	1
V	158	157	109	62	133	142	145	143
Ga	16	20	20	21	17	17	18	21
Zn	70	69	57	80	62	58	66	61
K/Rb	490	515	452	483	270	393	502	486
K/Ba	36	36	35	31	18	28	27	26
Rb/Sr	0.0	0.0	0.1	0.0	0.1	0.1	0.0	0.0
Rb/Ba	0.1	0.1	0.1	0.1	0.1	0.1	0.1	0.1
Ba/Sr	0.7	0.6	0.7	0.7	0.9	0.9	0.4	0.5
Zr/Nb	11.6	11.8	19.0	17.2	14.6	12.0	11.6	14.0
Zr/Y	3.4	3.7	4.5	4.5	4.3	4.8	4.1	4.7
FeO*/MgO	1.30	1.31	2.33	2.41	3.35	2.46	1.74	1.86
Mg# (x100)	63	63	49	48	40	48	56	55

Total Fe as Fe2O3. CIPW norms calculated using Fe2O3/FeO = 0.3.

Appendix 4-2. Whole-rock analyses of CMVA lavas.

Lab. #	21854	21853	21883	21852	23240	23237	23238	23242
Sample #	GIN27	GIN265	CAM275	GIN26	BAL9	BAL2	BAL3	BAL11
Analysis #	49	50	51	52	53	54	55	56
SiO2 wt%	58.58	58.89	59.40	61.40	48.24	48.71	49.17	50.50
TiO2	0.59	0.58	0.59	0.48	0.95	0.90	0.87	0.91
Al2O3	18.42	18.33	17.85	17.93	19.32	18.90	18.40	18.25
Fe2O3	7.03	7.05	6.65	6.05	10.30	11.12	9.91	9.83
MnO	0.13	0.15	0.11	0.10	0.18	0.19	0.18	0.18
MgO	3.46	3.40	3.32	2.63	4.63	5.60	5.11	5.22
CaO	6.82	7.16	6.72	6.10	11.02	10.85	11.11	10.09
Na2O	3.54	3.63	3.71	3.67	2.79	2.84	2.51	3.05
K2O	1.20	1.19	1.59	1.33	1.55	0.98	1.48	1.51
P2O5	0.27	0.26	0.29	0.23	0.28	0.23	0.30	0.33
LOI	0.23	-0.24	-0.60	0.51	0.61	-0.23	0.60	0.00
Total	100.27	100.40	99.63	100.43	99.87	100.09	99.64	99.87
CIPW norm								
Q	11.38	11.02	11.03	15.84	0	0	0	0
or	7.09	7.03	9.4	7.86	9.16	5.91	8.86	8.92
ab	29.95	30.72	31.39	31.05	23.2	24.2	22.09	25.81
an	50.72	49.58	46.57	47.88	60.56	59.65	60.89	55.08
di	1.02	2.98	3.36	0.19	14.09	13.66	15.94	13.23
hy	15.29	14.26	13.33	12.66	0	5.05	7.08	8.75
ol	-	-	-	-	9.32	8.26	4.37	4.06
mt	2.16	2.17	2.04	1.87	4.48	4.89	4.38	4.28
il	1.12	1.1	1.12	0.91	1.8	1.82	1.69	1.73
ap	0.63	0.6	0.67	0.53	0.65	0.53	0.7	0.76
Cr ppm	39	39	39	26	9	43	34	38
Ni	20	21	19	16	18	27	31	22
Rb	20	21	34	25	28	15	23	20
Ba	395	399	463	448	250	176	250	657
Sr	790	826	825	777	756	708	729	717
La	17	12	18	11	6	7	8	12
Ce	21	21	32	24	8	11	10	20
Nd	11	18	14	20	45	39	41	45
Y	20	14	17	13	15	16	17	19
Zr	54	53	79	63	38	46	42	70
Nb	4	5	6	5	5	4	5	6
Pb	9	13	14	13	12	12	10	10
Th	1	1	1	1	2	0.1	0.1	3
V	151	145	138	111	339	316	317	243
Ga	21	17	20	18	11	15	14	17
Zn	64	65	62	57	66	70	73	60
K/Rb	502	470	388	445	465	548	541	631
K/Ba	25	25	29	25	52	47	50	19
Rb/Sr	0.0	0.0	0.0	0.0	0.0	0.0	0.0	0.0
Rb/Ba	0.1	0.1	0.1	0.1	0.1	0.1	0.1	0.0
Ba/Sr	0.5	0.5	0.6	0.6	0.3	0.2	0.3	0.9
Zr/Nb	13.5	10.6	13.2	12.6	7.6	11.5	8.4	11.7
Zr/Y	2.7	3.8	4.6	4.8	2.5	2.9	2.5	3.7
FeO*/MgO	1.83	1.87	1.80	2.07	2.00	1.81	1.77	1.69
Mg# (x100)	55	55	56	52	53	56	56	57

Total Fe as Fe2O3. CIPW norms calculated using Fe2O3/FeO = 0.3.

Appendix 4-2. Whole-rock analyses of CMVA lavas.

Lab. #	23239	23241	23243	23244	23247	23254	23246	23251
Sample #	BAL4	BAL10	BAL12	BIN1A	BIN2B	BIN9	BIN2A	BIN6
Analysis #	57	58	59	60	61	62	63	64
SiO2 wt%	52.50	56.84	59.58	50.33	52.40	52.59	54.09	54.14
TiO2	0.90	0.68	0.49	0.82	0.85	0.83	0.99	1.05
Al2O3	20.07	17.42	18.39	20.87	19.89	20.17	16.94	17.37
Fe2O3	8.08	7.15	5.12	8.53	8.23	7.99	9.61	9.79
MnO	0.13	0.13	0.13	0.16	0.14	0.12	0.22	0.20
MgO	2.90	2.86	1.64	3.50	3.01	2.88	3.11	3.31
CaO	9.38	6.88	5.65	10.24	9.28	9.36	7.09	7.05
Na2O	3.36	3.74	3.57	2.96	3.34	3.41	4.15	4.04
K2O	2.22	2.46	3.79	2.47	2.24	2.29	2.65	2.55
P2O5	0.44	0.32	0.35	0.42	0.42	0.41	0.59	0.57
LOI	0.47	0.03	0.70	0.00	0.14	0.37	0.30	-0.34
Total	100.45	98.51	99.41	100.30	99.94	100.42	99.74	99.73
CIPW norm								
Q	0.77	6.86	9.48	0	0.62	0.34	0.72	1.07
or	13.12	14.54	22.4	14.6	13.24	13.53	15.66	15.07
ab	28.43	31.65	30.21	25.05	28.26	28.85	35.12	34.19
an	53.81	42.59	43.19	59.22	53.61	53.33	36.02	38.86
di	8.67	7.03	2.3	9.59	8.75	8.88	9.55	7.85
hy	9.05	9.29	7.03	0.11	9.53	8.91	10.53	11.9
ol	-	-	-	7.76	-	-	-	-
mt	3.51	3.11	2.23	3.71	3.58	3.48	4.18	4.26
il	1.71	1.29	0.93	1.56	1.61	1.58	1.88	1.99
ap	1.02	0.74	0.81	0.97	0.97	0.95	1.37	1.32
Cr ppm	11	17	8	13	6	11	11	8
Ni	13	11	5	13	5	13	13	10
Rb	31	53	89	58	42	39	36	36
Ba	346	912	521	262	733	330	336	414
Sr	729	635	573	608	734	726	733	664
La	10	16	15	8	14	11	10	14
Ce	16	23	23	10	27	17	12	34
Nd	46	46	52	46	50	42	43	39
Y	19	17	19	18	28	19	20	29
Zr	64	101	114	46	89	62	66	91
Nb	5	6	7	5	5	5	6	7
Pb	12	14	13	8	13	12	14	15
Th	1	4	3	3	3	5	3	5
V	220	172	88	274	223	221	213	238
Ga	15	17	17	19	17	19	19	20
Zn	71	63	57	68	92	68	77	87
K/Rb	597	393	360	355	447	490	620	593
K/Ba	54	23	62	79	26	58	66	52
Rb/Sr	0.0	0.1	0.2	0.1	0.1	0.1	0.0	0.1
Rb/Ba	0.1	0.1	0.2	0.2	0.1	0.1	0.1	0.1
Ba/Sr	0.5	1.4	0.9	0.4	1.0	0.5	0.5	0.6
Zr/Nb	12.8	16.8	16.3	9.2	17.8	12.4	11.0	13.0
Zr/Y	3.4	5.9	6.0	2.6	3.2	3.3	3.3	3.1
FeO*/MgO	2.51	2.25	2.81	2.19	2.46	2.50	2.78	2.66
Mg# (x100)	47	50	45	51	48	48	45	46

Total Fe as Fe2O3. CIPW norms calculated using Fe2O3/FeO = 0.3.

Appendix 4-2. Whole-rock analyses of CMVA lavas.

Lab. #	23245	23253	23248	23250	23249	23255	23257	23256
Sample #	BIN1B	BIN8	BIN3	BIN5	BIN4	LUM1	ILI1B	ILI1A
Analysis #	65	66	67	68	69	70	71	72
SiO2 wt%	54.74	55.12	56.67	57.20	57.89	55.46	51.41	51.82
TiO2	1.00	0.98	0.77	0.97	0.98	0.97	0.83	0.81
Al2O3	16.96	16.97	17.39	16.81	16.92	18.02	16.51	15.59
Fe2O3	9.59	9.34	7.13	8.08	8.13	8.26	10.15	9.66
MnO	0.19	0.16	0.16	0.20	0.18	0.14	0.16	0.14
MgO	3.14	3.04	2.29	2.47	1.99	3.14	6.70	6.89
CaO	6.93	6.94	5.56	5.49	5.41	7.48	10.20	11.13
Na2O	3.95	4.04	4.17	4.56	4.63	3.75	2.99	2.91
K2O	2.69	2.63	3.78	3.08	3.13	2.37	0.49	0.59
P2O5	0.57	0.56	0.39	0.58	0.59	0.34	0.15	0.15
LOI	0.34	0.14	0.56	-0.20	0.47	0.00	0.33	0.63
Total	100.10	99.92	98.87	99.24	100.32	99.93	99.92	100.32
CIPW norm								
Q	2.34	0.94	2.82	3.84	4.86	4.08	1.21	1.15
or	15.9	15.54	22.34	18.2	18.56	14.01	2.9	3.49
ab	33.42	34.19	35.29	38.59	39.09	31.73	25.3	24.62
an	38.14	45.54	33.24	29.7	29.56	44.4	54.4	52.97
di	8.3	1.8	6.17	5.91	5.51	7.84	15.73	21.39
hy	11.13	13.85	8.16	9.34	8.39	10.13	17.23	14.53
ol	-	-	-	-	-	-	-	-
mt	4.17	4.06	3.1	3.51	3.55	3.59	4.41	4.2
il	1.9	1.86	1.46	1.84	1.9	1.84	1.58	1.54
ap	1.32	1.3	0.9	1.34	1.39	0.79	0.35	0.35
Cr ppm	7	7	8	7	7	21	142	193
Ni	9	7	5	4	5	16	76	85
Rb	45	39	69	52	56	53	8	10
Ba	382	414	496	457	481	414	103	90
Sr	639	667	534	600	614	539	512	521
La	14	16	12	15	16	11	10	6
Ce	29	28	29	28	31	27	5	5
Nd	43	42	41	46	46	42	35	38
Y	30	28	27	31	34	24	20	18
Zr	87	90	97	107	110	103	63	63
Nb	5	7	6	7	7	6	5	5
Pb	15	19	18	18	16	11	10	9
Th	2	0.1	4	0.1	3	2	2	5
V	220	225	153	140	144	218	259	236
Ga	14	20	14	16	15	22	14	16
Zn	91	84	82	87	87	69	75	72
K/Rb	502	549	466	498	467	374	519	498
K/Ba	59	52	65	57	54	48	40	55
Rb/Sr	0.1	0.1	0.1	0.1	0.1	0.1	0.0	0.0
Rb/Ba	0.1	0.1	0.1	0.1	0.1	0.1	0.1	0.1
Ba/Sr	0.6	0.6	0.9	0.8	0.8	0.8	0.2	0.2
Zr/Nb	17.4	12.9	16.2	15.3	15.7	17.2	12.6	12.6
Zr/Y	2.9	3.2	3.6	3.5	3.2	4.3	3.2	3.5
FeO*/MgO	2.75	2.77	2.80	2.94	3.69	2.37	1.36	1.26
Mg# (x100)	45	45	45	43	38	49	62	64

Total Fe as Fe2O3. CIPW norms calculated using Fe2O3/FeO = 0.3.

Appendix 4-2. Whole-rock analyses of CMVA lavas.

Lab. #	23258	23259	23264	23261	23263	23262	23260	23270
Sample #	BALi3	BAL4	BUT6	KAL8	QUE7	MUS15	KAT9	MAR5
Analysis #	73	74	75	76	77	78	79	80
SiO2 wt%	52.00	52.54	52.01	54.11	54.27	55.67	64.00	53.10
TiO2	0.86	0.83	1.10	1.00	0.83	0.74	0.58	0.84
At2O3	15.65	15.25	16.58	16.93	16.49	16.73	16.84	19.01
Fe2O3	9.86	10.03	10.30	8.24	7.91	7.69	4.36	9.85
MnO	0.16	0.17	0.16	0.14	0.13	0.14	0.09	0.19
MgO	7.49	7.71	7.45	4.65	7.76	6.07	2.18	4.12
CaO	10.18	10.40	8.59	7.34	7.63	7.25	4.39	7.48
Na2O	3.10	3.04	3.16	3.63	3.43	3.27	4.09	3.39
K2O	0.56	0.62	0.46	2.76	1.29	1.37	2.80	1.62
P2O5	0.15	0.16	0.15	0.61	0.24	0.27	0.26	0.40
LOI	-0.06	-0.26	0.43	0.17	0.41	0.86	0.71	0.38
Total	99.95	100.49	100.39	99.58	100.39	100.06	100.30	100.38
CIPW norm								
Q	0.26	0.64	1.98	1.02	1.65	6.41	16.29	3.1
or	3.37	3.72	2.78	16.31	7.62	8.1	16.55	9.57
ab	26.57	26.06	26.65	30.72	29.02	27.67	34.61	28.69
an	50.64	50.29	52.71	41.46	47.05	49.32	35.83	52.63
di	18.31	19.65	9.66	8.66	8.4	5.86	0.62	2.15
hy	17.92	17.83	22.08	13.48	21.37	18.33	8.3	17.12
ol	-	-	-	-	-	-	-	-
mt	4.3	4.37	4.66	3.58	3.44	3.34	1.9	4.28
il	1.56	1.61	2.13	1.9	1.58	1.41	1.1	1.6
ap	0.35	0.37	0.35	1.41	0.56	0.63	0.6	0.93
Cr ppm	169	192	216	104	280	233	30	11
Ni	78	78	114	53	162	87	20	19
Rb	10	11	7	86	30	25	102	21
Ba	100	114	61	392	238	305	345	471
Sr	495	472	306	487	454	441	497	663
La	7	7	9	16	9	8	16	14
Ce	6	5	9	43	16	18	40	20
Nd	37	38	36	49	41	45	52	41
Y	15	16	22	28	17	21	25	21
Zr	56	66	81	163	83	101	184	67
Nb	4	5	6	10	10	6	9	4
Pb	10	10	7	12	7	9	15	9
Th	0.1	4	1	3	4	3	8	3
V	212	233	165	207	172	172	82	197
Ga	15	18	19	20	15	16	16	16
Zn	67	68	86	78	63	68	46	74
K/Rb	465	468	557	269	360	462	229	652
K/Ba	46	45	64	59	45	38	68	29
Rb/Sr	0.0	0.0	0.0	0.2	0.1	0.1	0.2	0.0
Rb/Ba	0.1	0.1	0.1	0.2	0.1	0.1	0.3	0.0
Ba/Sr	0.2	0.2	0.2	0.8	0.5	0.7	0.7	0.7
Zr/Nb	14.0	13.2	13.5	16.3	8.3	16.8	20.4	16.8
Zr/Y	3.7	4.1	3.7	5.8	4.9	4.8	7.4	3.2
FeO*/MgO	1.19	1.17	1.29	1.59	0.92	1.14	1.80	2.15
Mg# (x100)	66	66	65	59	71	67	56	51

Total Fe as Fe2O3. CIPW norms calculated using Fe2O3/FeO = 0.3.

Appendix 4-2. Whole-rock analyses of CMVA lavas.

Lab. #	23271	23269	23278	23274	23273	23277	23275	23279
Sample #	MAR6	MAR4	APO7	APO3	APO2	APO6	APO4	APO8
Analysis #	81	82	83	84	85	86	87	88
SiO2 wt%	54.28	55.59	59.87	60.17	61.60	62.23	62.90	63.87
TiO2	0.74	0.90	0.66	0.68	0.62	0.50	0.60	0.58
Al2O3	19.20	17.11	17.93	16.58	16.65	15.73	16.24	16.14
Fe2O3	8.85	7.50	6.29	6.16	5.35	4.39	5.19	4.86
MnO	0.18	0.11	0.11	0.15	0.12	0.10	0.12	0.10
MgO	3.34	3.54	2.07	3.15	2.62	2.20	2.34	1.83
CaO	8.06	7.14	5.28	5.98	5.42	5.17	5.29	4.63
Na2O	3.32	3.65	3.73	3.47	3.64	2.66	3.63	3.65
K2O	1.72	3.63	2.70	2.81	2.91	3.39	3.26	3.41
P2O5	0.41	0.33	0.28	0.20	0.20	0.18	0.21	0.19
LOI	0.20	-0.03	0.76	0.54	0.56	2.23	-0.20	0.63
Total	100.30	99.47	99.68	99.89	99.69	98.78	99.58	99.89
CIPW norm								
Q	5.09	1.25	12.06	11.63	13.96	19.16	14.68	16.71
or	10.16	21.45	15.96	16.61	17.32	20.03	19.27	20.15
ab	28.09	30.89	31.56	29.36	31.22	22.51	30.72	30.89
an	53.57	38.8	43.41	42.12	39.46	48.23	37.45	36.28
di	4.03	11.15	0.13	5.69	4.34	2.85	5.29	3.4
hy	13.49	8.91	9.92	9.83	8.56	7.44	7.19	6.53
ol	-	-	-	-	-	-	-	-
mt	3.85	3.26	2.74	2.68	2.33	1.91	2.26	2.11
il	1.41	1.71	1.25	1.29	1.14	0.95	1.14	1.1
ap	0.95	0.76	0.65	0.46	0.46	0.42	0.49	0.44
Cr ppm	13	36	11	36	22	19	15	19
Ni	19	18	9	27	14	12	11	11
Rb	34	75	47	57	60	109	70	76
Ba	446	280	435	498	527	785	570	570
Sr	759	465	549	448	496	490	497	441
La	13	15	18	12	12	11	12	12
Ce	18	26	30	23	19	18	15	22
Nd	44	48	45	47	43	47	45	45
Y	19	26	29	22	15	16	16	17
Zr	77	180	125	99	120	114	118	119
Nb	7	7	6	6	6	7	7	8
Pb	10	14	12	9	12	13	12	10
Th	0.1	5	4	3	6	3	7	4
V	151	177	151	159	133	99	121	98
Ga	15	19	19	17	17	10	15	13
Zn	82	60	62	70	52	47	49	49
K/Rb	422	406	484	414	408	268	389	377
K/Ba	32	109	52	47	46	37	48	50
Rb/Sr	0.0	0.2	0.1	0.1	0.1	0.2	0.1	0.2
Rb/Ba	0.1	0.3	0.1	0.1	0.1	0.1	0.1	0.1
Ba/Sr	0.6	0.6	0.8	1.1	1.1	1.6	1.1	1.3
Zr/Nb	11.0	25.7	20.8	16.5	20.0	16.3	16.9	14.9
Zr/Y	4.1	6.9	4.3	4.5	8.0	7.1	7.4	7.0
FeO*/MgO	2.38	1.91	2.73	1.76	1.84	1.80	2.00	2.39
Mg# (x100)	49	54	45	56	55	56	53	49

Total Fe as Fe2O3. CIPW norms calculated using Fe2O3/FeO = 0.3.

Appendix 4-2. Whole-rock analyses of CMVA lavas.

Lab. #	23276	23272
Sample #	APO5	APO1
Analysis #	89	90
SiO2 wt%	64.31	64.91
TiO2	0.51	0.47
Al2O3	16.14	15.82
Fe2O3	4.67	4.19
MnO	0.10	0.1
MgO	1.85	1.88
CaO	4.75	4.37
Na2O	3.64	3.71
K2O	3.39	3.47
P2O5	0.18	0.15
LOI	0.30	1.22
Total	99.84	100.29
CIPW norm		
Q	17.11	17.8
or	20.03	20.51
ab	30.8	31.39
an	36.48	34.13
di	3.86	3.62
hy	6.3	6.13
ol	-	-
mt	2.03	1.82
il	0.97	0.89
ap	0.42	0.35
Cr ppm	18	16
Ni	10	11
Rb	75	76
Ba	567	600
Sr	455	430
La	13	10
Ce	21	14
Nd	43	47
Y	16	15
Zr	118	122
Nb	6	7
Pb	11	15
Th	6	6
V	114	91
Ga	17	17
Zn	46	45
K/Rb	379	379
K/Ba	50	48
Rb/Sr	0.2	0.2
Rb/Ba	0.1	0.1
Ba/Sr	1.2	1.4
Zr/Nb	19.7	17.4
Zr/Y	7.4	8.1
FeO*/MgO	2.27	1.98
Mg# (x100)	50	53

Total Fe as Fe2O3. CIPW norms calculated using Fe2O3/FeO = 0.3.

APPENDIX 5 CRYSTALLISING CONDITIONS

Conditions at which crystals equilibrated with host melts are summarised in Table 5-1 (Chapter 5). Magmatic temperatures, pressures and H_2O contents were calculated using phenocryst core and bulk-rock compositions thus giving parameters at the time of crystallisation.

5.1. BACKGROUND AND THEORY

5.1.1. TEMPERATURE

The basaltic phenocryst assemblage olivine + plagioclase + clinopyroxene + magnetite allows the use of olivine-liquid geothermometry. For andesites and dacites, hornblende-plagioclase equilibria define magmatic temperature. Two-pyroxene thermometry is applicable only for central Camiguin Island owing to lack of equilibrium between mineral and melt in other localities.

The logarithm ratio of FeO, MgO and MnO between olivine and liquid varies linearly with temperature in the range of basaltic compositions (Roeder and Emslie, 1970). Using FeO_{ol}/FeO_{liq} and MgO_{ol}/MgO_{liq} ratios (Roeder and Emslie, 1970; Roeder, 1974; Bender, 1978) yields temperature between 1,090^{o} to 1,161^{o}C. The distribution coefficient for selected analyses varies from 0.28 to 0.36, which are within the range of K_D values (O.26 - 0.36) used to calibrate the olivine-liquid geothermometer. Barton and Wyers (1991) ascribed an uncertainty of ± 50^{o}C to this method. Application of the modified Evans-Frost olivine - spinel geothermometer (Fabries, 1979; Fisk and Bence, 1980) to Butong basalt (sample BUT6, analysis 75, Appendix 4) yields 1,123^{o}C, in general agreement with the olivine-liquid thermometer.

The hornblende-plagioclase geothermometer of Blundy and Holland (1990) calculates temperatures up to 1,100^{o}C for andesites whereas dacites have

equilibration temperatures around 1,050°C. These values are probably accurate because mean temperature calculated independently using olivine-liquid equilibria for a hornblende andesite (analysis 6, Table 3-2) is similar (1,030°C) to estimates for the same rock. The uncertainty of the hornblende-plagioclase geothermometer is ± 75°C. Crystallising temperatures of dacites can be further verifed using the mica geothermometer of Luhr and Carmichael (1980) because biotite is abundant in Mt. Apo. Assuming total FeO = FeO^*, temperatures vary from 1,031°C to 946°C, with an uncertainty of ± 23°C. The lower temperatures assigned to dacites probably reflect higher water contents than basic lavas.

5.1.2. P_{TOTAL}, P_{H2O} AND H_2O CONTENTS

Pressure of crystallisation (P_{TOTAL}) can be estimated using two methods assuming equilibrium between phase assemblages. Method 1 uses standard-state thermochemical data and activity-composition relations between olivine, clinopyroxene and plagioclase to derive SiO_2 activity (α_{SiO2}) and P_{TOTAL} for mafic lavas. Method 2 uses Al contents in hornblende, appropriate for acid andesites and dacites.

Assuming equilibrium between olivine and pyroxene, α_{SiO2} in the melt can be determined from the reactions:

$$Mg_2SiO_{4(Ol)} + SiO_{2(melt)} = Mg_2Si_2O_{6(En)} \quad \text{(Nicholls et al, 1971) (1)}$$

$$CaAlSiAlO_{6(CaTs)} + SiO_{2(melt)} = CaAl_2Si_2O_{8(An)} \quad \text{Wood (1976) (2)}$$

where En is enstatite, CaTs is Ca-Tschermak's molecule and An is anorthite. The thermodynamic equations for Gibbs energy change for the above reactions are:

$$\Delta G/RT = \Delta G^o/RT - \ln \alpha_{SiO2} - \ln \alpha\, Mg_2SiO_4 + \ln \alpha\, Mg_2SiO_{6(px)} \quad (3)$$

$$\Delta G/RT = \Delta G^o/RT - \ln \alpha_{SiO2} - \ln \alpha\, CaAlSiAlO_{6(CaTs)} + \ln \alpha\, CaAl_2Si_2O_{8(An)} \quad (4)$$

where ΔG^0 is the standard Gibbs energy of reaction, R is the gas constant and T is temperature (^{0}K). Since at equilibrium $\Delta G/RT = 0$, α_{SiO2} in the melt can be expressed in two independent equations:

$$\ln \alpha_{SiO2} = \Delta G^0/RT + \ln \alpha\, Mg_2SiO_{6(px)} - \ln \alpha\, Mg_2SiO_{4(Ol)} \quad (5)$$

$$\ln \alpha_{SiO2} = \Delta G^0/RT + \ln \alpha\, CaAl_2Si_2O_{8(An)} - \ln \alpha\, CaAlSiAlO_{6(CaTs)} \quad (6)$$

If $\Delta G^0/RT$ and mineral compositions for each reaction are known, equations (5) and (6) can be solved simultaneously for unique values of PTOTAL, using temperature obtained from olivine-liquid geothermometry. For reaction (5) α_{SiO2} was defined in the equivalent form:

$$\log \alpha_{SiO2} = \log K + \log [\alpha\, Mg_2SiO_{6(px)} / \alpha\, Mg_2SiO_4](Ol)$$

De Paolo (1979) (7)

where $$\log K = \frac{A}{T} + B + \frac{C}{T}(P-1) + \frac{D}{T}(P-1)$$

Nicholls and Carmichael (1972)

and A, B, C and D are constants.

For reaction (6):

$$\Delta G^0 = 44530 + 6.30T - 1.456P$$

Gasparik and Lindsley (1980). (8)

It is sufficient to treat the olivine solid solution as ideal, $\alpha Mg_2SiO_4 = (X_{mg})^2$, where (X_{mg}) = Mg/Mg + Fe^{2+} (Ghiorso and Carmichael, 1980). $CaAl_2Si_2O_8$ and $NaAlSi_3O_8$ in plagioclase also mixes ideally (Kerrick and Darken, 1975) so $\alpha CaAl_2Si2O_{8(An)} = (X_{An})$. Since low Ca-pyroxene is absent in basaltic lavas of CMVA, an approximate activity model must be used for En and CaTs in clinopyroxene.

Expressions for En and CaTs are:

$$\alpha Mg_2Si_2O_6(px) = Mg^2 (Fe^{2+} + Mg + Ca + Na - 1) / (Fe^{2+} + Mg^{2+}) \quad \text{(Nicholls, 1976)} \quad (9)$$

$$\alpha CaAlSiAlO_{6(CaTs)} = 4(X^{M1}_{Ca})^2(X^{M1}_{Al})(X^{T}_{Al})(X^{T}_{Si})$$

(Powell, 1976; Herzberg, 1978) (10)

where superscripts M1, M2 and T are lattice sites.

Substituting mineral activities and constants into equations (5) and (6) and evaluating over different pressures and temperatures gives P_{TOTAL} for basaltic samples H51, BAL4 and BUT6 (Table 5-1, Chapter 5). Uncertainty in olivine-liquid thermometry of ± 50°C results in a pressure uncertainty of ± 1.0 kbar.

$P_{(H2O)}$ was determined independently of P_{TOTAL} using the plagioclase geothermometer of Kudo and Weill (1970), given temperature and compositions of coexisting plagioclase and liquid. $P_{(H2O)}$ values are poorly constrained because plagioclase compositions vary substantially within samples. Estimates are 0.75 - 0.80 kbar for basalts to 1.50 kbar for dacites, with uncertainties of about 0.50 kbar. These values are consistent in that $P_{(H2O)} < P_{TOTAL}$. Assuming $P_{(H2O)} = f_{(H2O)}$ (cf. Barton and Wyers, 1991), the molar fraction of H_2O (X_{H2O}) dissolved in the melt is calculated from the solution model of Nicholls (1980). Finally, X_{H2O} was converted to wt% H_2O using average gram formula weights for each magma. Calculated wt % H_2O are *initial* H_2O contents of the magma. Pre-eruption wt% H_2O can be estimated given total phenocryst modes (representing % of magma crystallised) in Table 3-1 (Chapter 3). Predicted pre-eruption H_2O contents of the groundmass (Table 5-1, Chapter 5) generally increase from basalt to dacite as expected for magmas which evolve in progressively shallower chambers.

5.2. APPLICATIONS: CALCULATION OF T, P AND H_2O CONTENTS

5.2.1. GEOTHERMOMETRY

The following geothermometers were used to calculate magmatic temperatures:

(i) Basalt

(a) Olivine-liquid equilibria (Roeder and Emslie, 1970; Roeder, 1974; Bender, 1978).

(b) Olivine-spinel (Fabries, 1979; Fisk and Bence, 1980)

(ii) Andesite

(c) Hornblende-plagioclase (Blundy and Holland, 1990).

a) Olivine-liquid Geothermometer

To use this geothermometer, there must be evidence of equilibrium between olivine and melt. Initially, petrography should show stability of olivine. Then, evaluate the relation:

$$(FeO/MgO)^{ol}\,(MgO/FeO)^{liq} = 0.3 \qquad \text{(Roeder, 1974)}$$

Table 3-2 can be used to test this relation. The MgO/FeO ratio of bulk rock sample CAM is 1.29. Coexisting olivine has an FeO/MgO ratio of 0.23. Therefore, predicted MgO/FeO of melt in equilibrium with olivine is 0.30/0.23 = 1.30, close to the actual value. The mol% of FeO and MgO in the liquid can then be plotted on Figure 3-12 to give the estimated temperature. In this example, FeO_{liq} and MgO_{liq} is 4.30 and 5.54 respectively, and returns a value of about 1,030°C.

b) Olivine-spinel Geothermometer

This method is based on Mg-Fe^{2+} exchange between olivine and spinel, originally calibrated by Evans and Frost (1975) from high-grade metamorphic rocks

and basalt pumices. Fabries (1979) modified this geothermometer to give the expression:

$$\text{temperature } T(^{o}K) = \frac{(4250\ (Y^{Cr,\ Spinel}) + 1343)}{(\ln K_D^{o} + 1.825\ Y^{Cr,Spinel} + 0.571)}$$

where $Y^{i,Spinel} = (i / Cr + Al + Fe^{3+})$ and

$\ln K_D^{o} = \ln K_D - 4.0(Y^{Fe3+,\ Spinel})$, with

$K_D = (X^{Fe2+} / X_{Mg})_{Spinel}\ (X_{mG}/X^{Fe2+})_{Ol.}$

Substituting values from:

Sample B6583, analysis 11 (olivine), Table A3-2a, Appendix 3-2 and spinel B6562, analysis 1, Table A3-4a, Appendix 3-2 gives $Y^{Cr,Spinel} = 0.39$ and $Y^{Fe3+,\ Spinel} = 0.23$, which gives $T = 1{,}123^{o}C$.

c) Hornblende-Plagioclase Geothermometer

Blundy and Holland (1990) calibrated a thermometer based on the Al^{IV} content of hornblende coexisting with plagioclase in SiO_2-saturated rocks. This method is applicable to rocks which equilibrated in the range 500^{o} - $1{,}100^{o}C$, with an uncertainty of $\pm\ 75^{o}C$. Because volcanic rocks were included in the experimental database, application of the hornblende-plagioclase geothermometer gives reasonable magmatic temperatures. In the case of olivine-bearing hornblende andesite (sample HIB20, analysis 28, Appendix 4), temperatures obtained by this procedure are comparable to values using olivine-liquid equilibria ($1{,}064^{o}C$ and $1{,}024^{o}C$ respectively). The complete formula is:

$$T\ (^{o}K) = (0.677P - 48.98 + Y) / (-0.0429 - 0.008314\ \ln K)$$

where P is pressure (Kbar) and Y is an expression for plagioclase non-ideality, $RT\ln(Y_{ab})$. $Y = 0$ for $X_{ab} > 0.5$ and $Y = -8.06 + 25.5\ (1 - X_{ab})^2$ for $X_{ab} < 0.5$. X_{ab} is the albite component in coexisting plagioclase and $K = [(Si - 4) / (8 - Si)\ (X_{ab})]$ is an

equllibrium constant. Si is the number of atoms pfu in hornblende. Applying these equations to a dacite from Mt Apo using P = 1.6 Kbar, Y = 0 since X_{ab} = 0.56 (plagioclase A6R703, Table A3-1d, Appendix 3-2), Si = 6.945 (hornblende analysis 4, Table A3-5b, Appendix 3-2) gives T (^{o}C) = 1,051.

5.2.2. GEOBAROMETRY

a) Fo-En-SiO_2 and An-CaTs-SiO_2 Equilibria

Solution of equations (5) and (6) is illustrated by using data from a basalt sample BAL4 (see analysis 57, Appendix 4 for bulk compositions):

Clinopyroxene: sample I4043, analysis no. 3, Table A3-3a, Appendix 3-2.
Olivine : sample I4493, analysis no. 2, Table A3-2a.
Plagioclase : sample I46305, Table A3-1a.

The activity of En in clinopyroxene (equation 9) is:

$$\alpha Mg_2Si2O_{6(px)} = Mg^2 (Fe^{2+} + Mg + Ca + Na-1)/(Fe^2 + Mg)^2$$

$$= 0.869^2 (0.237 + 0.869 + 0.789 + 0.023-1)/$$

$$(0.237 + 0.869)^2$$

$$= 0.570.$$

The activity of CaTs in clinopyroxene (equation 10) is:

$$\alpha CaAlSiAlO_{6(CaTs)} = 4(X_{Ca}^{M1}) (X_{Al}^{M1})(X_{Al}^{T})(X_{Si}^{T})$$

$$=4(0.789)(0.061)(0.065)(1.935)$$

$$= 0.024.$$

The activities of Mg_2SiO4 in olivine and $CaAl_2Si_2O_8$ in An are considered ideal:

$$\alpha Mg2SiO4_{(Ol)} = X^2_{Fo} = (0.77)^2 = 0.593 \text{ and}$$

$$\alpha CaAl_2Si_2O_{8\ (An)} = 0.663.$$

For equation (7), T is evaluated at say 1,273^{o}K and 3000 bars to give:

$$\log K = (A/T) + B + (C/T)(P-1) + (D/T)(P-1)^2$$

$= -1034/1273 + 0.597 + (-0.0416/1273)(2999) + (9.17E\text{-}8/1273)(2999)^2$

$= 0.332.$

Therefore, $\log \alpha_{SiO2} = -0.314 + \log (.570/.593)$

$= -0.332.$

For equation (8) at the same temperature and pressure:

$\Delta G^0 = -(44530 + 6.30T - 1.456P)$

$= -4.552$

Substituting in equation (6) using the activities of CaTs and An gives $\log \alpha_{SiO2} = -0.514$. The above procedure is repeated for varying temperature and pressure and the results are shown in Table A5-1 and Figure A5-1. Intersection of 2 sets of curves defines a line which satisfies both equilibria. At a defined temperature is a unique pressure which represents P_{TOTAL} at the start of crystallisation.

Table A5-1. Sample calculation of P_{TOTAL}

Sample BAL4

Clinopyroxene: sample I4043, analysis no. 3, Table A3-3a, Appendix 3-2.
Olivine : sample I4493, analysis no. 2, Table A3-2a.
Plagioclase : sample I46305, Table A3-1a.

	Log Activities		Site occupancies in clinopyroxene						
αSiO_2	Xmg	Xfe	Xca^{M2}	Xna	Xal^{M1}	Xal^{T}	Xsi^{T}	mg^{px}	mg^{ol}
-0.332	0.869	0.237	0.789	0.023	0.061	0.065	1.935	0.57	0.77
-0.298	0.869	0.237	0.789	0.023	0.061	0.065	1.935	0.57	0.77
-0.266	0.869	0.237	0.789	0.023	0.061	0.065	1.935	0.57	0.77
-0.236	0.869	0.237	0.789	0.023	0.061	0.065	1.935	0.57	0.77
-0.209	0.869	0.237	0.789	0.023	0.061	0.065	1.935	0.57	0.77
-0.364	0.869	0.237	0.789	0.023	0.061	0.065	1.935	0.57	0.77
-0.329	0.869	0.237	0.789	0.023	0.061	0.065	1.935	0.57	0.77
-0.296	0.869	0.237	0.789	0.023	0.061	0.065	1.935	0.57	0.77
-0.265	0.869	0.237	0.789	0.023	0.061	0.065	1.935	0.57	0.77
-0.237	0.869	0.237	0.789	0.023	0.061	0.065	1.935	0.57	0.77
-0.396	0.869	0.237	0.789	0.023	0.061	0.065	1.935	0.57	0.77
-0.360	0.869	0.237	0.789	0.023	0.061	0.065	1.935	0.57	0.77
-0.325	0.869	0.237	0.789	0.023	0.061	0.065	1.935	0.57	0.77
-0.294	0.869	0.237	0.789	0.023	0.061	0.065	1.935	0.57	0.77
-0.264	0.869	0.237	0.789	0.023	0.061	0.065	1.935	0.57	0.77
-0.428	0.869	0.237	0.789	0.023	0.061	0.065	1.935	0.57	0.77
-0.390	0.869	0.237	0.789	0.023	0.061	0.065	1.935	0.57	0.77
-0.355	0.869	0.237	0.789	0.023	0.061	0.065	1.935	0.57	0.77
-0.322	0.869	0.237	0.789	0.023	0.061	0.065	1.935	0.57	0.77
-0.292	0.869	0.237	0.789	0.023	0.061	0.065	1.935	0.57	0.77

Explanation: αSiO_2 is silica activity, X_i = i component in X (atoms pfu, in specified site).
Activities are calculated parameters discussed in text.

Table A5-1. continued

T (K)	P (bars)	Log αSiO_2	$\Delta G/RT$	Activities CaTs Cpx	An Pl
1273	3000	-0.514	-4.552	0.024	0.703
1323	3000	-0.452	-4.409	0.024	0.703
1373	3000	-0.394	-4.276	0.024	0.703
1423	3000	-0.340	-4.152	0.024	0.703
1473	3000	-0.290	-4.037	0.024	0.703
1273	4000	-0.454	-4.415	0.024	0.703
1323	4000	-0.394	-4.276	0.024	0.703
1373	4000	-0.339	-4.148	0.024	0.703
1423	4000	-0.287	-4.029	0.024	0.703
1473	4000	-0.239	-3.918	0.024	0.703
1273	5000	-0.395	-4.277	0.024	0.703
1323	5000	-0.337	-4.144	0.024	0.703
1373	5000	-0.283	-4.021	0.024	0.703
1423	5000	-0.233	-3.906	0.024	0.703
1473	5000	-0.187	-3.799	0.024	0.703
1273	6000	-0.335	-4.139	0.024	0.703
1323	6000	-0.279	-4.012	0.024	0.703
1373	6000	-0.228	-3.893	0.024	0.703
1423	6000	-0.180	-3.783	0.024	0.703
1473	6000	-0.135	-3.680	0.024	0.703

Reaction constants (after DePaolo, 1979), A = -1034, B = 0.597, C = 0.0416, D = $9.17E^{-8}$.

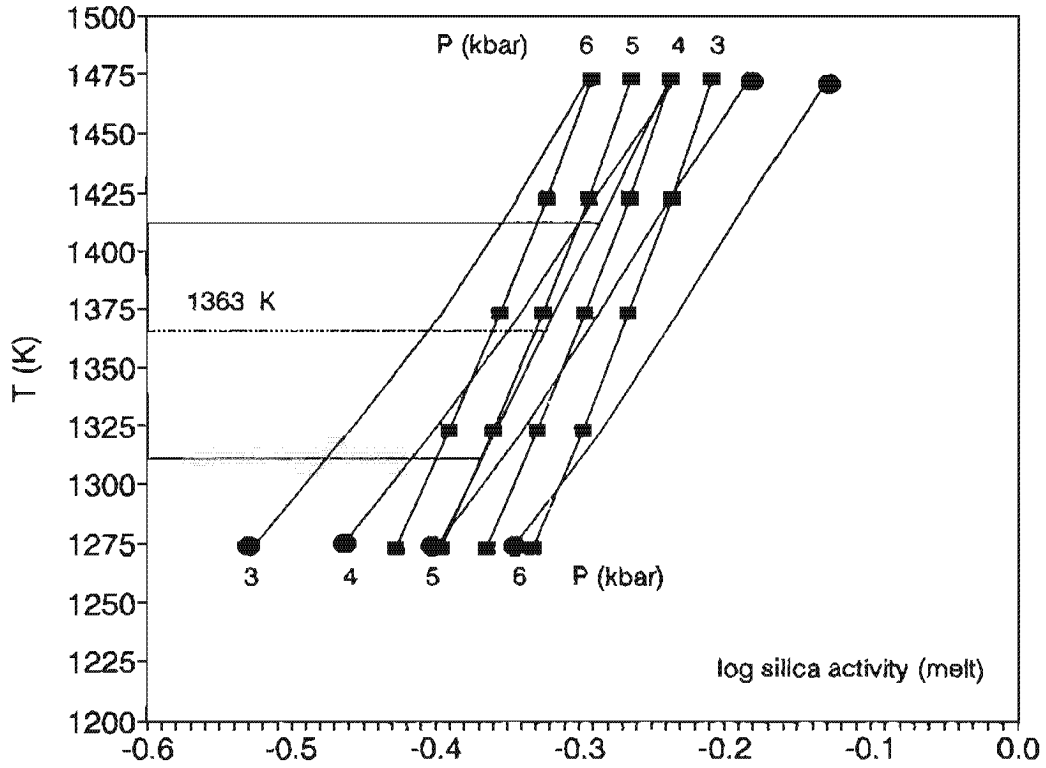

FIgure A5-1. Estimate of silica activity and total pressure from CaTs + SiO2 = An (lines connecting circles) and Fo + SiO2 = En (lines connecting squares) evaluated at various pressures and temperatures. Simultaneous solution of both equilibria yields P = 4.6 kbar.

b) Hornblende Geobarometer

The hornblende geobarometer of Johnson and Rutherford (1988) gives P_{TOTAL} for andesites and dacites. The expression $P = 4.28(Al^{TOT}) - 3.54$ results in 2.0 - 2.7 kbar for hornblende andesites and 1.6 - 1.8 kbar for dacites.

5.2.3. H_2O CONTENT

Solubility of H_2O in silicate melts was quantified by Nicholls (1990) using a regular solution model. The thermodynamic expression, based on equilibrium between a volatile phase and magma, is:

$$\mu^{o}_{H2O}/RT + \ln f_{H2O} - A/T - B - \varphi P = \ln X^{2}_{H2O} + (1-X_{H2O})^{2}\, \varphi/T.$$

where μ^{o}_{H2O} is the chemical potential in the ideal gas standard state of H_2O at 1bar. This term is defined as:

$$\mu^{o}_{H2O}/RT = 2.9147 \ln T - 9.6863E^{-4}T + 6.8593E^{-8}T^{2} + 77.8899T^{-0.5} - 28954.8T^{-1} - 2263.27T^{-2} - 15.8997.$$

A, B and φ are constants (-34345.9, 18.3527 and 4319.5 respectively) and the partial molar volume φP is:

$$\varphi P = (0.11T^{-1} + 4.432E^{-5} + 1.405E^{-7}T - 2.394E^{-11}T^{2})P + (7.337E^{-8}T^{-1} - 1.17E^{-8} - 9.502E^{-13}\,T)P^{2} + (1.876E^{-10}\,T^{-1} + 4.586E^{-13})P^{3} - 1.191E^{-14}\,T^{-1}\,P^{4}.$$

Substituting T, P_{TOTAL} and f_{H2O} for 2 hornblende andesites and 2 dacites gives X_{H2O} in Table 5-1.

Given X_{H2O}, initial Wt% H_2O in the melt is calculated from the relation:

$$Wt\%\ H_2O = GFW\ (100) / [1/X_{H2O} - (1\text{-}GFW)]$$

where GFW is the gram formula weight of (H_2O / melt). Burnham and Davis (1974) defined X_{H2O} with respect to 1 mole of silicate melt on the basis of 8 oxygens. This is because solubility of H_2O is dependent on melt composition at constant temperature and pressure, and to relate "activity" of H_2O with melt, there must be correspondence between "activity" of mineral components and melt composition. In silicate melts, such a correspondence does not occur (Glazner, 1984) because melts do not have fixed sites at which ions can mix randomly and because melts are not bound by stoichiometry. In the regular solution model the melt is considered to have a crystal structure. For example, Ghiorso et al (1983) treated the melt as a mixture of 8-oxygen units. Following the example of Nicholls (1980), oxides normalised to 8 oxygens are chosen as the components which comprise the melt. Using 73 as the mean atomic number and X_{H2O} = 0.1 (sample APO6) the above equation gives Wt% H_2O at equilibrium = 2.8. Pre-eruption H_2O contents of the groundmass can then be estimated using phenocryst modes as the crystallised fraction. Table 3-1 (Chapter 3) gives a total phenocryst mode of 64 vol% for dacite Type 2 (sample APO6, analysis 86, Appendix 4). Thus pre-eruption Wt% H_2O = 2.8/(1-0.64) = 7.8.

Table A5-2. Partition coefficients used in melting and fractional crystallisation models.

	Plagioclase	Olivine	Clinopyroxene	Orthopyroxene	Spinel	Amph
Rb	0.03 / 0.02	0.0002	0.0002 / 0.09	0.03 / 0.002	0.0001	0.05
Ba	0.15 / 0.06	0.0001	0.002 / 0.02	0.012 / 0.003	0.001 / 0.05	0.22
K	0.02	0.001	0.003	0.001	0.001	na
Sr	1.83 / 3.8	0.0002	0.01	0.02 / 0.01	0.0001	0.19
Nd	0.114	0.0013	0.09	0.0019	0.037	0.45
Zr	0.01	0.023	0.14	0.043	0.02	0.1
Y	0.05	0.13	0.69	0.30	0.10	na
La	0.219	0.0005	0.02	0.0005	0.029	0.2
Ce	0.169	0.0008	0.04	0.0009	0.032	0.26
Cr	0.01	2.4	7.5	8.7	150	30
Ni	0.05	10.0	1.7	7.3	6	8
V	0.00	0.0	1.1	1.1	20	6

Data mainly from Ewart and Hawkesworth (1987). For Nb, D_{Nb}^{cpx} = 0.02 (McCallum and Charette, 1978), others assumed equal to 0.001 (after Johnson et al, 1990). For minerals with dual values, the first coefficient is used for basic melts and the second for felsic magmas. Amphibole data (Kelemen et al, 1990) used only for least squares crystal fractionation models. Y was used only for partial melting models. Abbreviations: Amph, amphibole; na, not applicable.

GEOLOGIC MAP OF CENTRAL MINDANAO

9N
12330E

AGE SYMBOLS

Qal	Quaternary Alluvium
Qv	Quaternary volcanics
Qp	Pleistocene
Tpv-Qpv	Plio-Pleistocene volcanics
Tp-Qp	Pliocene - Pleistocene
Tp	Pliocene
Tpl	Upper Pliocene
Tml	Upper Miocene
Tmm	Middle Miocene
Tme	Lower Miocene
To	Oligocene
Tol	late Oligocene
Te	Eocene
pT	Paleocene
BST	Basement

LITHOLOGY SYMBOLS

- Clastics
- Limestone
- Volcanics
- Basement

STRUCTURAL SYMBOLS

- Lithological boundary
- Anticline
- Syncline
- Fault
- Normal fault
- Thrust fault
- Strike-slip fault

Butuan Bay
Gingoog Bay
Tpl
Qal
Tpv-Qpv
Tp-Qp
Mt Obulan
Qv
Mt Balatocan
Tml-Tp
Qal
Cabulic Canyon
Lanisi
Mt Pamalihi
Mt Mangaban
Tml-Tp
BST
Tagaloan
Qal
BST
BST
BST
Tpv-Qpv
Talakag
Pantalan
BST
Ticalan Plain
Mt Katanglad
Qv
MALAYBALAY
Tmm
BST
Kaulayanan
BST
Valencia
Qv
Mt Kalatungan
Kiharong
Qal
Qv
Qv
To-Tme
Lake Lanao
Tpv-Qpv
Qv
Mt Musuan
Qav
Qv
Quezon volcanics
Butong
To-Tme
Mt Kidonging
To
Tme
Tpv-Qpv
Mt Ragang
Qav
BST
Tpv-Qpv
Illana Bay
Mt Bita
Qv
Qv
Tml-Tp
Tml-Tp
Mt Malambo
Tmm
Tp
Tp
Tp-Op
Tpl
BST
Tml
Tpv-Qpv
Mt Tinanan
Tinanan Plain
Aracan Plain
Qv
Qv
Mt Carmen
Qal
Tp-Qp
Tp
Tme-Tmm
Kidapawan
Mt Talomo
Tpv-Qpv
Tp
Qal
Tme
Tmm
BST
Qv
Mt Apo
Mt Sibulan
Qp
Tp
Tml
Qal
Tp-Qp
To-Tme
Tml-Tp
Tml
Tp
Tml
BST
BST
BST
Tp-Qp
Qv
Qal
Mt Matutum
BST

0 40
km

7N
12330

GEOLOGIC MAP OF MINDANAO

AGE SYMBOLS

Q	Quaternary Alluvium
Qv	Quaternary volcanics
Qp	Pleistocene
Tpv-Qpv	Plio-Pleistocene volcanics
Tp-Qp	Pliocene - Pleistocene
Tp	Pliocene
Tpl	Upper Pliocene
Tml	Upper Miocene
Tmm	Middle Miocene
Tme	Lower Miocene
To	Oligocene
Tol	late Oligocene
Te	Eocene
pT	Paleocene
BST	Basement

LITHOLOGY SYMBOLS

- Clastics
- Limestone
- Volcanics
- Intrusives
- Metamorphics

STRUCTURAL SYMBOLS

- Lithological boundary
- Anticline
- Syncline
- Fault
- Normal fault
- Thrust fault
- Strike-slip fault

Modified after Philippine Bureau of Mines (1963, 1982).